Hermanus Magnetic Observatory
South Africa

PROCEEDINGS OF THE Xth IAGA WORKSHOP ON GEOMAGNETIC INSTRUMENTS DATA ACQUISITION AND PROCESSING

April 15-24, 2002

Editor: Louis Loubser

Issued by:
HERMANUS MAGNETIC OBSERVATORY
P.O. BOX 32
HERMANUS 7200
SOUTH AFRICA

Internet: http://www.hmo.ac.za

Photo of all the Delegates

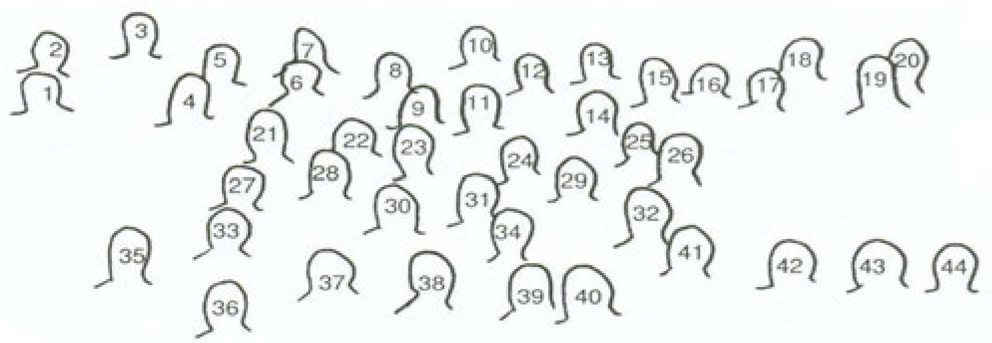

1 J. Carrigan
2 H-U Auster
3 G Schwarz
4 G Schulz
5 M Menvielle
6 J-J Schott
7 J Linthe
8 P Crosthwaite
9 M Váczyová
10 F Valach
11 I Hrvoic
12 W Worthington
13 P du Toit
14 L Loubser
15 A Rimi
16 Y Yamada
17 T Haile
18 J Rasson
19 A Berarducci
20 O Rasmussen
21 L Newitt
22 M Mandea
23 V Doumouya
24 M Mbemba
25 L McKee
26 P Kotzè
27 J Horacek
28 P Hejda
29 B Pretorius
30 T Arafa-Hamed
31 A Nhatsave
32 P Sutcliffe
33 K Pajunpää
34 A Patil
35 L Pedersen
36 M Kampine
37 RC Deka
38 D Gouws
39 G Overmeyer
40 H Theron
41 L Hegymegi
42 E Pulz
43 B Ginzburg
44 J Kultima

Absent: K Yumoto, E Moran, A Volker

Preface

During the XXII IUGG General Assembly at Birmingham, U.K. (July 1999) the proposal was accepted that the Hermanus Magnetic Observatory (HMO), South Africa should host Xth IAGA Workshop on Geomagnetic Observatory Instruments, Data Acquisition and Processing. The proposed Workshop took place during15 – 24 April, 2002 at the HMO Hermanus, South Africa and this publication is a report about the papers which were presented and the calibration results of the absolute instruments.

This was the first in this series of workshops to be held in Africa. It was attended by 40 delegates from 24 countries. The HMO was particularly pleased to welcome the largest ever delegation from the African continent to attend such a Workshop. African delegates from the Democratic Republic of the Congo, Egypt, Ethiopia, Ivory Coast, Morocco and Mozambique attended. This Workshop therefore not only served to promote geomagnetism worldwide, but also in Africa.

The wide international participation in the Workshop was made possible through the financial support provided by IAGA and INTERMAGNET.

The objective of the workshop was to do proper absolute magnetic field observations under controlled conditions, as well as to inter-calibrate equipment to detect possible instrumental, calibration or measurement errors. A further objective was to bring together the manufacturers and users of geomagnetic instruments.

The Workshop followed the same format as previous ones with a series of Measurement sessions and Presentation sessions.

During the practical sessions held over the first four days, 16 observers made a total of 83 absolute observations of declination and inclination using DI-flux magnetometers from their own respective observatories. Four pillars in the Absolute House were available for these observations. All absolute readings were reduced to the observatory base-line. Preliminary base-line values were presented to the observers during the course of the Workshop. Four proton precession magnetometers were also calibrated during this session.

The presentation sessions were held over three days during the second week. A total of 40 oral papers and 7 poster papers were presented. These papers addressed several outstanding issues related to observatory instrumentation and data processing.

A practical training session in the use of geomagnetic equipment was also conducted. Feedback from the participants indicates that it was a successful Workshop and that they benefited by acquiring experience and learning several new techniques.

The LOC wishes that an even successful workshop will be held in Japan in 2004.

Louis Loubser (Editor)

Obituary – Arthur Wallace Green, 1929 – 2001

Arthur Wallace Green, Jr., a retired brigadier general of the US Air Force, died of complications from surgery on December 12, 2001, at the age of 72. A native of Massachusetts, he enlisted in the Air Force in 1947 and was commissioned at Ellington Air Force Base as a navigator in 1950. He flew 56 combat missions in B-26s in Korea and was then assigned to SAC as an RB-36 navigator until his release from active duty in 1953. In the reserves, General Green served as a bombing and navigation instructor and held staff positions in the intelligence field. He was a life member of the Air Force Navigator Observers Association (AFNOA), serving as both 1st V-P and President.

In civilian life, General Green received a masters degree in Electrical Engineering from the University of Houston and a Doctorate of Philosophy in Physics from Texas Christian University. He was a senior scientist for Texas Instruments Company, associate director of the Marine Geology and Geophysics Group in Woods Hole, Mass., and a co-founder of the INTERMAGNET Geomagnetic Observatory Network, which consists of 75 observatories operating in 24 nations. At the time of his death, Dr. Green was President of Geomax, Leader of the U S Geological Survey Geomagnetism Group, and on the Board of Trustees of the U S Air Force Academy Falcon Foundation.

Dr. Green is survived by his wife Amy, sons Michael and Christian, stepchildren Louise Swanson and Hank Windmoeller, and seven grandchildren.

Bill Green was a special friend who will be missed but remembered by all for a long time.

(The above obituary appeared on the web site of the US Air Force Navigators and Observers Association. Thanks to Richard Ahrens, Editor, who gave permission to publish it in this Proceedings.)

Results of DI-flux and proton magnetometer comparison during the Xth IAGA Workshop.

L. Loubser
Hermanus Magnetic Observatory, National Research Foundation

1. DI-flux session

The reference for all DI-flux observations was the three component FGE-fluxgate, which is the standard magnetometer at the Hermanus Magnetic Observatory (HMO). It is a suspended fluxgate manufactured by the Danish Meteorological Institute, Denmark. It is situated in the Variometer House (see Fig.1).

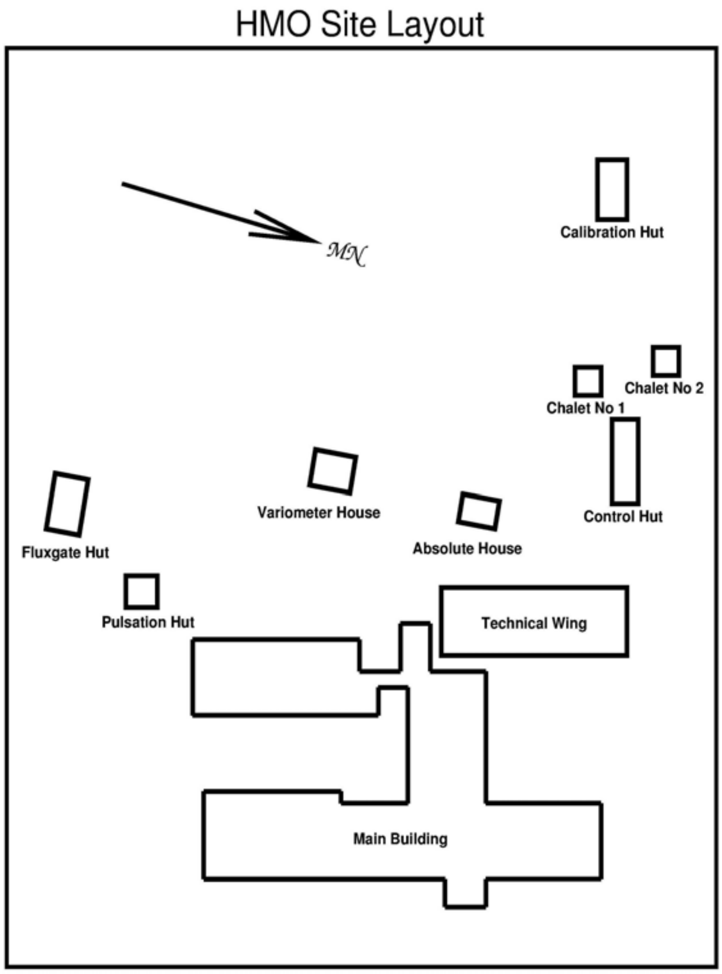

Fig 1 . Site Layout of HMO buildings

The Geometrics proton precession magnetometer, which is an integral part of the proton vector magnetometer, was used for total field values and is situated in Chalet no 2.

The absolute observations were carried out in the Absolute House. Besides pillar no 1 which is the primary observation pillar, pillars no 4,6 and 9 were also available for observations during the Workshop. The differences between the pillars were determined prior to the Workshop and Table 1 shows the values which should be added to the observed base-line values in order to refer it to the primary pillar no 1. In the case of F the value should be added to the recorded F value at the time of the observation. The standard deviation values are indicated by the symbol σ.

	D	σ	*H*	σ	*Z*	σ	*F*
	(min of arc)		(nanoteslas)		(nanoteslas)		(nanoteslas)
Pillar no 1	0.00		0.0		0.0		18.6
Pillar no 4	-0.33	0.09	-0.5	0.24	2.1	0.13	20.7
Pillar no 6	-0.07	0.05	-0.7	0.24	2.3	0.18	21.0
Pillar no 9	-0.20	0.07	-1.3	0.39	3.4	0.16	22.2

Table 1. Pillar differences

The observed DI-flux measurements were entered by observatory staff onto computer hard-disk and processed. The preliminary base-line values were presented to the observers during the Workshop.

Everyday during lunch-time of the first week of the Workshop, HMO staff also performed absolute observations in order to supply reference base-lines values for each day. Fig. 2 shows the stability of the base-line values at Hermanus for the period Jan - June 2002.

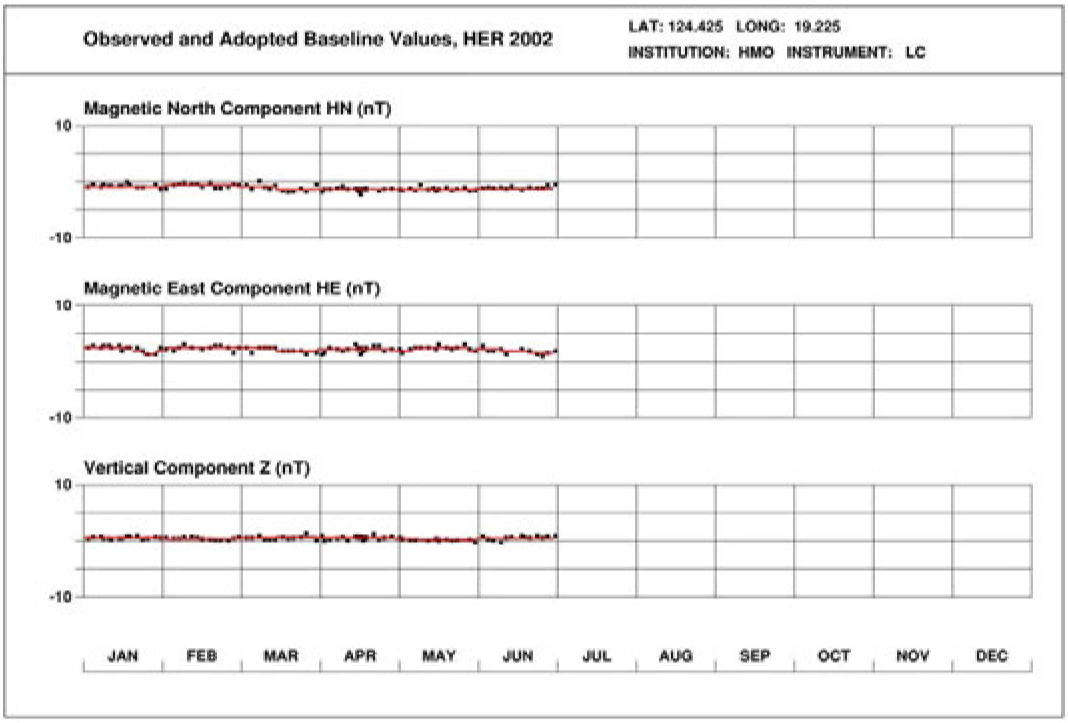

Fig.2 Observed and adopted base-line values.

The final results are presented in Table 2 . The first column of each element is the correction which should be applied to the observed base-line values in order to refer it to the standard observation pillar no 1. The standard deviation of the all observations for each observer is indicated by σ. The last row of the Table contains the results of the HMO staff.

	ΔD	σD	ΔI	σI	ΔH	σH	ΔZ	σZ
	(sec of arc)		(sec of arc)		(nT)		(nT)	
Auster	4.0	20.2	9.5	3.9	0.2	0.85	1.1	0.71
Berarducci	1.3	6.9	-1.0	3.2	-0.3	0.61	-0.2	0.36
Crosthwaite	4.2	6.1	0.1	1.9	0.0	0.23	0.0	0.26
Horacek	11.4	5.6	3.1	4.1	0.3	0.46	-0.2	0.81
Kampine/Nhatsave	-16.2	15.6	-0.8	9.9	-0.7	1.08	2.0	0.52
Kultima	-2.7	6.7	-1.6	2.3	-0.1	0.26	-0.3	0.25
Linthe	-16.0	6.9	-1.1	2.7	-0.1	0.36	-0.2	0.13
McKee	-8.7	11.5	5.4	3.3	0.6	0.46	0.3	0.25
Newitt	-2.3	14.8	3.4	1.9	0.4	0.20	0.2	0.32
Pajunpaa	-3.0	6.6	-1.0	2.2	0.0	0.15	-0.2	0.35
Pedersen	7.7	7.8	-0.6	1.0	0.0	0.15	-0.2	0.15
Rasson	5.0	12.8	-8.1	2.4	-1.0	0.32	-0.4	0.18
Vaczyova	23.0	1.7	-12.7	3.2	-1.4	0.34	-0.7	0.33
Valach	18.5	10.6	-11.0	6.4	-0.8	0.14	-0.7	0.42
Worthington	-3.8	11.5	0.2	2.7	0.0	0.32	0.0	0.29
Mean	**1.5**	**4.8**	**-1.1**	**2.2**	**-0.2**	**0.3**	**0.0**	**0.2**
HMO staff	0.0	3.4	0.0	1.5	0.0	0.14	0.0	0.17

Table 2

Although all absolute values giving residuals in excess of 30" (for *D* and *I*) and 2 nT (for *H* and *Z*) were discarded, this rule was not strictly adhered to. For example if an observer has a number of good residuals clustered and one bad value just short of this criterion, then this bad one was discarded.

The instrument used by Auster is not a traditional DI-flux but equipment developed by himself to measure the geomagnetic field vectors by using a scalar magnetometer and a three axis fluxgate magnetometer rotating about two defined axes.

Also note that Vaczyova and Valach used the same used DI-flux and also McKee and Newitt.

The two delegates from Mozambique, i.e. Kampine and Nhatsave used the DI-flux which is the property of J. Rasson. They received practical training during the Workshop and maybe they were not familiar with the equipment.

The mean differences above, i.e.,

Mean ΔD = +1.5 " σD = 4.8 "
Mean ΔI = -1.1 " σI = 2.2 "
Mean ΔH = -0.2 nT σH = 0.3 nT
Mean ΔZ = +0.0 nT σZ = 0.2 nT

indicates that the HMO's observatory reference DI-flux is within acceptable
limits. Fig. 3 shows the results in a graphical format. The value in brackets after each delegates name indicates the number of observations used after omitting bad readings.

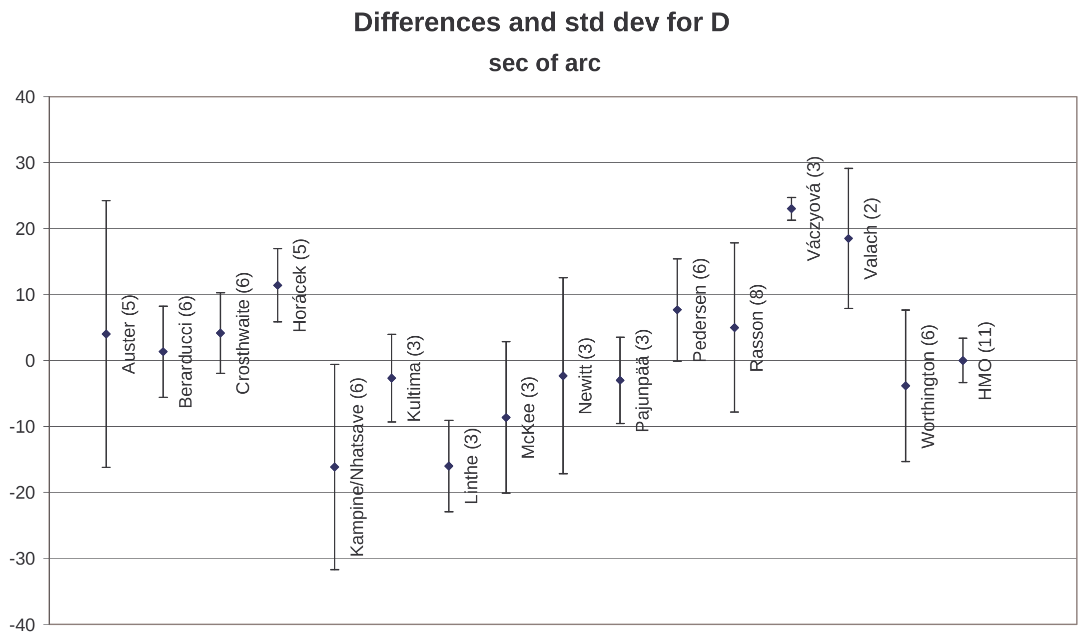

Fig 3 Magnetic declination

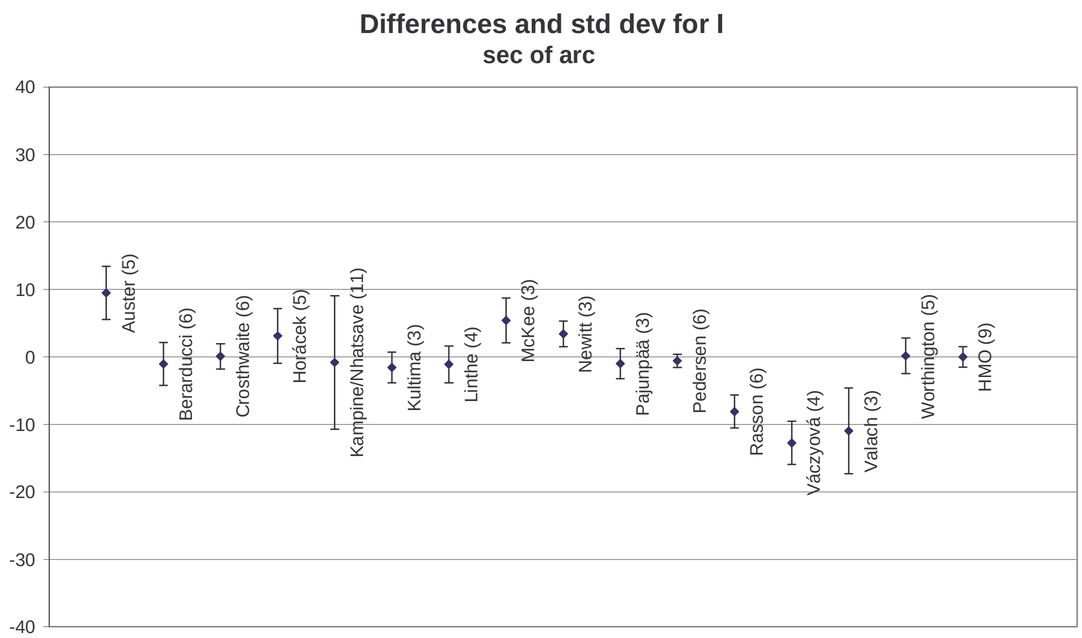

Fig 3 Magnetic inclination

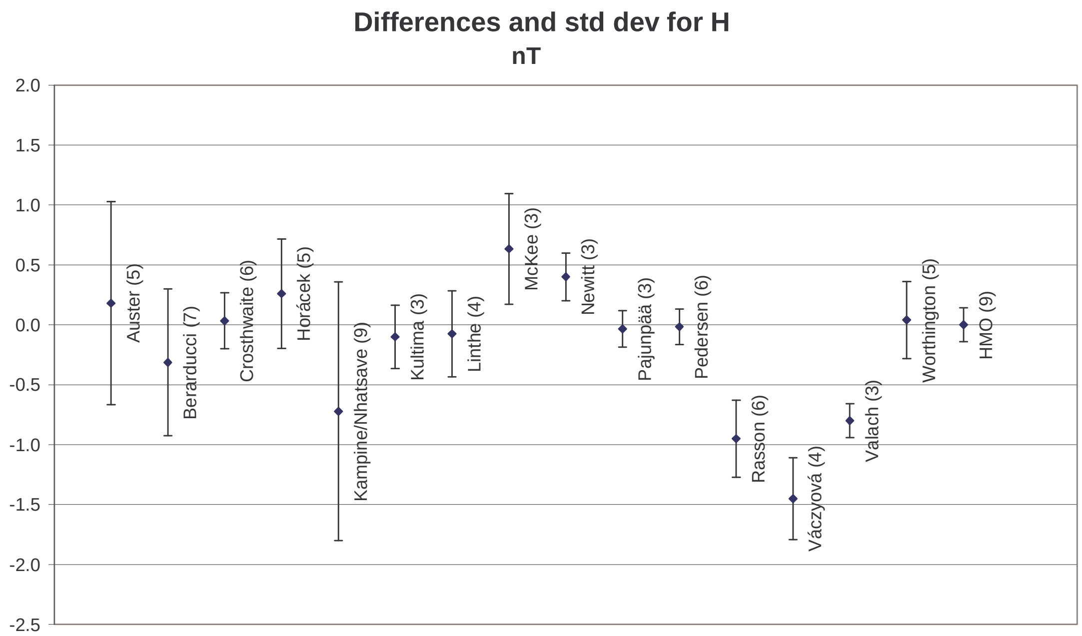

Fig 3. Horizontal Intensity

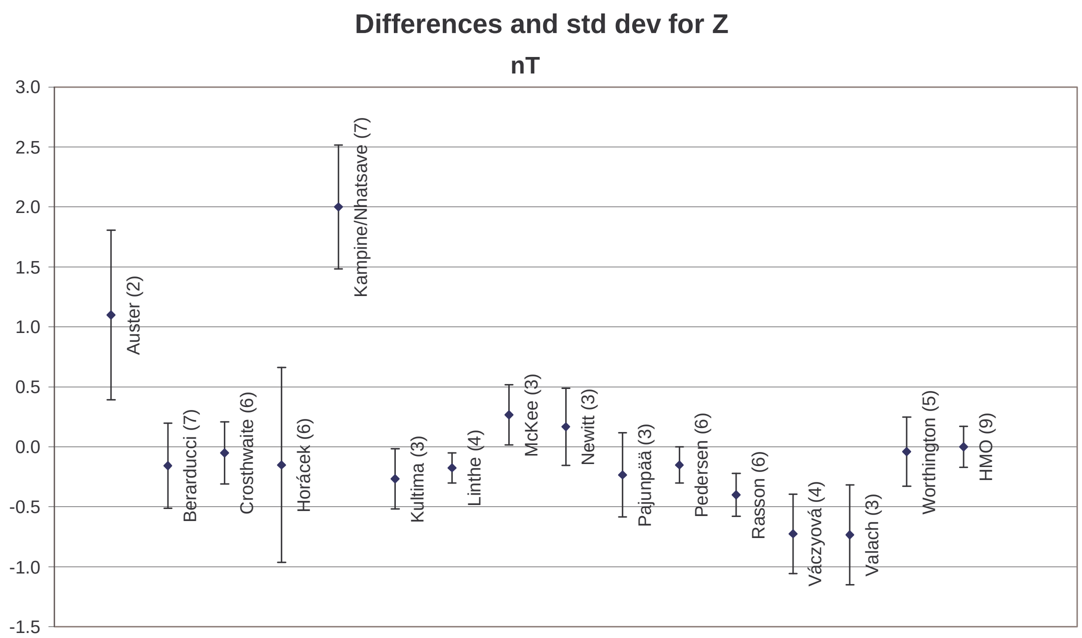

Fig 3. Vertical Intensity

2. Proton magnetometer session

The calibration of proton magnetometers took place on April 18, 2002 in a non-magnetic area between the Main building and the Variometer house. Four instruments were presented for calibration.

A Chemtron magnetometer tester G01, serial no. 8277 was used for this purpose. It was last calibrated on April 9, 2002. The error was then 0.011 nT at 30000nT.

The total field is given by

$$F = 2\pi \mathbf{f}/\gamma_p$$

where $\gamma_p = 2.6751525 \cdot 10^8 T^{-1} s^{-1}$ and **f** is the transmitted frequency in Hz.

Observer	Crosthwaite		Patel		Yamada		Kampine	
Country	Australia		India		Japan		Mozambique	
Instrument	GSM 90		IIG		Geometrics 856		Elsec 820	
Nominal *F* (nT)	Corr (nT)	σ	Corr (nT)	σ	Corr (nT)	σ	Corr (nT)	σ
25000	0.23	0.10	0.00	0.00	-0.43	0.19	0.06	0.16
30000	0.26	0.12	0.07	0.05	-0.51	0.23	-0.07	0.05
37500	0.33	0.15	-0.01	0.04	-0.60	0.26	-0.10	0.06
50000	0.45	0.20	0.00	0.00	-0.81	0.36	-0.17	0.08
60000	0.52	0.23	-0.01	0.04	-0.93	0.41	-0.19	0.09
75000	0.63	0.28	No readings		-1.13	0.50	-0.23	0.11

σ is the standard deviation.

Magnetic Observatory and Repeat Station Measurements in Moçambique

Jean L. Rasson,
Institut Royal Meteorologique (IRM), Centre de Physique du Globe, B-5670 Dourbes, Belgique

Francisco da Silva Sumbana, Manuel F. Kampine, Armindo A. Nhatsave,
Direcção Nacional de Geologia (DNG), Dept. de Geofisica Global, Caixa Postal 217, Maputo, Moçambique

and

John C. Riddick,
British Geological Survey (BGS), West Mains Rd., Edinburgh EH9 3LA, Scotland

Abstract

This paper will focus on the magnetic observatories of Maputo (LMM) and Nampula (NMP), presenting the current efforts deployed to operate them and examining the available data.

We will also examine some historical repeat station data and the measurements taken at the stations which were reoccupied during the 2001 field trip.

Introduction

The work described here is the result of collaboration between several people and organisations, all striving towards the same goal, i.e. to get high quality geomagnetic ground observations in the Republic of Moçambique and to establish a durable and sustainable infrastructure for the collection of these data in the long term.

A very useful framework for achieving this is the INTERMAGNET organisation, which has set standards for instrumentation, measurement protocols and data collection and transmission.

When inspecting a map of Sub-Saharan Africa, (Figure 1) where the locations of the various Magnetic Observatories is displayed, it is immediately obvious that there are not many observatories in this region, and that large gaps exist, with many countries having no magnetic observatory infrastructure at all. Sudan, Kenya, Somalia, Tanzania, Malawi, Zimbabwe, Zambia, Botswana, Angola and Democratic Republic of Congo form an enormous contiguous and adjacent group of countries where no magnetic information is systematically gathered. This large geographical void has a negative impact on many practical and scientific activities. It represents a strong hazard to people using a magnetic compass for navigation in those countries.

The distance between Hartebeesthoek (HBK) and Maputo (~500km) is the smallest between two observatories in Africa, and this is fortunate as those observatories cover a part of the continent where the spatial variation of the declination secular variation is the largest.

Nampula Observatory (NMP) was installed in the late seventies and was operative only a few years. We visited this station during this work and took preliminary steps to facilitate its reopening.

Francisco da Silva Sumbana, Manuel F. Kampine and Armindo A. Nhatsave are the observers in charge of Maputo and are responsible for the routine operations in the LMM geomagnetic observatory as well as the field-work.

John Riddick from BGS was the first to assist LMM in 1993 after a difficult period for the Republic and his involvement. This continues to the present day by facilitating equipment and advice to the LMM observatory. The British Geological Survey has been involved with the hand scaling of the LMM magnetograms since the late eighties. Jean Rasson made visits to LMM in 2000 and 2001 with the purpose of giving training in the use of DI-fluxgate’s for observatory and field use and to repair the variometers. He participated in a field trip to Beira and Nampula in July 2001. Dourbes, Niemegk and Hermanus Observatories invited the Mozambican scientists to their IAGA workshops in 1994, 1996 and 2002, and this helped greatly in the training, management and planning of the Observatory operation.

Figure 1: View of the Magnetic Observatories distribution in Africa and farther to the South. NMP is not operating and Beira is a repeat station. Orthographic projection centered on Maputo (LMM).

We cannot conclude these introductory notes without acknowledging the huge contribution of the Servicio Meteorologico Nacional (SMN) and other Institutions from Portugal. We appreciate the careful work of many individuals (let us mention Srs A.F.Paulo, F.Pastor, C.Gonçalves, Oliveires Barreiros, Ferraz, Mendes Victor) in planning the Geomagnetic Observatories and the fieldwork in the Mozambican territory. The archives of the DNG are witnesses of the excellent measurements taken by them over the past century.

Recent historical perspective

Magnetic measurements were first performed in Moçambique and in the adjacent seas by the early sailors and pilots en route from Europe towards the Indies. Some measurements are available from the seventeenth century.

Routine continuous observations started in 1957 with the building of the Magnetic Observatory in Lourenço Marques, the present Maputo. Below we will give some historical milestones. It is once more clear that successful magnetic observations result from stable political conditions.

1956	Construction of the Magnetic Observatory of Lourenço Marques (Maputo) by the SMN (Portugal) on the site of the International Airport
1957	Start of magnetic observations in Lourenço Marques

1960-1961	First field magnetic measurements at 22 national airports
1964-1966	Production of a magnetic map of Moçambique based on a network of 238 stations. The reference epoch was 1966.5. Temporary observatories were set-up in Vila Pery and Nampula. Secular variation was computed at the points also measured in 1960/61
1971	Starting the construction of Nampula Observatory.
1982	Start of observations in the Magnetic Observatory of Nampula.
1987	Magnetic Observatory of Nampula is closed.
1989	Stopped the observations in Maputo
1993	Contacts between DNG and BGS in order to restart the magnetic observations.
1994	Srs Sumbana and Matosse, in charge of LMM, participate in the IAGA Geomagnetic Instrument Workshop in Dourbes.
1996	BGS installs a digital variometer at the observatory of Maputo.

The LMM Magnetic Observatory

This Observatory is situated on the premises of the international airport of Maputo, in direct vicinity of the aircraft taxi and runways. It was built on fenced-off ground of 1 hectare in area, situated inside the closed zone belonging to the airport. This configuration is very satisfactory since it provides a double fencing for the observatory and it is completely encircled by land subject to international law.

The absolute house is a large L-shaped building, equipped with not less than 9 non-magnetic pillars, most having a view on suitable targets, one of the targets being a pillar inside the Observatory grounds. The variometer house (for a description, see the BGS report [i]) has two spacious vaults and two ground floor laboratories. The first vault is equipped with a large pillar. Vault 2 has two pillars which were built for the classical photographic variometer and recorder set-up. There is a second variometer house, a ground floor construction. Additionally, 3 more buildings are provided as living quarters for staff.

Variometric Instrumentation

Since 1996, a digital variometer consisting of an EDA DHZ tri-axial fluxgate, a BGS 16 bit data logger and an Olivetti laptop computer operated in the first vault of the variometer house. The correct timing is provided by a Motorola Oncore GPS receiver. The EDA sensor has been installed on a short aluminium pole cemented in the concrete floor near the large pillar in the southern extremity of the vault.

It is known that the EDA is not a high precision variometer as it has a high temperature coefficient, but with careful and frequent baseline control and efficient thermal isolation and high thermal inertia, this instrument can give satisfactory results. Further details relating to stability are given later in this paper.

Absolute Instrumentation

In August 2000, BGS donated an ELSEC 820 proton magnetometer and a Ruska DIflux besides a FLM1/B fluxgate electronics to Maputo Observatory. This was a much needed step since the Askania declinometer was out of order since the end of 1999, and the Scintrex Proton Precession Magnetometer MP2 was behaving erratically. Therefore, reliable baseline observations based on sound absolute measurements restarted effectively in August 2000.

The Ruska DIflux was converted from a Ruska nonmagnetic theodolite to a DIflux at Dourbes Observatory Instrumentation Laboratory. The theodolite was a gift from the Dourbes Instrument Pool by the US Geological Survey. To read the Ruska circles two microscopes 180° apart are used, each giving a resolution of 30 seconds of arc. This resolution on the reference mark sighting can be improved to nearly 15 seconds by the observer by taking readings on each side of the circles once with the vertical circle to the left and once to the right (a procedure called "plunging"), and using the mean of these four readings. A Pandect LFG-A13 fluxgate sensor was mounted in a V-groove in the sensor holder mounted on top of the telescope as shown in Figure 2. A 6 m cable connects it to the FLM1/B fluxgate electronics which have a 0.1nT resolution

The theodolite was carefully checked for residual magnetism, and magnetically cleaned where necessary. As a final check of the overall accuracy of the Ruska DIflux, (Serial Number RO1) a series of intercomparison measurements were performed in Dourbes Magnetic Observatory. These measurements were between RO1 and the observatory reference Zeiss 010 (Serial Number 116) DIflux, using both instruments to measure the D_0 and I_0 baselines of the ELSEC 8200 DIDD variometer. The results of this comparison are given in Table 1. The sensor collimation (ESI, EAZ) and magnetisation (ESO) errors as well as the vertical I gradient (GI) are given.

Date	D_0	ESO	ESI	EAZ	I_0	ESO	ESI	GI	**Instr**
Units:	°	NT	"	"	°	nT	"	"	
13-jul-00	-1.340	-1.	-17	73	65.457	3.5	-9	19	RO1
13-jul-00	-1.343	0.6	18	5	65.456	0.7	20	4	116
14-jul-00	-1.338	1.6	-17	85	65.458	2.1	-7	13	RO1
14-jul-00	-1.341	0.8	21	4	65.457	0.3	19	4	116
8-aug-00	-1.338	-1.	-19	74	65.458	-3.	-8	5	RO1
8-aug-00	-1.342	0.3	19	8	65.456	1.0	22.	4	116

Table 1. Intercomparison of Ruska RO1 and Zeiss 116 Difluxes by D and I baseline measurements in Dourbes. See text for column header description.

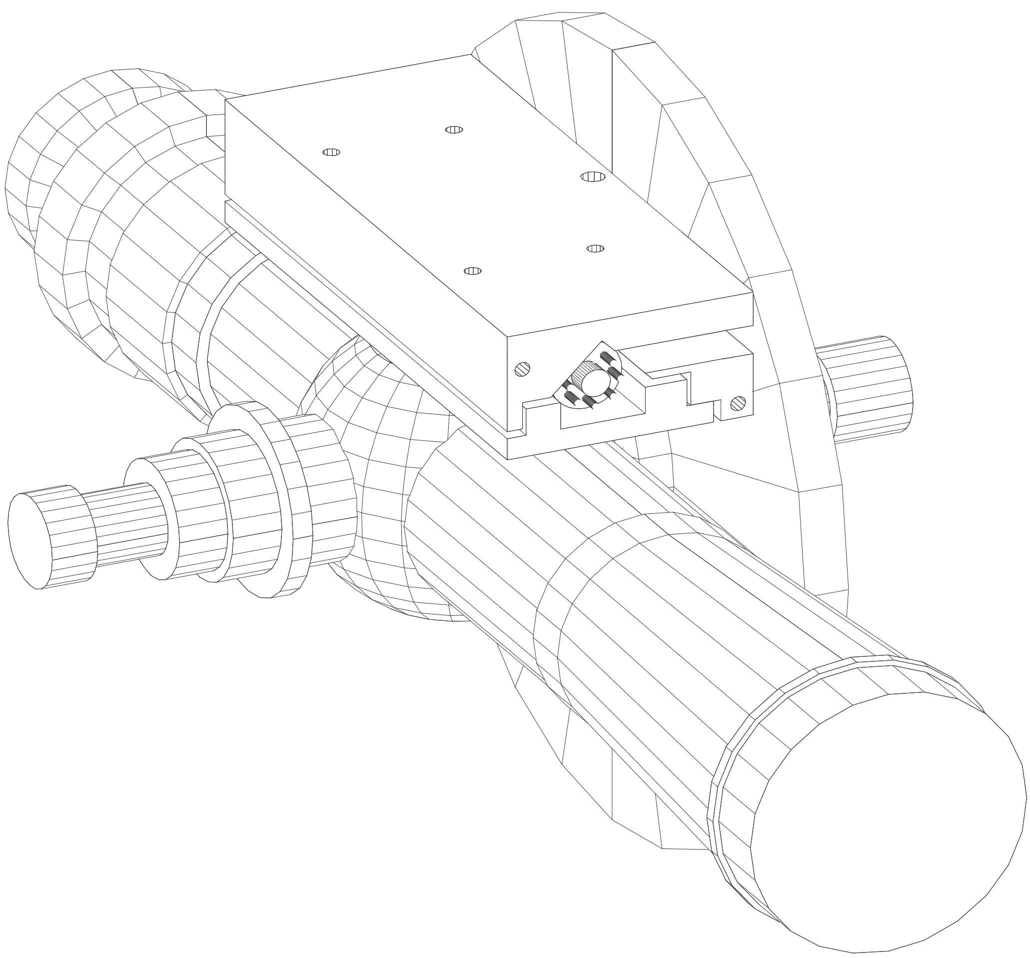

Figure 2. This shows the Ruska theodolite telescope with horizontal axis / vertical circle transformed for DIflux operation. The box for mounting the fluxgate sensor is screwed on the vertical circle, hence rotating with the telescope. Inside the box, in a V-groove, the Pandect fluxgate sensor can be seen.

Subtracting the mean baseline values obtained by the two instruments, we can assess the relative accuracies: D_0(RO1-116) = 0.0031° = 11” and I_0(RO1-116) = 0.0012°= 4”. As the 116 is known to be free from defects, we may safely conclude that the RO1 has the same quality, since the differences lie beyond the RO1 overall circle reading resolution.

The ELSEC 820 proton magnetometer was checked in the Dourbes Scalar Magnetometer Calibrator and found to be free from errors at the 0.2 nT level. See also the Hermanus 2002 Workshop scalar magnetometer tests in these Proceedings for further intercomparison measurements of this magnetometer.

Observatory Reference Changes

During the installation of the new absolute instrumentation (Aug 2000), all parameters of the observatory were checked and the most convenient pillar was selected as a new reference. This pillar is named "pillar 3". Figure 3 shows some of the pillars.

Change in F measurement as result of change in instrument from Scintrex MP2 #2 to ELSEC820 and change of pillar X to pillar 3	$dF = F_3 - F_x = +10.9$ nT.
Change in H measurement as result of change in instrument from QHM to DIflux RUSKA RO1 and change of pillar 2 to pillar 3	$dH = H_3 - H_2 = -16.2$ nT.
Change in D measurement. Presumed zero.	$dD = 0$

Table 2: Changes in the Geomagnetic field reference, resulting from moving observations from the old to the new instrumentation and pillars in the observatory.

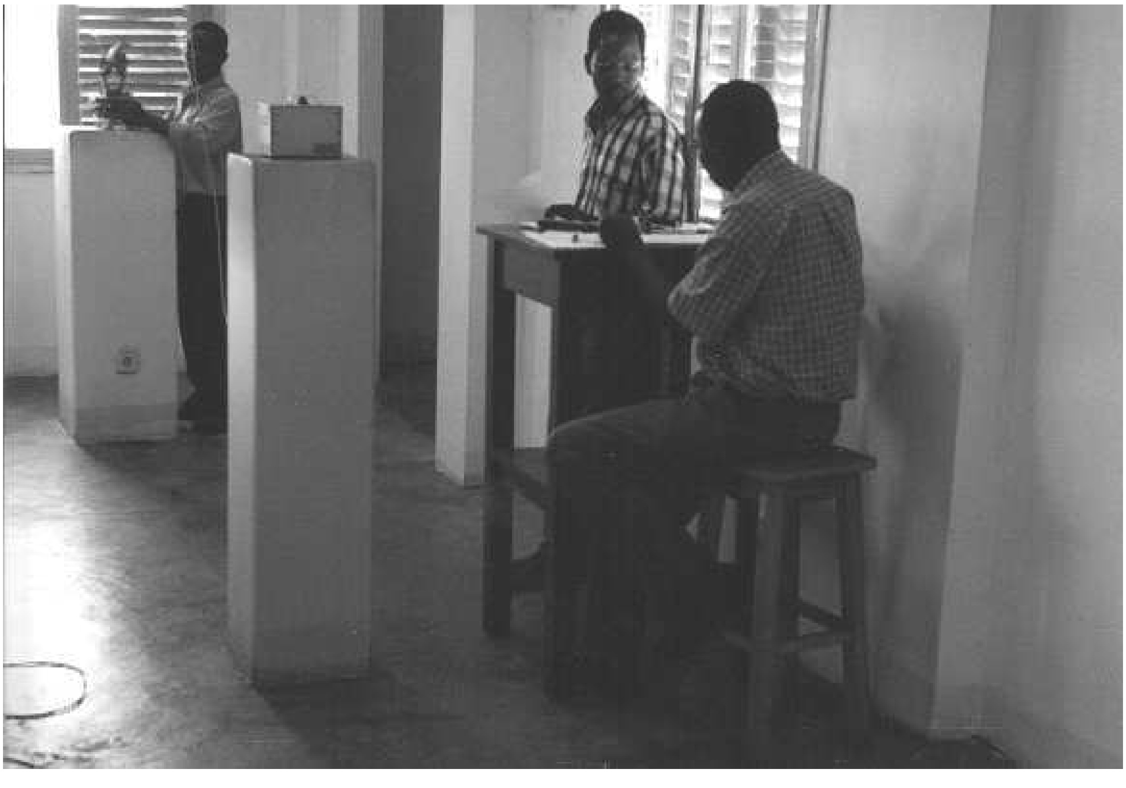

Figure 3. The Absolute House in the Maputo (LMM) observatory. The pillar in the foreground is pillar 2, used in the past for QHM measurements. In the background, with the Ruska DIflux, is pillar 3, presently the reference pillar for LMM.

As a result of this site change, the changeover from the Scintrex proton magnetometer to the ELSEC 820 and the discontinued use of the QHM as absolute instrument for H measurement, LMM observatory experienced a change in the H reference. In order to know the magnitude of this change the pillar differences were measured by using the new absolute instrumentation. The pillar differences are given in Table 2. It is noteworthy to mention that the Scintrex MP2 PPM #2 was calibrated in the Dourbes IAGA workshop in 1994 and had given the calibration equation:
$F = F_{Scintrex\#2} + (-4nT)$, for the field values in Maputo. This shows that the value of the F jump resulted partly from the correction of a calibration error of the Scintrex.

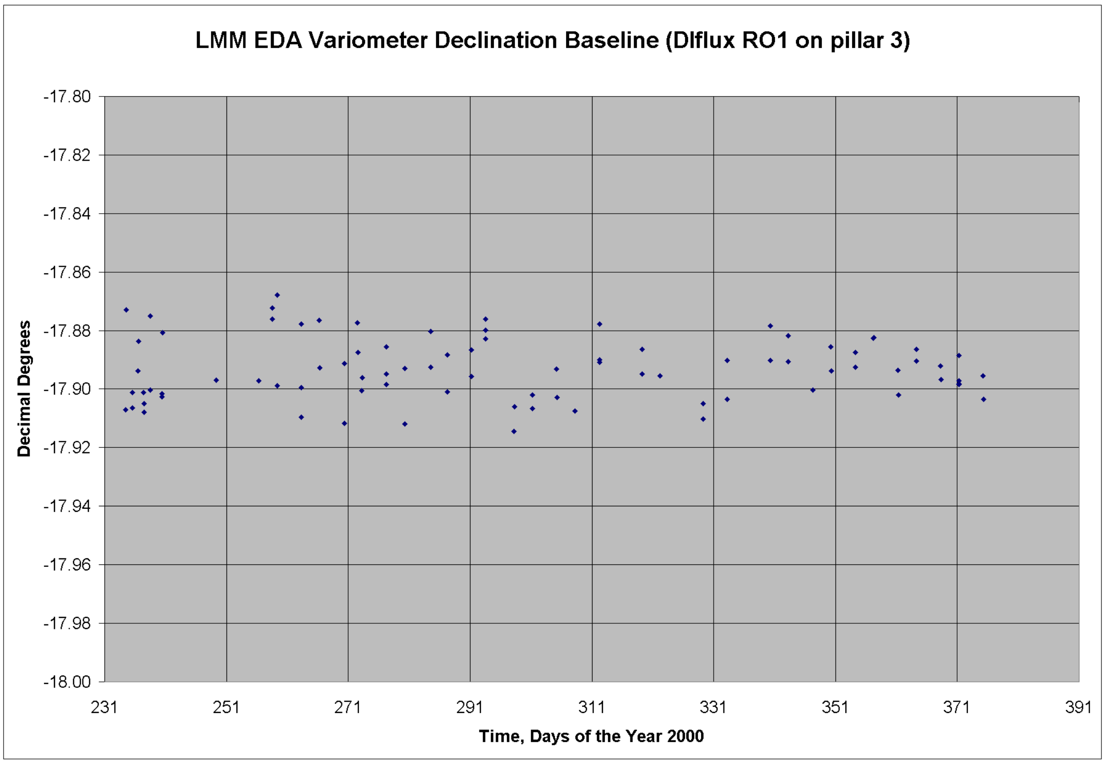

Figure 4

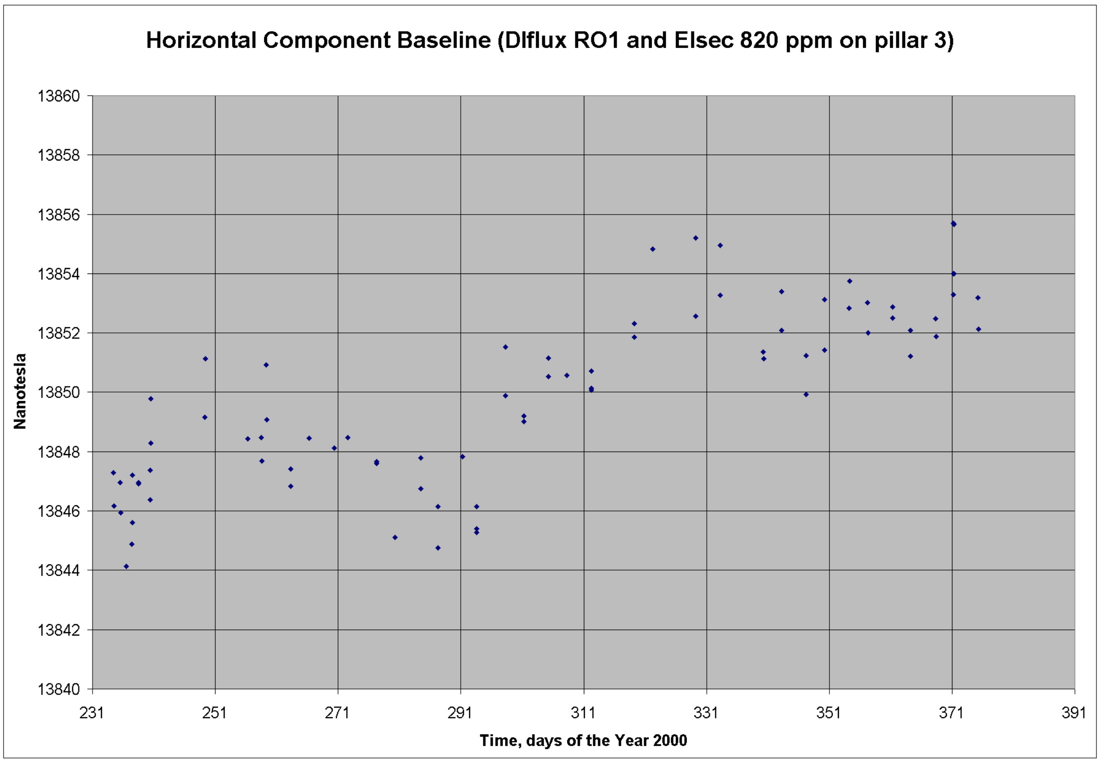

Figure 5

To the best of our knowledge there was no change in the D reference. This is because there was no pillar change, and the Askania declinometer must have been acceptable, as seen from inspection of the EDA baselines from September 1999 to December 1999. However, we cannot give any guarantee for this as the EDA D channel has been out of order since the beginning of 2000.

First Baseline Results with the Digital Instrumentation

In Figure 4 we show the D-channel baseline of the EDA variometer for the period August - December 2000. It can be appreciated that the stability of this channel is good: the stability is certainly better than 0.01° over the whole period shown. However, the dispersion of the successive measurements is more or less 1 minute of arc. This baseline noise is probably caused by the daily variation of the baseline due to diurnal temperature fluctuations.

In Figure 5, we give the baseline for the horizontal component during the same period. Here also the good stability of the measurements is noticeable, although a baseline shift of about 4 nT occurs near day 300. The dispersion of the successive measurements is less than 2 nT, indicating that the temperature influence on the H-channel is reasonably low.

Figure 6 gives the Z baseline. Here a 12 nT jump starting around day 300 compromises the stability record of the EDA instrument. Similarly, the dispersion of a few nT is similar to the H.

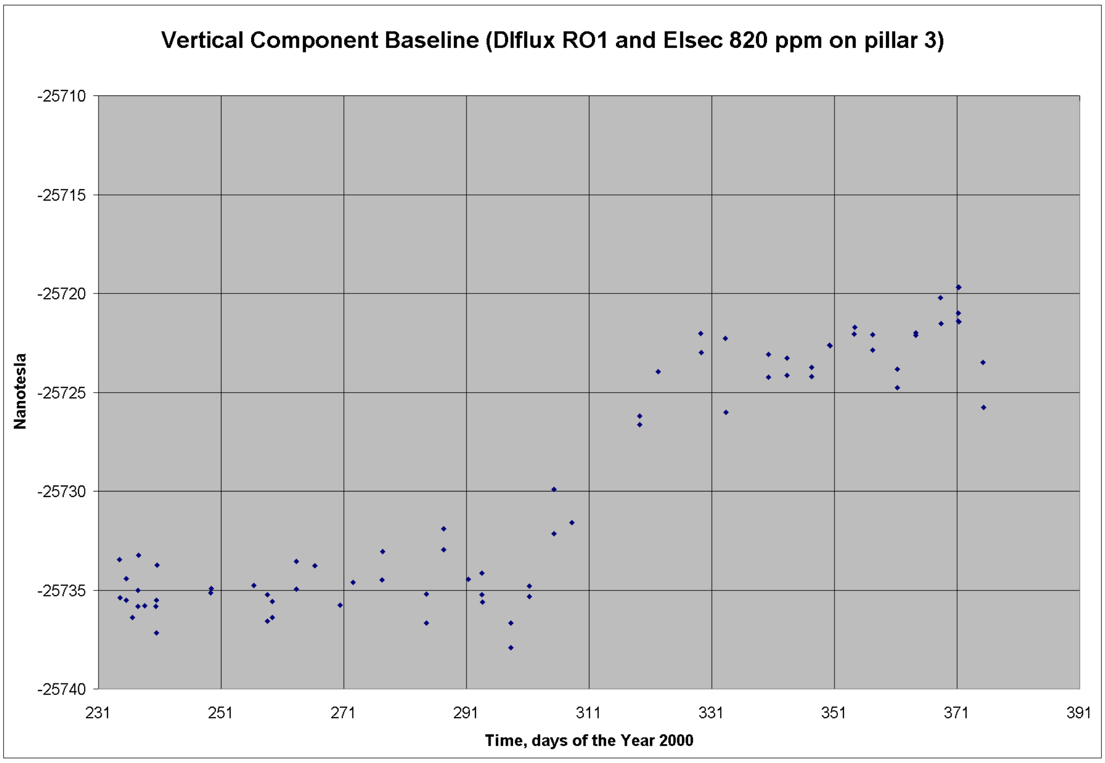

Figure 6

An essential routine task at the Observatory is the annual processing of the recorded data of the past year. It is good practice to have some tools to determine the good quality of the data processing. Thus, a final check when preparing these data for the observatory is the comparison of the definitive minute means data with the absolute spot measurements performed weekly for baseline computation. This check is a rather exhaustive one since any difference between the two data sets (minute means – spot measurements) will pinpoint errors in the absolute measurements as well as errors in the processing of the baseline and errors in the minute means. A simple way to compute the absolute spot measurements is to redo the baselines with zero variometer input. This check is illustrated in Figure 7 by investigating the magnetic declination for a section of the month of January 2001.

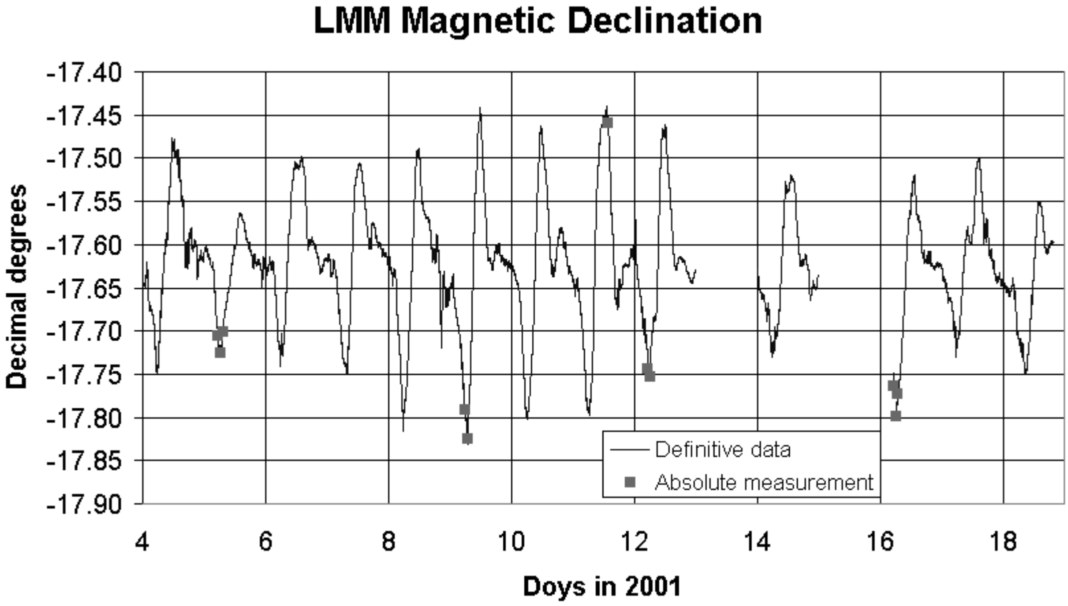

Figure 7. The intercomparison of the definitive minute means data and the spot absolute measurements taken regularly for the baseline determinations is a good check of the quality of the data. Any difference between the two sets will indicate errors in the measurement and/or processing of the data.

Difficulties Experienced in LMM with Data Acquisition

Also noticeable in Figure 7 are two gaps in the definitive data. They are caused by long (>10h) power failures in the observatory's electrical supply. Unfortunately this will increase during 2001 and culminate in May 2002, when observations will have to be stopped altogether due to the complete failure of the electrical mains supply. Now (August 2002) repairs to the cable supplying the observatory from the power transformer are programmed for the near future. An alternative solution to this problem would be the complete supply of the Observatory with solar power using photoelectrical panels. The financial estimates have shown that costs would be approximately the same for solar supply as for replacing the power cable. On the other hand, solar supply has a disadvantage, like yearly costs of battery replacements, and possible security problems. Also this would not solve the electrical supply of the rest of the observatory needs like room and premises lighting and living quarter's commodities.

Secular Variation in Maputo (LMM)

We give in Table 4 the monthly means for the Observatory of Maputo (LMM) obtained from the digital variometer and new absolute instrumentation. The final months of 2001 are not available for the reasons given in the previous paragraph.

The last published annual mean for LMM before this work began dates back to 1989, meaning a large gap of 11 years before restarting the observatory in 2000. In order to have an indication on the status of the magnetic field during this period, it is interesting to look in Figure 12 at the field in the neighbouring observatories of Antananarivo (TAN) in Madagascar and Hartebeesthoek (HBK) in South-Africa (see Figure 1 for the locations of these observatories). TAN has a very long series of observations dating back to the 19^{th} century and HBK is operating since 1973, nicely covering the period without data in Maputo.

Figure 12 illustrates the spectacular difference in declination secular variation between relatively close Magnetic Observatories in this part of Southern Africa. This problem will be dealt with in greater detail in the paper by P Kotze published in this Proceedings.

Repeat Measurements in Beira

Thanks to the interest and the financial support of "Aeroportos de Moçambique" (AOM), it was possible to implement a field trip to Beira and Nampula with the purpose of performing magnetic repeat measurements there. AOM asked us to perform additional True and Magnetic Heading measurements of their runways at the National airports of Beira and Nampula.

For setting-up our field stations, we needed a non-magnetic tripod, which was unobtainable in Maputo Observatory. Finally we located one in a warehouse to the South of Maputo owned by the DNG, where scientific equipment was stored. It is an Askania field galvanometer tripod. Unfortunately it was not possible to modify the length of the legs, so we had to accurately position the tripod level above the mark before mounting and levelling the theodolite. Furthermore, it was necessary to manufacture a small bronze adapter so that the Ruska Diflux could be securely fixed to it. Later we found two adjustable non-magnetic tripods in the NMP observatory.

We perused the archives of the DNG in order to find the exact location of the last repeat station measurements in Beira and Nampula and found nearly all the relevant repeat station information files about both sites. Unfortunately once on site it was impossible to find any markers left by the previous party in 1965. Therefore, we set up our station along the runways in Beira as exactly as possible on the same spot as described in the Beira repeat station file. This was done using the Lat/Long info and a detailed sketch found in the file.

For the benefit of future measurement sessions and field trips, we constructed a small concrete platform with a marker and 3 holes at 120°, into which the theodolite tripod feet should be placed (see Figure 8). In the Appendices of this survey report is the original report (in Portuguese) about this repeat station as well as the results of our repeat observations and runway orientation measurements. The results are reported in Table 3.

Figure 8. The newly constructed repeat station marker platform in Beira. The station is near the runways of Beira airport, exactly on the previous (1965) repeat station location. While the observer is measuring, the masons are enjoying a well earned break.

Examining the reduction of the Beira Estacion Magnetica spot measurements to the LMM baseline (5 last columns in Table 3), it is apparent that the 3 first observations performed at dusk on day 194 are preferred above those performed outside the diurnal variation period. This explains the H baseline jump of 17 nT on day 197, performed shortly before noon. However, in absence of any indication of the difference in field behaviour between Maputo and Beira, results have been computed as the straight mean of all measurements, but excluding the data of day 197. It is also noticeable from the results that the Beira runway is magnetically clean. The final results are given in the Appendix, as item 4.

Figure 9. Measuring on the runway in Nampula. Note the use of a double tripod configuration for supporting the DIflux.

Figure 10. View of the magnetic Observatory of Nampula. In the centre is the outdoor target pillar. Behind it the absolute house and to the extreme right the variometer house.

Visiting the Magnetic Observatory of Nampula, Repeat MeasurementsThe region of Nampula is quite spectacular with its many basaltic outcrops, emerging everywhere like strong towers from the ground. The horizon is therefore dotted with those steep rocks, not unlike the "meteors" from the Trikala region in Greece, the "mogotes" in Cuba near Piñar del Rio or even the "Pão de Azucar" in Rio de Janeiro. The outcrops are visible in Figure 9. However those geological conditions have an impact on the surface magnetism as basaltic rocks are magnetic. Previous magnetic measurements in the region have shown strong local anomalies and differences from point to point (up to 1.9° in declination). Therefore we were pleased to have the carefully selected and planned Magnetic Observatory of Nampula (NMP) for our use to process our measurements, even if no measurements had been made there since 1982.

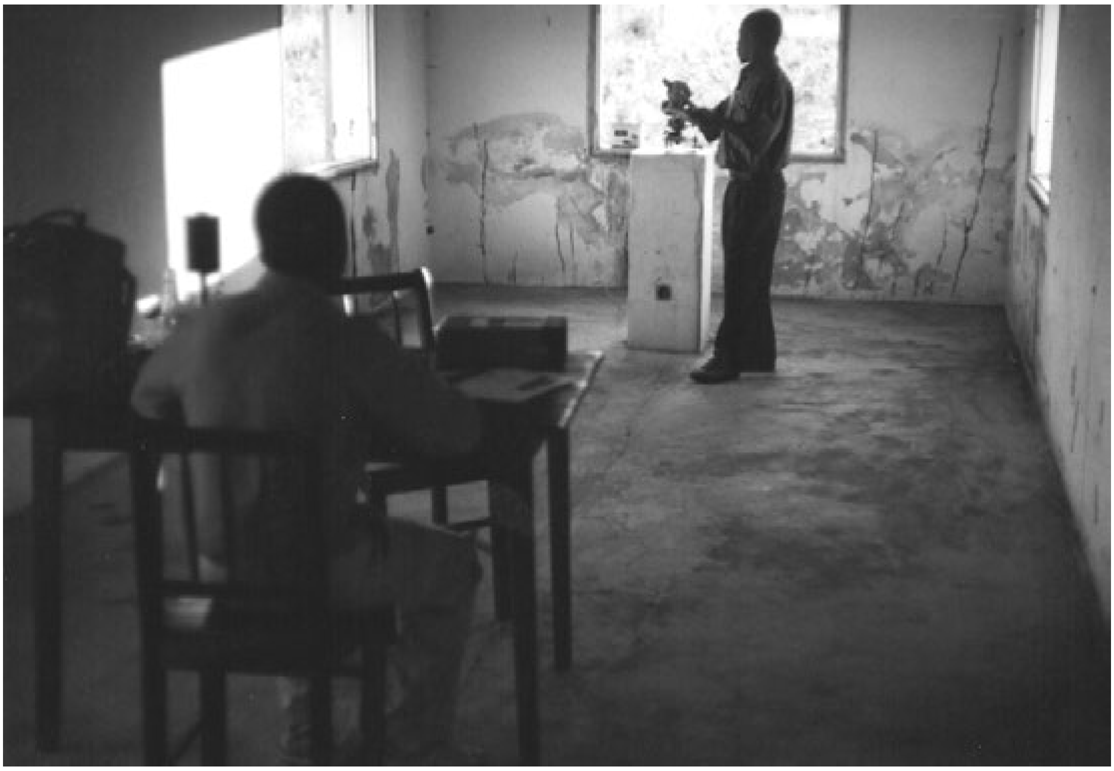

Figure 11. Measuring in the absolute house of Nampula Magnetic Observatory.

This NMP Observatory is a geophysical station with co-located seismic and geomagnetic facilities. The seismic part is presently actively operating. The Geomagnetic Observatory is equipped with a large absolute house, a variometer house, office space and a sturdy outdoor target pillar (see Figure 10). The conditions in the absolute house were still suitable for performing measurements. Although the windows had disappeared only a little cleaning was necessary before we could start the observations as shown in Figure 11. Excessive vegetation prevented us from observing the target from the D pillar. Therefore we measured D, I and F on the Z pillar, to the West in the absolute house. As in Beira, the observations taken at dusk seem to give a better reduction to the baseline in LMM, which is at a 1400 km distance (Table 3). But here also our computations are based on the straight mean of all measurements.

Realistic magnetic measurements on the runways of Nampula Airport were impossible, due to high gradients and therefore we measured only their true azimuth and computed their magnetic azimuth from the magnetic declination obtained in the nearby Observatory as explained in the Appendix.

Present and Past Data

With the availability of the recent measurements, it is worthwhile to try and summarise the whole geomagnetic field data-set available at the three stations of Maputo, Beira and Nampula. Therefore we visited once more the valuable archives of DNG, looking for an inventory of all the measurements taken at those places over time. We could indeed collect quite a few repeat station measurements; dating back to the late 19th century.

We realize that the quality of the measurements is not homogeneous and that the re-locations from one field measurement to the other can be bad or not cared for altogether. Nevertheless the data give us a rough idea of the secular variation during the whole 20th century at our three stations. The long series taken in Antananarivo gives a guideline to visually interpolate the noisy series (see Figure 12).

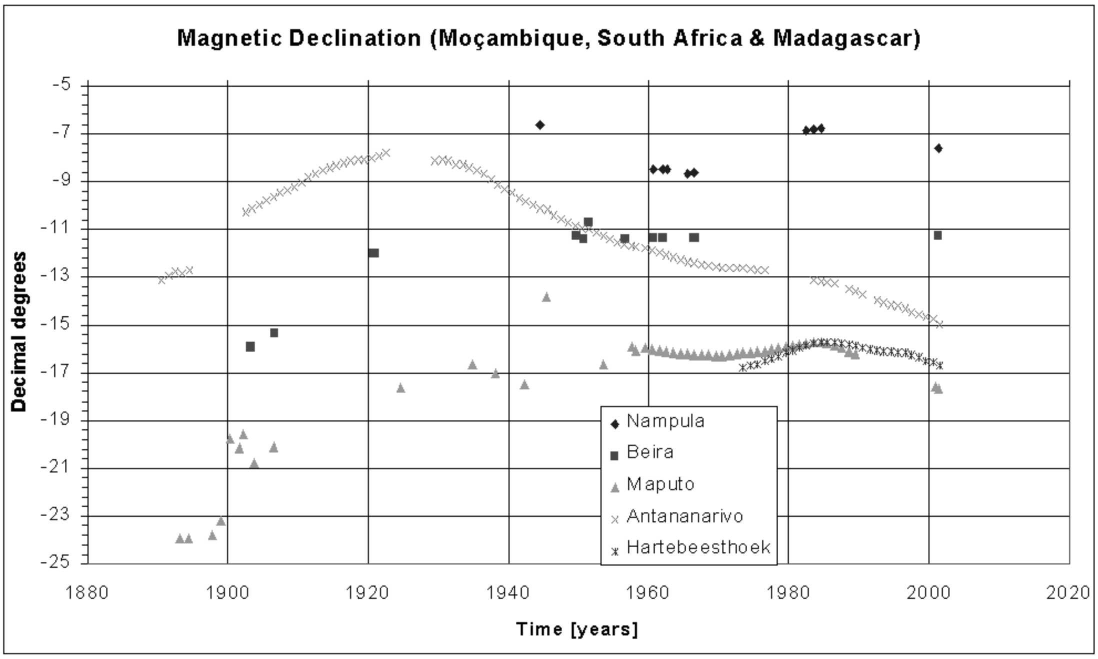

Figure 12. An attempt to summarise the available Magnetic Observatory data set for the Eastern part of Southern Africa. This is a mix of Observatory annual means and spot/repeat station measurements. Note the strong difference in secular variation for stations as close as HBK and LMM.

Comparisons between LMM and HBK for Rapid Variations

Since the digital data collected in LMM has been processed to get final results for the INTERMAGNET *.bin minute means format, it is quite easy to compare the minute data with neighbouring INTERMAGNET observatories, HBK for instance. As an example, daily plots for October 31th 2000 are given in Figure 13 and Figure 14. The similarity between both plots is striking, except for the Z channel. The Z rapid variation in HBK seems to be completely suppressed.

Conclusions

To conclude this work, it is important to point out once more that the observatory of Maputo is still at risk of being closed due to electrical mains disruption. The observatory of Nampula remains closed. We strongly recommend that the future of Maputo Observatory be guaranteed in the long term and that the observatory operations resume in Nampula.

We believe that this paper has shown the presence of both those observatories due to:

1. The excellent Magnetic Observatory infrastructure available in the Republic of Mozambique, complemented by the donated modern equipment,
2. The high level of expertise available both for observatory operations and field work,
3. The interest shown by the international scientific community for magnetic observations in a region with extreme secular variation gradients,
4. The strategic location of Nampula in a region with a shortage of magnetic observatories,
5. The interest shown by the commercial partners in Mozambique and

6. The possibility to export the Mozambican know-how to neighbouring countries.

Acknowledgements

We appreciated very much the contribution from “Aeroportos de Moçambique”, in the form of logistics, travel, financial support and most important, interest shown for the work described in this paper. The efficient help provided by their employees Sr Marcos Paulino, Sr Geraldo Sangue in Beira and Sr. Lopes in Nampula was very valuable.

INTERMAGNET paid the travel expenses for Jean Rasson for his flight from Belgium to Moçambique in 2001.

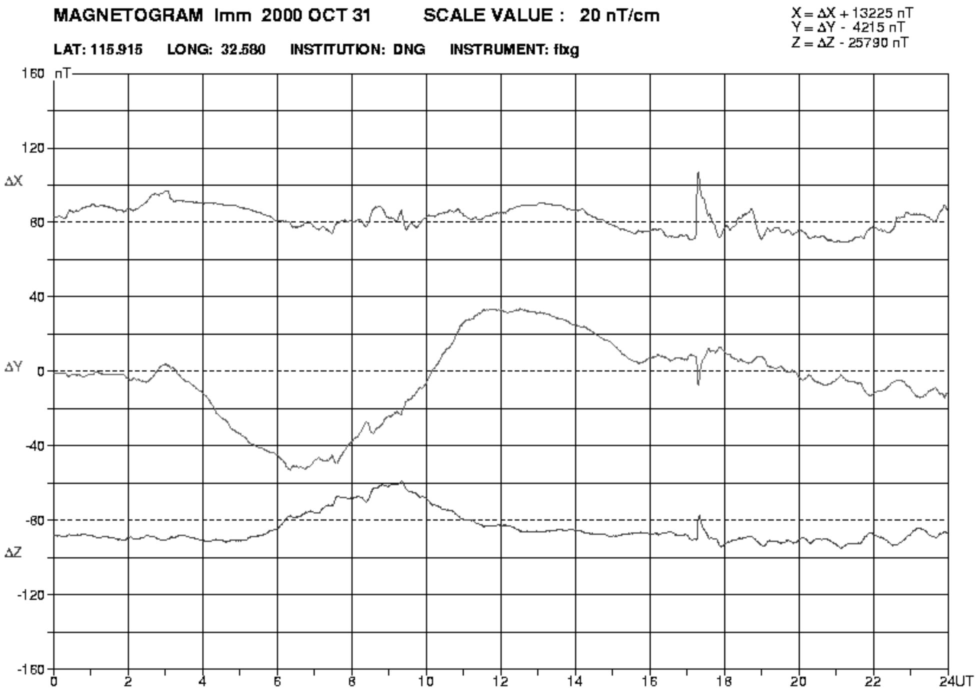

Figure 13

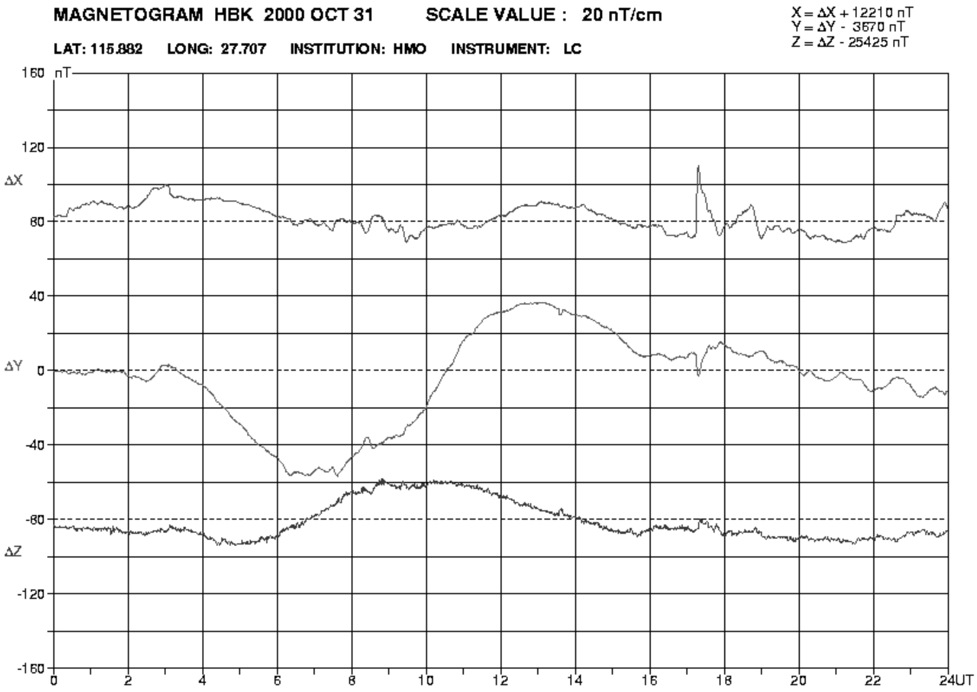

Figure 14

DINAGECA in Maputo kindly put its cartographic expertise at our disposal for clarifying some geographic coordinate issues.

We thank Dr Dias Joao in Nampula for helping with long term planning.

Dr Dani Ceuninck smoothed our way by judiciously flashing his diplomatic passport when appropriate.

We are indebted to Lee Pankratz from the US Geological Survey for donating the excellent Ruska Theodolite which would become the RO1 DIflux.

Finally we would like to thank our Parent Institutes (BGS, DNG and IRM) and their Directors who authorised those activities and contributed in no small way to the success of this project.

Appendix

Field report: Levantamentos de dados magnéticos nos Aeroportos de Maputo, Beira e Nampula em julho de 2001

1.- Descrição Geral

Chegado `a Beira `as 10 horas do dia 14 de Julho de 2001,uma brigada geofísica da Direcção Nacional de Geologia constituida pelos técnicos Francisco da Silva Sumbana, Manuel Farnela Kampine, Armindo Alberto Nhatsave e chefiada pelo tecnico Belga Dr. Jean L. Rasson Presidente do Grupo V-I de Trabalhos da IAGA (Associação Internacional de Geomagnetismo e Aeronomia) e de Instrumentos de Precisão, para vir dar continuidade dos trabalhos de treinamentos aos técnicos do Observatório Magnético do Maputo e bem como para efectuar levantamentos magnéticos da Declinação para a calibração em voo da informação radiada pelas estações e DVOR-DME e determinacao de Azimute magnetico nas pistas dos Aeroportos Internacionais de Maputo, Beira e Nampula para a melhor seguranca aerea dos aeronaves nas pistas dos Aeroportos Internacionais de Maputo, Beira e Nampula pedido das Empresas dos Aeroportos de Mocambique.

Chegado ao Aeroporto Internacional da Beira a brigada esteve acompanhado pelo tecnico das Empresas dos Aeroportos de Mocambique vindo de Maputo tambem o Sr.Marcos Paulino e o Sr. Geraldo Sangue tecnico electronico do Aeroporto da Beira, imediatamente a brigada dirigiu-se para o local a procura do marco da Estacao Magnetica, tendo sido feito buscas na pista principal nr. 12 a 75 metros do centro do cruzamento da pista TAXI (ver figura em anexo) e entrado em direccao ao Nordeste perpendicular a pista a 87,5 metros conforme a indicacao das informacoes anteriores de 1962 em mao e dado o facto de nao podermos encontrar o lugar exacto utilizado anteriormente, foi estabelecido a Estacao no lugar precisamente previsto medido por uma fita de medicao de 30 metros. Havendo a hipotese de ter sido retirado pelo tractor nos trabalhos de rotina de limpesa das pistas.

Pelo que foi necessario preparar no proprio lugar previsto uma plataforma da Estacao Magnetica da Beira, isto e foi feita um marco constituido por pedra, areia e cimento de uma forma triangular com um buraco no centro (introduzido um tubo de aluminio e nas tres extremidades tambem com tubos de aluminios para se poder assentar o tripe para observacoes no local feito este trabalho em 16 de Julho de 2001. Nas tres paredes do triangulo foi introduzido tres tabuas de madeira em contraplacado e cuidadosamente nivelado no seu assentamento. Dentro do betao foi introduzido tubos e alguns fios de bronze somente para a sua fortificacao.

Neste trabalho todo estiveram envolvidos os Srs. Alberto Malaidge e Manuel Cueija Joaquim “Well” ambos pedeiros, Dr. Jean L.Rasson, Francisco da Silva Sumbana, Manuel Farnela Kampine, Armindo Alberto Nhatsave, Marcos Paulino, Geraldo Sangue e alguns Bombeiros um dos quais o Sr. Angelo Miguel que trouxeram agua para os mesmos trabalhos .

Gradiante vertical na plataforma(ver figura) da Estacao Magnetica do Aeroporto da Beira com media de 2,6 nT.

Chegada a Nampula em 17 de Julho de 2001 as 15:15h vindo da Beira imediatamento foi solicitado um carro e cedido prontamente pelo Sr. Lopes da Delegacao da Empresa dos Aeroportos de Mocambique em Nampula, procurou-se a pista 05 para poder localizar o marco da Estacao Magnetica de Nampula e nao foi possivel localiza-la tendo se decidido seguir para o Observatorio Magnetico de Nampula.

As casas do Observatorio Magnetico de Nampula estao sem portas, janelas e tecto falso mantendo ainda a cobertura.

Na casa Absoluta foram encontados pilares e decidimos utilizar o pilar mais a Oeste para observacao do campo magnetico. Naquele pilar esta rodeado de tres janelas e tinhamos em vista o pilar da mira exterior que tinhamos identificado anteriormente. Constatou-se que o lugar estava sujo porque as pessoas defecavam, tendo sido necessario criar condicoes para se poder fazer observacoes magneticas dentro da mesma nos pilares, ja era noite seguiu-se para o Hotel para se pernoitar.

Nos dias 18, 19 e 20 de Julho de corrente ano continuou-se com os mesmos trabalhos de levantamentos magneticos no Observatorio Magnetico e nas pistas 05 e 32 respectivamente para a determinacao de Azimute e Declinacao Magnetica.

No dia 19 de Julho uma parte da brigada foi recebida pelo Sr. Director Provincial do MIREME em Nampula Branquinho Ferro Nhombe, Sertorio Azevedo M. Aurelio e Dias Joao tendo sido debrucado sobre a Estacao Sismografica e bem como a reabilitacao do Observatorio Magnetico de Nampula para poder receber novo equipamento doado pelo British Geological Survey do Reino Unido.

A Brigada regressou a Maputo no dia 20 de Julho de 2001 e em seguida ja em Maputo a brigada foi a Dinageca para confirmar as coordenadas geograficas dos pontos medidos durante acampanha magnetica, pelo que muito se agradece a boa colaboracao dada pelos tecnicos desta Instituicao.

Table 3. Results of our repeat observations and runway orientation measurements. The last five columns give the reduction of the LMM baselines.

Estacao	Data 2001	Lat	Long	GrV	Mira (Nome)	Azimuth	Azim Mag	D. média de
	(DOY)			nT		gr.d.	gr.d.	Julho 2001
Beira Aeroporto	194.5653	19° 47m 36s S	34° 54' 24" E	2.6	mira 2 lado	299.762		-11.288
Est Mag	194.5944				esquerdo			
	194.6208				torre C.			
	195.3472							
	195.4035							
	197.3465							
Beira Aeroporto	195.2910	19° 47' 37" S	34° 54' 12" E	-1.0	Linha central	104.931	116.242	-11.288
Pista 12	195.4278				da Pista 12			
	195.4431							
	195.4576							
Nampula OBS NMP	198.3069	15° 05' 15" S	39° 15' 16" E		pilar externo	166.773		-7.636
pilar 001 (Z)	198.6076							
	198.6271							
Nampula Aeroporto	200.2667	15° 06' 46" S	39° 16' 30" E		linha central	46.048	53.666	-7.636
Pista 05	200.2931				da pista 05			
	200.3042							
Nampula Aeroporto	198.4049	15° 06' 01" S	39° 17' 21" E		linha central	226.037	233.668	-7.636
Pista 23					da pista 23			
	198.4340							
Maputo Aeroporto	-189.6972	25° 55' 29" S	32° 34'13" E	-6.5	linha central	28.890	46.675	-17.699
Pista 05	-189.7076				da pista 05			
	-189.7014							
Maputo Observatorio	194-198	25° 54' 59" S	32° 34' 47" E		lado direito do	235.757		-17.699
LMM					edi.torr contr			

Table3 (continued)

Estacao	D	H [nT]	Z[nT]	F[nT]	I	D0	H0	Z0	F0	I0
	gr.d.				gr.d.					
Beira Aeroporto	-11.202	16439.4	-25561.0	30391.1	-57.253	-11.765	16403.3	-25566.0	30375.7	-57.315
Est Mag	-11.218	16435.3	-25563.8	30391.2	-57.263	-11.760	16399.6	-25568.1	30375.6	-57.324
	-11.253	16432.0	-25566.6	30391.8	-57.271	-11.764	16393.9	-25571.6	30375.4	-57.336
	-11.440					-11.771				
	-11.356					-11.746				
	-11.321	16475.9	-25542.0	30394.8	-57.176	-11.726	16411.4	-25559.0	30374.3	-57.296
Beira Aeroporto	-11.344					-11.747				
Pista 12	-11.326					-11.751				
	-11.293					-11.745				
	-11.279					-11.740				
Nampula OBS NMP	-7.676	20034.0	-23881.8	31172.1	-50.007	-8.113	19981.6	-23919.3	31167.3	-50.126
pilar 001 (Z)	-7.587	19997.1	-23895.0	31158.5	-50.075	-8.098	19957.7	-23900.5	31137.5	-50.137
	-7.614	19999.9	-23892.3	31158.2	-50.068	-8.101	19955.6	-23900.3	31136.0	-50.140
Nampula Aeroporto	-8.596					-9.035				
Pista 05	-8.623					-9.021				
	-8.652					-9.028				
Nampula Aeroporto	-8.300					-8.702				
Pista 23										
	-8.239					-8.668				
Maputo Aeroporto	-19.044					-19.427				
Pista 05	-19.067					-19.463				
	-19.035					-19.443				
Maputo Observatorio						-18.167	13928.0	-25865.0	29377.0	-61.698
LMM										

Table 4. Monthly means in LMM with the digital variometer and new absolute instrumentation

Date [Years]	D [°]	I [°]	F [nT]	H [nT]	X [nT]	Y [nT]	Z [nT]
2000.62	-17.5557	-61.6606	29405.2	13958.5	13308	-4210	-25881
2000.71	-17.5675	-61.6732	29392.2	13946.6	13296	-4209	-25873
2000.79	-17.5784	-61.6728	29396.4	13948.8	13297	-4213	-25876
2000.87	-17.6069	-61.6567	29397.2	13956.4	13303	-4222	-25873
2000.96	-17.6091	-61.6249	29402.9	13973.5	13319	-4227	-25870
2001.04	-17.6264	-61.6182	29401.9	13976.0	13320	-4232	-25868
2001.12	-17.6294	-61.6078	29400.1	13979.9	13323	-4234	-25864
2001.20	-17.6508	-61.6327	29392.5	13965.0	13308	-4234	-25863
2001.29	-17.6752	-61.6639	29386.8	13948.2	13290	-4235	-25866
2001.37	-17.6793	-61.6149	29393.4	13973.5	13314	-4244	-25860
2001.45	-17.6852	-61.6000	29393.7	13980.4	13320	-4247	-25856
2001.54	-17.6992	-61.5882	29394.4	13986.0	13324	-4252	-25854
2001.62	-17.7144	-61.5866	29390.7	13985.0	13322	-4255	-25850
2001.71	-17.7391	-61.5561	29394.4	14000.5	13335	-4266	-25846

No dia 24 de Julho a brigada trabalhou na pista principal 05 de Maputo. A pesar de vento forte e baixa temperatura fizemos observações de limpeza magnética com Magnetometer de Protões na pista 05 concluimos que a pista tinha maior Gradiente no campo magnético. Fizemos várias observações Astronómicas do Sol e magnéticas de Declinação. O resultado está na tabela. A diferença de 0.6 graus entre o Observatório de Maputo e a pista 05 confirma a falta de limpeza magnética da pista 05 do Aeroporto de Maputo por isso utilizamos a declinação medida no Observatório Magnético de Maputo para calcular o Azimute Magnético da pista 05.

Na tabela também damos a declinação média mensal de Julho do ano 2001.

Tem se a salientar a boa colabaracao dispensada na Beira,Nampula e Maputo pelos tecnicos que colaboraram para a boa execucao dos trabalhos desta Brigada Geofisica.

2.- Metodologia

1. Tratou-se de encontrar o marco deixada pela brigada anterior se existia. Fez-se de duas maneiras : perguntar as pessoas do mesmo lugar ou utilizar a informacao deixada pela brigada anterior. Se a marca nao fosse encontrada instalar a estacao no lugar identico segundo a informacao disponivel.
2. Averiguar a limpeza magnetica do lugar utilizando o magnetometro de protoes fazendo-se dois perfiles ortogonais intersectando pelo lugar da estacao. O perfil tem dez metros e com uma medicao em cada metro e com a distancia de 25 cm do solo . Adicionalmente fazendo a medicao de gradiante vertical no lugar da estacao: diferenca entre o campo total medido no solo com o campo medido em cima do tripe.
3. Depois de identificar as miras e conhecendo as coordenadas geograficas da estacao fazer a observacao do Sol para determiar os azimutes das respectivas miras. Deve ser utilizado um relogio em tempo universal com precisao de um segundo.Para a reducao das observacoes utiliza-se o software DOS Soleil.exe e o anuario Astronomico do periodo correspondente.
4. Fazer as observacoes absolutas da Declinacao e Inclinacao magnetica utilizando o Diflux fixado em cima do tripe.
5. Calcular o azimute magnetico da pista se necessario utilizando uma das duas formulas:

   Azimute magnetico = Azimute - Declinacao

   Azimute magnetico = Leitura da mira - leitura meridiano magnetico
6. Fazer a observacao absoluta da forca total utilizando o magnetometro de protoes fixado em cima do tripe na mesma altura que o eixo horizontal do Diflux.
7. Reduzir as observacoes de D, I e F calculando o campo magnetico instantaneo. Calcular a linha de base do variometro do observatorio mais proximocom as observacoes
absolutas da estacao. Calcular diferencas com a linha base do observatorio calculada com a medicao absoluta do observatorio.

3.- Detalhe dos resultados

Damos abaixo uma tabela com todos os resultados obtidos. Apesar de não poder localizar os marcos das estações magnéticas chegamos a uma precisão de relocalização de uns metros na

Beira. No aeroporto de Nampula encontramos dificuldades devido a anomalias magnéticas. Como indica a diferença de 0.3 graus na Declinação Magnética entre as extremidades da pista principal. Também tivemos dificuldades na medição naquela pista com Magnetometer de protões, o que indica o importante gradiente no campo magnético ambiente. Nos arquivos de DNG encontamos o mapa que indica também fortes gradientes (até 1.9 graus) na região de Nampula. Por esse motivo utilizamos a Declinação medida no Observatório Magnético de Nampula especialmente preparado para esta ocasião para calcular o Azimutes Magnéticos da pista principal de Nampula

4.- Diferenças entre o Observatório Magnético de Maputo e as Estações visitadas
Utilizando os valores médios das linhas de bases da tabela obtivemos as seguintes equações:

a) Estação Magnética do Aeroporto da Beira

D_{Beira}[graus] = D_{LMM} + (- 11.755 + 18.167)=D_{LMM} + 6.412

H_{Beira}[nT] = H_{LMM} + (16402-13928) = H_{LMM} + 2474

Z_{Beira}[nT] = Z_{LMM} + (-25566.2 +25865) = Z_{LMM} + 298.8

F_{Beira}[nT] = F_{LMM} + (30375.2 -29377) = F_{LMM} + 998.2

I_{Beira}[graus] = I_{LMM} + (- 57.318 + 61.698)=I_{LMM} + 4.380

b) Observatório Magnético de Nampula

$D_{Nampula}$[graus] = D_{LMM} + (-8.104 + 18.167)=D_{LMM} + 10.063

$H_{Nampula}$[nT] = H_{LMM} + (19965.0-13928) = H_{LMM} + 6037

$Z_{Nampula}$[nT] = Z_{LMM} + (-23906.7 +25865) = Z_{LMM} + 1958.3

$F_{Nampula}$[nT] = F_{LMM} + (31146.9 -29377) = F_{LMM} + 1769.9

$I_{Nampula}$[graus] = I_{LMM} + (- 50.134 + 61.698)=I_{LMM} + 11.564

5. – Recomendações
Para melhor segurança Aérea dos Aeronaves é necessária uma cobertura nacional pelos mapas magnéticos de Moçambique. Para obter esta carta é necessário reocupar várias Estações Magnéticas no interior do País e sobretudo as Estações fronteiriças. Estas últimas são importantes para evitar efectos de bordo durante a interpulação e extrapulação de mapas à actualizar. Por isso recomendamos a reocupação das Estações de Zumbo, Tete, Pemba, Lichinga e Quelimane. Essas Estações seriam o mínimo para poder chegar matematicamente a um mapa magnético actual a partir do mapa de 1975 como o último desponível actualmente. As Estações fronteiriças nacionais também permitiriam a D.N.G. prestar serviços e produtos magnéticos aos Paises visinhos

Experiences in the using of variometer recordings on-site for geomagnetic repeat station measurements

Hans-Joachim Linthe
GFZ Potsdam, Adolf-Schmidt-Observatory Niemegk
Lindenstr. 7
D-14823 Niemegk - Germany

Abstract

The accuracy of geomagnetic modelling depends on the quality of repeat station data. Besides the using of good modern instruments for the absolute measurements an accurate correction of the transient field variations is very important. These corrections can be well obtained by installing a variometer on-site and running the repeat station as a temporary observatory. Related to the IAGA recommendations to maintain repeat station measurements the Niemegk observatory purchased a field variometer for this purpose. The variometer was tested intensively and is in use since the measurements campaign in 1999-2000.
The tests are briefly presented and the experiences of the field applications are discussed.

Introduction

The first results of a regional magnetic survey are magnetic field values measured at the stations at different days within one or a few years. Such values are not directly comparable and cannot be used to produce any charts because of the variations of the geomagnetic field, both short-period external field variations and main field secular variation. The desired results are values of the internal magnetic field alone and for all stations for a common epoch, usually annual mean values which can be compared to those produced by geomagnetic observatories.

In the traditional method, observatory recordings are used for the reduction of the measured data to annual mean values:

$$C(x_i,t_{mean}) = C(x_i,t_i) - C(O,t_i) + C(O, t_{mean}) \qquad (1)$$

$C(x_i,t_i)$ is the value of geomagnetic component C at location x_i and time t_i, x being the repeat station, O the observatory, t_i the time of the observations at repeat station x and t_{mean} the annual mean centred at the desired epoch (e.g. Newitt et al., 1996). The difference $C(x_i,t_i) - C(O,t_i)$ will generally be an average of at least two absolute measurements at the station, in other words, averaged over several times t_i. This difference is the critical part to be determined correctly, $C(O, t_{mean})$ is the constant observatory annual mean value of the desired year.
Equation (1) is based on the assumption that all geomagnetic variations, both external and secular variation, are the same at the observatory and the repeat station. As this is not the case, errors arise. These reduction errors depend on the distance between the station and the observatory, the electrical conductivity beneath the two locations and the secular variation gradient. More detailed information on such errors is given by Newitt et al. (1996) and, with numerical examples for the mid-European region, by Korte (1999).
In general the secular variation gradient is small enough in Germany to make those errors negligible when reducing over time spans of less than one or two years. However, the differences in external field, and particularly differences in the resulting induced part of the magnetic field due to differences in ground conductivity are a real problem, as the examples will demonstrate later on.

Method using an in-situ Variometer

A variometer set up close to the survey points can minimise errors due to differences of external variations between repeat stations and observatories. The variations of, e.g. the components H, D and Z are measured as at an observatory for one to several days. The results of the absolute measurement are used to determine the base line and thus absolute values of the variometer recordings. To obtain an annual mean value it is still necessary to use the recordings of an observatory. However, it is now possible to use quiet night time values in equation (1) instead of the instantaneous values $C(x_i,t_i)$. The difference $C(x_i,t_i) - C(O,t_i)$ is now calculated as an average over many quiet night time values, e.g. hourly means of such values. The assumption now is that the night time displacement at the repeat station is the same as at the observatory. Quiet night time values come closer to the desired undisturbed internal field so the errors due to external influences should be significantly smaller than when using only instantaneous values (cf. Newitt et al., 1996).

The Variometer

For repeat station measurement purposes the Adolf-Schmidt-Observatory Niemegk purchased especially a three-component fluxgate magnetometer LEMI 008 with cardanic suspension of the sensor, manufactured at the Lviv Centre of the Institute of Space Research of the Ukrainian Academy of Sciences (LCISR). Flux-gate variometers are in use at observatories and at field surveys as well. The conditions at field surveys are completely different from those in observatories. Usually in the field there is no pillar, no hut, no constant temperature, but humidity and wind. It is extremely essential to use a variometer which guarantees a good base line stability under these conditions The long-term behaviour of the variometer directly influences the quality of the repeat station data. The knowledge of the long-term parameters is crucial for the use of the variometer.
Therefore, several parameter studies were carried out before the first use of the instrument The orthogonality, the transformation factors, the thermal behaviour and the efficiency of the suspension have been checked. The tests were carried out at the Niemegk observatory. The test equipment (Helmholtz coil system) and the standard observatory recordings were used for this purpose. The following parameters of the LEMI 008 were determined:

Orthogonality

	X – Y	Z - X	Z – Y
Orthogonality error	31.2'	20.1'	14.6'

Table 1: Orthogonality errors of the LEMI 008

Linearity of the transformation factors

	X	Y	Z
Maximum linearity error	0.03%	0.04%	0.17%

Table 2: Maximum linearity errors of the transformation factors

Thermal behaviour

	X nT/°C	Y nT/°C	Z nT/°C
Thermal coefficient of the sensor	0.18	0.25	0.10
Thermal coefficient of the electronic unit	0.08	0.08	0.08

Table 3: Thermal coefficients of the LEMI 008

Efficiency of the suspension

Tilt angle: **30'**	Tilting in North-South			Tilting in East-West		
	TE_c nT/'	TE_m nT/'	CF	TE_c nT/'	TE_m nT/'	CF
X	13	0.23	57			
Y				13	0.37	35
Z	5.7	0.083	69	5.7	<0.01	>500
Tilt angle: **3°**	Tilting in North-South			Tilting in East-West		
	TE_c nT/'	TE_m nT/'	CF	TE_c nT/'	TE_m nT/'	CF
X	13	0.12	108			
Y				13	0.19	68
Z	5.7	0.047	121	5.7	0.011	500

Where: TE_c : Calculated error in the magnetic field measurement caused by tilt in the case of suspension absence

TE_m : Measured error in the magnetic field measurement of the suspensed LEMI 008

CF : Tilt compensation factor

Table 4: Results of the tilt checks

The thermal tests have shown that temperature changes have an influence on both the thermal coefficients of the sensor and the behaviour of the suspension. To achieve a satisfactory long term stability it is recommended to operate the sensor under constant thermal conditions. For this purpose the sensor is buried in the ground about 40 cm deep and levelled horizontally. Due to the very small thermal coefficients of the electronic unit it can be operated under normal outdoor conditions.

Description of the Measurements

The German repeat station network consists of 45 stations (Fig. 1). Most of the sites have already been used in the earlier magnetic ground vector surveys of Germany and are well-defined by non-magnetic markers. The mean distance between the stations is approximately 150 kilometres. The measured field components are declination, inclination and total intensity. The absolute instruments used are a DI-fluxgate theodolite (Zeiss with Bartington magnetometer) for the measurements of declination and inclination and an Overhauser effect proton magnetometer GSM 19 for total intensity. Two sets of components are measured in the order F, D, I, D, I, F within a time span of 1 to 2 hours. During the angular measurements F was recorded with the proton magnetometer some metres from the station for control and comparison with the variometer recordings with a sample rate of 5 seconds. At several stations a gyro-theodolite GP1 2A was used to determine the azimuths.

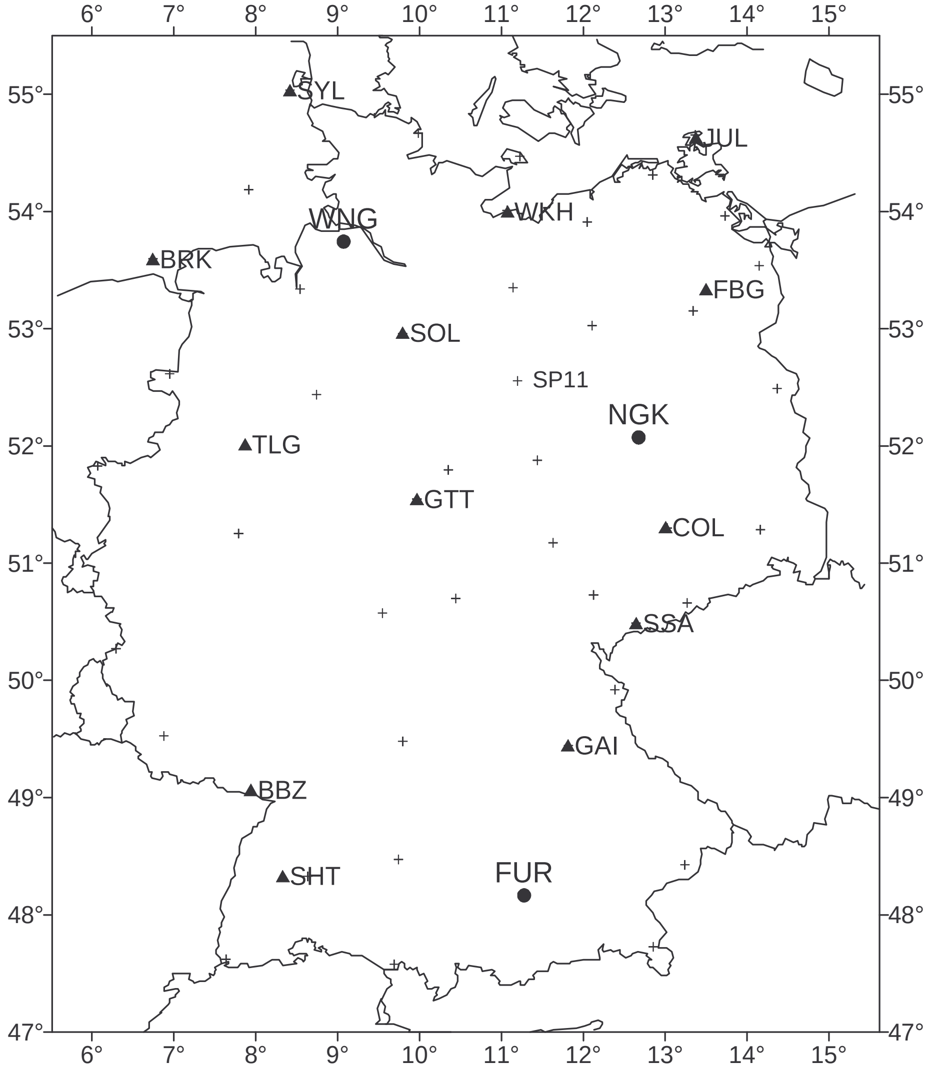

Fig. 1: Locations of repeat stations (crosses), variometer repeat stations (triangles) and the three German geomagnetic observatories Wingst (WNG), Niemegk (NGK) and Fürstenfeldbruck (FUR).

As the effort of putting up a variometer at every single one of the 45 stations for several days would be prohibitive, we had to compromise and use central variometer stations instead. A variometer station is set up at central repeat stations for several days while absolute measurements are done at the neighbouring stations. The distance between variometer and repeat stations does not exceed 150 km. The variometer was maintained long enough at one location for the recordings to include quiet night time values with K-index at the Niemegk observatory no greater than 1.

Processing and Comparison to Traditional Method

The situation is not quite so bad in other regions where gradients of conductivity are less strong. Table 5 shows examples of 3 repeat stations that all have been measured twice - once directly as variometer station and a second time when the variometer was recording at one of the neighbouring variometer stations. Additionally the values that would result using only the Niemegk observatory for reduction are given (momentary values). For the location of the three stations and the additional variometer stations see Fig. 1. The differences in the quiet night time results are less than 3 nT in H and Z and, except for GAI, not more than 0.3' in D. The variation of momentary values without any variometer is much more, e.g., at GAI in H by more than 10 nT. As expected even the average of those values can lead to results different by several nT’s from the results obtained by taking quiet night time values, as for example in the Z component of GAI.

Day/Variometer K-index	ΔH (nT) Quiet Night	ΔH (nT) Momentary	ΔD (′) Quiet Night	ΔD (′) Momentary	ΔZ (nT) Quiet Night	ΔZ (nT) Momentary
Repeat Station GAI						
211/SSA K=4	1374.0	1369.1 1381.8	-16.0	-15.8 -15.0	-1369.5	-1371.0 -1376.5
231/GAI K=3	1373.3	1372.0 1368.6	-16.7	-17.1 -17.5	-1366.7	-1375.1 -1374.1
Repeat Station COL						
214/SSA K=2/3	245.6	249.6 245.1	18.0	17.9 17.8	-300.8	-304.7 -302.8
172/COL K=2	244.3	244.6 243.3	17.9	17.8 17.8	-302.9	-304.2 -303.8
Repeat Station SHT						
223/BBZ K=2	2008.2	2013.5 2010.2	-71.1	-71.7 -71.4	-2173.1	-2179.9 -2178.1
239/SHT K=2/3	2005.9	2006.3 2007.6	-71.4	-71.3 -71.9	-2172.9	-2174.0 -2174.6

The values are the differences to the Niemegk observatory ($C(x_i,t_i) - C(O,t_i)$ from equation 1). Column 1 gives the day of the measurement and the variometer station used for reduction. The "quiet night" values are the values actually obtained using the variometer, the "momentary" values are the values obtained using no variometer station but only the Niemegk observatory recordings for reduction.

Table 5: Results for 3 stations if measured as variometer stations or with the variometer about 100 km away

Summarizing the results so far we can state that central variometer stations are an improvement above using only observatory values for reduction of repeat station measurements. However, we really should differentiate between the data from very high accuracy variometer repeat stations and the rest of the repeat stations.

Table 6 confirms numerically, that the differences of the quiet night time values really do not vary much and thus can be expected to well represent the difference between the undisturbed internal field at the two sites.

Date	UT	Hourly mean values ΔH (nT)	ΔD (′)	ΔZ (nT)
25.07.2000	22	-18786.2	-77.7	-45075.9
25.07.2000	23	-18786.2	-77.8	-45076.3
28.07.2000	21	-18786.4	-77.7	-45075.5
28.07.2000	22	-18787.0	-77.7	-45075.4
28.07.2000	23	-18786.4	-77.6	-45075.2

Table 6: Differences between variation recordings at TLG and Niemegk observatory values during quiet night times

Result Examples

The results of the measurement reductions are tables containing annual mean differences of the single repeat stations to Niemegk. From these tables magnetic maps are constructed by means of interpolation.
Fig. 4 shows maps interpolated from the results of the measurement campaign in 1999-2000 for horizontal intensity, declination and vertical intensity.

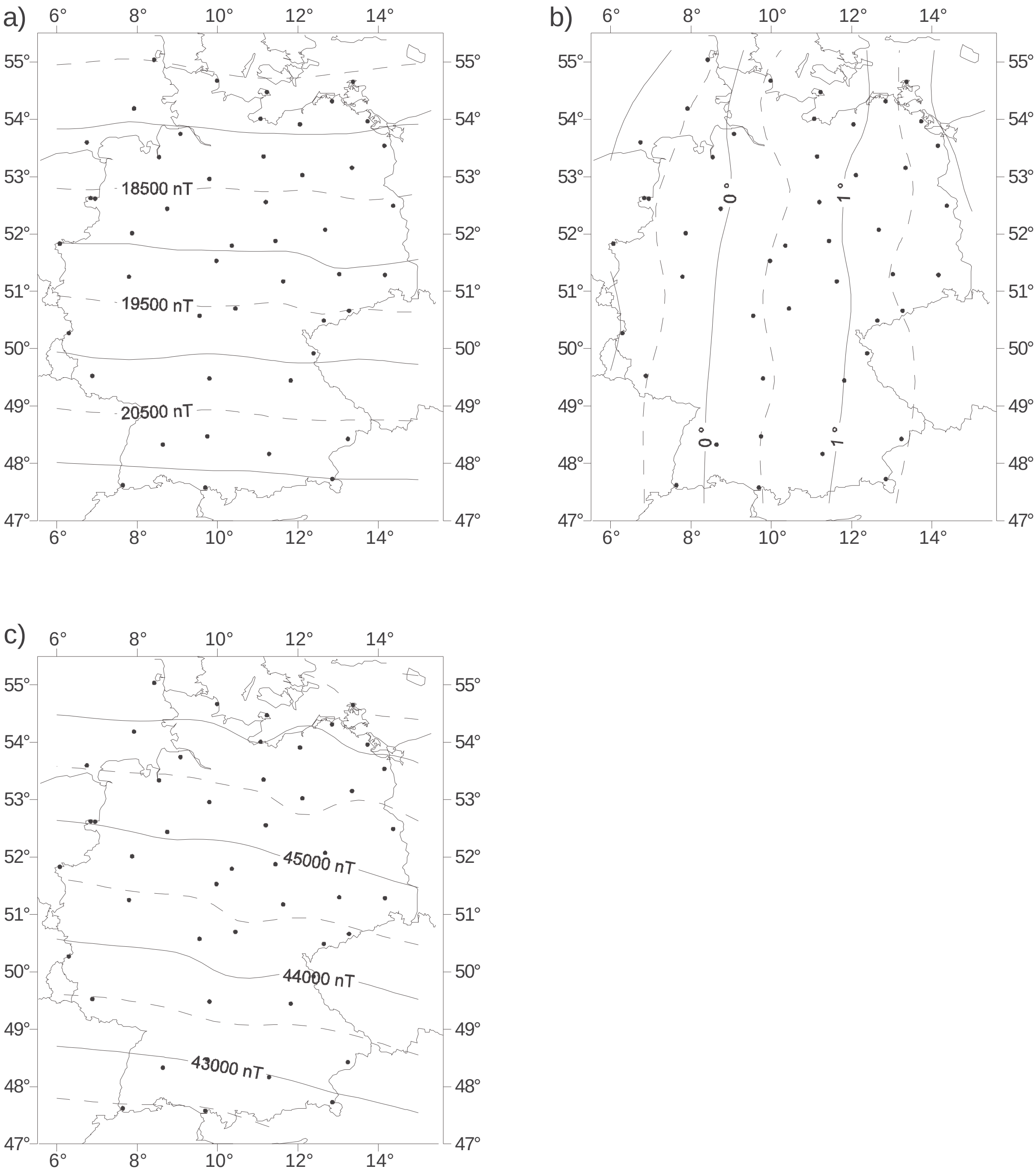

Fig. 4: Magnetic field in Germany 1999.5 as obtained by interpolation of the repeat station network.
a) Horizontal intensity, b) declination, c) vertical intensity.

Conclusions

The results of repeat station surveys can be improved significantly by using an on-site variometer. Provided the measurements are done sufficiently carefully, the accuracy of the measurements itself is less of a problem for the results than the non-homogeneity of the external and induced part of the magnetic field. Central variometer stations are an improvement in the traditional method using observatories only. However, in regions with high gradients of electrical conductivity such as northern Germany, even this is not enough. The accuracy that really is needed must also be taken into account. For obtaining interpolated maps of the magnetic components and an accuracy of several nT the spatial density of the stations should be good. For detailed studies of secular variation the accuracy has to be better, but we do not expect small scale features here. So a less dense network will do. With the method of central variometer stations we have achieved exactly these aims, i.e. a dense network of stations with quite a good accuracy and additionally a less dense but nevertheless well-distributed network of stations with excellent accuracy.

The projected reoccupation interval for the German repeat station surveys now is two years. Due to our experience with this survey and some practical problems with the locations of the stations the distribution of the variometer stations will change slightly during the next survey, but hopefully will be kept constant for a long time span afterwards.

References

[1] L. R. Newitt, C. E. Barton, Bitterly. J. (1996): Guide for magnetic repeat station surveys. International Assossiation of Geomagnetism and Aeronomy. Boulder

[2] M. Korte (1999): Kombination regionaler magnetischer Vermessungen Europas zwischen 1955 und 1995. PhD thesis. Freie Universität Berlin and Scientific Technical Report STR99/11. Potsdam

[3] M. Korte, M. Fredow (2001): Magnetic repeat station survey of Germany 1999/2000. Scientific Technical Report STR01/04. Potsdam

New Developments in Scalar Magnetometry

Dr. Ivan Hrvoic, GEM Systems Inc

In the past 22 years GEM Systems Inc has specialized in Earth's field quantum (scalar) magnetometry for various applications:

Geophysical exploration for minerals, diamonds and oil, archaeological and environmental surveys, long-term magnetic field monitoring at magnetic observatories and volcanological exploration, earthquake studies and defence (detection of weapons, submarines etc.) Overhauser and Potassium optically pumped methods have been developed and perfectioned.

Main features of both methods are high sensitivity and high absolute accuracy (implying long term stability). Both families of magnetometers are computerized and allow data storage, review of stored data, graphic display etc. They are, optionally equipped with Global Positioning system (GPS) boards for precise Universal Time and coordinates of position. Overhauser magnetometers are very low powered

Persistent research and development has recently resulted in a version 6.0 Overhauser and Potassium magnetometers based on Motorola "Cold Fire" microprocessor.

Vastly increased computing power has allowed us to develop new features that can be summarized as follows:

1. Improved sensitivity; it is now 0.015nT rms for "slow" readings Overhauser magnetometers and 1pT / √Hz for standard cell size Potassium magnetometers. This has been achieved by using a more complex algorithm for measurement of precession frequency and its conversion into magnetic field units.

2. Occasional "odd" readings or spikes have been eliminated by inspecting the quality of precession frequency zero crossings and selecting only the best interval; this is going to be very useful for operation in difficult environments, and, it will give clean long term records at observatories and in volcanological exploration.

3. New development also allows for a large memory, up to 32 Mbytes and further expandable to 128 Mbytes and storage of many millions of readings. Large memory is also needed if GPS post-processing is performed using inexpensive GPS boards, built-in in the magnetometer.

4. Updating and upgrading of software can now be done via Internet connections. This obviously includes any special software that the user may wish to order.

5. Comprehensive diagnostics of the instrument via Internet is also on agenda, although not implemented yet. This will be an equivalent of a worldwide service centre.

6. Preprogramming of future daily intervals of readings is available i.e. the magnetometer can be set to read from, say 8:00 in the morning to 5:00 in the evening every day. The rest of the time it is in low consumption sleep mode. Or, the reading intervals can be independently selected.

7. With the advent and maturing of satellite based Global Positioning System GEM has integrated a number of commercially available GPS boards with its magnetometers.

   Universal time with the precision of 1 microsecond and coordinates in different coordinate systems are available in various precisions, from some 5 meters in self-standing mode to centimetres in most sophisticated differential modes of operation. Local UTM coordinates can be rotated and a guidance system programmed in. User can specify a lane width along each survey line. When the lane boundary is crossed the instrument sounds an alarm and an arrow on the display advises the operator in which direction he / she needs to move to correct the error. Also, a large number of waypoints can be defined and transferred from a computer to the magnetometer. The magnetometer will guide the operator to the first waypoint and then from waypoint to waypoint indicating by a bar graph on the display how far the next waypoint is. This way the whole survey can be planned as needed and executed very efficiently.

   A number of auxiliary radio stations can be used for differential GPS like Omnistar, various beacons, WAAS systems in North America, EGNOS in Europe etc. The best DGPS is achieved by using a local base station and differentiate either in real time or in post processing mode.

   Since our magnetometers now command a large memory (up to 128 Mbytes) they are capable of storing all data for post-processing differential GPS. Of course, for observatories mainly <u>universal</u> time is of interest.

8. New free radicals, phosphorous based are being investigated for improved Overhauser gains. Phosphorous radicals have a potential of increasing this gain by up to 40 times but there are difficulties: stability is poor, size of molecules very large, EPR spectral lines wide.

   So far we succeeded in developing a stable free radical molecule with a potential of improvement of Overhauser gain of about 10 times but with wide electron paramagnetic resonance (EPR) lines. It is not (yet) clear what makes the lines so wide (6 Gauss), but a planned investigation will shed more light on the problem.

9. The first Potassium supergradiometer with 3 sensors and 0.03pT rms noise has been deployed in Israel in search of ways to predict earthquakes. Data collection and an assessment of the system is now underway.

10. We are also coming with the smaller Potassium sensor in an attempt to reduce heating requirements and increase a gradient tolerance in portable / stationary use. This model will also be of potential interest to magnetic observatories.

For further updating of our progress and other information, please visit our web site at www.gemsys.ca.

Magnetic mapping of Estonia 1992-2000 and new IMAGE station at Tartu

Kari Pajunpää (kari.pajunpaa@fmi.fi), Heikki Nevanlinna, Terttu Sallinen
Finnish Meteorological Institute
Geophysical Research Division
Johannes Kultima
Oulu University
Sodankylä Geophysical Observatory

Abstract

During the past five years the Finnish Meteorological Institute (FMI) has done magnetic measurements in Estonia. First, in summer 1998 declination at six Estonian airports was measured in co-operation with the Estonian Air Navigation Services. In 1999-2000 measurements of the magnetic field strength and direction were accomplished at 45 grid points all over Estonia. The data as well as some older observations were used to produce magnetic maps for Estonia. As a third phase, a permanent magnetic recording station was set up at the Tõravere observatory southwest from Tartu in September 2001. The new station is the southernmost of the IMAGE magnetometer network extending to Svalbard in the North. The short name of the station is TAR and it will serve as a reference station for magnetic measurements in Estonia and nearby areas. High stability is sought with a suspended FGE magnetometer in a temperature-controlled hut.

Measurements at airports and at grid sites

The magnetic declination was determined at six airports in Estonia in 1998. The airport reference point (ARP) on the runway was the desired site for the measurement. At two of the airports magnetic material in the concrete of the runway caused large disturbances in the magnetic field and the ARP was not suitable for the declination determination. The disturbance field was measured with a proton magnetometer, the declination with a DI-fluxgate and the azimuth by Sun observations.

During 1999-2000 the magnetic field components (declination (D), inclination (I), and total field (F)) were measured at 45 sites on mainland Estonia and on the islands (Fig. 1). The DI-fluxgate instrument together with the proton magnetometer was used similarly as in the observatory absolute measurements. The azimuth on each site was measured either by using Sun observations or by using two Trimble 4600LS GPS units. With a 100-200 meter base line the GPS-system had accuracy comparable to the Sun measurements. Both methods required post-processing of the data. The Sodankylä Geophysical Observatory took part in the field operation.

Declination map of Estonia

The observed results were reduced to the time epoch 2000.0 by using the Nurmijärvi observatory (see Fig. 3) in Finland. To extend the data coverage to the sea areas and neighbouring land areas, survey data, originally carried out in the 1920’s and 1930’s, were added after correcting it to the epoch 2000.0.

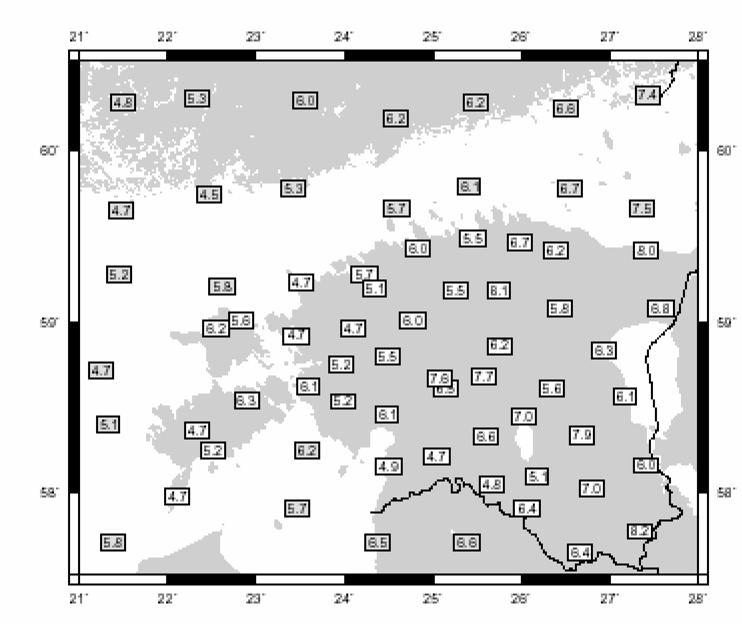

Figure 1. Measurement sites in Estonia marked with white background rectangles and the local declination value in 2000.0. The declination values in the rectangles with grey background are derived from other sources of data (see text).

Estonia is on the East European Platform, which is covered by Phanerozoic platform sediments. The sediment cover starts under the sea just north of Estonia and its thickness increases in Southeast Estonia up to several hundred meters. Due to the distance from the surface to the crystalline rocks the magnetic anomalies arising from the Precambrian rocks are attenuated and their scale lengths are increased. However, we found strong anomalies in the total field especially on the west coast of Estonia. The declination (Fig. 2) increases from +5 degrees (positive from North to East) in the West to +7 degrees in the East. There are many anomalies in the declination with over one-degree amplitude. The secular variation in the area is approximately +0.1 deg/year.

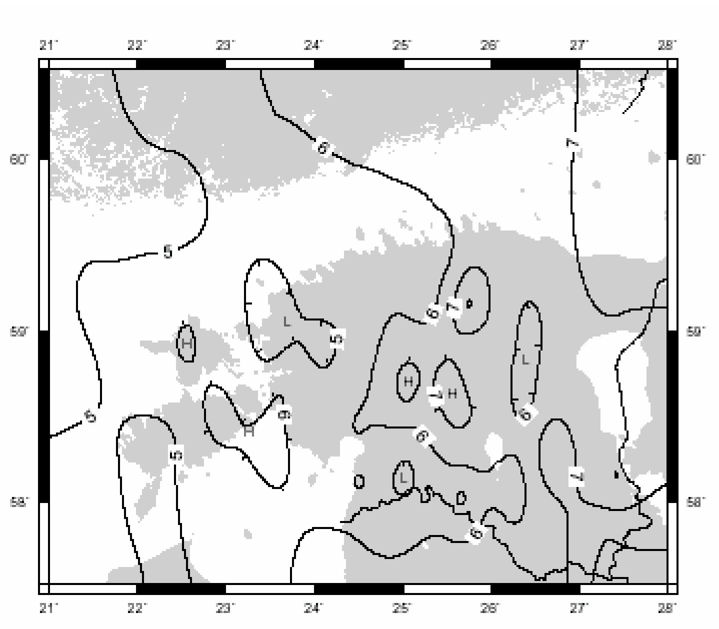

Figure 2. Declination isolines in Estonia for the epoch 2000.0.

The new magnetometer station at Tõravere (TAR)

The new magnetic recording station close to Tartu in southeastern Estonia was established for two main reasons: i) to serve as a reference station for future magnetic observations in Estonia and nearby areas, ii) to extend the IMAGE magnetometer network southward especially for studying space weather and large magnetic storms. A third purpose of the station will be to measure the secular variation. The absolute measurements in the future will show the stability of the station and its capability for serving as a magnetic observatory.

The station was put up in September 2001 at the Tõravere observatory some 20 km southwest from the old university town Tartu. The observatory is aimed for astronomical and meteorological observations. The geographical coordinates are: Lat. 58° 15.9' N; Lon. 26° 27.6' E. The Estonian partners are the Geological Institute of the Tartu University and the Tõravere observatory of the Estonian Meteorological and Hydrological Institute.

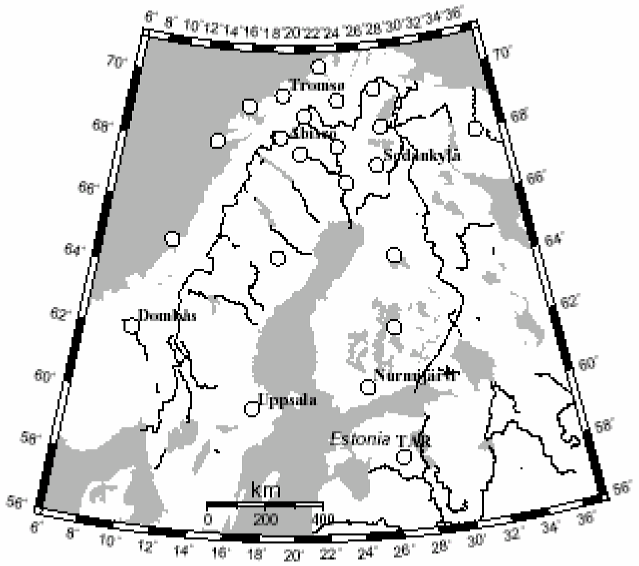

Figure 3. IMAGE magnetometer sites on the mainland northern Europe. Stations on the arctic islands are not shown here. The names of the magnetic observatories are shown together with the new station TAR.

The magnetometer site is similar to the other IMAGE sites of FMI. The magnetometer and the A/D-converter are installed in the temperature-controlled hut with a pillar for the sensor. The magnetometer is a Danish suspended FGE magnetometer. The Linux computer for data acquisition is installed in the meteorological building some 80 meters from the sensor hut. Data from the A/D-converter are transmitted by means of optical fibre. Time signals are obtained from a GPS receiver. The computer is connected to the local network of the observatory and data transfer and maintenance of the system is organized through the net. Absolute measurements will be done once per year in summer.

The data from TAR is processed together with data from other IMAGE stations at the Nurmijärvi Observatory. The data can be seen on the IMAGE web pages:
http://www.geo.fmi.fi/image/data.html.

Measuring the Geomagnetic Vector in the North Sea

T D G Clark, V B F Lesur, C W Turbitt, S M Flower, J G Carrigan and D J Kerridge (British Geological Survey, West Mains Road, Edinburgh, EH9 3LA, Scotland, UK)

Abstract

A marine vector magnetometer has been developed for measuring the strength and direction of the geomagnetic field from a ship. The system comprises a triaxial fluxgate magnetometer mounted on a rigid frame along with a GPS-aided ring laser gyro attitude and heading reference sensor. The attitude data can be used to rotate the magnetometer measurements into the geographic reference frame, once the relative alignments of the magnetometer and attitude sensor have been established by calibration. This calibration is achieved by rotating the frame through a range of attitudes at a location where the geomagnetic field is known. The system was mounted on a predominantly non-magnetic ship, constructed mainly from fibreglass and aluminium, but there was still a deviation field of about 200 nT at the magnetometer. This deviation field was accounted for by swinging the ship at a location on the tidal foreshore at high water where the geomagnetic field was accurately known from absolute measurements made at low water. The maximum errors estimated for this system are 0.25° in declination, 0.07° in inclination and 20 nT in total field intensity, with the main uncertainties being due to the accuracy of the attitude sensor and the ship's deviation field. This system was designed for use in the oil industry in connection with directional drilling (for which the above accuracies are sufficient), but may have applications in global secular variation modelling through the establishment of marine repeat stations if the accuracy can be improved.

A new method to perform an absolute measurement of the geomagnetic field

H.U.Auster,
IGM, TU Braunschweig, Mendelssohnstrasse 3, 38106 Braunschweig, Germany

V.Auster
Magson GmbH, Carl-Scheele-Strasse 14, 12489 Berlin, Germany

Abstract

The paper describes a method to measure the geomagnetic field vector using a scalar magnetometer and a three axis fluxgate magnetometer rotating about two defined axes. The proposed method is an alternative to the DI-flux measurement, which is based on a theodolite born one-component fluxgate magnetometer. The basic idea is, that the calibration of the magnetometer and the determination of the field in direction of the rotation axis can be done with the same procedure. Requirements concerning the three component magnetometer and the mechanics will be discussed. The presented method will be compared with the DI-Flux procedure.

Introduction

The term absolute measurement is attributable to Gauss, who was the first to express magnetic intensity in units of length, time and mass. The horizontal intensity of the geomagnetic field was measured by Gauss in 1832 with the help of two experiments. The first part of the experiment is the vibration experiment in which a bar magnet is suspended horizontally, and the period of small amplitude oscillation around the equilibrium N-S direction is measured. The period T is proportional $(1/MH)^{1/2}$, where H is the horizontal intensity of the magnetic field and M the magnetic moment of the bar magnet. The second part is the deflection experiment in which the ratio M/H is determined by suspending a second magnet (simply a magnet with a negligible moment like a compass needle) and noting its angular deflection from magnetic north when the bar magnet is placed at a known distance to the east or west. From the knowledge of MH and M/H , both the magnetic moment M and the horizontal intensity H could be deduced [Jacobs,1987], [Kertz,1969]. With the development of the proton precession magnetometer the field intensity could be measured by determining the frequency of free precession of protons. The measurement is absolute because the precession frequency depends only on the field intensity and the gyromagnetic ratio of the proton, which is an atomic constant. Scalar magnetometers like proton magnetometers can also be used to make vector measurements if bias fields in direction of the measured component are applied.
Therefore proton vector magnetometers (PVM) are equipped with precision coils generating an axial field of known magnitude controlled by the current fed to the coil. Application of a bias field, first in a positive sense and then reversed, allows the extraction of the field in a coil direction without the knowledge of the bias field intensity. If the magnetic and physical axes of the coil are collinear the alignment of the coil axis determines the accuracy of the measurement of the field component. Various coil setups are used for the direct measurement of H, X, Y and Z. Measurements in two or four positions eliminate tilting errors.
Since non magnetic theodolites are available, absolute measurement is mainly performed by a DI-Flux. A one component fluxgate sensor is mounted parallel to the telescope axis of a non magnetic theodolite. The sensor detects a zero field if it is aligned normal to the total force of the geomagnetic field vector. Declination (D) and inclination (I) are read from the horizontal and vertical circles of the theodolite. Adjustment and magnetometer errors are eliminated by measuring D and I for all four possible aspects of the sensor, and by adopting the mean value.

The DI-Flux absolute measurement is actually the standard method at all geomagnetic observatories. It will be used as reference method in this paper. The proposed method will be compared with the DI-Flux method in detail in chapter 4.

Fundamentals of the new method

The rotation of a three component fluxgate magnetometer about two well defined axes shall be used to determine the magnetic field along these axes. With two field components and the measurement of the field magnitude the field vector can be determined completely.
We shall show that a set of three measurements with a three component fluxgate magnetometer is sufficient to uniquely determine the Earth magnetic field component along any predetermined direction without needing to know anything about the geometry of the magnetometer. We take the direction in which we want to measure to be the Z-axis of a Cartesian reference system. We insert our magnetometer at the origin of the latter with an arbitrary orientation (see Figure 1) and measure B_{Magx} , B_{Magy} and B_{Magz} – the magnetic field components in the magnetometer system.

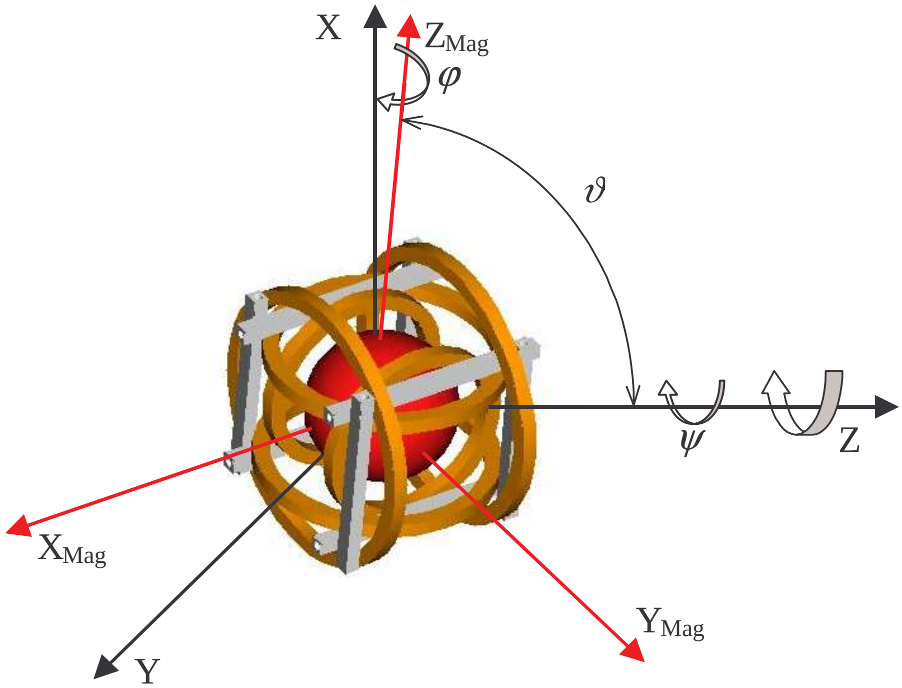

Figure 1

The magnetic field components Bx By and Bz in the reference system can be expressed by the measured ones with the following transformation:

$$\begin{bmatrix} \cos\varphi\cos\psi - \sin\varphi\sin\psi\cos\vartheta & -\sin\varphi\cos\psi - \cos\varphi\sin\psi\cos\vartheta & \sin\psi\sin\vartheta \\ \cos\varphi\sin\psi + \sin\varphi\cos\psi\cos\vartheta & -\sin\varphi\sin\psi + \cos\varphi\cos\psi\cos\vartheta & -\cos\psi\sin\vartheta \\ \sin\varphi\sin\vartheta & \cos\varphi\sin\vartheta & \cos\vartheta \end{bmatrix} \begin{pmatrix} B_{Mag\,x} \\ B_{Mag\,y} \\ B_{Mag\,z} \end{pmatrix} = \begin{pmatrix} B_x \\ B_y \\ B_z \end{pmatrix}$$

The transformation matrix uses Euler angles (φ, ϑ and ψ) with the following set of rotations: First we rotate the magnetometer about its Z_{Mag}-axis (ω_φ) until X_{Mag} gets identical with the node line of the X-Y and X_{Mag}-Y_{Mag} planes, next about this node line until Z_{Mag} coincides with Z and finally about the Z-axis until both coordinate systems overlap.
Note, that the field in the direction of the rotation axis (B_z) doesn't depend on the rotation angle ψ while the angles φ and ϑ remain the same (φ_0, ϑ_0). If we rotate the sensor in three positions (ψ_1, ψ_2, ψ_3), we derive for the field component in the Z direction the following vector equation:

$$B_z \begin{pmatrix}1\\1\\1\end{pmatrix} = \begin{bmatrix} B_{Mag\,x1} & B_{Mag\,y1} & B_{Mag\,z1} \\ B_{Mag\,x2} & B_{Mag\,y2} & B_{Mag\,z2} \\ B_{Mag\,x3} & B_{Mag\,y3} & B_{Mag\,z3} \end{bmatrix} \begin{pmatrix} \sin\varphi_0 \sin\vartheta_0 \\ \cos\varphi_0 \sin\vartheta_0 \\ \cos\vartheta_0 \end{pmatrix}$$

$$= \qquad \mathbf{MB}_{Mag} \qquad \hat{\mathbf{n}}(\varphi_0, \vartheta_0)$$

The matrix $\mathbf{MB}_{Mag}$ contains the measurement results of the fluxgate magnetometer. The vector $\hat{\mathbf{n}}$ contains the angles φ_0 and ϑ_0.. We rewrite the equation in the following form:

$$\mathbf{MB}_{Mag}{}^{-1} \begin{pmatrix}1\\1\\1\end{pmatrix} = \frac{1}{B_z}\ \hat{\mathbf{n}}(\varphi_0, \vartheta_0)$$

If we calculate the module of both sides of the equation the vector $\hat{\mathbf{n}}$ falls out because it is a unity vector. Therefore B_z can be expressed as:

$$B_z = \left\| \mathbf{MB}_{Mag}{}^{-1} \begin{pmatrix}1\\1\\1\end{pmatrix} \right\|^{-1}$$

The result shows that the field in the direction of the rotation axis B_z is independent from the rotation angles (ψ_1, ψ_2, ψ_3) as well as from the initial orientation (φ_0 ϑ_0) of the magnetometer. Thus, the field along the rotation axis can be derived directly from three vectors measured by the fluxgate magnetometer only. The knowledge of sensor orientation and rotation angles is not necessary.

The calculation of the field along the rotation axis is based on the assumption of an ideal fluxgate magnetometer measurement. Unfortunately scale values, non-orthogonality and offsets of fluxgate magnetometers are not stable in time and temperature. Therefore the error of the measurement depends on the quality and actuality of the magnetometer calibration.
The absolute measurement requires the rotation about two well defined axes and the measurement of the field magnitude. Auster et al [Auster, 2000] show that the rotation about two axes and the knowledge of the total field (measured by a scalar magnetometer) are sufficient to calibrate a magnetometer completely. So the rotation of the sensor can be used for both, first for the online calibration of the magnetometer and secondly for the determination of the magnetic field along the rotation axes. Consequently the calibration of the fluxgate magnetometer is always actual because the rotation of the fluxgate magnetometer during the absolute measurement can be used for the update of the complete set of calibration parameters. Calibration of the fluxgate magnetometer and absolute measurement can be done with one and the same procedure.

Realisation

Figure 2a shows the mechanics to rotate the sensor about one axis. The sensor is mounted in the middle of a tube which has two precisely manufactured treads at each end. The base plate is equipped with two parallel aligned bearing blocks. The base plate itself is mounted on a turntable which can be levelled by three foot screws.
To align the bearing blocks in the horizontal plane a spirit level mounted on a tailstock can be put on the treads. The error of the spirit level can be compensated by interchanging the ends of the

spirit level. Differences in diameters between both treads can be removed by interchanging the ends of the sensor tube.
To align the rotation axis in the direction of the meridian, the sensor tube has to be substituted by a telescope which also has two precisely manufactured treads at each end. With the telescope, true north can be established by observation of marks of known azimuth. The misalignment between telescope and treads axes can be determined by rotating the telescope in the bearing blocks. The reticule of the telescope draws a circle about the mark. Its diameter is proportional to the misalignment.

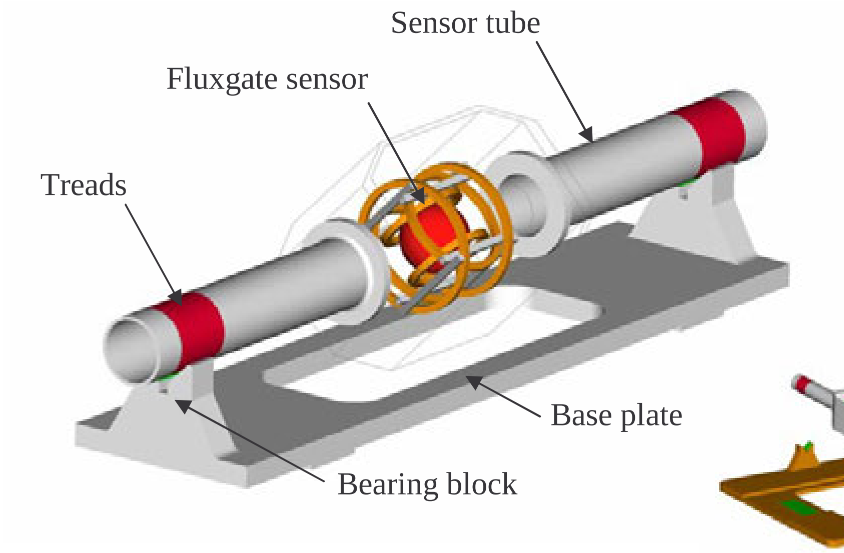

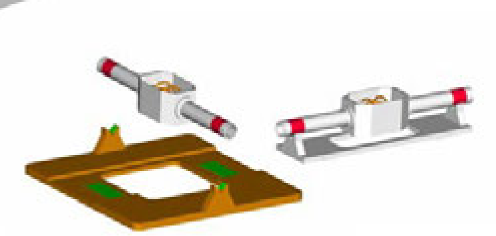

Figure 2b

Fiaure 2a

If a second base plate, also equipped with two parallel adjusted bearing blocks, is mounted perpendicular to the first one (see Figure 2b), the rotation of the sensor can be performed about two axis. The horizontal alignment has to be done in the same way as for the first axis. The angle between both axes has to be measured after fabrication of a turntable and bearing blocks under controlled condition e.g. using a theodolite. The deviation from 90° is a typical instrument error which has to be taken into account if the field components are calculated. It has to be recalibrated from time to time.
The first facility based on this method was manufactured by the Geomagnetic Observatory in Niemegk. Also the first absolute measurements were done in Niemegk.
Theoretically measurements at three rotation angles are sufficient for each axis. To have redundant results and to improve the magnetometer calibration we performed altogether 24 measurements, 12 for each axis. Using the opportunity to orientate the sensor inside the tube in various directions we always did six measurements at two sensor orientations. Simultaneously recorded variometer data are used to reduce the field variation between each set of three measurements. The total field was recorded by an Overhauser magnetometer.

Comparison with DI-flux

In the following table the equation used by the measurement procedure as well as the unknowns which have to be determined are listed for both methods.

DI-Flux:

Activity	*Number of equations*		***Number of unknowns***	
Proton magnetometer measurement	field magnitude F	1	Magnetic field:	
			$D_{a/b}$:	2
Rotation of a single component fluxgate sensor about the Z axis	theodolite angles in B_m=0 positions	4	$I_{a/b}$:	2
			Z:	1
			Sensor errors:	
Rotation of a single component fluxgate sensor about the D axis	theodolite angles in B_m=0 positions	4	***Offset:***	1
			Sensor orientation:	
			α_v, α_h:	2
		9		8

Presented Method:

Activity	*Number of equations*		***Number of unknowns***	
Proton magnetometer measurement	field magnitude F	1	Magnetic field:	
			X:	1
Rotation of a 3D fluxgate sensor about a horizontal axis along the direction of the azimuth mark	Three magnetic field vectors (minimum)	9	Y:	1
			Z:	1
			Sensor errors:	
			Offsets:	3
Rotation of a 3D fluxgate sensor about a horizontal axis perpendicular to the direction of the azimuth mark	Three magnetic field vectors (minimum)	9	Matrix:	9
		19		15

In both cases the number of equations exceeds the number of unknowns. At the DI-flux measurement declination and inclination are measured at two points (above and below the telescope) because the fluxgate sensor can not be located in the rotation centre. The single component magnetometer is used only as zero indicator. Furthermore the alignment of the fluxgate sensor has to be taken in account.
For the proposed method we need the full calibration set (12 unknowns) of the fluxgate magnetometer instead of only one parameter (offset) at the DI-flux measurement. On the other hand the method is completely independent from the orientation of the fluxgate sensor because neither the scalar calibration nor the calculation of the field in the rotation axis direction depends on the sensor adjustment. To increase the reliability the number of equations can easily be increased by additional measurements per rotation.

Measurement accuracy & first results

Three types of measurement errors have to be discussed.

- Firstly, we assumed that the field is constant during the rotation. The error depends on the geomagnetic activity and the duration of the sensor rotation. For a set of three measurements we need less than 1 minute. The reference value from the variometer is sampled at the second measurement. Thus the maximum error is the field variation about 30 seconds. This error can be estimated by the variometer records, typically it is less than 1nT.
- Secondly, the calibration is actual but still contains errors. The scalar calibration is based on a linear transfer function. The Magson digital magnetometers are highly linear because scale values and orthogonality depend only on the vector compensating feedback system. The 16 bit DA-converter used for the feedback in the Earth field range has a differential nonlinearity of

0.3nT (0.2LSB). This corresponds with the residuals in the magnitude calculated by the fluxgate components after calibration to about 1nT.

- Thirdly, all mechanical errors have to be summarized. Our colleagues in Niemegk have measured the errors of treads, bearing blocks and spirit level. All errors are less than 0.01mm which corresponds at bearing blocks distance of 250mm to an angle error of less than 10 arcsec and at an external field of 50.000nT to a measurement error of 2nT. Since this error can be eliminated by interchanging the ends of the sensor tube and spirit level, the overall mechanical error is also in the sub-nanotesla range.

All three types of errors are more or less of the same order. Therefore we can expect an overall error of about 1nT which might be further reduced by a larger number of measurements. All systematic errors can be eliminated by the measurement procedure.
A detailed description of the first measurements in Niemegk and an error determination is given by Eberhard Pulz.

The errors of the absolute measurements made during the X^{th} IAGA Workshop in Hermanus listed in the following table validate the error estimate.

	Pillar 1 22.04. 16:44	Pillar 4 19.04. 15:48	Pillar 4 19.04. 16:40	Pillar 6 22.04. 18:04	Pillar 9 23.04. 14:12
D	+1.0nT (19’’)	-1.1nT (22’’)	-0.7nT (-13’’)	+0.7nT (13’’)	+1.2nT (23’’)
H	-1.6	+0.1	-0.3	-0.1	+0.6

D and H were derived directly by the rotation about the axis in the direction of the azimuth mark and its perpendicular axis in the horizontal plane.

Summary

With the method presented in this paper an absolute measurement of the geomagnetic field vector without a non magnetic theodolite becomes possible. In comparison with the DI-flux we invest more efforts in the magnetic measurement technique - three components against one. This requires a magnetometer which can be operated in the full Earth field with a sufficient resolution and linearity. On the other side the mechanics is simpler and therefore more robust and less expensive. The error estimate and the tests in Hermanus show that the overall accuracy of the absolute measurement is about 1nT. The measurement procedure is easy and doesn’t depend on the qualification and experience of the operator.
The method has a large potential of automation, firstly because the sensor orientation is of no importance and secondly because magnetic field data can be simpler read out than angle values of a non-magnetic theodolite.

Acknowledgement

We would like to thank our colleagues Eberhard Pulz, Richard Winkler and Karsten Müller from the Geomagnetic Observatory in Niemegk. Eberhard organised the cooperation with the GeoForschungsZentrum, tested the equipment and he made the first absolute measurements with the new facility. Richard and Karsten have designed and manufactured the mechanics. They have contributed their experience in the processing of non-ferromagnetic materials and they brought in a lot of own ideas.

References

Jacobs, J.A. (1987), Geomagnetism, Volume 1, *Academic Press*

Kertz, W. (1969), Einführung in die Geophysik, *B.I. Wissenschaftsverlag*, Hochschultaschenbuch Band 275

Auster, H.U., K.H.Fornacon, E.Georgescu, K.H.Glassmeier and U.Motschmann (2002), Calibration of fluxgate magnetometers using relative motion, *Meas. Sci. Technol.* 13, 1124-1131

First Results of Absolute Component Magnetic Field Measurements without the use of a Theodolite

Eberhard Pulz and Oliver Ritter, GeoForschungsZentrum Potsdam, Germany

Abstract.

AUSTER [1,2] gives the theoretical background for a method to measure the absolute components of the Earth's magnetic field without a theodolite. Such non-magnetic theodolites are expensive, difficult to handle, and their operation requires highly trained personnel. The new measuring system is based on a device to support a three-component fluxgate magnetometer, which must be engineered with very high mechanical precision. In this paper, we report on first results of a prototype system which was manufactured and tested at the Adolf-Schmidt-Observatory, Niemegk of the GeoForschungsZentrum Potsdam. The first part of the paper describes the influence of mechanical tolerances and the measuring procedure. The comparison of the results with the observatory instruments indicates differences of less than 1.5 arc minutes for the declination (D) and the inclination (I). These results can be improved if more sophisticated correction procedures for the magnetic variation field are applied and the experiences are under consideration.

Introduction

The introduction of D/I-fluxgate magnetometers in the 1980's provided a simple way to determine the absolute components of the Earth's magnetic field. However, such absolute field measurements require a very accurate orientation of the magnetometer to the geodetic coordinate system. This is usually accomplished with a theodolite which must be free of magnetism. Such theodolites are expensive, difficult to operate and good results are generally only obtained if the observer is skilful and experienced [3].

To overcome this obstacle, AUSTER [1,2] proposed a device to determine the absolute components of the Earth's magnetic field which does not require a theodolite. This new instrument (called XYZ-instrument) consists of a stand-alone scalar magnetometer and a mechanical device to support a three-component fluxgate magnetometer. In this paper, we report on the first results of a prototype instrument which has been built by R. Winkler and C. Müller at the Niemegk Geomagnetic Observatory of the GeoForschungsZentrum Potsdam.

The Instrument

The method presented here to obtain absolute magnetic field measurements is based on (i) a scalar calibration of a three-component magnetometer and (ii) on the determination of the geomagnetic field in the direction of one well-defined axis using the same measuring procedure.

Fig. 1 shows the XYZ-instrument. It is made from aluminium and consists of a platform with three adjustable screws, and a turntable. Mounted on the turntable are two orthogonal pairs of support prisms which can hold the magnetometer or a telescope (see Fig. 2). The magnetometer is placed in a small container (or basket) which is situated at the centre of the turntable. Using the two pairs of support prisms, the *basket*-magnetometer can be rotated around the two orthogonal axes of the XYZ-instrument, respectively. The turntable can be orientated horizontally using a spirit level and a defined geodetic direction is taken from a known azimuth mark using the telescope. Naturally, such an instrument can never be built perfectly. It is therefore necessary to determine the influence of any mechanical tolerances on the measuring results.

The determination of mechanical tolerances

In order to determine the relative horizontal positions of the support prisms, the XYZ-instrument was installed on a platform together with a micrometer. Then, the tolerances of each support prism together with a test rod, the telescope, and the sensor basket can be measured relative to a fixed point. The results in Fig. 3 show only for one of the support prisms (P4) a significant deviation of 12 μm. The misalignment of the cylinder for the sensor basket is tiny; the deviation between the cylinders A and B is in the order of only 4 μm. Nevertheless, this knowledge has to be used for the correct levelling of the instrument (Fig. 4).

To measure the orthogonality between the support prisms, the instrument was installed at the centre of a flat meadow. Four target marks were fixed at distances of about 100 m and their directions were determined using the telescope (compare Fig. 2). Next, a Zeiss theodolite was installed at the centre of the turntable to measure the angles to the target marks. We found a deviation from orthogonality of 15 arc seconds between prism pairs P1/P3 and P2/P4 (Fig. 3). The standard deviation of these measurements was 1 arc second. A principal problem with this XYZ-instrument is that the telescope cannot be adjusted in the vertical direction which means, that in many cases it will be impossible to take an azimuth mark. This problem was overcome using a pair of adjustable mirrors which work like a scissors telescope. The mirrors were adjusted as follows:
An approximately 10m long and very thin plumb line was installed at a distance of approximately 50 m from the instrument. First, the plumb line was targeted without using the mirrors. Then, the mirrors were installed in such a way that we were able to look up and down the line without any deflection from the vertical axis. Obviously, we also checked all components for magnetic impurities prior to the experiments.

To summarise,

1. The horizontal alignment of the instrument can be done with an accuracy of some arc seconds which means that the z-axis is adjusted very well.
2. The deviation from orthogonality between the support prisms is 15 arc seconds. However, this can be taken into account when calculating the magnetic field components (see below).

Execution of the measurement

Firstly, the XYZ-instrument is levelled (Fig. 4). Then, the XYZ-instrument is orientated with respect to the geographic co-ordinate system by taking an azimuth mark by means of the telescope (Fig. 2). The total intensity of the magnetic field is measured with a proton-magnetometer. The result is stored on a GPS synchronized computer. The *basket*- magnetometer of the XYZ-instrument and an additional three-component fluxgate magnetometer are also connected to the computer via optical RS232. The second fluxgate magnetometer serves as a variometer. The additional measuring procedure is the following:

1. The *basket*-magnetometer is placed on support prisms P1 and P3 (see Fig. 1). In this position the first measurement is taken under computer control: three components of the *basket*-magnetometer and the three components of the variometer.
2. The *basket*-magnetometer is adjusted in steps of approximately 60 degrees, which means 6 positions for a full turn (positions 1-6 in Fig. 5). Note, we must ensure that a wide range of positions is covered, but it is not necessary to know the exact angles.
3. The measurements are repeated by using the second set of support prisms. Again, the basket-magnetometer is turned in 6 steps (Fig. 5, positions 7-12).
4. Steps b and c are repeated with the basket-magnetometer being rotated in the x-y plane (Fig.5, positions 13-18 and 19-24).
5. Optionally, the whole sensor basket rod is rotated by 180 degrees and steps 1-4 are repeated (Fig. 5, positions 25-48).

6. Three individual measurements (of the 48) are always analyzed to determine scaling factors, offsets, and non-orthogonality of the three components of the basket magnetometer. In total, we obtain 19 estimates (Fig. 6).

The whole cycle of measurement takes less than 30 minutes. The operation is simple; it involves rotating the instrument and pressing a computer button.

Results of the test measurements in Niemegk

A test suite of repeated absolute field measurements with the XYZ-instrument was carried out between March 7th and April 8th 2002. The instrument was built up and dismantled several times during this period. The mechanical tolerances were determined and the mirrors assembled. Both the measuring sequence and the calculating routine were changed, which means that the results have to be assessed differently. In the diagrams, individual experiments are numbered consecutively for simplicity.

The first results were derived from measurements, which contain only 24 positions of the *basket*-magnetometer and temporal magnetic field variations were not considered. The comparison with the recordings of the observatory instruments shows discrepancies in the order of 1.5 arc minutes for dI and dD (Fig. 7). A systematic bias on both traces indicates that the instrument was not correctly adjusted.

In order to improve these results, (i) a variometer was connected (at repeat point 21), (ii) the mirrors were assembled (at repeat point 26), and (iii) the mechanical tolerances of the instrument were considered (repeat point 34) and (iv) the interval of rotation steps was increased from 24 to 48 (repeat point 34). Throughout the second test period there was high magnetic activity (Ap=20 nT). It is therefore possible that large magnetic field variations are not reduced adequately if the time between individual readings is too long.

After readjustment of the instrument (repeat point 34) the correspondence to the Niemegk observatory measurements is clearly improving (Fig. 8).

Fig. 9 shows a comparison of F-values calculated from the *basket*-magnetometer and corresponding values calculated using the variometer. These values and the results of the Figs. 5 and 6 correspond to repeat point 38. The standard deviation of the differences is less than 0.5 nT.

Conclusions

A new instrument (XYZ) for measuring the vector components of the earth's magnetic field was manufactured and tested at the geomagnetic observatory of the GeoForschungZentrum in Niemegk. As a main advantage over existing instruments, the XYZ- instrument can measure the absolute magnetic field without an iron-free theodolite. Once the instrument is adjusted, it's handling is so simple that untrained people can reliably operate it. The quality of the results with the XYZ-instrument depends on very accurate targeting of the azimuth marks, precise determination of mechanical tolerances, and linear response of the three-component fluxgate magnetometer and a good reduction of temporal magnetic field variations. Nevertheless, these first results are so promising and we intend to use the XYZ-instrument routinely in addition to the traditional D/I flux measurements.

Acknowledgement

We are grateful to H.-U. Auster from the TU Braunschweig, Germany, for a very fruitful collaboration. For making the prototype instrument and their continuous support in all aspects of the engineering work, we would like to thank the members of the mechanical workshop in Niemegk.

References

[1] H:-U. Auster, K.-H. Fornacon, E. Georgescu, K.-H. Glassmeier and U. Motschmann
Calibration of flux-gate magnetometers using relative motion.
Meas. Sci. Technol. 13 No 7 (July 2002) 1124-1131

[2] J. Jankowski, Chr. Sucksdorff
Guide for magnetic measurements and observatory practice IAGA, Warschau 1996

[3] H.-U. Auster (in this volume)

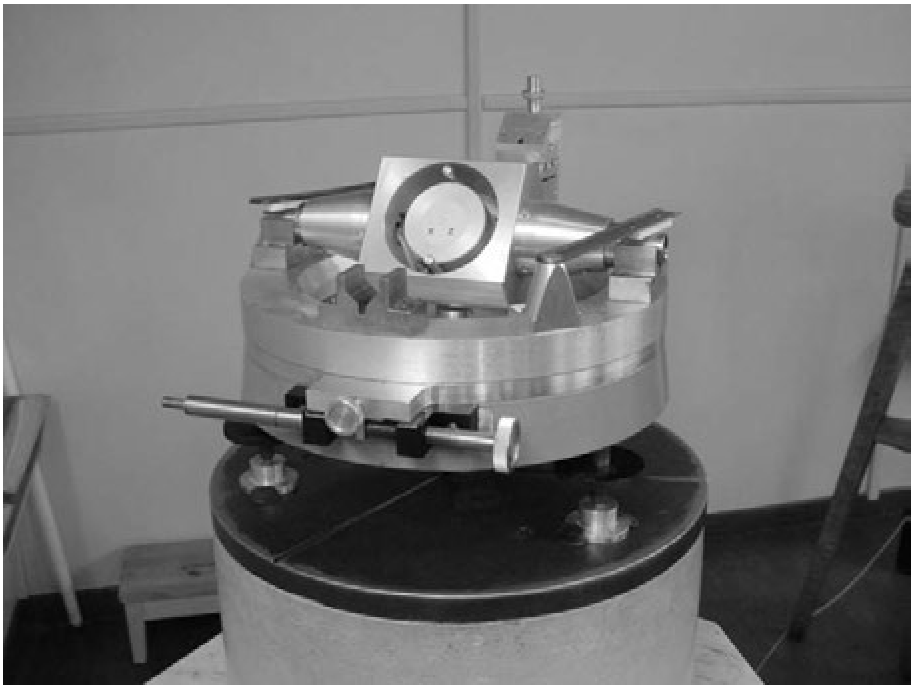

Fig. 1 The Instrument together with fluxgate magnetometer basket

Fig. 2 The instrument together with the telescope

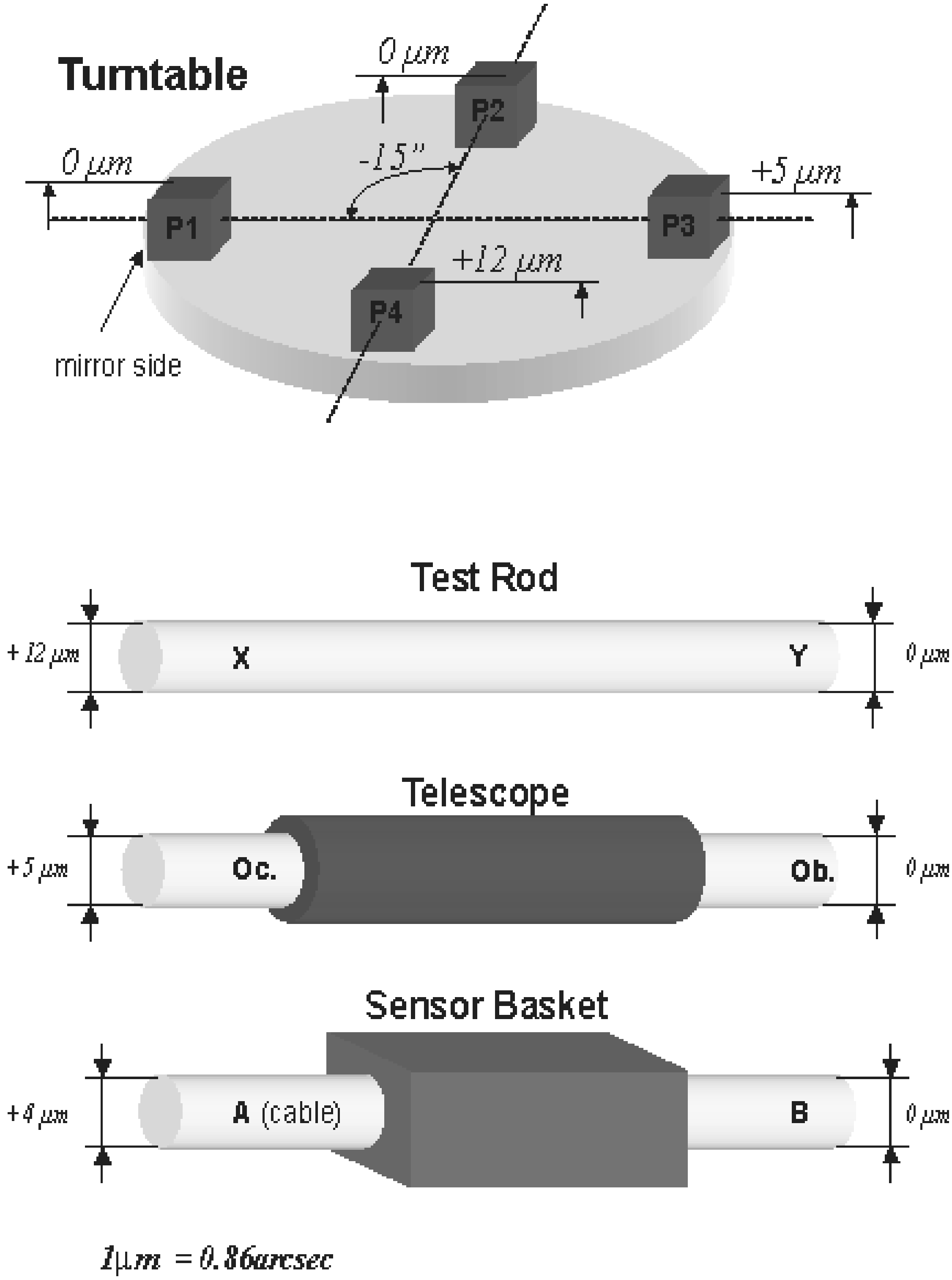

Fig. 3 Result of micrometer measurements (relative tolerances)

Fig.4 Levelling of the XYZ- instrument

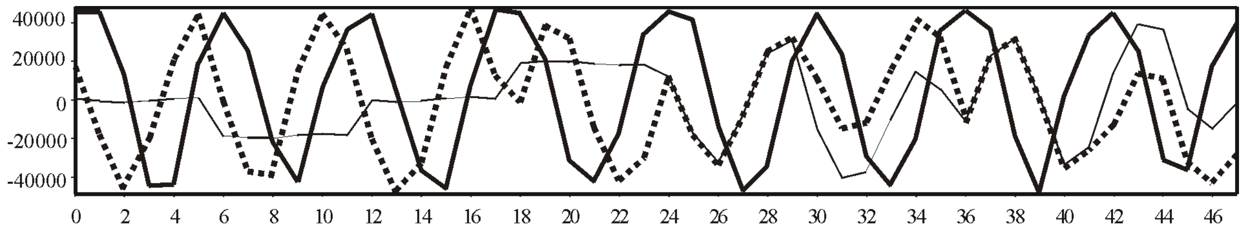

Fig. 5 3 component basket magnetometer: result of a complete measurement (48 single measurements)

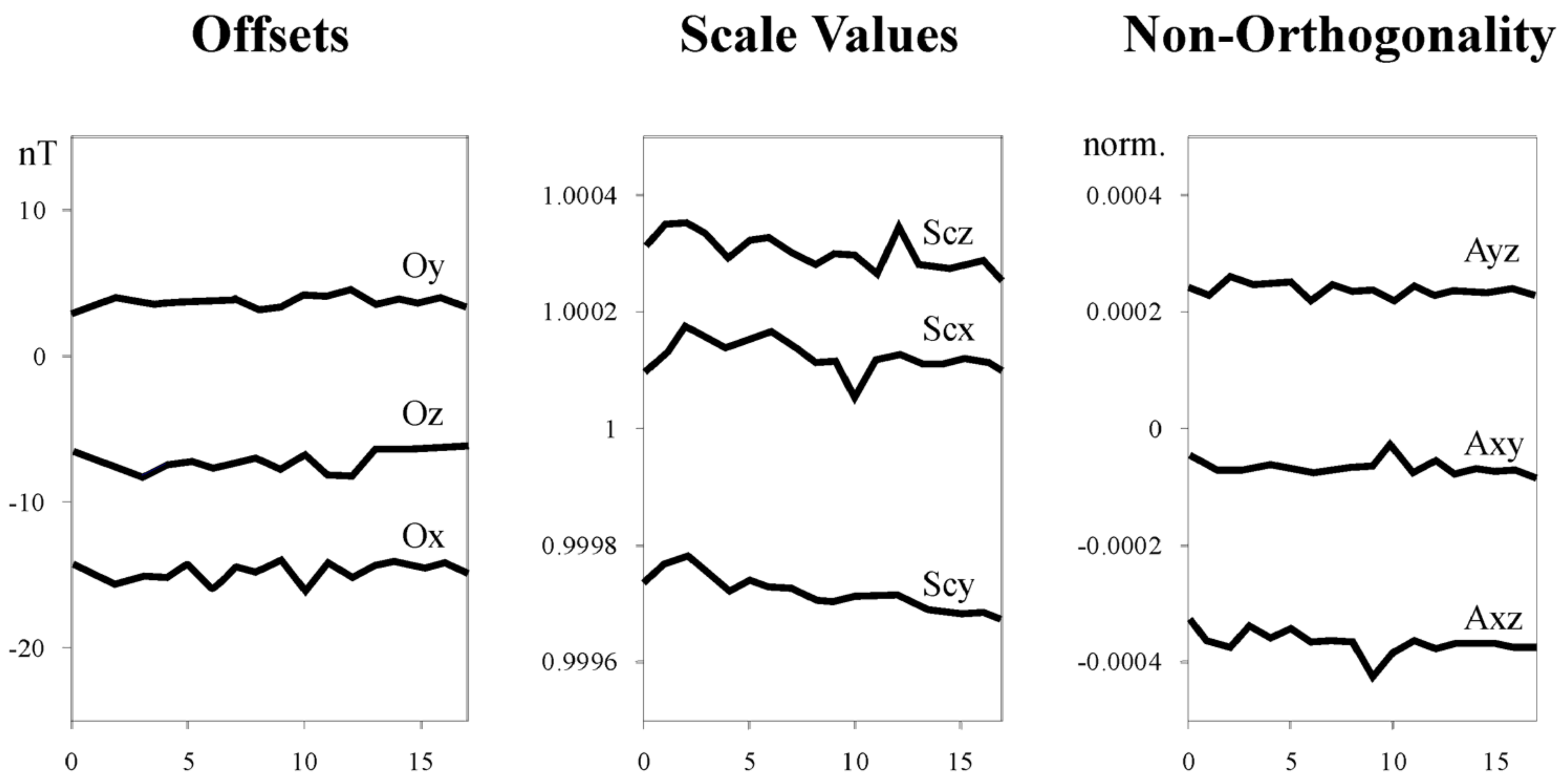

Fig. 6 Result of the basket magnetometer calibration during an absolute value dermination.

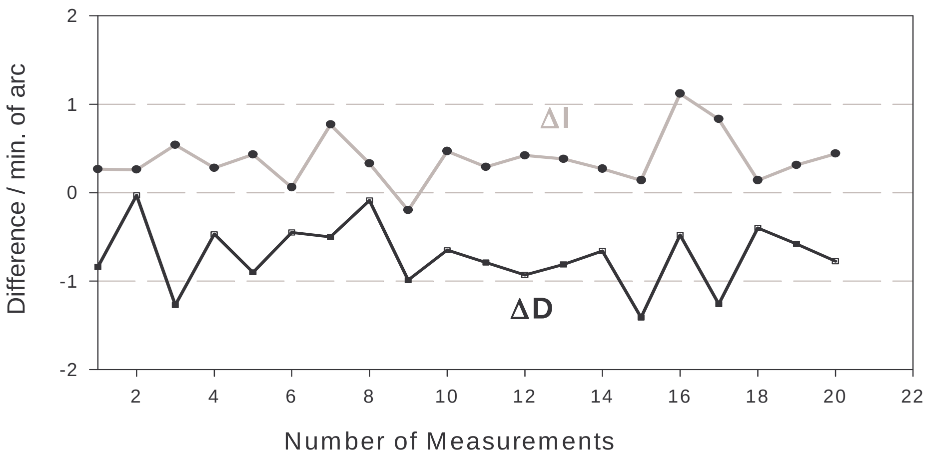

Fig. 7 Comparison of D and I with the Niemegk recordings without consideration of the variation

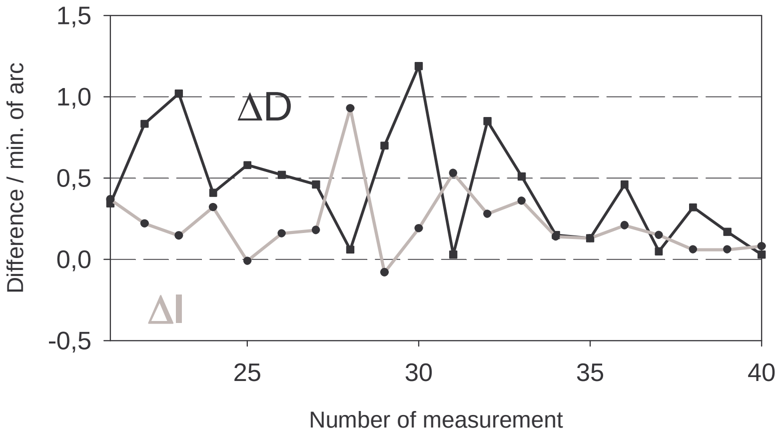

Fig. 8 Comparison of D and I with the Niemegk recordings under consideration of the variation

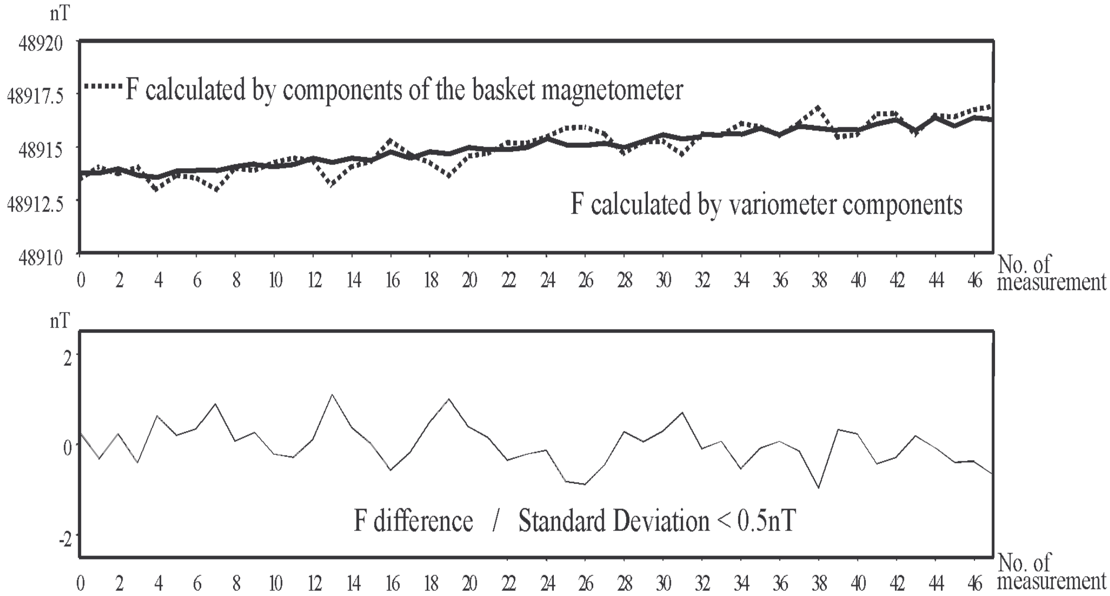

Fig. 9 F-Comparison between: variometer and basket magnetometer

Numerical techniques for proton magnetometers

Arun Patil and R. Rajaram
Indian Institute of Geomagnetism, Colaba, Mumbai – 5

Abstract

The problem of estimation of the precession frequency of the proton magnetometer has been addressed here. The precession frequency has to be determined from the successive zero crossings of the sinusoidal output signal induced in the coil by the proton rich fluid immersed in the earth's magnetic field. The dependence of the accuracy of the signal to noise ratio and decay of the signal is discussed. Least square methods and the robust median fit methods are used to estimate the signal period. It is found that the signal processing method using a robust technique gives superior performance when higher sampling is needed or the environmental conditions degrade the available signal to noise ration. For a five second sampling under ideal observatory conditions, even the least square technique provides a 0.1 nT accuracy.

Introduction

The proton precession magnetometer (PPM) is being used for measuring the geomagnetic field for many years now (Wienert, 1970). It involves measuring the sinusoidal oscillation frequency induced in the sensor coil by the precession of protons in the ambient geomagnetic field. The typical frequency for the magnetic field of the earth ranges from 1 kHz to 4 kHz. The protons are first polarized in a chosen direction with the help of a relatively large polarizing current. When the polarization current is withdrawn the proton's precession around the earth's magnetic field is initiated. The signal amplitude decays with spin-phase memory time constant T_2. This time constant depends on the liquid in which the sensor is immersed and on the gradient of the magnetic field across the sensor. Even in a uniform field, this time rarely exceeds two seconds. Initial signal amplitude at the sensor output is a few microvolts peak-peak. The task of the electronic circuitry along with its accompanying signal processing algorithms is to derive the period of precession frequency accurately with a measuring time of less than one second.

First generation magnetometers achieved this by using phase lock loop techniques. A phase lock loop locks on to the incoming signal and at the same time multiplies its frequency by a suitable factor. This process filters out the noise in the proton signal apart from reducing the measuring time. This method has its limitations. Apart from the fact that the phase lock loop takes a finite time to lock on to the incoming signal, the multiplying factor in the phase lock loop cannot be increased indefinitely to achieve an increase in measurement accuracy.

An accuracy of 1 nT (nano Tesla) can be achieved for a typical requirement of sampling period of 5 seconds but to attain greater precision a different approach has to be adopted. Sophisticated methods also become essential even for 1 nT accuracy when the sampling rates are around 1 second or less and the number of cycles available becomes too small to effectively weed out the errors generated by the noise component. In what follows, we discuss numerical data processing techniques that can be used to achieve such an objective. Two independent algorithms that can be used with the proton magnetometer output signal are discussed in detail. The numerical results focus on the typical output of a standard proton magnetometer but the same techniques are equally applicable to the Overhauser magnetometer as well. These include the standard least square signal for linear fit to the time progression of the zero crossings technique and the robust median technique.

Definition of the problem

The relation between the geomagnetic field and proton precession frequency is given by

$$B = gF_0 \qquad \textbf{(1)}$$

Where B – Geomagnetic field in nT

g – constant – 23.4874

F_0 – Proton Precession frequency

The period T_0, is estimated from the number of cycles of a higher frequency signal F_r measured during N number of signal cycles F_0. This involves recording the times of zero crossings of the signal voltage. If C is the total count of high frequency cycles of F_r, the period T_0 is given by

$$T_0 = \frac{C}{NF_r} \qquad \textbf{(2)}$$

Substituting this value in (1) gives

$$B = \frac{g}{C} NF_r \qquad \textbf{(3)}$$

We have tacitly assumed that the signal is pure and free from noise so that the zero crossings can be identified unambiguously. In reality we do have a noise component n(t). We can describe the signal Voltage V as (Hancke, 1990)

$$V = S.Sin(\omega t) + n(t)$$

Where S is the signal amplitude and n(t) is the noise component already defined. In principle any threshold level Δv can be used to estimate the period T_0 but as we shall see soon, the zero crossings are the most appropriate points for such estimations.

Let the signal S crosses the threshold level Δv at time t_1. Then

$$\Delta v = S.Sin\, \omega t_1 + n(t_1)$$

and

$$t_1 = \frac{1}{\omega} Sin^{-1} \frac{\Delta v - n}{S}$$

Let us assume that the pure sine wave would have crossed the threshold Δv at time t_2.

$$\Delta v = S.Sin\, \omega t_2$$

$$t_2 = \frac{1}{\omega} Sin^{-1} \frac{\Delta v}{S}$$

The error ΔT introduced by the noise is then given by

$$\Delta T = t_1 - t_2 = \frac{1}{\omega}\left[Sin^{-1}\frac{\Delta v - n}{S} - Sin^{-1}\frac{\Delta v}{S}\right] = \frac{1}{\omega}\left[\frac{-n}{S} - \frac{(\Delta v)^2 n}{S^3} + \frac{\Delta v n^2}{S^3} - \frac{n^3}{S^3}.....\right]$$

We get a minimum value for ΔT when $\Delta v = 0$ i.e. at the zero crossing point. This is not surprising as the slope of the sine wave attains its largest value at its zero crossings.

Thus to the lowest order we get

$$\Delta T = \frac{1}{\omega R} \qquad \textbf{(4)}$$

Where $R = \frac{S}{n}$ is the signal to noise ratio.

Thus measured period T_0 is accompanied by an error ΔT at every zero crossing of the signal. In addition to the error due to the noise, there is one more source error. The frequency Fr that is assumed to be a constant may not be so.

Taking into consideration these two sources of error we can use equation (3) to re-write the error in ΔB as

$$\Delta B = B\frac{\Delta F_r}{F_r} + B\frac{\Delta T}{T} \qquad \textbf{(5)}$$

The error caused by uncertainties in the reference frequency Fr can be taken care of by calibrating the crystal. But error arising from the fluctuations of the zero crossings generated by the noise component has to be treated using special techniques. This error can be minimized with different processing techniques.

In the real life situation the signal decays due to loss of coherence of the precession of the protons in the different parts of the sensor volume. The signal decay with time can be expressed through the degeneration of the signal to noise ratio R as

$$R = R_0e^{-t/T_2}. \qquad \textbf{(6)}$$

Here R_0 is the signal to noise ratio at time zero.

We note from the second term in equation (5) that the larger the value of T_2, the less will be the error in B. This would imply that the larger the value of N, the larger the accuracy in the magnetic field determination provided ΔT remains constant. We note form equation (4), that ΔT is inversely proportional to R and this error will manifest itself as we increase the number of cycles N. There should be an optimum N. To get this N, we substitute R from equation (6) into equation (4) to get ΔT and use this value of ΔT in equation (5) to get the error in B. This is differentiated with respect to N and put equal to zero. We get

$$N= \frac{T_2}{T_0}$$

N gives the optimum number of cycles for which the error in the estimated field is a minimum. But in practice the number of cycles available may be less and one has to make do with a smaller value of N.

Processing techniques

Two techniques that are used for processing the signal are described here. Both the methods attempt to retrieve the exact period of the wave from the N measured crossing. The period has to be determined from N values tp (p=0 , N) of observed times of the zero crossings each having a variance of σ_p. As the signal amplitude decays, the variance increases, though in most practical applications it is often neglected. We retain this feature in the basic formalism although we present numerical results with the simplified scenario. If T_c is the exact time period then

$$t_0 + pT_c = t_p \qquad \textbf{(7)}$$

Where p = 0, 1, 2…………N and t_0 is the uncertainty in the timing of the first crossing.

The techniques used derive T_c in such a way that its variance is as small as possible.

The standard technique used attempts to minimize the mean square difference of the actual zero crossing times and those computed from the estimated fit. This is referred to as the least square method here. We shall note that the least square technique, with suitably chosen algorithms, has the advantage that it requires a relatively smaller number of computations and with suitably defined algorithms it can be used in real time. However, the method is susceptible to strong biases generated by outliers. A median fit becomes more reliable and may be a preferred method with smaller samples. We describe both the methods in some detail here.

(1) Least square method – In this method time is measured from the first zero crossing of the signal up to N number of zero crossings. s^2, the sum of the square of the difference between the observed time and fitted value of the zero crossings is given by

$$s^2 = \sum_0^N \frac{\left(t_0 + pT_c - tp\right)^2}{\sigma_p^2}$$

Differentiating the above expression, with respect to T_c and putting the result equal to zero we get

$$t_0 \sum_0^N \frac{p}{\sigma_p^2} + T_c \sum_0^N \frac{p^2}{\sigma_p^2} - \sum_0^N \frac{ptp}{\sigma_p^2} = 0$$

A similar operation with respect to t_0 gives

$$t_0 \sum_0^N \frac{1}{\sigma_p^2} + T_c \sum_0^N \frac{p}{\sigma_p^2} - \sum_0^N \frac{tp}{\sigma_p^2} = 0$$

T_c can be obtained from the two equations given above and can be written as

$$T_c = \frac{S_A S_E - S_B S_D}{S_A S_C - S_B^2} \qquad \textbf{(8)}$$

Where

$$S_A = \sum_{p=0}^{N} \frac{1}{\sigma_p^2}$$

$$S_B = \sum_{p=0}^{N} \frac{p}{\sigma_p^2}$$

$$S_C = \sum_{p=0}^{N} \frac{p^2}{\sigma_p^2}$$

$$S_D = \sum_{p=0}^{N} \frac{tp}{\sigma_p^2}$$

$$S_E = \sum_{p=0}^{N} \frac{p\ tp}{\sigma_p^2}$$

The variance of T_c is given by

$$\sigma\left(T_c\right) = \sqrt{\frac{S_A}{S_A S_C - S_B^2}}$$

The expressions provided by Hancke (1990) can be retrieved if it is assumed that the variance in the estimates of the time of zero crossings remains constant right through the measurement cycle. After some manipulations it is possible to express T_c in the form

$$T_c = \sum_0^N \alpha_p t_p \qquad \textbf{(9)}$$

Where

$$\alpha_p = \frac{p.S_A - S_B}{\sigma_p^2.(S_A.S_C - S_B^2)} \qquad \textbf{(10)}$$

The form given in equation (10) is more convenient to implement in real time micro-controller computations. If we ignore the variation of the signal amplitude with time, σ_p is independent of p and can be replaced by some typical value σ_0 and α_p takes a simple form

$$\alpha_p = \frac{6.(2.p - 1 - N)}{N.(N^2 - 1)} \tag{11}$$

This is identical to the expression provided by Farrel et. al. (1965) using a somewhat different approach. α_p can be stored in a suitable array to enable quick real time computations.

(2) Robust estimation using the median fit: It can be shown (Press et al, 1992) that the median value of a given set of numbers is a truly representative value of the sample as the sum of its absolute difference from the set of points is the minimum. This property can be used to obtain a robust estimate of the linear fit (cf. Press et. al., 1992). We use this technique estimate period. Following the reference cited above, we use the least square estimate as a starting value to get the median of the distribution. This method minimizes the effect of outliers in a distribution. As we shall note later the use of robust technique is not recommended when large number of cycles are available for the estimation of the time period, as the computational overheads are not justified by the corresponding accuracies in the estimation. For smaller samples however, the robust estimate provides more reliable values.

Results

The least square algorithms have been implemented both in a PC based system as well as in a micro-controller based instrument. The micro-controller-based PPM was taken to the Xth IAGA workshop on instrumentation at Hermanus for inter-comparison and calibration and shown to generate field values accurate to 0.1 nT. We present here some results obtained using the PC-based system to demonstrate its sensitivity. The instrument was operated at the Alibag observatory and the results were compared with a standard fluxgate magnetometer developed by the Danish Meteorological Observatory with 0.1 nT accuracy. Figures 1 and 2 provide a good account of the sensitivity of the PPM.

ALIBAG DEC 24-25 2001 TIME IN MINUTES UT

Fig 1. Plot of F, the total magnetic field variation at Alibag from the PPM and the corresponding value derived from fluxgate magnetometer developed by the Danish Meteorological Observatory with 0.1 nT . The offset in the figures is because of different location of the instruments.

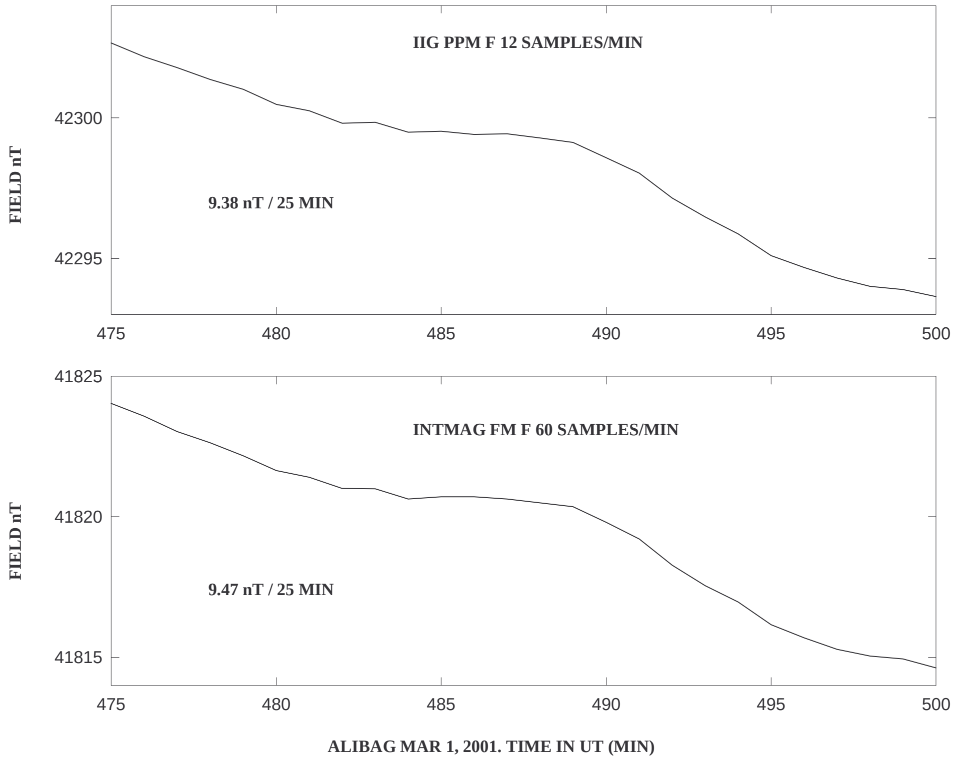

Fig 2. Same as Figure 1 but confined to a shorter period to demonstrate the authenticity of the short period variations of the PPM.

These plots show field variations at Alibag (18.64° N, 72.87° E geographic co-ordinates). Here the plotted values are one minute values that are averages of 60 samples in case of the Digital Fluxgate Magnetometer (DFM) and 12 samples in case of the PPM. The number of signal cycles of the proton precession utilized was 1000. The signal to noise ratio was 10 in the beginning and the signal decay time T_2 was around 1.5 seconds ensuring that over the entire measurement period the signal to noise ratio was above 6. The remarkable similarity in the long period variations and trends (Figure 1) and in the short data segment (Figure 2) brings out very effectively the authentic response of the PPM to changes even of the order of 0.1 nT. A DC offset between the two instruments is due to the different locations.

Very often a PPM output is required with a sampling rate of one per second or higher. In such cases the number of cycles available could be as low as 300. The signal to noise ratio also may not be as high. We therefore examine how the two methods described in the last section perform when only short periods of a signal output is available and the signal to noise ratio is also weaker. A standard signal source of very high stability with a frequency corresponding to 46974.3 nT was used to simulate the proton output. The signal to noise ratio was maintained at around 4 and the utilized measuring time for the data was varied to examine how the number of cycles used, controls the reliability of the measurement. Sixty independent samples were taken and using 300, 600 and 1000 cycles, the ‘field’ was computed for each of the sixty samples. The standard deviation and the probabilities of the computed field deviating (a) by more than 1 nT and (b) by more than 0.1 nT was estimated. The results of the computations are presented in. Table 1

Number of samples	Least Square estimates % Points outside			Robust Estimates % Points outside		
	σ(Tc)	0.1nT	1 nT	$\sigma(T_C)$	0.1 nT	1 nT
300	**1.286**	**98**	**13**	**0.357**	**58**	**1**
600	**1.116**	**96**	**18**	**0.206**	**41**	**0**
1000	**0.021**	**0**	**0**	**0.027**	**0**	**0**

Table 1. Performance summary for the least square and robust techniques.

We note that when 1000 cycles are available, the least square estimates lie within 0.1nT of the expected values and no advantage is gained by using the more time consuming but robust median fit. The variance is also not significantly different between the two methods. But the situation is dramatically different when a smaller number of cycles are used. The variance in the estimated periods is drastically less when a robust estimation is used.
When only 600 cycles are used, only 4% of the observations lies within a 0.1 nT window for the least square estimate and as many as 18% of the estimates lies outside 1 nT. On the other hand 59% of the points lie within the 0.1 nT window, and all the estimates are accurate to better than 1 nT.
When 300 points are used, only 2% of the least square estimates lies within 0.1 nT while 42% of the robust estimates lies within this window. 87 % of the least square estimates lies within 1 nT while in the case of the robust estimates 99% of the observations lies within 1 nT.

Conclusion

Using sophisticated numerical techniques; the accuracy and the sensitivity of the PPM measurements can be enhanced. For 5 second sampling, the PPM estimates based on least square algorithms can generate values reliable up to less than 0.1 nT. However, when a higher sampling rate is desired or when the signal to noise ratio is less due to the environmental conditions, the robust median fit is the right choice and can provide more reliable and accurate values.

References:

Farrel E.J.,Grosch ,C.B.,Proceedings of IEEE, 1965, p 2163.
Hancke G.P.,Transactions on Instrumentation and measurement, Vol. 39 No.6. December 1990.
Press, W.H., S.A. Tuecolsky, W.T. Vetterling and B.P.Flannery, Numerical Recipes in C - Art of Scientific Computing, Cambridge University Press, p 703, 1992
Wienert K.A., Notes on geomagnetic observatory and survey practice, United Nations Educational, Scientific, and Cultural Organisation, 1970.

A Review of the Methods to Determine True North for Measurement of Declination.

J G Carrigan. (British Geological Survey, West Mains Road, Edinburgh, EH9 3LA, Scotland, UK)

Abstract

This paper describes the various methods used in the determination of a true north bearing in the field or at a magnetic observatory. It investigates the use of the north-seeking gyro and discovers that there a range of options available, such as the Wild GAK-1 gyro currently used by BGS, the Sokkia GP1-2A and the Gyromat 2000. The hourglass method and the altitude method are compared in the determination of a true bearing using sun observations and advice and information for writing software for reducing the measurements is given. The use of twin Leica System 530 differential GPS receivers to acquire an accurate true bearing using post-processing techniques is discussed. Also described is the use of a handheld GPS receiver for determination of a true bearing over longer baselines to establish exact position fixes in conjunction with data from a global network of fixed GPS stations. This paper reveals that, when compared to the expense of higher grade GPS equipment, the use of the handheld receiver is a much more economical method of obtaining a true azimuth without much reduction in accuracy. Each technique is compared by making measurements on a known baseline established in Edinburgh. In addition, the practicality and financial feasibility of each method is considered.

Introduction

In making a precise measurement of magnetic declination (D), the determination of a true north bearing is just as critical as measuring the direction of the magnetic meridian. This paper is intended to be a practical guide for geomagnetism organisations who wish to review the way they determine true north at repeat stations or who simply wish to cross-check their existing fixed-mark azimuths at observatories using a different method. Also it will be useful to those organisations who are proposing setting up a repeat station network or who simply wish to make impromptu one-off measurements at sites they do not intend to visit again. Three different methods will be discussed: the north-seeking gyro; astronomical methods; and the use of the Global Positioning System (GPS). Each method is discussed not just in terms of practicality but also financial feasibility, as some of the equipment used for surveying true north can be very expensive. The emphasis in this discussion will be on the gyro technique which is used less frequently, and GPS which is a modern innovation. On the other hand, using sun observations to determine true north is widely used with procedures, accuracy levels and error values generally well known, so it will be discussed relatively briefly in this paper. The methods are tested using calibration baselines at Eskdalemuir and a newly established baseline in Edinburgh. The baseline at Edinburgh was established recently for this project by using a survey grade GPS system. As GPS features largely in this project it is important to firstly describe its principles and accuracy levels.

Principles of GPS

GPS is a satellite-based positioning system consisting of a constellation of 26 satellites (in 2002) orbiting the earth at height of 20,200 km on precisely determined orbital paths. These paths are defined so that at least 5 satellites are visible anywhere on the earth at any time. Each satellite transmits signals which allow the distance between a receiver and the satellite to be calculated. By calculating the distance from at least four satellites whose positions are precisely known then an accurate position for the receiver can be established. A wide range in the sophistication of GPS receivers is available and to understand their capabilities it is important to have some knowledge of the signals broadcast from the satellites.

Each satellite has a very accurate atomic clock on board which is used to generate the satellite signals at a fundamental frequency of 10.23 MHz. The satellites broadcast two carrier waves: the L1 carrier at 1575.42 MHz (10.23 * 154); and the L2 carrier at 1227.60 MHz (10.23 * 120). Modulated on these two carrier frequencies are much lower frequency codes referred to as Code phase which is a pseudo-random code used for matching satellite and receiver signals for measurement of range. This code also contains information about the satellite, including an accurate position. The code is used to synchronise the receiver clock with the atomic clock on the satellites by measurement of the offset due to receiver clock error from at least 4 satellites. Once receiver clock error is accounted for, the remaining time displacement is due to the distance the signal has to travel. When this is measured from several satellites a position for the receiver can be acquired. However, as the code phase has a relatively large period the results can be in error by several metres. This is the method used by the more basic handheld receivers which are generally used for recreational purposes.

Much greater positional accuracy can be achieved by using the carrier phase which has a frequency 1000 times greater than code phase and a wavelength of a few centimetres. However, as the carrier frequency is a simple sine wave, the pseudorandom code phase is still required for synchronisation. Thus the most sophisticated receivers use the code phase to get an approximate position and then the carrier phase to get a much more accurate position. This method is used by survey grade receivers which have a positional accuracy of around 10 cm or better.

Positional errors can occur due to the refraction effects of the ionosphere and the troposphere, which is the reason two carrier frequencies are useful. The more sophisticated receivers, which are able to receive the two carrier frequencies, can estimate positional error due to atmospheric refraction. A technique called Differential GPS involves twin receivers; the base receiver is installed at an accurately known position and the apparent location error used to correct the remote receiver which is tracking the same satellites. Thus any error which is common to both receivers is accounted for. This can be done in real time with corrections being transmitted from the base to the remote receiver or it can be done by post-processing data from each receiver.

Networks of permanent Differential GPS stations have been installed all over the globe with data often available free of charge. Data is available in standard format called the Receiver Independent Exchange Format (RINEX). This allows for the differential processing of data from a range of different receivers. The great disadvantage of GPS is that as the satellite signal is quite weak, line of sight from the receiver to the satellite is essential. Therefore GPS cannot be used indoors or in areas where a clear view of the sky is not possible such as in forests, next to tall buildings or in deep valleys. Great care should always be taken in positioning GPS receivers and when using twin receivers ensuring each receiver can track the same satellites.

True Bearing Calibration Baselines

In addition to an existing calibration baseline at Eskdalemuir Observatory, a second baseline was established at British Geological Survey offices in Edinburgh (Figure 1). The method used was carrier phase differential GPS in conjunction with a permanent GPS station. Twin Leica GPS 530 receivers were set up at either end of the baseline. They are dual frequency, code and carrier phase receivers with the option of real time processing of data through a radio link between the two receivers. This system represents top-of-the-range, high specification GPS equipment.

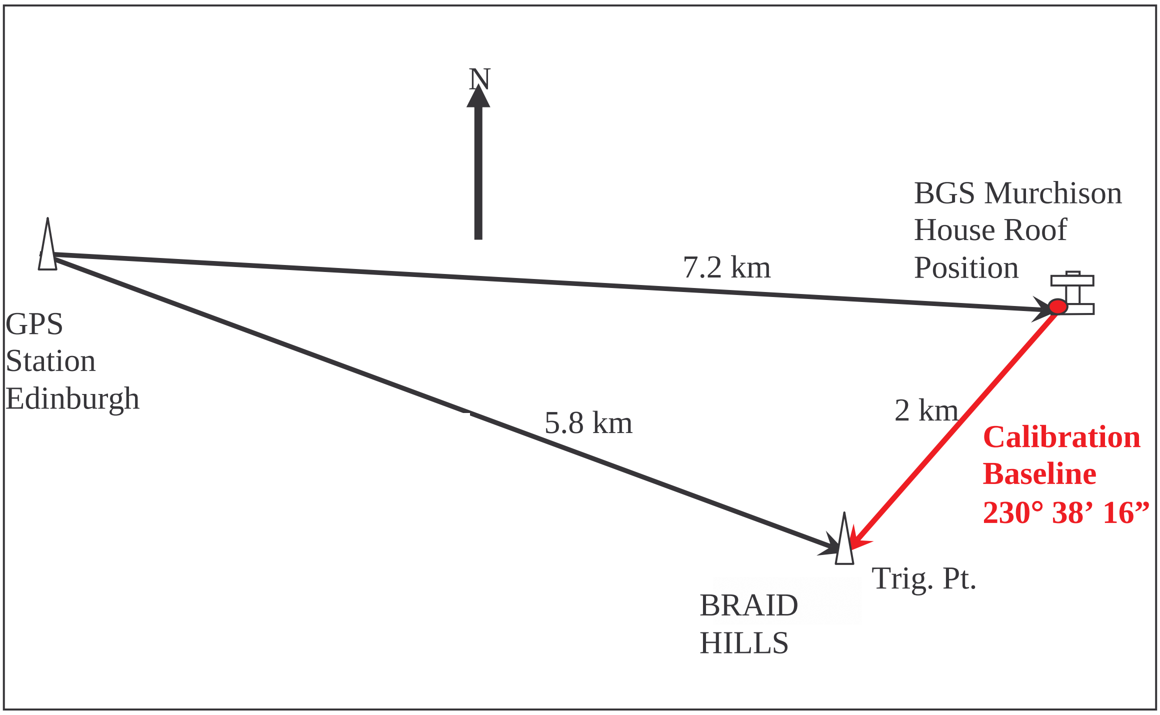

Fig 1 True Bearing Baseline

An existing GPS station in Edinburgh (EDIN) operated by the Ordnance Survey, the principal mapping agency in Great Britain, was used as the permanent reference station. This station is part of a dense network of permanent GPS reference stations throughout the UK. Data are stored in RINEX format in near real time on the World Wide Web, free of charge (www.gps.gov.uk). Data were logged in RINEX format at each GPS receiver on the baseline for more than one hour and then post-processed using Leica's proprietary software in conjunction with data from the permanent reference station. Accurate absolute positions of less than 1 cm uncertainty in the WGS84 datum are then obtained for the position at Murchison House and at Braid Hills. The true bearing from Murchison House to the Braid Hills triangulation point was measured to be 230º 38' 16". Repeatability over a number of independent measurements was less than one second of arc. The triangulation point on Braid Hills can be viewed easily through a theodolite telescope from the Murchison House station. Thus an accurate and practical baseline is established for calibration and testing of true bearing measurement systems. Using a permanent GPS station is not essential for obtaining an accurate position when using GPS equipment which is as sophisticated as the Leica 530 system. It is simply good practice to “tie” positional measurements into an established network.

The North-seeking Gyro

The north-seeking gyro is mounted on the theodolite and consists of a rotor suspended on a tape which, when not in use, is held in a clamp (Figure 2). When the rotor is spun up to about 22000 rpm and unclamped it is allowed to swing freely. Initially it tries to maintain its initial spinning plane but because it is earthbound it is influenced by the Earth's gravitational field and rotation. The spinning gyro rotor attempts to align itself with the Earth's axis of rotation. However due to its inertia it does not align itself perfectly but oscillates about it in regular periods. The position of the tape can be viewed on a graduated scale through an optical system. There are different methods of using the gyro to obtain a true azimuth. The method used by BGS is the clamped transit method (Kerridge 1984). The gyro is orientated approximately true north by tracking the tape to obtain the two turning points of the oscillation and calculating the centre point. The theodolite is locked in this position and the gyro is again released so that it is oscillating within the range of the graduated scale. The turning points are recorded as well as the timing of the tape through marks close to the centre of oscillation. The non-spin position of the tape is also recorded at the start and end of the observation and accounted for in the calculations. A true bearing azimuth with a specified accuracy of within 10 arc seconds is obtained by this method in about 45 minutes. BGS has developed software which can run on a portable PC to help operate the gyro and process the results (Carrigan 1996).

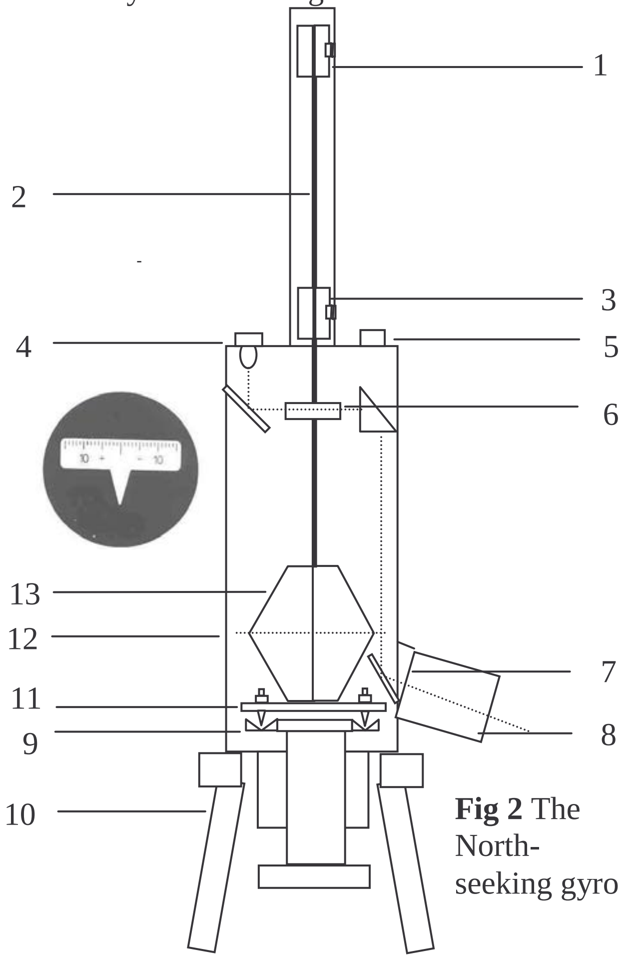

Fig 2 The North-seeking gyro

1. Upper Tape Clamp
2. Suspension Tape
3. Lower Tape Clamp
4. Lamp
5. Cable Connetion Socket
6. Optical Indicator
7. Reticle Plate with graduated scale
8. Observation Tube
9. Clamping Plate
10. Bridge
11. Damping Device
12. Gyro Spin Axis
13. Gyro Rotor

The BGS has been using this technique for several years for magnetic survey work and it has produced accurate and reliable results. Each gyro/theodolite system is checked regularly on calibration baselines at Eskdalemuir and Edinburgh. From these results the accuracy of the system is measured to be 15 arc seconds which is slightly worse than the quoted accuracy of 10 arc seconds.

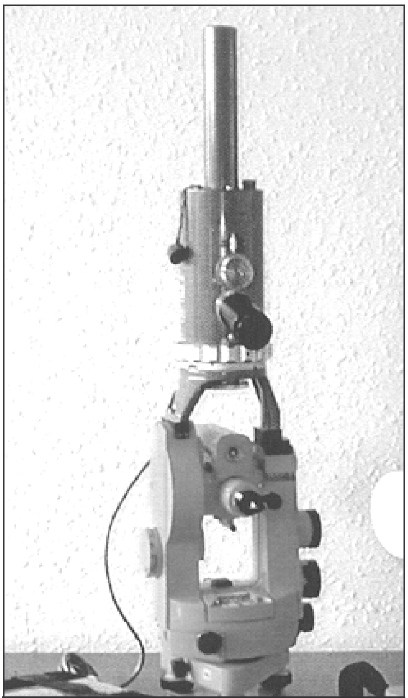

Fig 3 Wild GAK-1 North-Seeking Gyro

Fig 4 SOKKIA GP1-2A Gyro Station

The gyro attachment used by BGS is a Wild GAK-1 (Figure 3). Although no longer in production, it may be possible to obtain previously-used instruments at a much reduced price (approximately 5000 Euro(€)). They have been traditionally used in mining surveying and tunnel construction - one of the instruments belonging to BGS originally belonged to the national coal authority.

Another type of gyro/theodolite combination, the GP1–2A gyro station is produced by SOKKIA (Figure 4), and is available new. This gyro is operated using a similar technique to that of the Wild GAK-1. However the system has a built in computer to perform the calculations. Whereas the Wild GAK-1 can be mounted directly on the Carl Zeiss non-magnetic theodolite, the SOKKIA GP1-2A is supplied with the theodolite and gyro as a set. Therefore true north measurements must be carried out on a separate system to that of the magnetic observations. SOKKIA have indicated that they are willing to consider supplying the gyro attachment separately so that it can be mounted on the Carl Zeiss theodolite. This would result in a reduced cost than if the complete system was supplied. Calibration of the system would then be the responsibility of the user. The cost of the GP1-2A complete set including the theodolite and computer is €57000; the cost of supplying only the gyro attachment is €43000. SOKKIA say that it is currently not possible to supply the system on a rental basis as it is such a specialised and expensive instrument.

The disadvantages of using a north-seeking gyro are that it is expensive and requires some skill and care in transporting and handling. The advantages over other methods are that measurement can be made almost anywhere at any time. The exception to this is that the gyro will not work at the Earth's poles and there is no information available as to how the system will perform at very high latitudes (above 80º N/S).

The Gyromat 2000 instrument provides a very fast and accurate means of obtaining true north (3 arc seconds in only 10 minutes). However, this instrument is extremely expensive and difficult to obtain for testing and was therefore not considered in this study.

Sun Observations

Amongst the astronomical methods available for determining true north this paper will deal briefly with sun observations only, which is the technique most commonly used. There are two methods of obtaining a true azimuth from sun observations: the altitude method and the hour angle method. The main difference between the two methods is that the altitude method requires an accurate vertical angle to the sun whilst the hour angle method requires very accurate timing of solar transits. The altitude method is the traditional method because in the past sub-second time accuracy was difficult to obtain in the field. Nowadays with the widespread availability of accurate timepieces such as handheld GPS receivers, the hour angle method is favoured. Also parallax error and the refraction effects of the atmosphere can make the accurate measurement of a vertical angle to the sun difficult – although these errors can be modelled to a certain extent.

Any measurement involving astronomical bodies requires accurate and up-to-date ephemeris data which should be integrated into software used for the calculations. Information and ephemeris data required for processing of sun observations is available in a handbook which is published annually by SOKKIA (Elgin, Knowles and Senne). Software can also be purchased from Elgin, Knowles and Senne at cost of $150. The accuracy of the system is a function of user skill, latitude, time of day and accuracy of the timepiece. With care, accuracies of around 10 arc seconds should be achievable using the hour-glass method. It is good practice to make at least 2 separate sets of sun observations to confirm the accuracy of the resultant true bearings. This would give an observation time of approximately 20 – 30 minutes.

The advantage of using sun observations to obtain a true azimuth is that the system is light and portable and, apart from a few steep-sighting lenses and sun filters, does not require much in the way of additional expensive or bulky equipment. The system is accurate when appropriate conditions are fulfilled and care is taken. The disadvantages are that good weather conditions and a clear view of the sky are required and this is not guaranteed when planning survey work. Also, accuracy is dependent on the time of the day with accuracy reduced when the sun is too close to the horizon or too close to zenith. Mid-morning or mid-afternoon is the optimum time.

Using GPS to determine True North

The use of GPS to determine a true bearing for measurement of D is a relatively new technique. The use of two types of GPS equipment will be discussed which are representative of the broad spectrum in sophistication of receivers. The Leica 530 system consists of a pair of dual frequency, carrier phase GPS receivers. This represents the top of the range in survey grade GPS equipment and has a specified positional accuracy of 5 – 50 mm. The Garmin GPS II, on the other hand, is a relatively basic handheld receiver which is most often used for recreational purposes. In normal use this has a positional accuracy of only about 10 metres. However through the use of special data acquisition software it will be shown that the accuracy can be improved to 100 mm.

The Leica GPS 530 system was tested at the Braid Hills which is on the Edinburgh true bearing calibration baseline. The test site is an exposed area on top of a hill with a clear view of the sky and represented optimum conditions for the use of GPS.

One of the receivers is set up on the calibration baseline; the other receiver is set up about 25 metres away. The receivers are operated in differential mode with data being

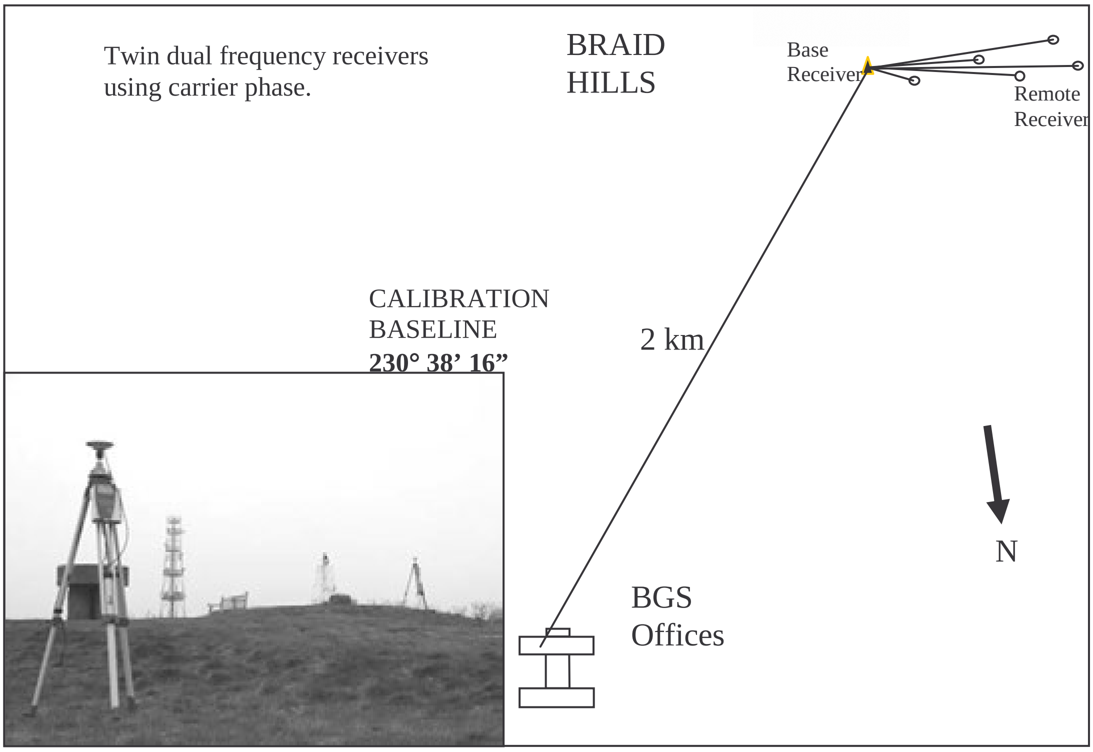

Fig 5 Leica GPS 530

logged simultaneously for ten minutes on each receiver. The lack of obstructions in the area ensures that each receiver can track at least the same four satellites. The data are then post-processed using Leica’s Ski-Pro software. Ten minutes of data seems to be sufficient for the software to resolve ambiguities in the number of carrier phase wavelengths from each satellite. Data processing results in high relative positional accuracy and a true azimuth from the base to the remote receiver is calculated. The base receiver is then removed and replaced with the Carl Zeiss theodolite. Great care was taken to ensure that the theodolite was placed in exactly the same position as the GPS receiver. The results from the GPS are then compared with the known baseline value. The test was repeated several times on a 25-metre baseline length. These tests were then duplicated but baseline lengths were increased to 50m, then 100m, 150m, and 200m. During the tests each receiver was monitored to check that the number of satellites and the satellite positional geometry was sufficient to give reliable results.

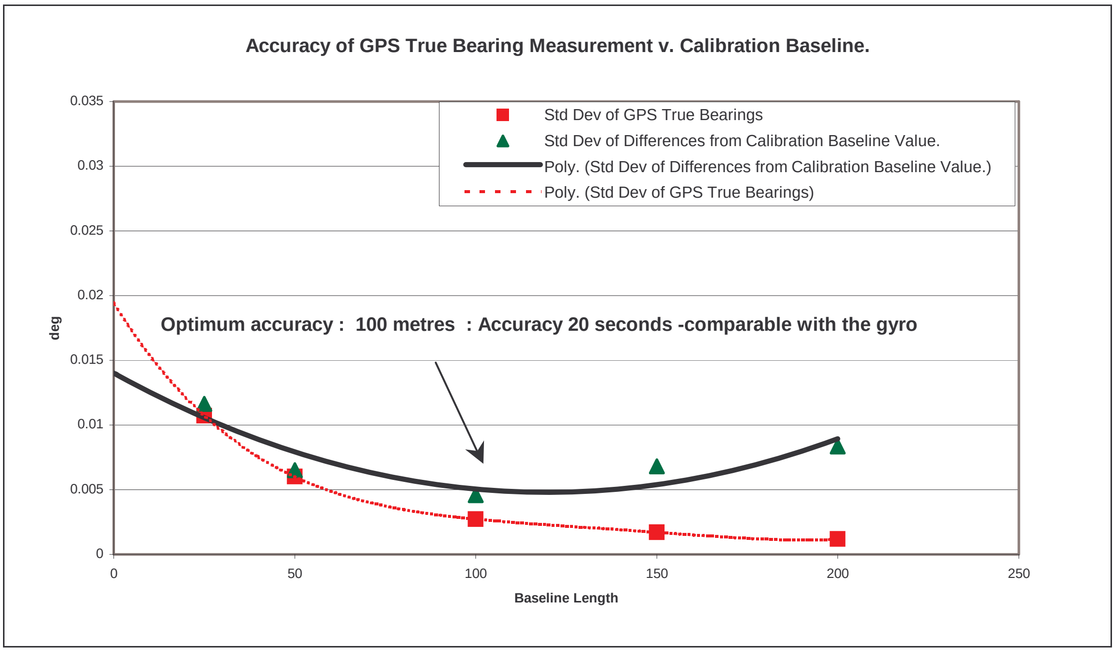

Fig 6 Leica GPS 530 Results

The results show that, as would be expected, as the distance between receivers increases, the standard deviation in values is reduced. The rate of improvement is small at separations greater than 50 metres. When the results are compared to the known calibration baseline value, the accuracy improves up to an optimum at just over 100 metres. Accuracy seems to degrade at lengths greater than this which may be due to difficulty sighting on the remote antenna over larger distances. During the tests, sightings were made on the neck of the receiver below the centre of the antenna which was not an ideal target. It is now possible to replace the antenna with a surveyor's target which makes sighting on the receiver much easier and much more accurate. From the results it can be seen that over a baseline of 100 metres a true bearing azimuth can be obtained to an accuracy of less than 20 arc seconds. This is close to the accuracy of the north seeking gyro method and sun observations. The cost of the Leica GPS 530 system in 2002 is €45000 for twin receivers. However dual frequency receivers are not essential for this application since the baseline lengths required are very short. It is sufficient to use single frequency receivers which are available at a reduced cost of less than €8000.

The GARMIN GPS II was tested on the Edinburgh calibration baseline with data logged to a laptop PC using special software developed by the University of Nottingham's Institute of Engineering Surveying and Space Geodesy (IESSG). This software is called the GPS RINEX generator (GRINGO) which stores data from the GARMIN GPS II in the standard RINEX format.

In normal operation the GARMIN GPS II receiver uses the code phase of satellite signals to establish the ranges to satellites which results in a positional accuracy of approximately ten metres. The IESSG have deciphered undocumented GARMIN protocols which consist of the raw code phase and carrier phase measurements. The raw carrier phase data is used to reduce the error in the code phase pseudoranges. When this data is post-processed differentially with RINEX data from the permanent GPS station, a positional accuracy of 0.1 m or better is obtained.

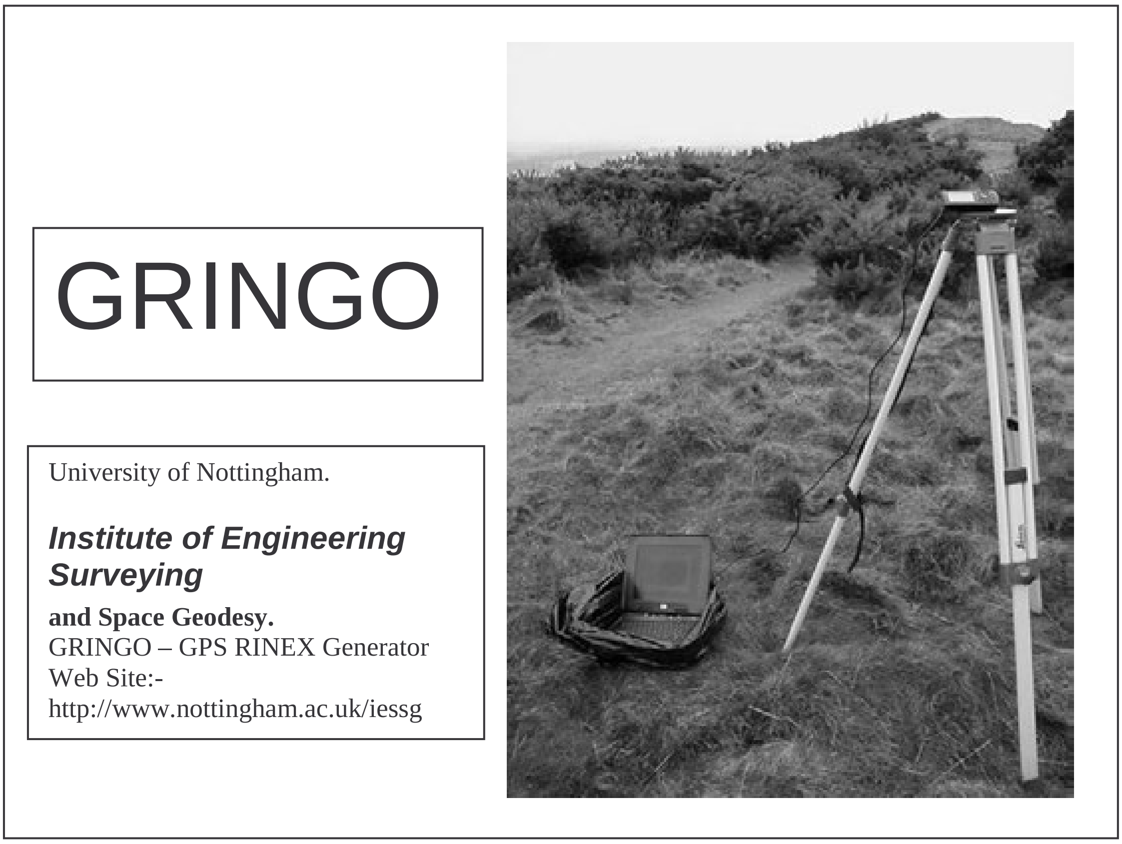

Fig 7 Use of the Garmin handheld GPS receiver

The accuracy of this system was checked by setting up the Garmin precisely over the positions on either end of the Edinburgh calibration baseline. Data were logged for one hour and then post-processed with the Edinburgh GPS station data using Leica's Ski-Pro software. The optimum statistical solution provided by this software is able to resolve carrier phase ambiguities if the data is of sufficient quality. If the ambiguities are unresolved the software resorts to other solutions so a position is always obtained.

Table 1 shows the results of these tests which confirm the accuracy of about 0.1m quoted by the IESSG.

Date	Difference from known position (m)	Location
18/02/2002	0.2779	roof
22/03/2002	0.2076	bh
03/04/2002	0.0616	roof
16/04/2002	0.0342	roof
17/04/2002	0.0229	roof
Average	0.12084	
Stand. Dev.	0.114894791	

Table 1 Comparison of Garmin/Gringo positions with known positions on the Edinburgh baseline

For the application of obtaining a true bearing for measurement of D to an accuracy of one arc minute, a positional accuracy of 0.1m at both the observing position mark and the remote location would require a baseline length of 486 metres. Note that the separation distances given on Page 41 of the IAGA Guide for Magnetic Repeat Station Measurements (1996) assume that the position of the observing mark is known precisely. In reality this is never the case. The baseline length of 486 metres is longer than the length required when using the Leica 530 system, but it is still possible if line of sight is available over this distance at the measurement site. The procedure would be to set up a tripod over the observing position mark using the optical plummet on the Carl Zeiss theodolite. Set up the Garmin GPS II on the tripod with the antenna in the centre over the mark. Measure the height of the centre of the antenna to the ground. The exact height is required for input in the post-processing software. Attach the GPS II serial cable to a portable PC, run the Gringo software and log data for at least one hour. Repeat this procedure at the remote location which should be greater than 486 metres away. Care should again be taken in siting the receiver accurately over a mark in the ground. When the data has been collected the GPS receiver should be replaced with a surveyors target which facilitates sighting on the remote position. Once the data has been collected at each position the Gringo RINEX data is post-processed with RINEX data from a reference station on a GPS network to obtain an accurate position.

Examples of networks of active GPS stations with World Wide Web links are shown in Figure 8. GPS networks are being implemented increasingly at a national level in many countries. It should be noted that when using GPS, as observation time and accuracy are mainly a function of baseline length, then baseline lengths and observation times should be maximised whenever possible.

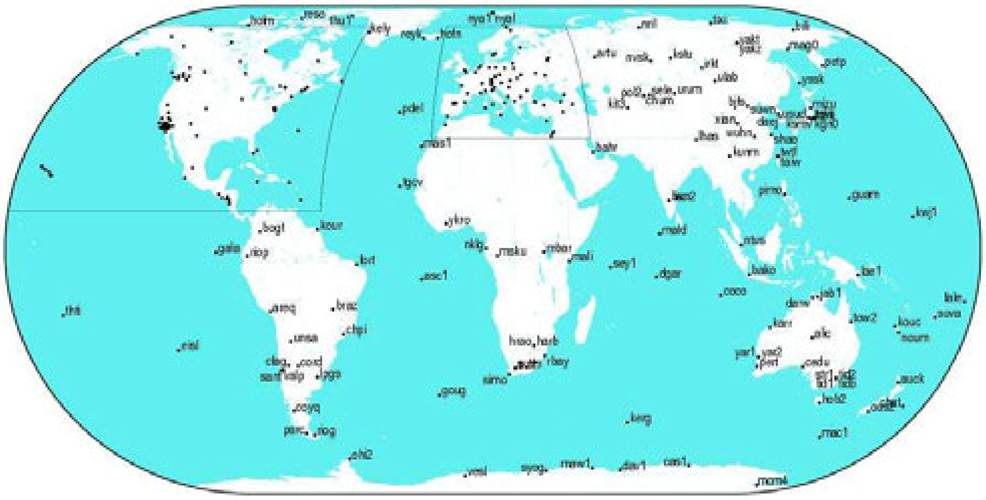

IGS (Global network): - http://igscb.jpl.nasa.gov/index.html
EUREF (European network):- http://epncb.oma.be/
CORS (US territories):- http://www.ngs.noaa.gov/CORS/

Fig 8 GPS networks. (Map reproduced courtesy of NASA)

With two GARMIN GPS II receivers and two copies of the GRINGO software it may be possible to obtain a true azimuth through processing of concurrent data that is as accurate as the Leica 530 tests. Further work is required to test the feasibility of this technique with this equipment. Very good relative positional accuracy between the two receivers may be obtained by this method without the need to use data from a GPS network.

The tests of the Garmin GPS II/GRINGO system to obtain true bearing, by establishing accurate absolute positions at either end of the baseline, show that this method is accurate over baseline lengths of greater than 486 metres. However care should be taken in ensuring collection of a sufficient length of time series data, positioning the receivers with a clear view of the sky, and ensuring that the GPS antenna is sited accurately over the mark. The cost of a Garmin GPS II receiver is around £450, and the cost of the GRINGO software is £160. When financial constraints are foremost in the purchase of instrumentation, this method is certainly worth considering.

In conclusion, the use of GPS provides accurate and practical methods for obtaining a true bearing to the required accuracies. The disadvantage over other methods is that a good clear view of the sky in all directions is required. Out of eleven repeat station visits made by the Geomagnetism section of BGS in 2001, it was not possible to use GPS for this purpose at four of these sites due to adjacent trees. GPS is a continually developing technology which has great potential for the future. Ever improving accuracy of receivers, falling costs, and further GPS constellations make consideration of this technology for geomagnetic surveying applications essential.

Conclusion

Table 2 summarises the advantages and disadvantages of each method of obtaining a true bearing. The gyro is the best all round technique with the only disadvantage being the cost of the equipment. The disadvantage of sun observations is that observation times are restricted by weather conditions. However, it is an accurate technique not requiring much in the way of additional equipment. The use of the GPS is restricted to outdoor areas with a clear view of the sky. It is not generally constrained by weather conditions, apart from poor visibility, and the use of lower specification receivers can alleviate the expense. Appendix A lists contact details for suppliers of equipment.

	Gyro	**Sun Obs.**	**GPS Survey Grade**	**GPS Garmin Handheld**
Cost	Expensive	Inexpensive	Expensive	Inexpensive
Clear Sky	Not Required	Required	Not Required	Not Required
Clear View of	Not Required	Required	Required	Required
Good Visibility	Not Required	Required	Required	Required
Ease of	Moderate	Good	Moderate	Good
Speed	Slow	Fast	Fast	Slow
Location	Anywhere	Restricted	Restricted	Restricted
Time of Day	Anytime	Restricted	Restricted	Restricted

Table 2 Summary of advantages/disadvantages of different methods of obtaining a true bearing

References

Carrigan J.G., 1996. Software for Geomagnetic Absolute Observations Using a Fluxgate Theodolite and Gyro Theodolite, *Brit. Geol. Surv. Tech. Rep.*, WM/96/22.

Elgin R.L., Knowles D.R., Senne J.H., 2001 Celestial Observations Handbook and Ephemeris, *Published by SOKKIA.*

Hill, C J; Moore, T; Dumville, M; Gringo, 2000. Recording RINEX Data from Handheld GPS Receivers, *Proc GNSS 2000, 4th European Conference on Global Navigation Satellite Systems*, pp 12, Edinburgh, May 2000.

Hill, C J; Moore, T; Dumville, M; Carrier Phase Surveying with Garmin Handheld GPS Receivers, 2000. *Proc ION GPS 2000, 13th International Technical Meeting of the Satellite Division of the Institute of Navigation*, 8 pages, Salt Lake City, USA, 2000.

Hofmann-Wellenhof B., Lichtennegger H, and Collins, J., GPS Theory and Practice. ISBN 3-211-82839-7 Springer Verlag.

Kerridge D.J., 1984b. Determination of true north using a Wild GAK-1 gyro-attachment, *Brit. Geol. Surv. Tech. Rep.*, WM/84/16.

Newitt L.R., Barton C.E., Bitterly, J 1996. Guide for Magnetic Repeat Station Surveys. *International Association of Geomagnetism and Aeronomy (IAGA).*

Appendix A: Equipment/Software Suppliers

GYRO

Wild GAK-1
Only previously used instruments available – from survey equipment suppliers.

Garner Survey Equipment Ltd.,
Unit 10, Bartlett Park,
Gazelle Road, Lynx Trading Estate,
Yeovil, Somerset, BA20 2PJ.
UK.

Tel: (44) 1935 431069

Leica UK Ltd.,
Davy Avenue,
Knowlhill,
Milton Keynes MK5 8LB.
UK.

Tel: (44) 1908 609992

SOKKIA GP1 – 2A Gyro Station

SOKKIA CO., LTD.,
1-1, Tomigaya 1-Chome,
Shibuya-Ku,
Tokyo, 151-8511,
Japan

Tel: +81-3-3465-5201
http://www.sokkia.co.jp

Gyromat 2000

Deutsche Montan Technologie GmbH,
Am Technologiepark 1,
45307 Essen, Germany.
Tel: +49 (201) 1 72-01
www.dmt.de

Fax: +49 (201) 1 72-14 62

Sun Observations

Software available from:

Elgin, Knowles and Senne Inc.,
310 East 6th Street,
Rolla, Missouri,
65401-3343
USA.

Tel: (573) 364-4785
http://www.rollanet.org/~eksi

GPS

Leica Geosystems AG,

Heinrich-Wild-Strasse,
CH-9435 Heerbrugg,
Switzerland,
Tel: (41) 71 727 31 31
Fax: (41) 71 727 47 02
www.leica-geosystems.com

SOKKIA CO., LTD.,
1-1, Tomigaya 1-Chome,
Shibuya-Ku,
Tokyo, 151-8511,
Japan

Tel: +81-3-3465-5201
http://www.sokkia.co.jp

Institute of Engineering Surveying and Space Geodesy, The University of Nottingham, University Park, Nottingham, NG7 2RD
Tel +44 (0) 115 9 513 880,
Fax +44 (0) 115 9 513 881,
Email iessg@nottingham.ac.uk
http://www.nottingham.ac.uk/iessg/

Collaborative Effort to Record Cleaner Geomagnetic Pulsation Data in South Africa

P R Sutcliffe, P J duToit, E J J Julies, B J Pretorius, H Theron, D R Wright
Hermanus Magnetic Observatory (HMO), Hermanus, South Africa

R Holme
GeoForschungsZentrum (GFZ), Potsdam, Germany

P Fourie
South African Astronomical Observatory (SAAO), Sutherland, South Africa

Introduction

During 2001 it was decided that the GeoForschungsZentrum (GFZ) and the Hermanus Magnetic Observatory (HMO) should commence a collaborative research project in geomagnetism. The initial phase of this project is to commence the recording of ULF geomagnetic pulsations on a continuous basis at the GFZ's geodynamic facility on the South African Astronomical Observatory's (SAAO) site at Sutherland.

The geomagnetic pulsations most commonly observed during local daytime at low to middle latitude stations, such as Hermanus, Niemegk, and Sutherland, are Pc3 pulsations. The frequency of oscillation is generally in the range 25-100 mHz and amplitudes typically range from 0.1-1.0 nT. The pulsations most commonly observed during local nighttime are Pi2 pulsations, which are impulsive, damped oscillations of the geomagnetic field in the frequency range 5-30 mHz and with amplitudes in the range 0.25-2.5 nT. The 24-hour pulsation plot in Figure 1 shows examples of Pc3 pulsations between 14 and 18 UT and Pi2 pulsations between 22 and 23 UT.

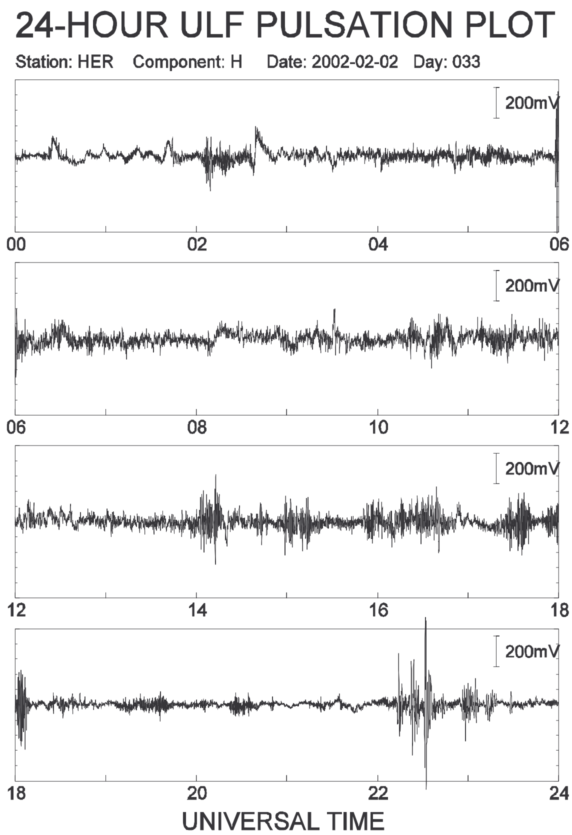

Fig 1. Plot of geomagnetic pulsation data recorded by the induction magnetometer at Hermanus.

The HMO has recorded geomagnetic pulsations at Hermanus for many years; however, in recent years the data have been adversely affected by anthropogenic noise, probably due to the Cape Peninsula electric railway system. Although the data are still useable, cleaner data are extremely desirable, particularly for distribution to the international research community. It was therefore decided that the HMO should set up a duplicate geomagnetic pulsation recording system at Sutherland with financial and infrastructure support from the GFZ and SAAO respectively.

Installation and Equipment

Drs Richard Holme (GFZ) and Peter Sutcliffe (HMO) carried out an initial inspection visit to the SAAO's Sutherland site on 19 to 20 April 2001; Figure 2 shows an aerial view of the Sutherland site. A follow-up feasibility study to determine the suitability of Sutherland as a site for geomagnetic pulsation observations was carried out by two HMO technicians from 7 to 9 August 2001. These investigations determined that the site was suitable for the recording of geomagnetic pulsations on a continuous basis.

Fige 2. Aerial view of Sutherland site. The yellow dot indicates the location of the pulsation equipment.

Construction of the facility and installation of the geomagnetic pulsation equipment took place from November 2001 to January 2002. A schematic diagram of the pulsation equipment, which is similar to that operated in Hermanus, is shown in Figure 3.

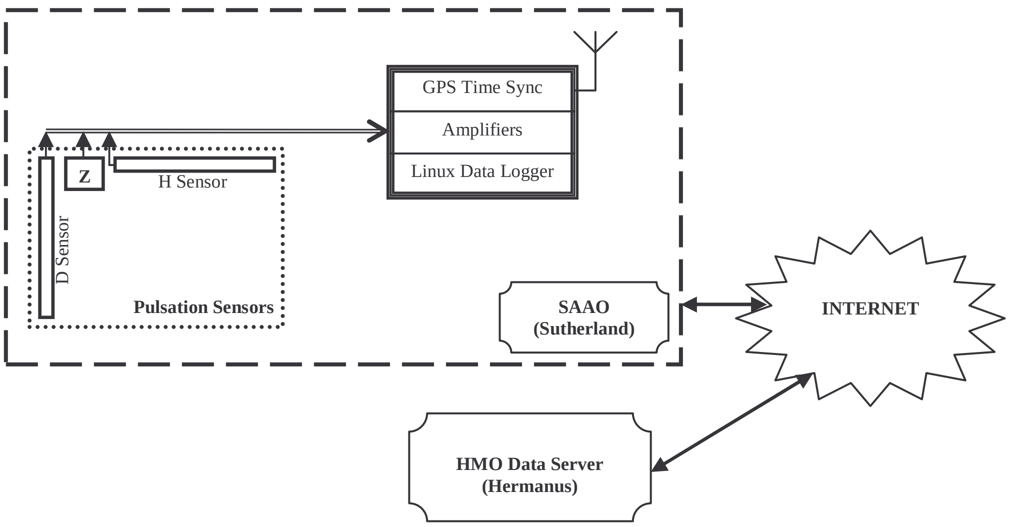

Fig 3. Schematic diagram of the geomagnetic pulsation equipment

The geomagnetic pulsation equipment consists of the following:

- Three induction sensors (2m long mu-metal rods wound with 100000 turns of copper wire) oriented magnetically N-S, E-W, and vertically. The sensors are located about 100m from the GFZ geodynamics facility building and mounted in concrete plinths with weather-proof covers, as shown in Figure 4.
- The associated electronics comprises amplifier/filter modules, a GPS module (for time signal), interface module with 16-bit analog to digital signal conversion, and PC for logging the data, as shown in Figure 5. The electronics are housed in the GFZ geodynamics facility building. The digital H, D, and Z component data are logged at 1 Hz and transferred to Hermanus via Internet connection. The system operates from mains power but contains battery backup to enable continued operation during short breaks in mains power supply.

The continuous recording of data was commenced on 1 February 2002.

Fig 4. Plinths for pulsation induction sensors during construction (left) and final pulsation induction sensor installation (right) at Sutherland site.

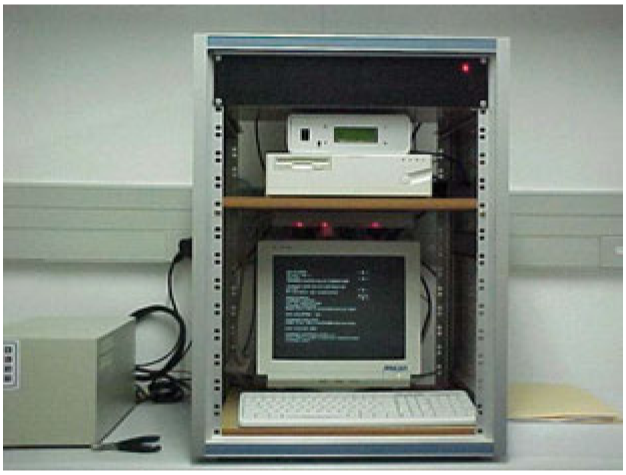

Fig 5. Pulsation magnetometer electronics and recording equipment.

Comparison of Hermanus and Sutherland Data

An interval during which there was relatively little geomagnetic pulsation activity but when there was significant anthropogenic activity was selected to compare the Hermanus and Sutherland data. Data for the interval 2200-2230 UT on 23 February 2002 as recorded at Hermanus and Sutherland are plotted in Figure 6. The disturbing spike-like activity at Hermanus is clearly visible; however, these disturbances are completely absent at Sutherland.

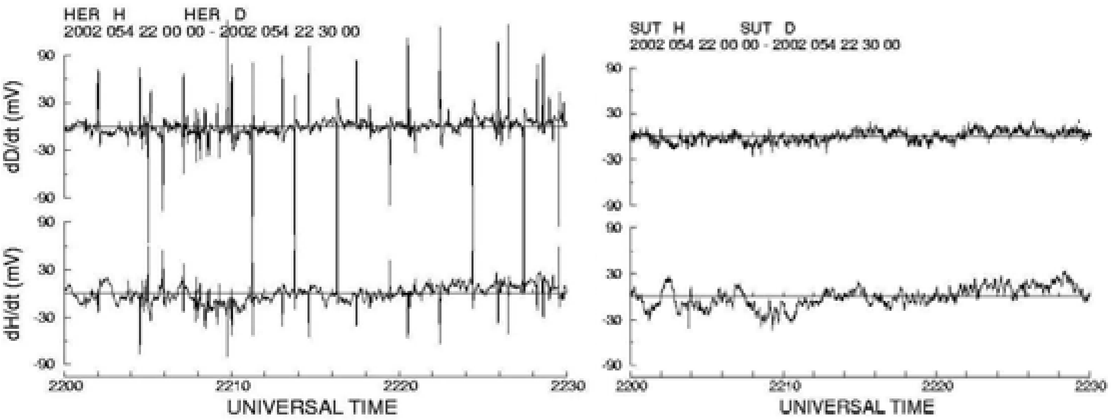

Fig 6. Induction magnetometer data recorded at Hermanus (left) and Sutherland (right) on 23 February 2002. Man-made, spike-like disturbances are clearly visible at Hermanus but absent at Sutherland.

A shorter interval of the Hermanus data is plotted in Figure 7. It should be noted that since the data are recorded using an induction sensor, the output is proportional to the time rate of change of the magnetic field variations, i.e. dB/dt as plotted in Figure 7(a). The data can be compensated for the frequency dependent amplitude and phase of the induction sensors and electronic filters, thus effectively integrating the data, i.e. B as plotted in Figure 7(b). It is seen that the alternate spike-like disturbances in dB/dt appear to be caused by the switching on and off of a disturbing magnetic field B. The origin of this disturbing field is unknown; however we surmise that it may be due to the Cape Peninsula electric railway system, which lies about 100 km from Hermanus.

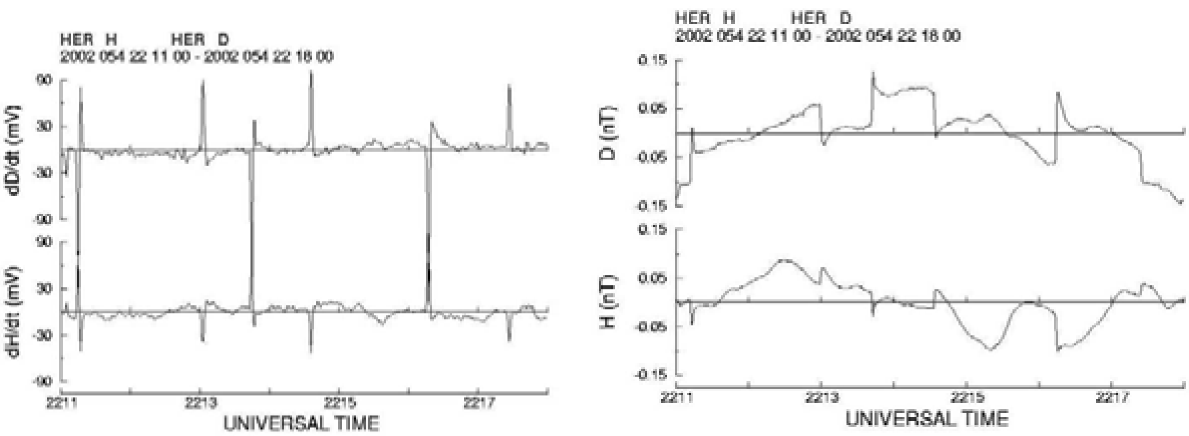

Fig 7. The diagram on the left shows the typical induction sensor output that is proportional to the time rate of change of the magnetic field variations, i.e. dB/dt. The diagram on the right shows the data after compensation for the frequency dependent amplitude and phase of the induction sensors and electronic filters, thus effectively integrating the data, i.e. B.

Two intervals during which both geomagnetic pulsation activity and anthropogenic noise were present are used to further compare the Hermanus and Sutherland data. Data for the interval 1100-1110 UT on 19 February 2002, showing a Pc3 pulsation, as recorded at Hermanus (lower curve) and Sutherland (upper curve) are plotted in Figure 8. Data for the interval 0120-0130 UT on 16 February 2002, showing three cycles of a Pi2 pulsation, as recorded at Hermanus (lower curve) and Sutherland (upper curve) are plotted in Figure 9. The man-made, spike-like disturbances in the Hermanus data are again clearly visible while the disturbances are completely absent from the Sutherland data.

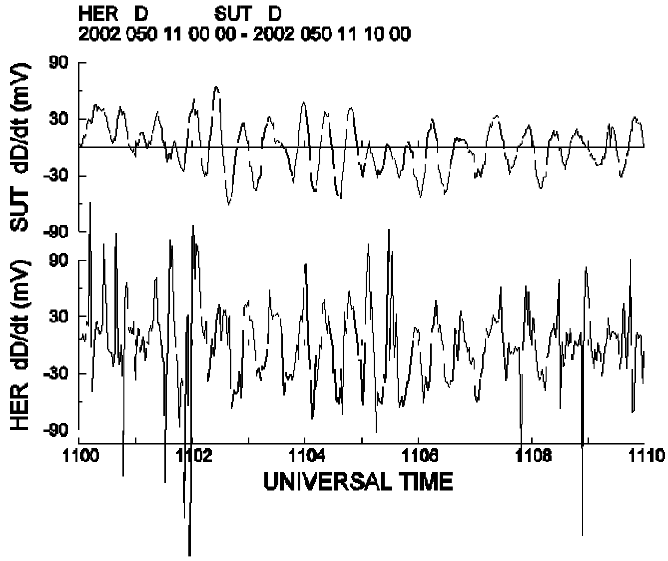

Fig 8. Pc3 pulsation recorded at Hermanus (lower curve) and Sutherland (upper curve).

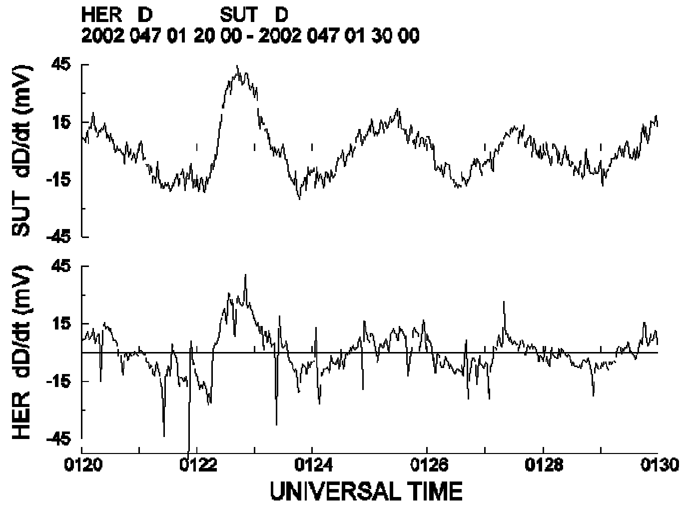

Fig 9. Pi2 pulsation recorded at Hermanus (lower curve) and Sutherland (upper curve).

Conclusion

The HMO has recorded geomagnetic pulsations at Hermanus for many years; however, in recent years the data have been contaminated with man-made noise. The decision to set up a duplicate geomagnetic pulsation recording system at Sutherland has resulted in noise free data. Although the Hermanus data are still useable, the cleaner Sutherland data are extremely desirable for the local and international research communities. At present the source of the noise in the Hermanus pulsation data is unknown, although thought to be due to the Cape Peninsula electric railway system. An investigation to determine the source of the noise in the Hermanus pulsation data is planned for the near future.

Acknowledgements

Financial and infrastructure support provided by the GFZ and SAAO respectively are acknowledged.

Applied Services of the Hermanus Magnetic Observatory

DJ Gouws, Hermanus Magnetic Observatory, Hermanus, South Africa (dgouws@hmo.ac.za)

Since its forerunner was first established in Cape Town in 1932, one of the main functions of the Hermanus Magnetic Observatory (HMO) has been to generate mathematical models of the Earth's magnetic field for the southern African region. These models, based on regional magnetic surveys executed at regular intervals, in due course found their way onto magnetic navigation maps. As a result navigators in southern Africa probably started relying on the work of the HMO many decades ago - most likely without even being aware of the existence of a facility like the HMO in South Africa.

In time, however, the support rendered by the HMO to the defence and aerospace industry and to other users became more direct. This started in 1964 when the SA Air Force (SAAF) began submitting their Watts Datum landing compass, used in the swinging of Shackleton maritime reconnaissance aircraft, to the HMO for calibration. Since then the support services to the local aerospace community, and specifically to the magnetic navigation sector, have expanded dramatically and currently include the following:

- **Magnetic Navigation Ground Support.** The main activities are the calibration and maintenance of landing compasses used during aircraft compass swings, as well as the magnetic survey of compass swing bases where the actual aircraft compass swings are executed.

- **Magnetometer Systems Support.** This involves the evaluation and calibration of magnetometers, the integration of magnetometers in systems and the use of the regional geomagnetic field in practical applications.

- **The application of Signal Processing techniques** in the development of navigation and orientation algorithms and systems, as well as the development of specialized algorithms that add value to magnetic field measurements.

- **Low-cost Sensor Integration.** Inertial and other sensors are integrated with systems using optimization algorithms.

The supply of regional geomagnetic data and mathematical magnetic field models to clients, which is a very important aspect of the services, will not be discussed in this publication.

Compared to many other magnetic observatories, these external services provided by the HMO are quite unique. The main reasons for the HMO performing these services are the following:

- For several client-specific requirements the HMO is the only facility in southern Africa capable of performing these services;

- As a National Facility the HMO needs to guarantee the availability of certain expertise, services and information on a continuous basis to industry;

- It creates valuable additional external funding for the HMO (clients are invoiced at commercial rates);

- It expands the general scientific, engineering and management capabilities of HMO staff;
- The interaction with clients requires quality standards that are very important in terms of long-term quality management of the information and services provided by the HMO.

Magnetic Navigation Ground Support

Currently the following services are provided:

- **Calibration and maintenance of several types of landing compasses.** This includes the Watts Datum Compass, the Wild TO Compass Theodolite, the Wild B3 Compass, SIRS, SESTREL and various other hand-held landing compasses. According to the current arrangement, landing compasses from SAAF squadrons are calibrated at six-monthly intervals, while compasses from civilian users are calibrated annually. The calibration interval is not based on the rate of wear-out of landing compasses, but is designed to prevent compasses, damaged as a result of misuse, from becoming a flight safety risk at centers of operation.
- **The survey of compass swing areas.** The magnetic characteristics of compass swing bases may change over time for a variety of reasons. For example, lightning strikes at or near the compass base may change the magnetization of sub-surface ferro-magnetic material (e.g. dolerite dikes), or civil engineering works may introduce ferro-magnetic material (e.g. storm water pipes with reinforced steel) after the initial survey. The HMO therefore executes a re-survey program at five-year intervals. Furthermore, if any compass swing base becomes suspect (i.e. if swing results suddenly become questionable), a special interim magnetic survey of such a base is usually arranged. This re-survey policy is broadly in agreement with Royal Air Force (RAF) policy, where some compass bases are re-surveyed at 6-yearly, and some at 4-yearly intervals.

  During a compass base survey the variation of magnetic declination over the compass swing area (generally between 60 and 100 meters diameter) is measured with D-I declinometers mounted on accurate non-magnetic theodolite circles. A reciprocal bearing method is used, with measurement point intervals not more than 6 m apart, to eliminate the effect of temporal variations of the natural magnetic field. The compass swing bases are surveyed from the center position to 6 meters outside the outer perimeter of the base.
- **The presentation of training courses** on the execution of aircraft compass swing procedures. These courses deal with the basic physics of geomagnetism and aircraft magnetism, the actual execution of aircraft compass swings (including the practical use of landing compasses), the calculation of the swing data and the interpretation of the swing results in terms of problematic conditions on the aircraft. The courses are normally presented to avionics technicians and navigators.
- **Consultation on magnetic navigation technology.** Through the years the HMO has been approached on many occasions to investigate and advise on problems experienced with magnetic navigation procedures and aids at SAAF Bases and civilian operational centers. These problems usually manifest themselves as problematic aircraft compass swings. Typical problems dealt with have been:
  - The landing compass operator not being fully demagnetized (i.e. not all Ferro-magnetic material removed from his person);

- Ferro-magnetic material being used in or near the aircraft compass mountings;
- Unserviceable landing compasses or aircraft compasses;
- Questionable procedures and calculation errors.

Some examples of particular support services are the following:

- Development of a tripod with slider for the SIRS hand-held landing compass to facilitate its use to a higher accuracy;
- Change of the magnetic inclination adjustment on mechanical compasses to be used at geographic locations where the magnetic inclination is considerably different from that in South Africa. For example, the preparation of landing compass used by helicopter support personnel at the Sanae Base in Antarctica.

The quality of the HMO's services is verified at regular bi-monthly intervals by QA staff members from the Armaments Corporation of South Africa (Armscor). The HMO has also recently obtained approval from the SA Civil Aviation Authority (SACAA) to function as a certified aviation processing, testing and training facility. This implies yet another level of independent quality assurance audits.

It is clear from the above that many of the HMO's services are directed towards ensuring the maintenance of an infrastructure conducive for accurate aircraft compass swings. These swings are executed to calibrate the electronic and mechanical compasses installed in the aircraft against an external reference. Such swings are generally done every six months, depending on the aircraft compass system and other factors (e.g. whether maintenance was done on the aircraft that could have changed the magnetic properties of the aircraft at the compass position). A serviceable and calibrated landing compass provides the reference for accurate aircraft compass swings – thus the need for regular landing compass calibrations.

Fig 1:

SIRS landing compass mounted on a tripod and slider developed by the HMO.

Magnetometer Systems Support

The HMO's magnetometer evaluation and testing services are available to organizations and individuals using magnetometers for navigation, orientation, remote sensing and similar applications. The following facilities are available:

- Dedicated non-magnetic outbuildings with precision surveyed observation pillars and beacons to provide an accurate evaluation and calibration environment;

- Large 3-axis Helmholtz coil system (2.5 m side length) in which any magnetic field vector on Earth or in space may be generated;

- Non-magnetic climatic chamber in which small magnetometers can be evaluated over a temperature range of -20ºC to +50ºC;

- Specialized automated systems for the calibration of magnetometers;

- Continuous and absolute magnetic field measurements acquired on a regular basis.

Related services and development provided are:

- **Tests on avionics/marine equipment**. The following tests can be executed:

    - Magnetic effect tests on avionics equipment according to the RTCA/DO-160C (Section 15) test specification;

    - Magnetic effect tests on avionics equipment according to the 3G.100: Section 2, test specification;

    - Magnetic effect tests for marine craft according to the International Standard IEC 945/1966-11 test specification.

- **Magnetic evaluation of munitions systems.** It is often required that the permanent and induced magnetism of munitions, which contains a magnetometer subsystem, be determined. This information is used to optimize the use of the magnetic sensor in such a magnetically unfriendly environment.

Fig 2:

Magnetic evaluation of munition systems.

- **Development of systems around magnetometer subsystems.** Recent projects include the mini degaussing range developed for the SA Navy (SAN) and compass test bench developed for the SAAF. The degaussing range is used for the measurement of the magnetic signature of diving equipment during the degaussing process of the equipment. The compass test bench is used for the functional verification of aircraft compasses and magnetic sensing units before installation in aircraft. Both can be supplied as commercial products.

Fig 3:

Magnetic test bench developed for the evaluation of standby and electronic compasses before installation on aircraft systems.

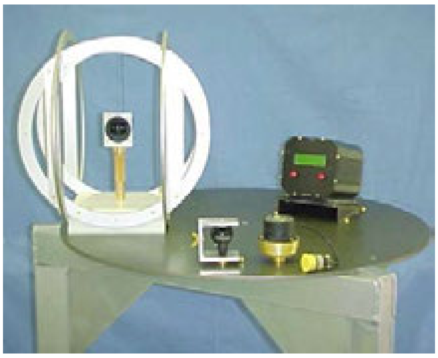

- **Development of specialized coil systems.** A coil system was recently developed to compensate the standby compass of a specific aircraft type for disturbance effects caused by nearby DC current looms. During several upgrades of the aircraft over the last two decades, a number of looms carrying DC currents were mounted in close proximity to the standby compass. The magnetic fields of these DC currents severely affected the readings on the compass. In certain instances deviations of up to 65° were recorded! The HMO developed a system where the magnetic fields caused by these DC currents were detected. Compensation currents were then generated and applied to specially designed coils around the standby compass. Compensation of the disturbing magnetic fields was achieved to within ±1º under laboratory conditions. During operational conditions on the aircraft the deviations were compensated to within ±5º, which is within the reading accuracy of the particular standby compass.

Fig 4:

Specialized compensation coil system developed for the standby compass of an aircraft system.

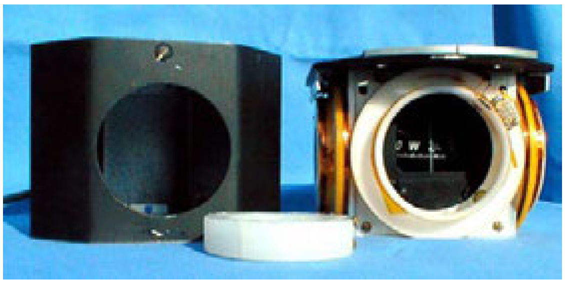

- **Development of mathematical models** of the magnetic field of a marine vessel. These models are used successfully to calculate the observable magnetic signature of particular marine vessels in their vicinity, and thus give an indication of their magnetic detection risk.

- **Electronic compass auto-calibration routines** which compensate for the magnetic properties of the host platform. The technology can be used in automobiles, marine- and unmanned aircraft.

- **Development of magnetic fuses for weapon systems.** It is sometimes required that a weapon system should be able to identify a potential target as a valid target. In the HMO's application this is realized by identifying the magnetic properties of the target (e.g. tank or armored car) in the presence of a background geomagnetic field and magnetic variations caused by platform motion.

- **Construction of fluxgate magnetometers for satellite orientation control**. The HMO developed both a scientific and an orientation control magnetometer for the South African SUNSAT I satellite. The orientation control magnetometer was critical for the flight control of the satellite during the initial de-spinning phase and functioned flawlessly for the lifetime of the satellite. The HMO also supplied orientation control magnetometers that were used successfully on board two of the German *Safir* satellites. An orientation control magnetometer was recently supplied for integration in a satellite developed by the SUNSAT team for a foreign client.

Application of Signal Processing Techniques

Signal processing (DSP) techniques have for many years been a mathematical tool used in fundamental research and for the processing of geomagnetic data at the HMO. During recent years the HMO has become a leader in southern Africa regarding the application of certain DSP techniques and a large amount of current high technology contracted development work is based on the HMO's DSP experience. These include:

- **Kalman filtering**, used in the development of navigation systems for ground vehicles and unmanned aircraft. Recently a navigation sub-system was developed for the SKUA high speed target drone of Kentron, a division of Denel. This was accomplished using the Kalman filter integration of low-cost onboard inertial and other flight control sensors. Furthermore, a Kalman filter, used for altitude estimation, was developed that permitted very low flight above the sea surface;

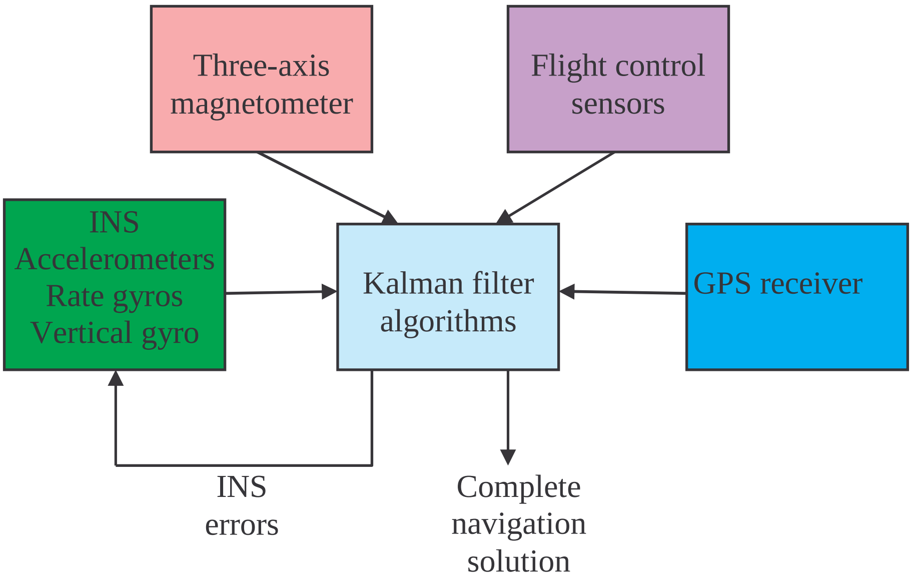

Fig 5: *Kalman filter integration of GPS and flight control sensors used in the development of a navigation subsystem for an unmanned aircraft.*

Fig 6:

The HMO developed a navigation Subsystem for the SKUA unmanned aircraft of Kentron, (Division of Denel)

- **Data Adaptive filtering** is used for the extraction of small magnetic signals, hidden in large amplitude geomagnetic noise. This technique is used for the determination of K-indices and for analysis of aeromagnetic survey data.

- **Artificial neural networks and wavelet analysis** are used for identification of magnetic ULF pulsations and for development of a pattern recognition system for an electronic chemical nose.

Low Cost Sensor Integration

Worldwide trends indicate that declining defence budgets require lower cost sensors to be used in defence systems. Unfortunately these low cost sensors are prone to large drift rates and inaccuracies. Therefore, in order to use these sensors successfully, several complementary sensors have to be integrated to calibrate (remove drift) in real time.

The following projects were executed in recent years:

- **Real-time calibration algorithms for an electronic compass**. These algorithms eliminate the need for compass swings on an electronic compass. The software automatically adapts to any changes in the magnetic effects of the host platform, therefore calibrating itself should magnetic changes in the load or host platform occur. A typical example is the use of an electronic compass on a military arms delivery vehicle. As weapons and ammunition are added or removed from the vehicle, the magnetic properties or signature will change dramatically. By integrating a magnetometer with a GPS, the magnetometer could be calibrated "on the fly" when a GPS signal is available.

- **Development of a software vertical gyro**. The attitude determination (pitch, roll and yaw angles) of a platform is a complicated and expensive task. It is usually obtained using an expensive inertial measurement unit (IMU), or a mechanical vertical gyro. In the first instance the solution is obtained by integrating high quality (and highly priced!) rate gyros exhibiting little drift. The mechanical vertical gyro used in the second option also has it own set of complications. It is expensive, easily damaged through improper handling, and is still classified as sensitive hardware with regards to importation from overseas. The most important drawback of a mechanical vertical gyro is the limitation that causes them to "lock-up" during highly dynamic manoeuvres. This has catastrophic implications for unmanned aircraft. However, the HMO developed algorithms which integrate rate gyros and accelerometers to replace the mechanical vertical gyro with a software version based on inexpensive sensors.

- **Attitude determination using a magnetometer and accelerometer**. By using a three-axis magnetometer to resolve the Earth's magnetic field into body coordinates, as well as a three-axis accelerometer to resolve the Earth's gravitational field into body coordinates, the attitude of a space vehicle is determined very accurately. This technology provides a low cost attitude determination solution and adds significant value to magnetometer measurements that are normally only used for heading calculation.

Future Activities

The following capability-development activities are envisaged for the near future:

- **Signature management** using advanced digital signal processing techniques. A typical example to be investigated is the monitoring of no-go zones for military activity. These zones or areas are established after peace treaties have been signed and no military activity is allowed in a specific area. Digital signal processing techniques may be used to discriminate between military and civilian vehicles and other activities.

  Another example is the development of an “electronic back-pack” for the future infantry soldier. It is anticipated that the soldier will carry a large array of sensors (magnetic, acoustic, infra-red etc), which detect signatures in his/her environment. DSP algorithms may allow automated friend-or-foe identification in the presence of surrounding noise.

- The **determination of the total electron content (TEC) in the ionosphere** from differential global positioning System (DGPS) data. The HMO will attempt to use Kalman filtering and other DSP techniques to calculate this information. If it proves feasible, one may be able to derive HF frequency prediction for communications, as well as HF direction finding support, from the information.

Conclusion

The HMO has found its long association with the local defense and aerospace industry to be stimulating, challenging and enjoyable. It is hoped that it may continue into the future to the benefit of all parties. The author can be contacted if any information regarding the above services is required.

The Current Status of Misallat Observatory (MLT) and the Necessity of an Additional Magnetic Station On the Egyptian Borders

Tarek Arafa-Hamed

National Research Institute of Geophysics and Astronomy, Helwan, Egypt
misallat@netscape.net

Abstract:

The Misallat Magnetic Observatory is the only one in the north-eastern corner of Africa. During the last three years, the observatory has been well developed by up-to-date digital instruments that give high resolution and accurate records of the geomagnetic field. The new status of geomagnetic measurement at MLT and its importance to the global network of observatories is reported.

It is known, that there is a large gab in the north-eastern part of Africa as a result of the absence of geomagnetic observatories in Sudan, Libya, and all of the Arabian Peninsula. A proposed network of unmanned magnetic stations at the Egyptian borders to cover the existing gab in Africa will be discussed. An observatory in southern Egypt about 1000 km south of MLT would cover the gab in Sudan. Another one at the western border would cover the gab in Libya. An Observatory in the southern Sinai Peninsula would somehow compensate for the gab in the Arabian Peninsula.

Introduction

Misallat magnetic observatory belongs to the Egyptian “National Research Institute of Geophysics and Astronomy (**NRIAG**)” which has its central location in Helwan city near Cairo. NRIAG has been grounded in 1903 to conduct geomagnetic, seismological, as well as solar research. Subsequently NRIAG became the largest research Institute of Geophysics and Astronomy in the Middle East with its nine laboratories listed in Figure 1. Geomagnetic observations in a specially prepared building at Helwan are one of the main responsibilities of the laboratory of Geomagnetism since the termination of the research institute in 1903 (Picture 1).

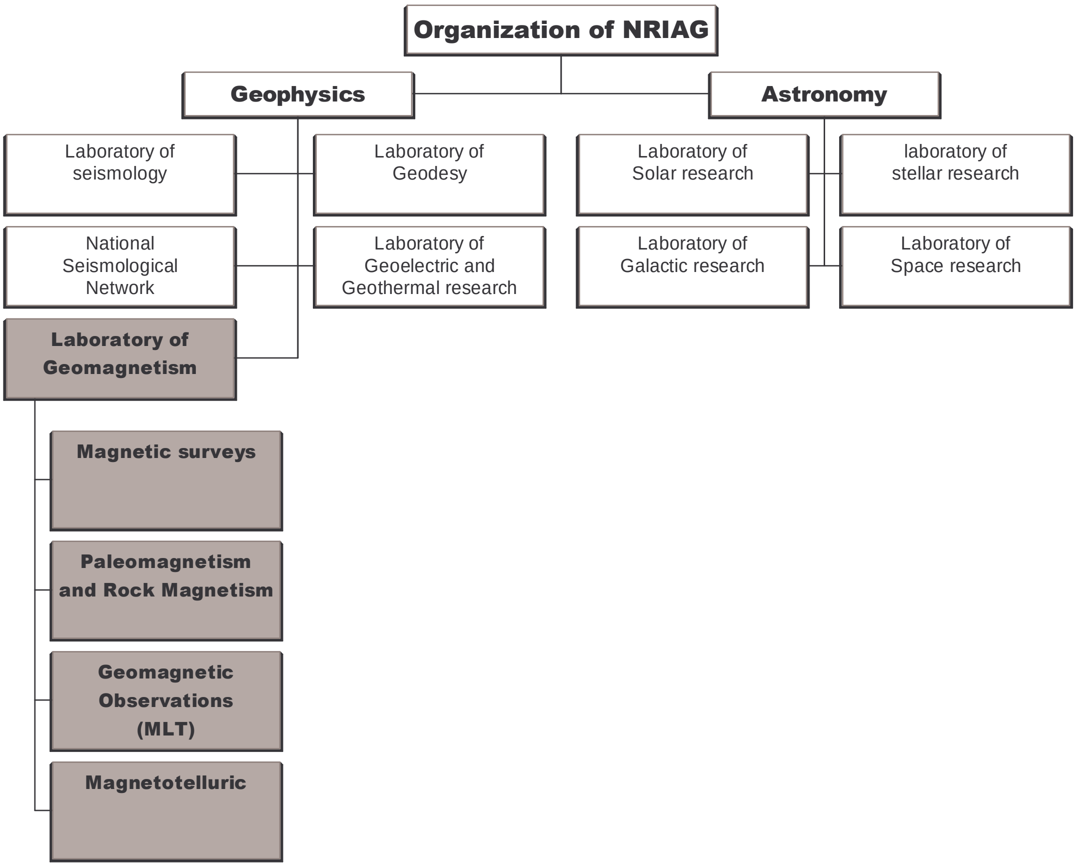

Figure 1: Chart showing the present organization of NRIAG and the main activities of the laboratory of Geomagnetism

Picture 1 : Building of the former magnetic observatory at NRIAG, run from 1903 to 1960.

Various instruments have been installed in the building since 1903 including: Schuster-Smith H-magnetometer, Potentiometer arrangements, Kew magnetometer (Picture 2), Dover-Dip Circle, and Lacour magnetometer.

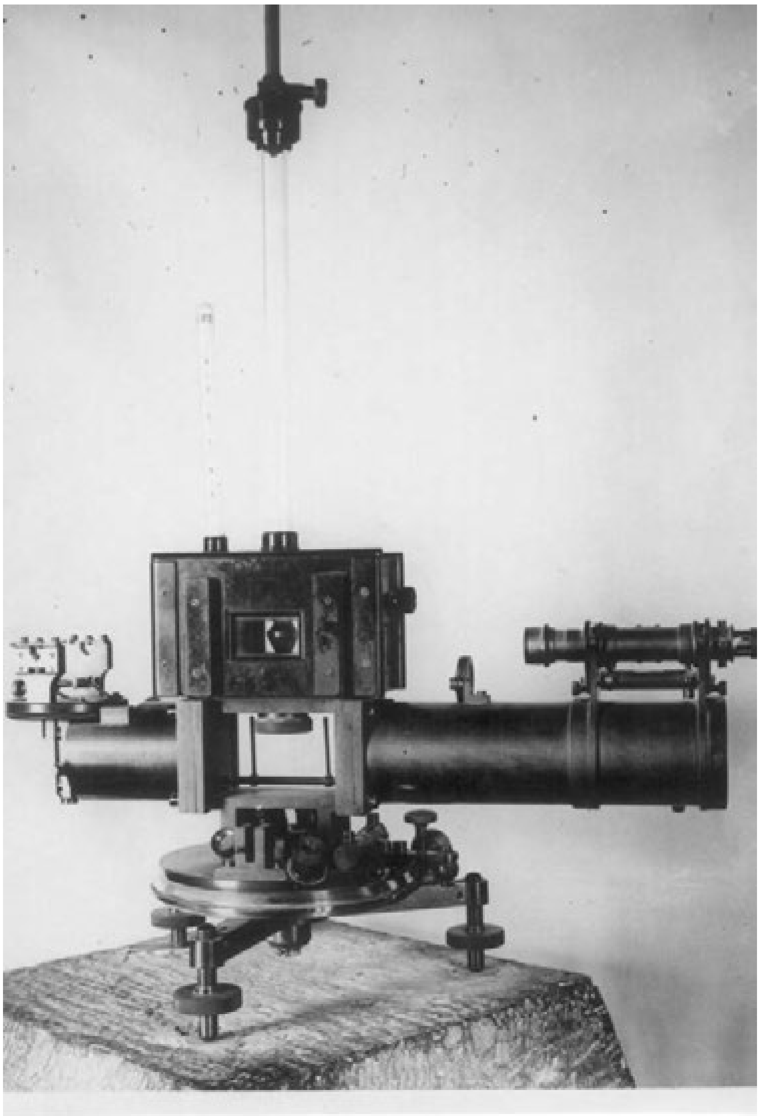

Picture 2: The Kew magnetometer used in Helwan till 1960

However, the gradual encroachment of the industrial area in Helwan towards the observatory and the clear effects of the newly established electrical tramline on the magnetic records have led to a decision to shift the Geomagnetic observatory to another location in 1960.

Grounds of MLT observatory

A new magnetic observatory was established in the village of Misallat in 1960. Misallat is north of Fayoum city and Fayoum city is located 72 kilometres south of Cairo. Although Misallat was a remote area its stability and high magnetic homogeneity made it a suitable location for the new magnetic observatory, which has the code MLT and coordinates 29°30´N, 30°53´E. The instruments building at Misallat has a construction similar to an old Egyptian temple and have double walls to keep variations of the temperature inside the building to a minimum. (Picture 3).

Picture 3: Building of the magnetic observatory at Misallat established in 1960 northern Fayoum and 72 Kilometres southern Cairo.

When the recording of data started, old instruments available in Helwan have been reinstalled in MLT and, as far as possible, new equipment was brought to the station. Unfortunately, MLT had a non-functioning period as a result of instrumentation failure and power supply problems in the remote area of Misallat. Since 1997 intensive development in both magnetometers and power supply equipment have been carried out to improve MLT observatory to the highest standards of recording and to solve its earlier defects.

Instrumentation currently in use at MLT observatory

The following instruments are currently running continuously at MLT and deliver quit accurate data:

Fluxgate Variometer (Picture 4a, b)

- 5 sec. Sampling rate
- Saving of 5 sec. and 1 min. records
- Suspended sensors
- DC backup battery for 7 hr.

Picture 4a: Suspended 3axis of the fluxgate magnetometer

Picture 4b: Low power consumption electronics and storing computer of the Fluxgate magnetometer

Digital fluxgate magnetometer (Picture 5)

- 1 sec. Record data saving
- Automatic compensation
- Long-term thermal stability
- Sensor and electronics temperatures recording

Picture 5: Sensor and electronic box of the high-resolution 3-axis digital fluxgate magnetometer.

Proton Vector Magnetometer

- Manual measurement of F, H, I

D/I fluxgate magnetometer (Picture 6)

- Mounted on nonmagnetic Zeiss Theodolite

Proton Magnetometer

- Continuous measurement of F

<u>Electrical Power sources:</u>

- Mains
- UPS: 6 KW for 30 minutes
- Automatic starting generator

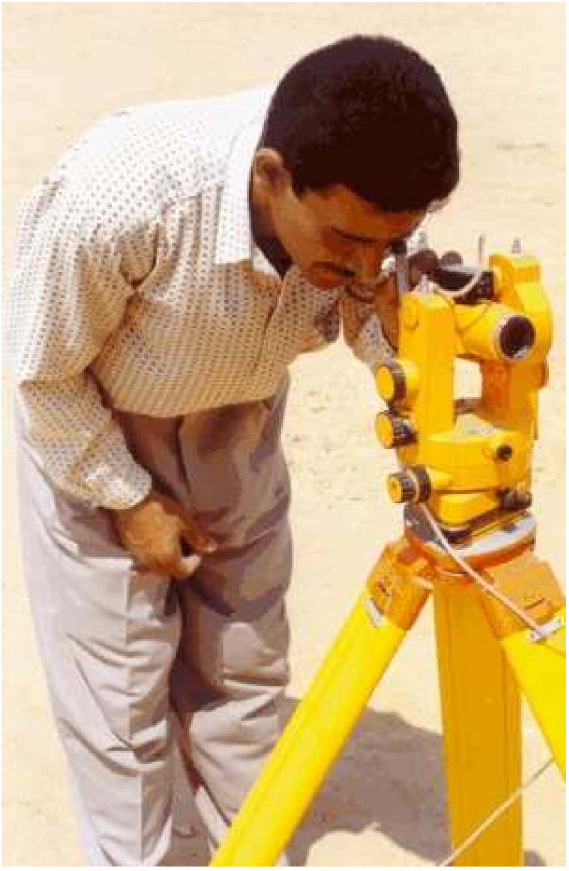

Picture 6: Single axis D/I Fluxgate magnetometer used for absolute measurements at MLT.

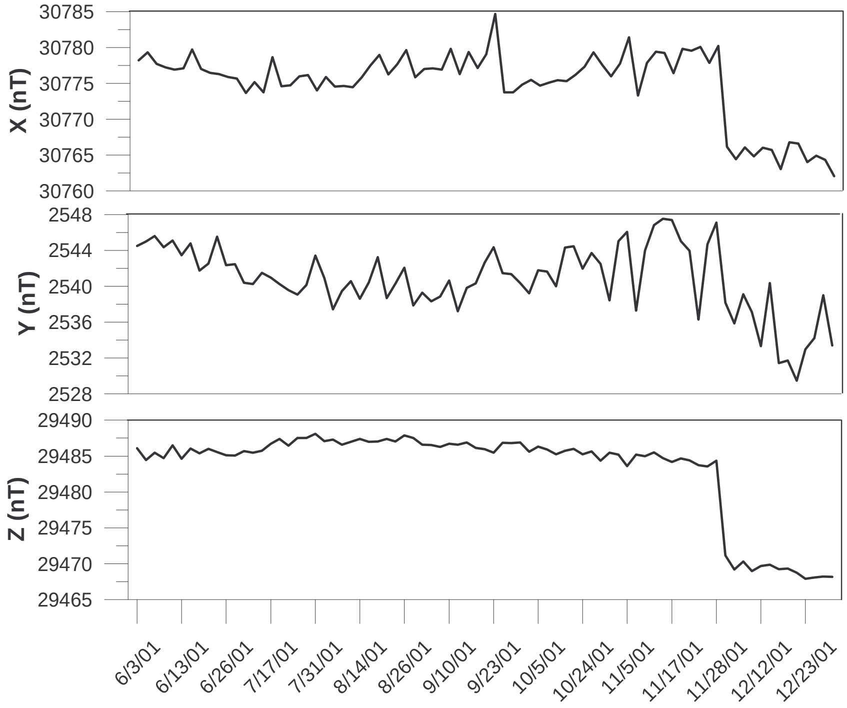

Figure 2: Base line of MLT observed in the second half of the year 2001.

Plans for a new magnetic Observatory in Egypt

For future development of magnetic observations in Egypt an additional station is in the planning stages to fill the gabs between MLT and the neighbouring observatories in Africa and the Middle East, as well as providing more accurate base station records for regional magnetic surveys carried out to the interest of the oil industry. However, the main problem is to find the optimal location to implement the new station. A series of possible locations for a new observatory are shown in Figure 3 as well as the locations of IMO’s surrounding Egypt.

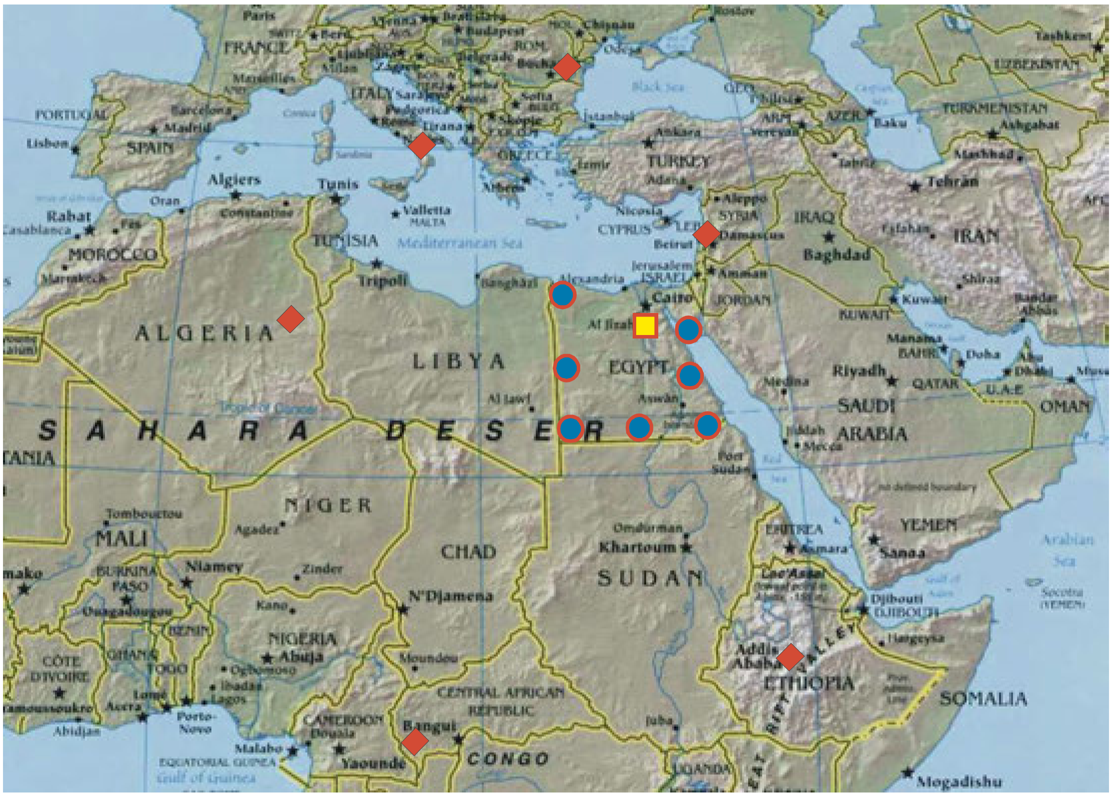

◆ Intermagnet Observatory ● Proposed observatories ■ MLT

Figure 3: Proposed Locations of additional Magnetic Observatories in Egypt and the available IMO's in the Middle East.

Stations on the western borders of Egypt would fill the gab of observatories in the Libyan and/or in Sudan. However, the installation there is very difficult because of the rough conditions, harsh climate and the absence of infrastructure in the Egyptian-Libyan Sahara.
To establish a magnetic observatory on the western bank of the Gulf of Suez would still leave a gap on the Arabian Peninsula. Furthermore, the Red Sea Mountains are known to be unstable and cause unfavourable magnetic disturbances.

Two other locations are more favourable to establish a further magnetic station. The first one is in the most southern part of Sinai and the second one is near Abu-Sumbul which is in the southern Egyptian territories. This is a distance of about 180 km from the High Dam of Aswan. The advantages of the first area, is its location near the Arabian Peninsula and the middle of the Red Sea, which may be interesting for a continuous magnetotelluric station to study the magneto-tectonics of the region, even if this would affect the stability of the magnetic measurements. In addition, the south Sinai area is supported by a good infrastructure and has a moderate climate throughout the year. The location at Abu-Sumbul is magnetically homogeneous and would represent the nearest observatory to the wide Sudan territories. In spite of the high temperatures dominating there during most of the year, Abu-Sumbul is the most favourite place for the new observatory in Egypt that will be connected to Helwan via the Cellular phone network to download the daily records.

Acknowledgement: I would like to express my thanks and appreciations for IAGA, INTERMAGNET and the Hermanus Magnetic Observatory (HMO) for the invitation and the support to participate in the workshop.

Geomagnetic Observations in Morocco

Abdelkrim Rimi
Scientific Institute
Department of Earth's physics
Geomagnetism and Geothermics group
B.P. 703 Ibn Battouta Avenue Rabat Agdal 10106 Morocco
Tel: +212-7-37774543/ Fax: +212-7-37774540
email: rimi@israbat.ac.ma / rimi_krimo@yahoo.com

Abstract

The presence of anomalous variations of the magnetic field in Morocco is observed since 1960. Geomagnetic measurements at the observatories and also during deep geomagnetic soundings, revealed main tectonic structures in Morocco. These experiments indicate conductive layers at different depths in the crust and the lithosphere. It is evident from recordings from the Averroes and Tiouine magnetic observatories that a large conductivity anomaly exists in the Rif and High Atlas mountains respectively. These anomalies are related to a regional network of conductive structures. These major structures might correspond to the boundaries of the units which make up the continental lithosphere in the region.

Introduction

Because of its geographical position, Morocco presents an outstanding Precambrian to Neogene tectonic evolution that has been the result of continuous interactions between the main lithospheric plates, namely the American, the African and Eurasian plates. The Iberian-African plate boundary region is characterized by large lateral variations in the lithospheric structure. A reliable estimate of the geophysical properties within the crust and the lithosphere is a relevant indication for a better understanding of this complex structure.

Geomagnetic measurements in observatories as well as during deep geomagnetic soundings and aeromagnetic surveys make possible an abundant resource of data which highly contribute to such purposes. On the other hand maintaining geomagnetic observations in Morocco plays a major role for the precision of the IGRF model because of the rare number of observatories in this part of Africa.

The geomagnetic measurements started in Averroes Observatory during 1967. The recording of the components of the terrestrial magnetic field in Morocco was in continuous service at the Averroes observatory from 1975 to 1994 and at the Tiouine observatory between 1985 and 1993.

The recording of the variations of the components of the magnetic field was done on photographic paper (imported from France) at both observatories (LACOUR device). For seven years, the operational budget of the Earth's Physics department could not acquire the necessary funding for these type of recordings.

The management of the LACOUR device becomes expensive in comparison with systems of digital recording available on the market.

In this paper we show what contribution geomagnetic measurements contributed to the knowledge of the complex lithospheric structure of Morocco.

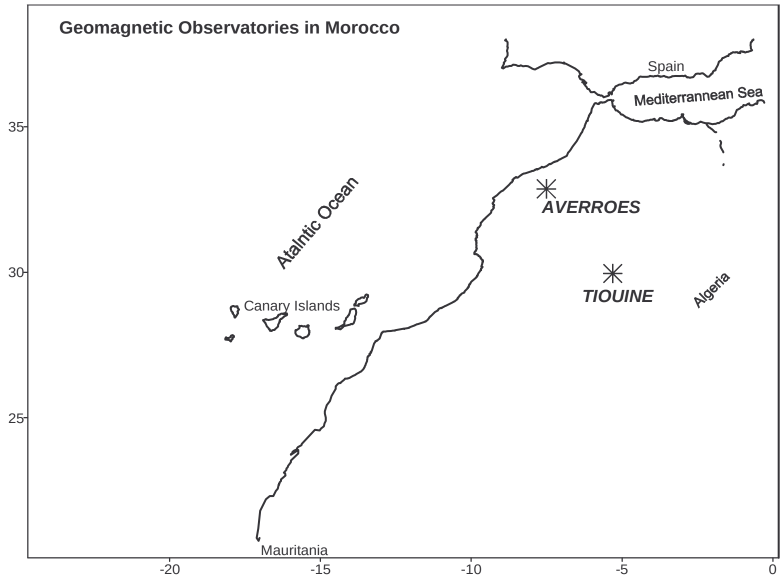

Figure 1: Moroccan Geomagnetic observatories Avverroes and Tiouine

Electrical Anomaly structures in Morocco

Rif

In 1969 Sibuet tried to study the oceanic effect on the magnetic recording quality in Averroes, by a comparison of magnetograms recorded in Averroes with those in operation at neighbouring observatories evidenced an electrical anomaly.

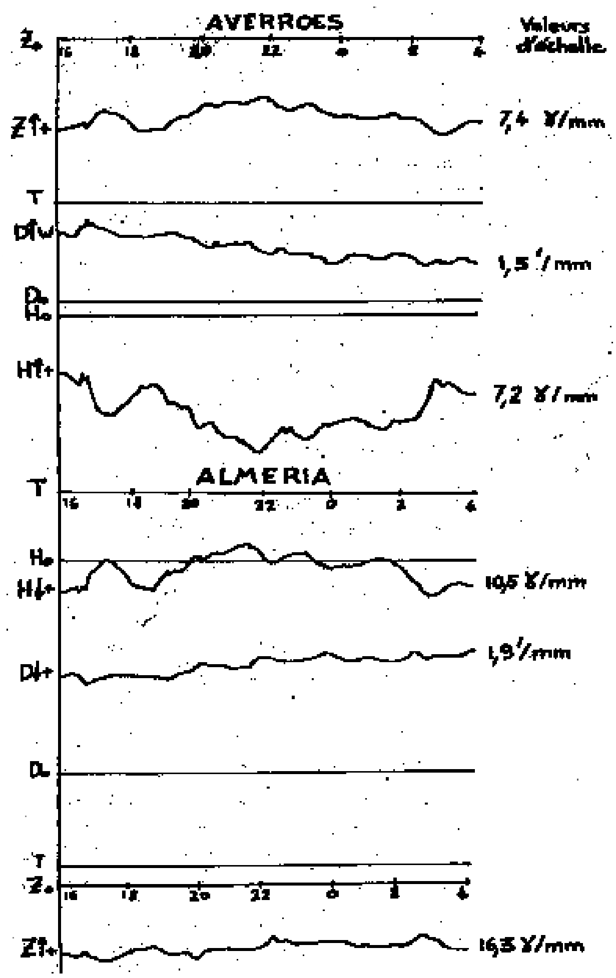

Figure 2: Transient variations in Averroes compared to neighbour Observatories

The existence of this anomalous electric structure was confirmed later by an aeromagnetic survey in northern Morocco (Demnati, 1972).

For a precise description of the anomaly in northern Morocco, deep geomagnetic soundings was conducted in 1975 by a Moroccan French team in the Rif belt (Figure 3 a and 3 b). They recorded the variations of the magnetic field along three components X, Y and Z.

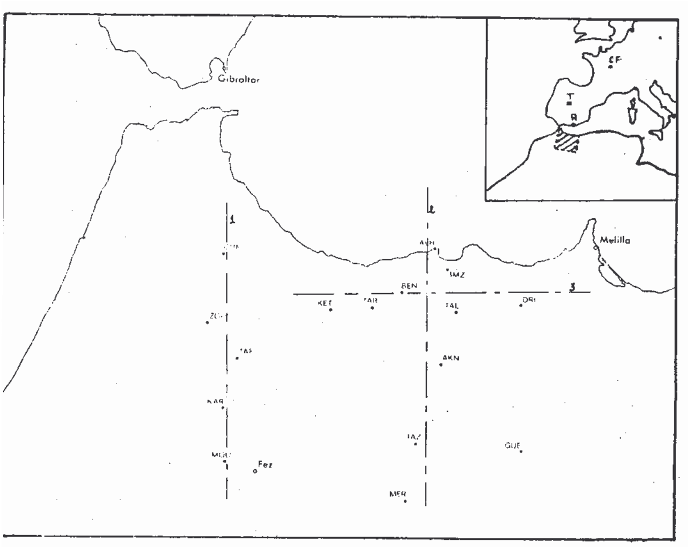

Figure 3 a: 3 profiles of geomagnetic soundings were conducted in 1975.

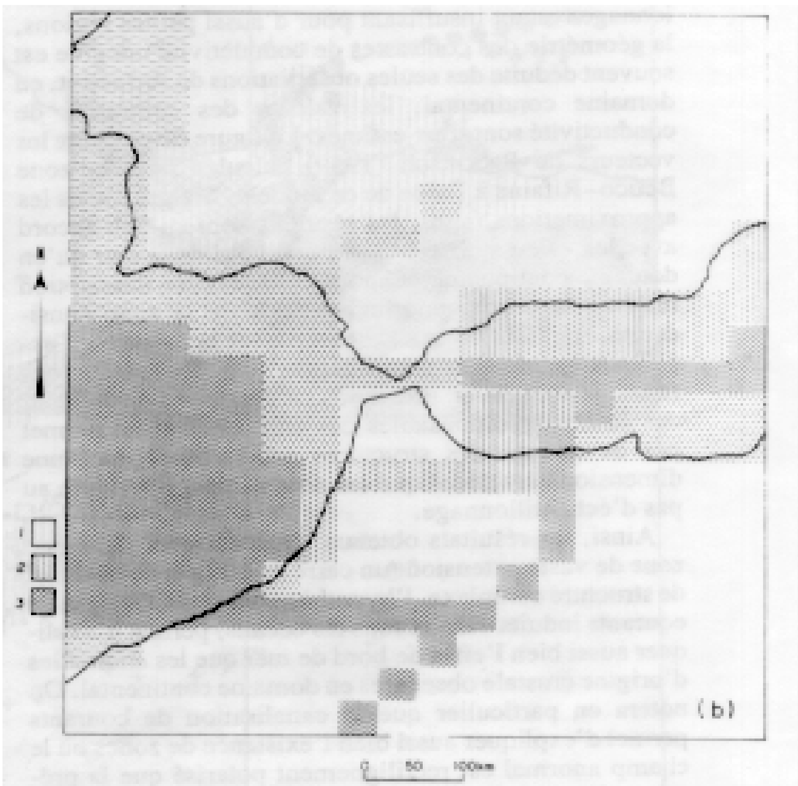

Figure 3 b: Distribution of the electrical conductivity heterogeneities in the crust (Menvielle and Rossignol, 1982)
1 resistant domain σ= 0.25 Ω-1 m-1, 2- intermediate domain σ =1.25 Ω-1m-1, 3-conductor domain σ = 4 Ω-1m-1

In order to precise the topography of the conducting levels in the Rif, we are digitizing the magnetic field variations analog recording, for an application of modern 2-3D thin-sheet algorithms that link surface and deep-seated processes.

Eastern High Atlas and Middle Atlas

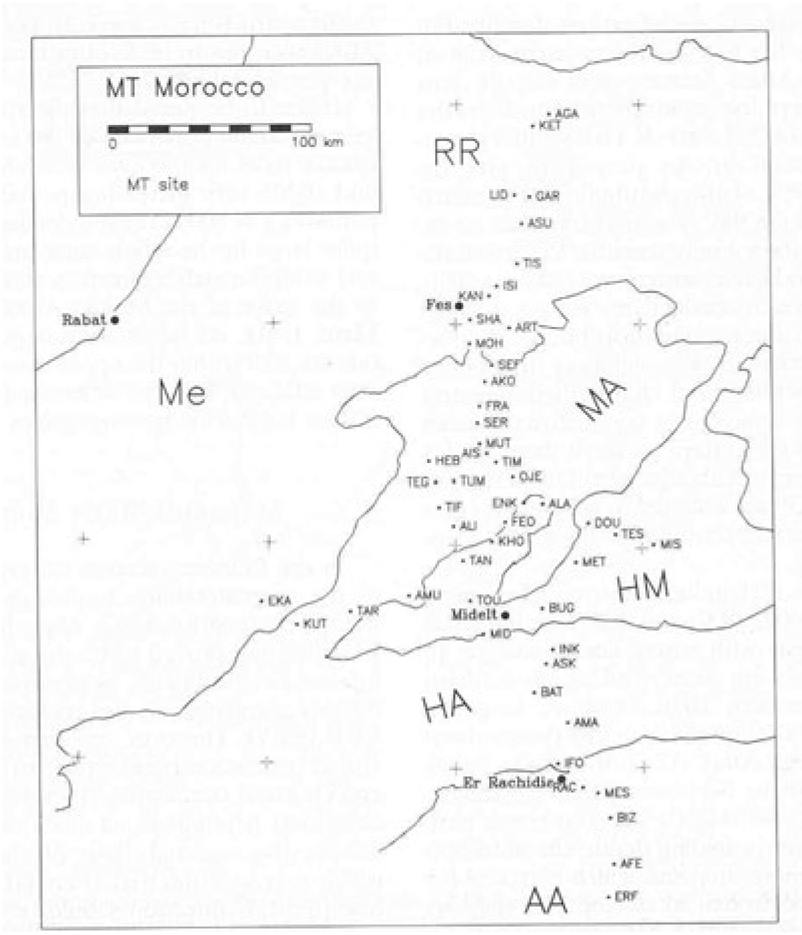

Figure 4: Deep Magnetic and Magnetotelluric profile across the Eastern High Atlas and the Middle Atlas.

Geomagnetic induction arrows from the Anti Atlas to four periods (200, 600, 1800, 3000 s) of the Rif indicates the lateral extent of well-conducting structures at upper to lower crustal depth. The induction arrows serve as the reversed pathfinders for lateral changes in electrical resistivity, i.e., almost perpendicular to, and pointing away from well-conducting structures. They reach their maximum in length where the gradient in resistivity is the largest. Two areas with high contrast in electrical conductivity can be identified: the Rif Ridges (RR) north the Middle Atlas (MA) and the southern area of High Atlas (HA).

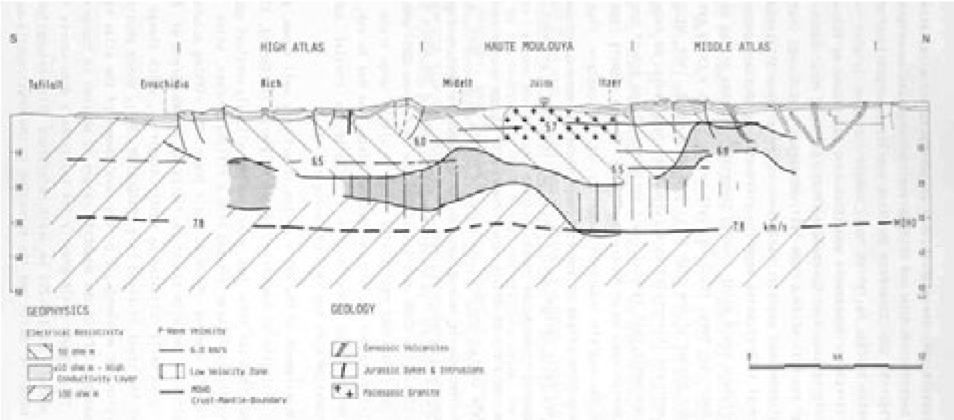

Figure 5: Crustal section showing the high electrical anomaly zone (in grey) in the crust beneath the Eastern High Atlas and the Middle Atlas.

Western High Atlas

As in the Rif, the temporal variations in the anomalous field recorded on December 7, 1982 in Tiouine Magnetic observatory revealed a large conductivity anomaly in the High Atlas (Menvielle and Le Mouel, 1985).

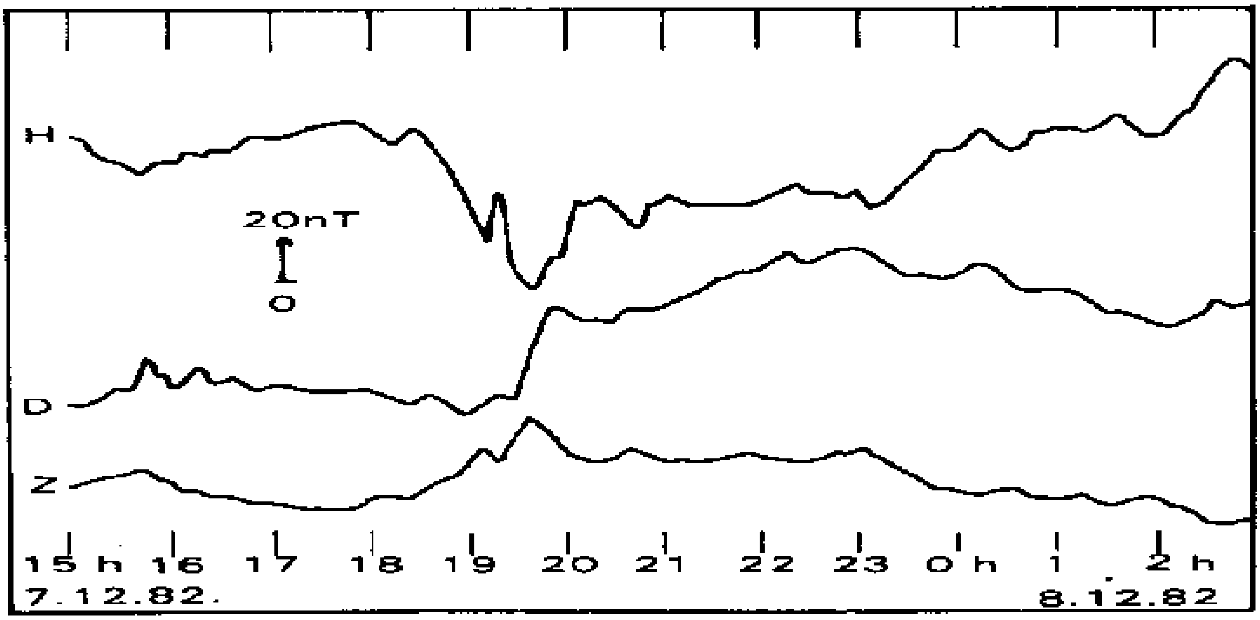

Figure 6: Magnetic variations recorded on December 7, 1982 in Tiouine.

Deep geomagnetic soundings in the Western High Atlas were conducted in 1987. Despite the correlation existing between discontinuity in the crust and magnetic observations, the relatively short recording time of the available data does not allow a good estimate of the conductive structure depth (Rimi & Menvielle, 1994).

Conclusion

It appears from this report that geomagnetic observations had been highly contributing to the knowledge of deep geophysical Moroccan structure. Therefore, it is essential that the Earth's Physics Department maintain and renew the recording equipment this year.

References

- BULLETINS MAGNÉTIQUES DU MAROC 1968-1973
- LEGSP & DMGM, 1977. Premiers résultas d'une campagne d'enregistrement des variations géomagnétiques dans le nord du Maroc. *Ann. Geophys.* t.33, fasc **1/2**, 225-236.
- MEM, 1959-1978- Unpublished Reports of the Ministry of Energy and Mining in Morocco.
- MENVIELLE M. & ROSSIGNOL J. C. (1982) - Conséquences tectoniques de l'existence d'une anomalie de conductivité électrique au nord du Maroc. *Can. J. Earth Sci*., **19**: 1507-1517.
- MENVIELLE M. & LE MOUËL J. L. (1985) - Existence d'une anomalie de conductivité dans le Haut Atlas marocain et concentration de courants telluriques à l'échelle régionale. *Bull. Soc. géol. France*, t, I, **4**: 553-558.
- RIMI, A., 1987. *La Grande Encyclopédie du Maroc*. Vol. n°3 "*Géographie physique*", pp.51-74.
- RIMI, A., & MENVIELLE, M., 1994. Résultats préliminaires des sondages magnétiques dans le Haut Atlas occidental - Maroc. *Rapport inédit*.
- SCHWARZ G, MEHL HG, RAMDANI F & RATH V (1992) - Electrical resistivity structure of the eastern Moroccan Atlas System and its Tectonic implications. *Geol. Rdsch*, 81/**1**: 221-235.
- SIBUET J.C. 1969.Etude des variations transitoires du champ magnétique terrestre à l'observatoire Averroes (Maroc) et dans les observatoires environnants. Diplôme d'Ingénieur Géophysiciien, Strasbourg, France. Unpublished.

60, 59, 58 ...How many minutes for a reliable hourly mean?

Mioara Mandea, Institut de Physique du Globe de Paris, 4 Place Jussieu, 75005 Paris, France
Email: Mioara@ipgp.jussieu.fr

Abstract

In the present study we will discuss the following question: if one computes hourly means using one-minute values and there are missing data, what percentage of data should be available to obtain a representative hourly mean? This question, addressed in July 2001 by Louis Loubser (Hermanus Magnetic Observatory), different answers were received (Laszlo Hegymegi: "our proposal is to use a secondary recording instrument and in case of data gaps in recording of primary instrument to replace the missing data from the secondary recording"; Ole Rasmussen: "if the gap in the particular hour is 20 min or more we do not calculate the hourly means"; Ellen Clarke: "hourly values are calculated from one-minute values unless more than 10% (6 mins) are missing"; Angelo De Santis: "in my opinion for most typical kinds of quiet and moderate magnetic activity, it would be probably better to have 1 data every three (i.e. 33% of data only) instead of having just the first half of the whole period but nothing of the rest (i.e. 50% of all data)").

I analysed 120 days for the 1999. These days are chosen as the quietest and the disturbed days of each month. In order to get an idea about how the field amplitude influences some artificial gaps (from one-minute to half an hour) are created and some statistical comparisons with the whole datasets are made. Finally, the improvement which such computations bring in terms of averaging the magnetic data, is discussed.

1. Introduction

For a very large period of time, the highest resolution in geomagnetic data provided by observatories was hourly mean value. This situation changed during the last part of the XXth century, when digital recording instrumentation was developed and installed at observatories, instead of the old photographic paper recordings. In modern times one-minute values are recorded and subsequently hourly, daily, monthly and finally annual means are computed. It is well known, that the first step in getting accurate means starts with getting a representative hourly mean. So, the aim of this study is just to find out how to compute hourly means using one-minute values when there are missing data, and what percentage of data should be available to obtain a representative hourly mean.

2. Data analysis

The data used in this study are the one-minute values over 120 days of the year 1999. For that we take one-minute values of the three components of the field during the year 1999, for four observatories, as available on the INTERMAGNET CDROM 1999. These observatories are: a high-latitude observatory, Resolute-Bay (RES), an equatorial observatory, Bangui (BNG), and two middle-latitude observatories, one in the Northern and one in the Southern hemispheres, Chambon la Foret (CLF) and Hermanus (HER). Their coordinates are given in Table 1.

No	Name	IAGA code	Latitude	Longitude
1	Resolute Bay	RES	74.69	265.11
2	Chambon la Foret	CLF	48.02	2.27
3	Bangui	BNG	4.33	18.57
4	Hermanus	HER	-34.43	19.23

Table1. Observatories used in the present study (from North to South).

To appreciate the effect of external contributions I selected, for each observatory O_i two subsets of 60 days each, D_i containing the most disturbed day and Q_i containing the five quietest days of each month of 1999. The selection of days is made from Kp indexes on the basis of three criteria for each day: the sum of the eight *Kp* values, the sum of squares of the eight Kp values, the maximum of the eight *Kp* values --- for more detail see: http://www.gfz-potsdam.de/pb2/pb23/GeoMag/niemegk/kp_index . It should be noted that these criteria only select the quietest or more disturbed days of a given month. As the general disturbance level may be quite different for different years and also for different months of the same year, the selected quietest days of a given month may sometimes be rather disturbed; a similar remark holds for the selected most disturbed days. It is to avoid as much as possible such a situation that we chose a year (1999) far from the minimum and maximum of the solar cycle 23.

Using this series of data hourly means have been computed with 60, 59, ..., 30 one-minute values, for all three components *X, Y, Z*, and for all D_i and Q_i days of 1999. Thereafter differences between the full hourly mean computed with all 60 one-minute values (HM_f) and the hourly means computed with only 59, 58, ...,30 (HM_{59}, HM_{58}, ..., HM_{30}) one-minute values have been obtained. I consider that when differences $| HM_f - HM_{59} |$, $| HM_f - HM_{58} |$, ..., $| HM_f - HM_{30} |$ are smaller than 1 nT, the hourly mean computed with less one-minute values than 60 is a reliable mean.

3. Results and discussions

An example of differences $HMf - HM_{59}$, $HMf - HM_{58}$, ... $HM_f - HM_{30}$ are shown in figure 1. For all four observatories the 24 differences are plotted for two days of July 1999, one quiet and another disturbed. For the same observatory the vertical scale is kept, but it differs by more than an order of magnitude from RES to HER. The differences (*dX*, *dY*, *dZ*) for the three component hourly means computed with 60 one-minute values (HM_f) and the hourly means computed with only 59, 58,..30 one-minute values (HM_{59}, HM_{58}, ..., HM_{30}) are plotted (circles for D_i and squares for Q_i days).

Some simple computations show how much the number of hourly means is changing when less than 60 one-minute values are used to compute the mean. For the 60 D_i and Q_i days of the year 1999, a number of 1440 HM_f are respectively computed for each observatory. If the hourly means HM_{59}, HM_{58}, ..., HM_{30} are as well computed, the total number of hourly means for an observatory is 41760. Taking into account the above consideration ($| HM_f - HM_{59} |$, $| HM_f - HM_{58} |$,..., $| HM_f - HM_{30} |$ are smaller than 1 nT) it is possible to find out how many hourly means are reliable. Table 2 summarises this computation.

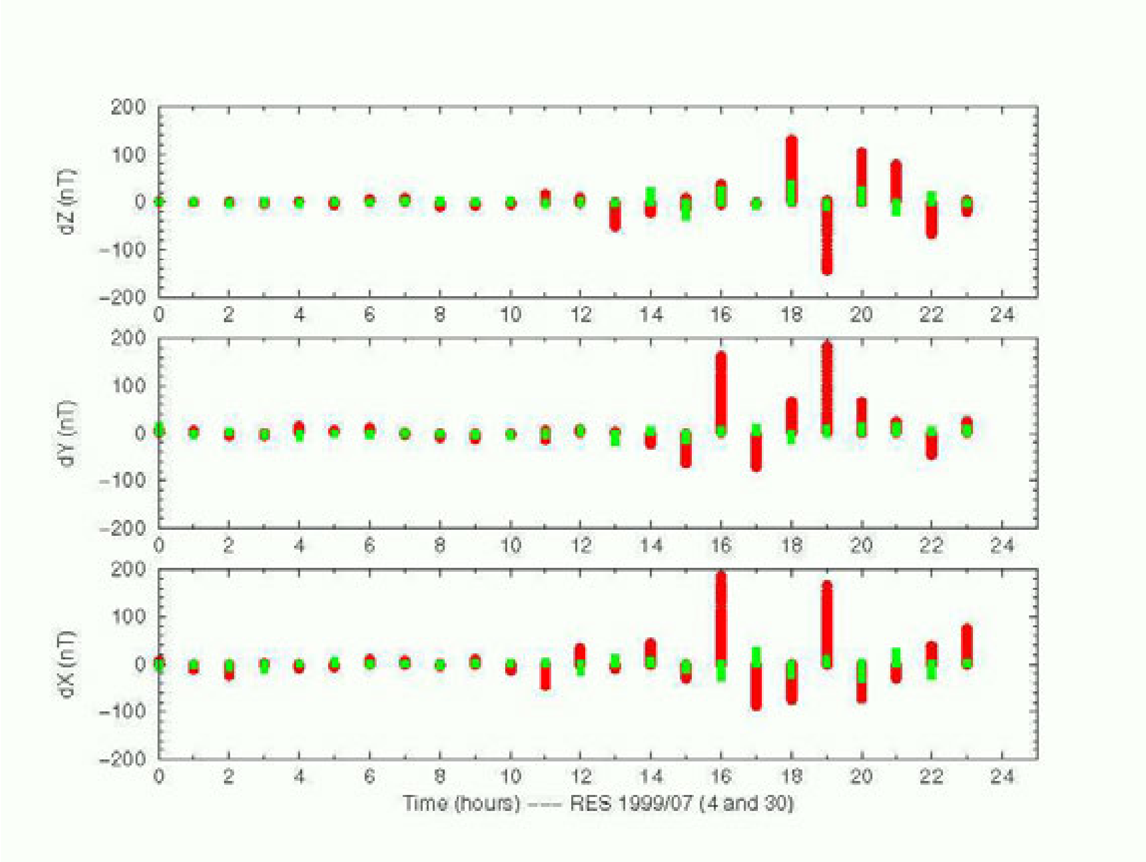

dZ (nT)
dY (nT)
dX (nT)
Time (hours) --- RES 1999/07 (4 and 30)

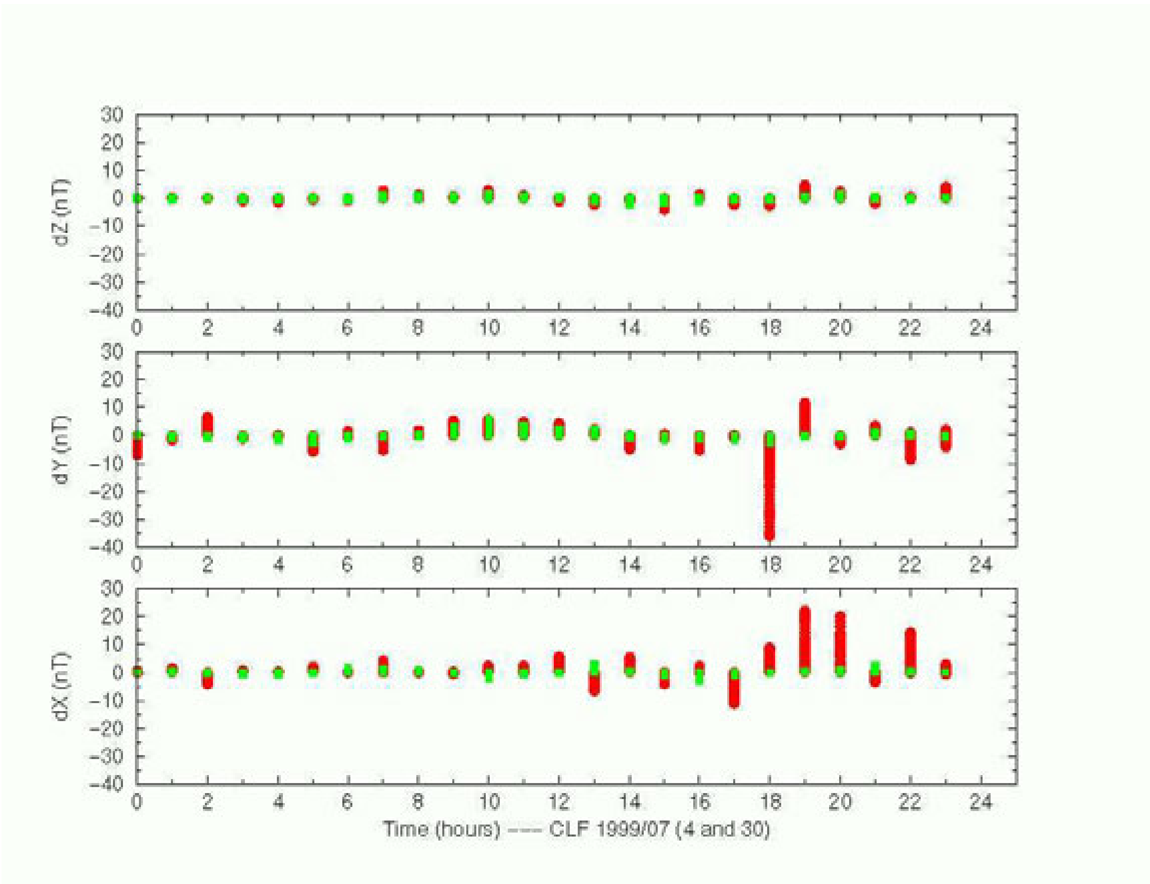

dZ (nT)
dY (nT)
dX (nT)
Time (hours) --- CLF 1999/07 (4 and 30)

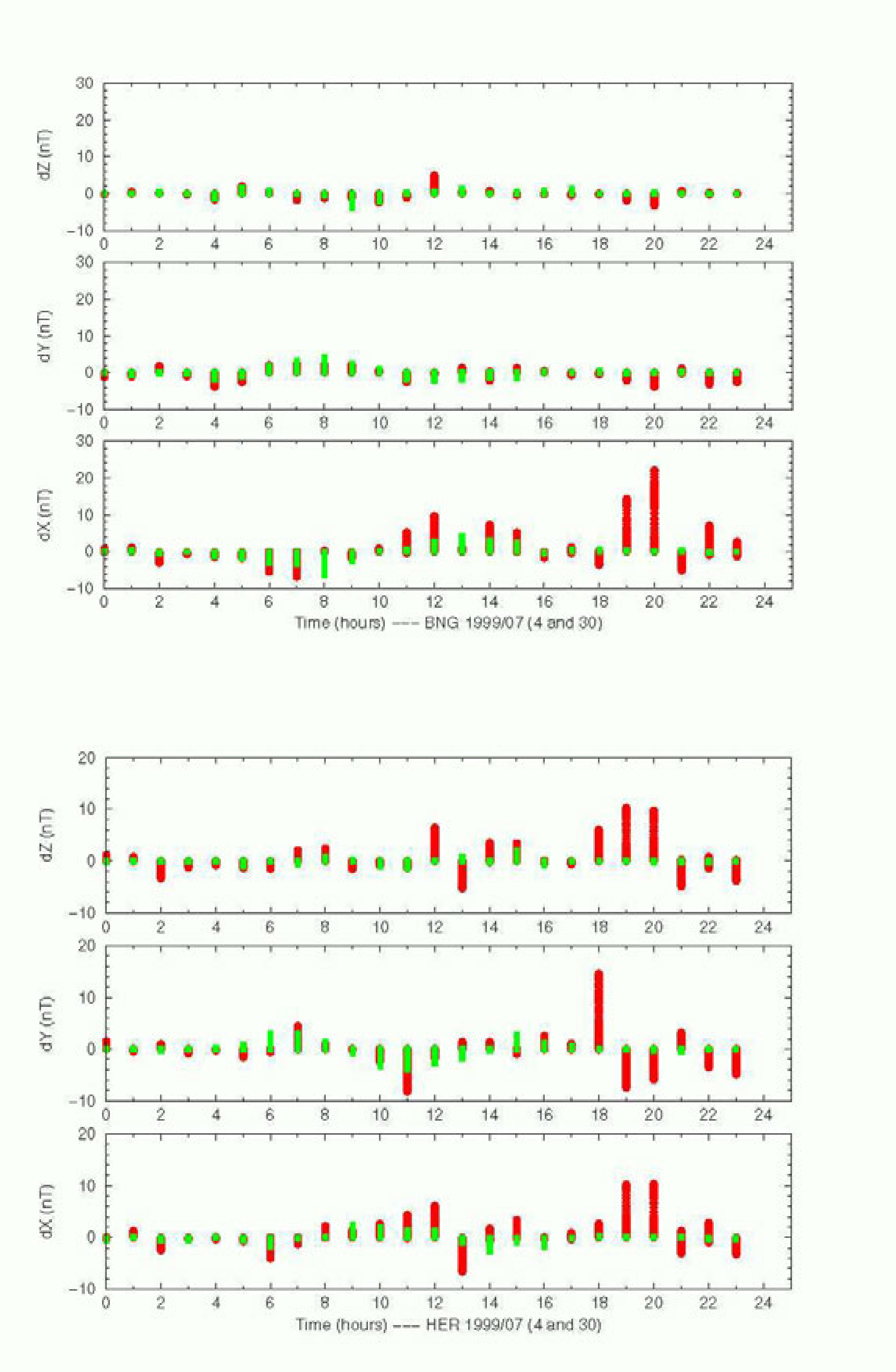

Fig1.Hourly mean differences dX, dY, dZ for *Di* (circle) and *Qi* (square) days.

Observatory	D_i	Q_i
RES	5394	11978
CLF	15364	31636
BNG	20393	31590
HER	17771	31619

Table 2. Number of hourly means with | HM_f - HM_{59} |, | HM_f - HM_{58} |,... | HM_f - HM_{30} | < 1 nT, over the total number of 41760 means (see text for details).

Figure 2 shows how the number of hourly means is decreasing for D_i and Q_i days, in each observatory. The graphs present a large difference between the quiet and disturbed periods. When data over only a few minutes are missing (less than 5one-minute values), the differences between the D_i and Q_i days are not important for observatories situated at low or middle latitude. However, for RES observatory the situation is completely different, important differences in the total number of data appearing with only a couple of one-minute values missing.

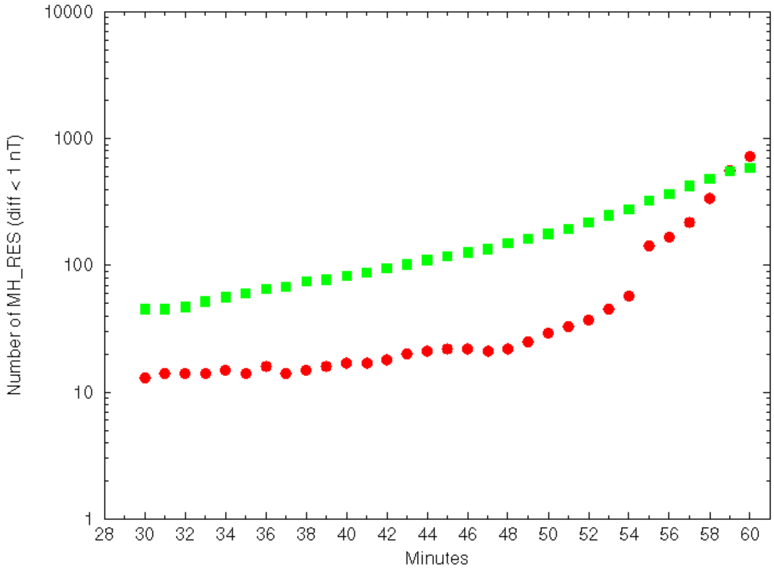

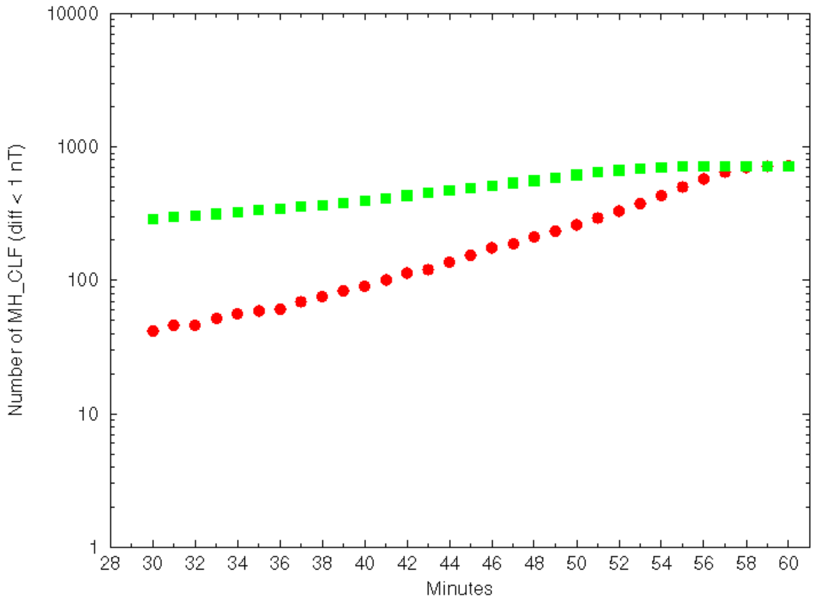

10000
1000
100
10
1
28 30 32 34 36 38 40 42 44 46 48 50 52 54 56 58 60
Minutes
Number of MH_CLF (diff < 1 nT)

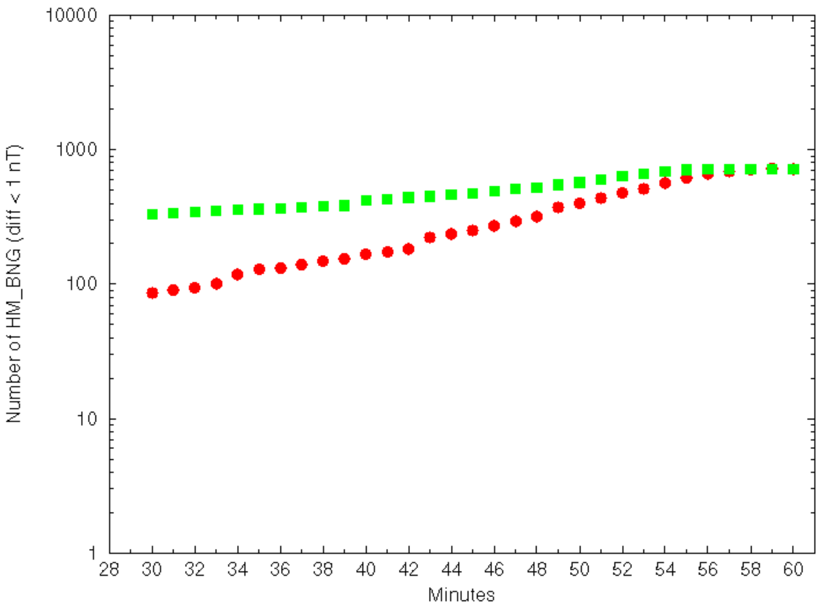

10000
1000
100
10
1
28 30 32 34 36 38 40 42 44 46 48 50 52 54 56 58 60
Minutes
Number of HM_BNG (diff < 1 nT)

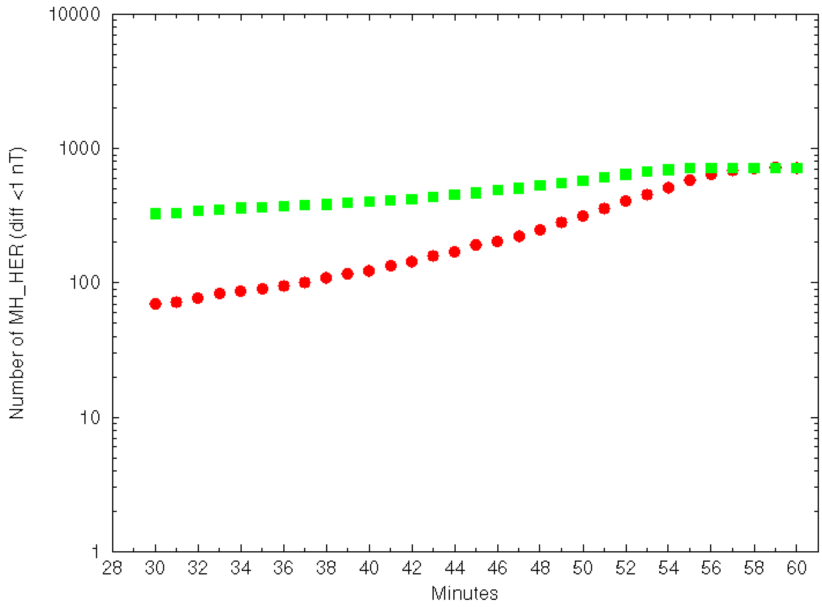

Fig2. Number of reliable hourly means for *Di* (circles) and *Qi* (squares) days.

Finally, in order to summarize the presented tests, some histograms have been computed and drawn in figure 3. Of course a compromise has to be accepted between the reliability of the hourly means and the accepted missing hourly means over one year.

I have indicated a level of 90% in all graphs. The upper panel of this figure (Fig 3a) shows the percentage of hourly means which are considered reliable for disturbed days. It appears again that for disturbed periods only gaps of a few one-minute values can be accepted. And again for RES observatory the situation is more difficult as at this high-latitude observatory the variations due to external fields are dramatically important from one minute to another one. The situation is much better during the quiet period (lower panel, Fig 3b), when the number of reliable values is really greater, even for RES observatory.

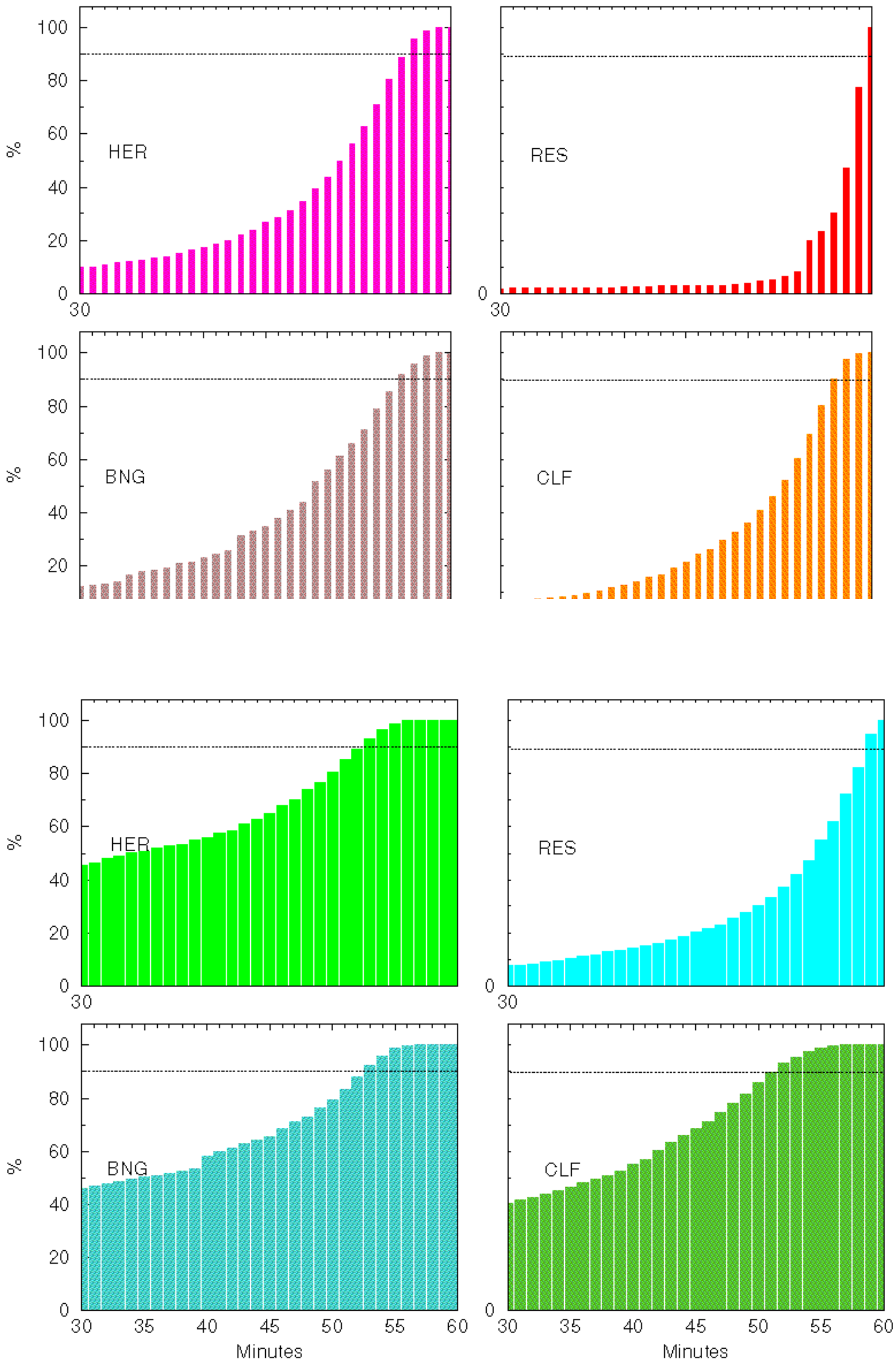

Fig 3. Histograms for *Di* (upper panel) and *Qi* (lower panel) days.

4. Conclusions

In this new epoch when a quasi-continuous measurement of the three components of the Earth ‘s magnetic field is recorded by satellites, the magnetic observatories are still, and will always be, absolutely necessary to provide, at the same site, continuous records of data of quality suitable for studies of the secular variation of the main field or external perturbations. Another obvious outstaying advantage of magnetic observatories is that they provide series of data starting long ago and thus permit to study changes in the magnetic field during at least the past century. Previously only annual means have been used but recently monthly and even hourly means are used. This is why the present study was undertaken just to show how reliable the hourly means are.

This study clearly shows that it is difficult to give a solution available everywhere. However, a general rule can be considered, i.e. reliable hourly means can be computed from one-minute values if less than 10% of data are missing. Nevertheless, individual users or team research scientists must themselves inspect the data before using them in different studies.

The present study should be continued. Firstly a larger number of observatories distributed around the world and during different magnetic conditions have to be taken into account. Another point is to consider a random distribution of gaps, with different length. And finally a study over a full solar circle will be welcome.

- *Processed data are available from M Mandea on request.*

USGS Magnetic Observatory on Midway Atoll

Alan Berarducci
Geomagnetism Group
U.S. Geological Survey
Box 25046, MS966, Federal Center
Denver, CO 80225 USA

Introduction

The geographic coverage of the US Geological Survey's (USGS) geomagnetic observatory array was significantly enhanced with the installation of a station on the remote mid-northern Pacific atoll of Midway in February 2000. Midway Atoll is located in the North Pacific Ocean, 2000 kilometers west-northwest of Honolulu, Hawaii and is part of the Hawaiian Island chain. Midway is a typical Pacific Atoll. It was originally a volcanic island, but today the original basalt island lies under more than 150 meters of carbonate material. The atoll consists of a breached barrier reef with three small islands inside the lagoon. The largest, Sand Island is 1200 acres.

Background

Midway was annexed by the United States in 1867, but remained unoccupied until 1903 when the Commercial Pacific Cable Company began operating the first trans-Pacific telegraph cable. Further development occurred in 1935 when Pan American Airlines began the first scheduled trans-Pacific air service. Major development on the island began in 1938 when the US Navy built a base there. In the 1960's and 1970's, 3000-4000 servicemen and dependants were stationed at Midway.

In 1996, the US Navy transferred ownership of Midway to the US Fish and Wildlife Service (USFWS), who today operate the Midway Atoll National Wildlife Refuge. The USFWS has an agreement with a contractor who operates the infrastructure.

The US Coast and Geodetic Survey fist collected geomagnetic data on Sand Island in the mid-1960's. The USGS collected repeat station data on Sand Island from 1980 until 1999. The USGS Midway Magnetic Observatory was established at Midway Atoll National Wildlife Refuge in February 2000.

Observatory Location

The observatory is located in the western part of Sand Island, about 600 meters west-southwest of the airport terminal, just west of the intersection of emergency runway 15-33 and the taxiway to the terminal on an area paved with asphalt that has since become overgrown. The area was paved to prevent birds from nesting close to the runway, as they are a hazard to aircraft. The paved area has become overgrown with trees and weeds, some of which are 15 meters tall. Approximately 7000 m^2 has been cleared of vegetation for the observatory equipment. Trees surround 3 sides of the observatory and serve as a wind block. The USFWS has agreed to a 200-meter buffer zone around the site and agrees to consult with the USGS Geomagnetism Group before building within the buffer zone.

The geographic coordinates of the magnetic observatory are N28.2076 degrees and W177.3824 degrees.

Observatory Layout [Figure 1]

The Midway Magnetic Observatory is a prototype for remote, solar powered observatories. There are several new innovations:

1. The observatory is powered exclusively by 4-60 watt photovoltaic solar panels, and 2-12 volt, 110 AH batteries. There is no connection to the mains power grid.
2. The fluxgate magnetometer electronics has been removed from the usual electronics box location and placed in an underground, plastic, insulated, waterproof tub.
3. The electronics box contains the DCP (Data Collection Platform), Geometrics G-856 Proton Magnetometer, DIDD (Delta I Delta D) control, and other electronics. It is mounted on a pole, outside, and exposed to the elements.
4. The only external communication with the DCP is through a laptop computer. There is no internet or telephone connection.

Station Electronics and Power

Solar panels, station electronics, and batteries are located about 30 meters from the edge of the emergency runway. The solar panels are mounted on a steel post, as is the station electronics box. The station electronics box is shielded on the south, east and west sides with plywood and on top by the solar panels [Figure 2]. The solar panels and plywood prevent direct sunlight from heating the electronics box for most of the day. The electronics box door opens on the north side. The electronics box contains the DCP; Geometrics G-856 proton magnetometer electronics, power buss, DIDD control, and interface control.

The battery box sits on a concrete pad below the electronics box and contains 2-12 volt batteries. The batteries are air shippable and designed for solar applications.

A green plastic tub is buried in the ground adjacent to the electronics box. The tub contains a Narod fluxgate magnetometer electronics and insulation.

A small box containing the solar charge controller is mounted on the pole above the electronics box.

The entire station electronics and solar power system are enclosed in a cage made of PVC pipe covered with a green plastic mesh [Figure 3]. The cage is to protect the solar panels and station electronics from flying Laysan Albatross and other birds.

Fluxgate, Proton and DIDD Magnetometers

A Narod triaxial fluxgate magnetometer, USGS model, measures the H, D, and Z (horizontal, declination, vertical) components of the vector field. The fluxgate sensor is housed on a pier comprised of 1 cubic meter of concrete poured around and inside a plastic, waterproof, insulated tub [Figure 4]. The fluxgate magnetometer electronics are in a plastic, insulated tub buried near the station electronics.

A Geometrics G-856 proton precession magnetometer measures the total field strength. The proton magnetometer sensor is suspended inside a DIDD coil on a pier identical to the fluxgate magnetometer pier. The proton magnetometer and DIDD electronics are located inside the station electronics box.

The magnetometer piers are about 30 meters apart. Magnetometer signals are transmitted via cables buried in PVC conduit to the station electronics box.

Data Collection Platform

A Synergetics Data Collection Platform (DCP) collects, stores, and transmits data. The DCP consists of three modules and a transmitting antenna. The GIM (Geomagnetic Interface Module 3455) collects data from the fluxgate magnetometer, the proton magnetometer and the

DIDD and forms it into 12-minute data blocks. The MCM (Master Control Module 3401) acquires a data block from the GIM and controls when the transmitter sends it. The Satellite Transmitter Module (GOES Module 3421A) transmits the data block via the GOES-West (Geostationary Operational Environmental Satellites) satellite to the USGS Data Collection Center in Golden, Colorado. The transmitting antenna is a Yagi type antenna located 18 meters south of the station electronics. The antenna is connected to the transmitter via an RG-214 cable buried in PVC conduit and is mounted near the ground. A cage made of PVC pipe and green plastic mesh surrounds the antenna to protect it from flying Laysan Albatross [Figure 5].

Temperature Sensors

Four temperature sensors are logged by the DCP. The sensors are located with the fluxgate magnetometer electronics, the fluxgate magnetometer sensor, the DIDD/proton magnetometer sensor, and the DCP.

Absolutes Magnetometer, Pillar and Shelter

A Zeiss-Jena 020B theodolite with a FLM 1/B electronics DI-flux magnetometer measures absolute values of declination and inclination. Absolute readings are comprised of four independent measurements of declination and inclination. The contractor makes absolute measurements once per week.

The absolutes pillar and shelter [Figure 6] are located 27 meters from the station electronics. The pillar is constructed of sand and cement poured into a 25 cm diameter PVC pipe topped with a 30x30x15 cm limestone cap. The pillar extends 1.2 meters into the ground anchored by a 1.2 m^2 block of concrete.

A concrete pad 2.4x1.8 meters surrounds the pillar, but is separated from the pillar by about 2 cm. The space is filled with backer rod and caulking. The pillar is 1.3 meters high.

A shelter over the pillar consists of a redwood frame and a heavy-duty tarp. The shelter serves to keep the sun off both the DI Flux and the observer. It also protects the observer in light rain.

Logistics

The USGS Geomagnetism Group pays a contractor to operate the Midway Magnetic Observatory. Two observers alternate the weekly work, and substitute for each other when one is off the island. Both observers have been trained in the full operation of the observatory. The weekly routine includes:

1. Making absolute measurements.
2. Computing baselines.
3. Retrieving data files.
4. Transferring data and baselines via FTP or email to the Golden, CO office.
5. Troubleshooting and diagnosing problems, replacing and repairing equipment as directed by the Golden, Co office on an as needed basis.

Transporting repair parts to the Midway Magnetic Observatory can take from one to four weeks due to limited air service. It is necessary to keep some repair parts on site.

Successes

1. Extensive testing for stability and reliability of the station electronics and magnetometers was done at the Boulder Magnetic Observatory. After installation on Midway, no unplanned outages of the station electronics occurred during the first 14 months of operation. The baseline stability at Midway is very good.
2. The solar power system has worked very well at Midway. The 4 solar panels and 2-110 amp hour batteries have provided ample power for the observatory.

Problems

1. The absolutes pillar was originally built on a magnetic anomaly and magnetic gravel was used in the concrete. The contractor failed to install the absolutes pillar to USGS specifications.
2. The solar charge controller caused some interference to the proton magnetometer readings. The interference showed up in consecutive proton magnetometer readings and ranged from more than 1 nT, and up to 3 or 4 nT. The interference occurred each day after the batteries had fully charged and lasted until the sun was low enough that the solar panels no longer charged the batteries.
3. After several days of heavy rain in April of 2001, the sensor houses and fluxgate electronics were flooded. The station was not operational for 108 days.

Solutions

The technical and design problems encountered during the construction and initial 2 years of operation of the Midway Magnetic Observatory have been overcome.

1. The original absolutes pillar was removed and a new pillar was built in a non-anomalous area with non-magnetic sand and cement in a 25cm PVC pipe. The new location and materials have been suitable.
2. Charge controller interference with the proton magnetometer, which occurred during the first 10 months of observatory operation, was prevented by the installation of a regulated power supply in the proton magnetometer power circuit.
3. Steps to prevent sensor house flooding were undertaken after the flood in April 2001. Loops of 1-meter high flexible conduit were placed in line with the PVC conduit just outside the sensor houses to prevent flooding through the conduit.

Future Modifications

In the future, USGS plans to move the observatory to a new location about 900 meters away. At that time, a small building will be built to house the station electronics.

Conclusions

The Midway Magnetic Observatory significantly enhanced the geographic coverage of the US Geological Survey’s magnetic observatory network. The planned Shumagin Magnetic Observatory in the Aleutians Islands will complement the Midway Magnetic Observatory and further enhance the sparse magnetic observatory coverage in the North Pacific Basin.

Midway Atoll is a strategic location for the USGS and other scientific organizations and commercial companies. Boeing Aircraft Company has an interest in keeping the airfield on Midway in operation as an emergency runway for trans-Pacific flights. A GSN (Global Seismic Network) seismic station operates on Midway and a GPS station measures continental drift. Fish, sea bird, and sea mammal research is carried out in conjunction with the US Fish and Wildlife Service who operate the Midway Atoll National Wildlife Refuge.

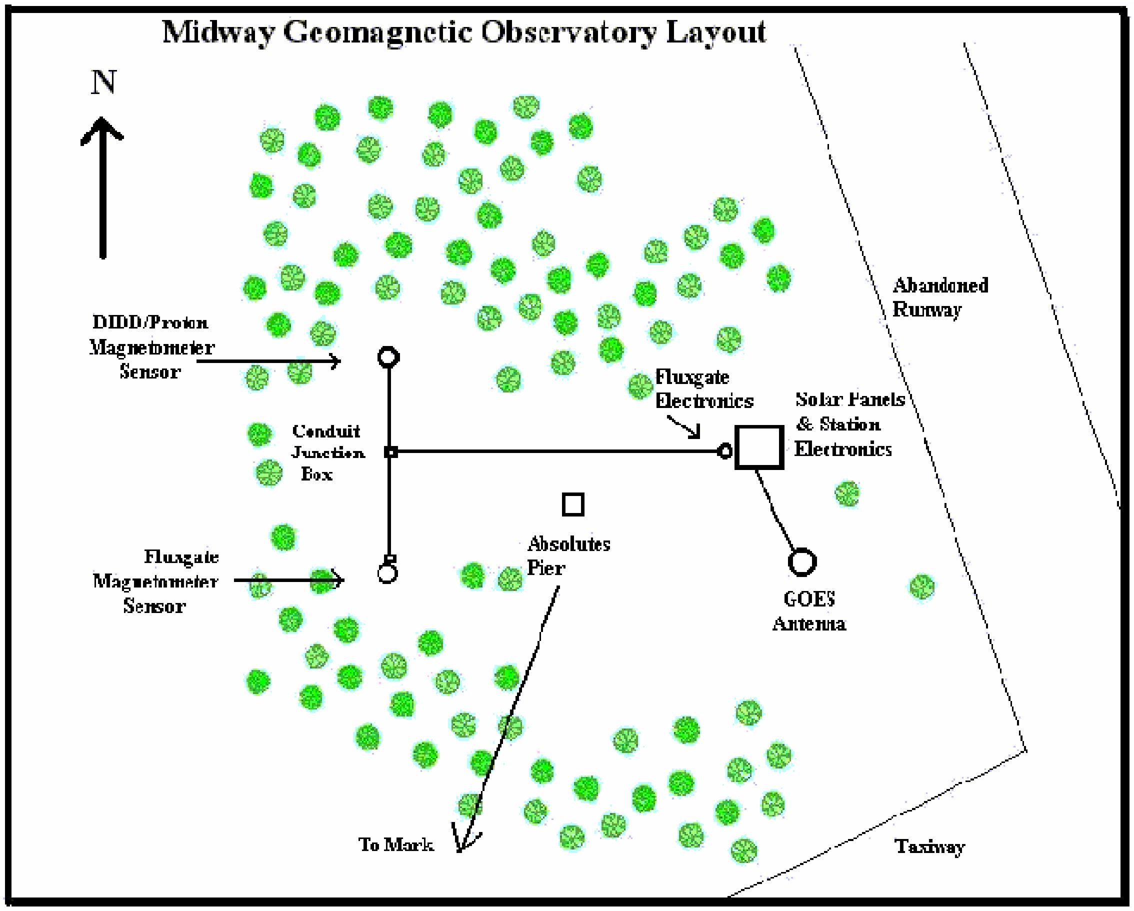

Figure 1

Figure 2

Figure 3

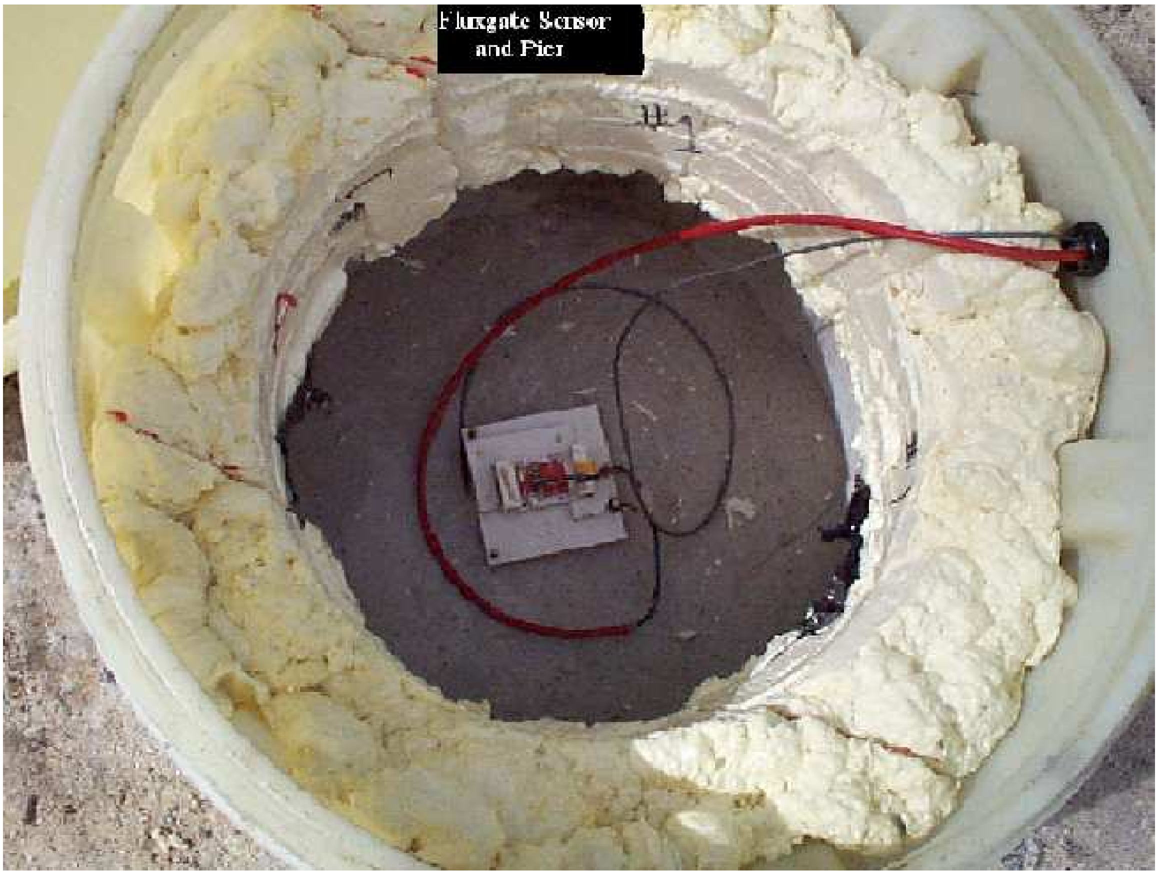

Figure 4

Figure 5

Figure 6

Geomagnetic observational activities at Alibag India

R.C.Deka and B.M.Pathan
Indian Institute of Geomagnetism , Mumbai- 400 005, India

Abstract

Before the introduction of the INTERMAGNET system (July, 1994) for nearly a century a geomagnetic observational schedule with digital magnetic observations (DIMARS) at Alibag (Lat 18° 37'N and Long 72° 52'E) was in operation. Since then the one minute digital data have been used to check and countercheck the manual scaling of photographic records, K-indices derivation, and baseline stability for both digital and analogue recordings with respect to VPPM absolute values. After the installation of 'INTERMAGNET' it became very easy to check any artificial shifts in the data. Absolute values for the horizontal, vertical, declination and inclination (H,Z,D,I) geomagnetic elements observed from different instruments such as the VPPM, BMZ, QHM, DIM, NO-7 old etc., are continuously checked before supplying the data to WDC (IIG), Mumbai. Special software routines are developed for checking the accuracy of the observations made by more than one standard and all observers will strictly adhere to the checking of the correctness of the data.

Alibag observatory attained a special status with all checks to perform on the various absolute instruments and continuous recording units of the geomagnetic field kept under an ideal electromagnetic environment. Also, the geomagnetic instruments available are periodically calibrated according to international standards and the same calibration facilities are extended to all the geomagnetic observatories functioning in the country under different agencies. Standards and facilities existing at Alibag are highlighted in this presentation.

Introduction

The study of the Earth's magnetic field is one of the oldest scientific disciplines with a history going back to Thales of Miletus (Circa 500 B.C.) who first noted the repelling action of lodestones. Ancient texts from India mentioned the specific property of iron being attracted by magnets. The Purans (4^{th} century A.D.), in defining the devotion to the Supreme, compare it to the attraction of a magnet for an iron needle. Although magnetic materials were known long back but it only became popular with the publication of Sir William Gilbert's *De Magnet* in 1600 mentioning that the "The Earth globe itself is a great magnet". Alexander von Humboldt was the first to discover the dependency of magnetic intensity on latitude based upon measurements taken during his voyage through the America's from 1799-1805. The scientific study of the spatial and temporal structure of the Earth's magnetic field is referred to as Geomagnetism. In the 19^{th} century, C.F. Gauss made use of mathematics to show that 99% of the observed geomagnetic field originates in the Earth's interior, and the remaining 1% comes from external sources. It was suggested that the external source lay in the electrical currents flowing in the Earth's upper atmosphere (now known as ionosphere and magnetosphere), and that the observed daily variations in the geomagnetic field reflected regular variations in these atmospheric currents. Simultaneous observations of the Earth's magnetic field were made at 50 different locations during 1836-1841, marking the beginning of the magnetic observatory system under the Gottingen Magnetic Union. Three of these locations were at Madras, Simla and Trivendrum in India. These observatories were subsequently discontinued after the project. The history of geomagnetism in India is discussed in detail in Rajaram and Pisharoty (1998).

The purpose of this presentation is to highlight the history of one of the oldest magnetic observatories in the world along with the observational procedure at this observatory.

Establishment of Magnetic Observatory at Colaba, Bombay

A regular magnetic observatory was built in Colaba, Bombay in the year 1841. This observatory was an outcome of a fortunate accident. Due to lack of proper facilities at Aden, the magnetometers meant for the observatory at Aden were diverted to the Astronomical observatory at Bombay in 1840 (both being under the control of East India Company). It took 5 years for working out the regular system of observations. The observations continued until 1905 without interruption. Initially the absolute values of horizontal intensity were determined by a unifilar magnetometer. Declination measurements commenced only in 1868. Self recording magnetographs were received in 1870 and the photographic recording commenced in 1872 and continued until 1905. The 60 years' data collected were analysed by Moos (1910 a, b) and the results were summarized in two volumes. These two volumes represent a monumental work (Chapman and Bartels, 1962).

Establishment of Alibag Observatory

In early 1900, Bombay decided to convert ordinary tram lines to electric traction. The proposed traction was within 3 km of the observatory site and hence the magnetic observations were bound to be seriously affected. Moos realized that the situation would worsen. Consequently, a farsighted decision was made to establish a new observatory at some protected site in the close neighbourhood of Bombay as early as possible, which would allow operation undisturbed from technical and urban influences for the foreseeable future. A suitable site was selected at Alibag (Lat $18^o37'$ N, Long 72^o 52' E) about 27 km SSE of Bombay, which is distant enough to be beyond the influence of electrification but near enough to have similar and comparable geomagnetic conditions, and after parallel operations of observatories for two years in 1904-05, the Colaba observatory was finally closed in 1906.

The absolute values of the geomagnetic field showed significant differences mainly due to the distances between the two locations (maximum in Z which was about 600 nT). The comparison of simultaneous observations revealed that the diurnal and seasonal variation of magnetic elements were in close agreement (to within +/- 2 nT for H and Z and 0.1' for D).

The variometers are housed in a special nonmagnetic room with effective insulation to keep the daily change in temperature inside close to zero and seasonal changes to within 3-4^o C. For thermal insulation a thick wall and a wooden wall with packed saw dust and air corridor were built.

Magnetic measurements at Alibag

Various instruments for absolute and variation measurements were used at Alibag observatory since its inception as discussed by Rangarajan (1992). The old kerosene lamped variometers were subsequently replaced by the modern variometers. Presently, Bobrov quartz sensors are used to get photographic records of variations in H, Z and D. This system is still functioning as the primary variometer and is extensively used. In 1994, Alibag observatory became a part of INTERMAGNET and a Narod ring core fluxgate magnetometer was installed. The data from this system is transmitted to Kyoto in real time using a satellite facility. Although the data is made available to the International community in near real time, the same magnetic weather could not be monitored at the station in real-time. Thus, in 2001 a Danish Meteorological Institute (DMI) fluxgate was installed to monitor magnetic weather in real-time. All the variometer sensors (Quartz, Narod, DMI) are installed in triangular positions in the same room with a separation of about 8 meters between them to avoid any interference.

The old Kew pattern magnetometers for measuring H and D and the Earth inductors for measuring I have been replaced by Quartz Horizontal Magnetometers (QHM) and Zero Balance Magnetometers (BMZ) in 1950. Now modern electronic magnetometers like a Declination-

Inclination Magnetometer (DIM) and Vector Precession Magnetometer (VPPM) are used to measure the absolute values of various components of the magnetic field. These absolute instruments are used to carry out observations at least twice a week (DIM every alternate day, and VPPM thrice a day) and are checked with different baseline values obtained from photographic and digital ordinates. If any shift of baseline data is noticed, a fresh observation is made to get a new absolute. After satisfying the validity of both the absolute and variations, the data is forwarded to the Indian Institute of Geomagnetism (IIG), Mumbai for further processing and publication.

Results and Discussion

The most important features of measurements carried out at Alibag during more or less the last hundred years are summarized here:

a) The annual means of H, Z and D at Colaba and Alibag Observatories for the period 1848 to 1995 are shown in the Fig.1. Abrupt changes seen in the year 1906 are due to the relocation of the observatory from Colaba to Alibag as mentioned earlier. It is clearly seen that H attained a maximum value in the year 1965 and since then it is decreasing at the rate of 20 nT/ year. Declination was easterly till the year 1926 and became westerly after that. It was at a westerly maximum around the year 1965 and then a gradual decrease was seen after that. Z attained its maximum value around 1930 and shows a near sinusoidal secular trend with an 80 year periodicity as reported by Bhardwaj and Rangarajan (1997). 11 year solar cycle variation or the jerk observed at many observatories in 1969-70 is not clearly evident at Colaba and Alibag observatories.

b) As mentioned earlier different magnetometers are used to carry out absolute measurements. Vector proton precision magnetometer (VPPM) is used to measure absolute H and Z while declination and inclination are observed by a Declination Inclination Magnetometer (DIM). The inclination measured with the DIM is used to estimate H and Z using total field (F) measurements with PPM. Quartz sensors are used as the primary variometers while the narod fluxgate magnetometer (INTERMAGNET) is basically a backup variometer for the observatory. Combinations of various absolute instruments and variometers are found to provide quite stable baselines. The base lines for some observations using these combinations are shown in Fig. 2. Monthly mean base lines for the period August 1995 to July 2001 are drawn in Fig.3. It can be seen that the quartz variometer has frequent adjustments due to seasonal changes.

c) As mentioned earlier three different variometers are operated simultaneously to avoid any data loss. The output of these variometers is seen to be well correlated even during severe magnetic storms. The magnetic storm of 23 March 2002 recorded at Alibag by the INTERMAGNET system is shown in Fig. 4. All the finer features of the storm are clearly evident in the magnetogram. The correlation between variations of individual elements H,Z and D of the same magnetic storm recorded by the INTERMAGNET and DMI fluxgate systems are shown in Fig.5. It is clearly seen that the two systems provide identical outputs during the disturbances.

Other services

The Alibag observatory caters also the needs of other observatories and organizations in calibrating their magnetic instruments. The observatory facilities are also used to calibrate magnetic aspect sensors used on board rockets, datum and landing compasses.

Conclusion

It is well known that the objective of a geomagnetic observatory is to record continuously the time variation of the magnetic field and to maintain accurate absolute standards of measurements over a long term.

The geomagnetic observations at Colaba which began in 1841, and became very regular and systematic from 1846, has given a continuous record till now - a span of more or less 160 years. This is despite the fact that the magnetic observatory shifted from Colaba to Alibag in 1904, and the continuity of the data recording has been maintained through simultaneous measurements during 1904-1906. The importance of such a long continuous time series of data can not be overstressed. From a mere magnetic observatory in 1904, Alibag has become a calibration centre where all the instruments used in geophysical and space studies are calibrated. The observatory is scheduled to have a celebration for completing 100 years of continuous measurements at low latitudes. Only three other observatories on the Earth share this honour but they are all at high latitudes. The data collected at this observatory has been extensively used in studying the daily, seasonal, annual and secular changes in the magnetic elements, day-to-day variability, the solar control and lunar daily variations of the changes. The vertical field measurements at Alibag are used to study the coastal induction effects as it is situated on the Arabian sea coast. The one minute digital data from this station is used in deriving ASY and SYM indices.

Acknowledgements

The efforts of the staff of Magnetic Observatory, Alibag, for getting good quality of data are highly acknowledged. The authors are thankful to Prof D.R.K.Rao for his critical suggestions.

References

Bhardwaj SK, G.K. Rangarajan , 1997. Geomagnetic secular variation at the Indian observatories, J. Geomagn. Geoelectr., 49, pp. 1131-1144.

Chapman S. and J. Bartels 1962. Geomagnetism Vol. II, Oxford University Press U.K., p. 941.

Moos N.A.F. 1910a. Magnetic observations made at the Government Observatory, Bombay for the period 1846 to 1905 and their discussion. Part I: Magnetic Data and Instruments, Government Central press, Bombay. pp.263.

Moos N.A.F. 1910b. Magnetic observations made at the Government Observatory, Bombay for the period 1846 to 1905 and their discussion. Part II: The phenomenon and its discussion. Government Central press, Bombay. pp.776.

Rajaram G. and R.P. Pisharoty 1998. The Earth’s magnetic field, Oxford and IBH Publishing Company Pvt. Ltd., New Delhi and Calcutta. pp. 373.

Rangarajan G.K. 1992. Proceedings of the symposium on Modern trends in geomagnetic at low latitudes, held at Bombay, India during 2-4 December 1991, pp xxvii-xxxvi.

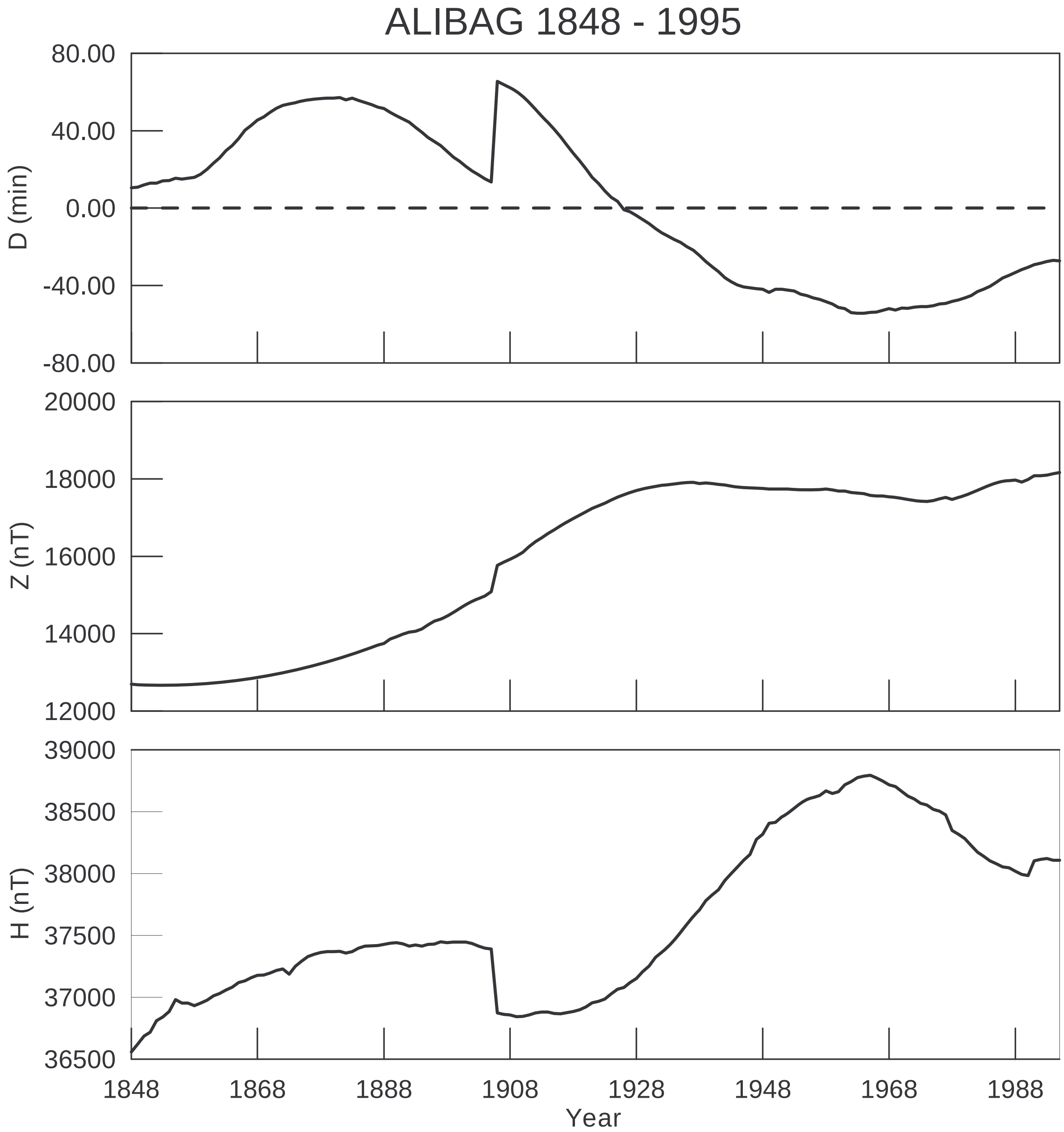

Fig.1: Annual mean of H, Z and D observed at Colaba and Alibag Observatory during the period 1848- 1995.

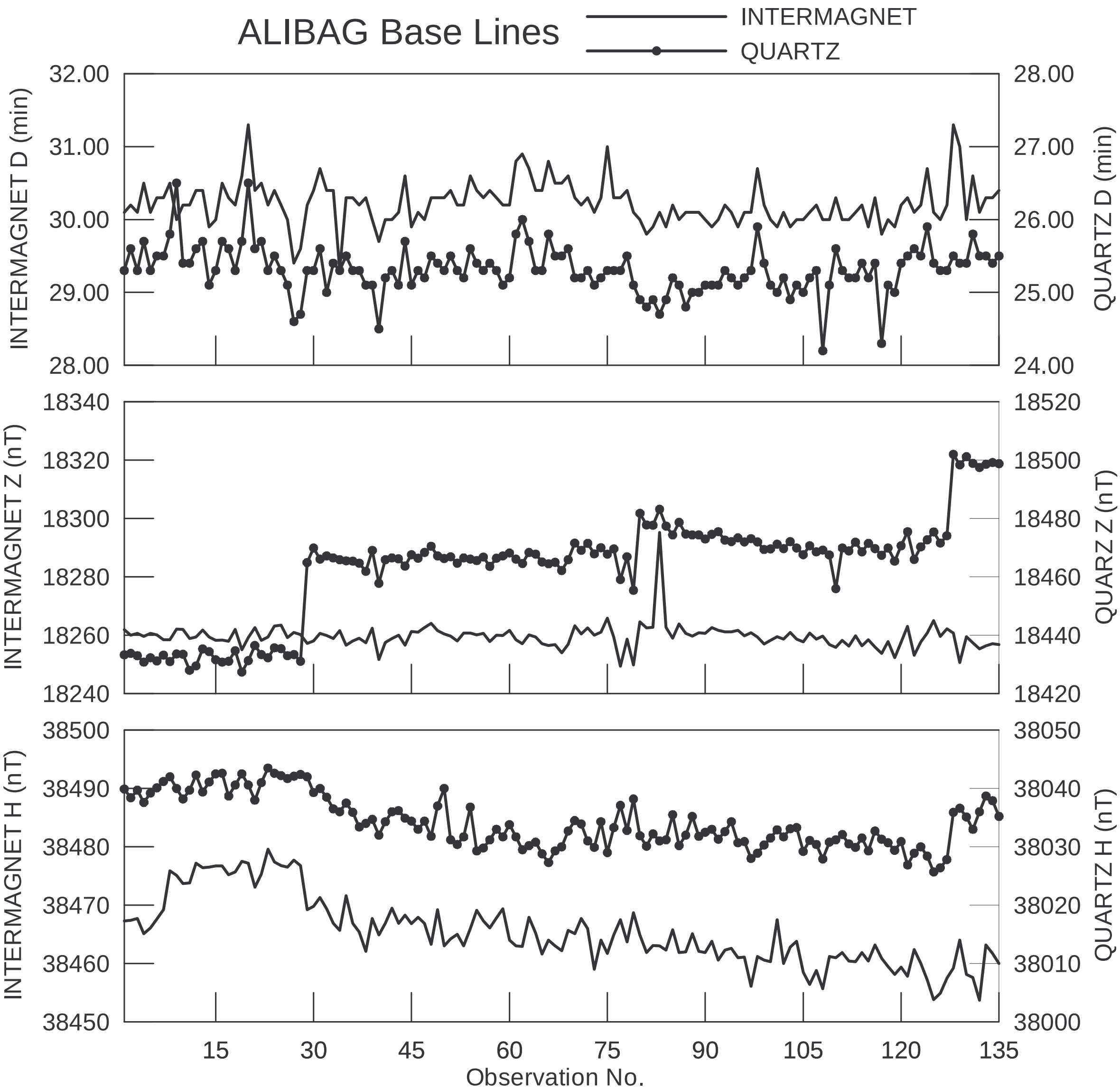

Fig.2: Base lines of H, Z and D computed using quartz and INTERMAGNET systems for some specific days. Absolute measurements were carried out with DIM and PPM.

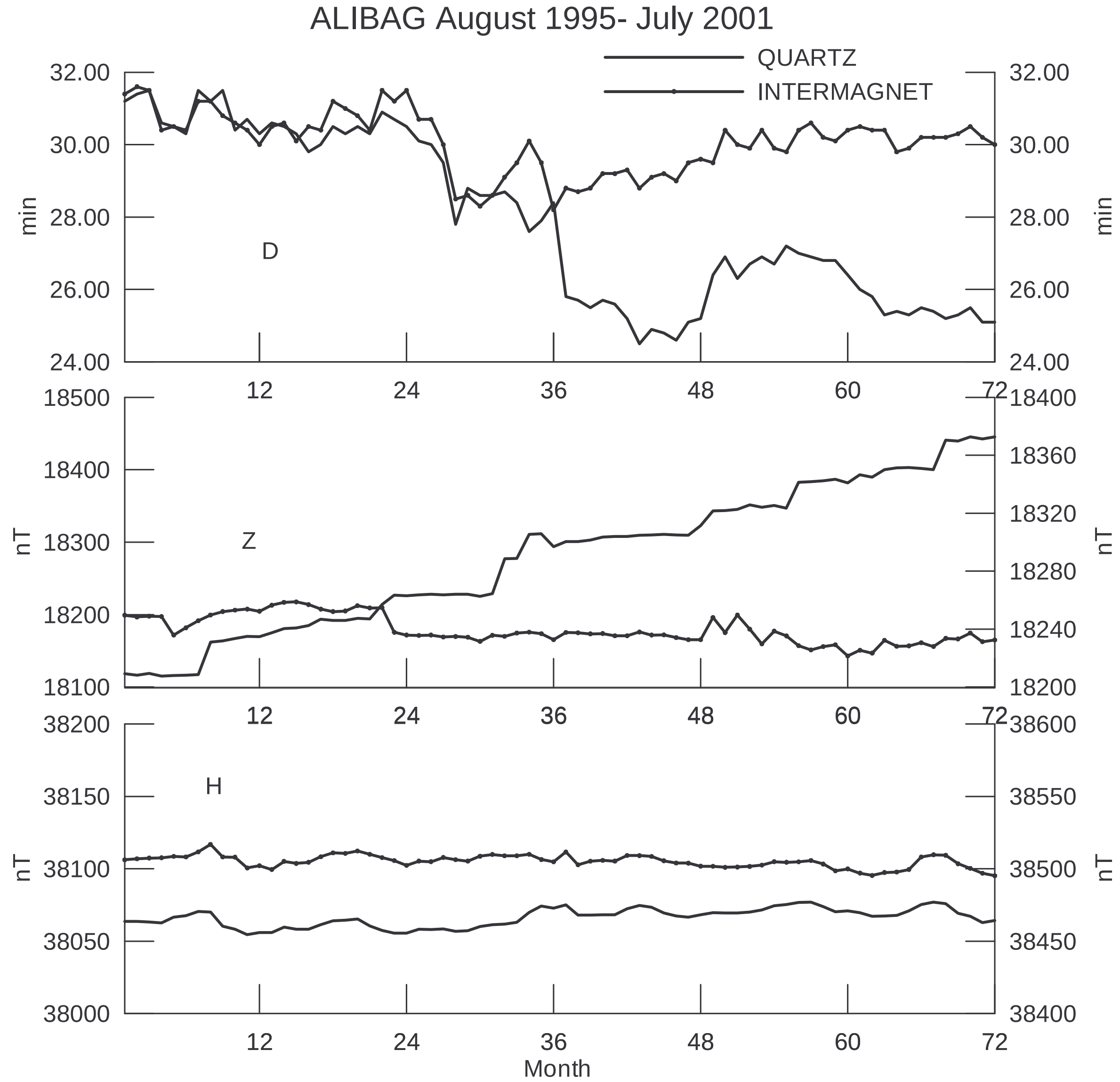

Fig. 3: Monthly mean Base line values of H, Z and D at Alibag during the period August 1995 to July 2001 with different measuring and recording systems.

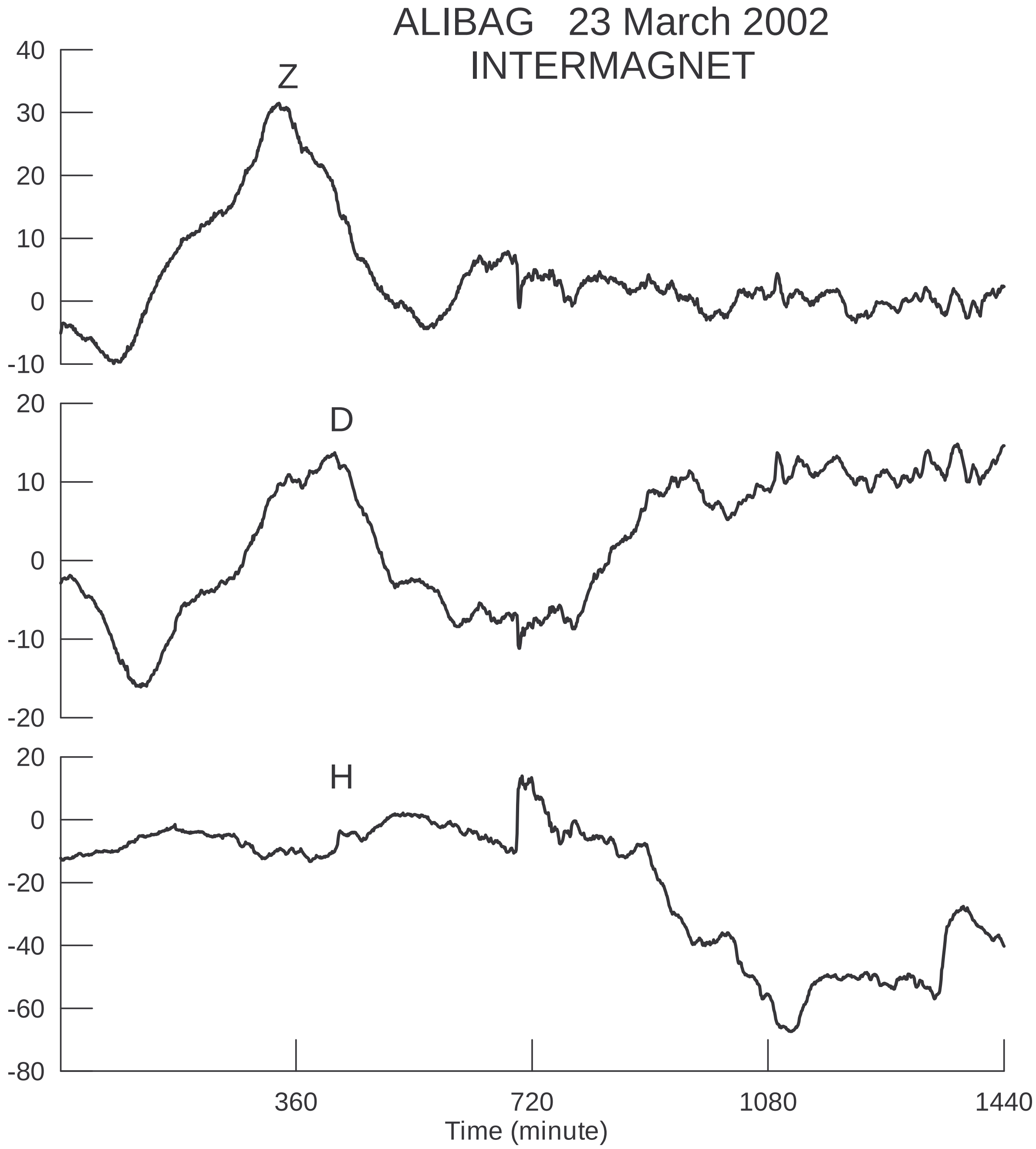

Fig.4: Variations in H, D and Z recorded by INTERMAGNET system at Alibag on 23 March 2002.

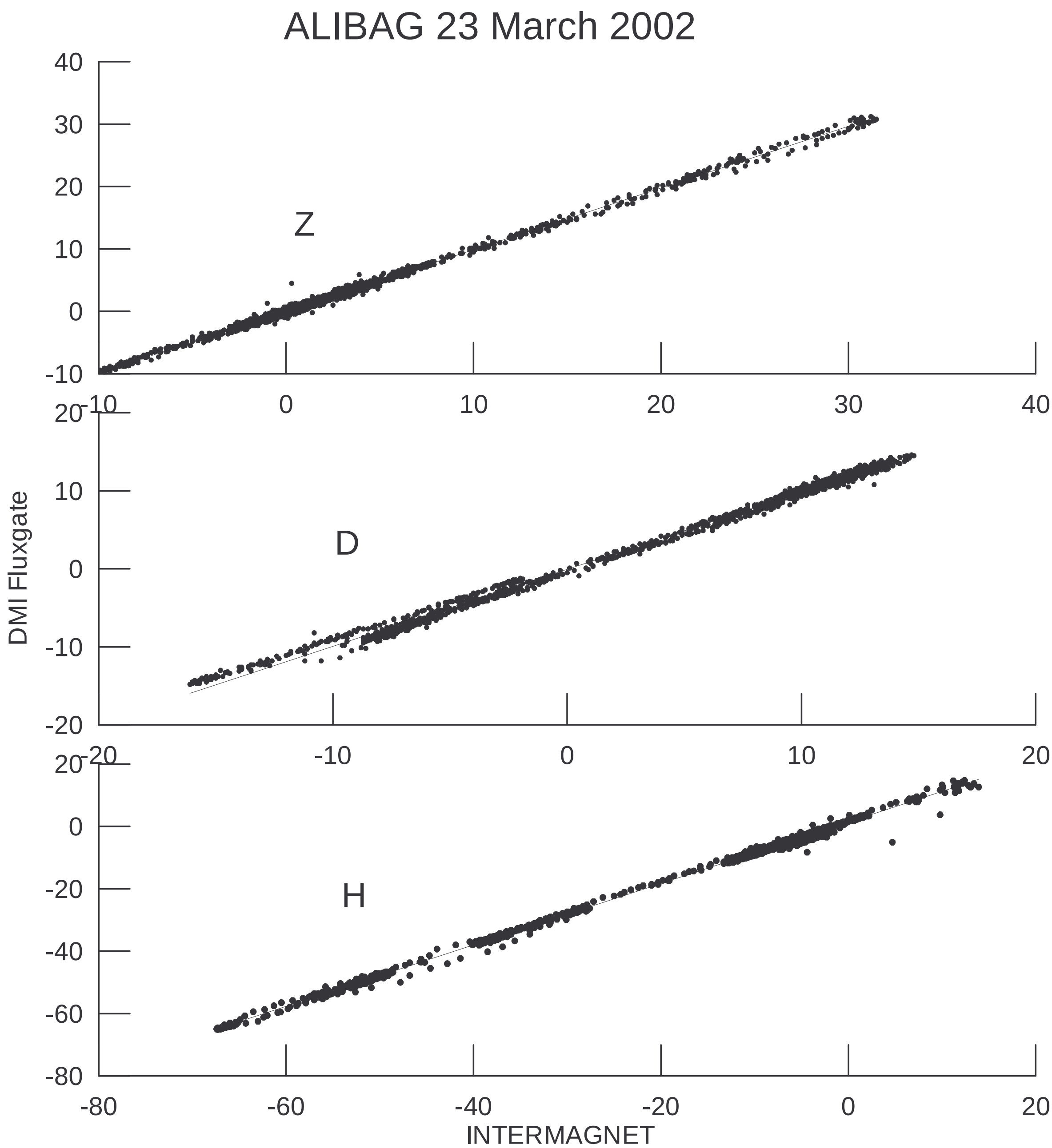

Fig.5: Correlation between H, D and Z on 23 March 2002 recorded by INTERMAGNET and DMI fluxgate magnetometers installed at a distance of 8 meters apart at Alibag . Correlation coefficients were 1.00 for all the three elements even during the magnetic disturbances.

The First Decade of INTERMAGNET Data.
A Producer and User View.

Alpar Kormendi, Papai Reformatus Kollegium, H-8500 PAPA, Marcius 15. ter 9, HUNGARY, e-mail: alpar44@freemail.hu

Mioara Mandea, Institut de Physique du Globe de Paris, 4 Place Jussieu, 75005 Paris, FRANCE, e-mail : mioara@ipgp.jussieu.fr

1. Introduction

The authors initialised the INTERMAGNET Project in the autumn of 1988 during an observatory meeting. A few pictures taken during the INTERMAGNET Pilot Experiment (between the US and UK) were presented. Military trucks moved big parabolic antennas on the pictures and the logo on the antenna consists of characters half a meter in size: ***US Airforce…*** The Berlin Wall seemed to be undestructible, yet in those days tanks were killing students on the Tian'anmen Square some months later. We were rather sceptic on the future of projects like INTERMAGNET. However, INTERMAGNET evolved into an important organization playing a definitive role in the community of magnetic observatories.

The present paper focusses on long-term stability using the base-lines of the variometers of selected IMOs whose data were published on INTERMAGNET CD ROMs between 1992 - 1999. As is noted in the INTERMAGNET Technical Reference Manual, 1999, an IMO must try to meet the following recommendations for vector magnetometers:

Resolution:	0.1 nT
Dynamic Range:	6000 nT Auroral & Equatorial
	2000 nT Mid Latitude
Band pass:	DC to 0.1 Hz
Sampling Rate:	1 Hz
Long term stability:	5 nT/year.

Considering these recommendations, we analysed the stability of base-lines over 7-9 years.

2. Data analysis
2.1. The observatories selected for base-line analyses

The "INTERMAGNET Magnetic Observatory Definitive Data 1991" or simply the first INTERMAGNET CD ROM, contains no base-line values. The base-line values are parts of the INTERMAGNET CD ROMs from 1992 due to the resolutions of the INTERMAGNET Operations Committee. On the second CD ROM (1992) there are data from 44 observatories of 10 countries (for comparison, the CD ROM 2000 has two volumes, with data of 78 observatories from 32 countries). The authors selected 38 observatories from the 1992 CD ROM and they added 11 observatories having continuous (undisturbed) records from 1993 – 1994 mainly to show their special instrumentation (like TPMs in Belsk or the Narod ring-core fluxgate variometer in Budkov, the only Narod magetometer in Europe) and at last the HMO of Hermanus observatory starting in 1995. The list of the 50 observatories included in the base-line analysis is presented in Table 1.

Table 1: Observatories used in this study.

Country	IAGA CODE	IMO B-L Start	Variometers
Algeria	TAM	1993	GEOMAG
Australia	CNB	1992	Narod
Canada	BLC	1992	Narod
	CBB	1992	Narod
	FCC	1992	Narod
	MEA	1992	Narod
	OTT	1992	Narod
	RES	1992	Narod
	STJ	1992	Narod
	VIC	1992	Narod
	YKC	1992	Narod
Central Africa	BNG	1992	La Cour/GEOMAG
Czech Repubic	BDV	1994	Narod
Denmark	BFE	1992	DMI
	GDH	1994	DMI
	NAQ	1994	DMI
Finland	NUR	1992	TPM/EDA DMI
	SOD	1992	TPM
France	AMS	1992	VFO31
	CLF	1992	TSA/VFO
	CZT	1992	VFO31
	DRV	1992	VFO31
	PAF	1992	VFO31
	PPT	1993	Vect. Proton GEOMAG
Germany	WNG	1994	EDA/DMI
Hungary	THY	1993	Quartz/FGA/DMI
Japan	KAK	1992	KASMER
	MMB	1993	FG (Japan)
Madagascar	TAN	1993	VFO31
New Zealand	EYR	1994	FG (DSIR)
Poland	BEL	1993	TPM
Senegal	MBO	1993	La Cour/VFO31

South Africa	HER	1995	FG (HMO)/ DMI
Sweden	LOV	1992	FG (TRIX)/DMI
United Kingdom	ESK	1992	EDA/DMI
	HAD	1992	EDA/DMI
	LER	1992	EDA/DMI
United States	BOU	1992	Narod
	BRW	1992	Narod
	BSL	1992	Narod
	CMO	1992	Narod
	DLR	1992	Narod
	FRD	1992	Narod
	FRN	1992	Narod
	GUA	1992	Narod
	HON	1992	Narod
	NEW	1992	Narod
	SIT	1992	Narod
	SJG	1992	Narod
	TUC	1992	Narod

Notes on variometers:
a) Flux-gate magnetometers: DMI, EDA, FGA = FG Afanasyev, TSA, VFO with linear core;

b) Narod has low noise ring-core;

c) GEOMAG has ring-core and linear core versions;

d) FG (DSIR), FG(HMO), FG(TRIX) are developed and/or manufactured by the observatory, HMO and TRIX serve as back-up system now, the geometry of core is not published on CD ROMs;

e) KASMER: Vector Magnetometers, Optically Pumped later Overhauser (GEM Systems) Proton magnetometers in Helmholz/Braunbeck coils;

f) La Cour: classical photorecording variometers;

g) Quartz: Bobrov-type variometers with photoelectric transducer, made in IZMIRAN.
TPM: Torsion Photoelectric Magnetometers from Poland (Bobrov Quartz variometers improved by J. Marianuk).

2.2. The compilation of base-line data.

The processing of annual base-line data is simple in principle: one should attach the **adopted** base-line files of the variometers from year to year. The practice was a little complicated and tedious, as:

- sometimes the site or the instrumentation of the observatory has been changed;

- sometimes the "philosophy" has been changed, what to build into the base-lines, producing thousands of nT jumps at change of year; a good luck that the observers prefer to shift the necessary interventions (intentionally made jumps), for instances re-adjusting the HDZ systems, to 31 Dec/1 Jan and to indicate that in the comments given to the base-line files, anyhow, these are break-points as well;

- sometimes we found that the comments on base-lines are copied from one year to the next year and the complementary information could be achieved from the printed yearbook (if it exists);

- it happened that we found irregularities – less or more than 365 lines in the file of a regular year.

All these facts make the programmatic compilation impossible. After visually checking the base-lines and compiled the files manually, we have a graphical database for a period of 7 – 9 years.

2.3. Some results and plots.

The presentation of 3 x 50 base-line plots is only possible as monographs. In the present paper, we chose some figures as examples of base-line behaviour. We summarises our analysis with the following remarks:

a) The 5nT/year recommended base-line stability is very difficult to achieve over the considered period. However, very good base-lines are provided by observatories as KAK and PAF (the required stability was achieved over the entire 9-year period) or by AMS, BDV, BEL, BFE, CLF, SOD. Figure 1 shows the plots for KAK, PAF and SOD.

b) For some observatories, when their out-dated variometers were replaced, their base-line stability improved remarkable, e.g. GDH, NAQ, THL, ESK, HAD, LER, LOV, NUR, WNG, BNG, MBO. Figure 2 shows the plots for ESK, BNG and MBO.

c) Nearly half of the magnetometers analysed in this study (23 from 50) are Narod Ring Core Fluxgates, they cover the whole North American Continent from the Caribbean and from Hawai to the vicinity of the North Pole. In accordance with their different locations, they have a wide variety of base-line drifts. Regardless of their individual behaviour they can be classified in two classes: a "USGS-type" and a "GSC-type" of irregularities. The only one European station, BDV follows the "canadian pattern".

Figure 3 shows the plots for GUA, CMO and OTT.

3. Is the base-line a measure of geomagnetic data accuracy?

The analysis of the base-lines suggests that the adoption of modern standards is one of the most difficult objectives of the INTERMAGNET program. The use of base-lines as quality indicator of the observatories can somehow be misleading, so we must treat it carefully.

Generally speaking, base-line values was truly the "Great Idol" for geomagnetic observatories in the second half of the 19th and in first half of the 20th centuries. In modern times this scope must be revisited. The so-called classical observatories collected data and tried to explain the phenomena existing behind the data, sometimes with a delay of years in decadal scale. In the present era, the physical models are much more evolved and we must put the emphasis on the prediction instead of the explanation (to forecast the space weather). The second important difference is that the classical observatories had some “aristocratic” characters (sometimes they litterally received their funds from the king, i.e. from noble personalities), but the modern observatory network tries to inforce the global characters: to move from a beautiful garden to subpolar, to subantarctic and now to submarine areas. One consequence of the global character is that there are nearly as many geological and climatic environments as observatories, given the constrains of the variation in base-lines.

Let’s take SOD declination (Figure 1) as an illustration as it is nearly horizontal. This Finnish observatory is situated on the granite of the Fenno-Scandinavian Shield. If a *djinn* (wicked or benevolent?) would place the whole observatory with its excellent instruments and staff onto the basaltic sheets of Kerguelen Island (CZT), the observatory base-lines would then onwards have a large annual variation amplitude inspite of unchanged technical and human factors.

Let’s analyse another aspect when using the adopted base-line as a quality indicator. On occasion, due to different systems, observatory staff sometimes has to intervene by introducing different base-line values. If it is done on Dec 31st, the method, applied in our analysis, just ignores it. If it is done in October, as for KAK declination 1998 (Figure 1), it appears as a jump, however the quality of data has not been changed.

Being producers and users of geomagnetic data, we could follow the efforts of the INTERMAGNET Operations Committee to find adequate definitions and requirements to balance between being “ideal” and “realistic” during the past ten years. To overcome difficulties originating in tradition and to extent the IMO network globally, the INTERMAGNET OpsCom focussed on “good base-line control” instead of “base-line”. The INTERMAGNET Technical Reference Manual gives instructions on data quality control in Chap. 6. Among several topics, it deals with the ratio of the *measured* base-line and of *adopted* base-line, ie the scattering of the individual points around the adopted base-line instead of the “geometry” of the adopted base-lines itself. It recommends the use of statistical parameters, variance and confidence limits, as quantitative measures of accuracy. Unfortunately, the statistical procedure requires fitting of adopted baselines by computer and not by hand, as it is done traditionally at many observatories.

Finally let’s quote the opinion of J. Bitterly — senior member of the INTERMAGNET Operations Committee, with a long observatory practice. He estimates that the standard accuracy for definitive data on the INTERMAGNET CD ROMs is ±5 nT. The explanation of “base-line stability” is in fact the comparison of the observed and the adopted base-line values. Considering a linearly interpolated point (a hypothetical point) between two succesive observed values, the difference between this interpolated (hypothetical) point and the adopted base-line must be less then 5 nT in 95% of cases. Once again, we underline the important role which absolute measurements play. Only a good set of absolute measuremensts, taken at a minimum twice a week, helps in getting stable and good base-line values for an observatory.

4. Conclusion

Magnetic observatories are characterized by the production of long-term continuous records of quality data, at the same site, suitable for studies of the secular variation of the main field, or external perturbations. The high quality of data is achieved by making regular absolute measurements in order to determine the base-lines for continuous recordings. INTERMAGNET program has now clearly demonstrated this. In more than 10 years INTERMAGNET has grown into an international federation of agencies running magnetic observatories.

Today, about half of the world’s observatories are members of INTERMAGNET. However, the quantity has not outdated the quality, and INTERMAGNET also helps to improve the quality and avalability of data. Nevertheless, users, as individuals or a team of research scientists, must investigate the data before using them in different studies.

- *Processed data are available from M Mandea or A Kormendi on request. Data are stored as Tab separated variables in individual text files for each observatory; the size of the 50 uncompressed text files is approx. 5MB.*

QUALITY IMPROVED by CHANGE of MAGNETOMETERS, 1994 - 1996
ESK: EDA replaced by DMI 1996, BNG: La Cour by GEOMAG 1996, MBO: La Cour by VFO31 1995

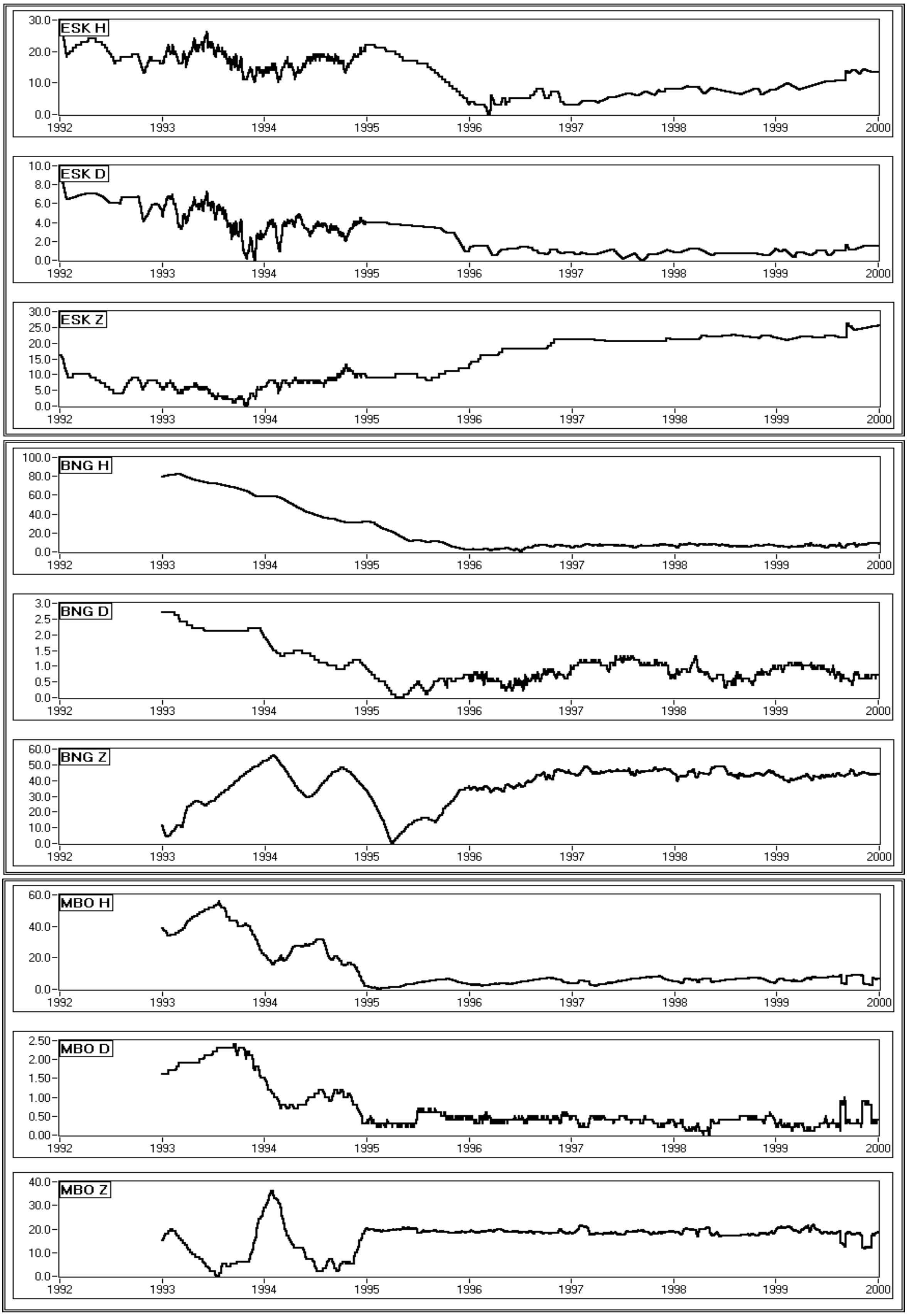

D in Arc Minutes, H, X, Y, Z in nT

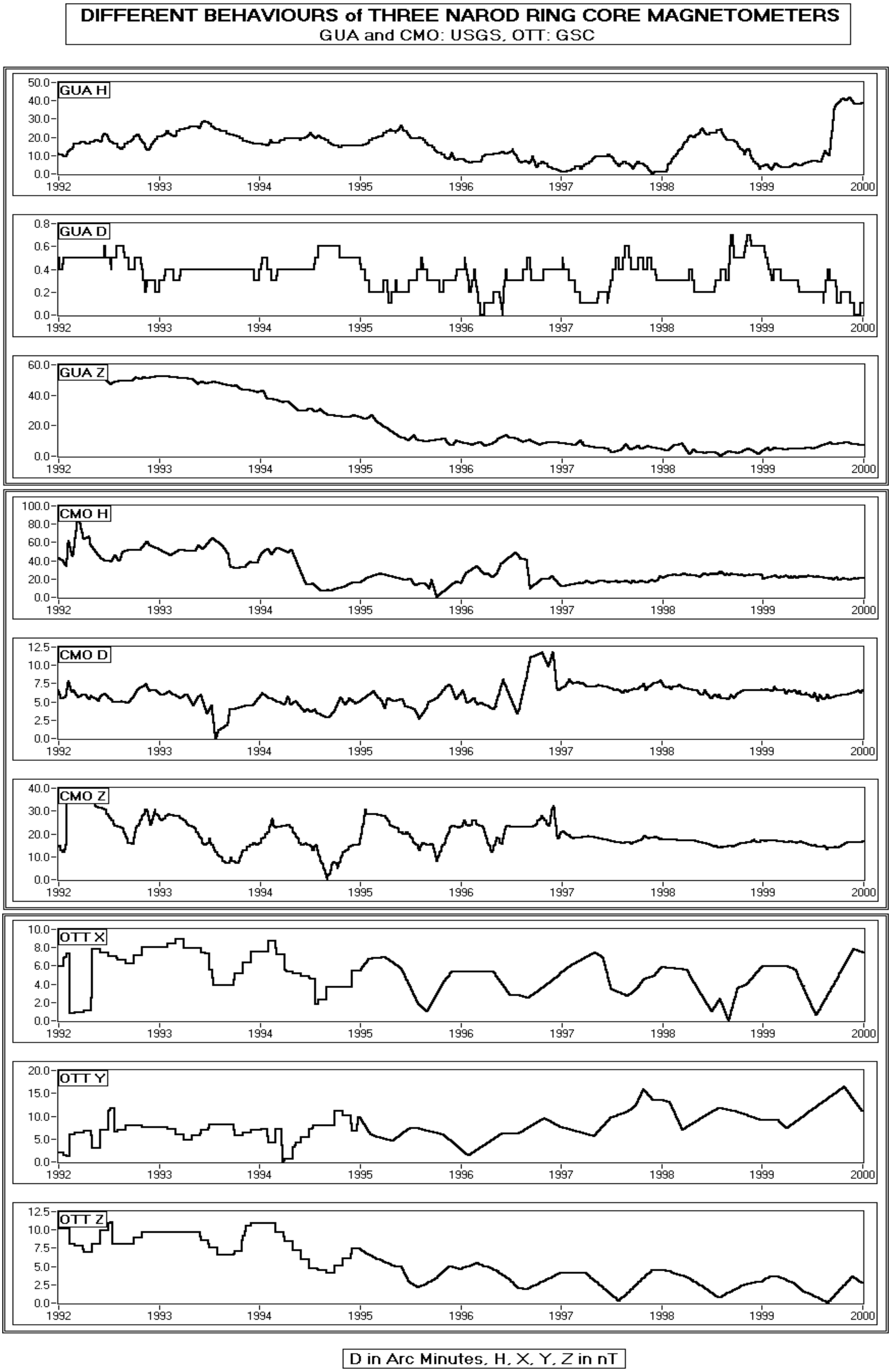

DIFFERENT BEHAVIOURS of THREE NAROD RING CORE MAGNETOMETERS
GUA and CMO: USGS, OTT: GSC
GUA H
GUA D
GUA Z
CMO H
CMO D
CMO Z
OTT X
OTT Y
OTT Z
1992
1993
1994
1995
1996
1997
1998
1999
2000
D in Arc Minutes, H, X, Y, Z in nT

French Contribution in Monitoring the Magnetic Field

M Mandea, J Bitterly, J-L Le Mouël (Institut de Physique du Globe de Paris, France), R Louat (Institut de Recherche pour le Développement, Bondy, France), J-J Schott (Ecole et Observatoire des Sciences de la Terre, Strasbourg, France)

Abstract

Three French institutions have combined their actions in the "Bureau Central de Magnetisme Terrestre" (BCMT) and are scientifically responsible for 15 magnetic observatories located in French territory or maintained in cooperation with different foreign countries. This effort represents the French participation to the INTERMAGNET program. The 14 observatories are located in Metropolitan France (CLF), French Polynesia (PPT), French Guyana (KOU), French sub-Antarctic Islands (AMS, CZT, PAF), Antarctica (DRV) and in Algeria (TAM), Madagascar (TAN), Lebanon (QSB), Senegal (MBO), Centrafrica Republic (BNG), Ethiopia (AAE), Vietnam (PHU), China (LZH). All these observatories operate under the same specifications (INTERMAGNET standards).

We describe the used instruments and procedure of geomagnetic observations. We also present the status of data transmission and statistics provided by the Geomagnetic Information Node (GIN) in Paris. We finally discuss the comparison of the baselines provided by these observatories, in term of instrument quality and data accuracy.

The DIDD as Quasi-Absolute Instrument : Reliability and Limitations

J.J. Schott, A. Pérès and J.M. Cantin (Ecole et Observatoire des Sciences de la Terre, Strasbourg, France)

Abstract : a complete algorithm for processing DIDD measurements is presented and illustrated with synthetic as well as real data. In the present state of the art, the major drawbacks are the extreme sensitivity of the instrument to temperature variations and the steady drift of the variometer base lines calculated with the DIDD records due to the drift of the DIDD reference frame.

1. Introduction

The development of unmanned ground magnetic observatories remains a major concern and challenge for the geomagnetic community. At the observatories equipped with fluxgate sensors, the accurate recording of the total field (not only of its variations with respect to an arbitrary base line, as in chains of magnetic observatories devoted to external field studies) relies upon the accurate calibration of the sensors, which cannot be done easily once the instrument is in operation. The DIDD (Deflected Inclination, Deflected Declination –see Herzog (1990) for the origin of the acronym) -instrument analysed in this paper originates from an idea first proposed by Alldredge (1960). It was developed further by Sauter, 1991, and the Geophysical Institute of Budapest, Hungary, (Csontos et al., 2001), with the hope that it could become a reliable absolute instrument, needing no manual absolute measurements for its calibration. The presently available proton magnetometers allow high rate sampling and therefore high rate calculation of the total magnetic field with the DIDD device (every 5 seconds, for instance) so that the DIDD could by itself provide the magnetic measurements required from a standard observatory. At E.O.S.T., Strasbourg, due to the particular operation of the magnetic observatories of AMS, CZT, DRV, PAF, and observers been replaced every year, the aim is to incorporate a DIDD-type device and abandon the need for frequent manual absolute measurements and dispose of independent, reliable, fluxgate base line estimations and to interpolate accurately between two successive manual measurements and thus provide a control on these measurements.

2. Description of the algorithm

2.1 Reference frames

Four reference frames are involved in DIDD record processing. The main reference frame is the usual geographical frame OXYZ, the three others being defined with respect to it. As the variometer records are involved in the processing too, its reference frame $OX_vY_vZ_v$ has to be taken into consideration (in a standard orientation, OX_v and OY_v are horizontal, and orientated approximately along the local magnetic North and East, respectively. We assume here that the axes of the three sensors are orthogonal). As to the DIDD, for computational convenience, we define two reference frames: one, which we will refer to as "intermediate" and designate by $Oe_1e_2e_3$, is an orthonormal frame, with Oe_1 approximately along the field direction (hence with positive or negative inclination, according to the hemisphere), and Oe_2 horizontal. Its orientation conforms to the theoretical orientation of the instrument. In this ideal case, Oe_2 and Oe_3 would be orientated along the D-coil and I-coil axes respectively. In addition, Oe_2 and OY_v would be perfectly aligned. The real situation may be different, due to imperfect orthogonality of the D-coil and I-coil axes and to misalignment between Oe_2 and OY_v. In order to account for these various defaults, we define a so-called "physical" reference frame $Oe'_1e'_2e'_3$ where Oe'_2 and Oe'_3 are along the D-coil and I-coil axes respectively, Oe'_1 being orthogonal to each of them. In the most general case, Oe'_2 is not horizontal, Oe'_2 and Oe'_3 are not orthogonal and there is a deviation between the horizontal projection of Oe'_1 and OX_v, although the angles are supposedly small.

2.2 Field and base line computation

Let us assume, is this section, that the intermediate and the physical reference frames are known. This assumption means that **R**, the matrix rotating the geographical reference frame towards the intermediate frame, and the matrix ρ mapping the intermediate reference frame onto the physical frame are known. Define **X** as a vector in $\Re^5$ built up with the three components of the field in the $Oe_1e_2e_3$ reference frame and the two deflection fields applied along the D-coil and I-coil axes respectively. **X** is the solution of the implicit equation:

$$\mathbf{R_X}.\mathbf{X} = \mathbf{G}(\mathbf{X},\mathbf{p}) \qquad (1)$$

where $\mathbf{R_X}$ is a 5x5 identity matrix, apart from the terms $R_X(2,1) = \rho(1,2)$, $R_X(2,2) = \rho(2,2)$, $R_X(2,3) = \rho(3,2)$, $R_X(3,1) = \rho(1,3)$, $R_X(3,2) = \rho(2,3)$, $R_X(3,3) = \rho(3,3)$. **G** is a function mapping $\Re^5$ to $\Re^5$ essentially defined in Schott et al (2001a), apart from terms accounting for field variation during the DIDD sequence defined in that paper. **p** stands for the five parameters determining the orientation of the physical reference frame with respect to the intermediate frame (three Euler angles plus one angle accounting for the non-orthogonality of the Oe'_2 and Oe'_3 axes) and the misalignment between Oe_2 and OY_v. Equation (1) may be solved iteratively by the fix-point method (Bass, 1971), starting from the approximate solution where $\mathbf{R_X}$ is the identity matrix and the field variations are neglected (note that this is the first-order solution given, for instance, in Sauter, 1991). The iterative process, which must be repeated for each DIDD sequence, converges within two or three iterations. Having found the total field components in the intermediate reference frame, it is trivial to compute them in the geographical frame thanks to the knowledge of the matrix $\mathbf{R}^{-1}$. The variometer base lines are first computed in the intermediate reference frame after mapping of the relevant variometer components onto that frame, and then rotated back to the geographical frame.

2.3 Estimation of the intermediate reference frame orientation

The estimation of the intermediate reference frame is based upon the comparison of simultaneous true absolute measurements made in the geographical reference frame and components calculated in the intermediate reference frame. In order to compare accurately the two sets of data, the field difference between the location of the DIDD and the absolute measurements has to be known, especially when the field is heterogeneous. The algorithm yielding the estimation of the angles D_0, I_0 defining the orientation of the Oe_1 axis is described in Schott and Leroy, 2001(b).

2.4 Estimation of the physical reference frame orientation

This estimation includes the angle between Oe_2 and OY_v, that is the estimation of the whole parameter vector **p**. It is based upon the observation that, if **p** is wrong, the base lines and deflection fields display disturbances strongly correlated with the field variations. Hence, the estimation of **p** is all the more reliable as the level of field disturbance is high during the interval selected for the estimation. The estimated **p** minimizes the functional

$$\sigma^2 = \frac{1}{5}\sum_{i=1}^{5}\frac{1}{N-1}\sum_{n=1}^{N}\left(S_{i,n} - \tilde{S}_i\right)^2 \qquad (2)$$

where $S_{i,n}$ include the base line components in the intermediate reference frame and the deflection fields, that is five time series indexed by n, and $\tilde{S}_i$ stands for the mean value of each of these time series over the selected interval. σ^2 is non-linear in **p**, and therefore an iterative scheme is needed, starting from an initial guess of **p**, which may be 0. In addition, the solution is not unique, due to the fact that the orientation of the physical reference frame, which is unique indeed, is defined by the product of the matrices **R** and ρ defined in section 2.2. Each of these matrices can be changed to some extent without modifying the orientation of the physical frame. In order to stabilize the inversion process, we may add a constraint consisting of minimizing the matrix which rotates the variometer reference frame towards the physical frame, with respect to its expression when **p** is null. This constraint leads to the incorporation of a quadratic form $\mathbf{p}^t\mathbf{.W.p}$, where **W** is a 5x5 matrix resulting from second order development of ρ with respect to **p**.

3. Influence of temperature variations

As a result of the processing of DIDD records provided by PAF observatory, the base lines and deflection fields show a daily variation which may be attributed to temperature influence. We have noticed that the base line and deflection field variations are quite similar. This observation supports the use of the deflection field variations to model the base line variations. The model would be merely:

$$\tilde{b}_{i,n} = c_i + \alpha_i \tilde{u}_{D,n} + \beta_i \tilde{u}_{I,n} + \varepsilon_i \qquad (3)$$

where $\tilde{b}_{i,n}$ stands for the ith base line component in the intermediate reference frame, smoothed by a polynomial approximation in order to remove the noise due to round-off errors and residual influence of field variations, $\tilde{u}_{D,n}$ and $\tilde{u}_{I,n}$ being the smoothed D-coil and I-coil deflection fields respectively. It is interesting to note that this simple model is fairly efficient in removing the daily variations observed in the base lines. However, this modelling may change the daily mean value of the base line, according to the reference level adopted for the deflection fields. Our conservative approach is to choose the daily mean value of the deflection fields as reference level for the daily variations brought about by temperature changes.

4. Examples of processing

The algorithm outlined in sections 2 and 3 has been tested on synthetic values built up with real variometer records and real base lines yielded by the PAF observatory, with 0.1nT Gaussian noise added, and given parameters D_0, I_0, **p** and deflection fields. In order to simulate temperature variation, **p** has been modulated with a sinusoidal daily variation, as well as the deflection fields (it is interesting to note that a variation of **p** alone has no influence on the calculated deflection field. On the other hand, provided that the deflection fields are constant over a DIDD sequence, their variation does not corrupt the calculated base lines).

Figure 1 illustrates the behaviour of the calculated base lines when the parameters **p** are set to 0 instead of their actual values and when the influence of the temperature is not accounted for (solid curves). The daily sinusoidal variation as well as the field variations clearly disturb the base lines from their expected constant values. The removal of the temperature influence by the modelling outlined in section 3, partly reduces their daily variation (dash-dot lines). The polynomial fitting of the base lines, preliminary to this modelling, is shown by the dashed lines. Crosses show the values of simulated manual absolute measurements, corrupted with a gaussian noise of 2nT.

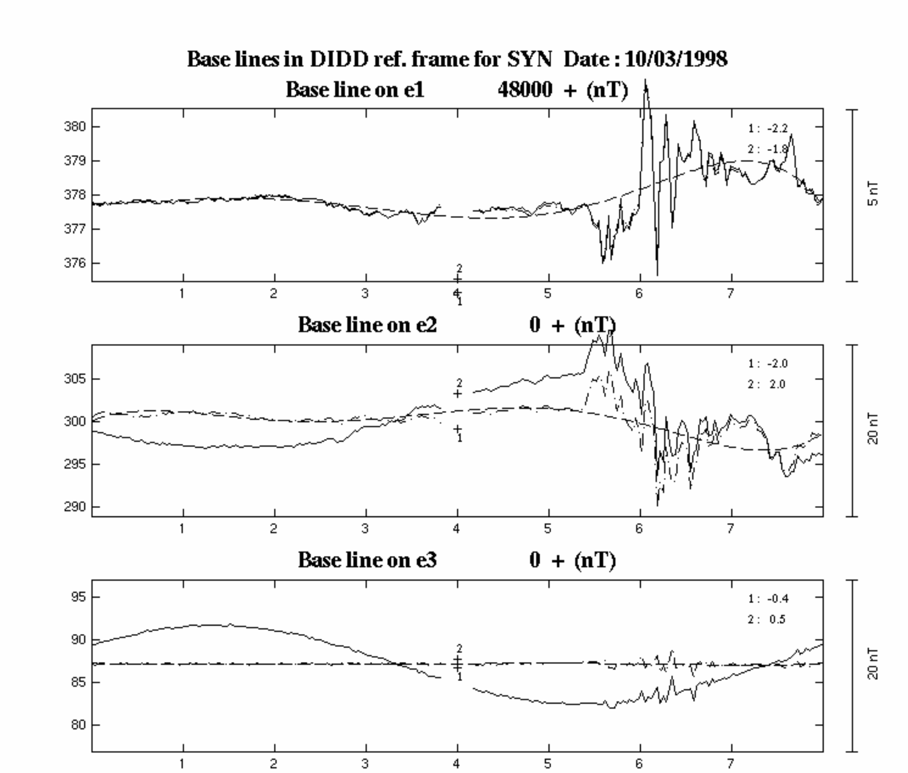

Fig.1 Synthetic example of DIDD data processing without physical reference frame estimation. See text for legend.

Figure 2 show the results obtained after estimation of the parameters **p**. **p** is estimated on the interval 16h-23h59 which is the most disturbed part of the magnetic field for the selected day. The solid curves display the results when the temperature influence is not removed whereas the dash-dotted lines show the final results when the algorithm is fully applied. This is of course the result we aim at, i.e. the base lines are horizontal and the agreement with the manual base values is excellent.

In figure 3 are displayed, in stereographic projection, the true and estimated directions of the intermediate and physical reference frames. Full symbols (resp. open symbols) stand for positive (resp. negative) inclinations. On the scale used, the true and estimated directions of the physical reference frame cannot be distinguished. The deviation of the estimated intermediate reference frame from the true one illustrates the

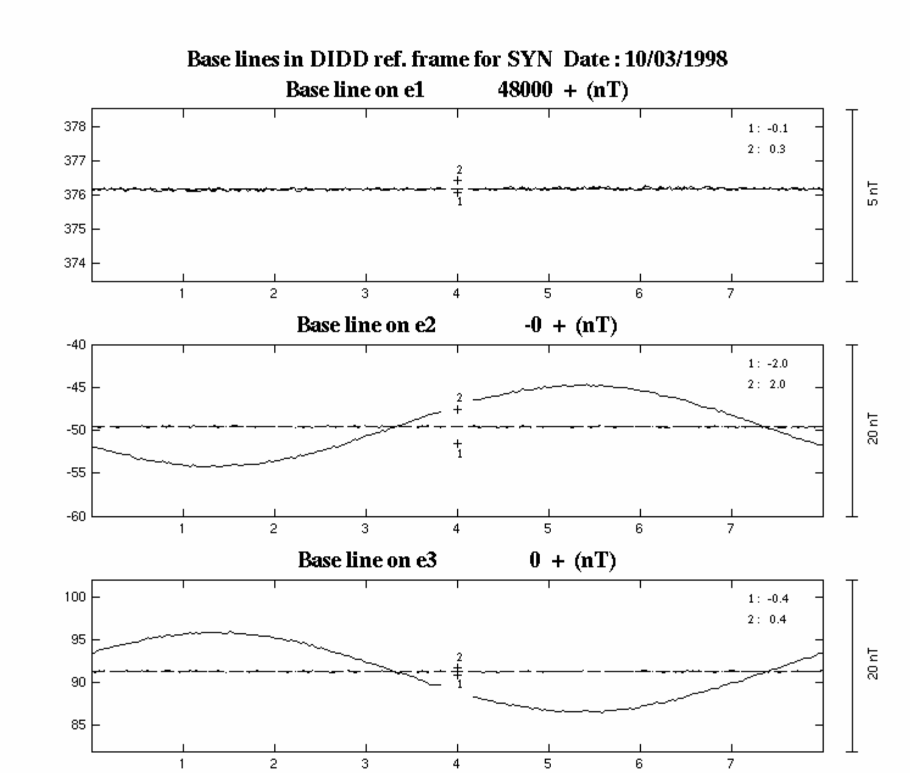

Fig.2. Synthetic example of DIDD data processing with physical reference frame estimation. See text for legend.

non-uniqueness of the inverse problem involved in the separate estimation of the matrices **R** and ρ, mentioned in section 2.4**.** On the other hand, the excellent agreement between estimated and true physical reference frames demonstrates the uniqueness of the product
R . ρ.

Figures 4 and 5 are similar to figure 1, but with an example of real data, provided by PAF observatory. Figure 4 displays the results of the processing when the parameters **p** are not estimated (their values are kept to their initial guess, i.e. zero). In figure 5 are shown the base lines obtained when the processing includes these features. The disturbances correlated with the field variations (especially during the interval 19-24h) and the daily variations due to temperature

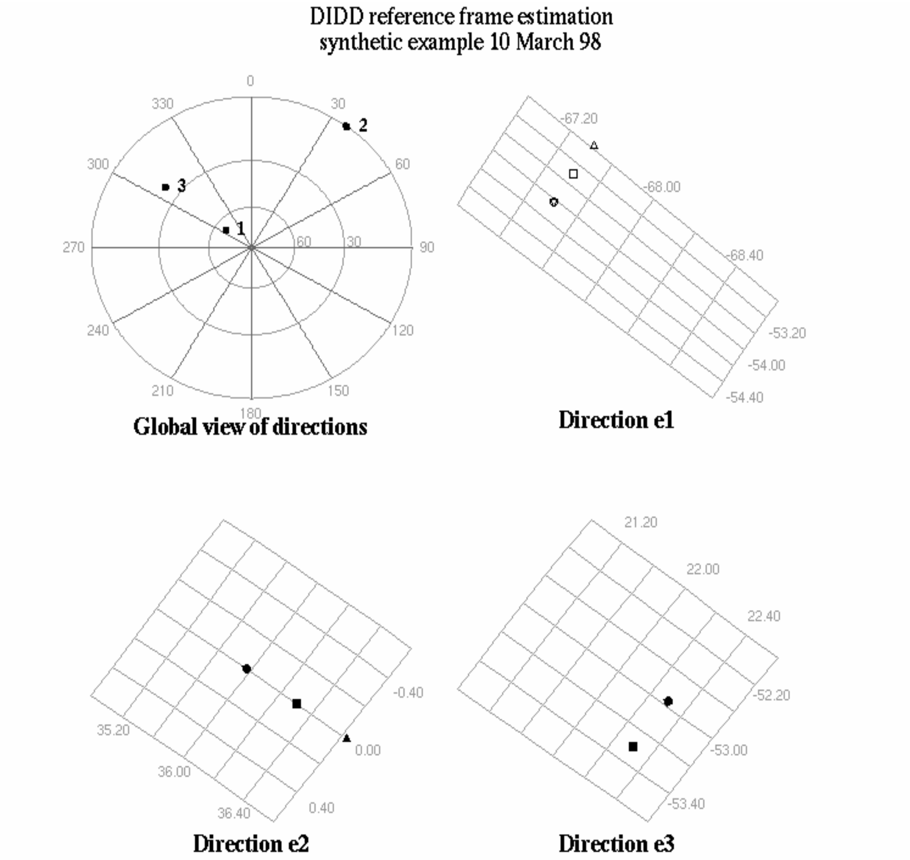

Fig.3. Directions of the intermediate and of the physical reference frame axes. Square: true intermediate reference frame; upward pointing triangle: est. int. r.f.; circle: true physical r.f.; downward p. triangle: est. phys. r.f. See text for further comments.

influence are reduced within about 0.3 nT standard deviation. However, we note that the agreement with the base values yielded by absolute measurements is not completely satisfying, especially in H and Z. In our opinion, the persistent misfit is due to inaccurate measurements of the field difference between the absolute measurement pillar and the location of the centre of the DIDD coil system. The discrepancy could be removed by a slight change of the inclination of the field at the DIDD location.

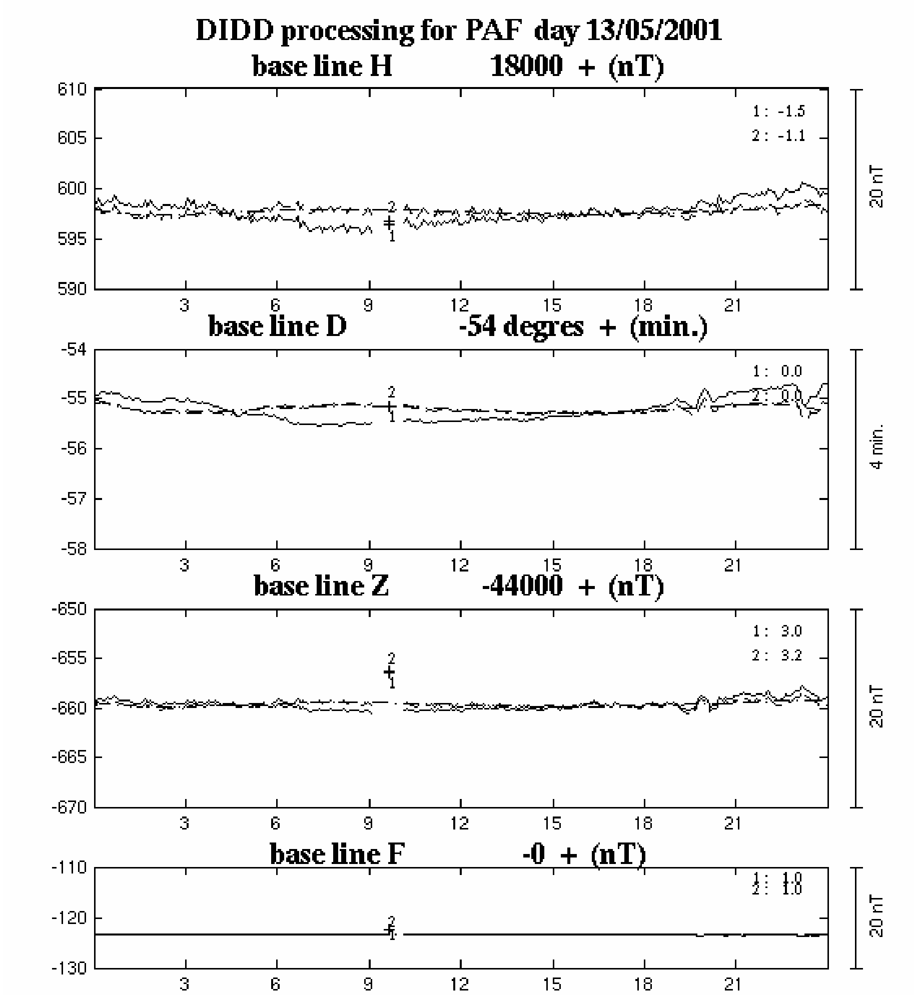

Fig 4. Example of processing with real data. Note the disturbances in the 19-24h time interval due to wrong values of parameter **p** (they are set to zero). Same legend as fig. 1.

Figure 6 shows the hourly mean values of the base lines estimation with the DIDD, without (solid curves) and with (dashed lines) removal

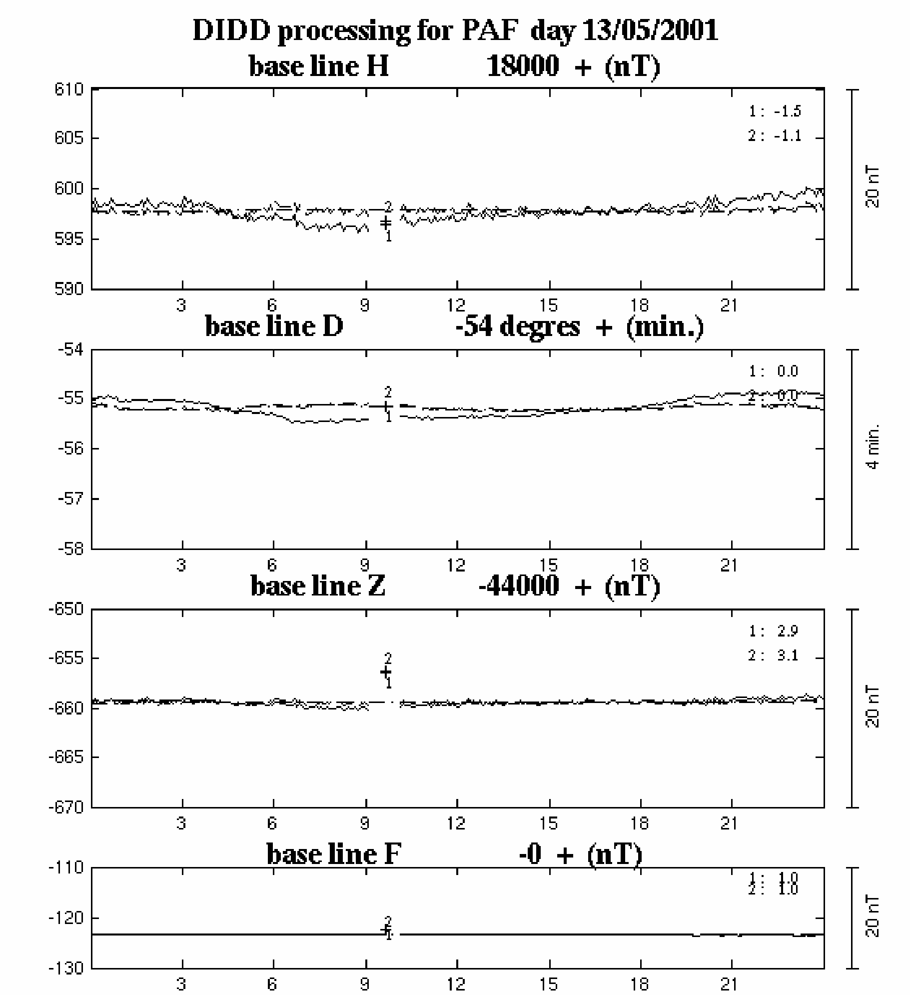

Figure 5. Example of processing with real data, and estimation of the parameters **p**. Note that the correlation with the field variation in the interval 19-24h observed on fig.4 is nearly removed. Same legend as fig.1.

of temperature influence. The results yielded by the modelling of temperature effects are better but not completely satisfying, particularly due to the jumps between two successive days. These jumps are likely to be due to slight variation in the inclination I_0. This assumption

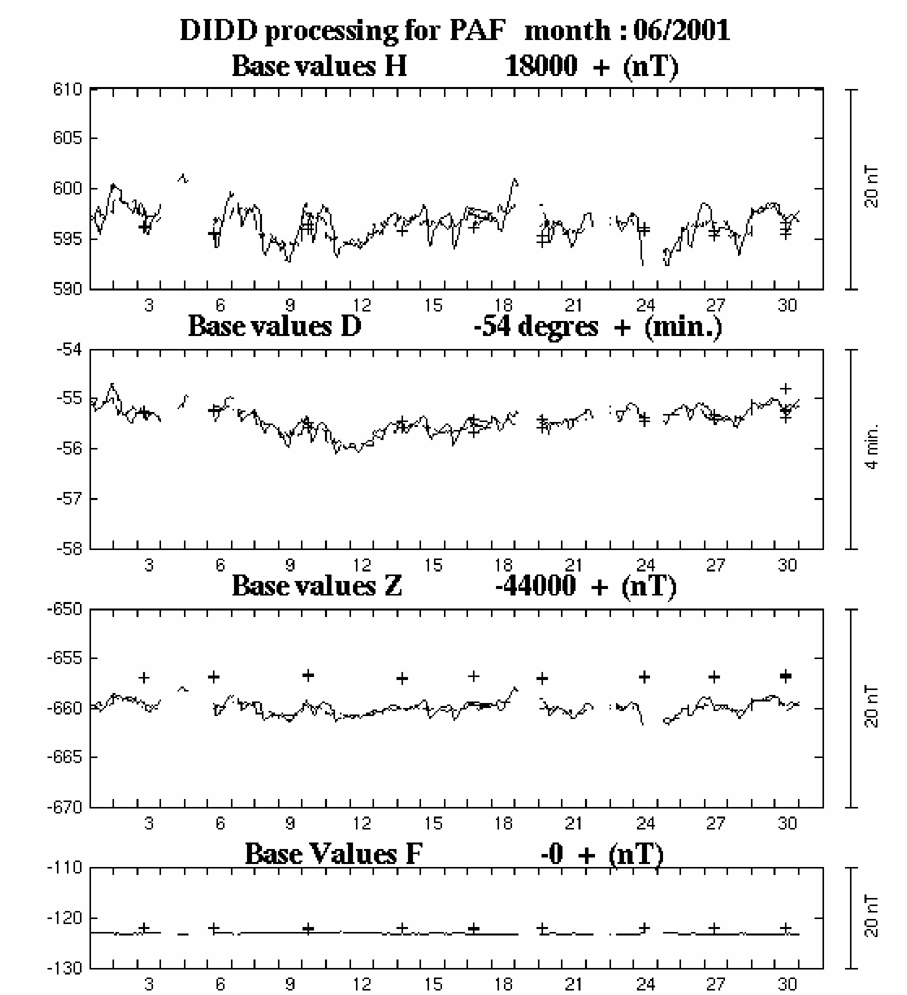

Figure 6. Hourly mean base values for June 2001, PAF observatory. Solid curves: without temperature correction; dashed curves: with temperature correction. See text for further comments about the jumps and discrepancies with the manual base lines.

is supported by the fact that the jump in H is between two and three times larger than the jump in Z. The jump in H is proportional to $\sin I_0$, which value is 0.93 for I_0 equal to 68 degrees, whereas the jump in Z is proportional to $\cos I_0$, which is 0.37. These results show the limitations of the temperature influence modelling: it could be safely carried out only thanks to a knowledge of the continuous variation of the intermediate reference frame orientation (especially inclination). In turn, this knowledge would require frequent absolute measurements, which is precisely what we would avoid with the use of the DIDD.

5. Conclusions

The synthetic as well as the real examples show the efficiency of the algorithm outlined in sections 2 and 3 for the processing of the DIDD data and the estimation of the various parameters needed to assess the orientation of the reference frames. The ability of estimating the orientation of the reference frames (intermediate and physical) is an advantage above the DIDD instrument over other recording systems, for instance triaxial fluxgate variometers, which orientation is more difficult to know within a few minutes with respect to the geographical reference frame. In addition, its calibration is easy to carry out, whereas the calibration of the triaxial variometer is hardly done once the instrument has been installed, the usual check being to compare calculated and estimated total field intensity.

However, the DIDD instrument has obvious weaknesses, which ultimately refer to its high temperature sensitivity. The influence of the temperature variation is probably twofold: on one hand, it induces a variation of the coil size which can be monitored by the variation of the deflection fields. On the other hand, it entails a variation of the orientation of the reference frame (both effects being possibly linked to an interaction between the variation of the coil size and the base which the external coil rests on). The first deformation has no influence upon the base lines as long as the deflection fields remain constant over a sequence of measurements. But the second effect is most inconvenient. Our tentative modelling of the temperature induced drift relies precisely on an interaction between the two kinds of deformation. The results show that it is only partly efficient, so that it is recommended to avoid the temperature influence as much as possible. One way is to improve the mechanical stability of the device (fixing of the coils of the sensor, of the way the basement supports the external coil), another way is to put the DIDD in a thermally insulated box with accurate temperature control. A third way is to suspend the coil system instead of placing it on a basement (Hegymegi, this issue), which would probably disconnect the coil size variation from the orientation variation.

Acknowledgements. The discussion of the advantages and drawbacks of the DIDD benefited from the experience of the Tihany observatory team (L. Hegymegi, A. Csontos and B. Heilig) who are gratefully acknowledged. This work was supported by the Centre National de la Recherche Scientifique (CNRS), UMS 830, and by University Louis Pasteur, Strasbourg, PPF Observatoires.

References

Alldredge, L.R., 1960: A proposed automatic standard magnetic observatory. J. Geophys. Res., **65**, 3777-3786.

Bass, J., 1971: Cours de Mathématiques, tome 3. Masson et Cie, éditeurs, 405 p.

Csontos, A., Hegymegi, L., Heilig, B., and Körmendi, A., 2001. The test results of the delta „I“ delta „D“ (DIDD) measurement system at the Tihany Geomagnetic Observatory of ELGI. Contributions to Geophysics & Geodesy, **31**, 83:90.

Herzog, D.C., 1990: An evaluation of the accuracy of geomagnetic data obtained from an unattended, automated, quasi-absolute station. Phys. Earth Planet. Inter. **65**, 112-118.

Sauter, E. A., 1991: An automatic, quasi-absolute, geomagnetic calibration system. U.S. Geol. Survey, open file report 91-350.

Schott, J.J., V. Boulard, Peres, A., and Cantin, J.M., 2001a. Magnetic component measurements with the DIDD. Contributions to Geophysics & Geodesy, **31**, 35:42.

Schott, J.J., and Leroy, P., 2001b. Orientation of the DIDD magneto-meter. Contributions to Geophysics & Geodesy, **31**, 43:50.

Absolute measurements at Wingst Observatory – a retrospective view of the past few years

G. Schulz (Wingst Geomagnetic Observatory, Germany)

Abstract

Besides a first generation proton vector magnetometer (Askania/Varian), a second generation instrument (Zeiss/Magson) has been in use at Wingst observatory since the late 1990s. Together with a DI-flux (Zeiss/Bartington), a set of three independent devices for base-line measurements has been available since then.

During this period, comparative measurements reduced according to the variations of the observatory's highly stable Danish FGE-type systems have been evaluated. The scattering of base-line values seems to reflect inadequacies of the absolute instruments and/or interference at the location of the absolute house rather than fluctuations of the variometers used.

Short-term series of consecutive observations show the performance of the three absolute devices of different generations and different techniques.

Key words: Instruments, absolute measurements, comparison measurements

Introduction

In order to monitor the stability of the observatory standard, two methods have been used at Wingst in the past:

1. Direct comparisons:

Fig 1 shows the results of comparative measurements which have been carried out in the past two decades either using Wingst instruments at other observatories (circles) or instruments from other observatories at Wingst (dots). Ignoring some outliers and assuming - in the worst case - that all differences are attributable to errors at our own observatory, the following measurement uncertainties are obtained for Wingst:

$\delta\mathbf{D} = 0.22'$ $\delta\mathbf{I} = 0.16'$ $\delta F = 1.2$ nT

2. Indirect comparisons:

A similar order of magnitude is obtained using the so-called momentary value comparison between European stations (Schulz, 1998) as a basis.

$\delta\mathbf{D} = 0.2'$ $\delta\mathbf{F} = 1$ nT

Momentary values are samples taken simultaneously during quiet night times on the ten least disturbed days of the month. Fig 2 shows the 1994 standard deviation of the monthly mean differences of D between Wingst and the other participating observatories, plotted against their distance from Wingst (dots). Differences in the secular variations, which may falsify the results, are assessed and eliminated beforehand.

In our case, the axis of intercept of the regression line is of interest. It forms the extrapolated value of the seasonal fluctuation at WNG and constitutes a measure of the uncertainty of the Wingst D standard.

While a direct comparison allows conclusions as to the quality of the base-line instruments' absolute scale, an indirect comparison via momentary values only provides data on their relative fluctuations. However, the latter also covers changes in the environment of the measurement location (absolute house), which means both methods complement each other.

The fact to be noted is that in an international comparison it is hardly possible to reduce the limits of uncertainty below 1 nT or a few 0.1´. In other words: the maximum limits of measurement uncertainty of the base-line instruments used are expected to be of the same order of magnitude.

The three base-line instruments at Wingst Observatory

When a physical quantity is measured using several instruments of the same standard simultaneously, more questions are usually raised than answered. Nevertheless, each additional measuring device further validates the result and offers a chance to detect and possibly eliminate inadequacies of individual instruments of the ensemble.

Since 1997, it has been possible at Wingst Observatory to determine base-lines using three independent devices:

1. PVM1 (Askania/Varian), since 1969: F, Z, H and D_{rel}
2. DI-flux (Zeiss/Bartington), since 1983: U, V, Z and F
3. PVM2 (Zeiss/Magson), since 1997: D and I

Fig 3 shows the two PVM located in the absolute house. While the PVM1 is operated with a double coil system of type Braunbeck (vertical and horizontal), the new PVM2 instrument only has a relatively small horizontal cylinder coil with a variable density of turns (Auster, 1991). Unlike the PVM2, the PVM1 also allows measurements of H applying the compensation method (Voppel, 1972.

Let us take a look at the first series of measurements using the PVM2, from August 1997 to August 1998 (Fig 4). The Z base-line of the variometer of type FGE125 (DMI) is shown: The correspondence between the two base-line instruments PVM1 (crosses) and PVM2 (dots) is striking; also the fine structure at the end of 1997 is resolved by both devices. The bias of 1 nT has two (unknown) components: the difference of the instruments and that of the pillars. The two outliers can be traced back to incorrect operation of the new device.

The results of D are less satisfactory (Fig 5): A quasi-periodic fluctuation of about three months indicated by both the PVM1 (Fig 6a; dots) and the DI-flux (circles) cannot be found in the respective results of the PVM2 (Fig 6b; crosses). It should be noted that D can only be measured relatively by both PVM.

A closer investigation of the microstructure could not be carried out because of the asynchronous nature of measurements in the period concerned, which had been made on different days. The situation did not improve until February 2001, after a modification of the PVM2 electronics.

Fig 6 shows D for this period. While half the difference of D (in terms of PVM1 minus PVM2) appears unstructured (Fig 6b), the quarterly period seems to continue in the diagram of mean values (Fig 6a).

Looking at the horizontal intensity H (Fig 7), it is evident that the certainty of measurement is clearly reduced for both methods – compensation field method (PVM1), on the one hand, and addition field method (PVM2), on the other hand – as expected in higher geomagnetic latitudes. Fig 8 shows that the scattering has to be attributed to the PVM: Half the difference of both variometers used, in terms of FGE125 minus FGE126, shows a considerably smoother slope.

The total intensity F shows a contradictory behaviour (Fig 9a): The strong initial drift of the PVM2 (dots) by more than 3 nT within six months may be due to aging of the quartz crystal. The comparatively small drift of the F-difference in terms of F(measured) minus F(calculated) supports this assumption (Fig 9b; dots). The F-difference remains constant even in case of frequency changes. However, the conspicuously parallel course of a third proton magnetometer of type PPM105 (EDA), also installed inside the absolute house (crosses), contradicts this assumption.

A brief look at inclination I (Fig 10). Its measurement allows a comparison between the three base-line instruments on an absolute level. The scattering of all readings has the same order of magnitude; a correlation cannot be recognised.

To assess the instruments´ performance largely independent of possible influences of undiscovered base-line fluctuations between the weekly measurements, short-term series of 10 consecutive measurements were carried out with each method. Fig. 13 shows the results. The following values have been calculated for the uncertainties (Table 1):

	D	**I**	**F**	**K**	**duration**
PVM1	0.08´	0.03´	0.2 nT	1-3	54 min
DI-flux	0.07	0.02		2	42 *)
PVM2	0.10	0.05	0.2	1	34

(* with an additional person taking the minutes).

Table 1 (see text above)
The geomagnetic K values and the duration of a single measurement have to be taken into account when assessing the results.

Conclusion

The measurement uncertainties of all three base-line instruments are clearly below the limit values that are obtained using the intercalibration methods. This can be concluded from a qualitative evaluation of the base-lines in the Figures, on the one hand, and from the results of the series of consecutive measurements, on the other hand. The best results are obtained using the DI-flux (Zeiss/Bartington). Improvements to the PVM2 (Zeiss/Magson) are to be expected in the near future: the manufacturer is currently working on an improvement of the signal/noise-ratio.

Acknowledgement: I would like to thank V. Auster for the development of the new PVM and for many fruitful discussions.

References

Auster, A., 1984: Kernresonanz-Komponenten-Meßtechnik. Adilf-Schmidt-Observatorium für Erdmagnetismus, Jahrbuch 1983

Auster, A., 1991: Vektor proton magnetometer system for different uses in the geomagnetic measuring technique. HHI, Proceedings of the International Symposium, 100 Years Geomagnetic Observatory Potsdam-Seddin-Niemegk

Schulz, G., 1998: Results of the momentary value comparison between European observatories – a summary of the last two decades. GFZ Potsdam, Scientific Technical Report STR98/21

Voppel, D.,1972: The proton vector magnetometer at Wingst Observatory – technical data and application. DHI Hamburg, Erdmagnetisches Jahrbuch No 17

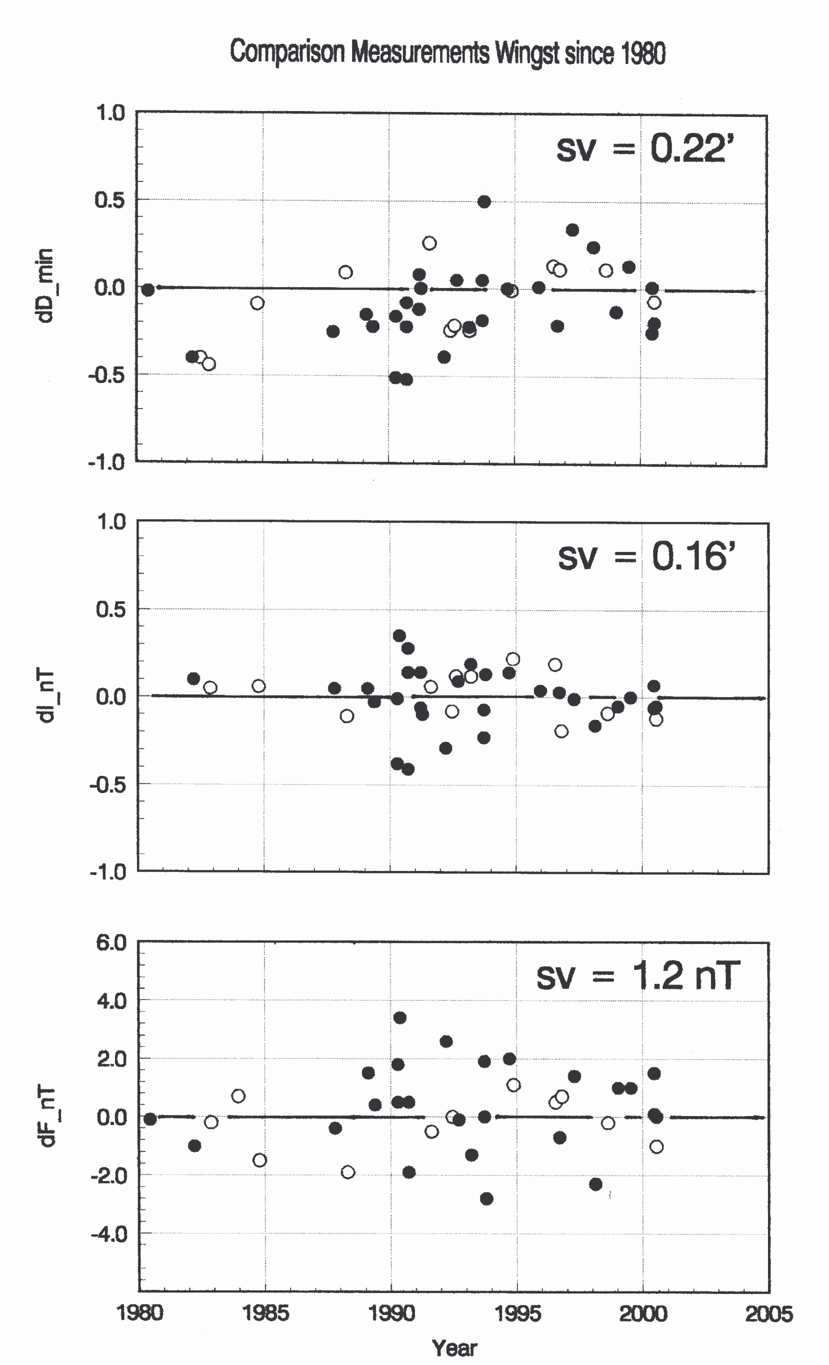

Fig 1

Comparison measurements Wingst since 1980 (see text)

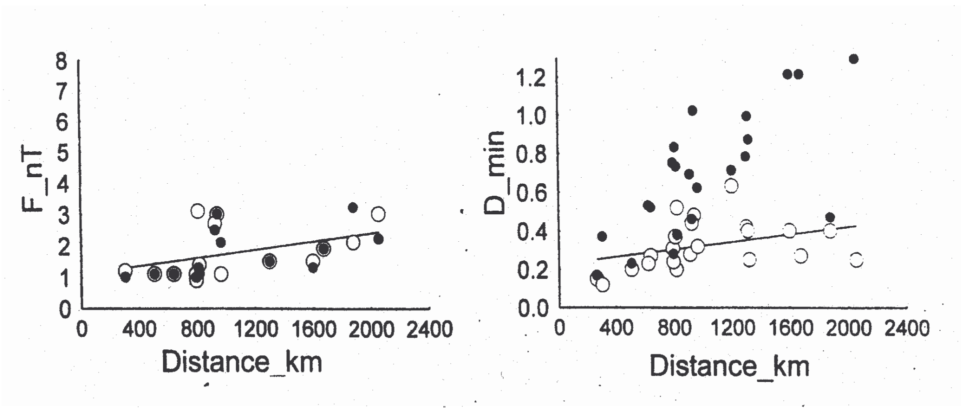

Fig 2

Standard deviation of monthly mean differences of raw (dots) and SV-reduced (circles) 1994 momentary values for D and F between Wingst and the other participating observatories, plotted against their distances from Wingst (See Schulz, 1998)

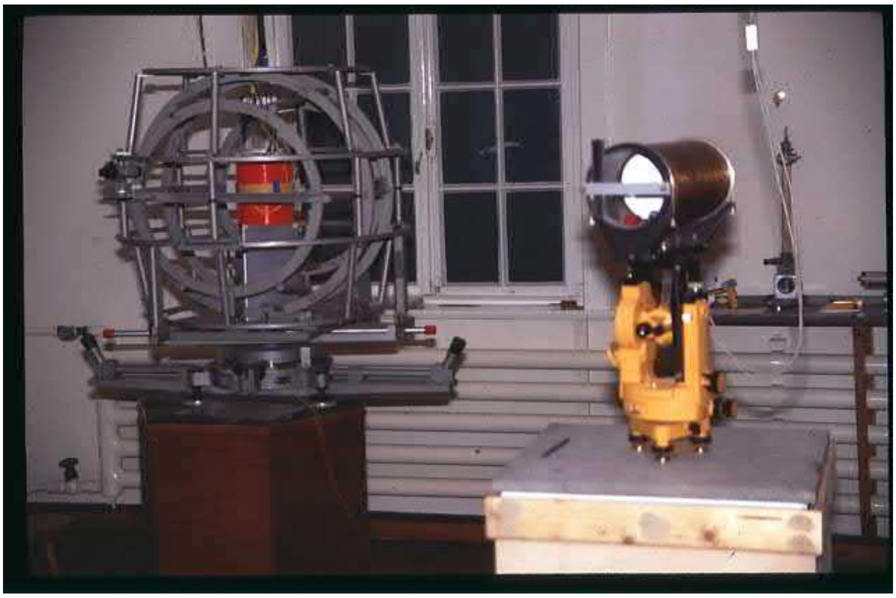

Fig 3

PVMs of type Askania/Varian and Zeiss/Magson at Wingst Observatory:

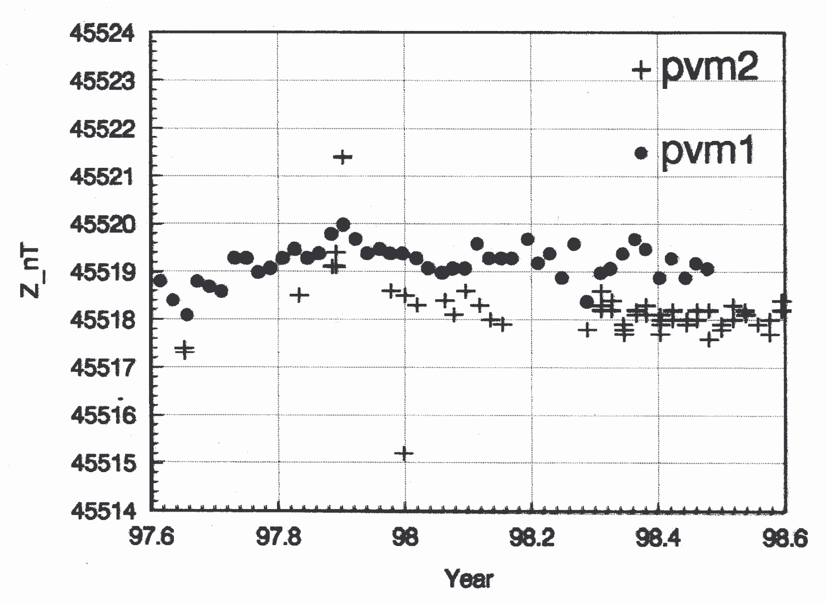

Fig 4

FGE125 Z base-line measurements from Aug 1997 to Aug 1998

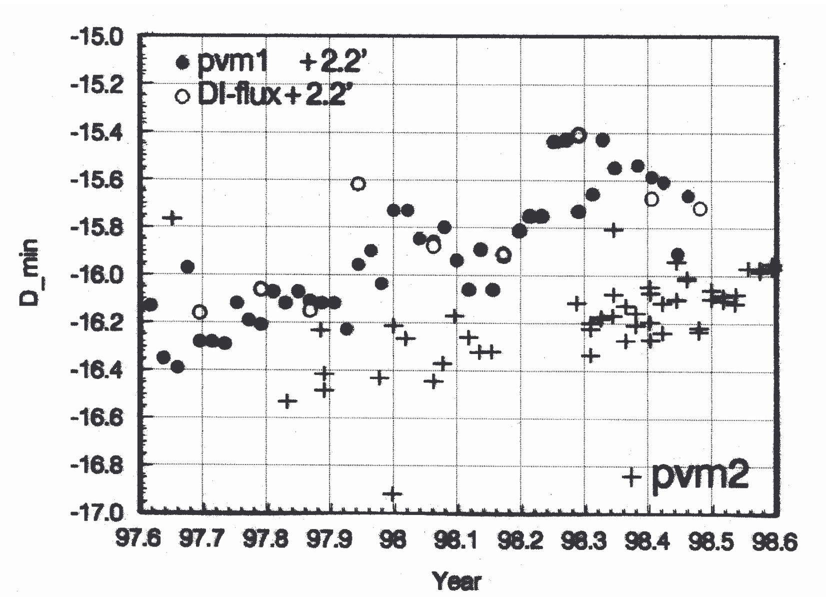

Fig 5

FGE125 D base-line measurements from Aug 1997 to Aug 1998

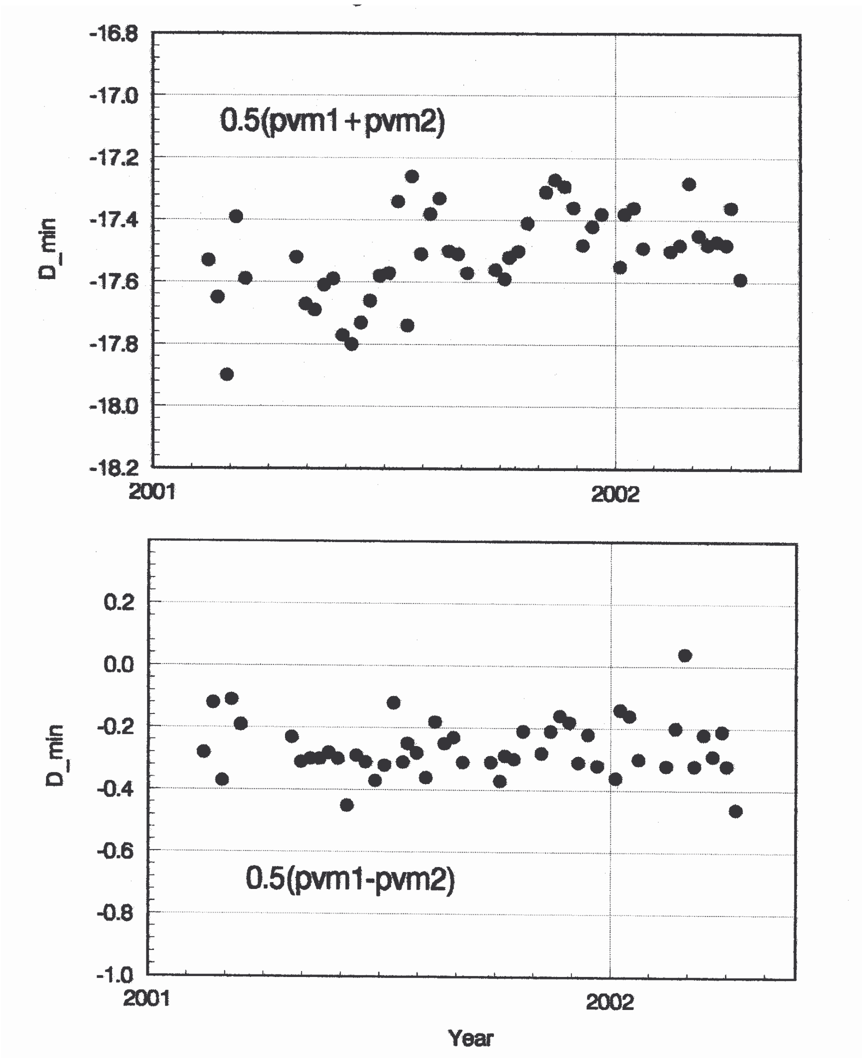

Fig 6a (top) and b (bottom)

FGE125 D base-line measurements from Feb 2001 to Mar 2002 and differences in terms of PVM1 minus PVM2

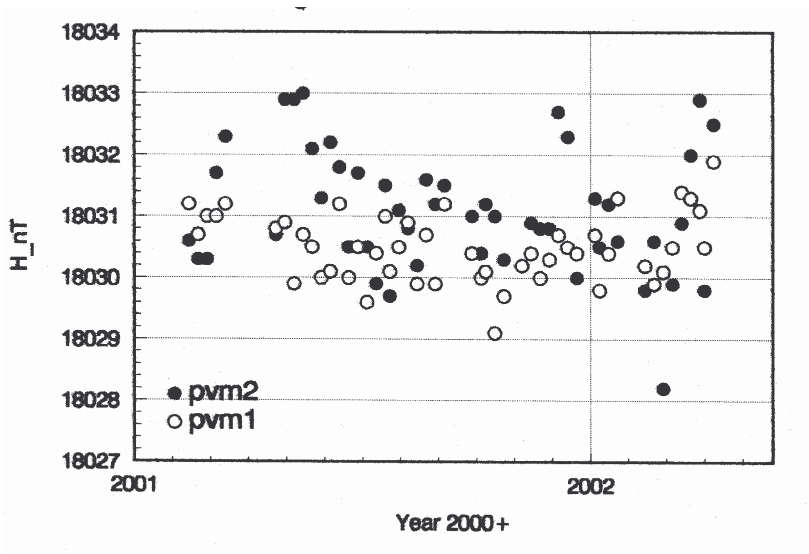

Fig 7

FGE125 H base-line measurements from Feb 2001 to Mar 2002

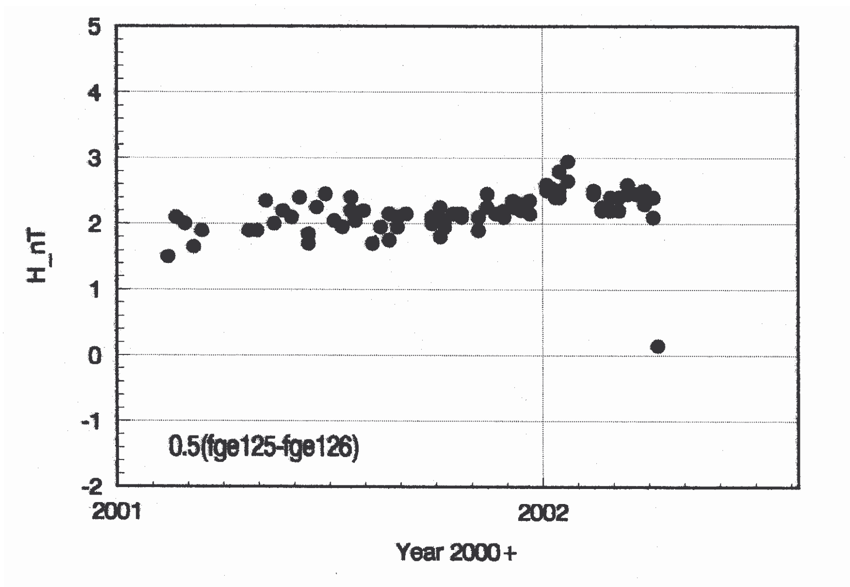

Fig 8

FGE125 H differences in terms of FGE125 minus FGE126 from Feb 2001 to Mar 2002

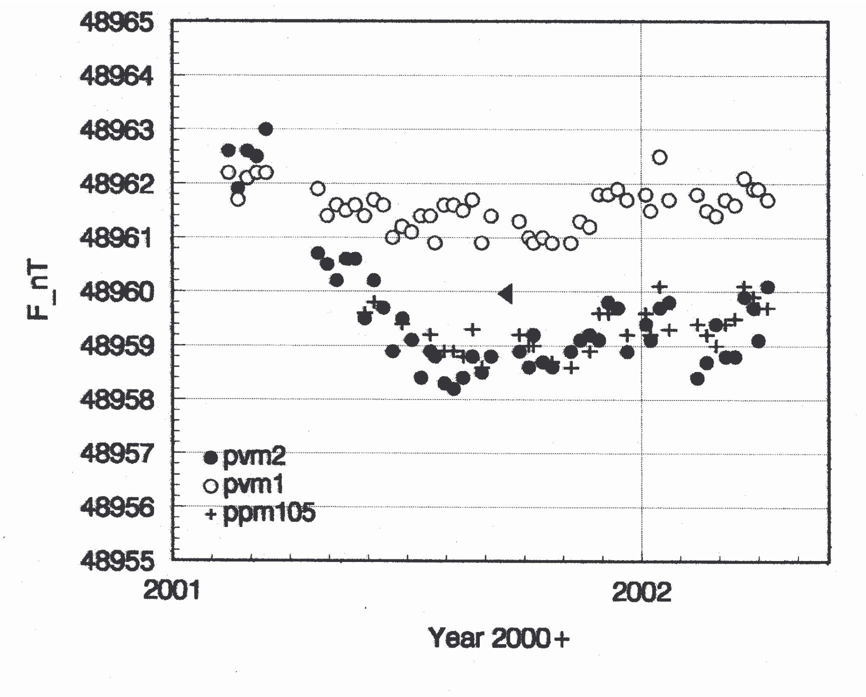

Fig 9a

FGE125 F base-line measurements from Feb 2001 to Mar 2002

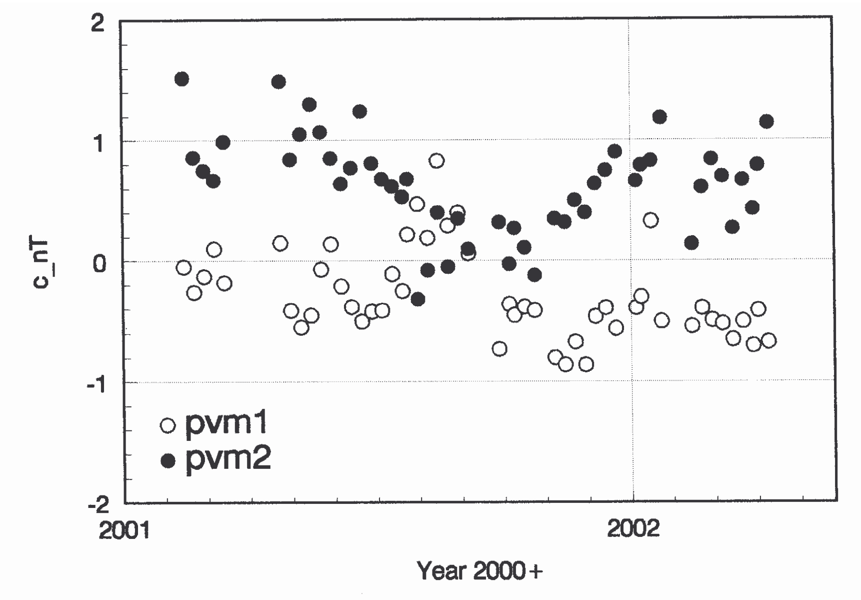

Fig 9b

F differences in terms of measured minus calculated from Feb 2001 to Mar 2002

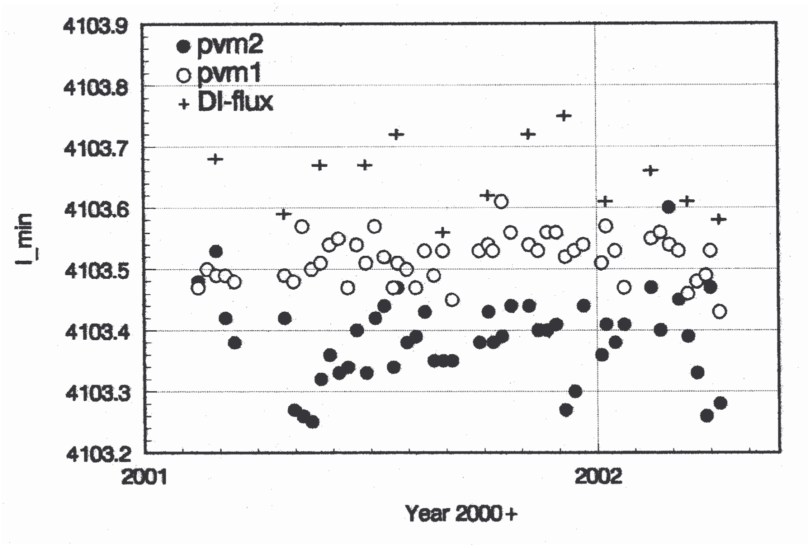

Fig 10

FGE125 I base-line measurements from Feb 2001 to Mar 2002

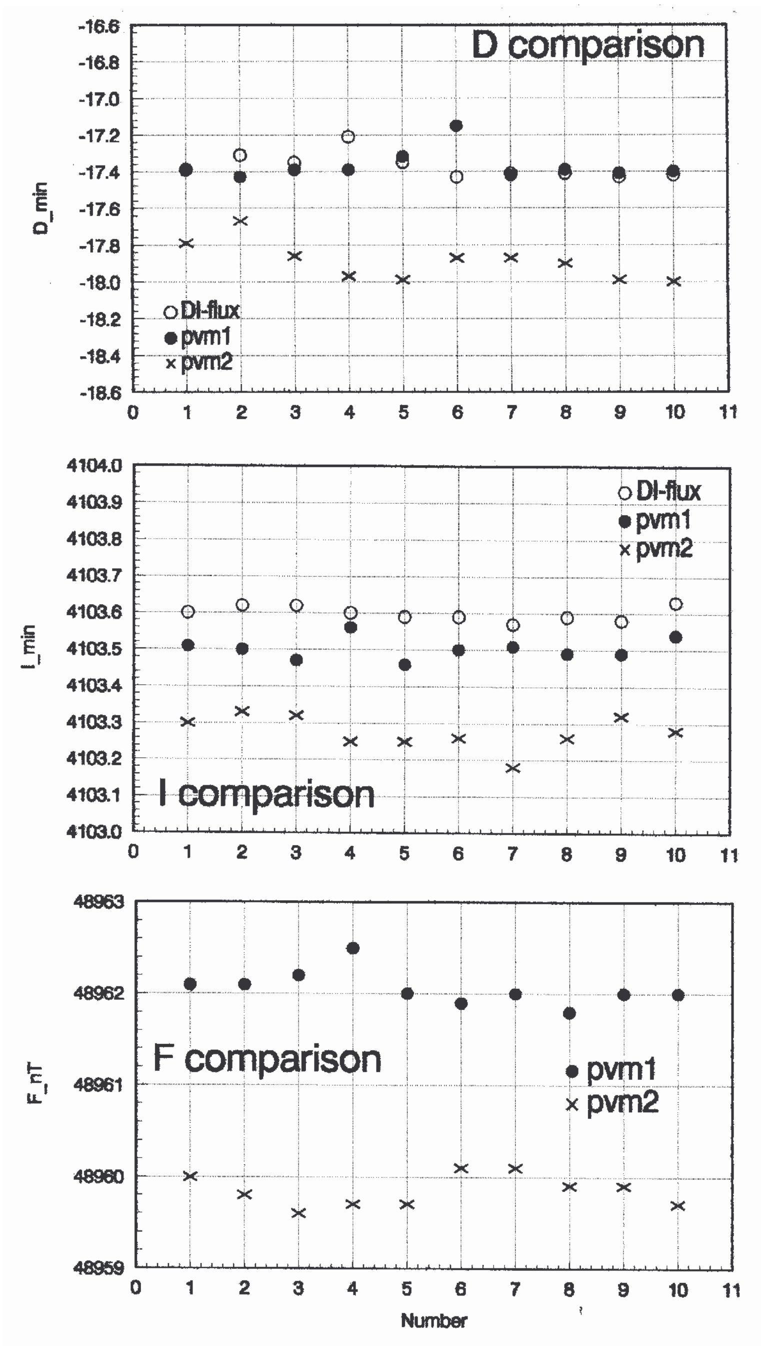

Fig 11

Short term series of consecutive measurements of D, I and F (see Table 1)

Processing of Scalar Magnetometer/Gradiometer Survey Signals by Decomposition in the Space of Orthonormalized Functions

B. Ginzburg, L. Frumkis and B. Z. Kaplan

Abstract.

The work is devoted to the analysis of magnetic survey signals caused by the presence of a magnetostatic dipole in the vicinity of the survey line. Processing of the acquired signal can be carried out by its decomposition in the space of orthonormal functions (orthonormal basis) constructed with the help of a Gram-Schmidt procedure. In the case of a magnetic gradiometer a set of five functions is found to be sufficient for an accurate signal description in a wide range of distances between the gradiometer and the dipole. The dipole energy signal in the chosen basis is found to be a convenient function for the data processing. The usage of the developed approach allows considerable increase in signal-to-noise ratio.

Introduction.

The present work deals with methods where scalar magnetometers are employed as magnetic anomaly detectors (MAD) both in a mono sensor and in a dual sensor gradiometric configuration. It is usual practice to install MAD systems on a platform scanning a search area by moving along straight survey lines [1]. Regarding the location of the target, it is expected to be either in a fixed position (e.g. a sunken ship) or moving much slower than the MAD platform. Depending on the mutual position of the target relative to the survey line, and direction of the target magnetic moment in relation to the Earth's magnetic field, the waveform of a MAD signal can take a variety of different (and a priori unknown) shapes, which results in considerable difficulties with signal processing (especially when the signal-to-noise ratio is rather low). Such uncertainty hampers application of effective correlation processing methods and optimal filtering. We intend to show that the set of the orthonormal functions developed in the present work for representing the dipole signal is helpful in improving the SNR of the MAD raw signal, when additive noise is considered.

An advantage of the developed approach is that a dipole energy signal is almost independent of the dipole orientation and diversity of dipole waveforms. This paves the way for making use of common data processing strategy for a wide variety of signal shapes.

Theory and Numerical Estimations

a) Single-sensor MAD

The hidden object in the present work is assumed to be a magnetic dipole. The dipole approximation is justified, since for practical hidden objects the higher order pole fields fall rapidly, and the dipole field prevails at distances larger than three to five times of the object maximal dimension.

The magnetic field $\boldsymbol{B}$ generated by a point dipole with a moment $\boldsymbol{M}$ at distance $\boldsymbol{r}$ from the dipole is

$$\boldsymbol{B} = \frac{\mu_0}{4\pi} r^{-3} [3r^{-2} (\boldsymbol{M} \cdot \boldsymbol{r}) \boldsymbol{r} - \boldsymbol{M}] \qquad (1)$$

where $\mu_0 = 4\pi * 10^{-7}$ H/m is the permeability of free space.

The signal S_1 of a scalar magnetometer is regarded as the projection of $\boldsymbol{B}$ onto $\boldsymbol{T}$ (the ambient Earth's magnetic field), provided that $|\boldsymbol{T}| >> |\boldsymbol{B}|$. Namely,

$$S_1 = (\boldsymbol{B} \cdot \boldsymbol{T}) \,/\, |\, \boldsymbol{T} \,| \tag{2}$$

The MAD signal is actually the small change of the total magnetic field registered along the survey line. Figure 1 describes the geometry related to the sequence of measurements along track *D*. The sensor is assumed to be moving along the straight-line track parallel to the *X*-axis. The dipole is located at the origin of the coordinate system. R_0 is the distance between the dipole and the track. It is the so-called CPA (closest proximity approach) distance. One can obtain this by substituting (1) in (2) that [2]:

$$S_1 = \frac{\mu_0 M}{4\pi R_0^3} \sum_{n=1}^{4} b_n \varphi_n(w) \tag{3}$$

where

$$\varphi_1(w) = w^2/[1+w^2]^{-5/2}, \quad \varphi_2(w) = w/[1+w^2]^{-5/2},$$

$$\varphi_3(w) = 1/[1+w^2]^{-5/2}, \quad \varphi_4(w) = 1/[1+w^2]^{-3/2},$$

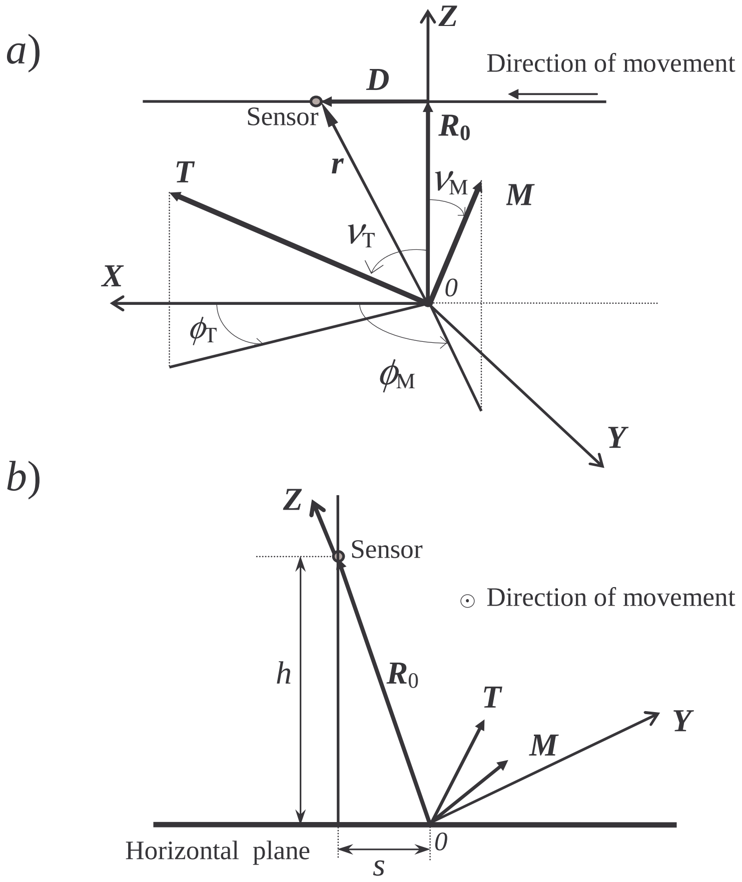

Fig. 1. Relative position of the dipole ***M*** and the sensor. The dipole ***M*** is located at the point of origin. The movement of the sensor is along the *D* track, which is parallel to the *X* axis.

a) A view where the track *D* lies in the drawing plane. ***T*** is the Earth's magnetic field.

ϕ_M and ϕ_T are the angles between the *X* axis and the projections of the vectors ***M*** and ***T*** onto the *XY* plane.

b) A view where the track *D* is perpendicular to the drawing plane.

$$b_1 = 3\sin\nu_M \cos\phi_M \sin\nu_T \cos\phi_T\,,\quad b_2 = 3(\cos\nu_M \sin\nu_T \cos\phi_T + \sin\nu_M \cos\phi_M \cos\nu_T)\,,$$
$$b_3 = 3\cos\nu_M \cos\nu_T\,,\quad b_4 = -\sin\nu_M \sin\nu_T \cos(\phi_M - \phi_T) - \cos\nu_M \cos\nu_T\,,$$

and $w = D / R_0$, w is a dimensionless coordinate along the track of the magnetometer movement. It can easily be shown, that $\varphi_4(w) = \varphi_1(w) + \varphi_3(w)$. The remaining three functions $\varphi_1(w)$, $\varphi_2(w)$, and $\varphi_3(w)$ are linearly independent, and can be orthonormalized. The Gram-Schmidt ortonormalization process [3] leads to various triplets of orthonormalized functions. The triplet chosen as an orthonormal basis for the representation of S_1, is as follows:

$$f_1(w) = \varphi_1(w)\sqrt{\frac{128}{3\pi}}\,,\quad f_2(w) = \varphi_2(w)\sqrt{\frac{128}{5\pi}}\,,\quad f_3(w) = [\varphi_3(w) - (5/3)\varphi_1(w)]\sqrt{\frac{24}{5\pi}}\,. \qquad (4)$$

In this case

$$S_1 = \frac{\mu_0 M}{4\pi R_0^3}\sum_{n=1}^{3} a_n f_n(w)\,, \qquad (5)$$

where

$$a_1 = \sqrt{\frac{3\pi}{128}}[(b_1 + b_4) + \frac{5}{3}(b_3 + b_4)], \qquad a_2 = b_2\sqrt{\frac{5\pi}{128}}, \qquad a_3 = (b_3 + b_4)\sqrt{\frac{5\pi}{24}}. \qquad (6)$$

These functions satisfy usual conditions:

$$\int_{-\infty}^{+\infty} f_i(w) f_j(w) dw = 0 \quad \text{for} \quad i \neq j, \text{ and } \int_{-\infty}^{+\infty} f_j^2(w) dw = 1, \qquad i, j = 1, 2, 3.$$

Following [2] we construct a criterion function for a primary detection algorithm as:

$$a_1^2 + a_2^2 + a_3^2.$$

This expression can be interpreted as the energy of the signal S_1 in the space of the chosen basis. The coefficients a_j can be obtained in the following way:

$$a_j = \left(\frac{\mu_0 M}{4\pi R_0^3}\right)^{-1} \int_{-\infty}^{\infty} f_j(w) S_1 dw \qquad (7)$$

The measurements are usually performed in a sequentially discrete manner while the magnetometer moves along the D track. The integration and the related multiplications associated with (7) are performed for a series of measurements between w_{m+k} and w_{m-k} as shown in Figure 2. The raw data $S_{1r}(w_i)$ in Figure 2 may include noise as well. The point number m can be regarded as the current point of signal processing. The processing related equations are as follows:

$$\alpha_j(m) = \sum_{i=-k}^{+k} f_j(w_i) S_{1r}(w_{m+i}) \Delta w, \quad j = 1, 2, 3, \qquad (8)$$

where $\Delta w = w_{i+1} - w_i$ is the length of spatial sampling. The limits of summation in (8) unlike the integration limits of (7) cannot be infinite. Furthermore, for practical reasons it is desirable to minimize the width of the observation window (and the value of k respectively) both to prevent excessive real time calculations and to get detection warning with a short time delay. Our analysis shows that a relatively small value of k is sufficient for satisfactory MAD signal representation since the $f_j(w)$ functions rapidly decay with large $|w|$. The numerical examples of the present work rely on the summation between $w_{-k} = -2.5$ and $w_{+\kappa} = 2.5$ (see Figure 2). The α_j's replace the theoretical a_j's in the measurement process. When there are no noise and disturbances, they are proportional to the latter a_j's. The sum $\alpha_1^2 + \alpha_2^2 + \alpha_3^2$ can be regarded as the energy E of the measured signal $S_{1r}(w_i)$, namely:

$$E = \alpha_1^2 + \alpha_2^2 + \alpha_3^2 \qquad (9)$$

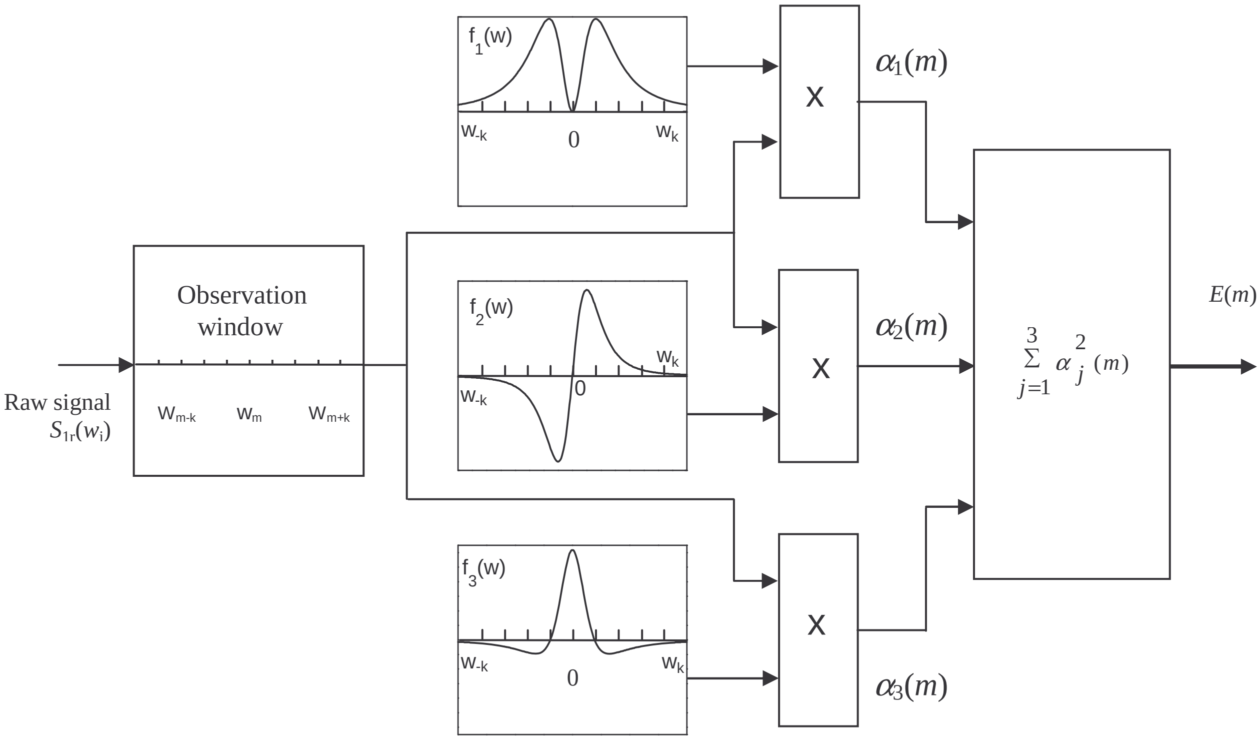

Fig. 2. Scheme of the single sensor magnetometer signal processing.
The basis functions $f_1(w)$, $f_2(w)$ and $f_3(w)$ employed for the data processing are shown as embedded in the system. These functions are multiplied step by step by the raw signal flowing through the observation window. The three multipliers are represented in the scheme by the **X** blocks. E (m) is regarded as the energy of the raw signal in the equation (9).

The signal processing procedure assumes some specific value of R_0. However, the actual value of R_0 is not known a priori. Hence, the signal processing procedure should be implemented in a multi-channel manner for several possible values of R_0. Our estimations show 4 - 6 channels of parallel processing being sufficient in practice. It has been found that the maximal energy in (9) is obtained when the assumed R_0 is close to the actual distance between the track and the dipole.

b) gradiometer MAD

Figure 3 describes the measurement scenario for a dual sensor gradiometric configuration.

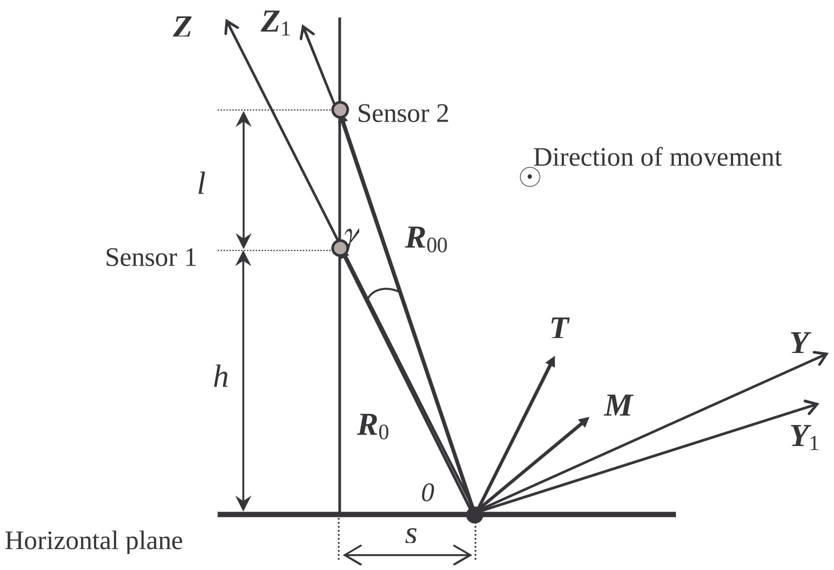

Fig. 3 The relative position of the dual sensor vertical gradiometer and the dipole ***M***. ***T*** is the Earth's magnetic field. R_0 is the distance between the dipole and the track of sensor 1. R_{00} is the distance between the dipole and the track of sensor 2. The sensors are located on vertical line with the separation of l between them.

The lower sensor with its coordinate frame ***X Y Z*** is the same one as that treated in the previous section. Therefore its signals, generated while moving in the ***X*** direction, are the same as those in (5). The signal of the second sensor, which accompanies the first sensor at a distance l above it, can be expressed in a similar manner. However, the distance R_{00} between the dipole and track and the proper angles are different. The signal of the second sensor is expressed as

$$S_2 = \frac{\mu_0 M}{4\pi R_{00}^3} \sum_{n=1}^{3} a_{Vn} f_{Vn}(w), \tag{10}$$

where

$$R_{00} = R_0\, c^{-1}, \quad c = \{[h^2+s^2] \,/\, [(h+l)^2+s^2]\}^{1/2}, \tag{11}$$

$$a_{V1} = \sqrt{\frac{3\pi}{128}}[(b_{V1}+b_{V4}) + \frac{5}{3}(b_{V3}+b_{V4})], \qquad a_{V2} = b_{V2}\sqrt{\frac{5\pi}{128}}, \qquad a_{V3} = (b_{V3}+b_{V4})\sqrt{\frac{5\pi}{24}}, \tag{12}$$

$$b_{V1} = 3\sin(\boldsymbol{MZ}_1)\sin(\boldsymbol{TZ}_1)\cos(\boldsymbol{MX}_1)\cos(\boldsymbol{TX}_1),$$

$$b_{V2} = 3(\sin(\boldsymbol{TZ}_1)\cos(\boldsymbol{MZ}_1)\cos(\boldsymbol{TX}_1) + \sin(\boldsymbol{MZ}_1)\cos(\boldsymbol{MX}_1)\cos(\boldsymbol{TZ}_1))$$

$$b_{V3} = 3\cos(\boldsymbol{MZ}_1)\cos(\boldsymbol{TZ}_1), \tag{13}$$

$$b_{V4} = -\sin(\boldsymbol{MZ}_1)\sin(\boldsymbol{TZ}_1)\cos(\boldsymbol{MX}_1 - \boldsymbol{TX}_1) - \cos(\boldsymbol{MZ}_1)\cos(\boldsymbol{TZ}_1)),$$

($\boldsymbol{MZ}_1$) is the angle between the moment of the dipole ***M*** and $\boldsymbol{Z}_1$ axis etc. The cosines of the angles are given below. The expressions for the $f_{Vn}(w)$'s in (10) are similar to those of the $f_n(w)$'s in (4),

$$f_{V1}(w)=\varphi_{V1}(w)\sqrt{\frac{128}{3\pi}}\,,\;\; f_{V2}(w)=\varphi_{V2}(w)\sqrt{\frac{128}{5\pi}}\,,\;\; f_{V3}(w)=[\varphi_{V3}(w)-(5/3)\varphi_{V1}(w)]\sqrt{\frac{24}{5\pi}}\,, \qquad (14)$$

where

$$\varphi_{V1}(w)=c^5w^2/[1+(cw)^2]^{5/2}\,,\;\; \varphi_{V2}(w)=c^4w/[1+(cw)^2]^{5/2}\,,$$

$$\varphi_{V3}(w)=c^3/[1+(cw)^2]^{5/2}\,,\;\; \varphi_{V4}(w)=c^3/[1+(cw)^2]^{3/2}\,. \qquad (15)$$

The gradiometer signal S is obtained by subtracting S_2 from S_1. This signal is now expressed by six functions $f_1(w)$, $f_2(w)$, $f_3(w)$, $f_{V1}(w)$, $f_{V2}(w)$, and $f_{V3}(w)$, which constitute a set of linearly independent functions. This is due to the fact that their Wronskian is not equal to 0 in the region of interest [4]. Therefore these six functions can be now transformed by the Gram-Schmidt procedure to get an orthonormal basis. The number of orthonormalized functions obtained in this way should be equal to the number of the initially linearly independent functions. Hence, the gradiometric signal S can be expressed as a weighted sum of six orthonormalized functions. However, as a result of our detailed calculations, one of these functions turned out to be a negligible component so that, for all practical cases, the number of basis functions can be reduced to five:

$$S=\frac{\mu_0 M}{4\pi R_0^3}\sum_{n=1}^{5}A_n u_n(w)\,, \qquad (16)$$

where $u_n(w)$, n=1,2…5 is the orthonormal basis:

$$\int_{-\infty}^{+\infty}u_i(w)u_j(w)dw=0 \quad \text{for} \quad i\neq j\,, \text{ and } \int_{-\infty}^{+\infty}u_j^2(w)dw=1, \quad i,j=1,2,\ldots 5, \qquad (17)$$

Our approach to compute the basis functions, $u_j(w)$, is based on a series expansion of integrals appearing in the Gram-Schmidt orthonormalization procedure. These alternating series rapidly converge for $l/R_0 \leq 3$ [5], so that three terms of the series have been found to be sufficient for accurate presentation of the gradiometer signal S. It means that the convergence covers all practical cases. These computations result in the following form for gradiometer basis functions:

$$u_1(w)=f_1(w),$$

$$u_2(w)=(f_{V1}(w)-f_1(w)\,F_1)\,F_2,$$

$$u_3(w)=f_2(w), \qquad (18)$$

$$u_4(w)=(f_3(w)+f_1(w)F_1(F_2)^2F_3-f_{V1}(w)\,(F_2)^2F_3)\,F_4.$$

$$u_5(w)=(f_{V2}(w)-F_5\,f_2(w))\,F_6,$$

The cosines of the angles between the magnetic dipole moment $\boldsymbol{M}$, the Earth’s magnetic field $\boldsymbol{T}$ and the coordinate axes $\boldsymbol{X}_1$, $\boldsymbol{Z}_1$ are as follows,

$$\cos(\boldsymbol{MX}_1)=\sin(\nu_M)\cos(\phi_M),\;\; \cos(\boldsymbol{MZ}_1)=\sin(\nu_M)\sin(\phi_M)\sin(\gamma)+\cos(\gamma)\cos(\nu_M),$$

$$\cos(\boldsymbol{TX}_1) = \sin(\nu_T)\cos(\phi_T),\ \ \cos(\boldsymbol{TZ}_1) = \sin(\nu_T)\sin(\phi_T)\sin(\gamma) + \cos(\gamma)\cos(\nu_T),$$

where

$$\cos\gamma = \cos\{\mathrm{atan}[(l+h)/s] - \mathrm{atan}(h/s)\}.$$

Coefficients A_n and F_j appearing in equations (13), (16) and (18) are as follows:

$A_1 = a_1 - a_{V1} c^3 F_1 - a_{V3} c^3 F_6$,

$A_2 = (F_2)^{-1}[a_{V3} c^3 F_1 (F_2)^2 F_6 - a_{V1} c^3 + a_{V3} (F_2)^2 F_5]$,

$A_3 = a_2 - a_{V2} c^3 F_3$, $A_4 = (F_7)^{-1}[a_3 - a_{V3} c^3 F_7 F_8]$, $A_5 = -a_{V2} c^3 (F_4)^{-1}$

$F_1 = (128/3\pi) I_1$, $F_2 = [c^{-1} - (F_1)^2]^{-0.5}$, $F_3 = (128/5\pi) I_2$, $F_4 = [c^{-1} - (F_3)^2]^{-0.5}$,

$F_5 = (32/\pi\sqrt{5})\,[cI_2 - (5/3)\,I_1]$,

$F_6 = (32/\pi\sqrt{5})\,[c^{-1} I_2 - (5/3)\,I_1]$,

$F_7 = [1 + c^{-1}(F_2)^4(F_5)^2 - 2(F_2)^2(F_5)^2 - (F_1)^2 (F_2)^4(F_5)^2]^{-0.5}$,

$F_8 = F_7\,[I_4 + F_1(F_2)^2 F_5 F_6]$,

$$I_1 = \frac{3\pi}{32\sqrt{c}\,(1+\beta(c))^2}\left[1 + \frac{1-\beta(c)}{24} + \frac{3(1-\beta(c))^2}{512}\right],$$

$$I_2 = \frac{5\pi}{32\sqrt{c}\,(1+\beta(c))^2}\left[1 + \frac{\beta(c)-1}{8} - \frac{5(\beta(c)-1)^2}{256}\right],$$

$$I_3 = \frac{35\pi}{32\sqrt{c}\,(1+\beta(c))^2}\left[1 + 5\frac{\beta(c)-1}{8} - \frac{35(\beta(c)-1)^2}{512}\right],$$

$$I_4 = \frac{24}{5\pi}\left[\frac{25}{9} I_1 - \frac{5}{3}(c + c^{-1}) I_2 + I_3\right], \qquad \beta(c) = \frac{1+c^2}{2c}.$$

As been mentioned, the five functions $u_n(w)$, n=1,2…5 give an approximate representation of dipole signal S (16). To estimate the approximation accuracy we have made computational comparison of (16) with the calculation of (S_1-S_2) through their exact expressions (5) and (10). It turned out that the maximal point relative error of 0.35% occurs for R_0/l = 1.25 with even lower values for more distant dipole locations. The relative root mean square error for w = -2.5…+2.5 interval does not exceed 0.1% for R_0/l > 0.1 and all possible dipole moment directions. Therefore, we regard the five-function orthonormal basis to be sufficiently accurate for representation (16) of the gradiometer signal for a wide range of dipole CPA distance R_0 relative to gradiometer base l.

The procedures of the gradiometric MAD signal processing is similar to (8) used for processing of the single magnetometer signal. It is based on the decomposition of the signal within a moving window:

$$\alpha_j(m) = \sum_{i=-k}^{+k} S(w_{m+i}) u_i(w) \Delta w, \quad j = 1, 2, 3, 4, 5, \qquad (20)$$

where w_{-k} = -2.5, $w_{+\kappa}$ = 2.5, $\Delta w = w_{i+1} - w_i$ is the normalized spatial sampling distance; and the calculation of the energy E in the form:

$$E = \alpha_1^2 + \alpha_2^2 + \alpha_3^2 + \alpha_4^2 + \alpha_5^2 \tag{21}$$

Examples of Application

The signal processing procedure presented in (8) and (9) is found to be rather effective in recovering the dipole signal when it is corrupted by additive noise. Figure 4*a* shows raw MAD data of a single scalar sensor where a dipole signal is corrupted by noise. Figure 4*b* shows the energy obtained through the procedures (8) and (9) where energy values are normalized to the maximal observed value. It can be seen that original signal to noise ratio of about 0.3 has been increased to 5 as a result of the developed data processing technique.

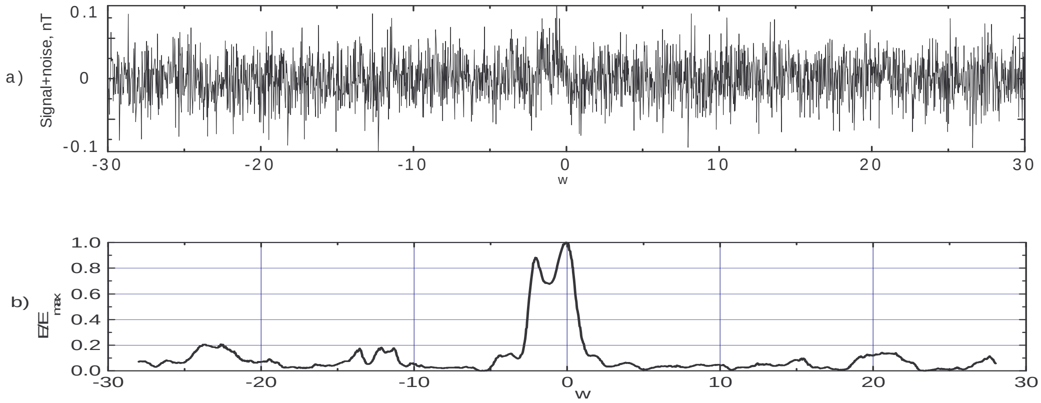

Fig. 4. Illustration of the signal recovery (single scalar sensor).
a) Computer simulated raw data where the dipole signal is corrupted by additive noise.
The dipole signal and the uniform noise are obtained by computer simulation. The noise samples are added to the signal samples and intensities are chosen so that the amplitude signal to noise ratio is about 0.3. The total number of sampling points along the *w*-axis is equal to 2400.
b) Result of the data processing. The S/N ratio has been increased up to 5.

Fig. 5 illustrates the signal recovery from raw data for another case. Here real data acquired on a survey line play the role of additive noise and the dipole signal is obtained by computer simulation.

Fig. 6 illustrates the signal recovery from gradiometer raw data. Here the additive noise is again real survey data while the dipole signal is obtained by computer simulation.

These examples confirm the effectiveness of the developed algorithm in recovering the signal from the noise.

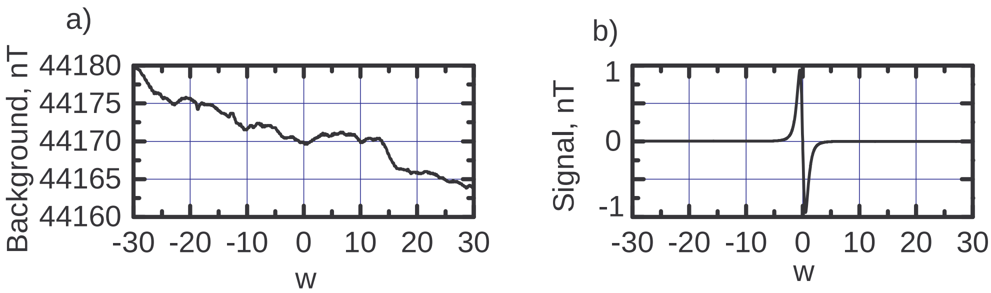

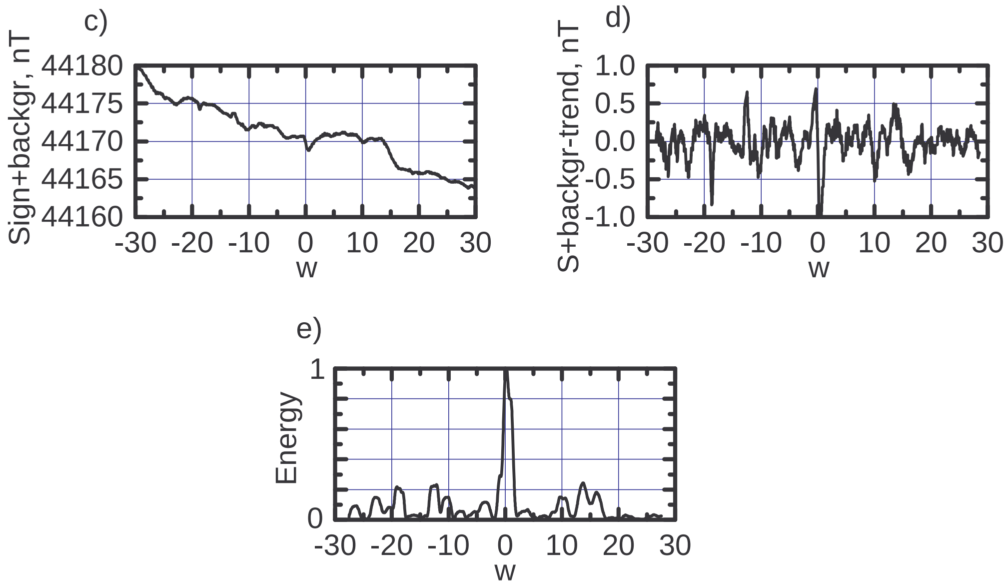

Fig. 5. Illustration of the signal recovery (single scalar sensor).

a) Real magnetic survey data (background). b) The dipole signal obtained by computer simulation. c) The sum of the background and the dipole signal - raw data for processing algorithm. d) The raw data after trend reduction. Trend $T_i(w) = a_i + b_i w$ (a_i and b_i are linear regression coefficients [6]) was calculated for each point i of the survey line in the interval [w_i – 1.5 ÷ w_i + 1.5]. e) The energy of the dipole signal (dimensionless) after signal processing.

As mentioned, a significant problem in the development of dipole detection algorithms is the great variety of the signal waveforms depending on dipole magnetic moment direction in relation to the Earth's magnetic field. The signal waveform can take various shapes – bell-shape, s-shape, intermediate shape, etc. which produces considerable difficulties in the application of effective correlation methods for extraction of the target signal and for optimal filtering.

It turned out that the present approach based on the decomposition of the MAD signal in the space of orthonormal basis functions allows a substantial advance in solving the problem. This is due to the fact that calculation of the energy in the manner of (9) or (21) provides an opportunity to obtain the target signal practically independent of the dipole magnetic moment direction. It is seen that even for substantially different dipole signal waveforms (Fig. 5 and Fig.6) their energy signal curves have a similar shape. This allows us to make use of single-channel optimal filtering methods and thus to avoid the necessity for complicated multi-channel correlative analysis, where each channel is matched to a specific signal waveform.

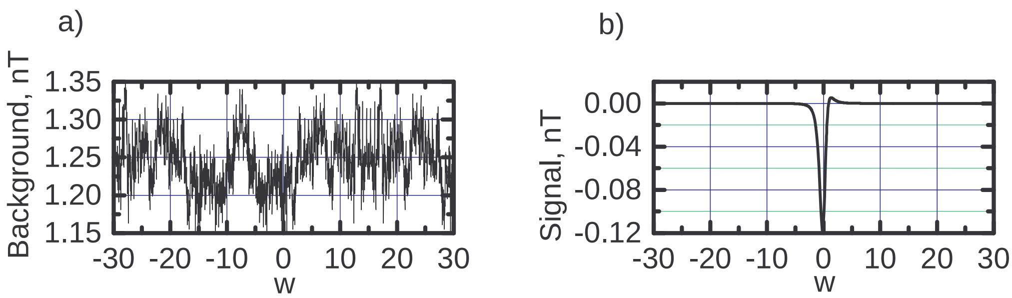

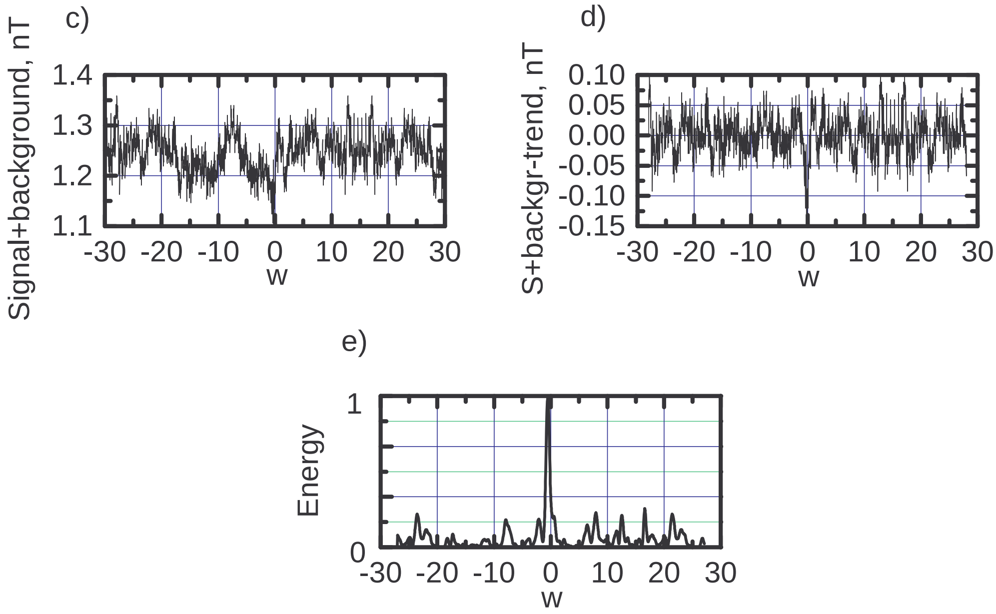

Fig. 6. Illustration of the gradiometric signal recovery.

a) Real magnetic survey data (background). b) The dipole signal obtained by computer simulation. c) The sum of the background and the dipole signal - raw data for processing algorithm. d) The raw data after trend reduction. See details in capture to Fig. 5. e) The energy of the dipole signal (dimensionless) after signal processing.

Conclusion.

An approach for gradiometric signal processing based on the decomposition of the MAD signal in the space of orthonormalized functions has been developed. A three-function set is sufficient for representing a single sensor total field magnetometer signal, while for the correct representation of a dual sensor gradiometer signal five functions are needed. The dipole energy signal in the chosen basis is found to be a convenient function for the data processing. The usage of this function allows increasing the signal-to-noise ratio and therefore improving detection characteristics.

The energy signal is found to be almost independent of the dipole magnetic moment orientation relative to the Earth's magnetic field and to the survey line direction. This paves the way for making use of common detection strategy for a wide variety of MAD signal waveform shapes.

Acknowledgement

The support of the Paul Ivanier Center for Robotics Research and Production Management is gratefully acknowledged.

References

[1] H. Zafrir, N. Salomonski, Y. Bregman, B. Ginzburg, Z. Zalevsky and M. Baram, *Marine magnetic system for high resolution and real time detection and mapping of ferrous submerged UXO, sunken vessels, and aircraft, Proc. UXO/Countermine Forum 2001, New Orleans, LA, Apr. 9-12, 2001.*

[2] Y. D. Dolinsky, Vliyanie osobennostei signala na strukturu optimalnogo priemnika pri obnaruzhenii namagnichennykh tel, Geofizicheskaya Apparatura, 97 (1993) 29-38 (in Russian).
[3] G. A. Korn and T. M. Korn, Mathematical Handbook for Scientists and Engineers, McGraw Hill, New York, 2nd edn., 1968, p. 491.
[4] *ibid.*, p.253.
[5] I. M. Ryzhik, Tables of Integrals, series and Products, Academic Press, New York, 4th edn., 1965.
[6] C. J. Brookes, I. G. Betteley and S. M. Loxston, Fundamentals of Mathematics and Statistics, John Wiley & Sons, New York, 1979, p. 426.

Geomagnetic Disturbances in the Periods Around the Solar Minimum and Maximum

Pavel Hejda, Josef Bochníček, Josef Horáček and Jaroslava Nejedlá
Geophysical Institute of the Academy of Sciences
141 31 Prague, Czech Republic

Abstract

The nature of the geomagnetic activity in 1995, the minimum of the (most recent) 23rd solar cycle, is compared with the nature of the geomagnetic activity in the year 2000, the maximum of the (most recent) 23rd solar cycle.
Although the average annual values of geomagnetic activity and the frequency of days on which $\Sigma Kp \geq 30$ was practically the same in both years the intensity of the disturbances and their physical causes differed markedly. Most of the disturbances recorded in 1995 were weak to medium whilst most of the disturbances recorded in the year 2000 were medium to severe. The predominant source of the geomagnetic disturbances in 1995 was coronal holes, whereas the predominant source of the geomagnetic disturbances in the year 2000 was irregular events.
It was also found that, as of the degree ‘active’, the level of the geomagnetic activity in Central Europe is lower than the world-wide level.

Introduction

Geomagnetic disturbances are caused by irregularities in the solar wind. The source of these

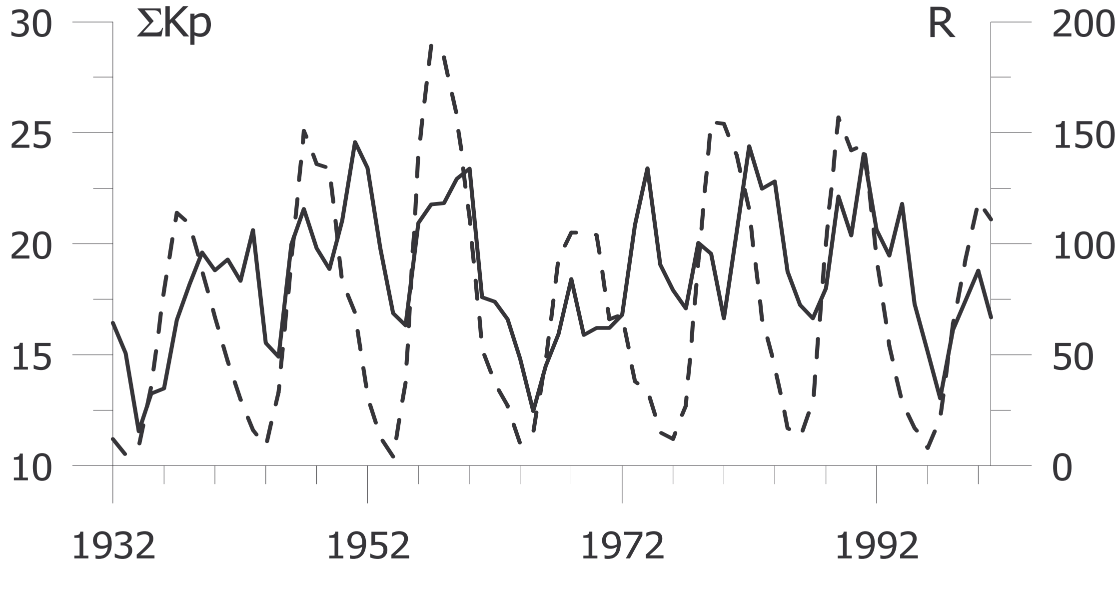

Fig. 1. Average annual values of geomagnetic and solar activity in the interval 1932 - 2000. The geomagnetic activity is expressed in terms of the daily sum of Kp-indices (full line), the solar activity in terms of Wolf’s number R.

irregularities is the processes on the Sun. The nature, intensity and frequency of the processes relates to the phases of the solar cycle - to solar activity. The correlation between the degree of disturbance of the geomagnetic field, i.e. geomagnetic activity, and solar activity, however, is not very close which is evidenced by the behaviour of the average annual values of the geomagnetic and solar activity in the interval of 1932 - 2000, shown in Fig. 1.

In this figure the geomagnetic activity is expressed in terms of the sum of the diurnal values of the Kp-index (this index was introduced in 1932), and the solar activity by Wolf's number R. As compared to the curve of the average annual value of solar activity, the curve of the average annual value of the diurnal geomagnetic activity is less regular, mostly displays two peaks, of which the second, higher as a rule, occurs 1 - 3 years after the solar activity maximum. Only the frequency curves of very severe geomagnetic disturbances display a closer correlation with the solar activity curve (Crooker and Siscoe, 1986) proof of which is the behaviour of the frequency curve of geomagnetically severely disturbed days ($\Sigma Kp > 45$) in Fig. 2.

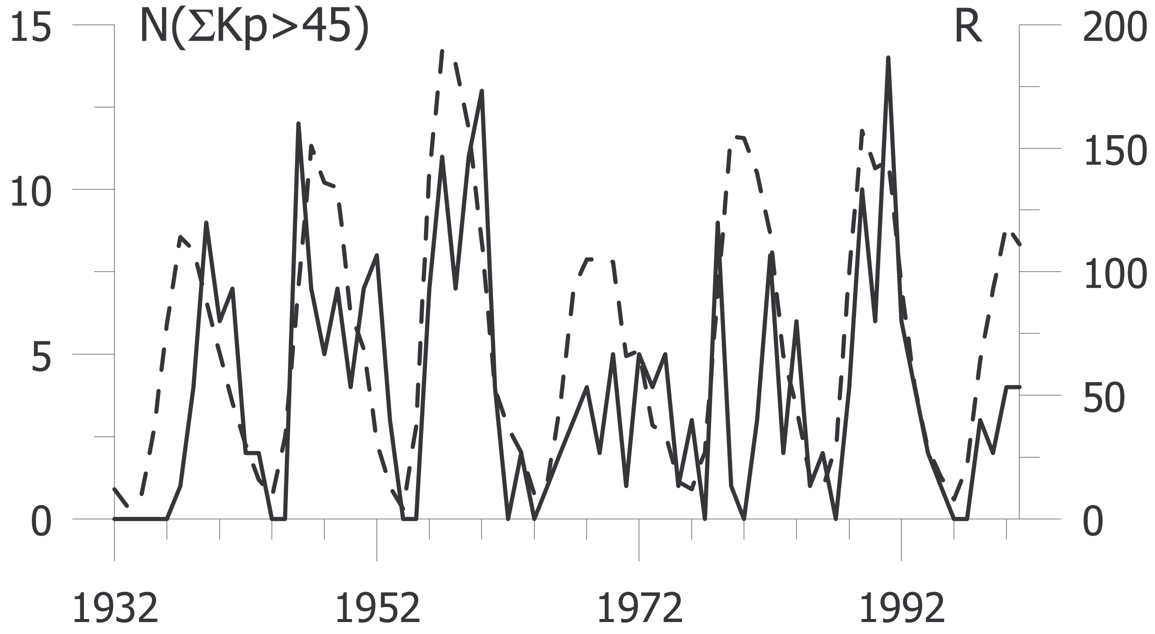

Fig. 2. The frequency of days on which the Kp index was larger than 45 (full line), and the average annual values of solar activity in the interval 1932-2000.

As one proceeds to time scales shorter than 1 year, the correlation between the averages of both activities diminishes rapidly, so that on a one-month scale it sometimes nearly vanishes altogether (Bochníček et al., 1996). The behaviour of the monthly averages in the course of the most recent solar cycle is shown in Fig. 3.

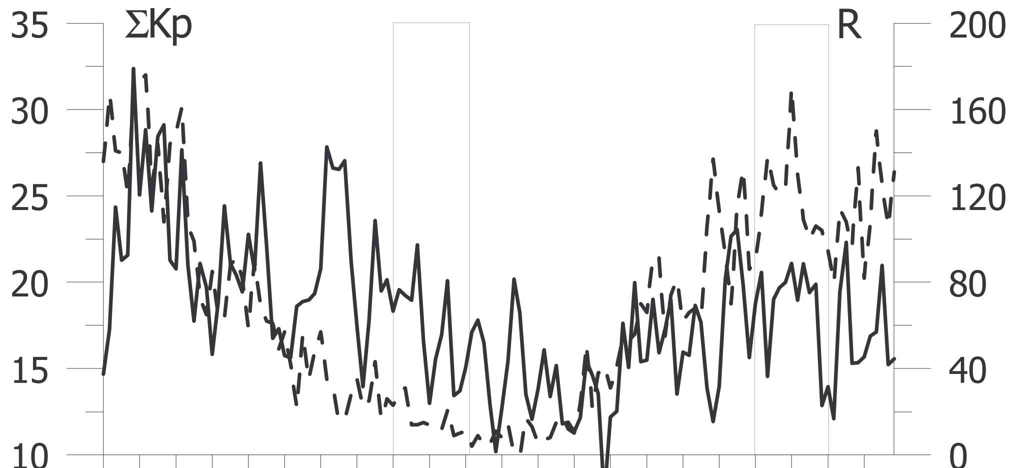

Fig. 3. Average monthly values of the diurnal geomagnetic (full line) and solar activity in the years 1991 - 2001.

Results

The purpose of this paper is to compare the nature of geomagnetic activity in the year of the minimum with the nature of geomagnetic activity in the year of the maximum of the most recent solar cycle. The years in question, 1995 and 2000, are marked by columns in Fig. 3. Although the average annual values of geomagnetic activity were practically the same in these two years, ΣKp = 17.3 in 1995 and ΣKp = 18.8 in 2000, see Figs 4 and 5, depicting the geomagnetic Kp-indices by individual Bartels rotations, they indicate that there is a principal difference in the nature of the geomagnetic activity between the two years.

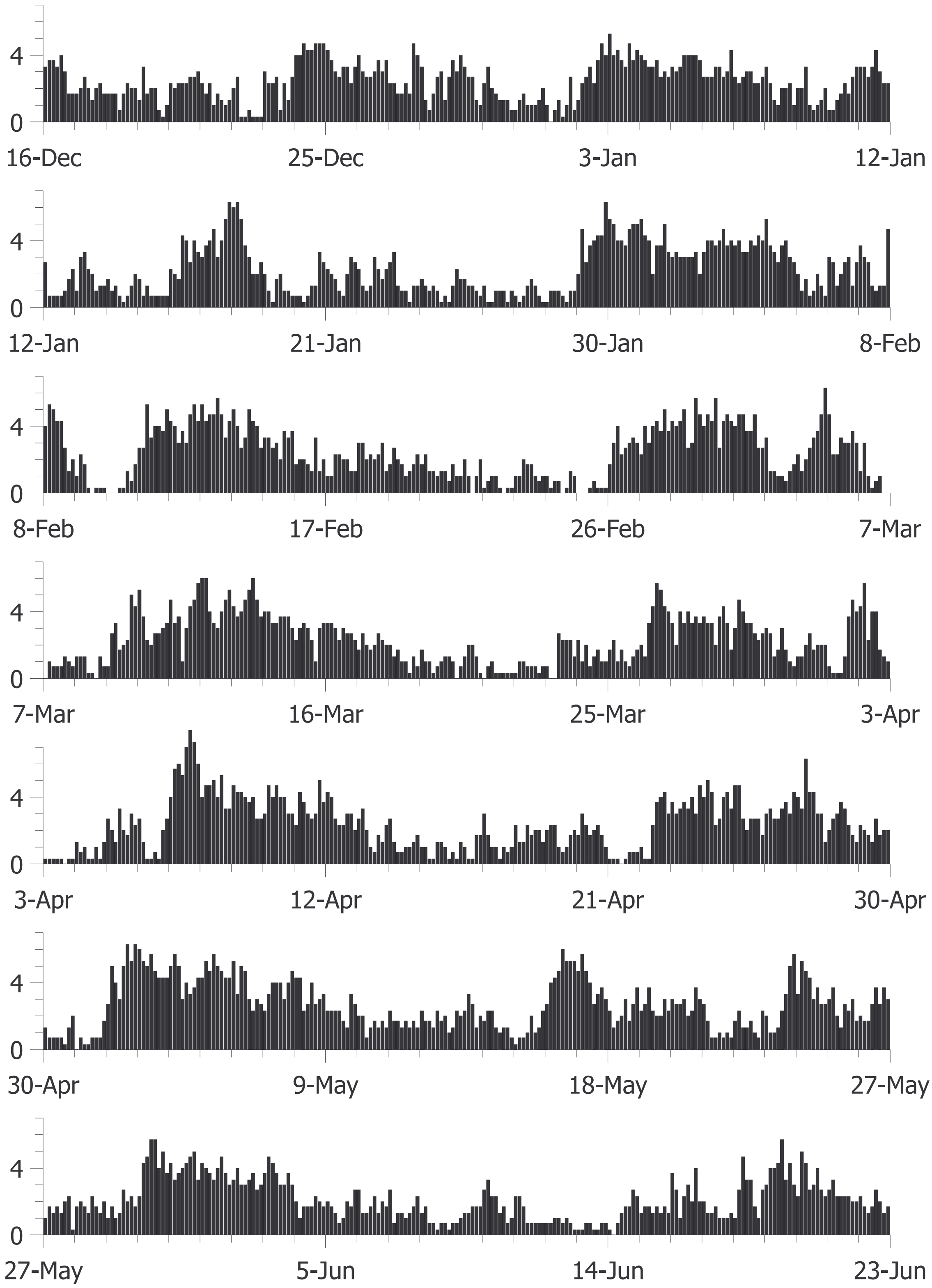

Fig. 4. Geomagnetic Kp-indices in 1995 (first half-year) by Bartels rotations.

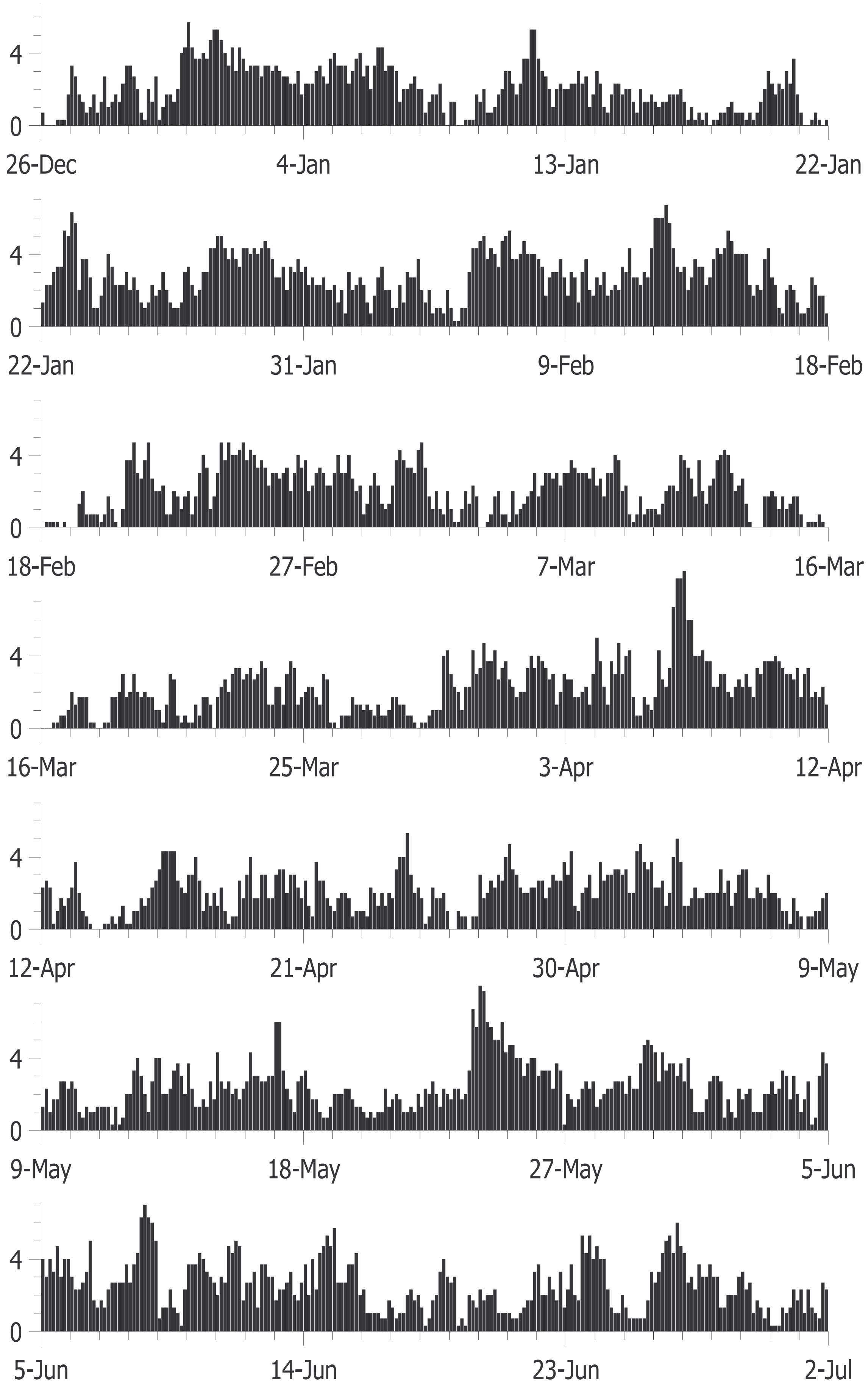

Fig. 5. Geomagnetic Kp-indices in 2000 (first half-year) by Bartels rotations.

The recurrent geomagnetic disturbances, mostly of medium intensity, in 1995 were replaced by non-recurrent geomagnetic disturbances, mostly of severe or very severe intensity, in the year 2000.
The recurrent geomagnetic disturbances are caused by high-speed flows, originating in coronal holes, and reflected on Yohkoh satellite soft X-ray images as places of very low intensity (Fig. 6).
Synoptic maps of coronal holes (Figs 7 and 8) plotted on the basis of the separate Yohkoh satellite

YOHKOH soft X-ray image in graphic form (GIF format)

contour maps made from digital format of the soft X-ray images allow better recognition of coronal holes

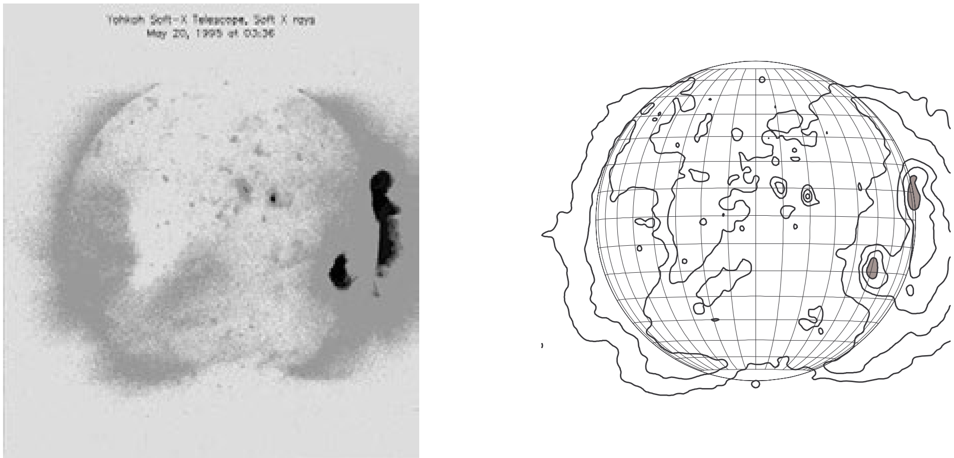

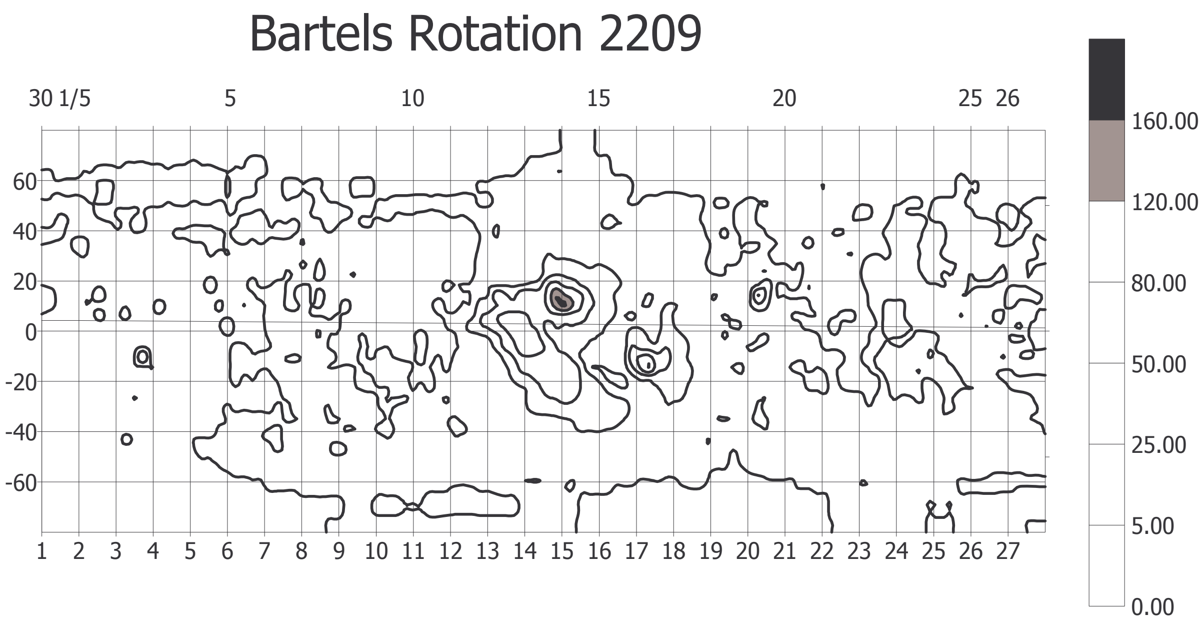

Fig. 6. Images of coronal holes in soft X-rays, and synoptic map of the solar surface constructed from the separate images.

images and supplemented with the relevant solar wind parameters, daily sums of the planetary Kp-index and K-index of the Budkov Geomagnetic Observatory, indicate that the velocity of the solar wind streams interacting with the Earth's magnetosphere, hence also the intensity of the geomagnetic disturbances, depends on the location of the coronal holes on the solar disk, their shape and area. As was shown by Bochníček and Hejda (2002) the areas of minimum intensity of the soft X-rays, associated with the high-speed streams, mostly have the shape of a wedge opened towards the pole and are located almost exclusively in the solar hemisphere facing the Earth (the Northern Hemisphere in autumn and the Southern Hemisphere in spring).

The CMP of the coronal holes was preceded by the occurrence of high-speed streams in the vicinity of the Earth's magnetosphere by about 3.5 days, i.e. the time required for the solar wind, whose velocity is about 600 km/s, to reach the Earth. At the leading edge of the high-speed stream, ion concentration n and the Bz-component of the IMF increase. The proton temperature Tp of the high-speed streams exceeds 10^5 K.

As the purpose of this study is a comparison of the changes in the intensity of solar soft X-rays with those of the values of selected solar wind parameters, the synoptic maps were not plotted in terms of Carrington rotations, but of Bartels rotations. In plotting the synoptic maps of the individual Bartels rotations, all the accessible images from satellite Yohkoh, corresponding to the time interval of the given rotation, were always used. The images were first spread out in a plane, provided with a system of co-ordinates whose equator was in the ecliptic plane. The central meridians of the images so transformed were then placed at the corresponding points of the time scales of the individual Bartels rotations, the images being cut so that they would always cover one half of the time interval preceding the foregoing or following image. The heliographic equator, which oscillates over an interval of ±7.2 degrees in the course of the year with respect to the equator of the co-ordinate system used, is marked in the synoptic maps by a line. As we are used to time axis increasing from left to right, mirror images of the synoptic maps have been used.

The scale of relative intensity was selected so that, by applying *Almg filter data and an exposure time of 5369 ms*, the 'coronal holes' on the synoptic maps would to a high degree correspond with the coronal holes as published by NOAA. For these reasons the 'coronal holes' on the synoptic maps were defined as regions with intensities of less than 5 relative units. Although many high-speed streams originate at high solar latitudes, our analysis based on the individual Yohkoh images indicated that all high-speed streams observed near the Earth's orbit were related to 'coronal holes' that extended below 60 degrees in the co-ordinate system mentioned above. The areas whose latitudes exceeded ±60 degrees were thus omitted.

Non-recurrent geomagnetic disturbances are caused by ejections of coronal matter, CME. Depending on the velocity of the ejection, CME's are divided into slow (~400 km/s) and fast (~1000 km/s). Slow CME's are very closely related to flare prominences whose visible manifestations are disappearing filaments, DSF. The travel time of a slow CME to the Earth's vicinity is about 4 days. Fast CME's, released as a rule from the fringes of active regions, are not related closely to any such visually distinct phenomenon, nevertheless LDE's (Long Duration Event - increase in X-radiation) lasting an hour and longer, and sigmoids (Hudson and Webb. 1997; Rust 1997) have been observed as their precursors. The existence of sigmoids is connected with twisted solar magnetic flux ropes. If the end-to-end twist of the flux rope exceeds ~2.5π, the rope becomes unstable and will kink. Its kink assumes a characteristic sigmoid shape, observable in soft X-rays as coronal brightening. The travel time of a fast CME to the vicinity of the Earth is about 2 - 3 days.

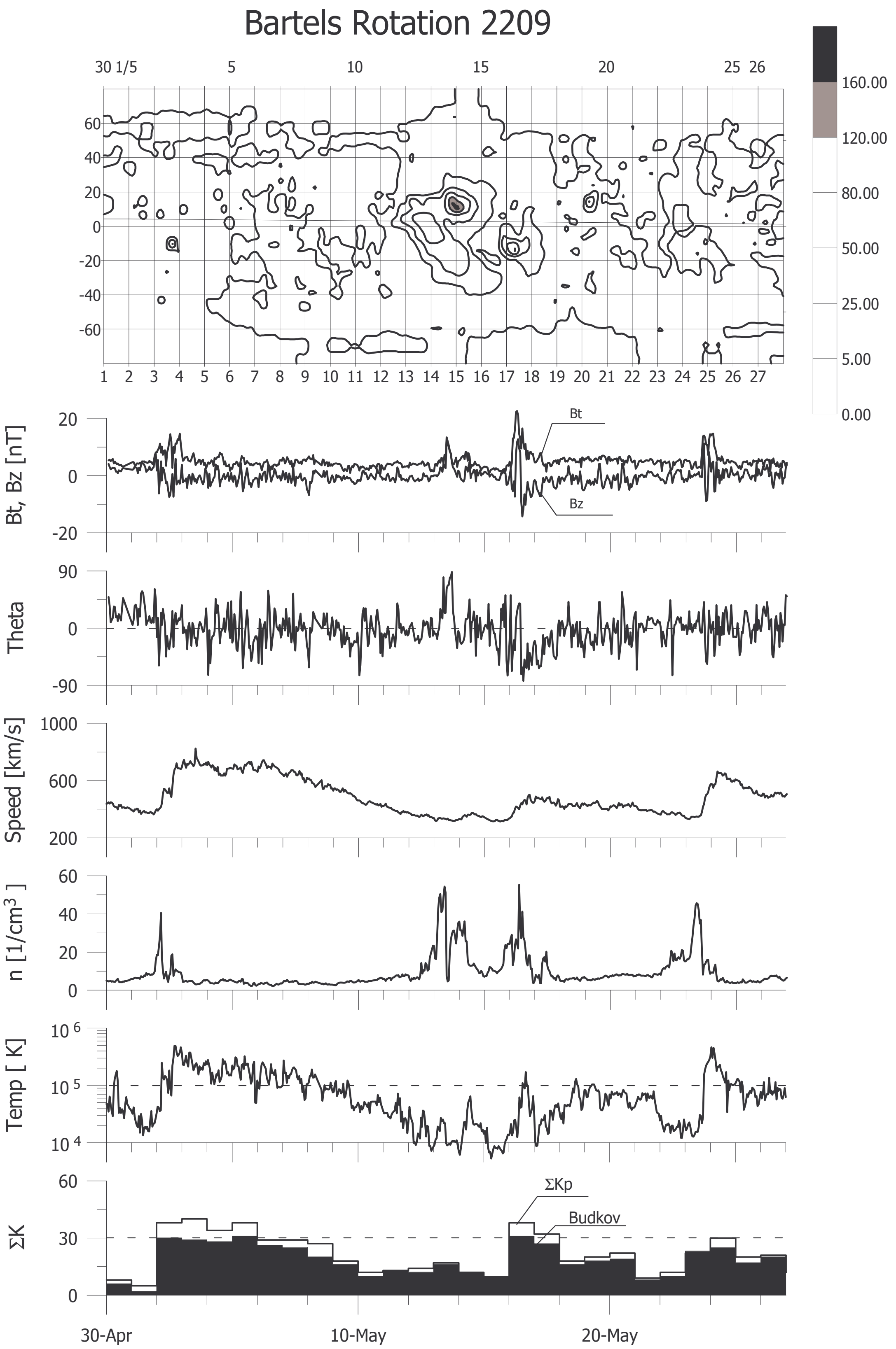

Fig. 7. Synoptic maps of coronal holes and active regions of Bartels rotation no. 2209, constructed from the separate images of the Yohkoh satellite, together with the curves representing the magnetic field, and velocity, density and temperature of the solar wind, as well as the daily sums of the planetary Kp-index and the K-index of the Budkov Geomagnetic Observatory.

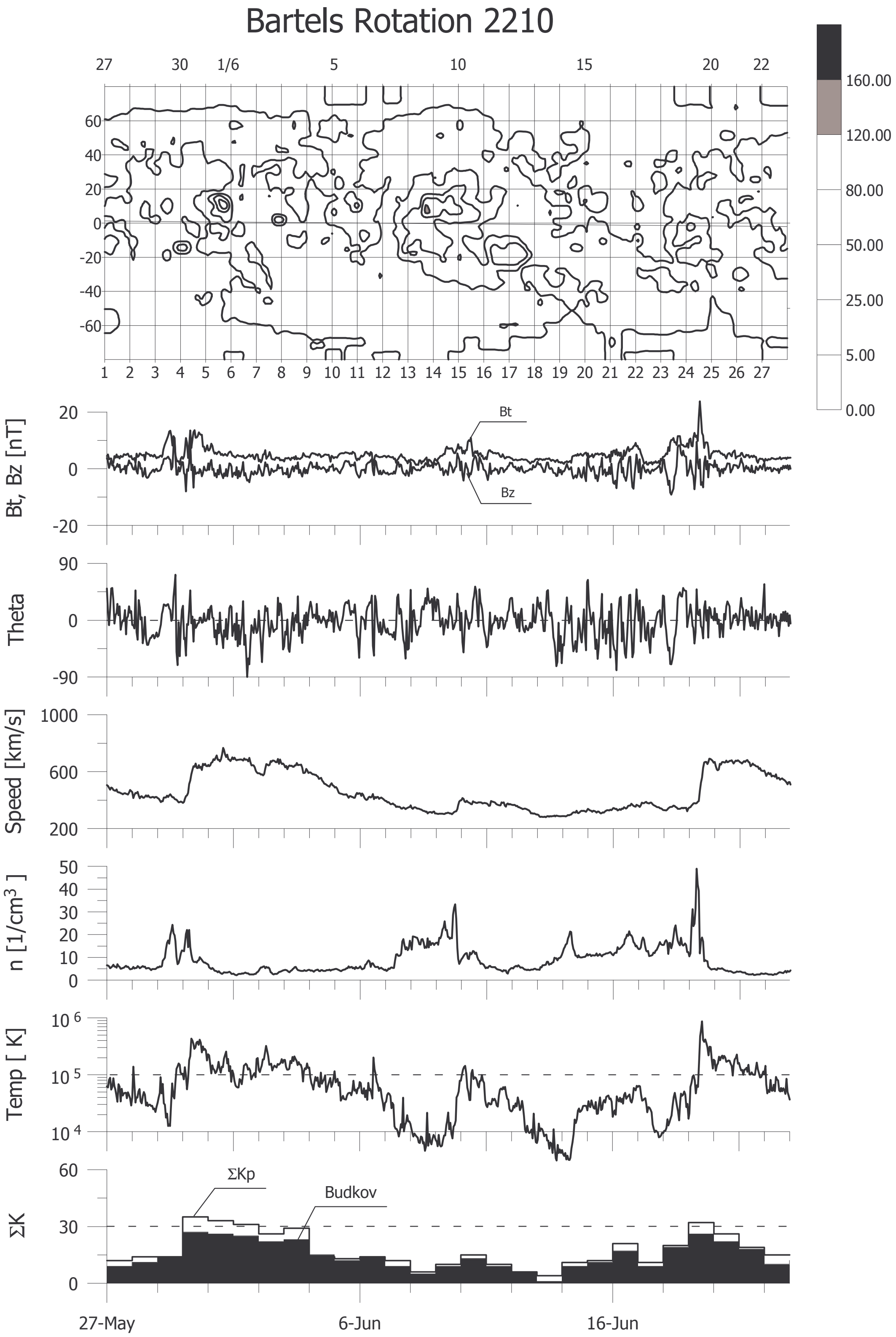

Fig. 8. Synoptic maps of coronal holes and active regions of Bartels rotation no. 2210, constructed from the separate images of the Yohkoh satellite, together with the curves representing the magnetic field, and velocity, density and temperature of the solar wind, as well as the daily sums of the planetary Kp-index and the K-index of the Budkov Geomagnetic Observatory.

A distinct feature of both types of CME is their low proton temperature Tp which does not reach 10^5 K. In comparison with the proton temperature of the high -speed streams it is thus lower (Neugebauer and Goldstein, 1997; Ness, 2001).

The shock wave, generated at the head of the CME, causes an increase in the IMF amplitude and the rotation of its total vector to the south. The amplitude of the CME magnetic field is distinctly higher than the average IMF amplitude. In the course of the interaction of the CME with the Earth's magnetosphere (sometimes lasting as much as tens of hours) the CME magnetic field rotates in the (y;z)-co-ordinate plane at a uniform rate through an angle $\theta = 180°$. This angle, equalling +90°, if the total vector is pointing to the north, and -90°, if the total vector is pointing to the south, thus changes linearly in the course of the interaction. The linearity of this variation indicates that, after one half of the interaction period, i.e. over a period of several hours, the CME magnetic field is pointing to the south. This orientation of the magnetic field of the shock wave,

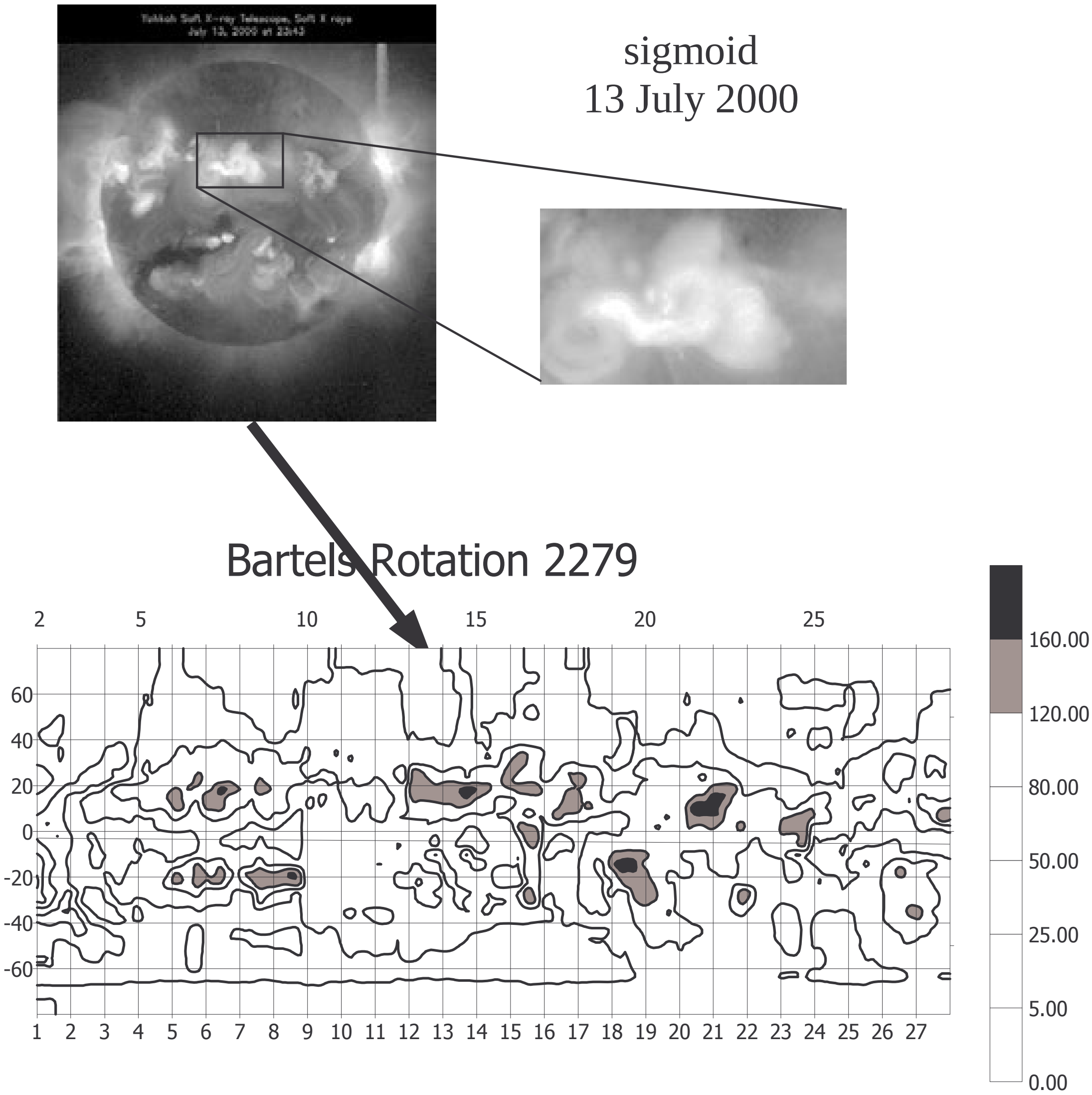

Fig. 9. The situation preceding the geomagnetic storm of July 15, 2001. Image of the solar disk taken by the Yohkoh satellite, detail of the sigmoid, and synoptic map of the solar surface in soft X-rays of the appropriate Bartels rotation. The intensity of the soft X-rays is given in relative units.

followed by the CME magnetic field pointing to the south for several hours, generates severe geomagnetic disturbances (Tsurutani and Gonzales, 1997). An example of such disturbances, which occurred during the most recent cycle, is the geomagnetic storm of July 15, 2000 (Figs 9 - 10).

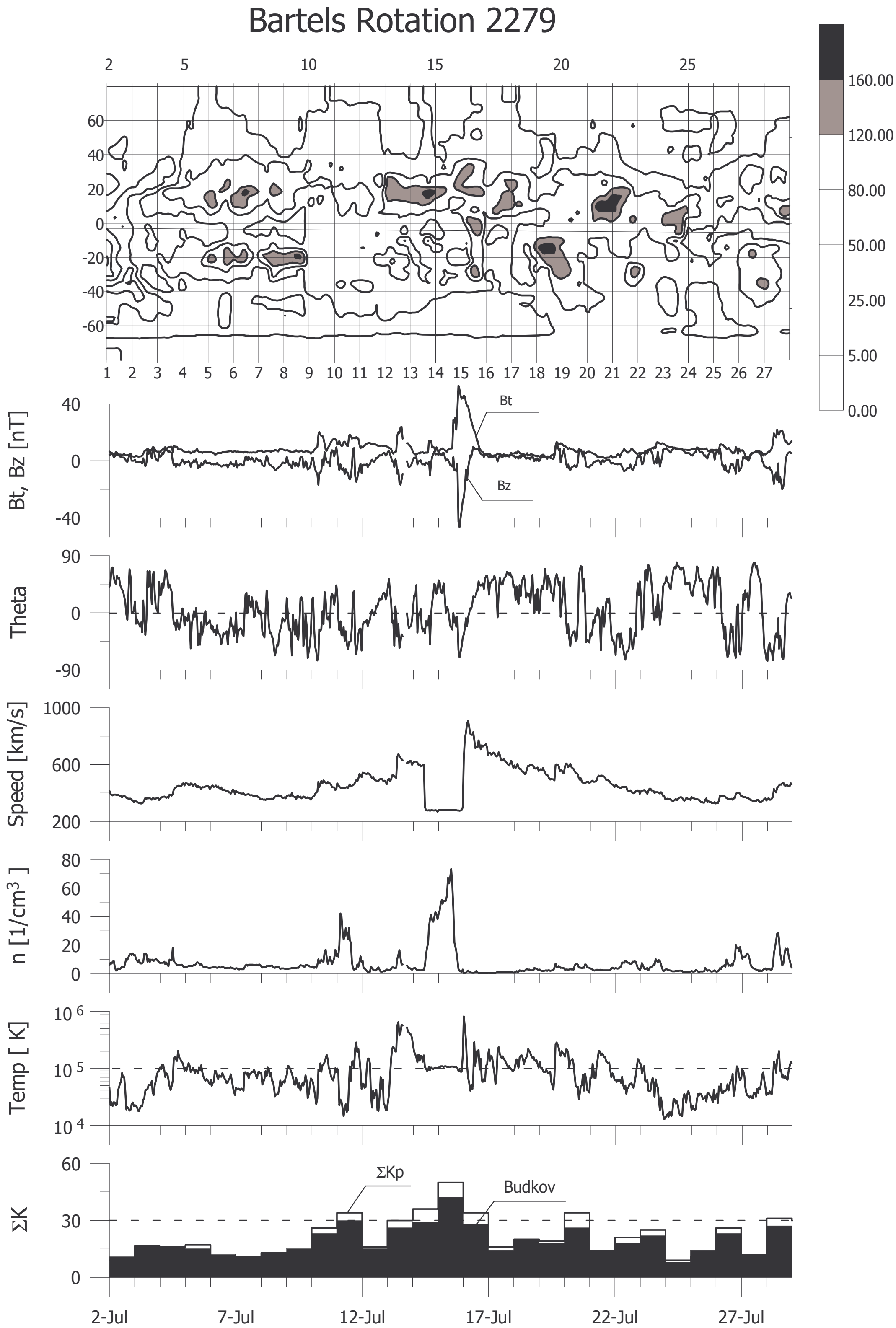

Fig. 10. Synoptic map of the solar surface in soft X-rays for Bartels rotation no. 2279, the magnetic field, and velocity, density and temperature of the solar wind, as well as the daily sums of the planetary Kp-index and the K-index of the Budkov Geomagnetic Observatory.

Discussion

If the geomagnetic activity in 1995 and 2000 are compared in terms of average annual values, negligible differences will be observed between the two years: $\Sigma Kp = 17.3$ in 1995 and $\Sigma Kp = 18.8$ in 2000. Similarly negligible differences will be found if the two years are compared in terms of the number of days on which geomagnetic activity reached or exceeded the level of $\Sigma Kp = 30$, i.e. 46 days in 1995 and 45 days in 2000.

However, if both years are compared in terms of the intensity of geomagnetic disturbances or with the purpose to find the physical causes of the geomagnetic disturbances, distinct differences will be found.

In 1995 there were only 2 cases of the total 46 cases of increased geomagnetic activity which were classified as a major or a severe storm, but in the year 2000 there were 16 cases out of a total of 45 cases of increased geomagnetic activity which were ranked as major or severe storms. Similarly distinct differences existed also in the physical causes of the disturbances.

In 1995 coronal holes were the cause of 37 and irregular events the cause of 7 cases of increased geomagnetic activity, whereas in the year 2000 coronal holes were the cause of 10 and irregular events the cause of 31 cases of increased geomagnetic activity. The dominance of coronal holes and the associated high-speed streams at the time of the solar minimum was replaced by the dominance of irregular events at the time of the solar maximum. These changes occurred because the relative quiescence of the heliomagnetic dipole field, favourable for the origination of geo-effective coronal holes, was replaced at the time of the solar maximum by the relative unrest of the multipole field, accompanied by an increased occurrence of active regions, frequently unstable from a heliomagnetic point of view.

A detailed review of the characteristics of the world-wide and Central European geomagnetic activity in the years 1995 and 2000 is given in Table 1.

	Year 1995 **Solar minimum**	Year 2000 **Solar maximum**
Number of days with ΣKp ≥ 30	46	45
The enhanced activity caused by		
- coronal holes	37	10
- coronal holes + irregular events	2	4
- irregular events	7	31
Level of geomagnetic activity		
- active	17	6
- minor storms	27	23
- major storms	1	13
- severe storms	1	3
Number of days with ΣK ≥ 30 in Central Europe (geomag. observatory Budkov)	9	18
- active	6	5
- minor storms	3	10
- major storms	0	3

Table 1

Table 1 clearly shows that the geomagnetic activity recorded at the Central European observatory of Budkov is slow than the world-wide activity. Long-term comparisons have disclosed this difference, discernible already from the degree 'active', increases with every subsequent higher degree. Hence, geomagnetic activity of the degree 'severe storm' is exceptional in Central Europe.
In view of the differences between the world-wide and regional geomagnetic activity, which differ from region to region, each and every regional forecast of geomagnetic activity should be based on the knowledge of extraterrestrial data, as well as on the knowledge of the long-term behaviour of the geomagnetic field in the region in question.
The Geomagnetic Department of the Geophysical Institute, which has been issuing daily forecasts of geomagnetic activity for Central Europe since 1994, thus bases these forecasts not only on information about solar activity and the solar wind, provided by Space Environment Boulder and satellites Yohkoh, Sohio and ACE, but also on the knowledge of long- and short-term trends in geomagnetic activity, observed at the Czech geomagnetic observatory of Budkov. The issuance of forecasts, financially sponsored by 'The Program for Supporting Targeted Research of the Academy of Sciences', provides a deeper insight into many aspects of the origin of geomagnetic disturbances.

Conclusions

The results of comparing the nature of geomagnetic disturbances which occurred in the years 1995 and 2000, i.e. in the year of the minimum and in the year of the maximum of the most recent solar cycle indicate that:

1) the average annual value of geomagnetic activity in 1995 did not differ very much from the average annual value of geomagnetic activity in the year 2000: ΣKp = 17.3 in 1995 and ΣKp = 18.8 in 2000,

2) the frequency of days on which ΣKp ≥ 30 was practically the same in both years: 46 cases in 1995 as opposed to 45 cases in the year 2000;

3) whereas most of the disturbances which occurred in 1995 were weak to medium (17 active, 27 minor storms, 1 major storm, 1 severe storm) most of the disturbances which occurred in the year 2000 were medium to severe (6 active, 23 minor storms, 13 major storms, 3 severe storms);

4) the predominant source of the geomagnetic disturbances during the solar minimum were coronal holes (37 cases out of 46), the predominant sources of the geomagnetic disturbances during the solar maximum were irregular events (31 cases out of 45);

5) the level of geomagnetic activity in Central Europe as compared to the world-wide level was lower, specifically as of the degree ‘active`.

Acknowledgements

This work was supported by the Project S3012007 of the Academy of Sciences of the Czech Republic and the Grant A3012105/01 of the GA ASCR.

References:

Bochníček J., Bucha V., Hejda P., and Pycha J., 1996: Relation between Northern Hemisphere winter temperatures and geomagnetic or solar activity at different QBOphases. J. Atmos. Terr. Phys. **58**, 883-897.

Bochníček J., Hejda P., 2002: Areas of minimum intensity of soft X-rays as sources of solar wind high-speed streams. J. Atmos. Solar-Terr. Phys. 64, 511-515.

Crooker N. U., Siscoe G. L. : The effect of the solar wind on the terrestrial environment. In: Physics of the Sun, edited by P. A. Sturrock, T. E. Holzer, D. M. Mihalis, and R. K. Ulrich, pp. 193-249, D. Reidel, 1986.

Hudson H. S., Webb D. F. : Soft X-ray signatures of coronal ejections. In: Coronal Mass Ejections, edited by N. Crooker, J. A. Joselyn and J. Feynman, pp. 27-38, AGU, 1997.

Ness N. F. : Interplanetary magnetic field dynamics. In: Space Storms and Space Weather Hazards, edited by I. A. Daglis, pp. 131-155, Kluwer, 2001.

Neugebauer M., Goldstein R. : Particle and field signatures of Coronal Mass Ejections in the solar wind. In: Coronal Mass Ejections, edited by N. Crooker, J. A. Joselyn and J. Feynman, pp.245-251, AGU, 1997.

Rust D. M. : Helicity conservation. In: Coronal Mass Ejections, edited by N. Crooker, J. A. Joselyn and J. Feynman, pp. 119-125, AGU, 1997.

Tsurutani B., Gonzales W. D. : The interplanetary causes of magnetic storms : A review, edited by B. Tsurutani, W. Gonzales, Y. Kamide and J. K. Arballo, pp. 77-89, AGU, 1997.

Southern Africa's Time-Varying Geomagnetic Field

P B Kotzé, Hermanus Magnetic Observatory, South Africa

Abstract

The geomagnetic field at any given epoch is a function of space coordinates, varying differently at each location with time. It has been known that secular change is a comparatively local phenomenon and that it does not proceed in a regular way all over the Earth, giving rise to regions where the field changes more rapidly than elsewhere, like for instance southern Africa.

The Hermanus Magnetic Observatory (HMO) routinely executes geomagnetic repeat surveys, which includes South Africa, Namibia, Zimbabwe and Botswana. Spherical Cap modelling of field survey data between 1970 and 1990 shows that a geomagnetic jerk occurred between 1980 and 1985 over southern Africa as evidenced by a plot of the $g_0^{0,i}$ SCHA internal field coefficient versus epoch. Solving simultaneously for internal and external field coefficients, we find that the $q_1^{1,e}$ external coefficient, which represents the field due to a ring current above the equator, is constant with time. This suggests that the jerk originated deep within the Earth, rather than due to some external source.

Introduction

The geomagnetic field of the Earth varies on timescales ranging from seconds to millions of years. Variations on short timescales are mostly dominated by external sources, while variations on longer timescales (~ 1 year and longer) are collectively known as secular variation (SV) and are predominantly of internal origin. It is also known that secular change is a comparatively local phenomenon and does not proceed in a regular way all over the Earth, giving rise to regions where the field changes more rapidly than elsewhere, as is the case for southern Africa. The observed high SV in southern Africa has been ascribed by *Bloxham and Gubbins* [1985] to rapidly drifting core spots. These intense patches normally occur in the Southern Hemisphere and drift westwards towards South America.

Several localised regions where abrupt changes in the secular variation have occurred are known to date. *Mizuno* [1980] examined the variation in the annual mean value of the north component of the Earth's magnetic field from 1964 to 1976 at the Kakioka Magnetic Observatory and observed abrupt changes in the secular variation rate around 1965 and 1974. Neither of these impulses was of global distribution, showing that regional abrupt changes in the secular variation rate with a time scale of 1 year do exist.

During 1983/1984 an abrupt secular variation change occurred in the southern African sub-continent where the Hermanus Magnetic Observatory routinely executes geomagnetic repeat surveys, including countries such as South Africa, Namibia, Botswana and Zimbabwe. A map showing the location of the various field stations can be seen in Fig. 1.

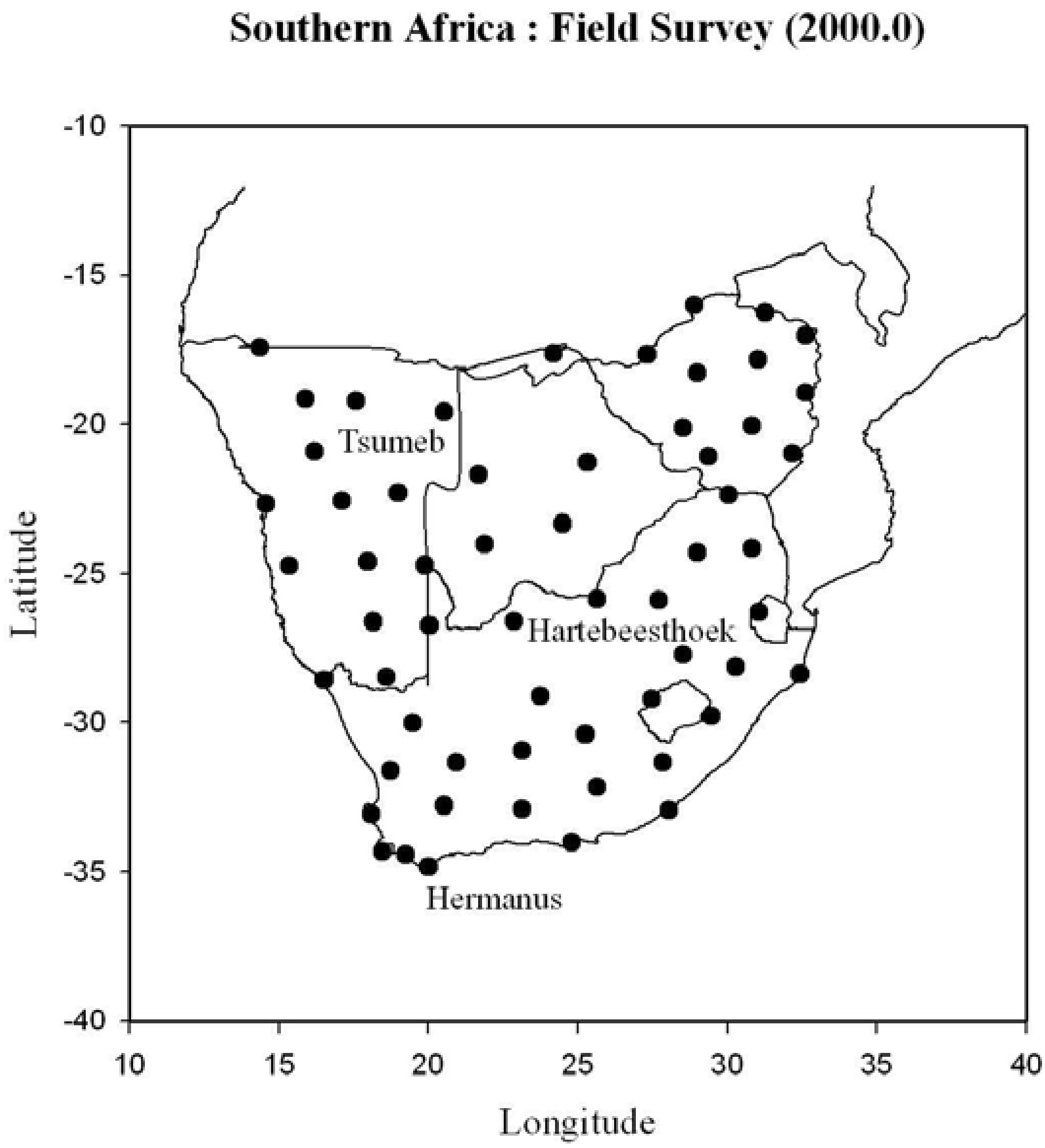

Figure 1. A map showing the various field survey stations for southern Africa as well as the 3 continuous recording observatories at Hermanus, Hartebeesthoek and Tsumeb.

The phenomenon was first observed in the data from the continuous recording stations at Hermanus, Hartebeesthoek and Tsumeb (Namibia), and was subsequently confirmed in results from regional surveys at epochs 1980, 1985, 1987 and 1990 as shown in Fig.2.

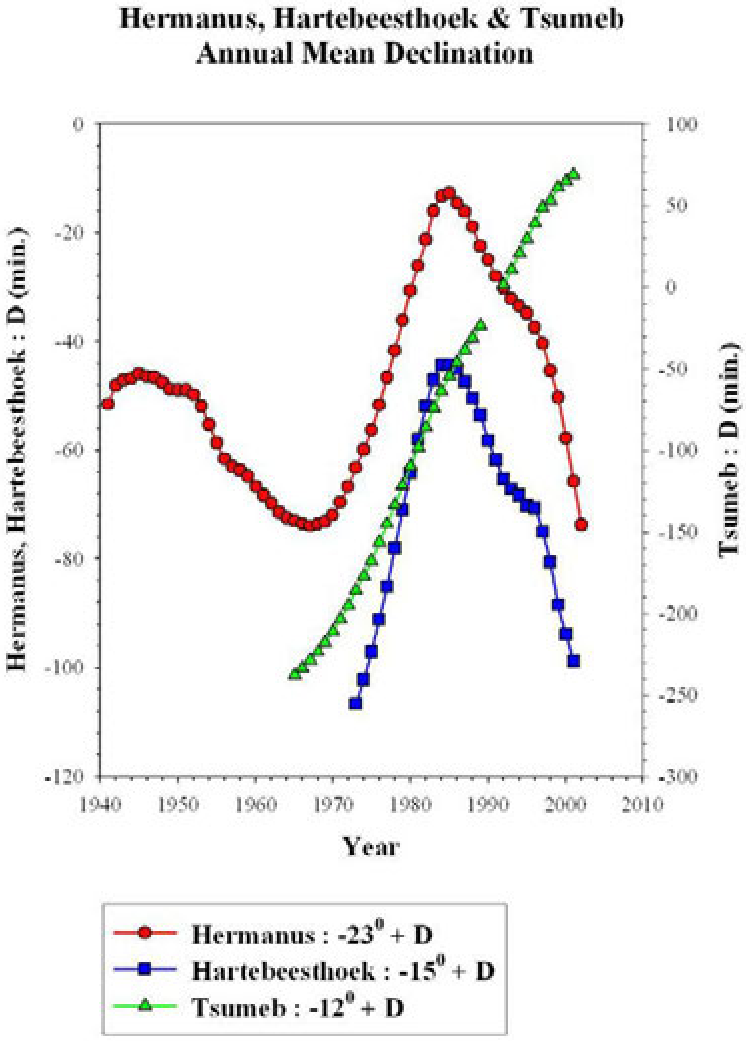

Figure 2. A plot showing the secular variation in declination (D) as observed at Hermanus, Hartebeesthoek and Tsumeb.

Data Collection and Field Surveys

Continuous recording of geomagnetic field variations are conducted at Hermanus (34º 25.5' S, 19º 13.5' E), Hartebeesthoek (25º 52.9' S, 27º 42.4' E) and Tsumeb (19º 12' S, 17º 35' E). The primary instrument for recording of magnetic field variations is the FGE fluxgate magnetometer, manufactured by the Danish Meteorological Institute in Copenhagen, Denmark. This instrument is based on three-axes linear-core fluxgate technology, optimised for long-term stability and records the components H, D and Z. Another system also in operation at all three stations has an integrated design for measuring the Earth's magnetic field by a sequence of firstly measuring the total magnetic field and then four biased values of the magnetic field with a Geometrics sensor mounted at the centre of a set of coils in order to obtain F, H, D and Z.

For field survey purposes, field stations are marked by concrete beacons, ensuring that all observation points are exactly reoccupied during surveys. All measurements are taken on a standard 1.2m pillar as shown in Fig.3. A DI fluxgate magnetometer was used as primary instrument during field surveys to obtain values of D and I, while a Geometrics PPM instrument delivered values of total field intensity (F). During field surveys a Quartz Horizontal Force magnetometer was employed to obtain the horizontal intensity (H). In order to reduce the influence of the geomagnetic diurnal variation, observations were carried out during the period 1800 – 2000 UT, necessitating the use of a special non-magnetic fluorescent lamp in the observation tent.

In our investigation we used only repeat stations that were occupied during all surveys conducted during 1975, 1980, 1985, 1987 and 1990. Corrections for diurnal variation and other disturbing effects were made by comparing field station observations with magnetic data obtained at the continuous recording observatories, Hermanus, Hartebeesthoek and Tsumeb. These field survey measurements were then reduced to a common epoch, by interpolating between the preceding survey (epoch t_1) and the present survey (epoch t_2).
For a particular magnetic field component K, the differential secular variation at field station (FS) relative to control observatory (CO) is given by:

$$\Delta S(K) = \{[K_{CO}(t_2) - K_{FS}(t_2)] - [K_{CO}(t_1) - K_{FS}(t_1)]\}/(t_2 - t_1) \quad \text{……… (1)}$$

where :

$K_{CO}(t_2)$ = value of K at control observatory at epoch t_2

The mean secular variation at the field station is then given by:

S(K) = (annual change at control observatory) – ΔS(K)

The value of a field component K at a particular field station at epoch t_3 is then given by:

$$K_{FC}(t_3) = K_{CO}(t_3) - [K_{CO}(t_2) - K_{FS}(t_2)] - \Delta S(K) * (t_3 - t_2) \quad \text{……….. (2)}$$

Since the surveys were conducted during 1980, 1985, 1987 and 1990, the time span for reduction of data amounts to less than 1 year.

Figure 3 : A picture showing a typical 1.2 m high field survey concrete beacon.

Modelling of Field Survey Data

Spherical Cap Harmonic Analysis [*Haines*, 1985] was used to model the field survey data sets between 1975 and 1990.
Spherical Cap Harmonic Analysis (SCHA) is mathematical technique developed specifically to model a potential field and its spatial derivatives, or a general function and its surface derivatives, on a regional scale in order to overcome the non-orthogonality problem in the case of global spherical harmonic models when applied to restricted areas. The SCHA modelling technique has also been used successfully to derive a regional field model over southern Africa, using vector data from the Ørsted satellite mission [*Kotzé*, 2001].

The solution to Laplace's equation over a spherical cap for both internal as well as external sources is given by :

$$V(r,\theta,\lambda) = a\sum_{k=0}^{K\,\mathrm{int}}\sum_{m=0}^{k}\left(\frac{a}{r}\right)^{n_k(m)+1} P_{n_k(m)}^{m}(\cos\theta) * \left[g_k^{m,i}\cos(m\lambda) + h_k^{m,i}\sin(m\lambda)\right]$$

$$+ a\sum_{k=1}^{Kext}\sum_{m=0}^{k}\left(\frac{r}{a}\right)^{n_k(m)} P_{n_k(m)}^{m}(\cos\theta) * \left[q_k^{m,e}\cos(m\lambda) + h_k^{m,e}\sin(m\lambda)\right] \ldots\ldots(3)$$

where :

r, θ, λ are the geocentric spherical coordinates radius, colatitude, and longitude;

a = reference radius;

$P^m_{n_k(m)}(\cos\theta)$ = associated Legendre function with integral order *m* and real degree $n_k(m)$;

k = ordering index, with Kint the maximum index for internal sources, and Kext the maximum index for external sources;

$g_k^{m,i}, h_k^{m,i}, q_k^{m,e}, h_k^{m,e}$ are the spherical cap coefficients.

If the half-angle of the spherical cap is denoted by θ_0, the $n_k(m)$ are determined as the roots of the equation, for given *m* :

$$dP^m_{n_k(m)}(\cos\theta_0)/d\theta = 0\,,\ k - m = \text{even} \quad \ldots\ldots\ (4)$$

and additionally, if differentiability with respect to θ is required :

$$P^m_{n_k(m)}(\cos\theta_0) = 0\ ,\ k - m = \text{odd} \quad \ldots\ldots\ldots\ (5)$$

If the expansion in Eq. (3) is truncated at k = K, the number of model coefficients is $(K+1)^2$.

When applying spherical cap harmonic analysis, it is recommended to remove a global spherical harmonic potential from the total potential in order to improve convergence as well as extrapolation beyond the spherical cap boundary [*Haines*, 1985]. In this study the IGRF (n = m =10) models were subtracted from the field survey component data, while K_{int} = 4, and K_{ext} = 2 model parameters were used to simultaneously determine internal and external modelling coefficients. A half-cap angle of 20º provided a best fit to data for all surveys.
Spherical cap modelling of the field survey measurements between 1970 and 1990 shows that a geomagnetic jerk did occur between 1980 and 1985 over the southern African region as evidenced by a plot (Fig. 4) of the $g_0^{0,i}$ internal field coefficient as a function of time.

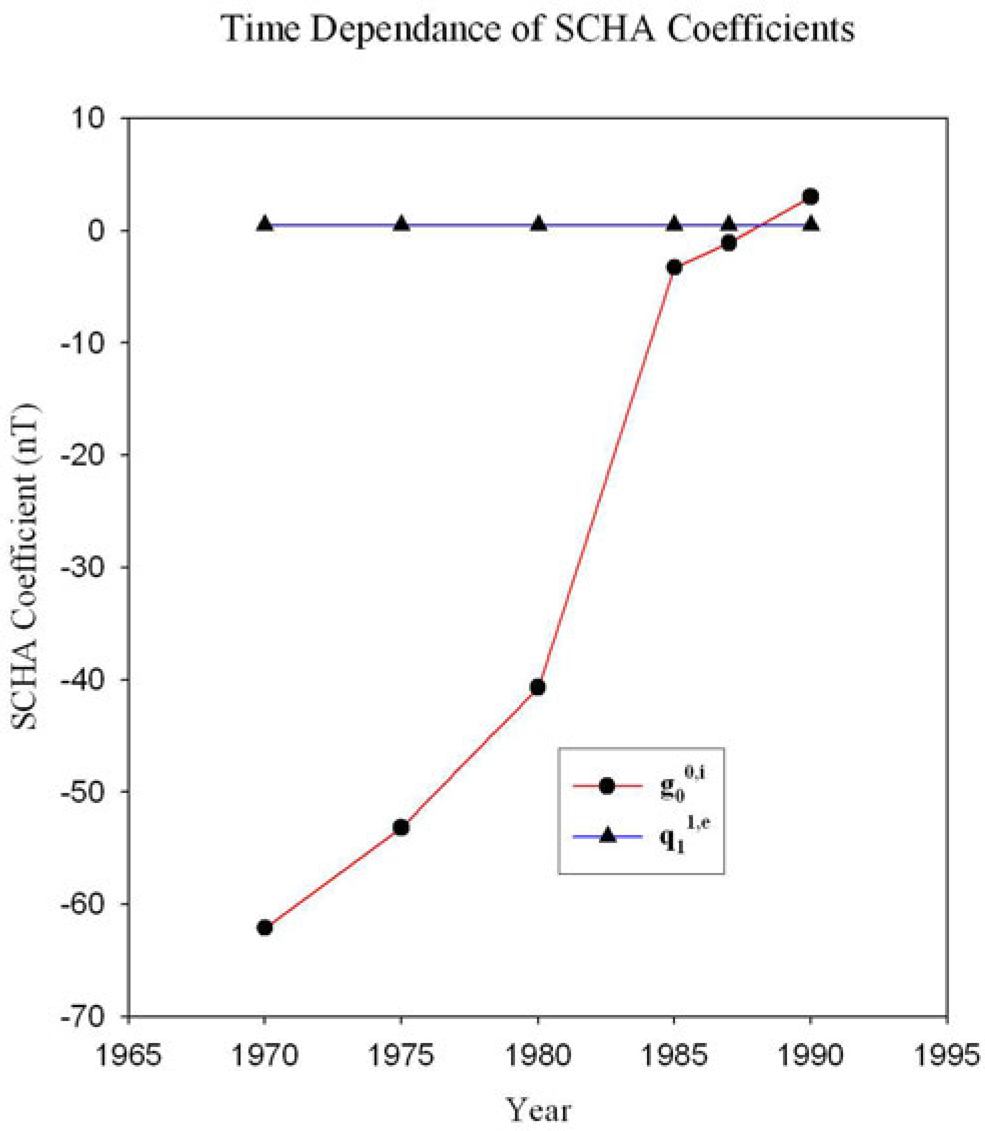

Figure 4. A plot showing the time dependence of both internal and external SCHA coefficients as derived from modelling field survey data between 1970 and 1990.

Solving simultaneously for both internal as well as external field coefficients, we find that the $q_1^{1,e}$ external coefficient is constant with time. This suggests that the observed jerk originated deep within the Earth, rather than due to some external source.

Discussion and Conclusions

The results obtained in this investigation confirm that internal sources can give rise to changes in the geomagnetic secular variation on time scales of 1 to 2 years, supporting previous results obtained by *Malin and Hodder* [1982], who argued that internal sources were responsible for the 1969 global geomagnetic jerk. Internal sources were therefore the major factor in the observed geomagnetic jerk that occurred in southern Africa around 1984.

It is also evident from Figure 2 that an acceleration process is busy taking place in the secular variation for declination as observed at both Hermanus and Hartebeesthoek. In contrast, however the secular variation as observed at Tsumeb shows no such behaviour, but is moving in the opposite direction of Hermanus and Hartebeesthoek. The consequence of this is that the gradient in declination over southern Africa is increasing with time. It is also evident that we will be able to measure the largest declination value at Hermanus since its existence in 1941.

References

Bloxham, J and D Gubbins, The secular variation of Earth's magnetic field, *Nature*, **317,** 777-781, 1985.

Haines, G V, Spherical cap harmonic analysis, *J Geophys. Res.* **90**, 2583-2591, 1985.

Kotzé, P B, Spherical cap modelling of Ørsted magnetic field vectors over southern Africa, *Earth Planets Space*, **53**, 357-361, 2001.

Malin, S R C, and B M Hodder, Was the 1970 geomagnetic jerk of internal or external origin ? *Nature*, **296**, 726-728, 1982.

Mizuno, H, Abrupt change in secular variation rate of geomagnetic north component observed in Japan, *J Geomag. Geoelectr.*, **32**, 413-420, 1980.

Elimination of Magnetic Perturbations Generated from a Warm-Water Heating System in Magnetic Measurement Buildings

E. Pulz, H.-J. Linthe

GeoForschungsZentrum Potsdam, Adolf-Schmidt-Observatorium
Lindenstr. 7
D-14823 Niemegk, Germany

Abstract

Geomagnetic observatories spend considerable effort to avoid artificial influences from the environment. However, it is even more important to avoid self-made disturbances. At Niemegk observatory, three buildings – the absolute house, the variometer house and the magnetic laboratory – are heated by a dedicated hot-water heating system. In 1993 the old coal-burning boiler was replaced by one, which runs on natural gas. From that time, disturbances of the magnetic recordings have been noticed. These disturbances became particularly obvious after more sensitive geomagnetic instruments came into use. Over the last ten years various methods were undertaken to find the physical reasons for the disturbances and to eliminate their influence. We describe the effect, its physical causes and the measures we have taken to eliminate the problem.

Introduction

Since the Adolf-Schmidt-Observatory in Niemegk was founded, the absolute house, the variometer house and the magnetic laboratory are heated by a dedicated hot-water heating system. Later, an additional electric heating system was installed because of the very good temperature control possibility. So an optimal working environment is obtained for the magnetic recording equipment. No influences on the magnetic recordings were observed during all the years. Classical magnetometers, fluxgate magnetometers, and Overhauser effect proton magnetometers are in operation in the variometer house. After replacing the old coal-burning boiler by one which runs on natural gas in 1993, we observed a large influence on the magnetic recordings. We undertook several measures to minimise this influence. Since 1996 two K-tandem magnetometers [1] are in operation in the magnetic laboratory, working like a gradiometer. Unfortunately these very sensitive magnetometers very obviously always recorded the disturbing influences of the heating system. We had no solution to suppress the perturbations unless to reconstruct the heating system extensively.

The Heating System

The heating house supplies three buildings – the absolute house, the variometer house and the magnetic laboratory – as the schematic drawing in Fig.1 shows. Up to 1993 an old coal-burning boiler was in operation. The copper pipes run undergrounds to the three houses. Within the buildings no ordinary radiators are used, but snaky copper pipes are installed instead. Fig. 2 shows the schematic arrangement. At Fig. 3 the detail is shown. Unfortunately, this construction of the heating radiators forms an electric coil with a vertical axis. So, if a current is flowing in this coil, a vertical magnetic field is generated.

In 1993 the coal-burning boiler was replaced by a modern type, which runs on natural gas. However, only the boiler was removed while the other parts of the heating system remained essentially unchanged.

The heating system is in use only during the heating period, if the outdoor temperature is for long periods less than approximately 5-8 degrees centigrade. For several months in summer the heating system is not in operation.

The Influence of the Heating System on the Magnetic Recordings

Up to 1990 exclusively classical methods were in use in the variometer house. Until this time nobody noticed any effect from the running heating system. Causes may be:

- The classical instruments were not sensitive enough.
- The running heating system generated only very tiny magnetic effects.

Afterwards we could not find any of these effects.
In 1991 the French GEOMAG recording system M390 (3-component fluxgate magnetometer and an Overhauser effect proton magnetometer SM90) was installed in the variometer house. In 1993 a 3-component fluxgate magnetometer FGE and a second Overhauser effect proton magnetometer GSM19 were added. Also nobody noticed any effect caused from the running heating system.
Then, after replacing the boiler we immediately observed a strong effect. The disturbances were clearly visible in data from all magnetometers in the variometer house There was a magnetic disturbance at every start processes of the natural gas burning boiler. Not immediately from the beginning it was clear, that thermoelectric currents flowing in the heating pipes are the main reason of the disturbances.
At first the electrical ignition was assumed being the reason of the disturbing effect. So the boiler was replaced by a boiler with low flame ignition. The magnetic disturbances were reduced however not eliminated. An improvement of this situation was achieved by installing of an isolating transformer between mains supply and the boiler. Further we tried to make short circuits between the forward and the backward pipes to suppress any current flowing in the heating pipes in the measurement rooms. The disturbances were reduced however not eliminated. Nevertheless the results of our measures show the correctness of our way. In 1997 we installed finally an electrical insulating piece of pipe immediately at the boiler into the forward and the backward pipe. The reduction of the magnetic disturbances looked at that time satisfying, but the disturbing effect could not be completely suppressed.
After finishing the VIIth IAGA Workshop on Geomagnetic Observatory Instruments, Data Acquisition and Processing in September 1996 we installed two optically pumped magnetometers (OPMs), a K-tandem magnetometer and a Cs-He magnetometer [1], in our magnetic laboratory. The distance between both of them was approximately 50 cm in E-W direction. The comparison of the recordings of both of them, and with the two proton magnetometers (PMs) in the variometer house showed that the disturbances caused by the heating system still exist. This can be demonstrated by means of Figs. 4-6. Fig. 4 shows a comparison between the OPM recordings when the heating system is out of operation; Fig. 5 shows the same comparison in case of the working heating system. At Fig. 6 a comparison between an OPM and a PM recording is shown also during the operation of the heating system. The disturbing effect at Fig. 6 has about the double size of that at Fig. 5. That means: the direction of the disturbing magnetic field at the magnetic laboratory is in opposite to that in the variometer house.
In spite being aware these perturbations on our magnetic recordings during several years it was impossible to resolve the heating problem because of financial limitation. During the wintertime 2001/2002 we remarked an increasing of the disturbances caused by the heating system; and therefore we decided to clear away the disturbances after all.

The Cause of the Magnetic Disturbances

We can imagine the following causes:

- Thermoelectricity at pipe connections with different metals
- Electrolysis or galvanic elements caused by polluted water in the pipes
- Ionisation of the flame inside the boiler
- Grate pollution

Different experiments were carried out to find out the causes, and to find out a cheap solution of this problem if possible. During all experiments two OPM sensors were situated inside the East room of the magnetic laboratory and a third one outside of the building. Three-second mean values were recorded. Fig. 7 shows the comparison of the recordings of the two OPMs inside the room. The interval mode operation of the boiler can be clearly recognized. Fig. 8 shows the comparison of the outside OPM and the inside OPM during a start of the heating process. The boiler temperature is shown in the lower diagram. A clear correlation is to be seen.
Fig. 9 shows the result of another experiment: We made a short circuit between the forward and the backward pipes (look at Fig. 2) inside of the room, which the both OPM sensors are situated in. The decreasing of the heating effect is clear visible, and simultaneously an additional offset occurs. From these results we calculated a coil current of 3 mA, which is necessary to generate this magnetic field. If we assume a resistance of <10 Ohm of the copper pipe, so there is a voltage of <0.3 mV necessary to drive this current. The resistance of water (even if it is strongly polluted) is at least thousand fold higher than that of the copper pipes. This would require a voltage of 300 V, which can be produced neither by the thermoelectric effect, nor by a galvanic element. So electrolysis and galvanic elements can be excluded from the reasons for the disturbing effect. Also the assumptions of ionisation of the flame inside the boiler and grate pollution can be excluded because of the galvanic disconnection of the boiler from the entire heating system by means of the non-metallic pipe pieces (see above).
A further experiment proved additionally our theory of thermoelectricity: During summertime the circulation pump was started in case of switched-off boiler burner. Even in that working mode the effect could be observed. This can be explained as follows: If the system is out of operation for longer periods, the water temperature in the pipes in buildings is nearly equal to the air temperature, while the water temperature in the underground pipes is determined by the ground temperature. Air temperature and ground temperature differ by several degrees. If the obviously cooler water flows from underground pipes through the warmer pipes in the buildings, temperature differences occur at connections of different metals and a thermoelectric current is produced. The disturbing effect on the magnetometers decreases; the more the water temperature becomes balanced in the entire heating system.
For sure only one effect - the thermoelectricity - could be proved. The only question is: Why are the disturbances only obvious in case of the new natural gas burning boiler, though all the further entire heating system remained unchanged? It can be explained as follows: During the heating period the old coal-burning boiler was heated nearly continuously, depending on the necessity (outdoors temperature). The circulating pump, which was obviously not very effective, transported the warm water rather slowly through the entire system. So the water temperature inside of the heating system increased slowly and remained nearly constant during a long period. After stopping of the boiler heating the entire system slowly cooled down. Because of this working regime strong temperature differences could not occur at any construction part of the heating system. So thermoelectric currents were not generated or if any occurred, they were so small, that they did not induce remarkable disturbing magnetic fields in the recording rooms.
Modern natural gas burning boilers work in an interval mode. So there are periods of rather strong warm water flowing in the system and periods of no flowing and cooling down of the water. This mode obviously causes temperature differences at construction parts of the heating system. There are different metals (copper, brass) directly connected in the heating system and so thermoelectric

currents are generated and flowing through the system. All our experiments clearly demonstrate this result.

The Reconstruction of the Heating System

The reconstruction of our heating system should be inexpensive and disrupt the operating of the observatory as little as possible. Therefore we made further tests to remain as large as possible portions of the old heating system. We replaced gradually more and more copper parts by plastic parts (Fig. 10). The magnetic disturbances were reduced more and more. But we finally decided on a complete replacement of all the copper pipes by plastic ones within the buildings anyway. We concluded not only in a simple replacement, but we further decided to avoid constructing the room heating in form of electrical coils. As shown schematic for one room at Fig. 11, the radiator pipes will be mounted in bifilar manner. This anti-parallel mounting of the pipe pairs suppresses the efficiency of any electrical current in the pipes.

Conclusion

It is rather a catastrophe, if a geomagnetic observatory disturbs its own recordings by self-made perturbations. No effort is too big, to avoid such a situation.

In our case the modernisation of a heating system suddenly showed problems, which never occurred before and which nobody expected. Such modern natural gas burning boilers are used in thousands in central heating systems and nobody notices any perturbation produced by the boiler. But the use in a geomagnetic observatory is so problematically! Unfortunately there is no gas or oil burning boiler available, which works in a similar mode, as an old coal burning one: burning continuously at a controlled temperature and transporting the warm water slowly through the heating system.

This report shows which high expense is necessary and how long it can take, to find the reason of self-made perturbations and to suppress them satisfying.

At present the reconstruction of the heating system is in progress.

Acknowledgement

We are grateful to R. Holme, the former director of the Adolf-Schmidt-Observatory, for the promotion of this job.

References

[1] E. Pulz, K.-H. Jäckel, H.-J. Linthe:
A new optically pumped tandem magnetometer: principles and experiences
Meas. Sci. Technol. **10** (1999) p.1025-1031

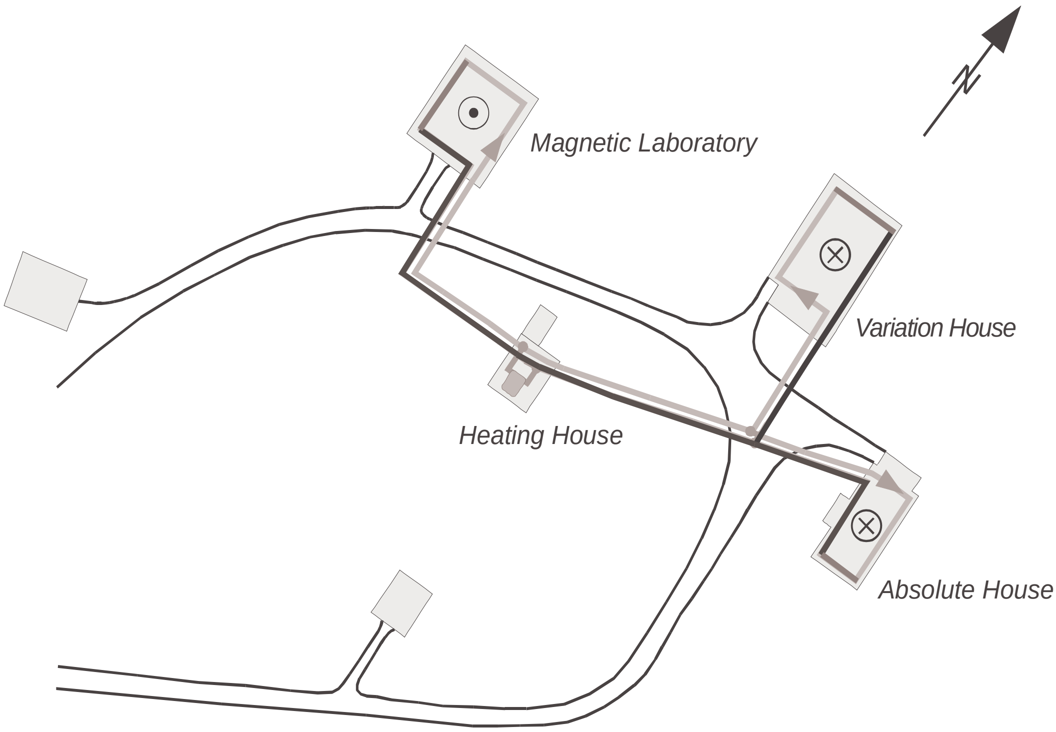

Fig.1 Schematic arrangement of the entire heating system

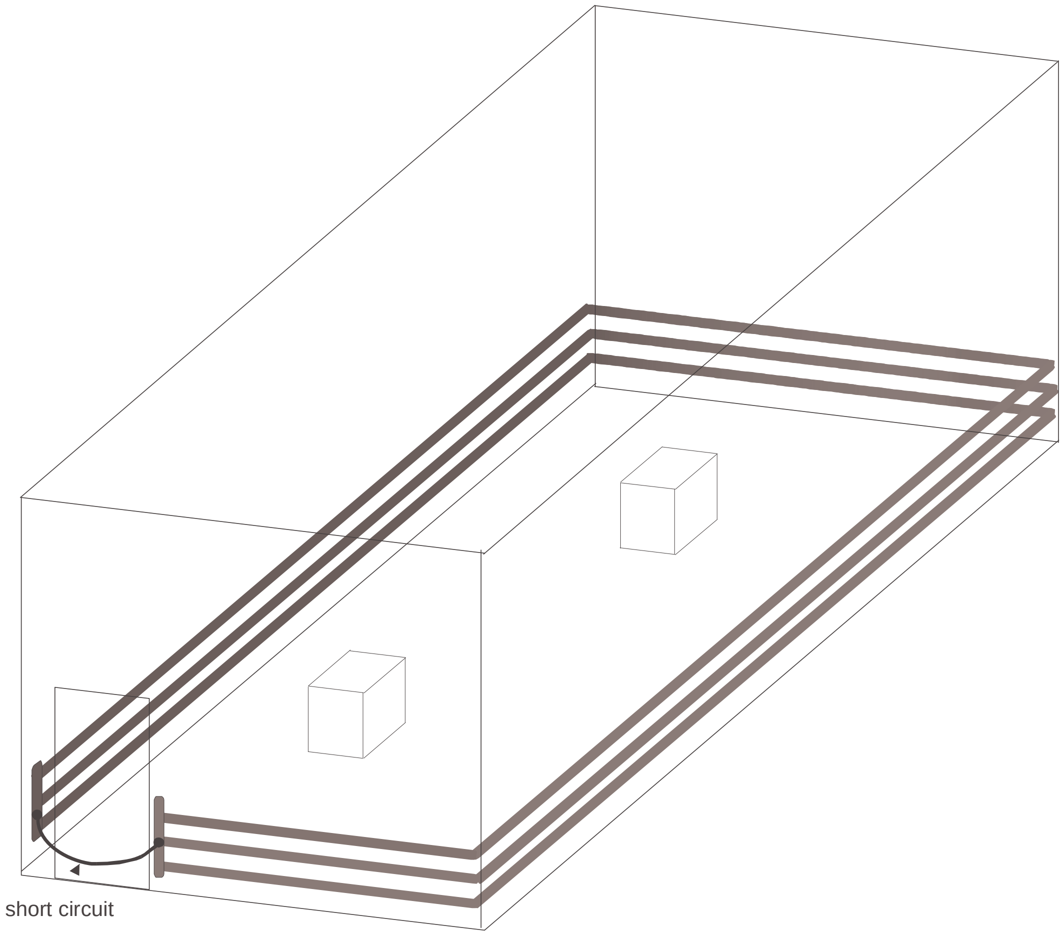

Fig. 2 Schematic arrangement inside of the building

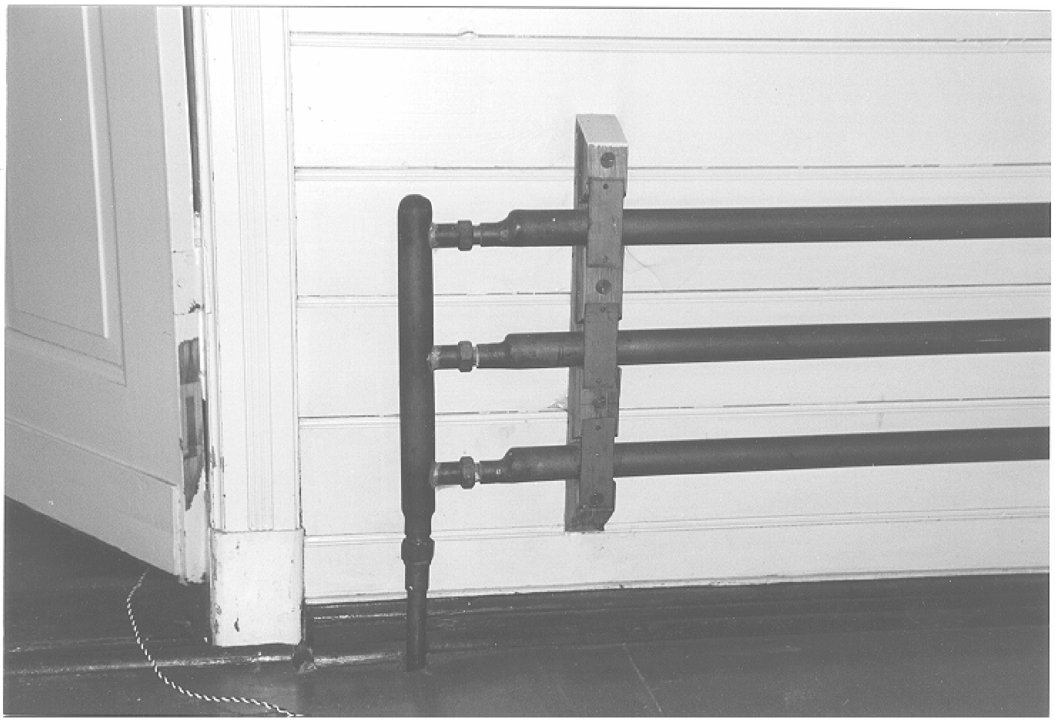

Fig. 3 Detail of a room

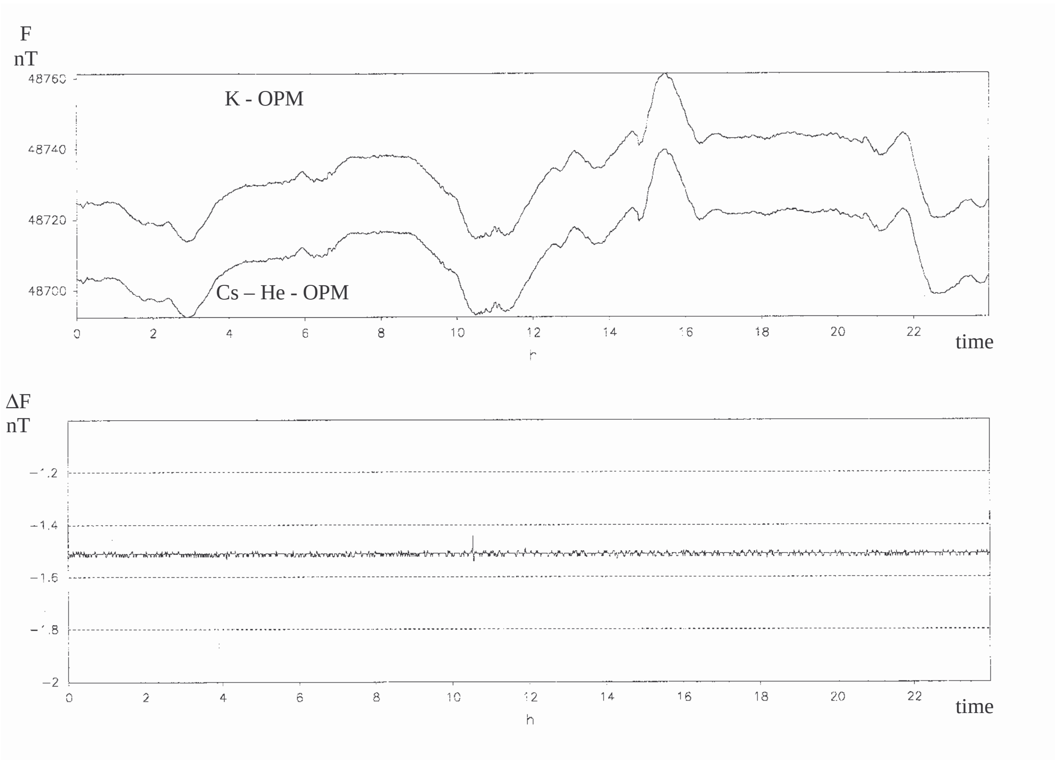

Fig. 4 Minutes mean values comparison of two OPMs when the heating system is out of operation. (at 19 October 1996)

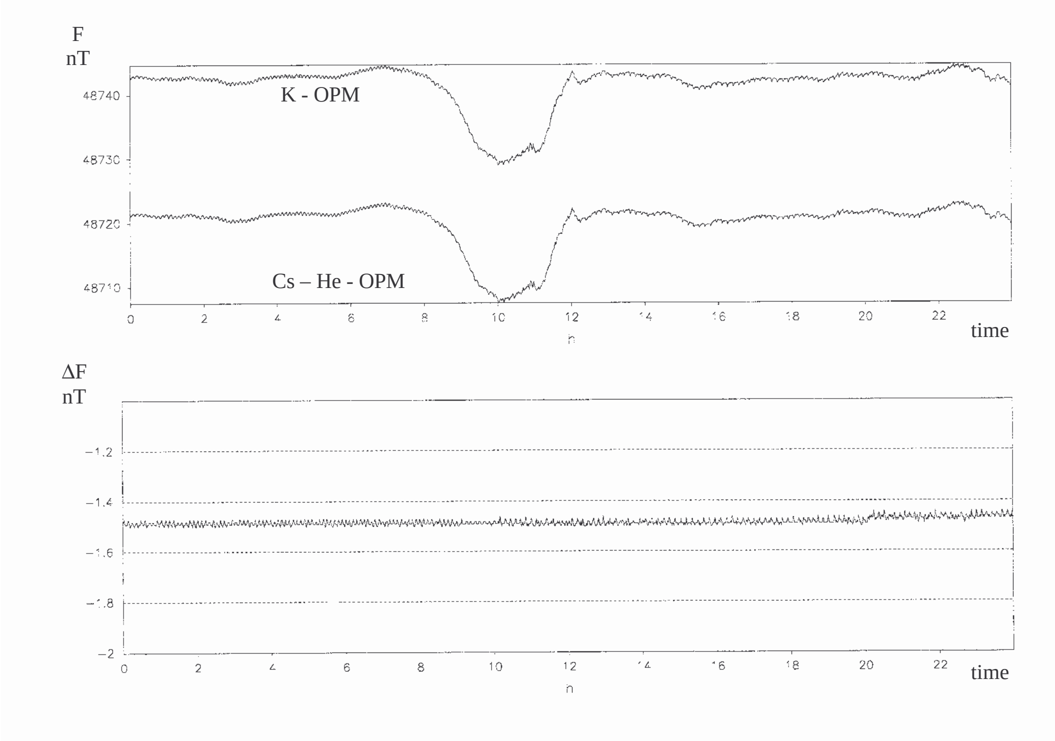

Fig. 5 Minutes mean values comparison of two OPMs when the heating system is in operation. (at 27 October 1996)

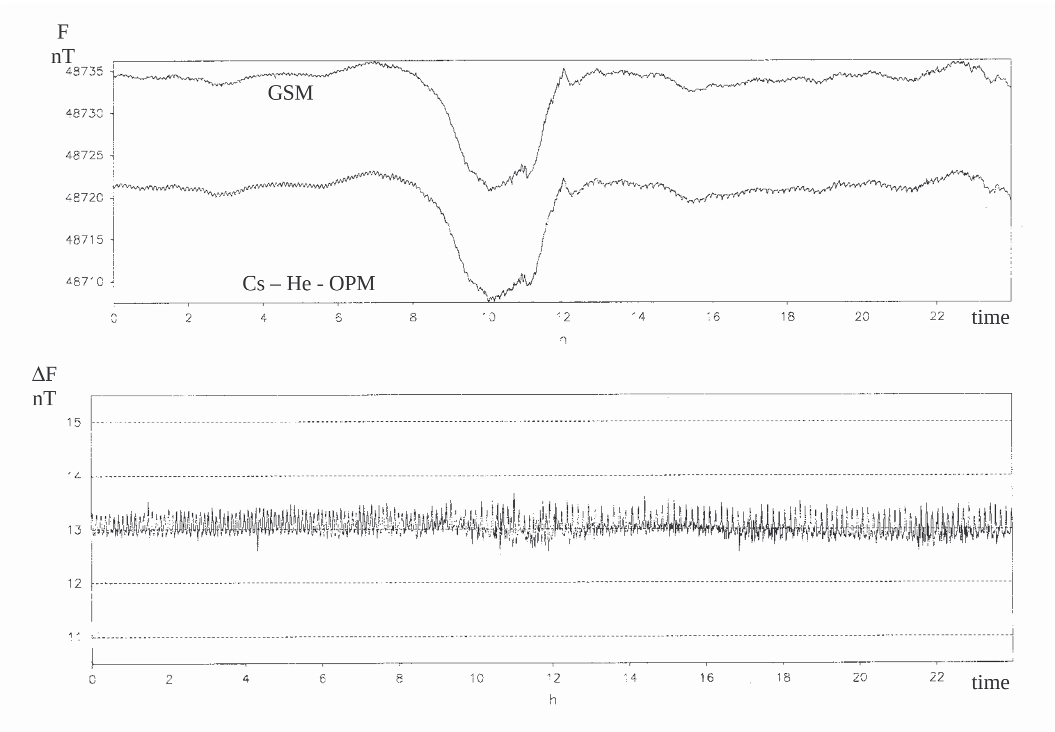

Fig. 6 Minutes mean values comparison of two magnetometers when the heating system is in operation. (at 27 October 1996)

The GSM is located in the variometer house while the OPM is in the magnetic laboratory.

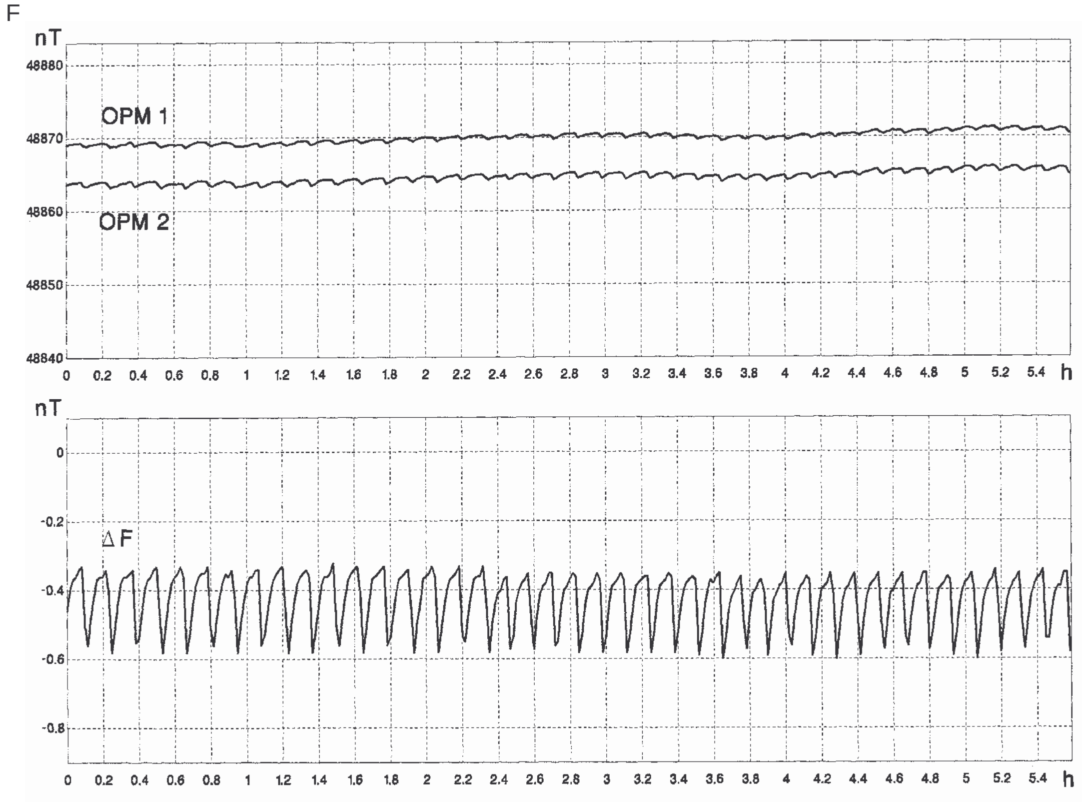

Fig. 7 Three second mean values comparison of two OPMs when the heating system is in operation. (at 9 January 2002)

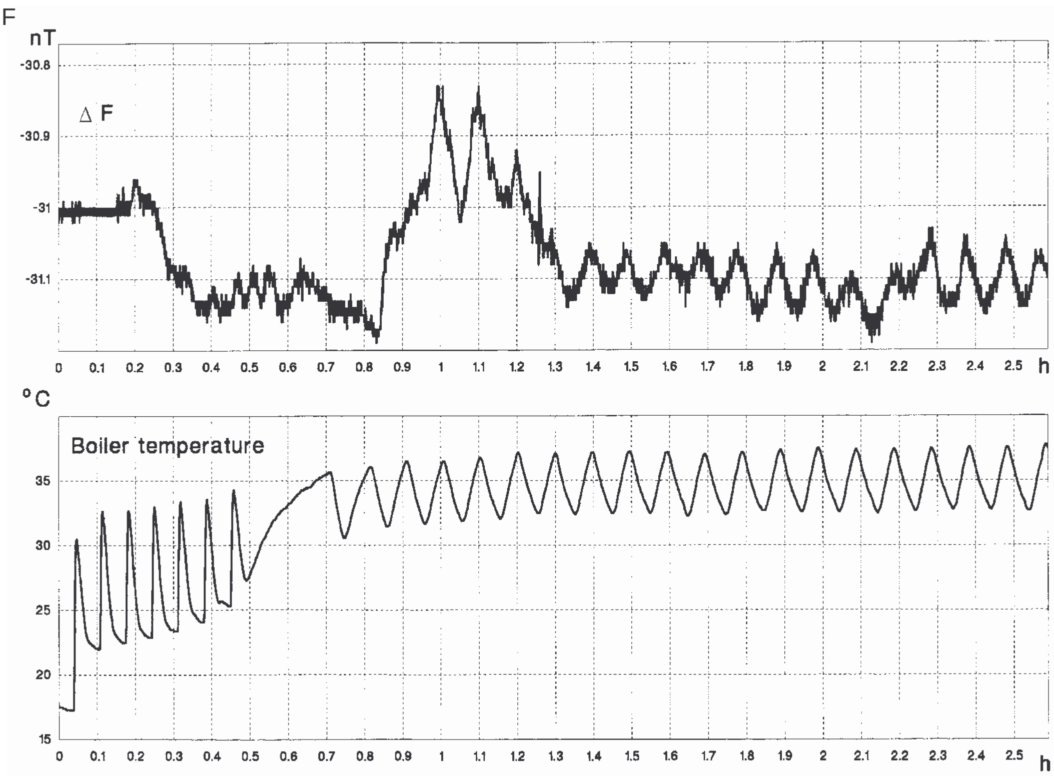

Fig. 8 Three second mean values comparison of two OPMs, one inside and the other outside the magnetic laboratory, during a start of the heating process. (at 10 January 2002)

The lower diagram shows the boiler temperature.

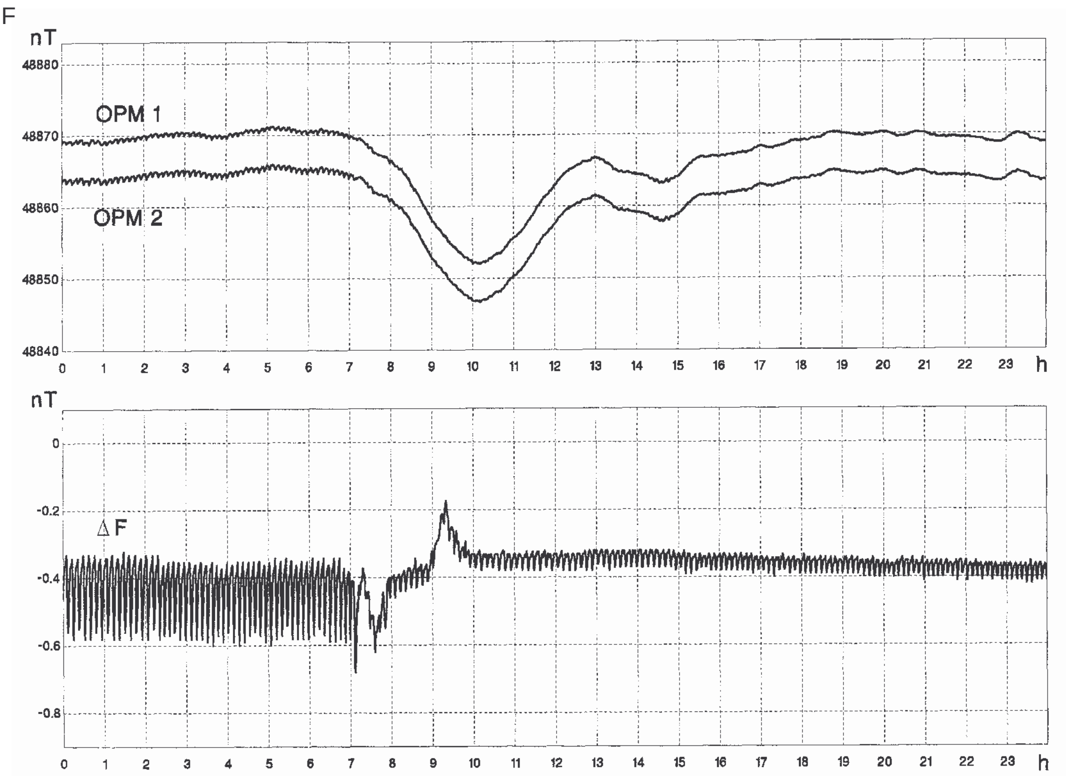

Fig. 9 Three second mean values comparison of two OPMs when the heating system is in operation. (at 14 December 2001)

A short circuit between the forward and the backward pipes is closed

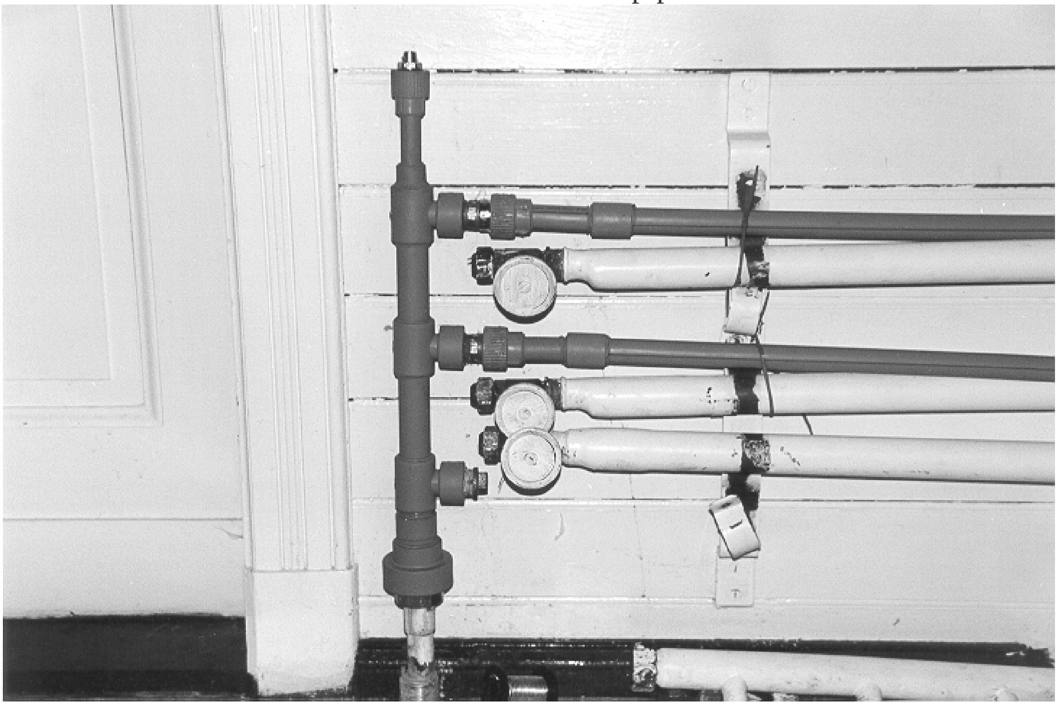

Fig. 10 Experiment at arrangement of a room heating

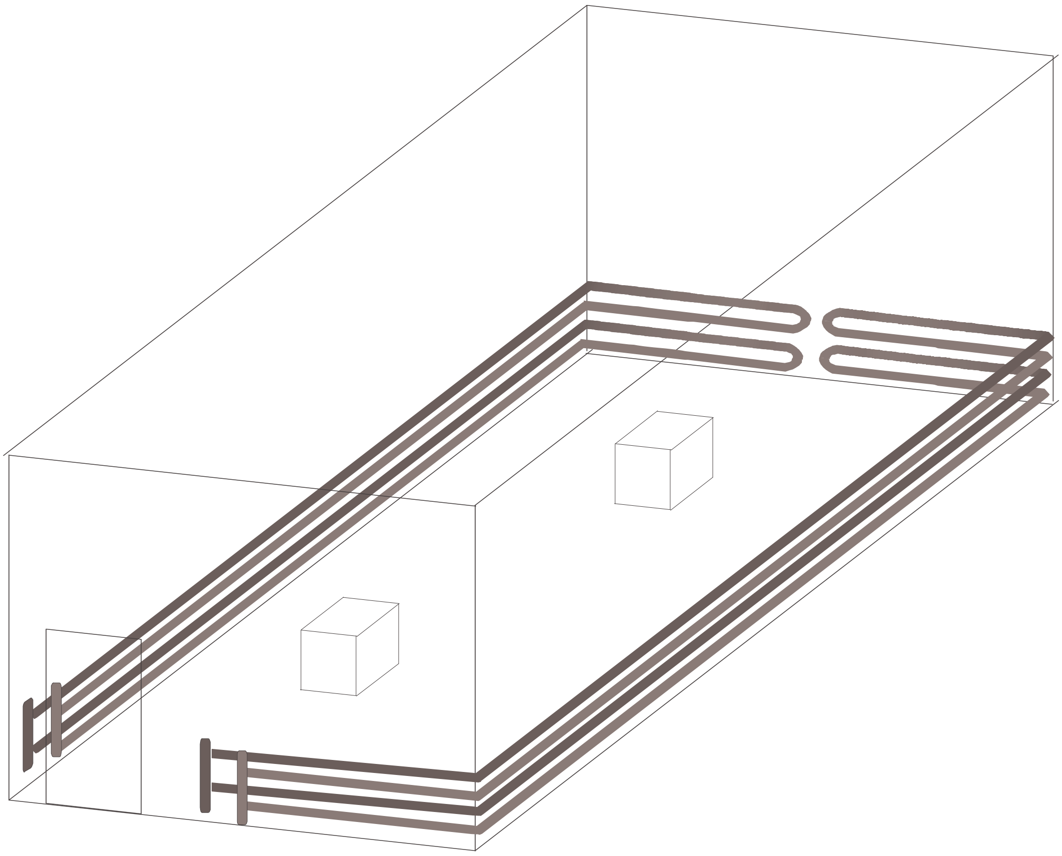

Fig. 11 New schematic arrangement for one room

The Optimum Spacing between Magnetic Repeat Stations for Regional Modelling

L.R. Newitt
Natural Resources Canada
Geological Survey of Canada
7 Observatory Crescent
Ottawa, Canada
K1A 0Y3

Abstract

Data from magnetic repeat stations are routinely used in the production of magnetic reference field models to augment the data from magnetic observatories. However, little has been done to establish the density of repeat stations actually needed. This question was investigated by producing spherical cap harmonic models of the secular variation over Canada and adjacent areas using synthetic data for different distributions of repeat stations. Approximately 40 repeat stations, with an average spacing of 456 km, were needed to produce an acceptable model. However, it was found that the model was sensitive to the distribution of data, and was affected by the lack of data in the oceanic areas.

1.0 Introduction

Magnetic observatories are the primary source of information about the secular variation (SV) of the earth's magnetic field. However, there are few regions where the density of observatories is sufficient to allow an accurate modelling of the spatial variation of SV. Therefore, many countries maintain a network of magnetic repeat stations to increase the density of data.

In this regard, Canada is no exception. However, the Canadian repeat station network has undergone a drastic evolution over the past 40 years (Newitt et al, 1985). In 1962 the network consisted of 103 stations occupied every five years. In 1979 the number of stations was reduced to 58, but the length of time spent at each station was increased from one day to three. The occupation interval was variable: two, four or 10 years, depending on the perceived importance of the station to the production of the magnetic reference field model. Since 1979, budgetary constraints and lack of personnel have resulted in a gradual decrease in the number of stations visited on a regular basis. Since 1995, only 5 stations have been occupied, at roughly two year intervals. Canada is not alone in being forced to reduce its repeat station program due to lack of resources.

When arguing for a revitalization of a repeat station program, a fundamental question is bound to arise: What density of repeat stations is really necessary? Among existing networks, the density, or station spacing, varies considerably from country to country – from 415 km to a remarkable 53 km, according to information gathered by Newitt et al. (1996). Such a large spread in station spacing suggests that a proper study of the optimum spacing remains to be carried out.

This paper tries to establish the density of secular variation stations (repeat stations and observatories) required for the purpose of determining secular variation. In the discussion that follows I assume that secular variation is of core origin and is therefore a long-wavelength phenomenon. Secular variation of tectonic origin is not considered. I also assume that the purpose of collecting the SV data is to produce some sort of mathematical model. Therefore, the station density should be consistent with the modelling procedure actually used. In the context of Canada this means using a spherical cap harmonic (SCH) model as a means of determining the station density.

2.0 Testing Procedures

Since 1985 the method of spherical cap harmonic analysis (Haines, 1985) has been used to produce the Canadian Geomagnetic Reference Field (CGRF, see for example Haines and Newitt, 1997). In the CGRF, secular variation is represented by a non-linear temporal function over a forty year time span whose coefficients are determined by using main field differences (Haines, 1993). Thus all data, regardless of year or location contribute to the solution. Although spherical cap harmonic analysis is the obvious modelling procedure to use in a test of station density, the means by which the SV data is treated must be greatly simplified in order to see how a change in station density actually affects the model. Therefore, a file of X, Y and Z annual change values was compiled as the basic data set. A small subset of this file was chosen and a spherical cap harmonic model of annual change was computed from this subset. The annual change computed from the model was compared with the true annual change over the spherical cap. Next, a larger subset of input data was chosen and another model computed. The procedure was repeated for an increasingly large set of input data until the RMS difference between the model and the real field became acceptably small. I consider, quite subjectively, acceptably small to be an RMS difference that does not exceed 2 nT/yr in any component. I often use the term "total RMS difference", which I define as

$\sigma_T = \sqrt{(\sigma_x{}^2 + \sigma_y{}^2 + \sigma_z{}^2)}$. An acceptable value of σ_T is 3.5 nT/yr.

The spherical cap for which the models were produced is the same as that used for the CGRF. It has a half angle of 30° centred at 65° N, 85° W. The spatial resolution of the model is determined by the spatial index K. A value of 10 was assigned to K for reasons outlined in Section 2.1.

2.1 Initial Considerations

In terms of spherical harmonic models, it is generally believed that the core field is represented by a maximum degree and order up to about 14 (Merrill et al., 1998, pg 36). (I used N=15 simply to create a test data set with a slightly shorter wavelength). The wavelength (in kilometres) corresponding to spherical harmonic degree N is given by *40000/N* (Bullard, 1967). Therefore, for N=15, the approximate wavelength of SV features is about 2700 km. The Nyquist interval would be 1350 km, which means that in theory only about 6 SV stations would be needed for Canada, which has an area of 10,000,000 square kilometres. However, the Nyquist interval must be considered a theoretical limit which applies to equally spaced samples. Its significance becomes less clear when data are not equally spaced. In any event, it is generally necessary to sample at more closely spaced intervals. Authors differ over the question of how closely spaced the samples need. Bendat and Piersol (1971), for example, recommend about twice the Nyquist frequency (or half the Nyquist interval), but I have also seen recommendations of 7 samples per cycle, and 10 to 20 samples per cycle. The corresponding station spacings for each of these options are listed in Table 1.

Table 1 Number of Stations vs Sampling Interval				
Sampling Interval (km)	Spherical Cap ($30x10^6$)	Landmass Area ($15x10^6$)	Canada only ($10x10^6$)	Approximate K max
1350 (Nyquist)	17	9	6	3
675 (Nyquist/2)	66	33	22	6
386 (Nyquist/3.5)	202	101	67	10
270 (Nyquist/5)	412	206	137	15
135 (Nyquist10)	1646	823	549	31

Taking a sampling interval in the middle of the range listed in this table (386 km) as a working value we see that 202 samples would be need over the entire spherical cap. This then allows us to estimate the spatial index that we should be using for the spherical harmonic models. Bullard recommended that the number of observations used in producing a model should be at least five times the number of coefficients in the model. In this context, one station yields three observations (X, Y, and Z). Therefore, for 202 stations, a spherical cap harmonic model with a K value of 10 (121 coefficients) seems reasonable. Most tests were, however, also carried out with K=8 and K=12 as well as 10.

3.0 Tests to Determine Optimum Station Spacing

3.1 The Data Set

Before any tests can be performed we need a set of data to use for modelling, plus a more extensive set of data against which the model can be compared. In practice, any set of observatory and repeat station data that can be obtained would not be complete, nor would it be error free. Of even greater importance is the fact that there is no other source of data against which the models can be compared. Therefore, I constructed two synthetic data sets by computing annual change values from an N=15 spherical harmonic model. The model coefficients up to N=8 were the IGRF2000 coefficients (Mandea et al, 2000). Coefficients for N=9 to N=15 were fabricated such that they produced a very dynamic, but not totally unrealistic pattern of SV. The coefficients were used to produce a file of X, Y and Z annual change values on a one degree geographic grid bounded by the spherical cap (the test file or set). A second file was produced which contained synthesized annual change values at locations of existing and former observatories and repeat stations in Canada, the United States, Greenland and Iceland (the input data file or set.) It is important to use the locations of real observatories and repeat stations since it is highly unlikely that the distribution of observatories will be changed, and it is unlikely that more than a few repeat stations will be relocated. Subsets of this file were the input data for the various tests described in the following sections. Figure 1 is a plot of the synthesized Z annual change data that form the test data set.

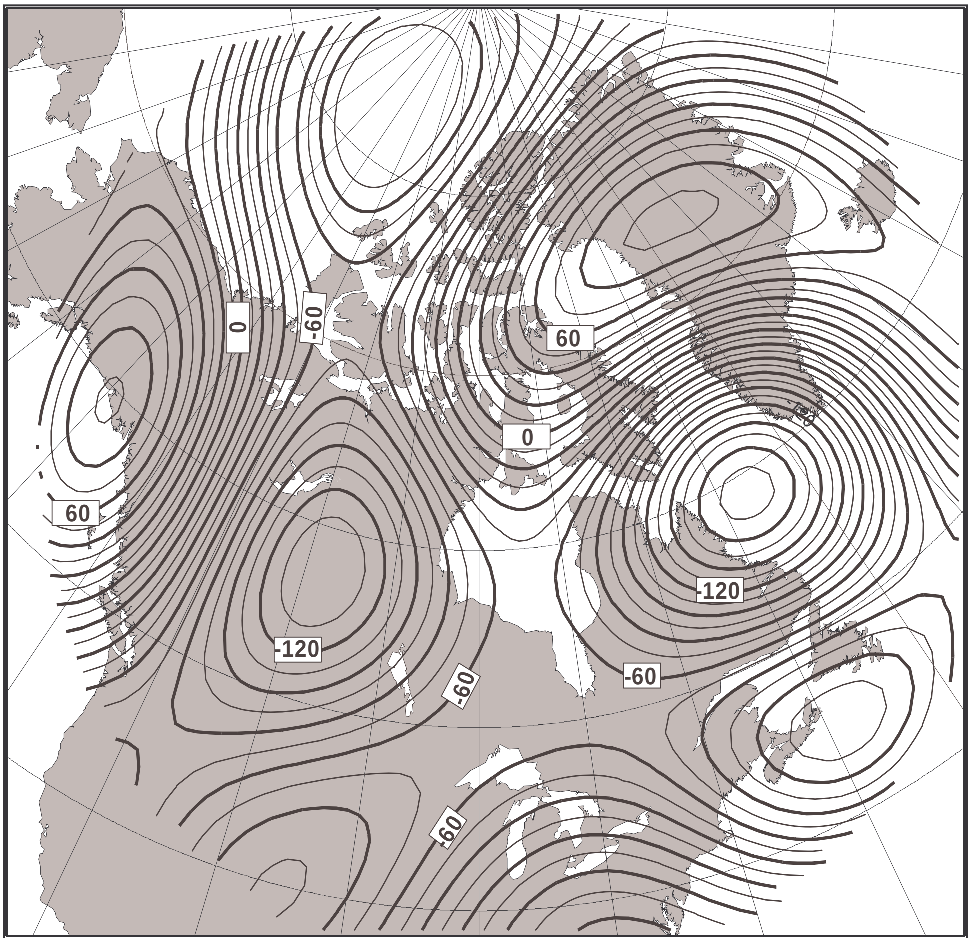

Figure 1

The Z component of the synthetic secular variation produced for modelling and testing with different distributions of repeat stations. Contour interval is 10 nT per year.

3.2 Preliminary Tests

Since the testing procedure consists of producing spherical cap harmonic models which are then compared against the test data set, it is important to establish that the test data set can be reproduced accurately by a spherical cap harmonic model. There are a total of 8498 points inside the spherical cap at a maximum spacing of 111 km. It should therefore be possible to fit the data almost exactly, given the right K value. Table 2 shows the fit to each component as K is increased from 8 to 16. It can be seen that the fit is almost perfect when Kmax=16, and that it is quite acceptable at Kmax=10.

In Section 2.1, I estimated that roughly 200 stations, distributed over the entire spherical cap, would be needed to model SV with an acceptable degree of accuracy. The validity of this assumption was tested using the test data set, which was progressively decimated by a semi-random selection of every Ith point where I ranged from 12 (giving an input file of 710 points with an average spacing of 206 km) to 96 (giving an input file of 89 points with an average spacing of 581 km). Note, however, that since these points fall on a latitude-longitude grid that includes the pole, the data are distributed very unevenly. Models with K=10 and 12 were produced for each decimated data set. A plot of total RMS difference versus decimation interval (Figure 2) shows that decimation should not exceed 64, which corresponds to 133 stations over the cap with an average station spacing of 475 km, or 2.8 samples per cycle. This is in rough agreement with our previous estimate. Thus, prior to carrying out the tests, expectations are that a minimum of 133 stations (observatory plus repeat), but maybe as many as 202, are likely needed to model the entire cap, or between 67 and 101 stations in the landmass area

Table 2 Fit of Test Data to Spherical Cap Harmonic Models of Different Spatial Indices

K	σ_X (nT)	σ_Y (nT)	σ_Z (nT)	σ_T (nT)
8	1.64	1.63	1.40	2.70
9	0.88	1.12	0.79	1.63
10	0.54	0.56	0.50	0.92
12	0.16	0.14	0.23	0.31
14	0.06	0.06	0.08	0.12
16	0.04	0.04	0.05	0.08

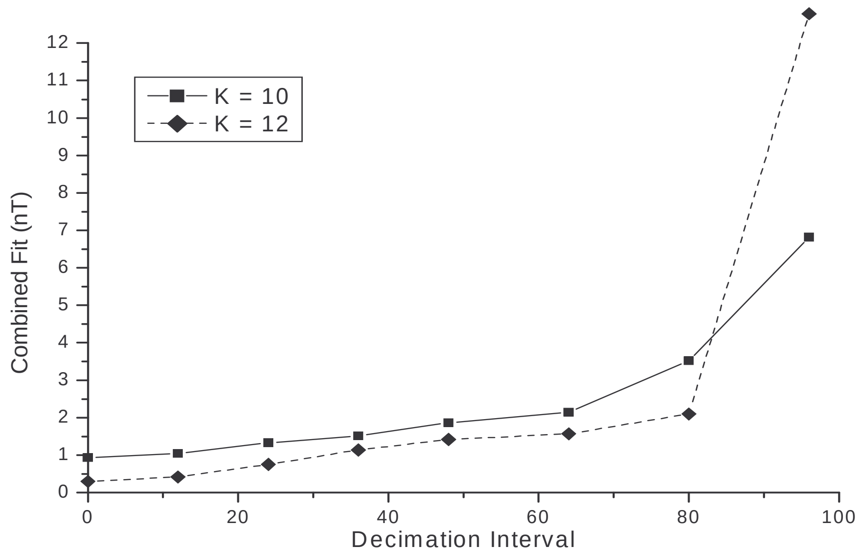

Figure 2

Total RMS differences between the test data set and models produced with decimated subsets of the test data.

3.3 SV Models 3.3 SV Models produced with Different Data Distributions

Canada currently runs a network of 13 magnetic observatories. In addition, 10 observatories in the US, Greenland and Iceland, and 6 current US repeat stations fall within the area of the spherical cap (Figure 3). This constitutes the base network of SV stations in the absence of any Canadian repeat stations. The average spacing is 719 km. I used this subset of the input data to produce spherical cap harmonic models with K=10 and K=12. Values computed from each of these models were then compared to the test data set. It comes as no great surprise that the fit is poor; σ_T = 43.7

nT/yr in the case of K=10, σ_T=43.1 nT/yr in the case of K=12. However, these are the RMS differences computed for the entire spherical cap. If the RMS differences are computed for an area that takes in only Canada and immediately adjacent areas (the “core” area; see Figure 3) we find that σ_T=9.2 nT/yr for K=10, σ_T =9.5 nT/yr for K=12.

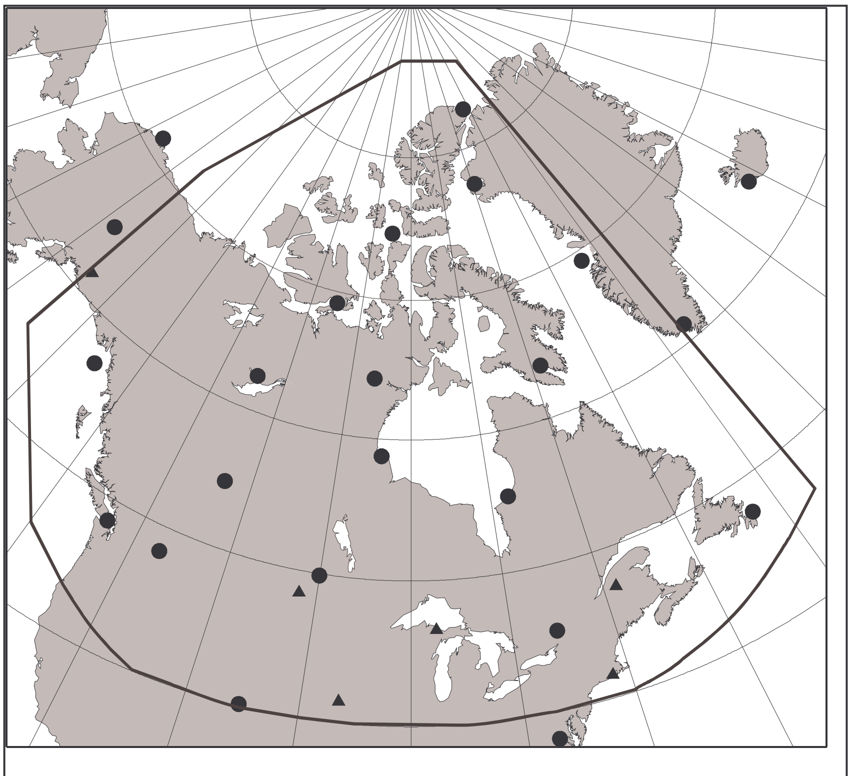

Figure 3

Initial distribution of observatories and repeat stations. Circles are observatories; triangles are US repeat stations. The area over which the RMS differences were calculated (core area) is outlined by a heavy solid line.

Next, models (K=8, 10, 12) were produced using the base network plus data for the 4 Canadian repeat stations that have been visited in recent years. The process continued with the number of Canadian repeat stations (Ns) increasing from 4 to 13, 20, 30, 43, 67 and finally 90. The fit of each model as a function of the number of repeat stations is given in Figure 4. Models produced for K=8,10,12 all have RMS differences better than the acceptance level of 3.5 nT when Ns equals 30. (However, in the case of K=12, the RMS difference for the Z component is greater than 2 nT.) It is interesting to note that the K=12 models normally fit the test data more poorly that do models with K=8 or 10. It is also noteworthy that when K=10 or12 the lowest RMS difference occurs when Ns=43. Increasing the number of stations beyond 43 results in an increase in the RMS difference. For the K=8 models, the RMS difference remains constant when Ns is greater than 43. The distribution of stations (Ns=43) is shown in Figure 5. Differences between the test data set and the Ns=43 models are shown if Figure 6 (K=8) and Figure 7 (K=10). Significant differences occur mainly near the spherical cap boundary and over oceanic areas.

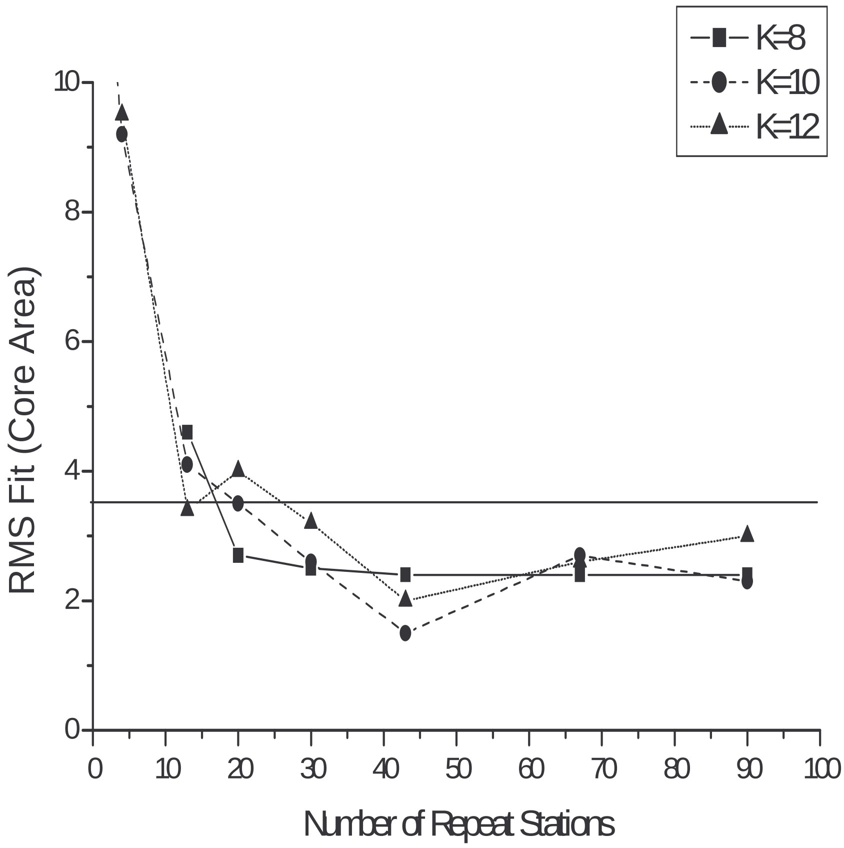

Figure 4

Overall RMS difference (nT/yr) between the test data set a spherical cap harmonic models plotted as a function of the number of repeat stations in the input file.

3.4 Sensitivity to Station Placement and Lack of Data in Oceanic Areas

Although the fit of all three models with Ns=43 to the core area is very good, there is reason to question the stability of the models. The ratio of observations to coefficients is only 1.8, and about half of the spherical cap is without observations. Both factors are likely to negatively affect the model solution. This leads to two questions: 1) Will the use of a slightly different data set lead to a significantly different model? 2) Can a model that is better and more stable in the core area, be achieved by adding artificial repeat stations in the ocean area?

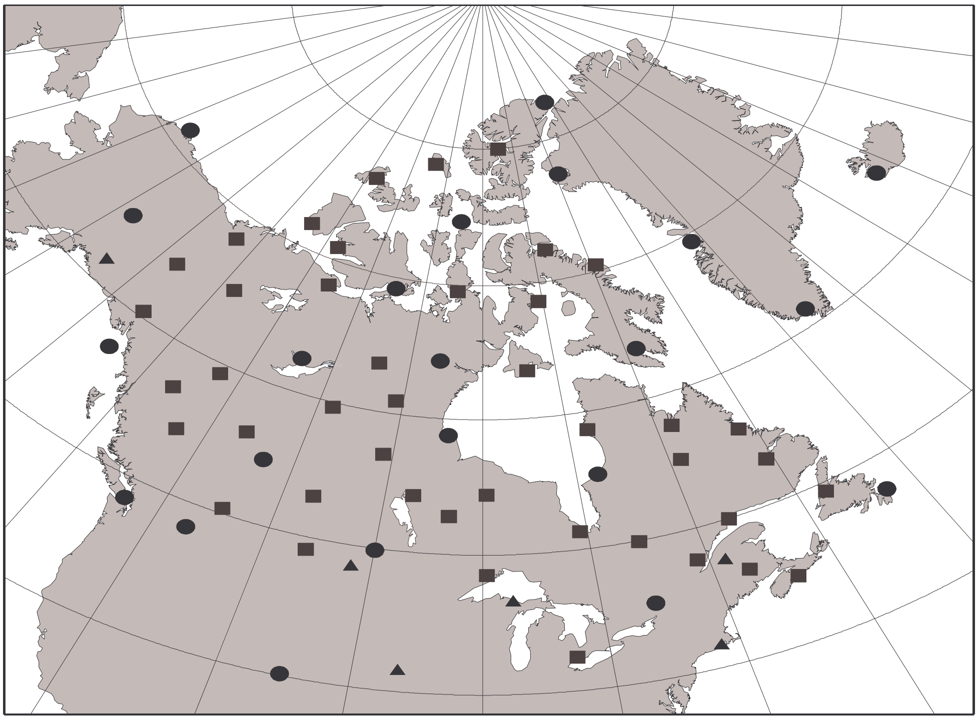

Figure 5

Distribution of SV stations for best fitting spherical cap harmonic models. The number of observatories (circles) is 23; the number of Canadian repeat stations (squares) is 43; the number of US repeat stations (triangles) is 6.

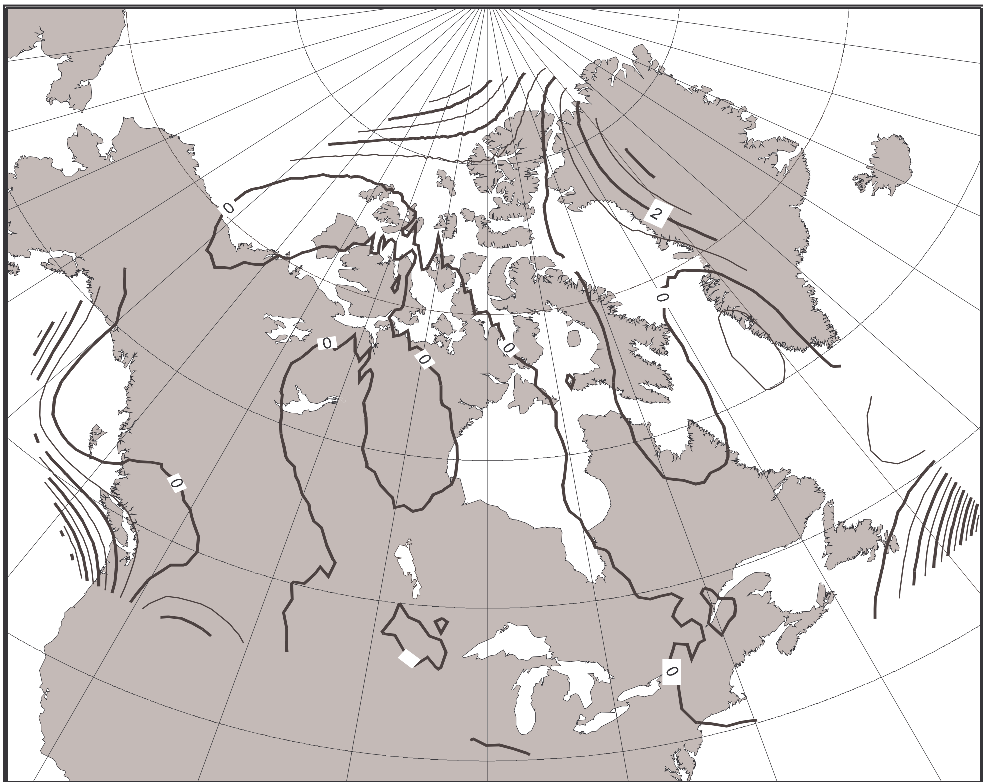

Figure 6

Differences between the K=8, N=43 model and test data, Z component; contour interval is 1 nT per year

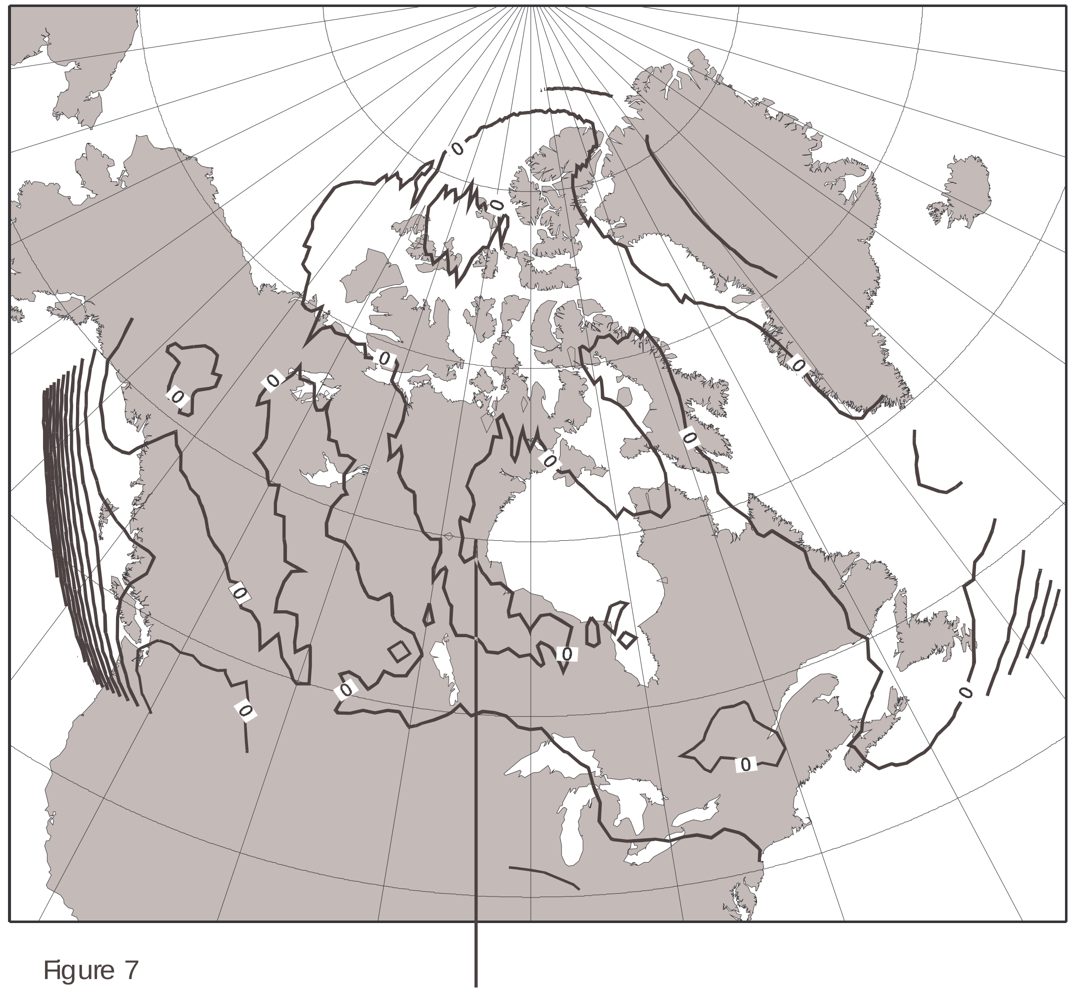

Figure 7

Difference between the K=10, N=43 model and test data, Z component.
Contour interval is 1 nT per year.is 1nT per year.

To test the first point I replaced the input file of 43 repeat stations with an alternative file containing data at 43 different locations. (All these locations were at one time actual repeat stations.) The RMS differences for models with K=8, 10 and 12 are given in Table 3. In all instances the use of the alternative repeat station data set results in models that fit the test data more poorly than the original file of repeat station data.

The observations in the second data set are not distributed as optimally as the original data set. This by itself would be expected to produce a worse fit. But the situation is compounded by the complete lack of data over fully 50% of the spherical cap. With no observations to constrain the solution in these regions, a relatively minor difference in the input data could result in a large change in the model value outside the area of data. In other words, if the spherical cap covers a region of 30,000,000 square kilometers, one would expect a more stable solution over the area of interest if there are data everywhere.

I therefore created 40 dummy repeat stations in the oceanic areas and remodelled for K=8, 10 and 12. The results are also summarized in Table 3. In all cases, adding dummy values in the oceanic areas reduced the RMS difference in the “core” area. In fact, the improvement in the K=12 model was so great that is now the best fitting model. The addition of dummy values did not completely eliminate the effects caused by the change in distribution; it did, however, reduced the degradation by a factor of about two.

Table 3 RMS Differences of Models Produced with Alternative Input Data Sets				
	σ_X (nT)	σ_Y (nT)	σ_Z (nT)	σ_T (nT)
K=8, original	1.6	1.4	1.1	2.4
K=8, alternative	1.6	1.5	2.7	3.5
K=8, original+ocean	1.3	0.9	1.5	2.2
K=8, alternative+ocean	1.5	1.1	2.1	2.8
K=10, original	0.8	0.5	1.2	1.5
K=10, alternative	1.8	1.2	1.8	2.8
K=10, original+ocean	0.8	0.4	0.6	1.1
K=10, alternative+ocean	0.9	0.6	1.2	1.6
K=12, original	1.6	0.6	1.1	2.0
K=12, alternative	2.0	1.1	1.6	2.8
K=12, original+ocean	0.2	0.2	0.3	0.4
K=12, alternative+ocean	0.3	0.3	0.5	0.7

4.0 Discussion and Conclusion

The tests described in the previous sections indicate that approximately 40 repeat stations are needed in Canada to supplement the 23 observatories located in Canada and adjacent areas. However, spherical cap harmonic models based on this relatively sparse set of data are very sensitive to the actual distribution of data. Introducing dummy repeat stations in the ocean area near the spherical cap boundary greatly improved the model fit and the stability of the model.

In Section 2.1 I estimated that the number of observations needed within the entire spherical cap would be approximately 200. Preliminary testing showed that the number might be as low as 133. The input data set that resulted in the best-fitting model consisted of 13 Canadian observatories, 10 foreign observatories, 6 US repeat stations, 43 Canadian repeat stations, and 40 dummy stations, a total of 112 stations, of which 72 are "real".

If we consider only the 15 million square kilometres in which there are data (the "landmass" area), the spacing between the 72 SV stations averages 456 km. Taking the entire spherical cap and including the dummy repeat stations give an average station spacing of 518 km. The ratio of observations to coefficients is 2.8. This ratio is smaller, and the sampling interval larger, than the theoretical and preliminary investigations had indicated. However, it must be remembered that I have used idealized data which is noise free. A logical extension of this study would be to investigate the effects of noise on the data.

In the meantime, the preliminary conclusion is that a network of 43 repeat stations, as shown in Figure 5, is required for Canada. Of the 43 stations, only 18 are accessible by road; 20 are accessible by commercial air craft, and 5 require charter aircraft. As a rough estimate, it costs about $1000 (Canadian) to occupy a repeat station accessible by road, $2500 to $4000 to occupy a station accessible by commercial air, and roughly $10,000 to $20,000 when it is necessary to resort to charter aircraft. These figures are based on 3 days at a station plus a day for travel for one person, except at the remote stations where due diligence requires a two person crew. Thus the total cost of surveying the network is about $168,000, or $42,000 (approximately $26,500 US) per year assuming a four year cycle. The magnitude of this sum makes it important to verify that the conclusions reached here are valid under more realistic situations. This requires a much more ambitious extension of this study that would emulate the actual methodology used to produce the CGRF.

5.0 References

Bendat, J.S. and A.G. Piersol, Random data: Analysis and measurement procedures, *Wiley-Interscience*, 1971.

Bullard, E.C., The removal of trend from magnetic surveys, *Earth Planet. Sci. Letts.*, **2**, 293-300, 1967.

Haines, G.V., Spherical cap harmonic analysis, *J.G.R.*, **90**, 2583-2591, 1985.

Haines, G.V., Modelling geomagnetic secular variation by main-field differences, *Geophys.J. Int.*, **114**, 490-500, 1993.

Haines, G.V. and L.R. Newitt, The Canadian geomagnetic reference field 1995, *J. Geomag. Geoelectr.*, **49**, 317-336, 1997.

Mandea, M., S. Macmillan, T. Bondar, V. Golovkov, B. Langlais, F. Lowes, N. Olsen, J, Quinn, T. Sabaka, International geomagnetic reference field – 2000, *Phys. Earth Plan. Int.*, **120**, 39-42, 2000.

Merrill, R.T., M.W. McElhinny and P.L. McFadden, The magnetic field of the earth, *Academic Press*, 1998.

Newitt, L.R., C.E. Barton and J. Bitterly, Guide for magnetic repeat station surveys, *International Association of Geomagnetism and Aeronomy*, 1996.

Newitt, L.R., R.L.Coles and J.F. Clark, Canadian magnetic repeat stations 1962-1983: instruments, procedures and observations, *Geomagnetic Series*, **29**, Ottawa, 1985.

Problems of observatory instrumentation and possible solutions

László Hegymegi, Eötvös L. Geophysical Institute, H-1145 Budapest, Columbus u. 17-23, Hungary

Introduction

Most geomagnetic observatories are not producing ideal records. From observatory to observatory the reasons for that are different but also the conditions are very different. In this paper we try to summarise the most common problems and make a suggestion how to improve recording quality.

General observatory configuration

Recently digital instrumentation is used at most magnetic observatories (Fig.1). The sensor part of the system is a triaxial fluxgate magnetometer giving three analog voltages on its output which are proportional to the measured field components. These signals are digitised and recorded by a data collection platform (DCP).

As the fluxgate magnetometer is a relative instrument we must use absolute instruments to determine the zero level of the variation curve. Generally this is done regurarly by a D/I theodolite and proton precession magnetometer (PPM) but in many observatories the PPM is part of the recording system to provide easy checking of the fluxgate magnetometer.

If we want to compare this instrumentation to the classical one, we have to mention the following main features:

Fluxgate magnetometer:
- simple instrument, no maintenance
- good resolution
- moderate noise
- continuous analog electrical output
- low power consumption
- relative instrument, needs calibration
- sensitive to temperature changes

Classical variometer:
- simple instrument
- low resolution
- no electric output
- relative instrument, needs calibration
- very sensitive to temperature changes

To demonstrate the above features let us look at some baseline curves of INTERMAGNET observatories (IMO) (Fig.2). These observatories have modern instrumentation and good ambient conditions. We can see that they are not straight lines as they would be in an ideal case but sometimes they have jumps, drift and periodic change over the plotted one year period. Source of these changes can be different but in most cases the baseline change is due to mechanical and temperature effects.

There are several methods to minimise or cancel disturbing effects. A classical solution to decrease temperature effects is to use good insolated buildings for the instruments. This is a good but not very cost effective solution. In such a building the yearly temperature variation can be less then ten centigrade. If this is not possible we can apply temperature control. With a well designed heating system the ambient temperature variation can be in the range of 0.1 centigrade.

Another disturbing effect can be the pillar tilt or any other mechanical change in the instrument position. In this case the position of the sensor changes relative to the magnetic vector and this will result the same output signal as a change in the position of the vector. Consequently we observe magnetic variation even if the field does not change.

An other common source of data errors or data gaps is the data acquisition system. In the past they were very often complicated instruments. Nowadays a PC or an embedded PC can be used to control the process. The process itself has two main parts the data recording and the data download.

Most common data recording and transmission problems are:

- A/D conversion errors
- timing problems
- power failures
- PC problems (program or operating system)
- recording media errors
- communication line problems
- errors by the operator

In the case of fluxgate magnetometers we have an electrical signal, proportional to the magnetic field as the instrument output. An A/D converter is used to convert the analog voltage to a digital number. Usually 12 to 24 bit A/D convertion are applied. The quality of the converter strongly affects the quality of the magnetic variation curve.

Time stamp on recordings is produced by the data acquisition system. This can be a PC or a dedicated hardware having an internal system clock. Long-time precision of system clocks can be poor to achieve ±5 sec/month precision.

Power failures can be serious problems in geomagnetic observatories. As geomagnetic recording can be undisturbed only in remote places where the traffic or industrial activity is low it happens very often that the mains is not reliable, there are shorter or longer power breaks. Such a situation can cause data losses or can even halt the recording system.

Recently digital systems very often apply a PC as a recorder. Stability of an ordinary tabletop PC is not always sufficient for the required stability at an observatory. More often this problem even disturbs our work if we use a Windows operating system.

It can happen that recorded data cannot be read due to recording media errors. This can result data loss if we make only one copy of our data.

There are different ways to produce output recorded data from data acquisition systems. Possible data download solutions are: satellite transmission, telephone line communication, internet or LAN connection or manual download. It happens very often that data are corrupted due to communication line problems.

It is not a usual case but it can happen that recorded data are deleted by an operator mistake. If we have only one recording system and we have no backup medium there is no way to replace missing data.

Examples giving solutions to these problems

Recording equipment

A classical solution to reduce baseline drift is to place the fluxgate magnetometer in a temperature insolated or controlled hut. As a fluxgate magnetometer have many components which are sensitive to temperature changes in such an environment one can get very stable baselines. Figure 3 shows underground instrument vaults in a stone building with old-style woven-rush roofing. This provides excellent environmental stability. This solution has the advantage that there are no energy costs but construction can be more complicated and more expensive. In the other case we need a nonmagnetic heating system and heat controlling device. Heating costs can be reduced using different hut temperatures for warm and cold seasons but this will cause a jump in the baseline.

To eliminate pillar tilt effects which changes the position of the sensor relative to the vertical direction and at the same time to the geomagnetic vector we can suspend the magnetometer. A general solution to this problem is to apply a Cardan-type suspension for the sensor. In this case even if the instrument frame is tilted together with the pier, the sensor position remains unchanged. The situation is the same if we have changes due to any deformation in the sensor's support.

Figure 4 shows a suspended fluxgate magnetometer. This instrument type exhibits excellent baseline stability, and in ideal case the baseline drift is less then 3 nT/year but only in a controlled environment. In a practical case the baselines are not so good. In Figure 2 we show baseline curves for INTERMAGNET observatories. The periodic change is due to the temperature change but long period drift is probably an instrumental effect.

It is a difficult problem to reduce temperature effects on magnetometers. The main problem in case of a fluxgate magnetometer is that the principle of the measurement is based on the physical characteristics of the core material. This feature is affected by temperature and sometimes by other long-term physical processes. These changes affect the long-term variations of the output signal which we cannot separate completely from variations resulted by magnetic variations.

A good solution to this problem to apply delta I – delta D (dIdD) measurement principle introduced by Alldredge in 1964 (Alldredge et al) (Fig.5). The biggest advantage of this method that most of the temperature effects could influence the measurement only in long term range and here the system is based on a proton precession magnetometer (PPM) which is an absolute instrument. PPM measurements are not affected by external conditions (at least in the range interesting for us). One dIdD measurement is really a series, consisting of five individual measurements. This can be carried out in a very short time. If we apply an overhauser magnetometer it needs only one second for this series. The only requirement for dIdD systems is to have the stability of the components for this time interval.

On the other hand any mechanical instability, especially tilting effects or torsionlike movements can produce long-term baseline changes in the measurements. This problem is bigger if the system has large dimensions. To avoid these inconveniences a compact spherical coil system was constructed in ELGI in the nineties (Pankratz et al.) (Fig.6). This coil was the base of the dIdD instrument constructed in cooperation with USGS and GEM Systems. This dIdD system has reduced temperature sensitivity and its baseline drift is nearly as good as in the case of the best fluxgate magnetometers. In order to localise sources of long-term baseline changes a suspended experimental version was constructed and built in ELGI (Fig.7). During the test measurement phase it was found that the new instrument has no temperature sensitivity and its baseline variation is smaller then the same for fluxgate magnetometers.

Main features of dIdD systems:

- simple instrument, no maintenance
- good resolution
- low noise
- direct digital electrical output
- low power consumption
- partly relative instrument, no calibration
- not sensitive to temperature changes

Data collection platform

A stable and low power data acquisition system, Magrec-1 was built with an embedded industrial PC (Fig.8). It runs under DOS and has a built in watchdog. If the system stops the watchdog reboots it in 15 seconds and the data acquisition can continue automatically.

The system is built around an RS485 bus. Such a system uses a twisted pair cable for communication between individual units. As A/D converter and multiplexer an ADAM 4017 (Advantech) 16 bit module is used. This module can be built into the magnetometer electronics and uses the same power source. Five input channels are connected to the output of three magnetometers, sensor and electronics temperature measuring elements. In this way there are no long cables for analog signals which would be another possible source of disturbance. Timing is done by the embedded PC. Its clock is synchronised by a built-in GPS module.

Data are stored on a flash memory module which has no data loss even in case of power failures. The data acquisition process organised in such a way that the data loss is minimised to the interval of power failure. To increase reliability, the whole system uses 12 V DC power permitting to use a backup battery.

The data acquisition system can be connected to a graphic display giving the possibility to make a fast check on the whole system. The variation curve is displayed for the last 24 hours together with numeric data for a period of the last few minutes.

Magrec-1 can be connected to a telephone line and this gives the possibility to carry out remote check of the system and data download without visiting the station and disturbing the data acquisition process.

Conclusions

There are several sources of disturbances which can make the life hard of a supervisor at a geomagnetic station. Part of this problem one can avoid by choosing the best configuration for the site. It is important to know what the temperature conditions are for the magnetometer, how stable is the pillar, what is the distance between the magnetometer and the data acquisition system, how stable is the mains (if there is any), is a local operator, telephone or internet connection available etc. This means that the same system can be perfect for one place and not very good for another site. One has to explore all the disturbing effects to find the solution which gives the best result for a certain site. We think that in our examples we show solutions which helps to improve the quality of geomagnetic data products.

References

Alldredge, L.R., Saldukas, I.: An automatic standard magnetic observatory, J. Geophys. Res., 1964. Vol. 69. pp. 1963-1979

Leroy W. Pakratz, Edward A. Sauter, Alpár Körmendi, László Hegymegi, The US-Hungarian Delta I – Delta D (DIDD) Quasi-absolute Spherical Coil System. Its history, evolution and future. Geophysical Transactions, 1999. Vol.42. No. 3-4, pp. 195-2002

Figures

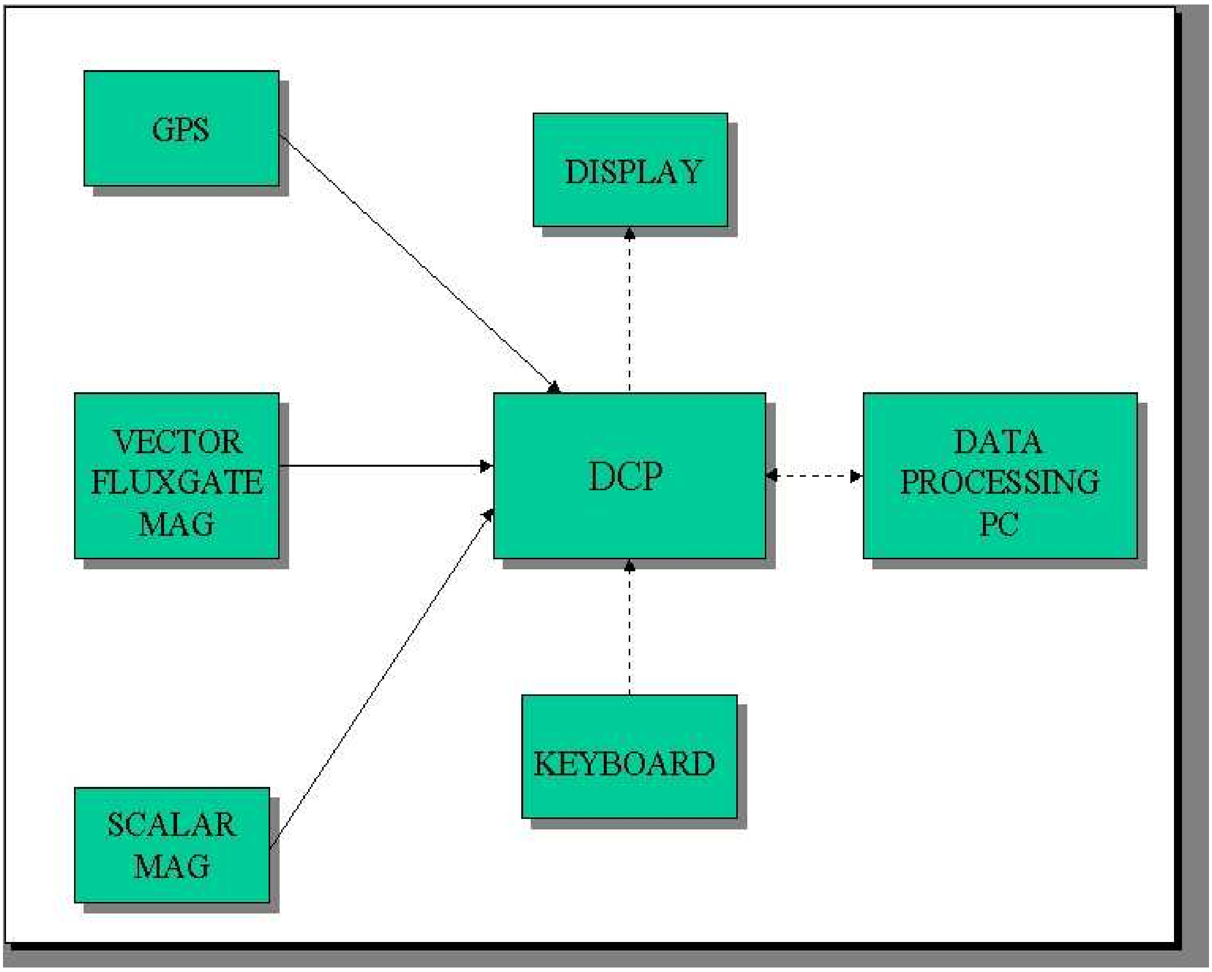

Fig.1 General schematic for a magnetic observatory

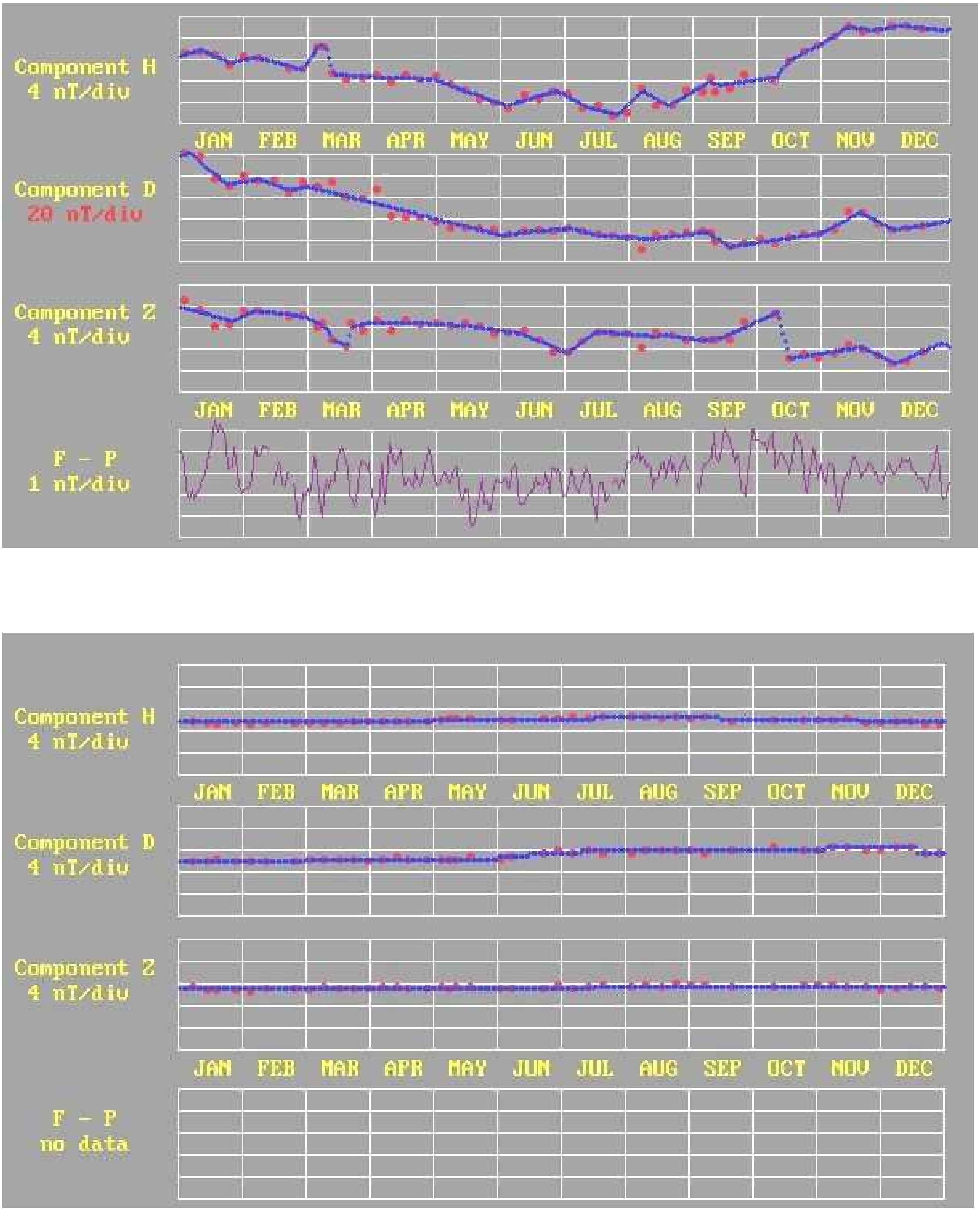

Fig.2 Baseline curves of INTERMAGNET observatories

Fig.3 Underground instrument vaults in stone building

Fig.4 Suspended fluxgate magnetometer

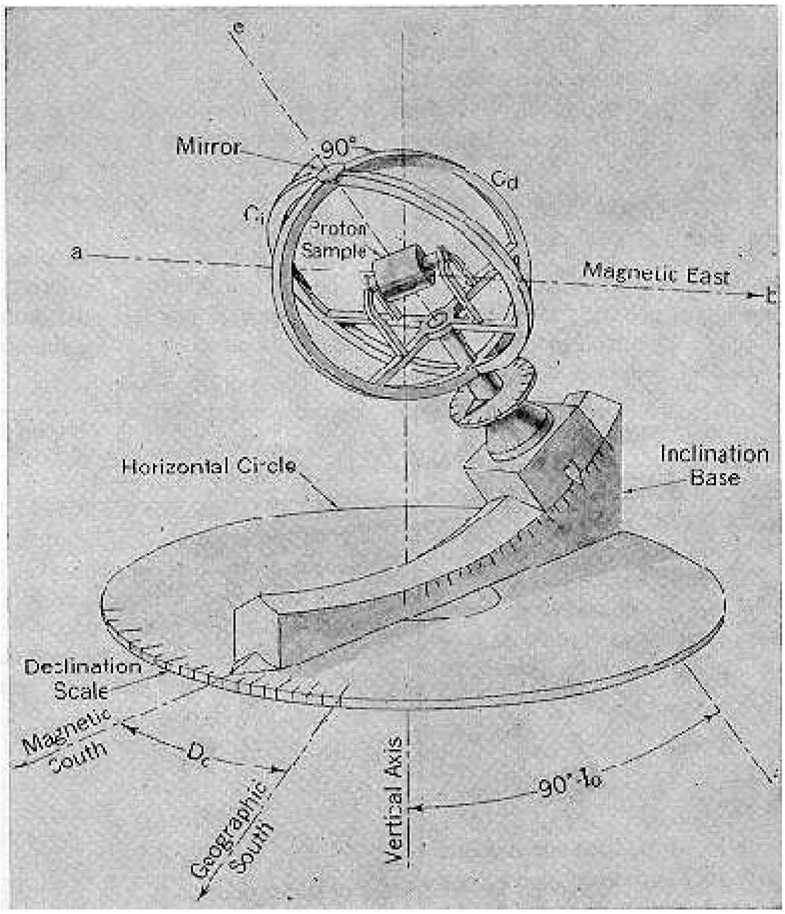

Fig.5 System proposed by Alldredge

Fig.6 ELGI-USGS-GEM Systems dIdD

Fig.7 Suspended dIdD

Fig.8 Magrec-1 DCP

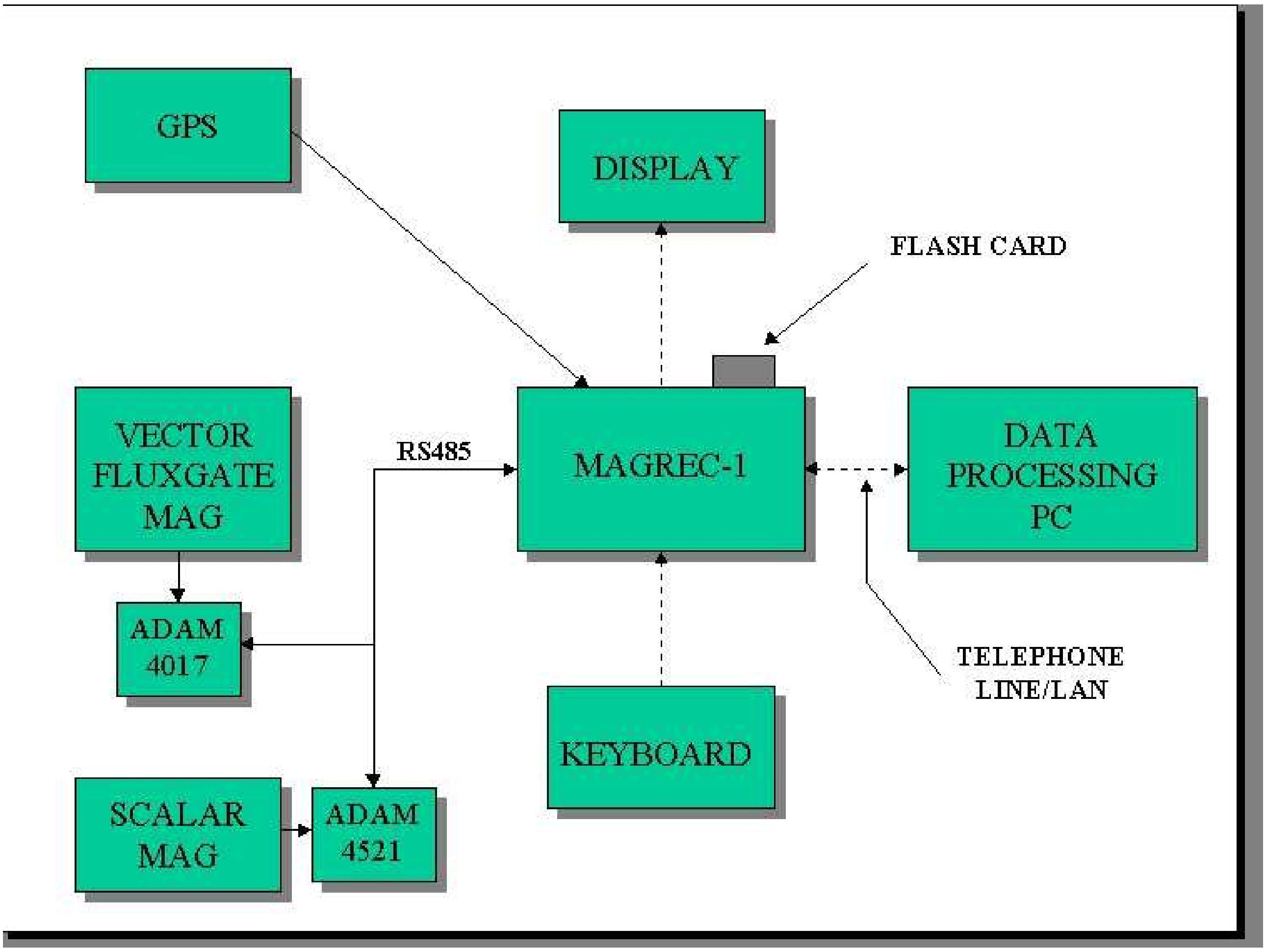

Fig.9 Schematic with Magrec-1

INTERMAGNET: A Global Network for Near-Real-Time Geomagnetic Data

Ole Rasmussen[1] and David Kerridge[2]

1) Danish Meteorological Institute, Lyngbyvej 100, DK 2100 Copenhagen, Denmark, or@dmi.dk
2) British Geological Survey, Murchison House, West Mains Road, Edinburgh, EH9 3LA, djk@bgs.ac.uk

ABSTRACT

For years, institutions in many countries around the world have been operating geomagnetic observatories with the aim of recording geomagnetic variations on time scales from seconds to decades, even to centuries. With the growing interest in having timely or even real-time access to digital data from a global network of geomagnetic observatories, the need for a federation of observatories able to supply high quality digital data in near real time became more obvious, and resulted in the establishment of the programme named INTERMAGNET. INTERMAGNET is now a global network of more than 80 observatories supplying near-real-time data to a group of data centres, Geomagnetic Information Nodes (GINs – see www.INTERMAGNET.org), where scientific users can access the data.

1. INTRODUCTION

The idea of establishing a global network of magnetic observatories under the name INTERMAGNET was born during the IAGA Workshop in Ottawa in 1986 when Bill Green (A.W. Green Jr.) of the US Geological Survey (USGS) and Bill Stuart of the British Geological Survey (BGS) agreed to start exchanging geomagnetic data between the US and the UK in near real time. The trial data transmission project proved successful and the Geological Survey of Canada and the Institute de Physique du Globe de Paris agreed to join in an effort to establish a programme, which was named INTERMAGNET.

The purpose of the programme was [1]:

"*to establish a global network of co-operating digital magnetic observatories, adopting modern standard specifications for measuring and recording equipment, in order to facilitate data exchange and the production of geomagnetic data products in close to real time.*"

The initiative to establish INTERMAGNET was supported by the International Association of Geomagnetism and Aeronomy (IAGA), and INTERMAGNET still works in close contact with IAGA's bodies with interests in magnetic observatories. In short, INTERMAGNET is an informal federation of institutions running magnetic observatories (INTERMAGNET observatories - IMOs) operating to agreed standards.

The characteristics of the INTERMAGNET observatories are:

High standards of absolute data quality and continuous recording maintained over many years at stable locations.

Producing data suitable for studies of changes in the main geomagnetic field, and long-term changes in geomagnetic activity.

This last characteristic is what geomagnetic observatories are all about and what distinguishes them from geomagnetic variation stations. It is accomplished by making regular absolute measurements to determine the baseline values of the recording magnetometers.

2. MANAGEMENT

INTERMAGNET management is taken care of by an Executive Council with, in 2002, members from each of the four founding organisations, and an Operations Committee with members from a number of countries. The Executive Council is responsible for policy and liaison with national and international scientific and governmental agencies. The Operations Committee advises the Executive Council on technical matters. It deals with subject such as:

Setting standards for the operation of INTERMAGNET observatories
Technical implementation and expertise
Providing practical assistance to members and prospective members
Production of the INTERMAGNET annual CD-ROM
Publication of the INTERMAGNET Technical Manual
Assessment of new applications

Assistance is given by the members of the committee to improve operations at non-member observatories to meet INTERMAGNET standards, and there is an emphasis on helping observatories in the less developed regions of the world.

3. OPERATIONS

INTERMAGNET operations are illustrated in Fig.1. The recommendation for IMOs is to run a three-component vector magnetometer and an independent scalar magnetometer. The sampling interval should be 10 seconds or shorter for the vector magnetometer and one minute for the scalar magnetometer. The resolution should be 0.2 nT or better, depending on the latitude of the observatory.

Preliminary data are transmitted to one of the INTERMAGNET GINs within 72 hours of recording. In fact many observatories send their data every hour or even more frequently. Today most observatories communicate directly with one of the Geomagnetic Information Nodes (GINs) via the Internet; e-mail and satellite transmission were the most common ways of sending data in the early days of INTERMAGNET.

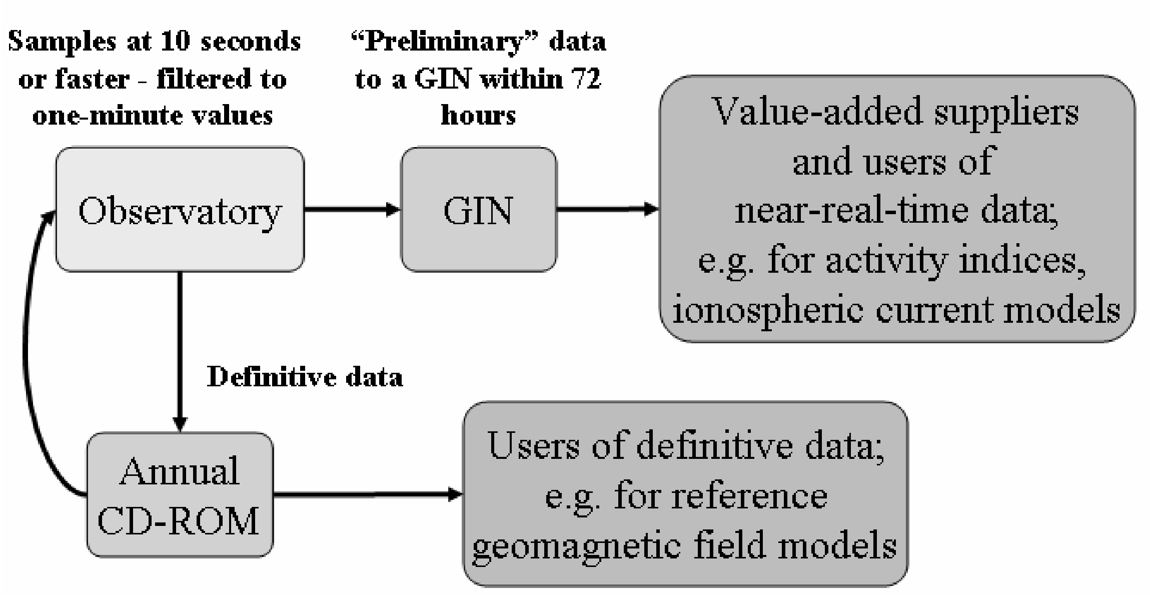

Fig. 1 Components of INTERMAGNET Operations

3. THE GINs

The original idea was that every observatory should send their data to one of six INTERMAGNET GINs, and that users could request data from any GIN by e-mail. Ten years ago that was the only way users from could access IMO data. Today the data are made available on the Web (via www.intermagnet.org), and a newly developed ftp-helper makes it very easy to download the near-real-time data. It is planned that all INTERMAGNET data shall be available at a few GINs so that a user does not have to access more than one GIN to obtain a global selection of data. Through the Web it is also possible to view on-line magnetograms and, in the future, magnetograms from all of the IMOs will be available using just one GIN.

In addition to the real-time data, the final or definitive data are now made available through the GINs, as soon as they have been processed. These final data will stay on-line until the data have been published on the annual CD-ROM.

The INTERMAGNET web pages provide a wide range of information on INTERMAGNET including contact details, the list of current IMOs and the participating institutions. The Technical Manual with all the information needed by prospective members can be found on-line. During the 2002 INTERMAGNET meeting it was further decided that photographs from all observatories should be available from the web pages.

4. THE GLOBAL NETWORK

The present network consists of more than 80 IMOs around the world, which is probably more than half of all the world’s observatories operating in 2002. The map in Fig.2 shows that large gaps exist in the network, especially in the Former Soviet Union (FSU), China, India, Latin America and in the Oceans.

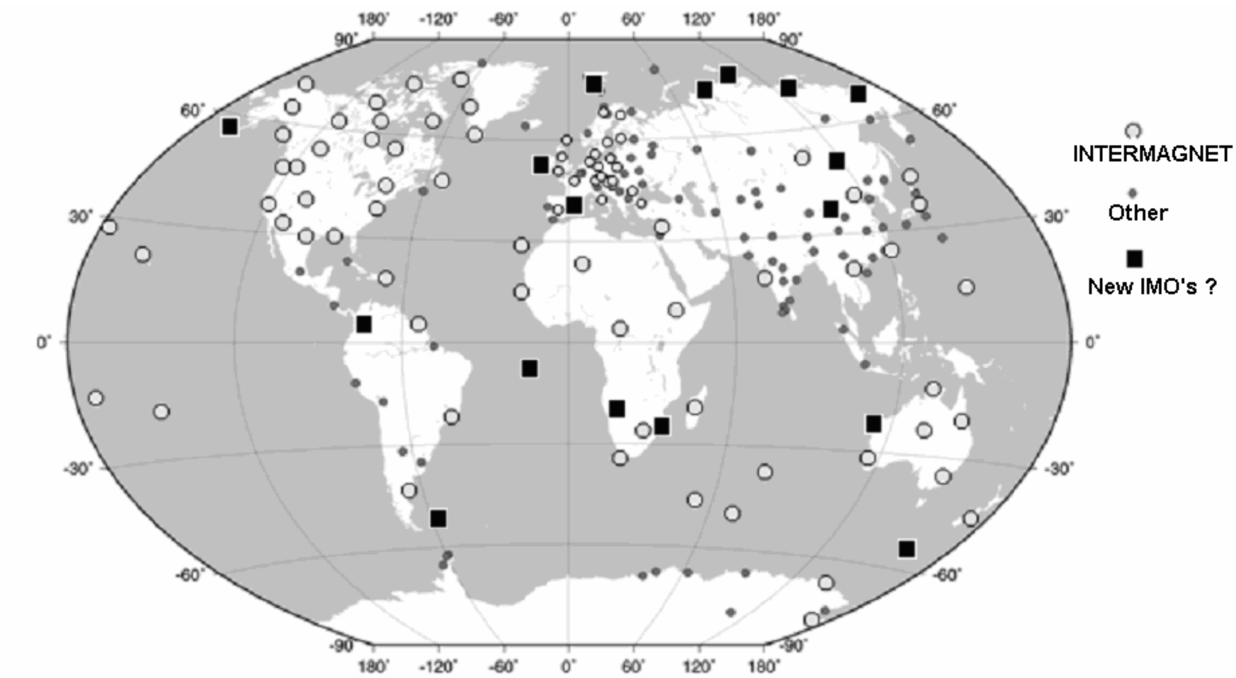

Fig. 2 Present and future IMOs

Fortunately, the situation is improving and within the next few years we can expect the number of IMOs to have increased to more than 100. On the map are shown some of the potential new members, some of which already applications under consideration.

5. ANNUAL CD-ROM's

Every year, the IMOs are required to submit their final one-minute data for publication on an annual INTERMAGNET CD-ROM. Ten CD-ROMs have been published. The first, for 1991, had data from 40 observatories; the 2000 CD-ROM holds data from 80 observatories from 32 countries.

As well as definitive one-minute data the CD-ROMs contain additional information including:

A *readme* file for each IMO and for each country
A map of each country
A graphic “About-screen” for each country
An annual mean value table for each observatory

The *readme* file has a mandatory section providing all the information commonly required by users. It also has sections for the history of the observatory, a diary of events at the observatory during the year and other relevant information. For this reason the CD-ROMs have, for many observatories, replaced the former yearbooks.

During the first years of INTERMAGNET the CD-ROMs were sold through the INTERMAGNET Sales Office in Paris. It has however recently been decided that the CD-ROMs should be made available to all scientific users free of charge. All scientists working with observatory data can request copies of the CD-ROMs.

6. STANDARDS

From the information found in the *readme* files on the INTERMAGNET CD-ROMs it is possible to summarize the status of the INTERMAGNET network. The *readme* files reveal that almost all IMOs are using the combination of a fluxgate-theodolite instrument (DIM), to measure declination and inclination, and a proton precession magnetometer (PPM), to measure field strength, as their primary absolute instruments. A few Japanese observatories use a magnetic theodolite with rotating coils and one observatory is using a DIM with a proton vector magnetometer (PVM). No INTERMAGNET observatories are using the previously very popular, but less precise, QHMs anymore. As for the variometers, most IMOs are using 3-component fluxgate magnetometers as the primary recording instrument. A few are using other instruments such as Bobrov quartz magnetometers. For sensor orientation, about 2 out of 3 observatories use the HDZ-orientation, probably as it is the easiest way to install a variometer. But since INTERMAGNET recommends giving the final one-minute data in the XYZ-orientation almost 2 out of 3 observatories are using this orientation for reporting the final data. (The reason for recommending the use of XYZ for the final data is that the declination scaling factor to convert from nT to angular measure varies by more than a factor of 10 from the equator to the near-polar observatories.)

The *readme* files also give information on the variometer resolution and dynamic range.
INTERMAGNET asks for a digital resolution of 0.1 nT for low and mid latitude stations, and allows 0.2 nT resolution at high latitude. INTERMAGNET recommends a dynamic range of 6000 nT at auroral and equatorial observatories, 2000 nT at mid-latitudes. Only very few IMOs do not meet these specifications.

7. DATA USE

An important use of observatory data is the derivation of magnetic indices, which are parameterisations of various types of geomagnetic disturbance. It was recognised early in INTERMAGNET's development that this application was important, and INTERMAGNET's strategy has been to recruit the observatories supplying data for the various indices. INTERMAGNET is not involved in the production of the indices but works to improve the timeliness of the data availability to the institutions responsible for computing the indices. The ***aa-index*** available since 1868 and the ***Kp-index*** available since 1932 are important and widely used. The observatories contributing data for these indices are all INTERMAGNET members. The ***Km/am index*** is computed from a number of observatories having a better global distribution than those contributing to the *Kp* index. Except for a few observatories in the FSU these observatories are also members of INTERMAGNET. The ring-current index ***Dst*** is derived from four INTERMAGNET observatories. Colleagues in Japan, the USA and Russia have worked very hard to modernise the observatories along the North Coast of Siberia, and have finally managed to install modern digital instruments at the four observatories contributing to the Auroral Electrojet index ***AE***. These observatories are now sending real-time data to Japan using the Japanese GMS-satellites. It is an INTERMAGNET goal that these observatories should soon be able to qualify as IMOs.

Another important use of ground-based data is for global modelling of the Earth's main magnetic field. One of the most recent models of the Earth's magnetic field [2] computed using data from the Ørsted satellite owes its high accuracy to the use of ground-based observatory data. Eighty of the observatories were IMOs. The PI for the modelling effort, Dr. Nils Olsen from the Danish Space Research Institute, has asked us to thank all the contributing observatories for their data and he also requests prompt processing of more recent data, covering the year 2001, and later, in order to produce even better models in the future.

Using the Ørsted data Olsen has succeeded in producing the first secular variation model using satellite data only. This model has been compared to the secular variation measured at the observatories and the model fits the ground based data very well at many sites, but in some regions, especially around China and Japan, the model does not agree very well with the ground-based measurements, showing the importance of the ground-based observations.

The study by Cain et al. [3] of secular variations over a longer time span shows a similar agreement between the ground-based and the satellite data, again with larger disagreements in East Asia.

Another application of the INTERMAGNET data is the use of near-real-time data by oil companies as a reference for directional drilling using magnetic sensors. The oil companies use the geomagnetic field as a navigational tool during the drilling of oil wells and the accuracy of the drilling depends on how well the geomagnetic field is specified at the site, as well as on information about geomagnetic activity. Both the British Geological Survey and the Danish Meteorological Institute are supplying the oil industry with relevant data.

Also, in the study of upper atmosphere physics the INTERMAGNET network is extreme useful. The INTERMAGNET network of observatories has been used at the Danish Meteorological Institute, in combination with the many networks of geomagnetic variations stations, to model ionospheric convection from the magnetic disturbance vectors [4].

8. CONCLUSIONS

INTERMAGNET has, since it began in the late 1980s, grown into a global federation of institutions running geomagnetic observatories. Today more than 80 observatories supply near-real time data to data centres, GINs, from which scientific users can easily obtain the data. More than half of all geomagnetic observatories are now members of INTERMAGNET. Each year INTERMAGNET publishes definitive data on CD-ROM. Ten CD-ROMs have been published up to now (1991 to 2000) and these are available free of charge to scientists. INTERMAGNET has put forward a set of standards for the operation of modern digital geomagnetic observatories, which have become the *de facto* standards for the global network of observatories, and in this way has helped to improve data quality. The data from the INTERMAGNET network are widely used by scientists working in areas including main field and magnetospheric modelling, and for applications including directional drilling.

9. ACKNOWLEDGEMENTS

The contributions of the INTERMAGNET Executive Council and Operations Committee and of the participating national institutions and observatories as well as the funding support from the International Council for Science (ICSU) are gratefully acknowledged.

10. REFERENCES

1. St-Louis, B.J., Sauter, E.A., Trigg, D.F., and Coles, R.L., INTERMAGNET Technical Reference Manual Version 4, 1999.

2. N. Olsen, A model of the geomagnetic field and its secular variation for epoch 2000 estimated from Ørsted data, Geophys. J. Int. (2002) 149, 454-462

3. Cain, J.C., D.T. Mozzoni, B.B. Ferguson, and O. Ajayi, Geomagnetic Secular Variation 1995-2000, J. Geophys. Res., Solid Earth, (2002).

4. Stauning, P. (Private communications)

A qualitative analysis of five years of am quick-look values

Josette Paris[(1)] and Michel Menvielle[(1,2)]

(1) Centre d'études des Environnements Terrestre et Planétaires, 4 Avenue de Neptune, F-94100 SAINT MAUR DES FOSSES, France
(2) Université Paris Sud, Orsay, France

Abstract

Am quick-look values are routinely calculated and made available on a daily basis by the ISGI Publication Office, since July 1st, 1996. The minute values are automatically obtained from the observatories on a daily basis through data transfer facilities like ftp procedure or e-mail. The K indices are then computed with the FMI algorithm, and stored. Quick-look values of K-derived planetary indices are finally computed when K indices from enough observatories are available. am (Kpm) and aa (Kpa) are expressed in terms of Kp units using the statistical relationship between these indices. All these indices (am and Kpm, aa and Kpa, longitude sector activity indices) are made available at the ISGI www page (http://www.cetp.ipsl.fr/~isgi/homepag1.htm). A qualitative analysis of the whole set of quick-look values is presented and discussed in terms of delay of dissemination and quality of the quick-look values.

Introduction

The data dissemination through electronic networks makes it possible to derive and distribute values of geomagnetic indices with delays that could not have been considered before. It actually opened a new era, and resulted in particular to a new approach of derivation and dissemination of geomagnetic indices.

It makes it possible to derive and disseminate quick-look values with a delay of a few days. We describe hereafter the derivation process for am quick-look values, and give a qualitative analysis of these values over a five-year time span.

Definitive, provisional, and quick-look values of geomagnetic indices

The definitive values of IAGA magnetic indices are computed from the definitive values of magnetic transient variations (AE and Dst indices), or of K indices (K-derived planetary indices: aa, am, Kp) provided by the observatories [*see Mayaud (1980) for a review*].

In the past, data were made available by the observatories as hard copy magnetograms or data sheets. Because many months were necessary to receive all the definitive data, provisional values were computed in order to circulate the indices within reasonable delays. They were, and are still computed using provisional data distributed by the observatories. Electronic data transfer facilities resulted for most of the indices in a shortening delay down to a few weeks necessary for provisional values derivation and dissemination (see Table 1). The purpose of these values is to provide estimates of the definitive values of the indices: the provisional data series have similar statistical properties as the definitive ones.

The increasing facilities for data dissemination led the *ISGI Publication Office* (for K-derived planetary indices) and the *WDC-C2 for Geomagnetism* (for Dst and AE indices) to consider the routine derivation of quick-look values of geomagnetic indices. Since 1996, these values are made available on-line via the *ISGI*[1] and *WDC-C2* www homepages within delays ranging from 12 hours to a few days depending on the indices. The quick look values aim at providing estimates of the definitive values, and the quick look data series should have similar statistical properties as the

[1] *ISGI Publication Office: http://www.cetp.ipsl.fr/~isgi/homepag1.htm*

definitive ones. The confidence interval for each individual estimate is however significantly larger for the quick look values than for the provisional ones.

Index	**Quick-look values**		**Provisional values**		**Definitive values**
	Data	**Dissemination**	**Data**	**Dissemination**	**Dissemination**
AE	Digital minute values	Daily basis delay: H+12	Digital minute values	often responding to demands of projects	yearly basis delay: few years
Dst	Digital minute values	Daily basis delay: H+12	Digital minute values	monthly basis delay: ~2 months	yearly basis delay: several month
Kp	Not derived	Not derived	provisional K values	twice a month, delay: few weeks	yearly basis delay: definitive K values availability
am, an, as	Digital minute values	Daily basis delay: D+2	provisional K values	monthly basis delay: few weeks	yearly basis delay: definitive K values availability
Aa	Digital minute values	Daily basis delay: D+2[2]	provisional K values	weekly basis delay: few days	weekly basis delay: definitive K values availability

Table 1: *Dissemination of provisional and definitive values of geomagnetic indices*

The am quick-look values

Derivation

Following *Berthelier (1993)*, the am derivation process can be described in terms of four components [see *Menvielle and Berthelier*, *1991*, for a review]:

- *The time interval*: 3-hour UT intervals (00-03, 03-06,… 18-21, 21-24);
- *The quantity to be measured*: K indices from stations of a network;
- *The network of stations*: 21 stations (12 North, 9 South) at subauroral latitudes. The stations are arranged in groups representing longitude sectors (see Table 2);
- *The derivation process*: For each longitude sector, K codes are averaged, and converted into range amplitudes. an (as) is the weighted average of those amplitudes for the northern (southern) hemisphere. am = (an + as) / 2 (unit: nT).

Northern hemisphere

MGD	PET	MMB	POD	SVD	HAD	NGK	OTT	FRD	NEW	TUC	VIC
		x			x	x	x	x	x	x	x
ursi	ursi	obs	ursi	obs	obs	obs	obs				obs

Southern hemisphere

EYR	CNB	AMS	GNA	CZT	HER	PAF	AIA	TRW	PST
x	x	x	x	x	x	x		x	x
obs	ursi	obs	obs	obs	obs	ursi	obs		

Table 2: am *network and data collection.*

x: minute values provided by the observatories, and K *computer derived at ISGI;*
ursi: K *provided by the observatory through ursi messages (delay: few days);*

obs: K *directly provided by the observatory (delay: 1 to 4 weeks).*

PST is a backup station added for quick-look values derivation..

In order to make it possible to derive and make available on line quick-look values within a D+2 delay, the am derivation scheme has been modified slightly. Backup stations have been added to

[2] *The* ISGI Publication Office *has assessed the possibility of* aa *derivation and dissemination less than 30 minutes after the end of the 3-hour interval. Such quick-look values of* aa *and* Kpa *indices will soon be routinely derived and made available on-line at the ISGI www homepage.*

the am network (see Table 2), and the sectors are alternatively determined with regard to the distribution of observatories from which data are available. The weighting factor is computed accordingly.

The minute values are obtained automatically from the observatories on a daily basis through data transfer facilities like *ftp* procedure or *e-mail*. Spikes and jumps are automatically removed, then the K indices are computed using the FMI algorithm [*see Menvielle et al. (1995) and references therein*]. am quick-look values are finally derived when K indices from sufficient observatories are available for defining three longitude sectors in each hemisphere.

Availability

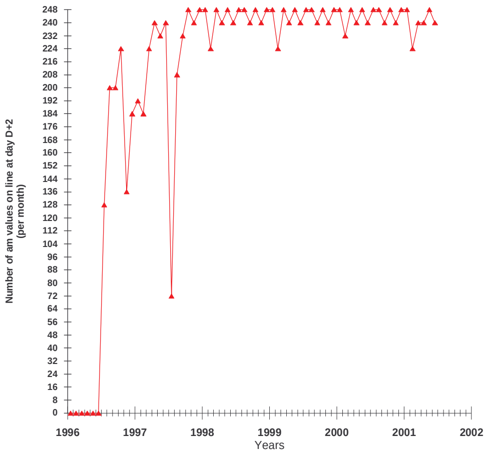

Figure 1: *Number of* am *quick-look values available on line at day D+2*

The quick-look values derivation routinely started on July 1996.

Figure 1 shows the monthly number of am quick-look values that have actually been made available on line at day D+2. During the first 12 months, we had problems to ensure routine derivation of am quick-look values at day D+2. After this period, quick-look values have been made available on-line at day D+2 for more than 95% of the 3-hour intervals.

In practice, missing data correspond to periods during which the ISGI system was down.

A comparison between am quick-look and provisional values

Let us consider 5 years of data, from July 1996 to June 2001 inclusively.

Figure 2 shows the comparison between the provisional and quick-look am values, for the whole data set. A comparison between provisional and definitive am values is also given in Figure 2, for a three-year data sample.

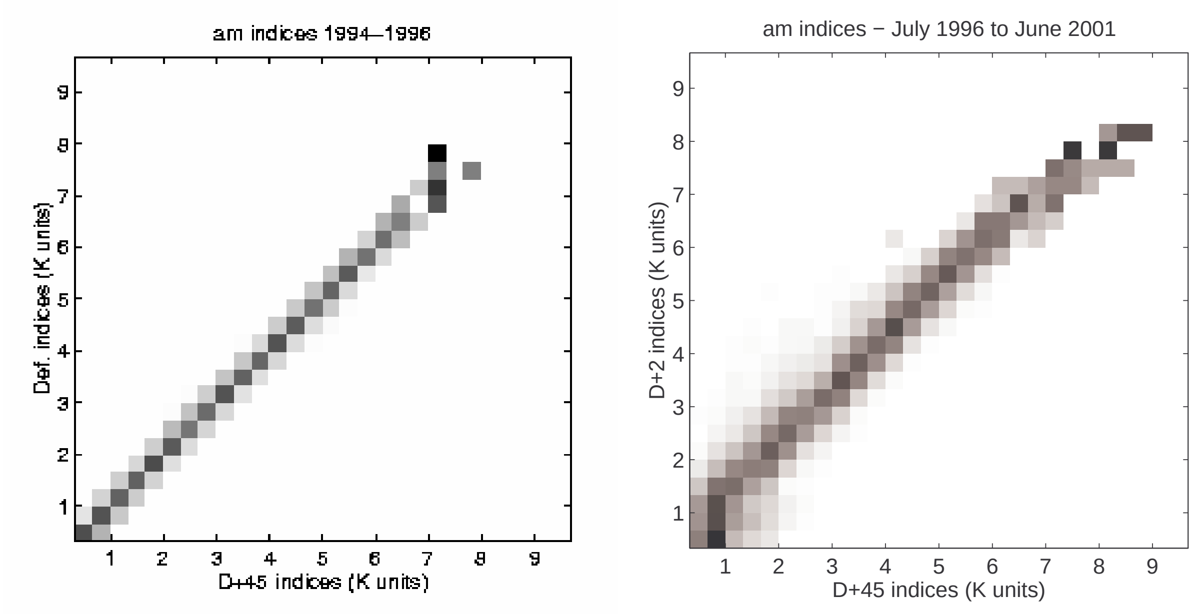

Figure 2: *Empirical joint probability distribution of provisional and definitive* am *values (left) and of provisional and quick-look* am *values. The level of grey in a pixel corresponds to the probability value: the darker the pixel, the higher the number. The scales are expressed in* K *units: the am values are converted back to* K *using the classical* am *to* Km *conversion table [see Table 3, and Menvielle and Berthelier (1991) for further details].*

This figure illustrates that definitive and provisional values do not differ by more than one third of K unit, except for a very limited number of 3-hour intervals. On the contrary, provisional and quick look values may differ by more than 1 K unit for a significant number of 3-hour intervals (about 5% in average for the whole data set).

This figure also shows that quick-look values are on average larger than the provisional values by about one third of a K unit.

am (nT)	0.0	1.4	3.4	5.4	7.4	10.4	13.4	16.4	20.4	26.4	33.4	40.4	50.4	50.4	60.4	70.4
3K	0	1	2	3	4	5	6	7	8	9	10	11	12	13	14	
am (nT)	70.4	86.4	103.4	120.4	146.4	173.4	200.4	243.4	286.4	330.4	386.4	443.4	500.4	611.4		
3K	15	16	17	18	19	20	21	22	23	24	25	26	27			

Table 3: *Conversion from* am*, expressed in nT, to* Km*, expressed in 3*K *units*

Figure 3 presents the comparison between am quick-look and provisional values for the three Lloyd's seasons (E: March, April, September, October; J: May to August; D: January, February, November, December), over the whole 5 years data set. No significant seasonal effect is observed.

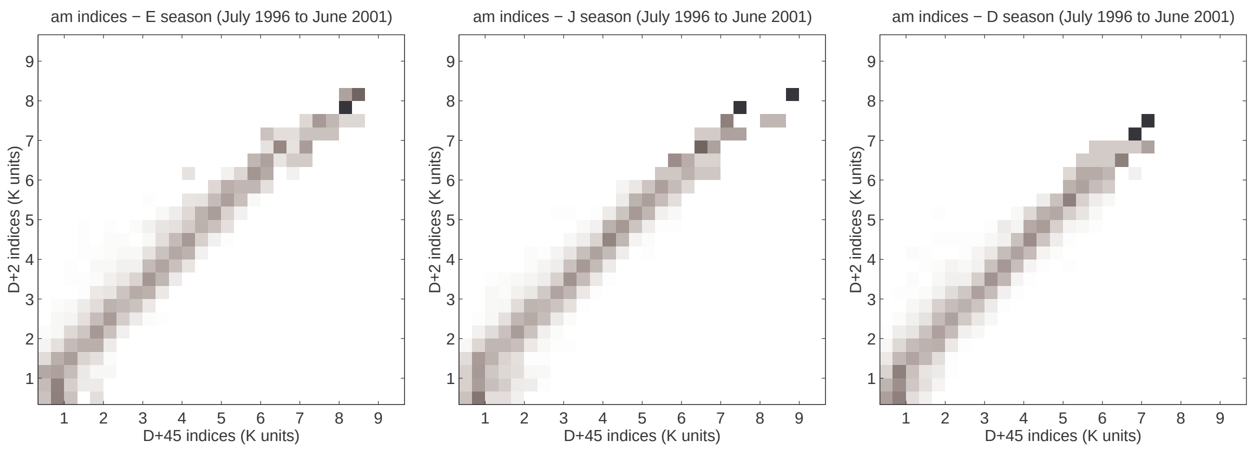

Figure 3*: Empirical joint probability distribution of provisional and quick-look* am *values for the equinox (E season, left), July (J season, centre) and December (D season, right) Lloyd seasons.*

The level of grey in a pixel corresponds to the probability value: the darker the pixel, the higher the value. The scales are expressed in K *units: the* am *values are converted back to* K *units using the classical* am *to* Km *conversion table [see Table 3, and Menvielle and Berthelier (1991) for further details]*.

Conclusion

am quick-look values are routinely calculated and made available on a daily basis by the *ISGI Publication Office*, since July 1st, 1996. The routine for their derivation and on-line dissemination makes it possible to have more than 95% of the individual 3-hour indices available on-line within a D+2 delay.

A five-year data set (from 1996, July 1st to June 30th, 2001) is considered in the present paper. A qualitative comparison between quick-look and provisional values shows that the quick look value differs from the provisional value by 1 K unit or less for 95% of the 3-hour intervals, on average over the whole data set. Furthermore, am quick-look values are not affected by any significant seasonal effect. However, these values are found to be on average larger than the provisional ones by about one third of K unit.

The statistical properties of the am quick look values can therefore be considered as similar to those of the provisional and definitive ones, with a larger confidence interval on each individual estimate. The observed systematic bias of quick-look values however deserves further investigations.

Bibliography

Berthelier, A., 1993: The geomagnetic indices: derivation, meaning and uses in Solar Terrestrial physics, in *STPW-IV proceedings*, Hruska J., Shea M.A., Smart D.F., and Heckman G., editors. US Gov. Publications Office, Boulder, 3-20.

Mayaud, P.N., 1980: Derivation, meaning and use of geomagnetic indices, *Geophys. Monogr 22,* 154 p., AGU, Washington DC.

Menvielle, M., and Berthelier, A., 1991: The *K*-derived planetary indices: description and availability, *Reviews Geophys. Space Phys.,* **29,** 415-432.

Menvielle, M., Papitashvili, N.E., Häkkinen L., and Sucksdorff, C., 1995: Computer production of *K* indices: review and comparison of methods, *Geophys. J. Int* , **123,** 866- 886.

On the possibility to monitor the planetary activity with a time resolution better than 3 hours

Michel Menvielle

Centre d'études des Environnements Terrestre et Planétaires, 4 Avenue de Neptune, F-94100 SAINT MAUR DES FOSSES, FRANCE, and Université Paris Sud, Orsay, France

Abstract

IAGA planetary geomagnetic activity indices are computed using K indices measured at a network of observatories. They do not keep up with requirements arising from operational Space Weather activities, in terms of time resolution and delay of dissemination. The routine availability of digital magnetograms makes it possible to derive planetary geomagnetic indices that could keep up with these requirements. Such a new index is proposed in the present paper.

Introduction

There is a clear request from some communities to get geomagnetic indices within delays smaller than 2 days. The need of their dissemination within delays ranging from about 20 minutes to a few hours is not clearly expressed. It is at present under investigation. Efforts have however been made to ensure in future the routine dissemination of planetary geomagnetic indices quick-look values within delays in the range 20 to 30 minutes.

The present IAGA planetary geomagnetic indices can however not keep up with requirements arising from operational Space Weather activities, in terms of time resolution – few tens of minutes – and on-line dissemination delay – few minutes if possible. Therefore it is necessary to build new planetary indices (i) that would have a better time resolution than (3 hours) of the present *am*, *aa*, and *Kp* indices, and (ii) that it would be available on-line within delays as short as possible.

The planetary geomagnetic activity indices

The irregular transient variations of the geomagnetic field at the Earth's surface are the signature of the currents taking place in the entire magnetosphere, under the influence of the solar wind. Many geomagnetic indices have been introduced to monitor these complex variations [see *Mayaud, 1980*, for an extensive review of geomagnetic indices]. Some of them aim at separating and quantifying the variations representative of an isolated effect: the ring current axis-symmetric variations are described by the *Dst* index; the auroral activity is monitored by the *AE* indices [*see Mayaud (1980) and references therein for further details*]. On the contrary, the planetary geomagnetic activity indices – *am*, *aa*, and *Kp* – aim at giving a global characterisation of the geomagnetic activity.

The present IAGA indices

The present planetary geomagnetic activity indices are derived from *K* indices measured at geomagnetic observatories. At subauroral latitudes (~ 40° to 55° in magnetic latitude) the observed morphology of the *K* variations (i.e. the deviations with respect to the Solar regular – S_R – variation) is actually such that the 3-hour ranges from which *K* indices are deduced, are related to the energy density embedded in the irregular geomagnetic variations (see e.g., *Menvielle, 1979*, *Menvielle and Berthelier*, *1991*, and references therein). *am*, *aa*, and *Kp* indices provide information on the global energy input in the magnetosphere.

Following *Berthelier (1993)*, their derivation process can be summarized in terms of four components [see *Menvielle and Berthelier, 1991*, for a review]:

- *The time interval*: 3-hour UT intervals (00-03, 03-06,… 18-21, 21-24);

- *The quantity to be measured*: *K* indices from stations of a network;
- *The network of stations*: 13 stations at subauroral and auroral latitudes (11 in North America and Western Europe, and 2 in Australia and New Zealand) for *Kp*, 23 stations at subauroral latitudes (13 in the North hemisphere and 10 in the South hemisphere, arranged in groups, each group representing a longitude sector) for *am*, 2 antipodal subauroral latitude stations for *aa*;
- *The derivation process*: weighted average of *K* equivalent amplitudes for *am* and *aa*, average of standardized *K* indices for *Kp*.

Quick-look values of *am* and *aa* planetary geomagnetic indices are at present routinely made available on-line on day D+2, at the ISGI www homepage[3]. The *ISGI Publication Office* has assessed the possibility of *aa* derivation and dissemination less than 30 minutes after the end of the 3-hour interval. Such quick-look values of *aa* and *Kpa*[4] indices will soon be routinely derived and made available on-line at the ISGI www homepage.

A possible new index

The next step, arising from operational space weather requirements, is to define new planetary geomagnetic indices that (i) would have a better time resolution than the *K*-related 3-hour interval, and (ii) would be available on-line within as short delays as possible.

The network

Because most of, if not all the software, used in space weather activities requires as input the existing IAGA planetary indices (in fact *Kp*), these new indices should be proximations of these indices. This requirement implies to consider *K*-variations observed at subauroral latitude stations.

What we learnt from the *aa* derivation and dissemination within a delay smaller than, or equal to 30 minutes makes it clear that routinely getting data within such short delays requires specific procedures for each station: the larger the number of stations, the more complicated the routine. The best possible network is of course the *am* network, since the stations are evenly distributed in longitude in both hemispheres (see e.g. *Menvielle and Berthelier, 1991*). Its fairly large number of stations (about 20) would however result in a quite complicated routine. On the contrary, the *aa* network (2 stations: Hartland, United *K*ingdom, and Canberra, Australia) would lead to the simplest possible routine, and is likely to be the best compromise.

The measured quantity

The time resolution of an index based on range measurements is the time interval on which the range is computed. Changing the time resolution of a planetary index based upon range measurements therefore requires changing the time interval on which the range is measured. As indicated above, the three-hour interval used to derive *K* indices is the best suitable for characterising *K* variations at subauroral latitudes. An index based upon ranges measured over a different time interval is then expected to be less significant at subauroral latitudes, and ranges are not worth being considered for deriving a planetary geomagnetic index with a time resolution smaller than 3 hours.

At subauroral latitudes, the *K* variations are sensitive to the field-aligned currents, the ring current and the dayside magnetopause currents: they are not under the predominance of one system of currents. The morphology of the *K* variations is accordingly difficult to interpret in terms of magnetospheric physics. The *K* variation waveform is then not worth being considered for deriving a relevant planetary geomagnetic index.

As stated above, *K* indices are related to the energy density embedded in the *K* variations. This suggests considering a quantity that is representative of this magnetic energy density. At station S_i and time t, this energy is proportional to:

$$E(S_i,t) = \left(\Delta B_x(S_i,t)^2 + \Delta B_y(S_i,t)^2\right)^{1/2}$$

[3] http://www.cetp.ipsl.fr/~isgi/homepag1.htm
[4] *Kpa is the aa index expressed in terms of Kp units*

Where $\Delta B_x(S_i,t)$ and $\Delta B_y(S_i,t)$ are the *K* variations in the horizontal geographic North and East magnetic components. The intensity of the *K* variations in the vertical component is negligible, except in the vicinity of lateral contrasts of conductivity in the conductive Earth where they result from induction in the Earth: they are not worth being considered here (see *Mayaud, 1980,* and *Menvielle and Berthelier, 1991* for further details).

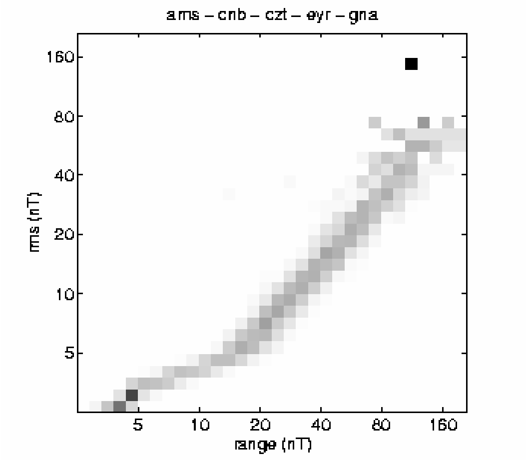

Figure 1*: Comparison between the ranges used for K derivation and the rms of the K variations in the horizontal components [S_R estimated using the FMI algorithm, see Menvielle et al. (1995) and references therein]. The level of grey in a pixel corresponds to the number of 3-hour intervals for which the range and the rms fall in the corresponding intervals: the darker the pixel, the higher the number. Data: minute values from the Amberley (AMB), Amsterdam (AMS), Canberra (CNB), Crozet (CZT), Eyrewell (EYR) and Gnangara (GNA) observatories, for 1996 and 1997.*

The average of $E(S_i,t)$ over a time interval of duration τ:

$$\alpha_\tau(S_i,t) = \frac{1}{\tau}\int_t^{t+\tau} E(S_i,t)\, dt$$

is thus representative of the mean energy density embedded in the *K* variations during the interval $[t, t+\tau]$; it is expressed in nT.

When the $[t, t+\tau]$ intervals correspond to the classical 3-hour UT *K* intervals, $E(S_i, t)$ and the range used to derive *K* indices are expected to be correlated. So it is observed, as illustrated in Figure 1. The $\alpha_\tau(S_i, t)$ quantity therefore ena-bles one to derive indices that monitor the en-ergy density embedded in the *K* variations over time interval of duration τ, and that would be approximations of the present planetary geomagnetic indices when the time intervals correspond to the UT 3-hour intervals used for *K* derivation.

The derivation process

The proposed index, named αa_τ is derived in a similar way as the *aa* index. It is the weighted average of the $\alpha_\tau(S_i, t)$ quantities computed for the Hartland (HAD) and Canberra (CNB) stations. For the sake of homogeneity with the *aa* index, the weighting coefficients are those used for the *aa* derivation:

$$\alpha a_\tau = \left(\lambda_{HAD}\cdot\alpha_\tau(\mathrm{HAD},t) + \lambda_{CNB}\cdot\alpha_\tau(\mathrm{CNB},t)\right)/2$$

with $\lambda_{HAD} = 1.059$ and $\lambda_{CNB} = 1.084$.

The time interval

As a result of the αa_τ definition, the time interval τ can be adjusted to get the best compromise with regard to the requirements. αa_{180} (i.e. $\tau = 180$ min.) is a proximation of *aa*; considering the present data transmission protocol from the Hartland and Canberra observatories to the ISGI Publication Office (10-minute data packets within a delay smaller than 10 minutes), note that any τ value that is not a multiple of 10 minutes is of no practical interest.

A first comparison between *aa* and □a indices

In order to give a first illustration of the αa_τ index behaviour, let us present in this section a comparison between αa_τ and *aa* indices for different τ values.

The data

The data are minute values recorded at the Hartland and Canberra magnetic observatories during a 14-day long period, between 2000 July 19th and August 1st, i.e. Julian days 200 and 213 inclusively.

The αa_τ indices are computed from *K* variations estimated for each observatory as the difference between the observed transient magnetic variations and the S_R estimated using the FMI algorithm.

τ = 180 minutes

Figure 2 shows the comparison between αa_{180} and *aa* indices. The two indices are quite well correlated, and gives an experimental confirmation of the results established by *Menvielle (1979)*, based on the αa_τ definition. The experimental average value of the αa_τ / *aa* ratio has been estimated for this data set: it is in the order of 0.4, thus providing an experimental confirmation of the 0.55 ± 0.3 estimate already proposed by this author from morphological considerations.

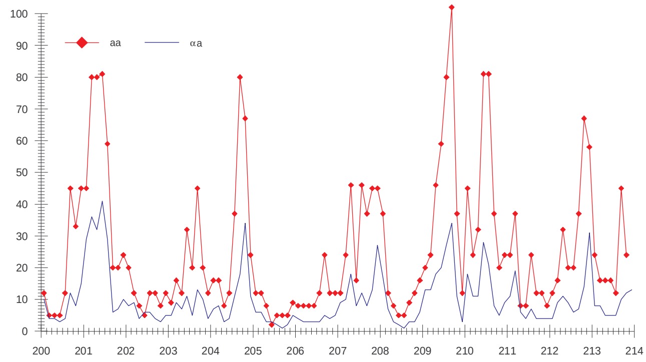

Figure 2: *Comparison between αa_τ and aa indices for τ = 180 minutes.*

τ < 180 minutes

Figure 3 presents the comparison between αa_τ and *aa* indices, for τ = 15, 30, and 60 minutes. Figures 2 and 3 show that the irregularity in the αa_τ variations increases with decreasing τ values. This is consistent with the commonly observed fairly rapid and large changes in the intensity of the *K* variations: such features are actually expected to be filtered out, and the αa_τ variations accordingly expected to be smoother when τ becomes larger than their apparent period.

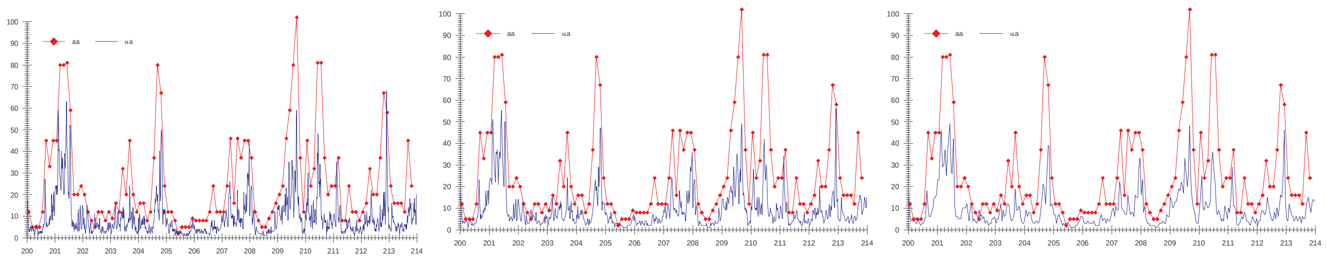

Figure 3: *Comparison between αa_τ and aa indices for τ = 15 minutes (left), 30 minutes (centre), and 60 minutes (right).*

Conclusion

The αa_τ index proposed in this paper allows keeping up with requirements arising from operational Space Weather activities, in terms of time resolution and on-line dissemination delay. Furthermore, the αa_τ index is an approximation of the *aa* index, when the time intervals correspond to the UT 3-hour intervals used for *K* derivation.

Bibliography

Berthelier, A., 1993: The geomagnetic indices: derivation, meaning and uses in Solar Terrestrial physics, in *STPW-IV proceedings*, Hruska J., Shea M.A., Smart D.F., and Heckman G., editors. US Gov. Publications Office, Boulder, 3-20.

Mayaud, P.N., 1980: Derivation, meaning and use of geomagnetic indices, *Geophys. Monogr 22*, 154 p., AGU, Washington DC.

Menvielle, M., 1979: A possible geophysical meaning of *K* indices. *Ann. Géophys.*, **35**, 189-196.

Menvielle, M., and Berthelier, A., 1991: The *K*-derived planetary indices: description and availability, *Reviews Geophys. Space Phys.*, **29,** 415-432.

Menvielle, M., Papitashvili, N.E., Häkkinen L., and Sucksdorff, C., 1995: Computer production of *K* indices: review and comparison of methods, *Geophys. J. Int* , **123,** 866- 886.

The Geomagnetic Field and its Secular Variation in Slovakia

M Vaczyova (Geomagnetic Observatory GPI SAS, Hurbanovo, Slovakia)

Abstract

The paper deals with the geomagnetic field and its secular variation in Slovakia and at Hurbanovo Geomagnetic Observatory during the last century based on four magnetic surveys. The secular variation of the geomagnetic field was derived in the form of a linear expression.

Introduction

The determination of geomagnetic field elements and their secular variation in certain region belongs to the fundamental problem. For this purpose, the data are provided by magnetic observatories and magnetic surveys. The results of the magnetic surveys are usually used to derive the average behaviour of the individual geomagnetic elements in dependence on the geographic latitude and longitude in the form of polynomials of a certain degree. Repeated geomagnetic surveys serve to determine the secular variation of the individual elements over a given time interval.

Magnetic surveys on the territory of Slovakia

The first survey in Slovakia was carried out in 1843-1851 [Kreil and Fritsch, 1850] as part of the survey of the Austro-Hungarian Monarchy. There were only 8 stations in the territory of Slovakia. More detailed magnetic surveys were executed in the years 1864-1879 [Schenzl, 1871,1881], 21 more stations were attributed. The next magnetic survey was in the years 1892-1894 [Liznar, 1898], only with 7 stations in Slovakia.

During the later activities neither the measurements in 1928-1929 [Cechura, 1934] nor in 1936-1937 [Behounek, 1939] had the features of a complete magnetic survey. Actually the Geomagnetic Observatory at Hurbanovo observed only declination at that time and the distribution of the network points was relatively low.

The first complete first-order survey was carried out in the years 1951-1953 and reduced to the epoch 1952.5 [Ochaba, 1959]. In the years 1957-1958, the Institute of Applied Geophysics in Brno (the former Czechoslovakia) carried out airborne mapping which was reduced to the 1958.0 epoch. The next completed surveys were in the years 1967-1968 [Krajcovic and Nemeth, 1972] reduced to 1967.5, after that in the years 1979-1982 [Podsklan, 1987] reduced to the epoch 1985.5 and the last in the years 1993-1995 [Vaczyova, 1999] reduced to the epoch 1995.5.

Secular variation

We used the normal field for the determination of the secular variation from the geomagnetic mappings, the measured values on the selected points from the geomagnetic mapping were not moved from the delimitation of the new network since 1951 or were just slightly moved (we interpolated these values by means of the normal field) and the observatory results from Hurbanovo (Fig. 1, Tab.1). The 14 points were selected on the territory of Slovakia.

No.	Name of station	Geographic latitude	Geographic longitude
1.	Hurbanovo	47.9°	18.2°
2.	Brusno	48.8°	17.2°
3.	Hajnacka	48.2°	19.6°
4.	Oravska Polhora	49.5°	19.5°
5.	Sastin-Straze	48.4°	17.2°
6.	Ubrez	48.8°	22.1°
7.	Turna n/Bodvou	48.6°	20.9°
8.	Pribylina	49.1°	19.8°
9.	Tisovec	48.7°	19.9°
10.	Svidnik	49.3°	21.6°
11.	Senec	48.2°	17.4°
12.	Pukanec	48.4°	18.7°
13.	Rajec	49.1°	18.6°
14.	Podolinec	49.3°	20.9°

Table1. The list of points and their geographical coordinates used for determination of the secular variation.

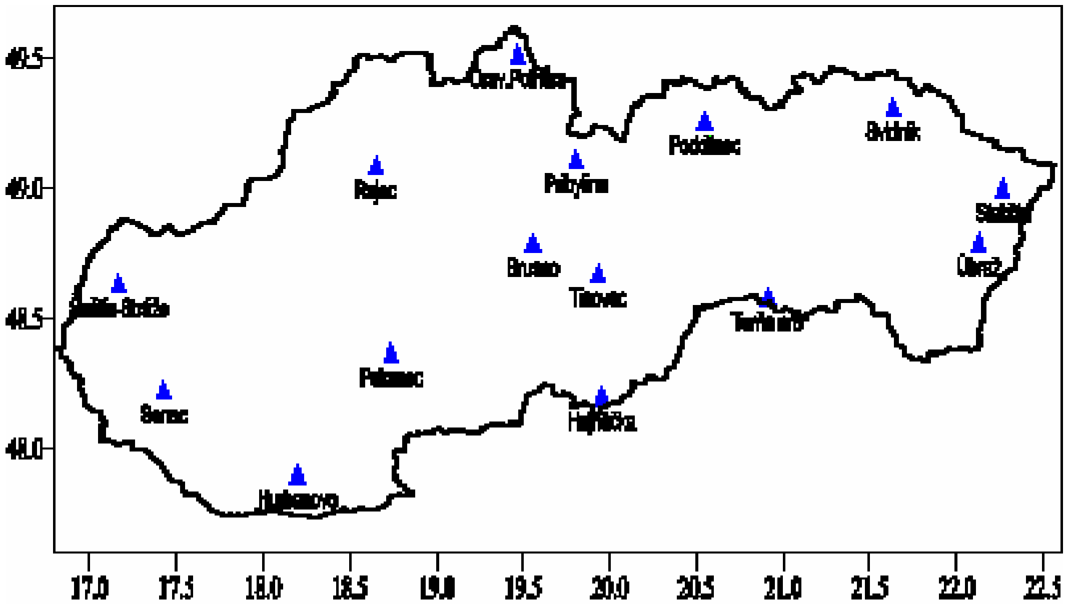

Fig. 1 Distribution of observation points for secular variation

The distribution of the secular variation was calculated in the form of polynomials of the first degree for the epoch differences :

1952.5 – 1967.5
1967.5 – 1980.5
1980.5 – 1995.5

The results are as follows:

from 1952.5 to 1967.5

$\Delta D = 2.85 + 1.23 * \Delta\varphi - 1.08 * \Delta\lambda$
$\Delta H = 10.32 + 2.16 * \Delta\varphi - 3.87 * \Delta\lambda$
$\Delta Z = 22.26 + 3.42 * \Delta\varphi - 0.25 * \Delta\lambda$

from 1967.5 to 1980.5
$\Delta D = 3.87 - 1.04 * \Delta\varphi + 0.61 * \Delta\lambda$
$\Delta H = 10.38 - 2.59 * \Delta\varphi + 1.60 * \Delta\lambda$
$\Delta Z = 26.59 + 0.46 * \Delta\varphi + 0.05 * \Delta\lambda$

from 1980.5 to 1995.5
$\Delta D = 3.48 + 0.15 * \Delta\varphi + 0.07 * \Delta\lambda$
$\Delta H = -2.89 - 2.00 * \Delta\varphi + 0.27 * \Delta\lambda$
$\Delta Z = 24.90 - 0.22 * \Delta\varphi + 0.08 * \Delta\lambda$

The point with the geographical coordinates $\varphi = 48.5°$ and $\lambda = 19.5°$ represents the middle of the territory of Slovakia ($\Delta\varphi = \varphi - 48.5°$, $\Delta\lambda = \lambda - 19.5°$).

The total secular change for epochs 1967.5-1952.5, 1980.5-1967.5 and 1995.5-1980.5 is also shown in the charts in Fig. 2 – Fig. 4.

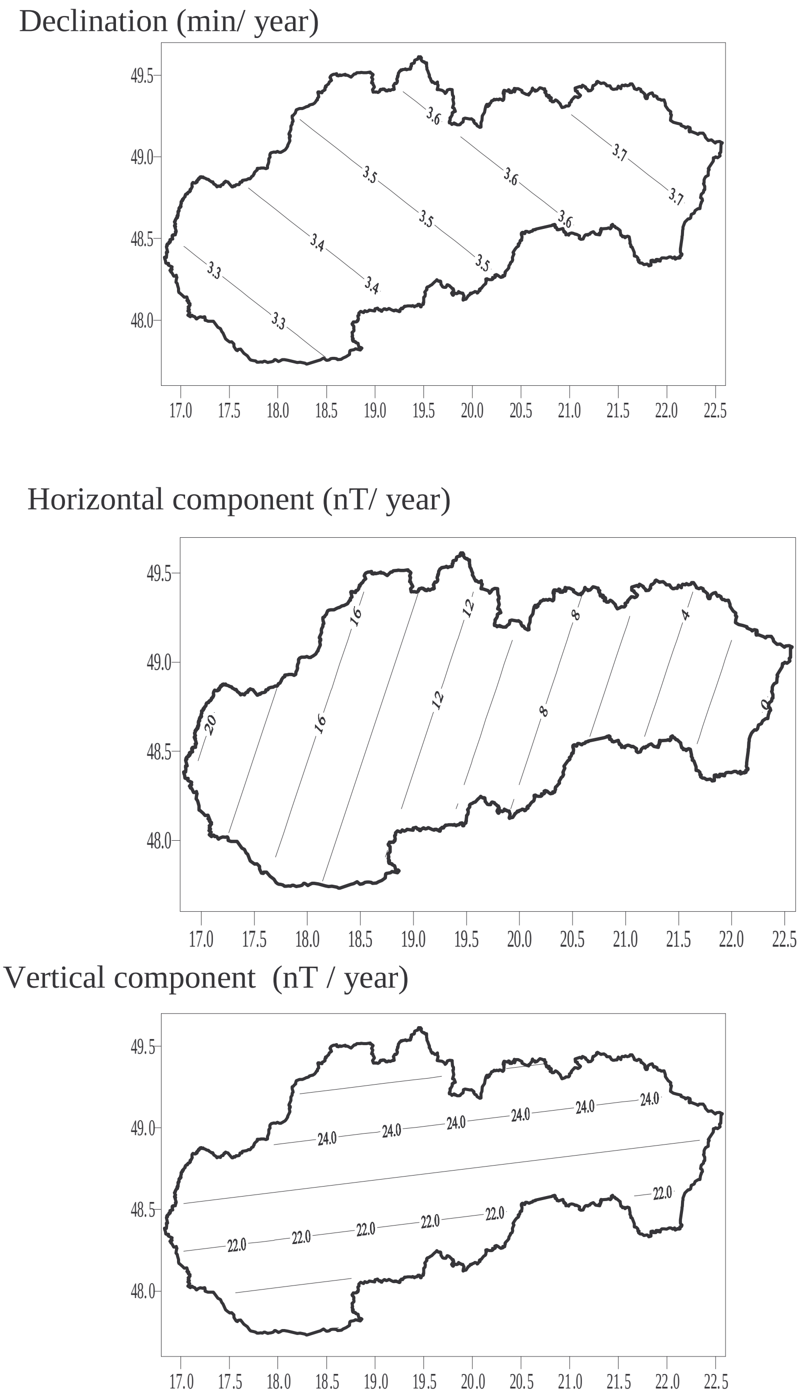

Fig. 2. Secular variation from 1952.5 to 1967.5, calculated from first-degree polynomials.

Declination (min/ year)

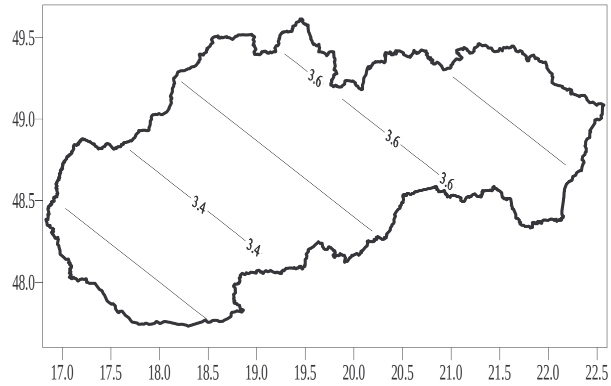

Horizontal component (nT/ year)

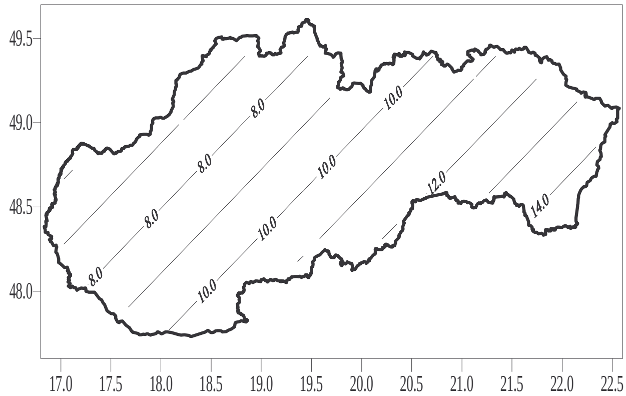

Vertical component (nT/ year)

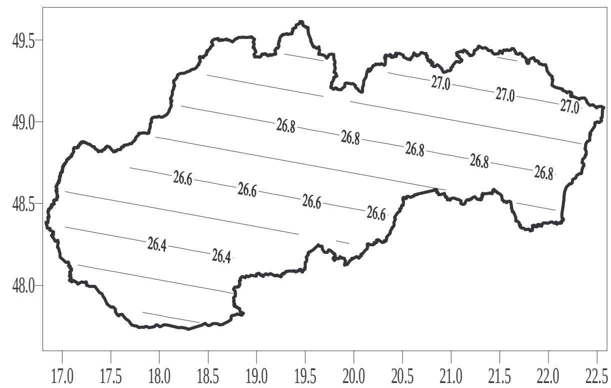

Fig. 3. Secular variation from 1967.5 to 1980.5, calculated from first-degree polynomials.

Declination (min/ year)

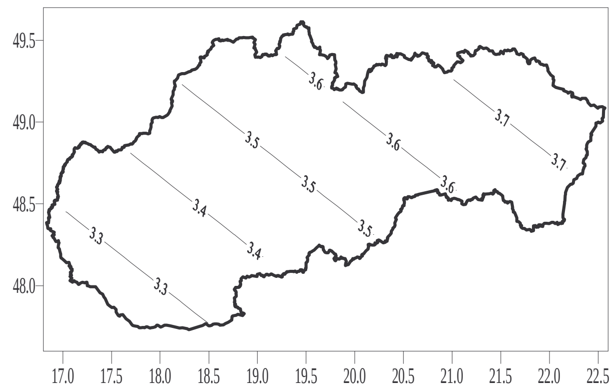

Horizontal component (nT/ year)

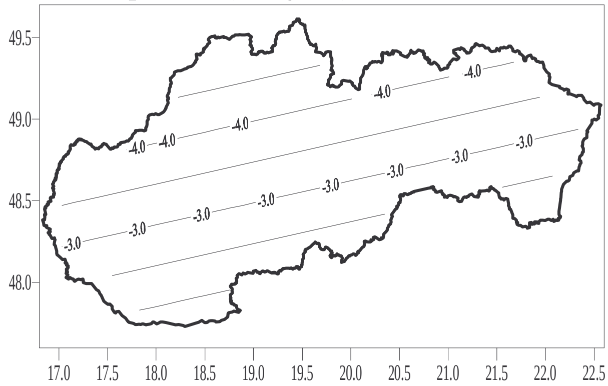

Vertical component (nT / year)

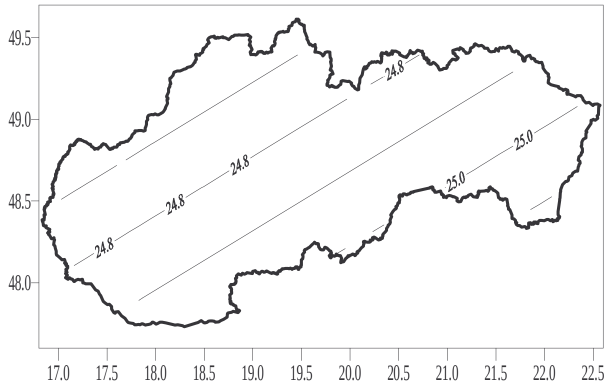

Fig. 4. Secular variation from 1980.5 to 1995.5, calculated from first-degree polynomials.

The next aim was to determine how the total values for the secular variation vary with the decreasing number of secular variation points. We calculated the secular variation from points 14, 10 and 6. The stations were distributed equally on the territory of Slovakia.

The secular variation was also calculated from the normal field and from IGRF. The observed and calculated values from individual models are in Fig. 5 – Fig.7.

Hurbanovo

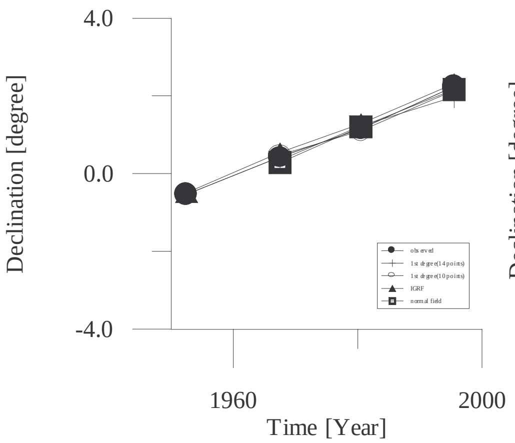

Brusno

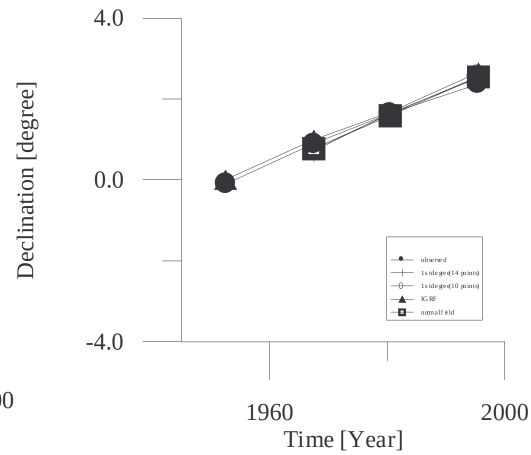

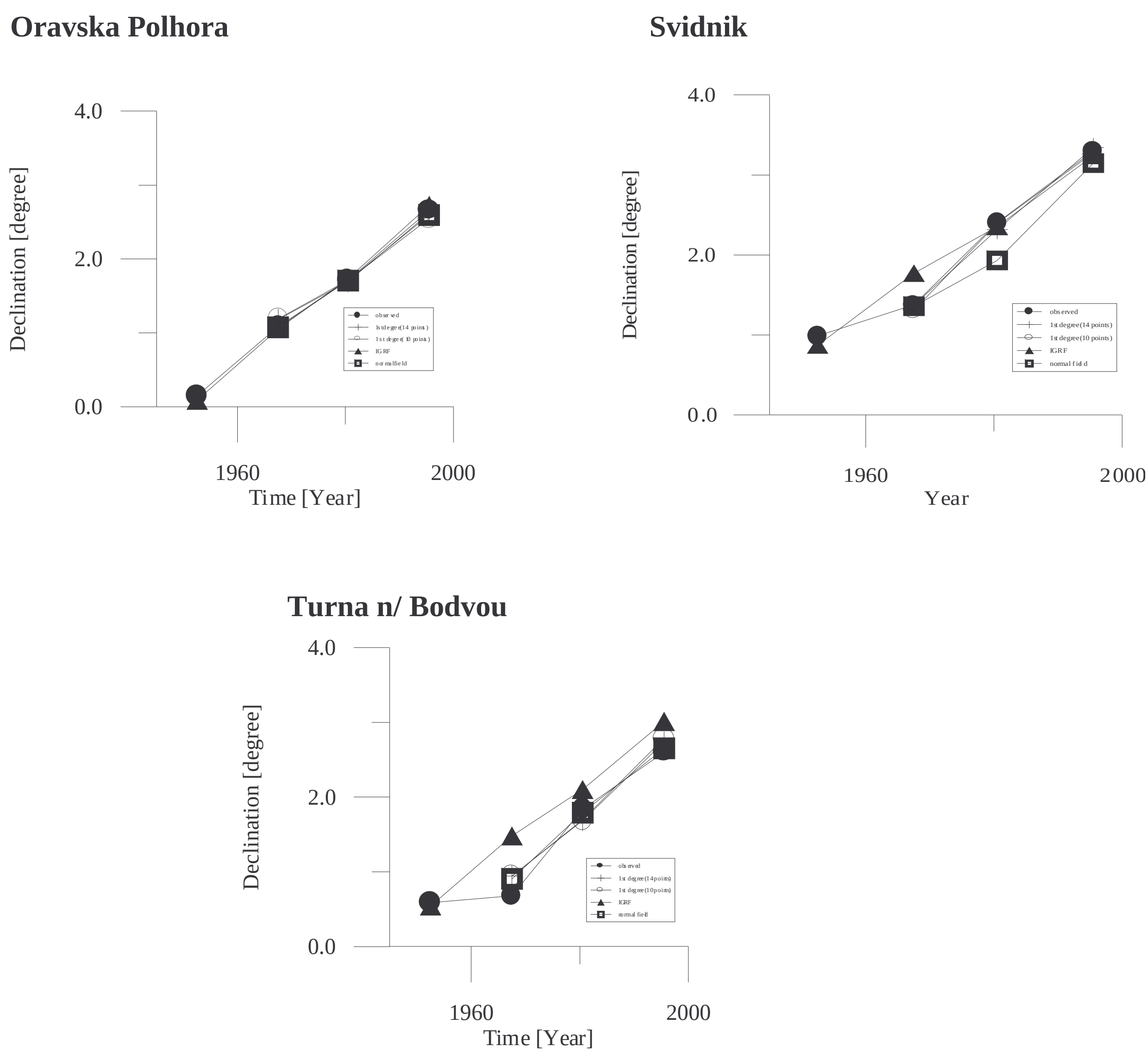

Fig. 5. The secular variation of the declination from 1952.5 to 1995.5 at five magnetic stations in Slovakia, calculated from several models.

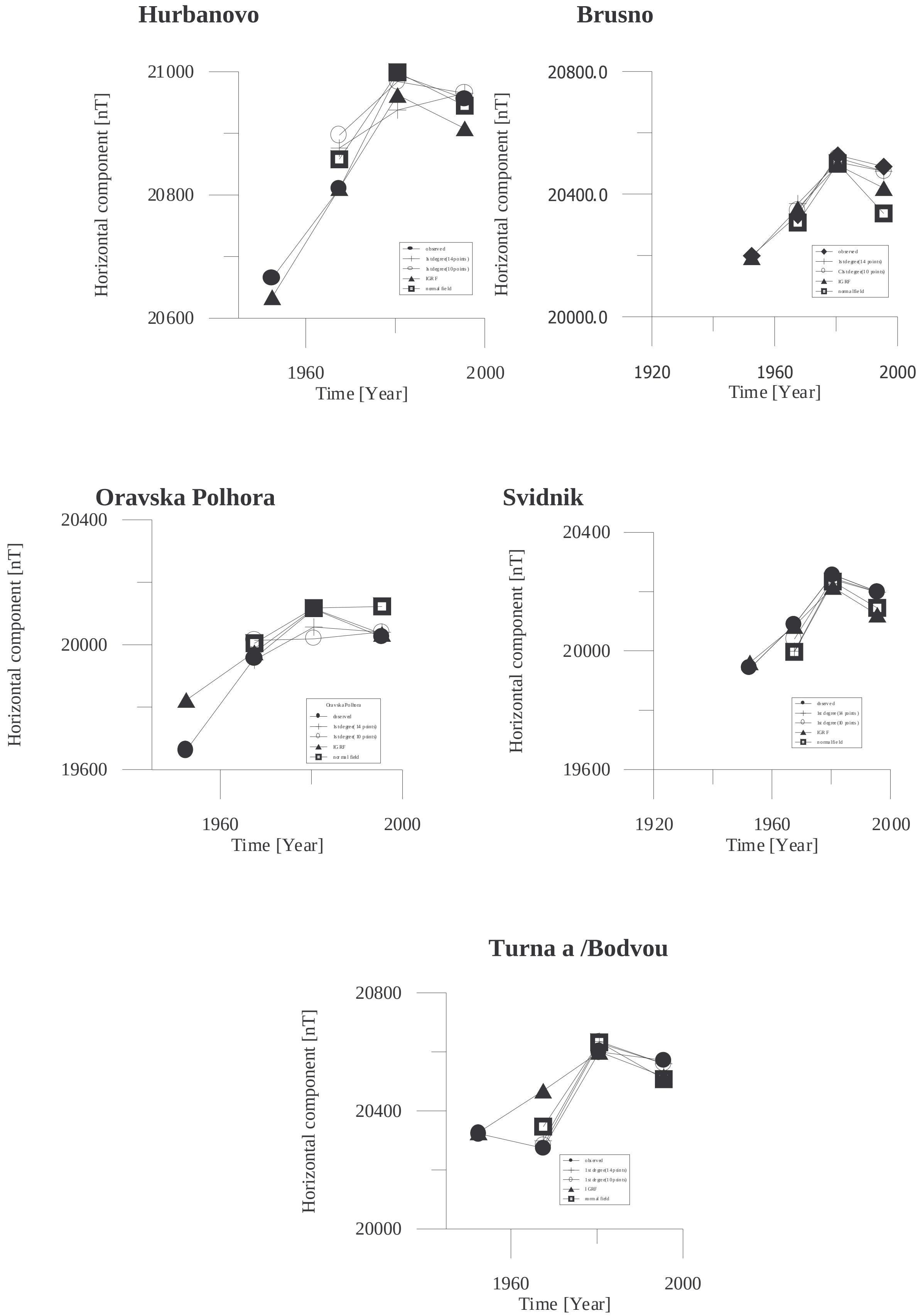

Fig. 6. The secular variation of the horizontal component from 1952.5 to 1995.5 at five magnetic stations in Slovakia, calculated from several models.

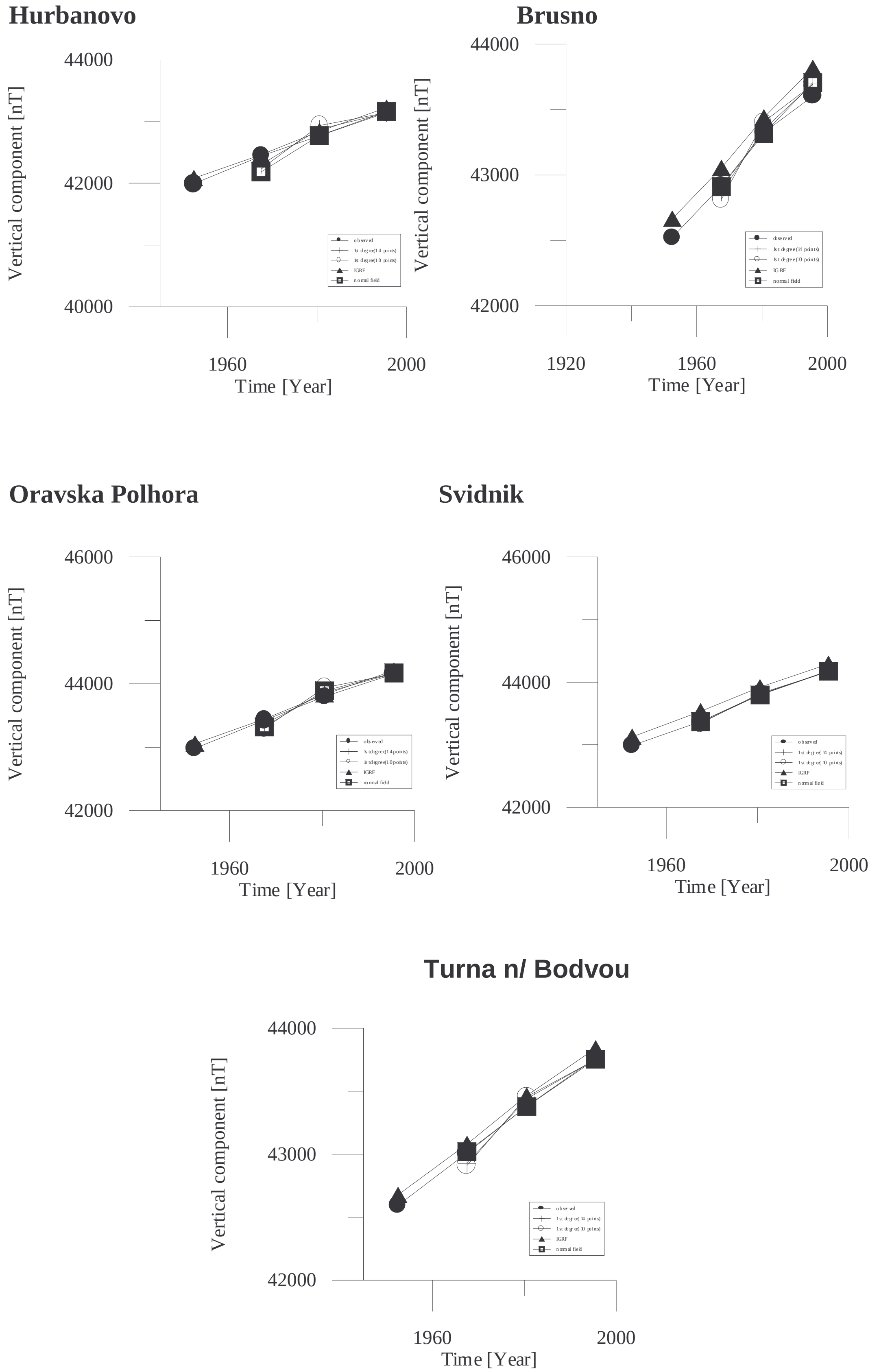

Fig. 7. The secular variation of the vertical component from 1952.5 to 1995.5 at five magnetic stations in Slovakia, calculated from several models.

The r.m.s - values for the individual models are:

Declination

	14 points	10 points	6 points	normal field
1967.5 – 1952.5	14.37’	13.14’	4.78’	24.44’
1980.5 – 1967.5	16.09’	14.94’	5.36’	22.50’
1995.5 – 1980.5	16.40’	5.69’	4.01’	18.17’

Horizontal component

1967.5 – 1952.5	167.96 nT	110.02 nT	76.87 nT	189.23 nT
1980.5 – 1967.5	127.84 nT	139.63 nT	131.42 nT	139.33 nT
1995.5 – 1980.5	9.90 nT	11.33 nT	13.49 nT	20.16 nT

Vertical component

1967.5 – 1952.5	143.47 nT	177.98 nT	135.69 nT	182.69 nT
1980.5 – 1967.5	139.21 nT	179.07 nT	129.81 nT	178.53 nT
1995.5 – 1980.5	41.27 nT	31.87 nT	38.62 nT	33.25 nT

Conclusion

The secular variation for various epochs was determined in five based points. On the basis of the diagrams of the secular variations. The following conclusions can be drawn.

(1) The values of magnetic components D and Z increased continuously on the territory of Slovakia. The values of the H component were rising up to 1980 and then started to decrease.

(2) The rate of change in D decreases from the western part to the eastern part of the country, and increases in Z. The rate of the H variation decreases from west to east in the rising period and increases in the falling period.

(3) The values of the magnetic components from IGRF are higher than the observed values. The values from the other models calculated with the last-squares method are smaller.

(4) The comparison of several models shows that six secular stations are sufficient for the determination of the secular variation on the territory of Slovakia.

Acknowledgements

The paper was prepared with the support of Agencyor Science VEGA grant 118/2000.

References

Behounek R., 1939: Magnetic measurements in Slovakia, Moravia-Slez region and Carpathian Ukraine, State Geophysical Institute, Prague, 49p.

Cechura F., 1934: Magnetic declination in Slovakia for the 1932.0 epoch (in Czech). Magazine of the Club for Nature Sciences in Kosice, II, 1933-1934,1-30.

Krajcovic S., Nemeth M., 1972: Distribution of the geomagnetic field in Slovakia for epoch 1967.5. Contr. Geophys. Inst. SAS, 3, 16-24.
Kreil K.,Fritsch K., 1850: Magnetische und geographische Ortsbestimmung im Österreichischen Kaiserstaate. Prag., 50 p.
Liznar J.,1898: Verheilung der Erdmagnetischen Kraft in Österreich-Ungarn. II. Theil, Wien1898, 90p.
Ochaba S., 1959: Geomagnetic field distribution in Slovakia for the epoch 1952.5 (in Slovak). Geophysical Issue, No. 72-78, Prague, 319-356.
Podsklan J., 1987: Distribution of the Earth magnetic field on the territory of Slovakia for the epoch 1980.5. Contr. Geophys. Inst. SAS, 17,111-141.
Vaczyova M., 1999: Distribution Of the Earth’s magnetic field on the territory of Slovakia for the 1995.5 epoch. Contr. to Geophysics and Geodesy, 29/4, 1999, 169-284.

A Calibration Facility for Search Coil Magnetometers

E. Pulz
GeoForschungsZentrum Potsdam, Telegrafenberg, D-14473 Potsdam, Germany

Abstract

A calibration facility for search coil magnetometers (SCMs) has been built at Niemegk Geomagnetic Observatory, GeoForschungsZentrum Potsdam. I describe here the commissioning of this facility. The usable frequency range of 10 mHz to 100 kHz enables calibration of all standard types of SCMs. The homogeneity is 0.1 % up to a diameter of 10 cm and up to a length of 2.5 m. Extensive test measurements showed broad agreement with theoretical calculations made before construction. As part of the testing, all SCMs in the GFZ geophysical equipment pool were checked. Several devices showed serious malfunctions, emphasising the value of such a calibration facility.

The calibration coil has been designed to be largely automatic, enabling non-specialists to operate it after short instruction. It can also be adapted to test other types of sensors with little effort (for example, fluxgate magnetometers). As a result, the facility should be of broad use for external institutions to calibrate their instruments, particularly Germany because there are a lot of SCMs in use at several institutes without the possibility of calibration.

1. Introduction

Varying electric currents in the ionosphere and magnetosphere generate magnetic fields which induce electric and magnetic fields within the Earth. Magnetotellurics is the study of the conductivity structure of the Earth using measurements of these magnetic and electric fields. Magnetotellurics [1,2] has made great progress during recent years, with complex models of Earth structure computed using modern computers. The successful calculation of such models requires very good input data. But the measurement of the magnetic field variations is not easy, because they are of small amplitude but have a very large frequency range [2]. Different instruments are more or less suitable for the recording of geomagnetic field variations. Search coil magnetometers (SCM) are highly suitable for the frequency range from a few mHz up to some kHz. These are highly complex devices with a ferromagnetic flux amplifier and with flux-feedback. However, to be used they must be transported great distances and repeatedly buried in the ground. Consequently, the mechanical demands on these instruments are great, and they can easily be damaged without such damage being clear in the measurements. Therefore, regular calibration is crucial to ensure that the geophysical measurements are not compromised.

To rectify this, a calibration facility for search coil magnetometers has been built at Niemegk Geomagnetic Observatory, GeoForschungsZentrum Potsdam.

2. Specification of the Problem

The required output of a magnetometer calibration is the frequency response function (FRF). The sensor is excited in the required frequency range, and the input excitation and output are compared, both in amplitude and in phase difference. The resulting response is a complex function of the frequency. To generate such a function, the calibration coil must clearly be large enough to contain the sensors, its magnetic field must be sufficiently homogeneous, and the coil must generate the required frequency range without phase shift. At present, search coil magnetometers are used up to 10 kHz, but to accommodate future developments, the frequency specification for the facility was chosen as 100 kHz.

3. Calculations and Estimations

The size requirements led to the choice of a cylindrical geometry–the required size of a Helmholtz coil would have been too great.

The required homogeneity is easily achieved with a cylindrical coil, but reaching the desired resonant frequency is much more difficult. To reduce the capacitance, we proposed to have chambers with one winding per chamber. We decided in favour of a diameter of 30 cm for the windings and a total calibration coil length of up to 5 m. Firstly, the magnetic flux density B was calculated [e.g., 3] in the direction of and perpendicular to the coil axis for distances between windings (chambers) of 5 cm, 7 cm, 8 cm, and 9 cm. The result for 8cm distance is shown in Fig.1. Then the resonance frequency was estimated for the different distances. There must be a phase shift near zero at 100kHz, from which it follows that the resonance frequency must not be smaller than 1MHz. A small experiment to test our results was carried out, and showed that the estimated resonance frequency was very pessimistic. Therefore, we decided on a distance of 8cm between windings.

In this case the homogeneity corresponds to the specifications of an instrument diameter of <6 cm. Search coil sensors have mostly a large diameter, but the core of such sensors consists of a magnetic flux amplifier (ferromagnetic material). That means the magnetic flux density outside of the centre is less important. Further the magnetic flux is averaged along the length, so the effects of non-homogeneity tend to cancel out.

4. Design and Construction

The basic structure was manufactured from a polyethylene sewage-pipe, with inner diameter 26 cm, and wall thickness 1cm. 54 PVC-rings (diameter 30 cm) were manufactured and pushed over the pipe, with 3 separators inserted between each pair of rings, to fix the exact distance between the rings. The connection wires are in one of these separators. The connections between the windings and the return wire (that closes the circuit) are placed anti-parallel to minimise the possible stray field.

The coil is 4.50 m long. The distance between the windings is gradually reduced towards the ends to improve the homogeneity there. The coil is mounted on a plastic support, which in turn is mounted permanently on a long stone pillar in a large wooden house - the observatory magnetic laboratory. The search coil under test is pushed into the calibration coil using a specially constructed sled.

Fig.2 shows the calibration coil before installation.

5. Measurements with the completed coil and comparison with the estimated coil parameters

The calibration coil was examined for short-circuits in the windings by connecting it in parallel with a capacitor and applying a high-frequency sinusoidal field. Each winding was checked using an analyser and a magnetic field probe. The electrical parameters of the calibration coil were determined. The magnetic flux density was determined using two different sensors: a Bartington MAG03 fluxgate sensor, and a small self-made air coil. For both, a lock-in amplifier eliminated the natural variation of magnetic field.

For results of the comparison see Table 1. As expected, the estimated and measured inductance agrees well. In contrast, the measured capacitance is five times less than estimated. These values lead to a resonance frequency of 1.6 MHz (the phase shift is only 0.2 degrees at 100 kHz).

	Resistance Ω	Inductance µH	Capacitance pF	Resonance frequency MHz	Scale Factor nT/mA
calculated	5.2	100	500	0.660	15.65
Measured at 15.5°C	4.6	109	90	1.6	15.65 ± 0.05

Table 1 Comparison of the electrical parameters

The MAG03 results suggest no significant deviations from homogeneity. Only a part of the measurement results are shown in Fig. 3. It shows the magnetic flux density inside the coil along the cylinder axis at x = 0 cm, 2 cm, and 4 cm over and under the axis. Further measurements were carried out at x = ± 6 cm and x = ± 8 cm, measured every 1cm because of a sinusoidal shape. It was tested for z = 0 cm, and z = ± 75 cm. The results do not indicate any construction defects. The homogeneity is 0.1% up to the diameter of 10 cm and up to a length of 2.50m. To test the reliability of the MAG03 sensor in this application, the experiments were repeated with a small, self-made air coil. The results confirm the high quality performance of the calibration coil. (For more details see [4,5]).
As mentioned above, the search coil sensor is an active system containing a ferromagnetic flux amplifier. This left open the possibility of interaction between search coil and calibration coil. However, tests with SCM METRONIX sensor [6] in situ gave identical results to those reported above; therefore any such interaction is so small as not to affect the calibration.
These results demonstrate that the new calibration coil satisfies the requirements for calibrations with respect to the homogeneity, and the frequency range up to 100 kHz.

6. The calibration facility

To perform the calibrations, the SR785 spectrum analyser is used. This has an internal signal source and two signal inputs, and allows measurements up to 100 kHz. The measurement arrangement is shown in Fig 4. The final output is a complete picture/ data set of the FRF, both the frequency dependence of amplitude and phase:

$$FRF = \frac{< FFT2^* > \cdot < FFT2 >}{< FFT1^* > \cdot < FFT1 >},$$

where FFT denotes the Fast Fourier Transformation. The asterisk indicates the complex conjugate value, and the number refers to the input number. The internal signal source of the SR785 is used. Alternating current is connected through the shunt (1 Ohm) to the calibration coil. The analyser allows the control of the AC level at input 1 by controlling the amplitude of the internal signal source. The calibration coil current is therefore constant even for temperature changes of the calibration coil. This option is very useful, allowing easy determination of the amplitude of the FRF in absolute units.
The result is graphically represented (phase and amplitude in dependence of the frequency) on the screen of the analyser after completion of the measurement. It is further possible to make a hardcopy, and the data can be saved on a diskette for further processing.
The frequency, amplitude, and the number of the test points can easily be selected, allowing general users to carry out the calibrations after receiving elementary instructions.

7. Results of calibrating measurements

As part of the testing, all search coil magnetometers in the GFZ geophysical equipment pool were checked. Examples of calibrating measurements of METRONIX coils from the GFZ equipment pool are shown as Fig. 5. These sensors can operate in both a low-frequency (LF) mode and a high-frequency (HF) mode. Correspondingly, two calibrating measurements must be carried out per device, in the LF mode of 0.1 Hz to 500 Hz and in the HF mode of 1Hz to 10kHz. While the LF measurement lasts for about 2 hours, the HF measurement takes only 30 minutes. The Frequency Response Function of the magnetometer No.46 is an example of a fully operational sensor. The peaks at f = 50 Hz and f = 16.66 Hz are not a malfunction of magnetometers, but are superimposed interference levels that are caused by the mains power supply and the electrified railway. The magnetometer No.35 in the LF mode and the magnetometer No.45 in the HF mode both show significant deviations from the required FRF. It is highly unlikely that such a problem would be recognised during a field survey, leading to the collection of useless or even worse misleading results. This confirms both the necessity of calibrations and the functionality of our system.

Acknowledgements

I thank V. Haak, R. Holme and O. Ritter, of the GeoForschungsZentrum Potsdam, section Deep Electromagnetic Sounding, for the motivation to built this facility, and H. Lühr for suggestions in designing the coil and for useful discussions.

References

[1] Kaufman, A.A. and Keller, G.V. — Magnetotelluric Sounding Method, Elsevier Scientific Puplishing Company 1981

[2] Vozoff, K., ed. M. N. Nabighian — The magnetotelluric method, Electromagnetic Methods in Applied Geophysics, Vol 3, p641-711, 1991

[3] Croizier, Stuart, Forbes, Lawrence K., Doddrell, David M. — A novel, open access elliptical cross-section magnet for paediatric MRI, Meas. Sci. Technol. 9 (1998), p. 113-119

[4] Pulz, Eberhard, Ritter, Oliver — Entwicklung einer Kalibriereinrichtung für Induktionsspulenmagnetometer am GeoForschungs-Zentrum Potsdam, Scientific Technical Report STR01/10, Potsdam 2001, http://www.gfz-potsdam.de/bib/pub/str0110/0110.htm

[5] METRONIX-Handboock, Broadbank Induction coil magnetometer MFS05

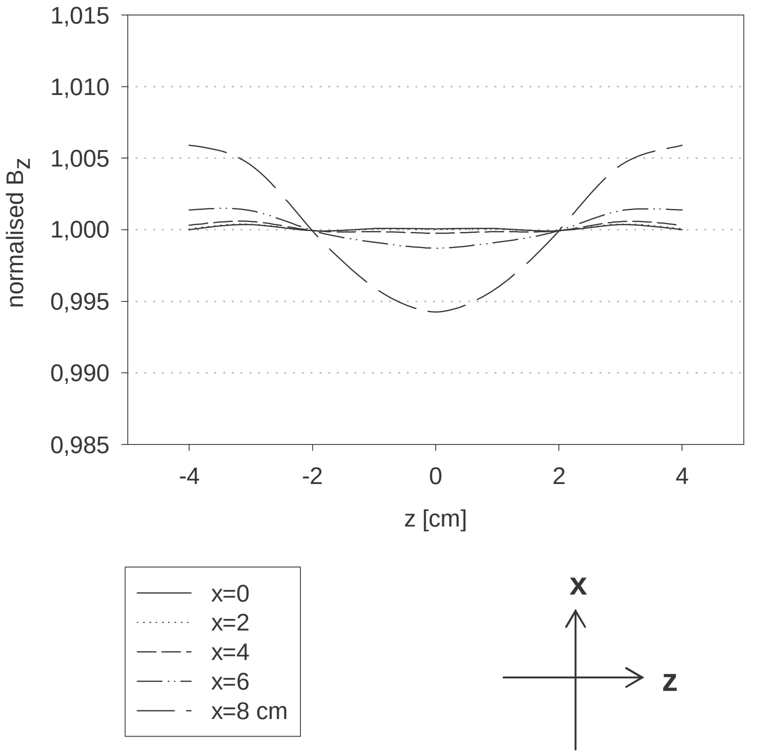

Fig. 1 Calculated magnetic flux density, z= component distance between windings 8 cm, ∅= 30 cm

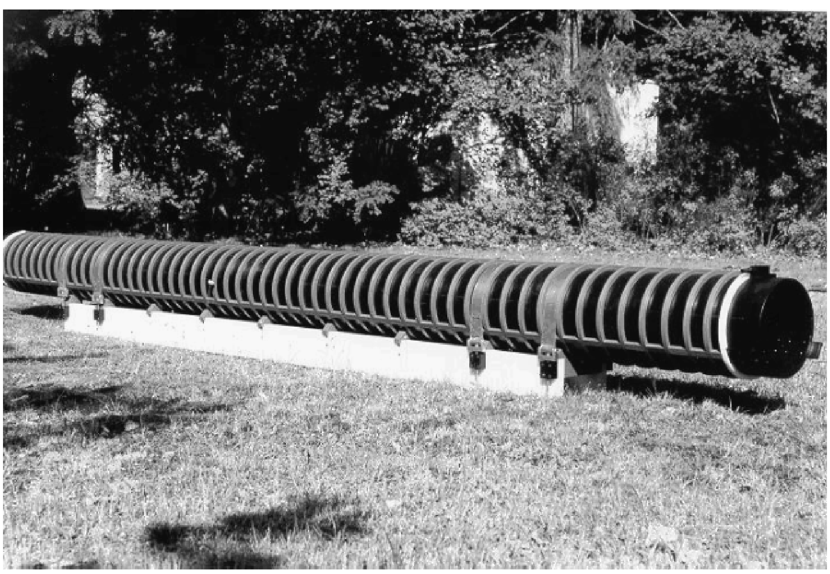

Fig. 2 Calibration coil before installation

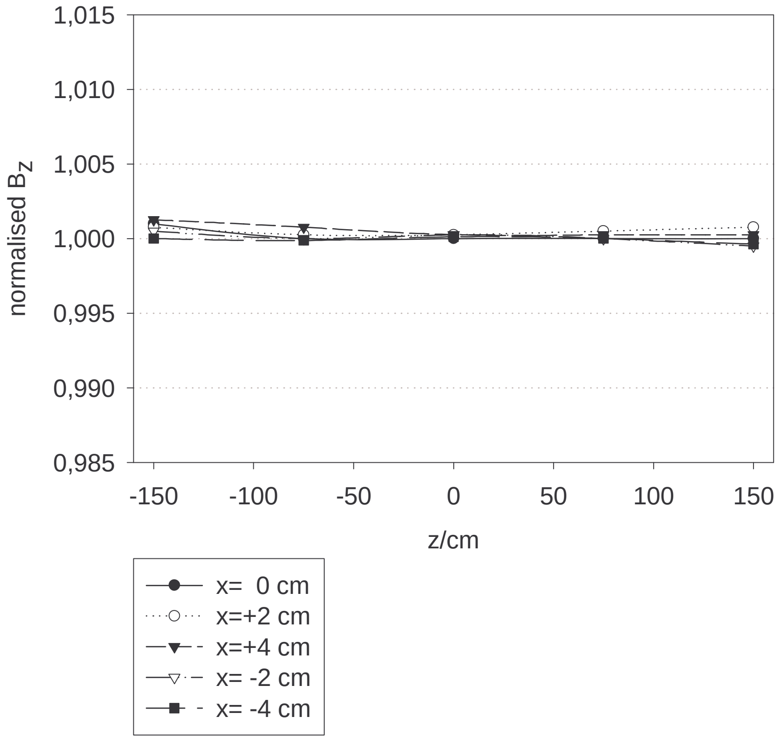

Fig. 3 Measured (MAG03) z- component

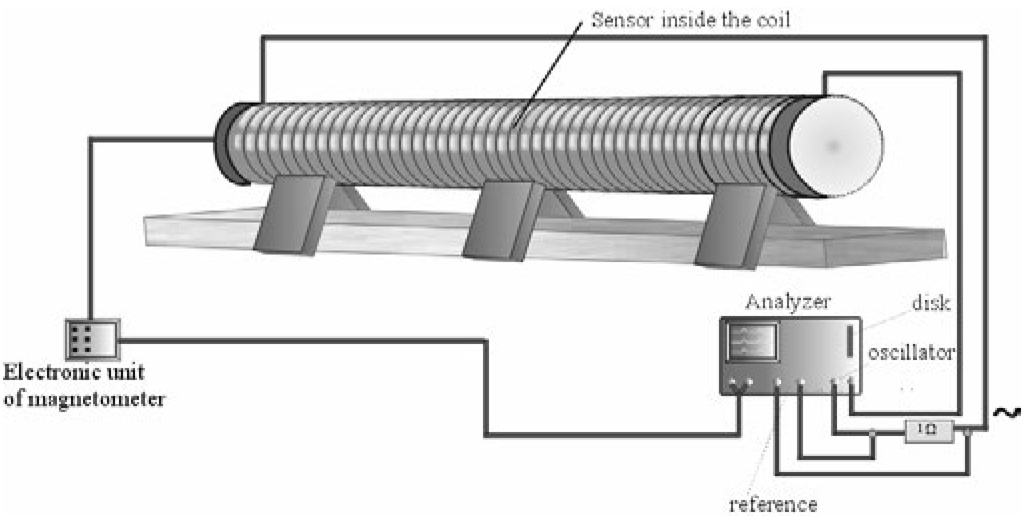

Fig. 4 Block diagram of the calibration facility

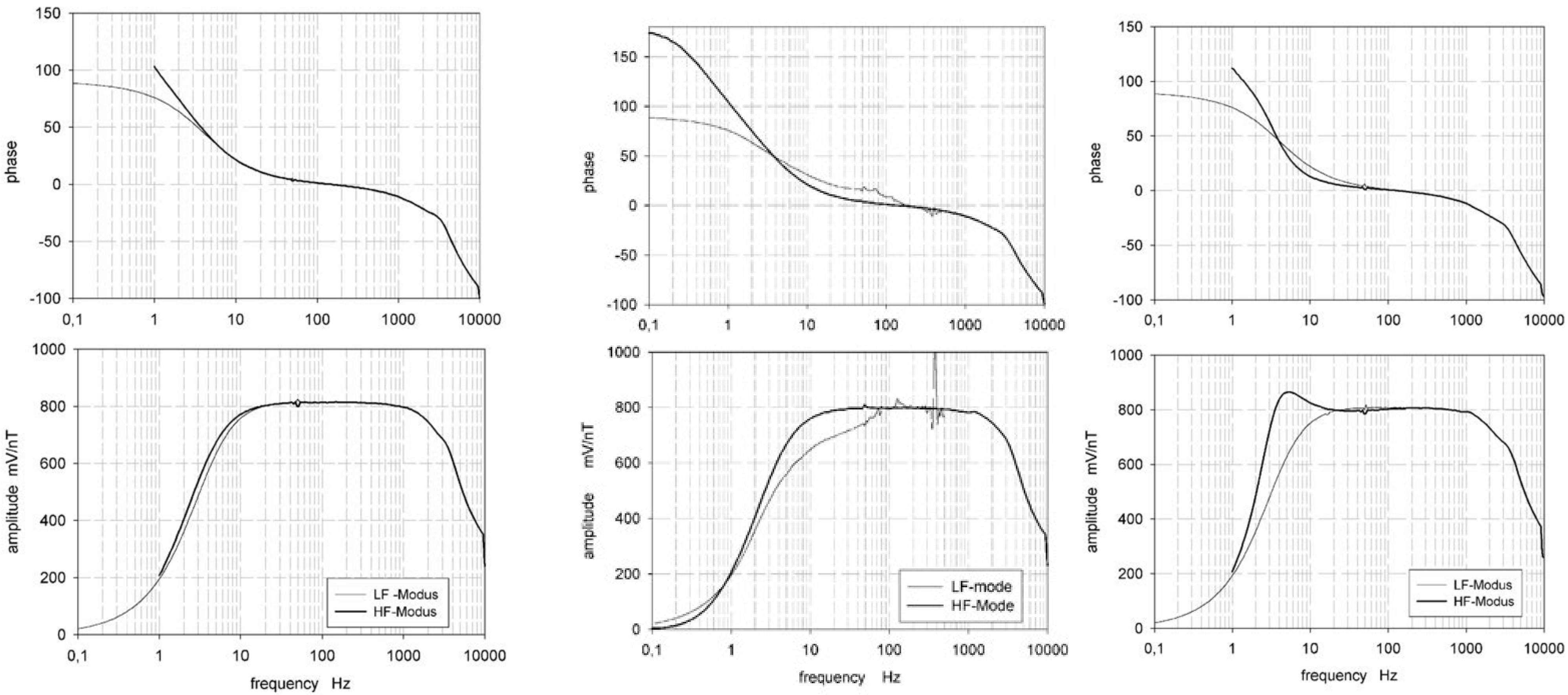

Fig. 5 Frequency response function of coil No. 46, 35, and 45

Additional Measurement Algorithms in the Overhauser Magnetometer POS-1

O.V. Denisova, A.Y. Denisov, V.A. Sapunov
(QM Laboratory of Ural State Technical University, Mira 19, Ekaterinburg, 620002, Russia)
J.L. Rasson
(Royal Meteorological Institute, B-5670, Dourbes, Belgium)

Introduction

The Quantum Magnetometry Laboratory produces the processor Overhauser magnetometer POS-1 since 1998. The magnetometer is a precision instrument for measurements of the geomagnetic field modulus with sensitivity up to 0.01 nT at an operational cycle of 3 s. Besides the field measurement the POS-1 has additional possibilities for continuous monitoring of the factors affecting its functioning. A statistical analysis of digitized periods of the nuclear precession signal in a single measurement gives with good accuracy the signal to noise ratio, the level and character of noise and the dynamics of period (frequency) changes. In particular, the knowledge of these parameters allows one to estimate the device sensitivity and the field behavior during a measurement, in fact to carry out the additional control for both the magnetometer and the ambient magnetic conditions.

Quality of Measurement Conditions

In modern weak field nuclear-precession magnetometers, algorithms are used which transform the signal precession frequency ω to the field modulus B (frequency-field conversion) by processing time-series of signal's zero crossing moments. In general, a measured period is a function of zero crossing time moments t_i:

$$T = F_N(t_0, t_1, \ldots t_N),$$

where N is the number of recorded zero crossings over measurement. In presence of noise, t_i differs from the proper value t_i^0. The standard deviation (SD) of the field calculated value for an undamped signal and uncorrelated Gaussian noise is:

$$\sigma_B = B\frac{\sigma_t}{T}\sqrt{\sum_{i=0}^{N}\left[\frac{\partial F_N}{\partial t_i}\right]^2},$$

where σ_t is the SD of the zero crossing time moments t_i. The SD σ_B is an unbiased parameter of measurement quality under similar conditions. The distribution law of the calculated field value is assumed normal. In this case, the above formula allows one to estimate the confidence interval under the given reliability index (confidence probability), i.e. to assess the data reliability.

The presented algorithm for the measurement random error estimation at a confidence probability 0.68 (in fact SD) is realized in the POS-1. This function is called the Quality of Measurement Conditions (QMC). At normal conditions and cycle of 3 s the POS-1 stores at least a thousand of crossings. This fact allows us to reliably estimate σ_t and thus to predict the SD σ_B for a series of the measurements carried out at similar conditions and at constant geomagnetic field. The QMC is determined by the POS-1 at every field measurement and is transmitted by the RS232-port with the field value. This parameter is intended for the continuous control of sensitivity, which depends on the internal device noise and external cultural disturbances. The QMC was experimentally tested using POS-1 magnetometer and POS-2 gradiometer.

A number of experiments were carried out at the natural magnetic field (Arty observatory), at RMI magnetic field standard (Dourbes observatory) and at the QMLab by the etalon signal transmission from the generator to the sensor head by means of a current loop. The results of the experiments showed that for the normal noise the QMC parameter was in a good qualitative agreement with the real magnetometer sensitivity, unambiguously reflecting the noise situation changes. Quantitative disagreement was up to 100% (the QMC predicted the best sensitivity). This can probably be explained by not having included the noise correlation in the QMC formula. However, such disagreement is acceptable for parameters of this kind.

At the Arty observatory the QMC and experimentally obtained SD were compared while the magnetic field variations were excluded by means of the POS-2 gradiometer. Fig. 1 shows an example of recorded geomagnetic field variations and field difference for sensors spaced 1.8 m apart. The SD over the presented time amounts to 0.013 nT and the QMC averages to 0.009 nT (the disagreement is 44%). Other data showed the same agreement. Similar results were obtained at the QMLab testing equipment by provoking variations of generator etalon frequency and signal amplitude corresponding to real signal/noise values and Gaussian noise (for example fig. 3a). However, when the signal/noise was approximately 5 and less, the QMC and SD showed an abrupt disagreement probably because of a abnormality of zero crossing times t_i. Also essential disagreements were observed for non-Gaussian external noise (especially impulse noise) at all signal/noise values. This is explained by the nature of the QMC, which is calculated for a normal noise only. The striking example is POS-1 testing in the Dourbes standard at 3 values of stabilized magnetic field (20 μT, 50 μT and 78 μT). The measurements were made by the manual freezing method: the field was stabilized and then frozen during the polarization and frequency measurement to prevent malfunction of the field stabilizer, which was perturbed by the POS-1 polarization magnetic field. According to testing results at 20 μT SD = 0.099 and average QMC = 0.022, at 50μT SD = 0,075 and average QMC = 0.020, at 78μT SD = 0.069 and average QMC = 0.040. It is the impulse noise disturbance that causes such essential disagreement.

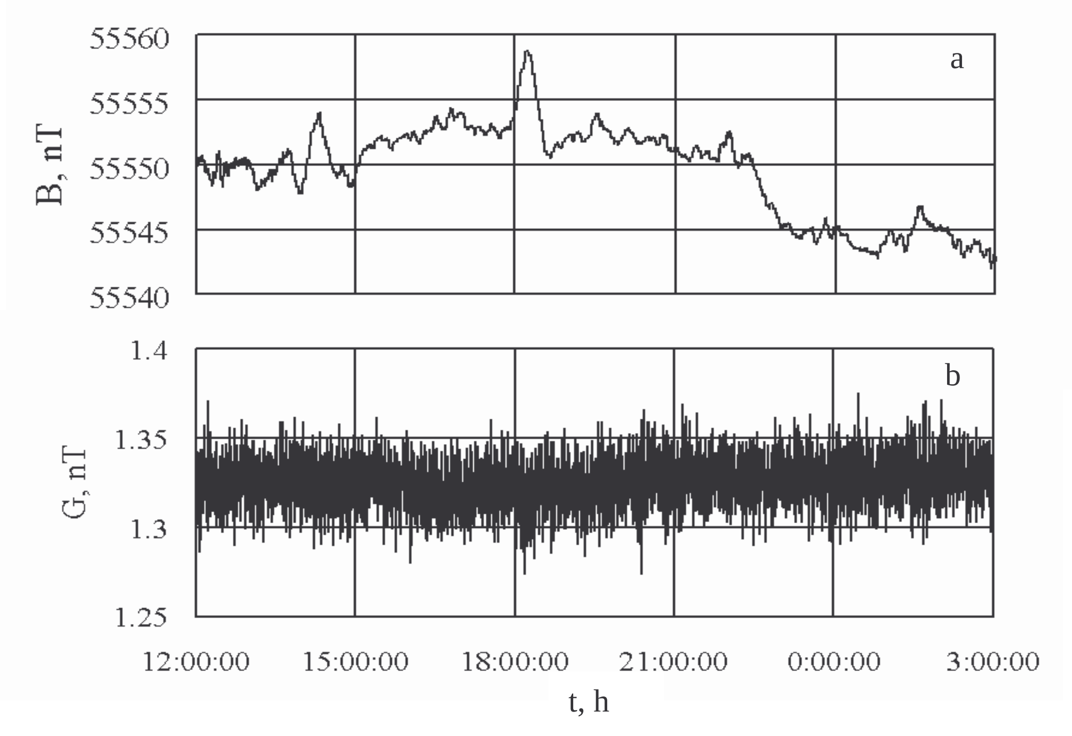

Fig.1. Natural geomagnetic field B (a) and field difference G (b) for sensors spaced 1.8 m. Arty observatory. One POS sensor: SD = 0.013 nT, QMC = 0.009

As a result of the QMC function discussion it must be noted:

1. In spite of some quantitative disagreement the QMC function reflects adequately the real measurement conditions at normal noise. This parameter allows one to control the quality and data authenticity, to estimate the ambient noise situation and to pre-tune the device. All standard magnetometers of POS family are supplied with this useful QMC function.
2. To increase the QMC function accuracy the development of another algorithm is necessary, in particular one, which takes into account the noise correlation.

Time Derivative Mode

The second feature to be tested is the additional function Time Derivative Mode (TDM), which is in a development stage. This function is intended for measurements of magnetic field variations. Besides the field measurement, the magnetometer has a processing algorithm for extracting the time derivative of field modulus (dB/dt) in a single measurement. The idea of TDM consists in using the zero crossing times array accumulated during measurement time for the calculation of field variations. This is realized by the calculation of two functions for average period determination by N_1 crossings with delay n ($n + N_1 = N$):

$$D \equiv \frac{\Delta B}{\Delta t} \cong \frac{B}{n}\left(F_{N_1}(t_0,t_1,...t_{N_1})^{-1} - F_{N_1}(t_n,t_{n+1},...t_{n+N_1})^{-1}\right).$$

The N_1 and n parameters are chosen such that the algorithm error is minimized. The theoretical estimations show that for a standard POS-1 sensor at a measurement time of 1.5 s (total cycle time is 3 s), the sensitivity (SD) for TDM is up to 0.05 – 0.1 nT/s.

For the algorithm evaluation the standard POS was equipped with the additional TDM function. The tests were carried out in the natural geomagnetic field of Dourbes observatory with an added sawtooth artificial field variation supplied by a coil system and by means of a current generator (see for example fig. 2-5). The results showed a good agreement of the TDM experimental sensitivity and theoretical prediction.

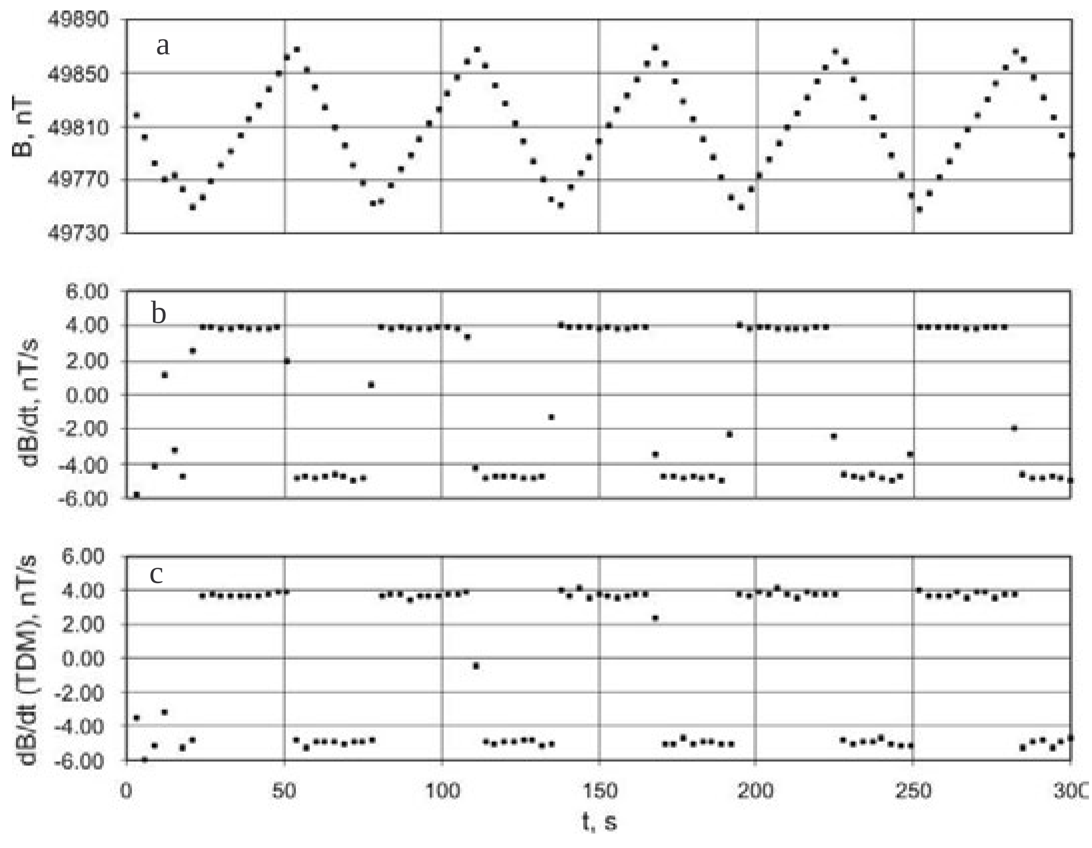

Fig.2. Natural geomagnetic field with added sawtooth artificial variation by the coil system. Dourbes observatory. Measured field modulus B (a). Derivative dB/dt determined by two sequential measurements (b). Derivative dB/dt calculated by TDM (c).

It is to be noted that for the long-time variation observation the TDM is at a disadvantage

n relation to the method using two sequential measurements (fig. 2-5, c and b). Theoretically, for equal cycle times, the TDM sensitivity is approximately smaller by a factor 11 than the

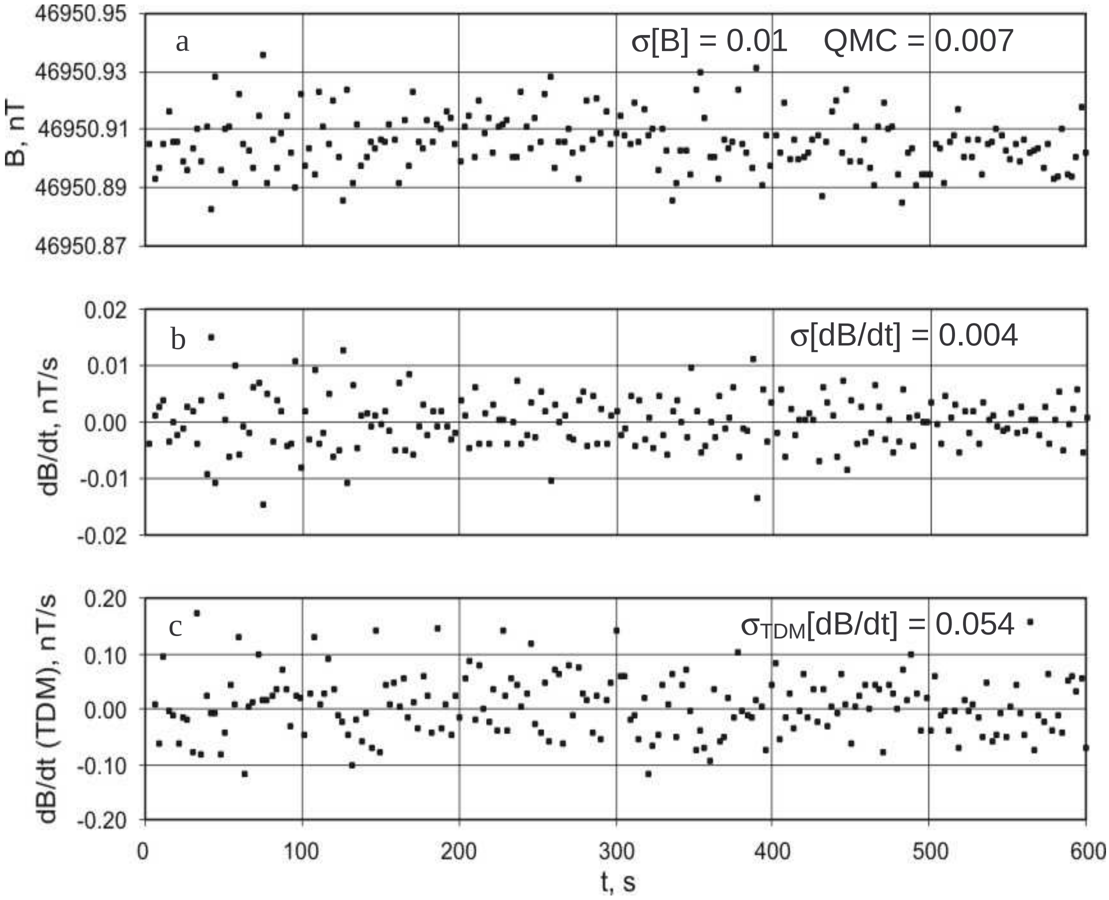

Fig.3. Example of records B and dB/dt at simulation of undamped proton signal by the generator signal. Signal amplitude appropriate to a working signal of the POS-1. Measured field modulus B (a). Derivative dB/dt determined by two sequential measurements (b). Derivative dB/dt calculated by TDM (c).

two-point method. If the cycle time for TDM is approximately 2.6 times as large as the cycle for the two-point method, the algorithm sensitivities are close. In fact, to achieve the sensitivity of the two-point method, a special sensor head with a relaxation time of the working substance 2.6 times as large as for the standard POS-1 head is necessary.

However, when assessing the TDM versus the two-point method, we must take into account that the latter may be strongly affected by aliasing errors, when one tries to compute the derivative for two measurements widely separated in time, whereas TDM will correctly estimate the two derivatives. The advantages of the TDM are the simultaneous determination of the derivative with the magnetic field measurement and correct response of the TDM function to rapid variations with periods of the order of the measurement time. The estimation showed that for the equal time interval Δt (on which derivative $\Delta B/\Delta t$ is calculated) for the both methods, the TDM function has an advantage factor of 1.4.

In conclusion it is possible to sum up the TDM analysis:

1. The TDM function showed results in agreement with the theoretical predictions. However the sensitivity of the TDM achieved by the standard POS-1 sensor is not enough for useful observation of standard variations of the geomagnetic field. The planned sensitivity can be achieved by employing of special sensor head with long relaxation time of proton signal.

2. The TDM function accuracy improvement is possible not only by way of sensor specialization, but also at the expense of algorithm improvement.
3. The TDM is at an advantage in comparison with the standard methods when measuring rapid variations (up to 40 %).
4. The TDM function can be used as an additional control parameter of external magnetic conditions for autonomous observatories with low cycle rates and for geological explorations.

5. The development of the TDM and the use of other estimations of the real magnetic situation are a major contribution to the creation of smart high-precision magnetic equipment

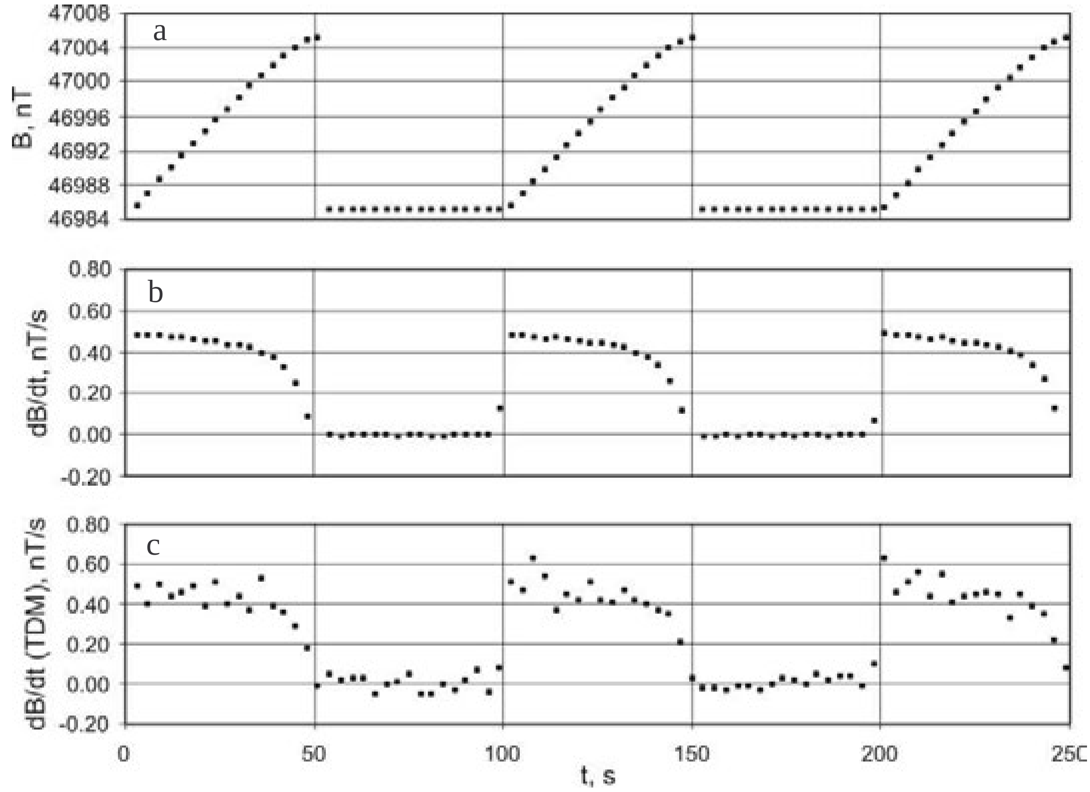

Fig.4. Simulation of field variation 0.5 nT/s by the generator signal, at which field was modulated by a sawtooth law. Measured field modulus B (a). Derivative dB/dt determined by two sequential measurements (b). Derivative dB/dt calculated by TDM (c).

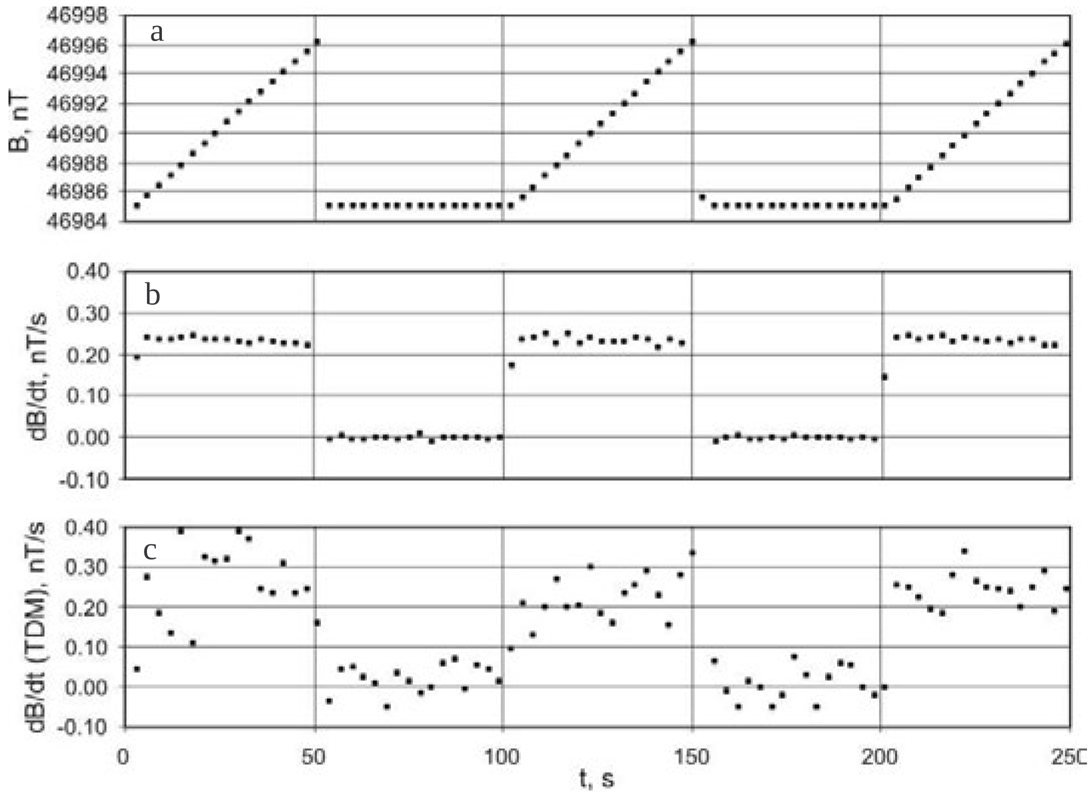

Fig.5. Simulation of field variation 0.25 nT/s by the generator signal, at which field was modulated by a sawtooth law. Measured field modulus B (a). Derivative dB/dt determined by two sequential measurements (b). Derivative dB/dt calculated by TDM (c).

Development of Testing Methods for Absolute Magnetometers and Some Test Results of the Overhauser Magnetometer POS-1

Jean L. Rasson (Royal Meteorology Institute, B-5670, Dourbes, Belgium),
Vladimir A. Sapunov (QM Lab. of USTU, Mira str., 19, Ekaterinburg, 620002, Russia)

Proton magnetometers are well known as precise instruments for the measurement of total magnetic field. Such position is based on the proton gyromagnetic ratio, a fundamental physical constant. In this report we discuss some general metrological aspects of the proton and Overhauser magnetometers which can be used for development and exploitation. This discussion is stimulated by researches of the new Overhauser magnetometer POS-1 that is intended for magnetic observatories and fieldwork.

The photos show two designs of the POS-1 namely a variant with a flexible cable and a hard-staff design. An example of the recording of geomagnetic variations in polar latitudes (Yakutia) is also shown.

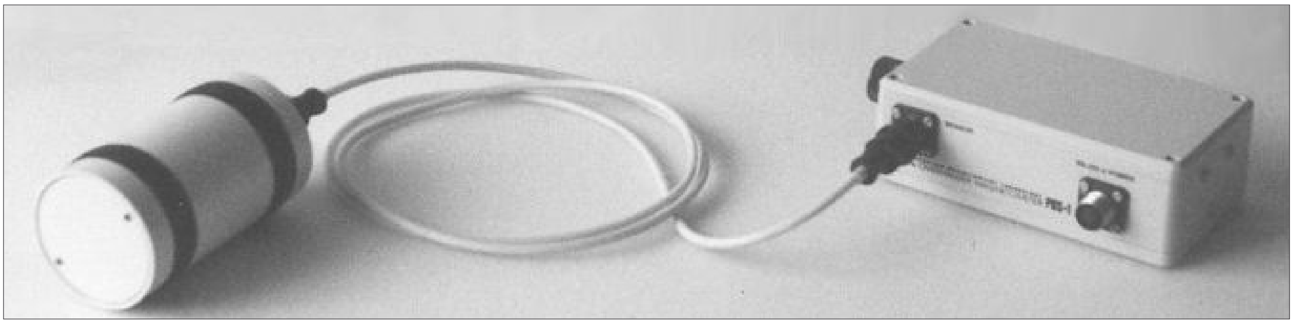

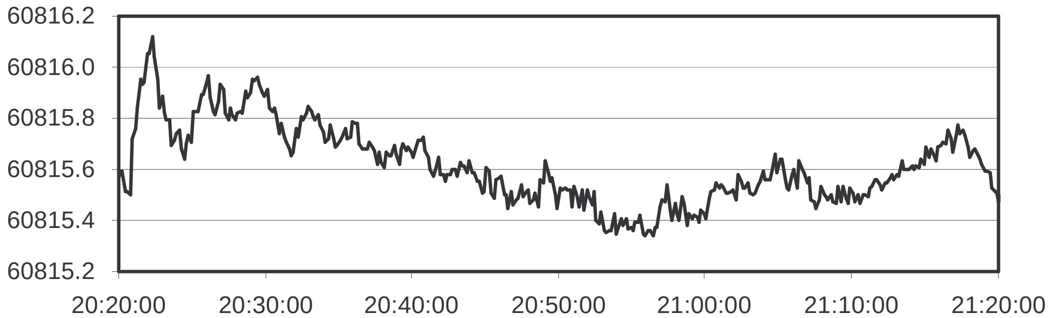

The manufacturer of the POS-1 magnetometer declares a high measurement sensitivity (up to 0.01nT at 3 s cycling rate or 0.1nT at 1 s) and an absolute accuracy of up to ±0.5nT. To check these parameters, tests in the RMI magnetic field standard were carried out. For low fields around 27 µT we have a noise level lower than 0.05nT, while for fields around 60µT the noise level is below 0.01nT.

On the other hand, we found a deficiency in the magnetic cleanliness checking methods at the manufacturer materials processing stage, which resulted in absolute and heading errors. Three cylindrical Overhauser sensors were tested. The orientation dependence of measurements for the sensor head rotation around the cylinder axis was measured. One sensor has an orientation dependence of ±0.5nT. Two faulty sensors have shown dependence of about ±3nT. Addressing this last problem, we made comparisons of several methods for magnetic impurity testing. A flux-gate magnetometer was found to be the most successful at the stage of sensor element control and preliminary check. The photo shows the RMI magnetic field standard and testing of a harmful field by the flux-gate magnetometer FLM1/B (0,1nT sensitivity).

The flux-gate magnetometer is set-up with the sensitive axis perpendicular to the geomagnetic field and inside the vertical plane (magnetic meridian plane). The flux-gate output is then essentially zero except for the variations due the magnetic inclination time changes. The Overhauser sensor under test (SUT) is approached with the sensor axis horizontal and perpendicular to the magnetic meridian till the cylinder surface is at 1 cm from the flux-gate extremity. Then the SUT is rotated around its axis and the readings of the flux-gate observed. We look for a sinusoidal signal in function of the rotation angle. The peak-to-

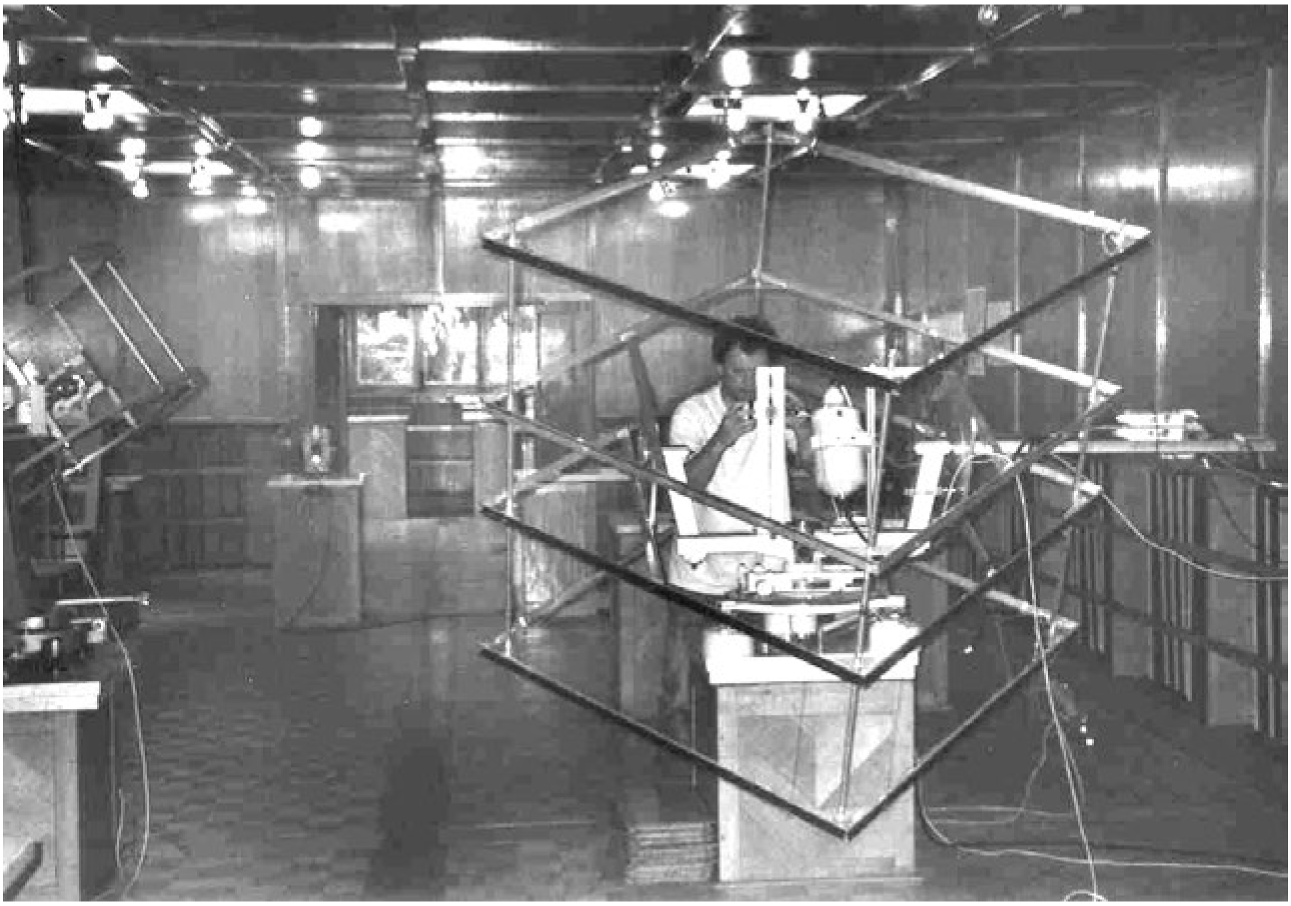

peak (p-p) sinus amplitude reading in nT gives the magnetic signal perturbing the cleanliness. For the POS-1#24
the p-p sinus amplitude was 3.0nT. For the POS-1#23 the p-p sinus amplitude was 3.3nT. As the + and - peaks are identified we put marks on the cylindrical surface of the sensor head. Actually it turns out that the peaks are separated by almost 180 degrees, showing dipolar behaviour. The strongest p-p amplitude is at the centre of the sensor.

The second stage of the general check of the POS-1 performs a comparison with a reference device and allows absolute error measurement. Comparisons were performed at 30, 50 and 70 µT. The SUT was each time measured in two positions: once with the perturbing dipole parallel (3 readings) and once anti-parallel (3 readings) to the stabilizer magnetic field vector. A self-oscillating optically pumped potassium vapour (39K) magnetometer stabilizes and controls the current in the coil system (Rasson 1996). The sensor position is adjusted at a previously determined gradient-free spot (H=760mm V=128mm) with the connector towards West. The free field value at the time of the experiment was 48144nT.

Stab. set-point	30000nT	50000nT	70000nT
SUT: POS-1#23 Parallel	30002.5 30002.5 30002.4	50001.7 50001.6 50001.7	70000.2 70000.2 70000.2
Antiparallel	29998.4 29998.2 29998.6	49997.7 49997.4 49997.6	69996.1 69996.3 69996.0
Mean (par-antipar)	4.1	4.1	4.1

Similar results were obtained for the POS-1#24 where the value of mean (par-antipar) was: 4.8, 5.3 and 4.8 nT. Thus the faulty POS-1 magnetometers have an orientation error around the sensor axis of 4.1 nT for POS1-#23 and 4.8 nT for POS-1#24, confirming the magnitude of the earlier measurement with the flux-gate (take into account the different distances).

The defective sensors were disassembled and it was established that a magnetic impurity in the cast plastic holder of the Faraday screen caused the pollution. It is indicative that a magnetic beam balance used by the manufacturer for the impurity control did not find out those significant effects notwithstanding the balance's capability to find out the diamagnetism of liquids. Obviously the volumetric distribution of impurity played an essential role here. The replacement of the impure holders resulted in errors below ± 0.5nT.

Similar researches and results were obtained in the laboratory magnetic field standard (four-layer magnetic screen and slender solenoid). The photo shows QMLab magnetic standard with the geological survey POS-1 under testing.

Unfortunately, the QM laboratory employees did not find the defects described above at the

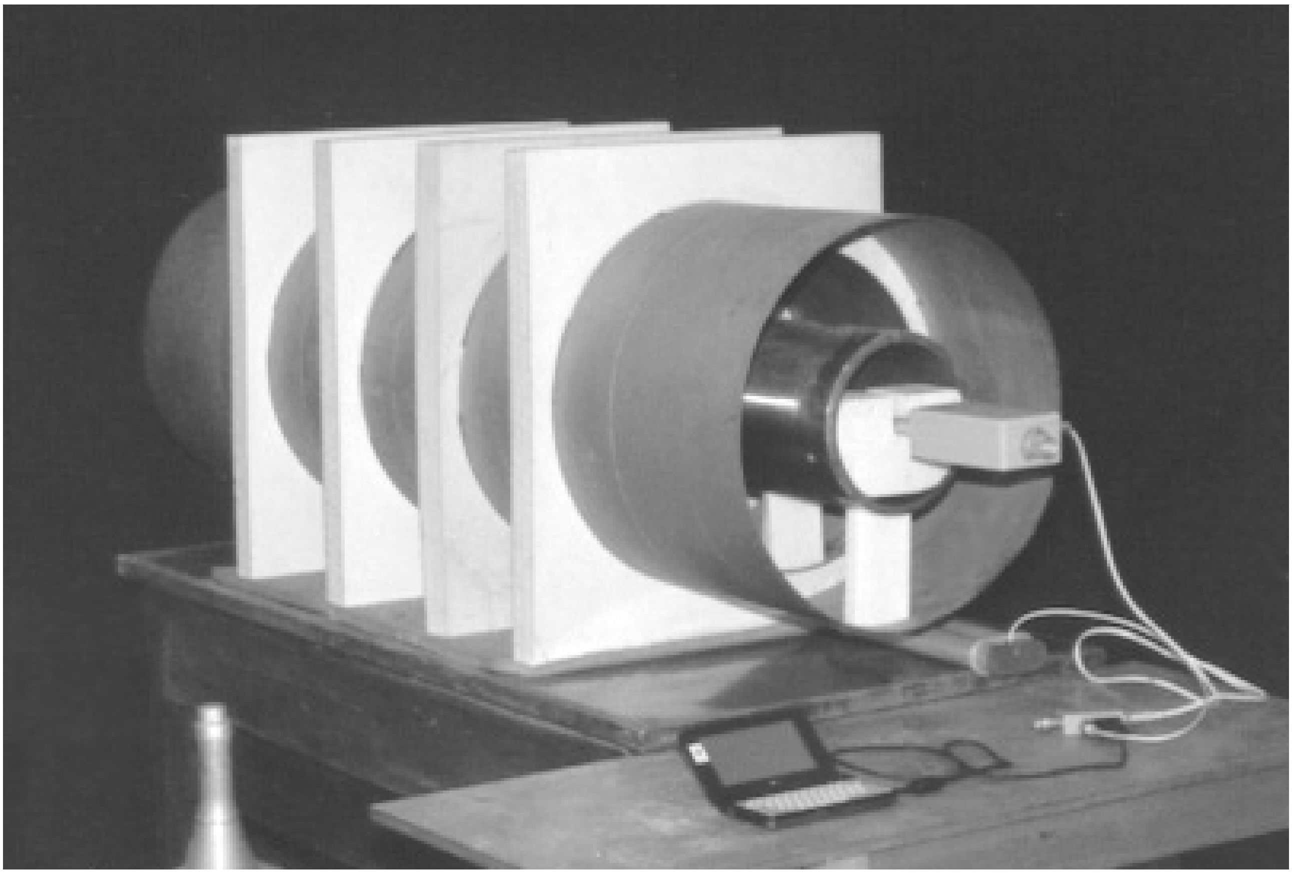

stage of manufacture. On the one hand it is caused by changes brought in the sensor design under observatory requirement and on the other hand by defect of laboratory technique. We observed additional deviations at the manufacture stage but it was explained by the influence of the polarization field on the screen magnetic shell and not by the magnetic impurity presence.

Due to joint efforts the technique of magnetic cleanliness test progressed. In particular the RMI transferred a flux-gate magnetometer FLM1/B to QM laboratory. This has permitted to carry out a number of interesting experiments described below. It is established that the magnetic field uniformity of the magnetic screen does not allow to supervise orientation errors better than ±0.5nT. From this point of view it is necessary to carry out metrological researches under systems similar to the RMI magnetic standard (coil system with active stabilisation).

In the second stage of research we investigated the reason causing residual orientation error. The value of the error was inexplicable as the magnetic cleanliness of the sensor head by methods described above was established. An hypothesis about a thermal origin of this error was put forward earlier. Within the framework of the submitted results the convincing proofs were found.

The main element of the Overhauser sensor of POS-1 magnetometer is the high-frequency resonator inside which there is a vacuum-processed glass ampoule with working substance. The high-frequency resonator is made as two copper coaxial pipes whose ends are connected by the crosspiece and capacitors. The general view is shown in the figure below. The ampoule has small size (diameter of 30, length about 70 mm). When a continuous high-frequency power of about 1 Watt is applied, that causes a temperature increase of about ten degrees. The basic heat-generating elements are the discrete capacitors that cause a temperature gradient as shown approximately in the figure.

Due to couples which are formed in the connecting-points of the capacitors with the outside shell, thermocurrents are generated due to the heating by the high-frequency power. The manufacturer of ampoules knows about this property and consequently declares some

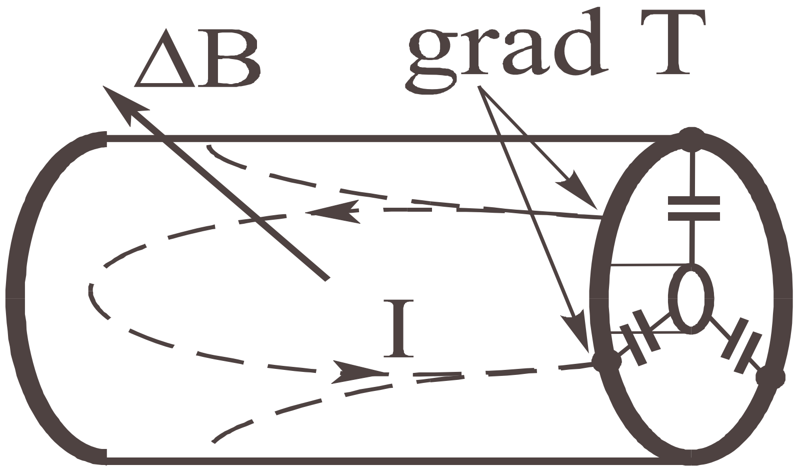

orientation error. This problem is caused partially by a small irregularity in the capacitor positions that does not allow to cancel completely out the thermogenerated magnetic fields. Some ways were used to research this effect. In particular, we have applied the flux-gate magnetometer to register the perturbing magnetic fields. The experiment was carried out in the above-mentioned magnetic screen at a magnetic field of about 0-10 nT. The flux-gate sensor was set-up parallel to the ampoule at a distance of 5 mm. The difference of measurements was registered when the high-frequency power was switched on and off. The figure shows the result of measurements (nT) at angular rotation of the batch production Overhauser ampoule.

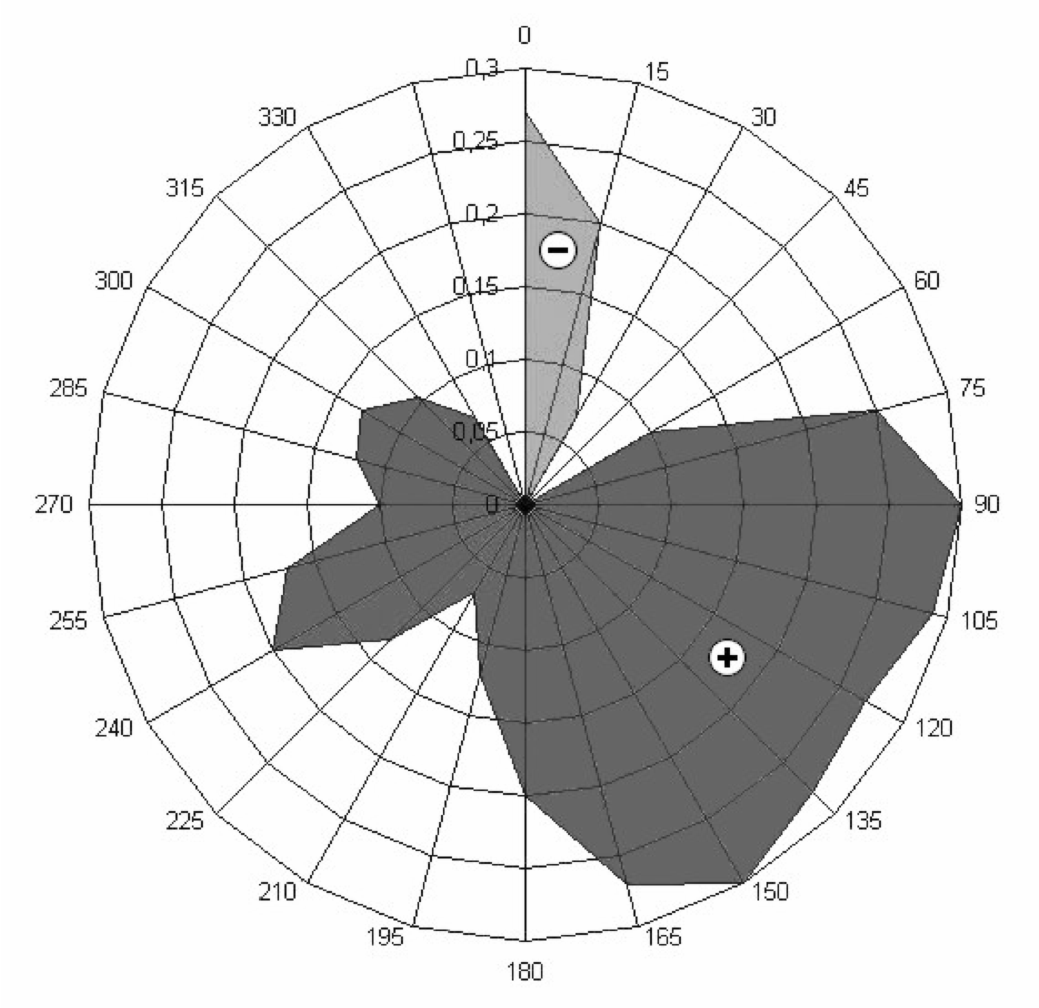

Thus the ordinary POS-1 magnetometers have an orientation error around the sensor axis confirming the magnitude of this result. Similar experiments were made with a new ampoule design, which has shown magnitude up to 0.1nT. However, the new ampoule is more difficult to manufacture.

The second experiment was aimed at the research of the integrated effect and revelation of the absolute errors caused only by the thermal effect. The laboratory field standard and usual POS-1 magnetometer was involved. To increase the heating effect, an Overhauser ampoule was powered from an external rather powerful HF-generator (up to 3 W). The time behaviour of the total field measurement from the beginning of the cyclic measurements was registered. The HF-generator worked continuously. The maximal magnitude for the usual ampoule was in a range from 0.2nT up to 2nT at the various sensor orientations in relation to the standard stable field of 20000nT. The time decay of this process was about 40 seconds. It is interesting to note that the curve has a small maximum caused by reduction of the temperature gradient after transient (we apologise for the absence of a figure for technical reasons). The new design of the Overhauser ampoule has shown a general change of no more than 0,5nT at a power of 3 W and 0.2nT at the standard power used in the POS-1.

Thus, the effect of thermal current generation in the conducting shell of the Overhauser sensor HF-resonator results in absolute errors and must be taken into account to meet of highest absolute accuracy. For the POS-1 magnetometer we offer to carry out a calibration of orientation dependence for example by the RMI reference equipment with marks of minimal absolute error directions.

In summary it is necessary to note that the considered themes are applicable to all types of absolute magnetometers and that this research is of interest to others in the field. Dedicated magnetic field standards and careful investigations of all measurement conditions of Overhauser magnetometers are necessary in order to reach absolute accuracies of the order of 0.1nT.

Rasson J.L. (1996). Coil system for the magnetic full field stabiliser, in Proceedings of the VIth Workshop on Geomagnetic Observatory Instruments, Data Acquisition and Processing (JL Rasson Ed.), Publ. Sci. et Techn. No 003, Institut Royal Meteorologique de Belgique, Brussels p87-93.

An Episode in the History of Geophysics Against the Background of World Events

D Voppel. and G Schulz (Buchholz/Nordheide, Germany; Wingst Geomagnetic Observatory, Germany)

Abstract

Three quartz horizontal magnetometers (QHM) ended up among the front lines of World War II but survived undamaged. After the war, they were used for base line and comparison measurements and as repeat station instruments at Wingst Observatory for over 20 years until their replacement by modern equipment like the proton vector magnetometer and fluxgate theodolite. After their origin had become known, the QHMs were returned to their legitimate owners.

Further undetected events may still lie dormant in archives. The present report could mark the beginning of a series of publications that may lead to a reappraisal of the history of geophysics in Germany during World War II, supplementing the so-called ”FIAT” report (Bartels, 1948).

Key words: History of Geomagnetism, instruments, absolute measurements

Introduction

It has generally been found difficult to close existing gaps in wartime history because the events tend to be covered by a veil of secrecy. In many cases, war-related events have become known only by chance. Sometimes small episodes have been the key to historic facts. Such an episode will be reported in this paper.

The authors are past and present observers at Wingst Observatory: D. Voppel from 1954 to 1973, G. Schulz (co-author) thereafter.

The coefficient of humidity

When D. Voppel started his work at Wingst Observatory in February 1954, he was assigned the task of experimentally determining the humidity coefficient of four quartz horizontal magnetometers (QHM) at different temperatures.

QHM’s were very useful, handy, and robust instruments. Their accuracy was very close to 1 nT , which was the measurement limit at that time (Fig 1; Kring Lauridsen, 1977)): The position of a small magnet, which was suspended by a quartz

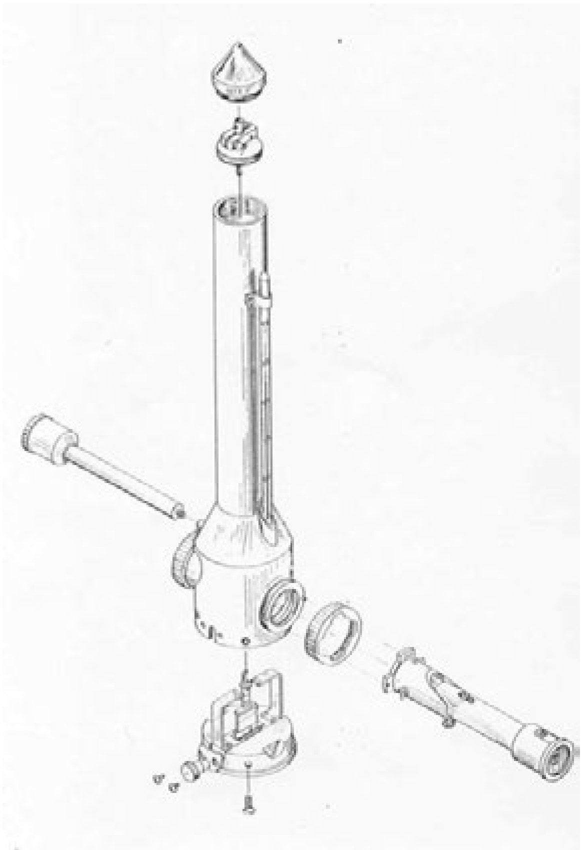

Fig 1 QHM (Kring-Lauridsen, 1977)

fibre within an non-magnetic metal tube of about 15 cm length and 2 cm diameter, was observed through a telescope using a mirror. For that purpose, the tube was mounted on that part of an iron-free theodolite which was rotatable about its vertical axis. With zero torsion, the magnet pointed to magnetic North. After rotating the theodolite about its vertical axis until the magnet could be observed again through the telescope, the fibre had been distorted by exactly 360°. The angle between the distorted and undistorted positions was a measure of the geomagnetic horizontal intensity, provided that the magnetic moment of the magnet and the torsion moment of the fibre were constant. The shape of the torsion fibre, invented by La Cour (1936), was the characteristic feature of the QHM: The fibre was considerably thicker at the clamping points than in the middle section (Fig 1). In this way, torsion occurred mainly in the middle section and was kept away from the clamping points. This contributed substantially to the stability of the fibre and thus to that of the measurement.

Back to the measurement of the humidity coefficient, which had been unknown until then. It could only be determined by comparing the base-line measurements carried out regularly, over many years, with several QHM and the station theodolite applying the method of deflection and oscillation after Lamont. Fig 2 shows the systematic annual

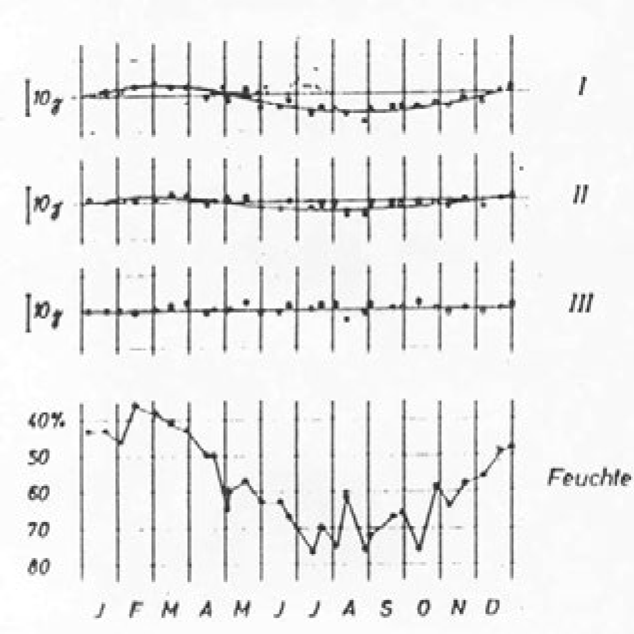

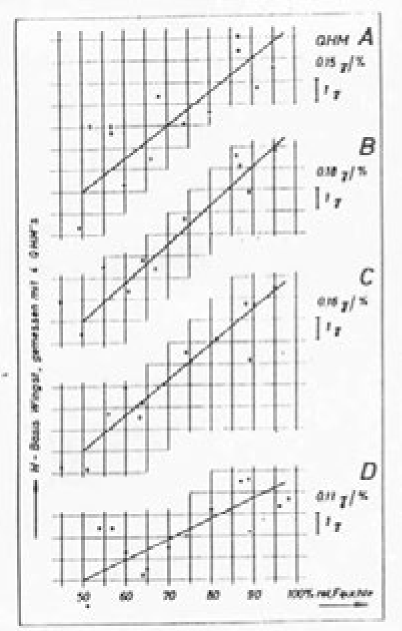

Fig 2 **Fig 3**

(both Meyer and Voppel, 1959)

drift of the mean horizontal intensity of the four QHM against the smoothed base-line of the 1954 measurements using the standard theodolite. Fig 3 shows the experimentally determined humidity coefficient of one of the QHM.

Looted instruments

When a publication was considered, the co-author (and predecessor of D. Voppel) of the planned paper, O. Meyer, surprisingly refused to indicate the series numbers of the QHM as usual but insisted on denoting them A, B, C and D. He stated that the origin of three of the four instruments was unknown, and that they had been looted during World War II. He pointed out that he did not know their origin. Only one of the four instruments, that with the series number 23, was listed in the observatory´s inventory of instruments and had been purchased when the observatory was founded in 1938. The QHM with the numbers 25, 26 and 27 obviously constituted war loot. As they had been in use at Wingst Observatory since June 1940, they could only originate from one of the countries that had been occupied by German forces beforehand.

The discovered humidity sensitivity (Meyer and Voppel, 1959) of the QHM was reported to their manufacturer, the Danish Meteorological Institute. Since then, only quartz fibres not showing any sensitivity to air humidity have been used in the production of QHM series. Also Wingst Observatory purchased three new QHM in the following years. So the old devices became museum pieces.

On 2 October, 1939, after Hel surrended, the invading „Kriegsmarine" troops destroyed the Meteorological-Magnetic Station. The measurement pavilions with recording and measuring instruments were devastated. The eyewitness of the events, captain Dziubiński, chief of 21 battery of 2 MDAPL, and the neighbour of the Station from the other side of the road, recalls: „... After this exchange of words, the Germans turned toward the meteorological station which was empty. When the troops were leaving, one could hear the butts knocking to the closed shutters and then the explosions of hand-grenades thrown into the building..." (Witkowski, 1973).

Fig 4 (Czyscek and Czyscek, 1983)

Note of the authors: The date of the event was probably September 2, 1939, because the attack on Poland started on September 15 and lasted 18 days

In 1983, Zofia and Waclaw Czyszek published a historical paper under the title Geophysical Observatory at Hel, 1932 – 1982 (Czyszek and Czyszek, 1983). They described the course of events at Hel Observatory, which is located on the Hela peninsula north of Gdansk, and particularly mentioned the observatory's destruction by forces of the German navy during the first days of the attack on Poland. Fig 4 shows an excerpt of this publication, which also includes an inventory of the observatory's instruments in 1937 - among them the QHM with the numbers 25, 26 and 27. This clearly proved the instruments' origin. The Polish colleagues at the observatory, who obviously were of the opinion that the QHM had been destroyed by a grenade exploding in the absolute house, were all the more surprised to learn that the instruments still existed.

The return of the instruments

During the past several decades, European observatories have routinely exchanged momentary values during magnetically quiet times (02 UTC) in order to mutually monitor their base-line instruments. Hel (today's international abbreviation: HLP) was one of the participants. Therefore, with a view to continued, mutually beneficial co-operation, it appeared logical to return the instruments to their legitimate owners. In 1988, the head of the Polish observatory HLP was informed about the history of the instruments, which had meanwhile been published, and of our intention to return them to HLP. The return was arranged via so-called short official channels in order to bypass bureaucratic and other obstacles. In 1990, G. Schulz brought state-of-the-art comparison instruments to Niemegk and extended the official journey via Warsaw to HLP, where he handed over the instruments to his Polish colleagues, who were delighted (Fig 5).

Fig 5

So the last piece has finally fallen into place after 50 years. The illegitimate change of ownership - as a result of the war – was at least useful to the scientific community in one respect, namely the discovery and proof of the humidity dependence of the older QHM series by O. Meyer, and the improvement of subsequent series of this instrument type. The latter has been achieved by Kring Lauridsen of the Danish Meteorological Institute (Kring Lauridsen, 1977).

Outlook

The purpose of this paper is to document existing gaps in the history of geophysics and to encourage others to take notice of occurrences during the last World War. Such topics have only been reported summarily in the volume Naturforschung und Medizin in Deutschland 1939 – 1946, the special issue for Germany of the FIAT REVIEW OF GERMAN SCIENCE, Vol.17, Geophysik, Part I, Editor Julius Bartels with the assistance of E.Bederke, W.Dieminger, F.Errulat, A.Graf, H.Israel, K.Jung, H.Reich, Wiesbaden 1948 (Bartels, 1948).

Of course, it covers only the most important scientific results of that time, leaving out other events that may be also have been typical of the development. A thorough appraisal of the war events and final collapse certainly has not been possible after such a relatively short time. Relevant reports may still lie dormant in archives, and their reappraisal may help to increase our knowledge of the history of geophysics.

References

Bartels, J. (Editor), 1948: FIAT Review of German Science, Vol.17, Naturforschung und Medizin in Deutschland, Geophysik, Part 1, 1939-1946, Vol. 17. Wiesbaden

Czyszek,Z. and W.Czyszek, 1983: Geophysical Observatory at Hel 1932-1982. Acta Geophysica Polonia, Vol XXXI, No 4

Kring Lauridsen,E., 1977: The QHM – contributions to the theory and practice of the quartz horizontal magnetometer. DMI, Geophysical Papers,R-50

La Cour, D., 1936: Le quartz-magnetometre QHM. Com.Magn.etc. No 15, Copenhagen

Meyer,O. and D.Voppel, 1959: Der Einfluß der Luftfeuchtigkeit auf erdmagnetische Messungen mit Quarz-Horizontal-Magnetometern. DHI, Ergebnisse der erdmagnetischen Beobachtungen im Observatorium Wingst in den Jahren 1955 und 1956, No 10, 143-148

Examples of Activities of GPI SAS for Practical Use in the Field of Geomagnetism

I. Túnyi, J. Vozár (GPI SAS, Bratislava, Slovak Republic)
P. Dolinský, F. Valach (Geomagnetic Observatory GPI SAS, Hurbanovo, Slovak Republic)

Abstract
In the paper two possibilities of employing standard geomagnetic practice for non-traditional tasks, mapping of artificial magnetic disturbances in cities and seeking for undisturbed areas, are presented.

Introduction

The modern age produces man-made sources of strong artificial magnetic fields. Many geomagnetic observatories moved from their old locations to remote ones because of these man-made disturbances. However, people stayed and they live in the modern industrialized cities. They are affected by strong artificial magnetic fields - "magnetic smog". The most substantial man-made disturbances in the geomagnetic field are due to the DC electric railways and similar transport systems [Jankowski and Sucksdorff, 1996]. The authors of [Hejda and Horáček, 2001] dealt with such magnetic noise at the observatory site not far away from the centre of Prague. They confirmed that the magnetic field is in the first place generated by currents in trolleys or tracks. The disturbances are mostly visible in the vertical component of the geomagnetic field. The aim of this paper is to describe the artificial magnetic disturbances over the territories of cities.

Seeking for areas with the smallest possible artificial magnetic disturbances and also with the minimum natural anomalies is necessary for practical purposes, too. Such areas are utilized for the compensation of compasses, e.g. in aeroplanes.

Magnetic noise over Bratislava and Košice

Figs 1 and 2 show the amplitudes of man-made disturbances in the vertical component of the geomagnetic field over Bratislava and Košice [Túnyi and Vozár, 2001]. Their frequencies are from the range of minutes. The maps were constructed on the basis of the recordings carried out during 1991-1992 in Bratislava (14 observational sites) and 1995-1996 in Košice (15 sites). A Bobrov variometer with an analog (at Bratislava) and digital (at Košice) recording system was used for the registrations. The disturbances disappear between 10:00 p.m. and 04:00 a.m., when electric traffic of the city stops.

Seeking areas with the minimum noise

If one intends to compensate compasses, the anomalies at the chosen area have to be less then the precision of the compass. One has to find such an area where it meets the demands as close as possible.

Firstly, in order to have information whether the place is plausible for practical utilization or not, measurements of total field with a PPM should be made. Simplicity and fastness are the main advantages of this procedure. Fig. 3 shows the map of total field over the area selected for the compensation. (Note the visible contours of the concrete circle - the brighter part near the centre.) Fig 4 shows the total field at the area recommended for the compensation purposes for the compasses of large aeroplanes.

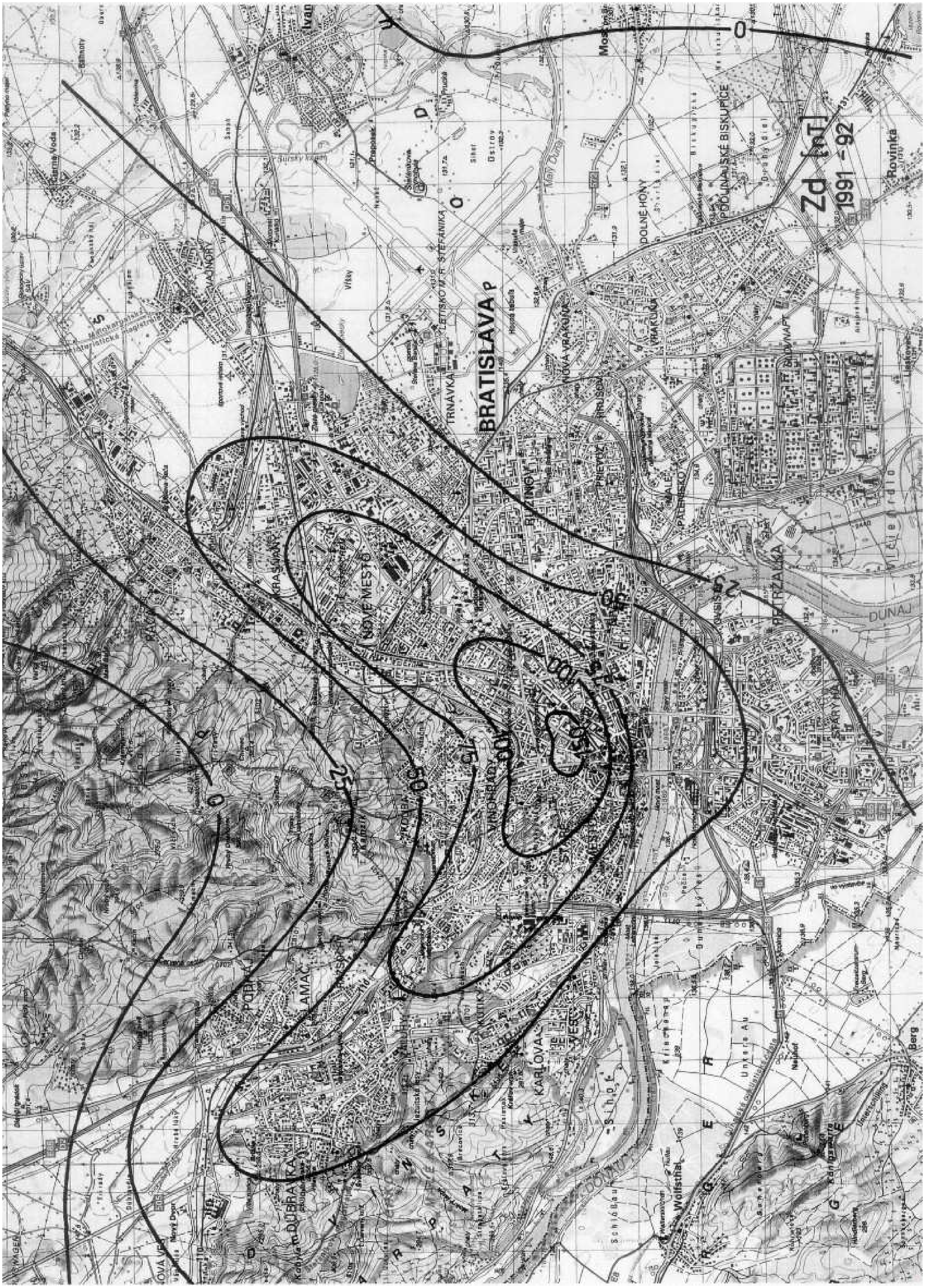

Fig. 1 The amplitude of disturbances *Zd* over the territory of Bratislava derived from the measurements of geomagnetic activity carried out in 1991-1992. *Zd* means the disturbances of Z-component of geomagnetic field which is generated by the city electrical traffic (trams and trolleybuses).

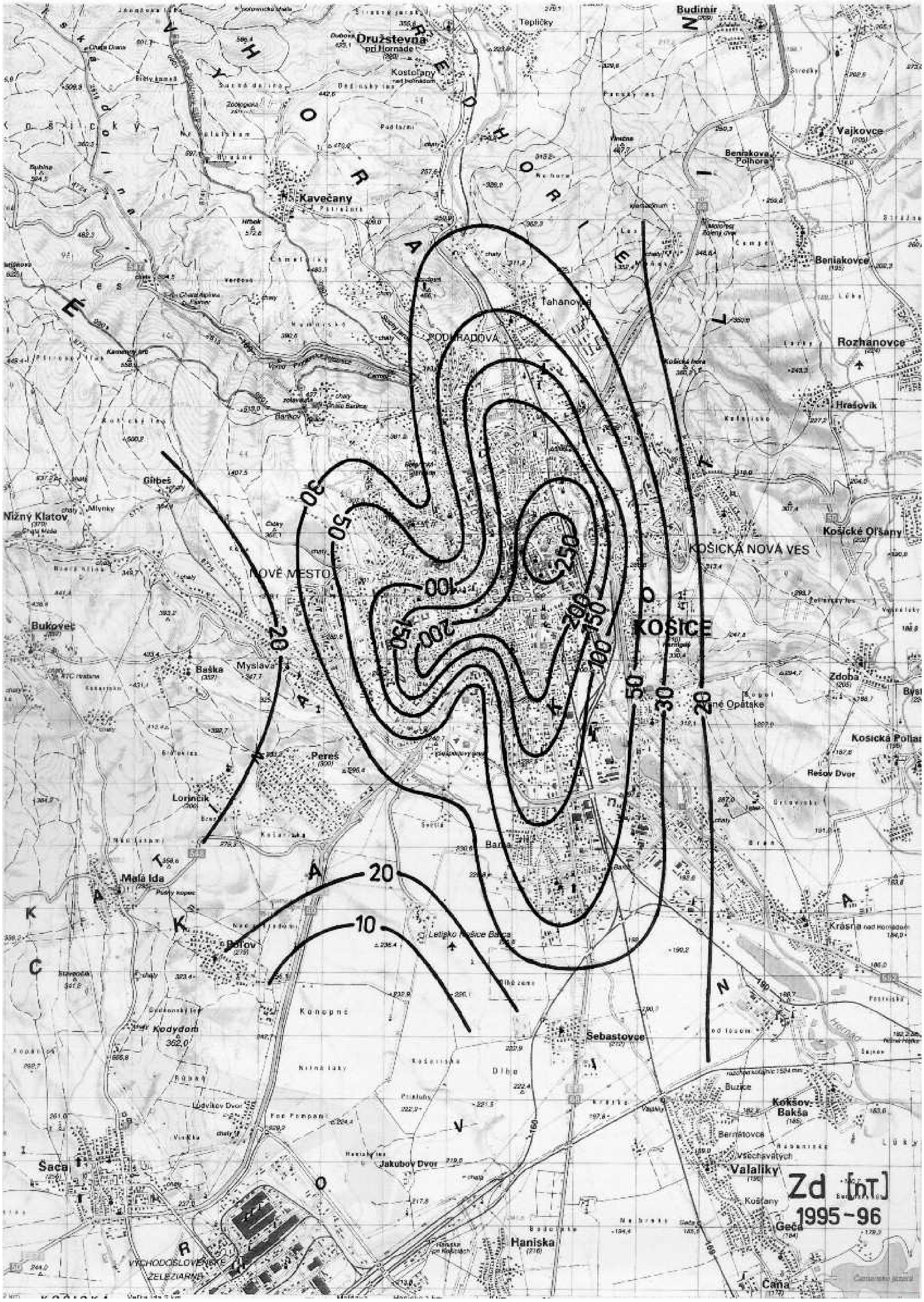

Fig. 2 The amplitude of disturbances *Zd* over the territory of Košice derived from the measurements of geomagnetic activity carried out in 1995-1996.

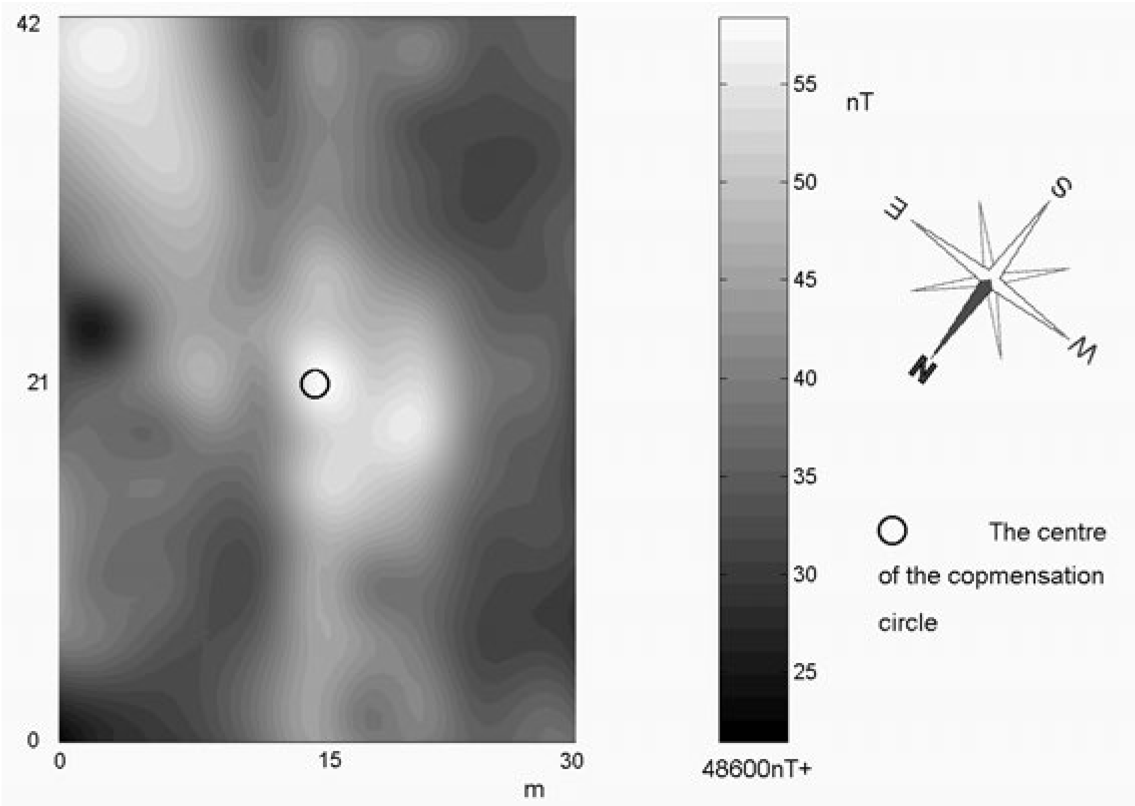

Fig. 3 The total magnetic field at the compensation circle.

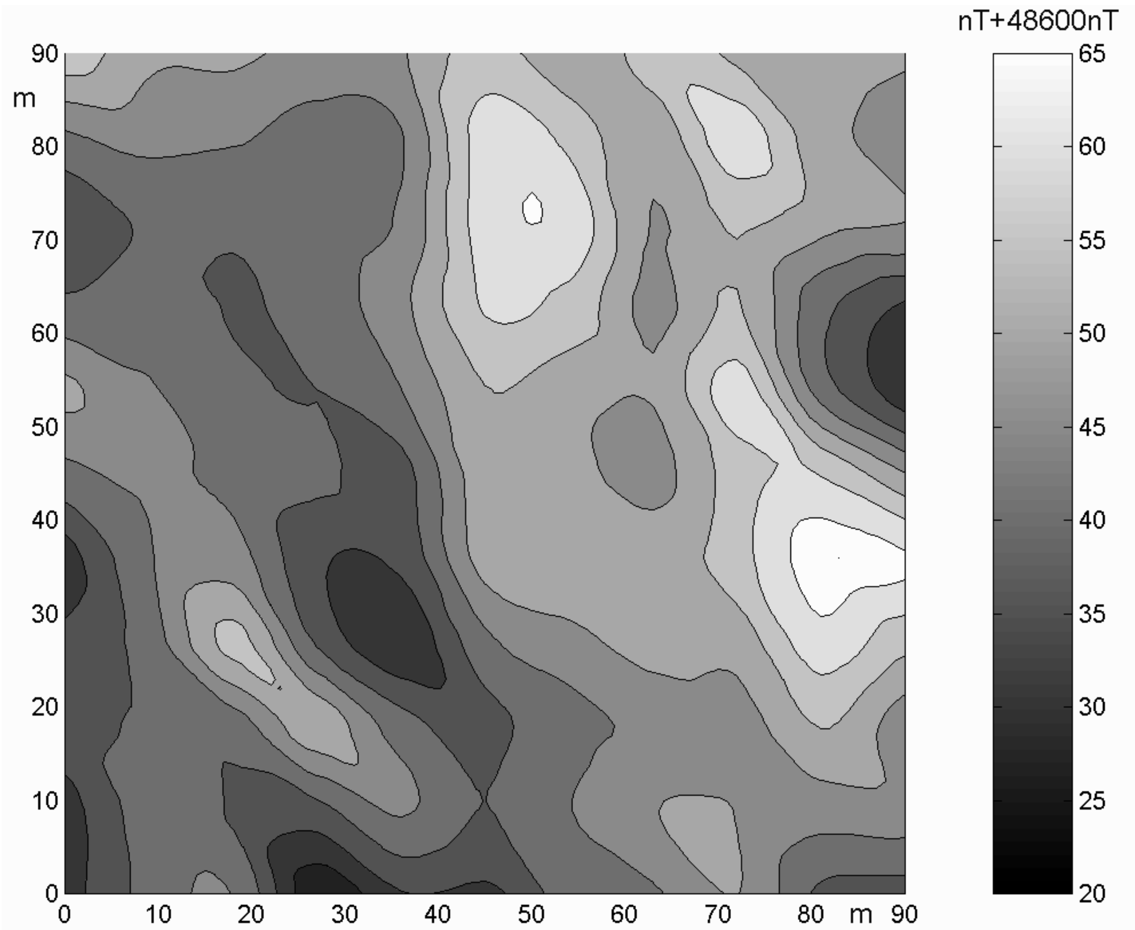

Fig. 4 Seeking for a suitable place for the new compensation circle (total field). The contour step is 5 nT.

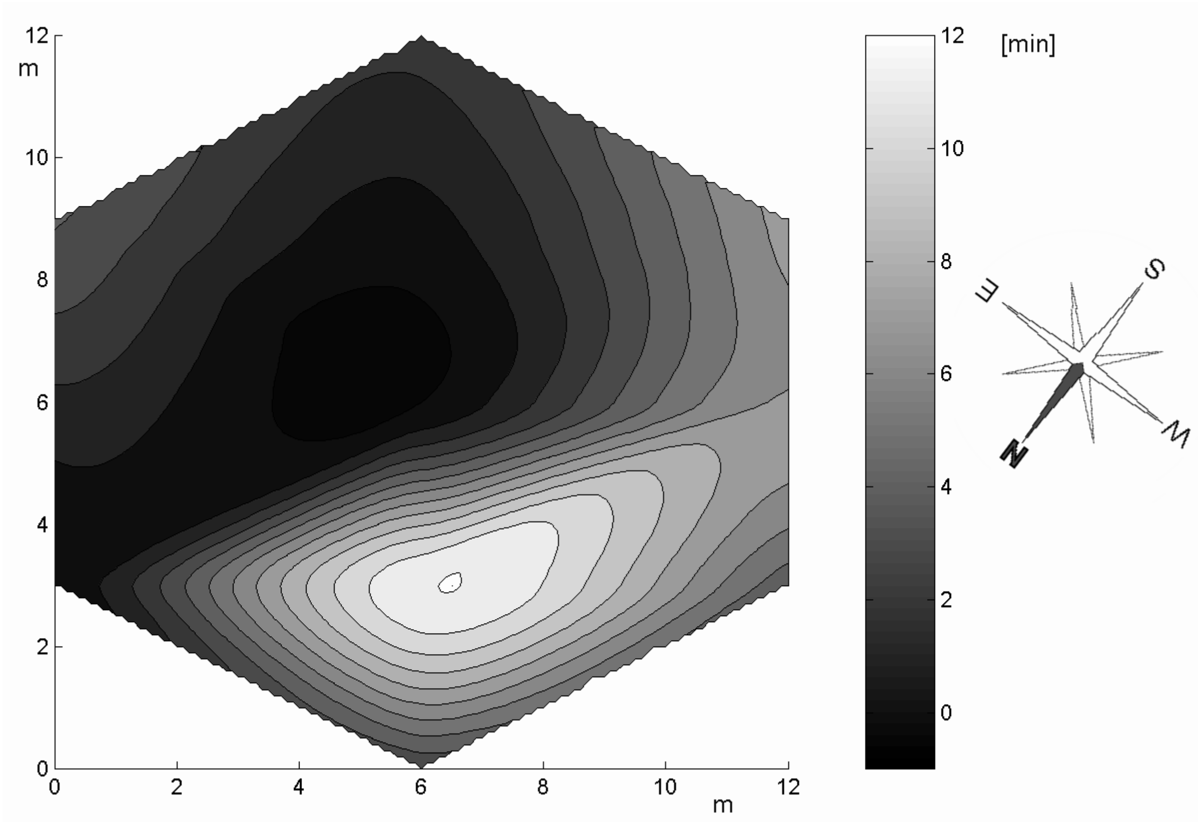

Fig. 5 A map indicating the anomalies of declination at the compensation circle. The isogon step is 1'.

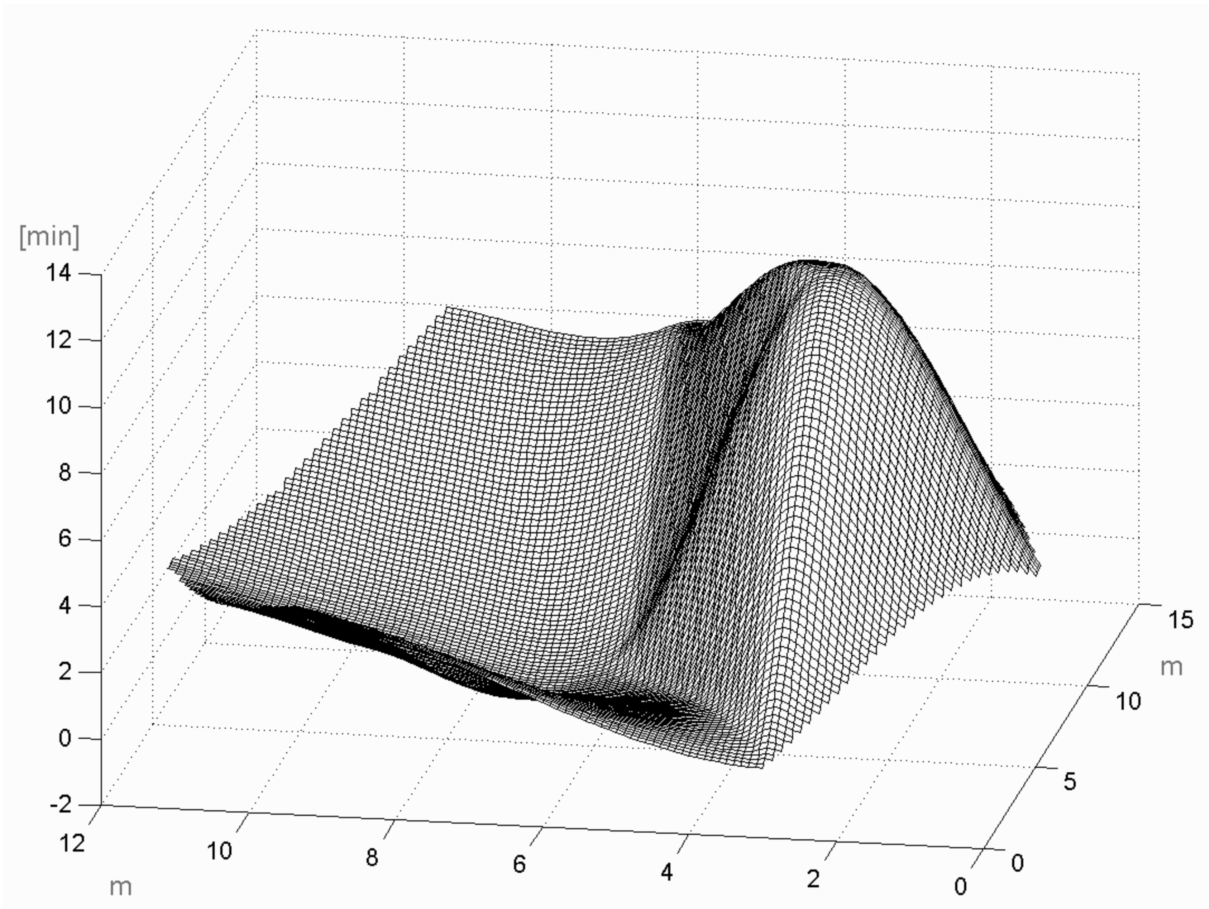

Fig. 6 **A** 3D map of the anomalies of declination at the compensation circle.

The measurements of declination were carried out in a network with sufficient density,. A quartz declinometer QD-21 was employed for this purpose. The data are treated as a usual

geomagnetic survey. For removing daily variations, the records of nearby observatories are taken into account. Owing to the small area of Slovakia, the records of the Hurbanovo observatory are representative for the whole country.
Figs. 5 and 6 show the anomaly maps of declination within the areas which are convenient for the compensating of compasses in small aeroplanes.
Besides the map of anomalies, the accurate absolute value of declination at the centre of the area must be determined, too. It is imperative to re-determine the absolute value from time to time (e.g. once per year) because of secular variation. Also the anomaly map should to be re-produced occasionally (e.g. every five years).

Conclusions

The paper was devoted to some practical utilization of geomagnetism, where the common observation practice can by employed in a direct manner.
The maps of artificial magnetic noise imply that a man-made magnetic field cannot be ignored when the geomagnetic activity influenced by human bodies is disputed.

Acknowledgements
The paper was prepared with the support of Agency for Science VEGA grant No. 1118/2000.

References

Hejda P. and Horáček J., 2001: On the industrial noise of the geomagnetic field in Prague. Contributions to Geophysics and Geodesy, 31, 159-163.
Jankowski J. and Sucksdorff C., 1996: Guide for Magnetic Observatory Practice. IAGA.
Túnyi I. and Vozár J., 2001: Magnetic Disturbances in Bratislava, Košice and in the Area of the Cyclotron Centre, Bratislava. Contributions to Geophysics and Geodesy, 31, Special Issue (Procc. of abstr. of the 4th Slovak Geophys. Conf.), Geophys. Inst. SAS, 39.

Secular Variations of the Geomagnetic Field at Hurbanovo

F Valach (Geomagnetic Observatory GPI SAS, Hurbanovo, Slovak Republic)

Abstract
In this paper a summary of the average annual values of the elements of the geomagnetic field observed at Hurbanovo is presented. The parts with period of hundreds of years and approximately 60 years were separated from the secular variation of declination. An analogous investigation carried out for inclination yields similar results. Because of a gap in Hurbanovo's records of inclination the data of other observatories were also taken into account. Considering the revealed sinusoidal variations, declination and inclination were estimated beyond the interval of true data.

Introduction

Since the 17th century it is known that the direction of the Earth's magnetic field lines depends not only on the coordinates but it also changes slowly in time. Halley [1692] estimated 700 years for a complete rotation of the magnetic field, implying a westward drift of 0.51° . yr^{-1}. Fig. 1 illustrates the secular variation of declination and inclination at five European sites in a zenithal equidistant projection - Bauer diagram (Soare et al., 1998).

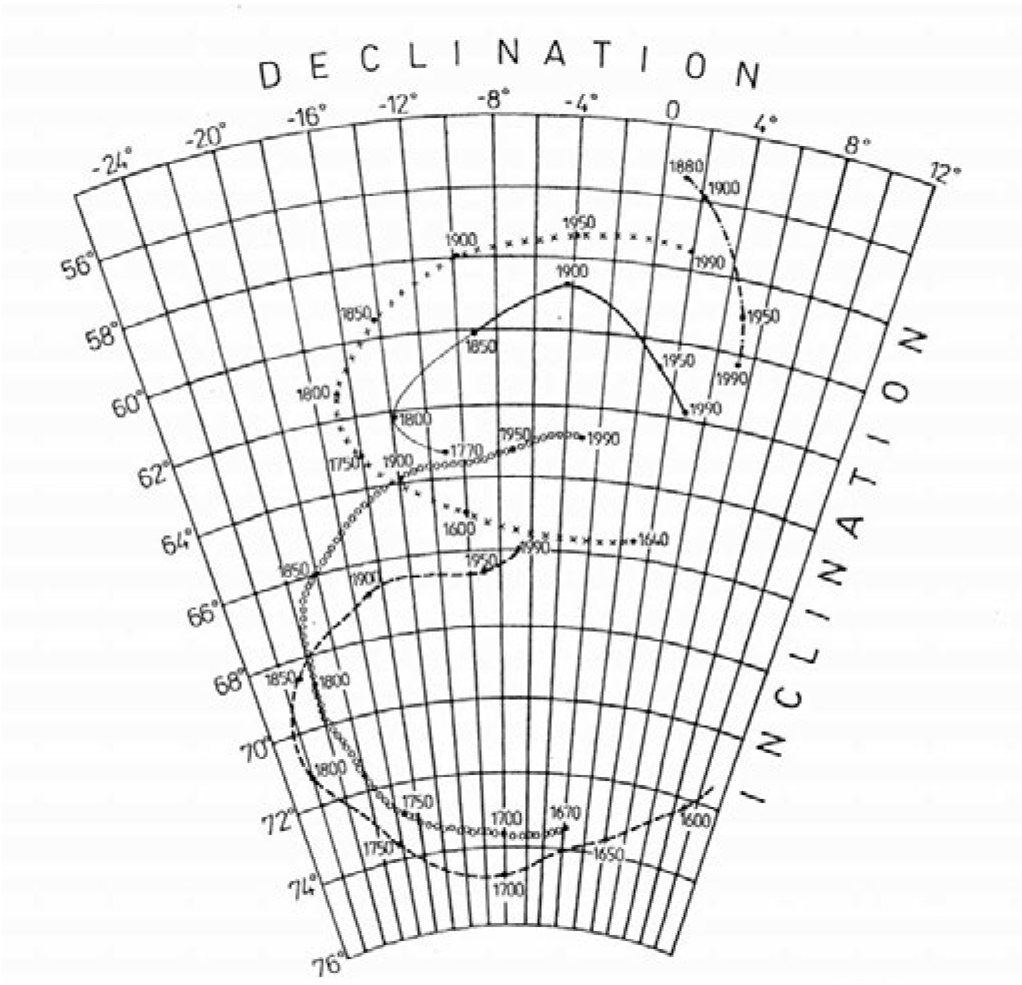

Fig.1 The direction of the Earth's magnetic field (Bauer diagram) for five geomagnetic time series: London (dashed line), Paris (open circles), Rome (crosses), Bucharest (solid line), Dusheti (dot-dashed line); points labeled every 50 years (except for the first and last). After (Soare et al., 1998).

Variations of the geomagnetic field with periods of hundreds of years are known from archeomagnetic results [Bucha, 1975]. These variations have approximately sinusoidal shapes and were found in declination as well as in inclination data. Hydromagnetic theory of the Earth's core suggests such a period, too [Merrill and McElhinny, 1983]. Previously, periods of tens of years were found in the geomagnetic elements series. The exchange of momentum between the mantle and core is considered as the cause of this variation [Podsklan, 1977, Barta, 1954, Vestine, 1953]. In this paper an attempt to identify such variations in the data of Hurbanovo (HRB) and Fuerstenfeldbruck (FUR) is made. Also an attempt to model the values of inclination and declination beyond the time periods of actually carried out observations is made here.

Data

The annual means of declination and inclination data for HRB are used in the paper (Fig. 2). There is a wide gap in the inclination series (1911 - 1941).

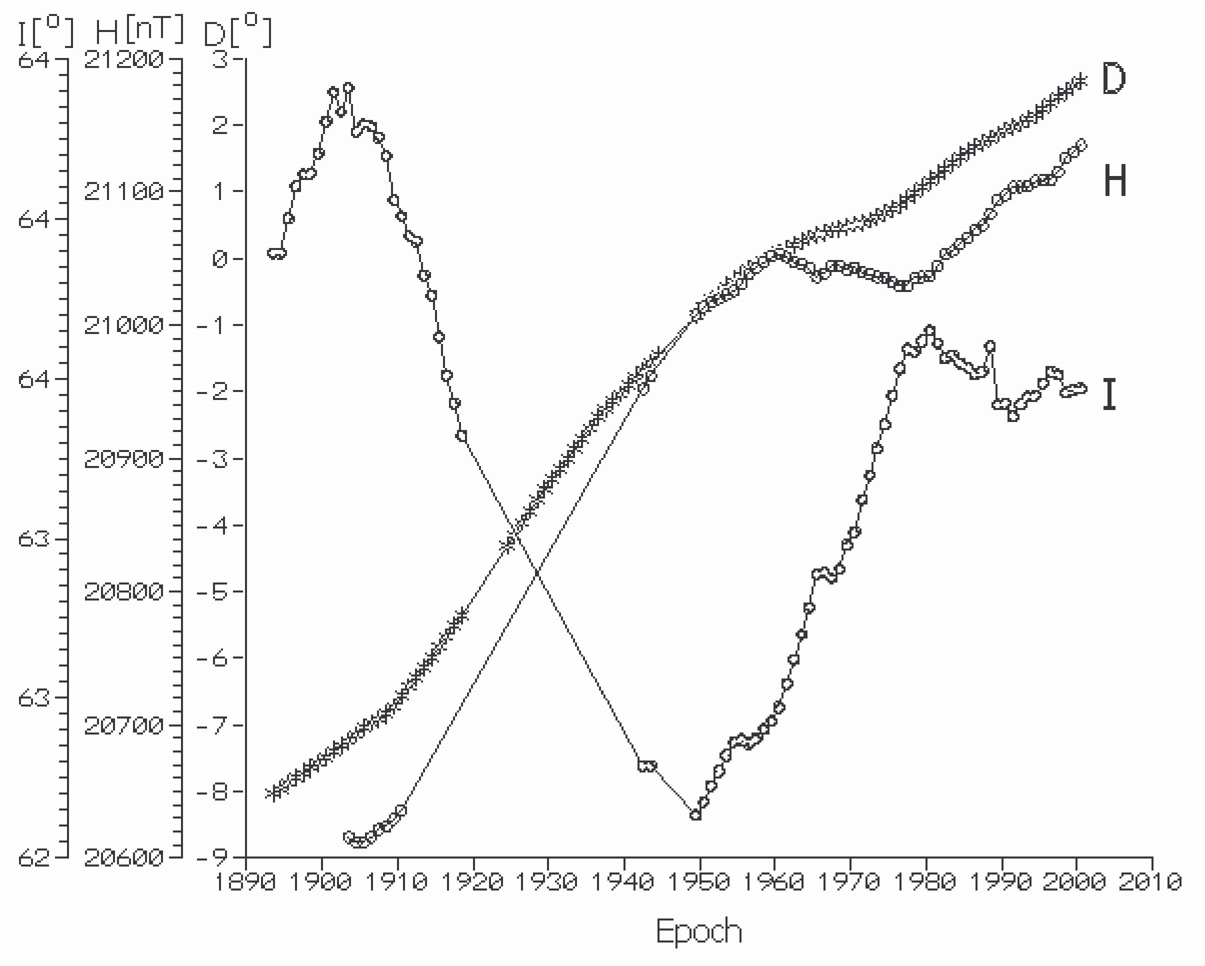

Fig. 2 The elements of the geomagnetic field (D, H and I) registered at Hurbanovo.

For this reason the HRB's data are not enough for intended purposes and also data of Fuerstenfeldbruck (FUR), Munich (MNH) and Maisach (MAS) will be used. These observatories were chosen because the geographic latitudes of them are almost the same as the latitude of Hurbanovo observatory is (Tab. 1).
A second reason is that their geomagnetic recordings are almost continuous for a very long time (since 1841). The data of MNH and MAS were reduced to FUR. Some of the results obtained from FUR's inclination were adopted for the variations of HRB's inclination .

	Latitude	Longitude
HRB	47.9 N	18.2 E
FUR	48.2 N	11.3 E
MNH	48.1 N	11.6 E
MAS	48.2 N	11.1 E

Tab. 1 The geographical coordinates of the observatories.

Methods and results

1. Using the least square method the variation with period T of several hundred of years were sought in the form

$$A \ \sin(2\pi \ t/T + B) + C \qquad (1)$$

In (1) time is indicated as *t*.
The period and amplitude of the variations of declination and inclination founded, are stored in Tab. 2 and Fig. 5. The original data and the fitted sinusoids are shown in Figs. 3a and 3b.

	Declination		Inclination	
	Period	Amplitude	Period	Amplitude
HRB	430 yr	9.74^o	690 yr *	5.20^o
FUR	470 yr	9.99^o	690 yr	4.52^o

Tab. 2 Periods and amplitudes of the long-term secular variation.
* The period T and the value of C found in FUR data were adopted for inclination of HRB.

2. The sinusoidal variations obtained in the previous were substracted from the original time series. In the new time series the previous procedure was repeated - using the least square method - the variation with period T of several tens of years were sought in the form (1). The founded periods and amplitudes of variations are stored in Tab. 3 and Fig.5. The time series and the fitted sinusoids are shown in Figs. 4a and 4b.

	Declination		Inclination	
	Period	Amplitude	Period	Amplitude
HRB	61 yr	0.40^o	115 yr*	0.49^o
FUR	71 yr	0.44^o	115 yr	0.37^o

Tab. 3 Periods and amplitudes of the shorter-therm secular variation.
* The period T found in FUR data was adopted for inclination of HRB.

Also the variations with the period of 58-yr and the amplitudes of 0.06° (HBR), and 0.10° (FUR) were founded in the inclination data after removing the 115-yr period but we consider it to be caused by a non-perfect removal of the 115-yr variation.

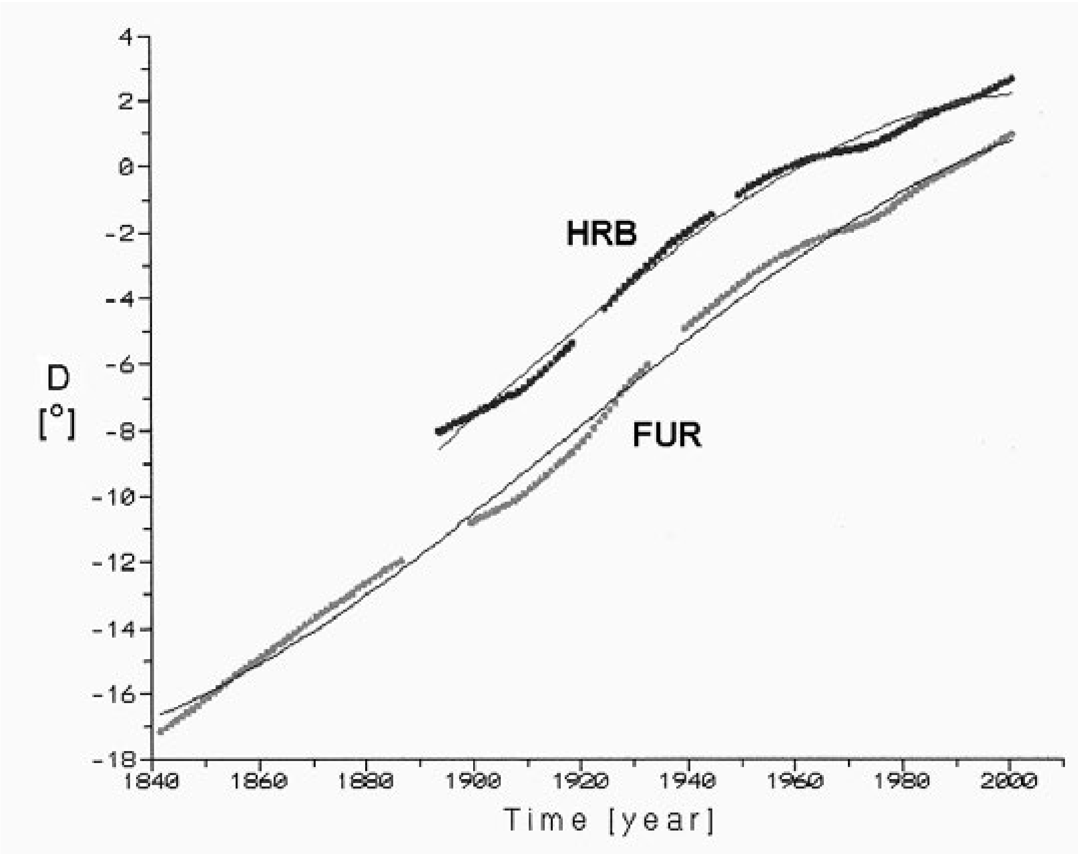

Fig. 3a Declination at HRB and FUR and fitted sinusoids (periods 430 and 470 yr, respectively).

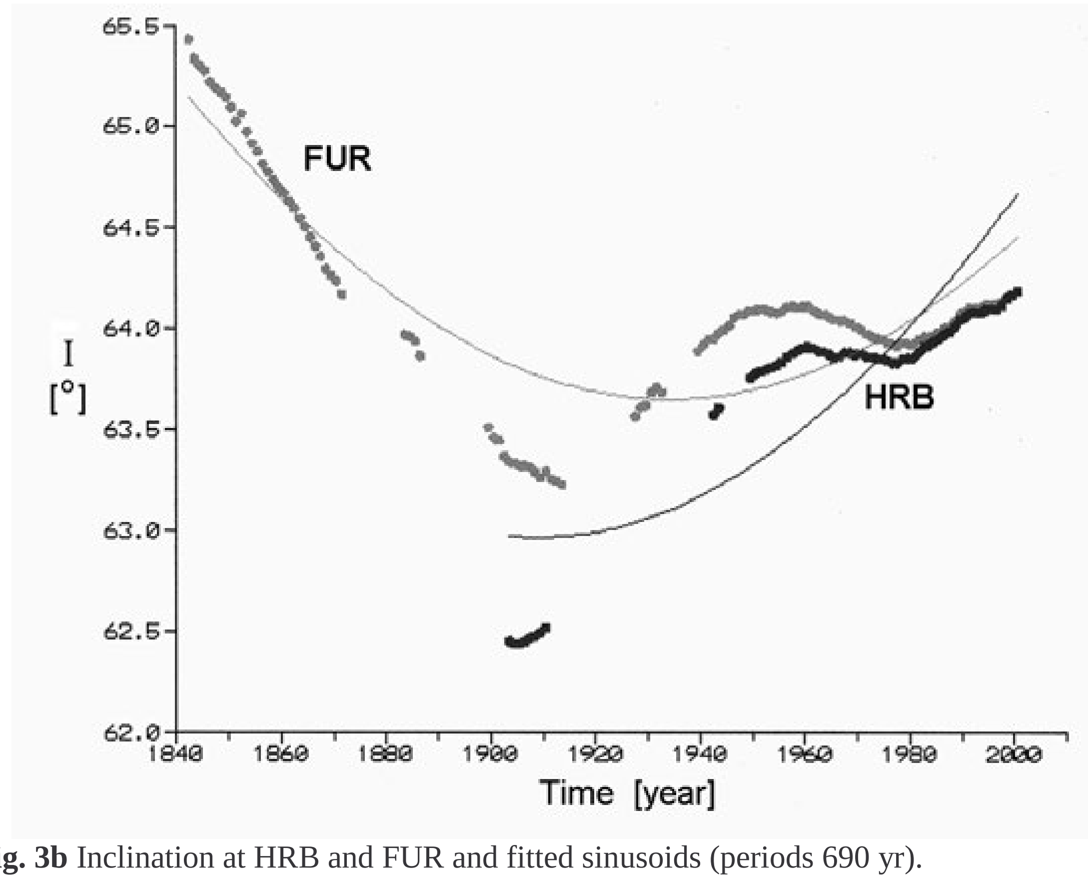

Fig. 3b Inclination at HRB and FUR and fitted sinusoids (periods 690 yr).

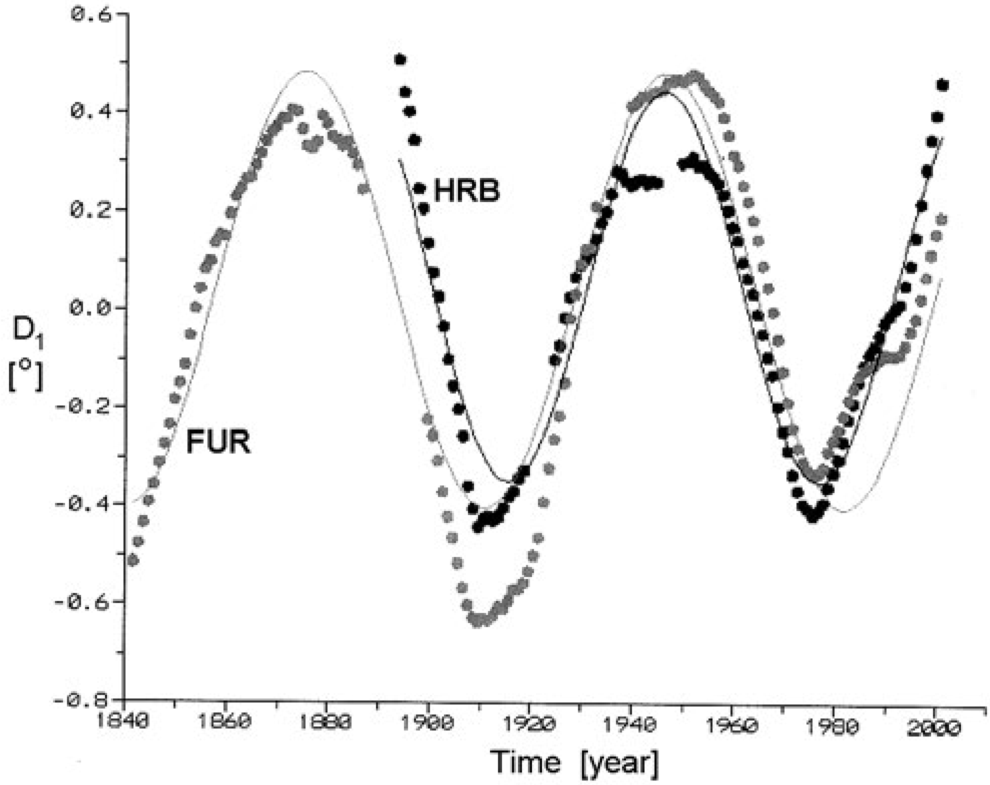

Fig. 4a Declination at HRB and FUR after removing the long-therm (hundreds of years) secular variation and fitted sinusoids with periods 61 and 71 yr, respectively.

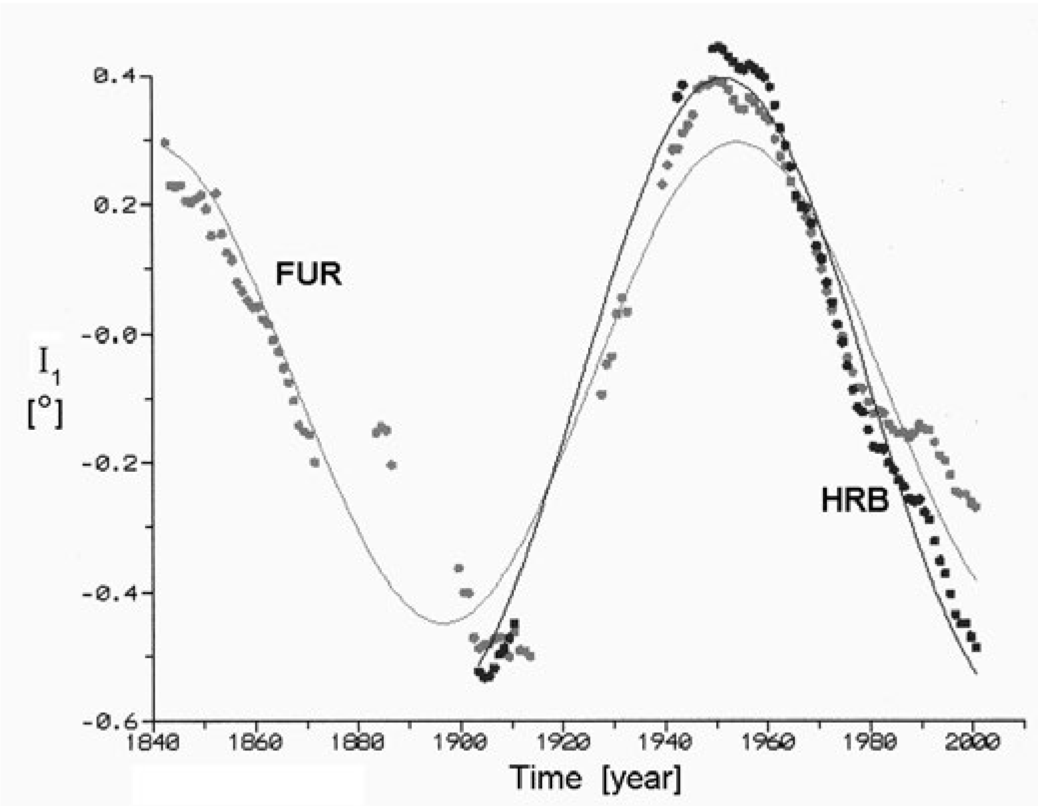

Fig. 4b Inclination at HRB and FUR after removing the long-therm (690 yr) secular variation and fitted sinusoids with periods of 115 yr.

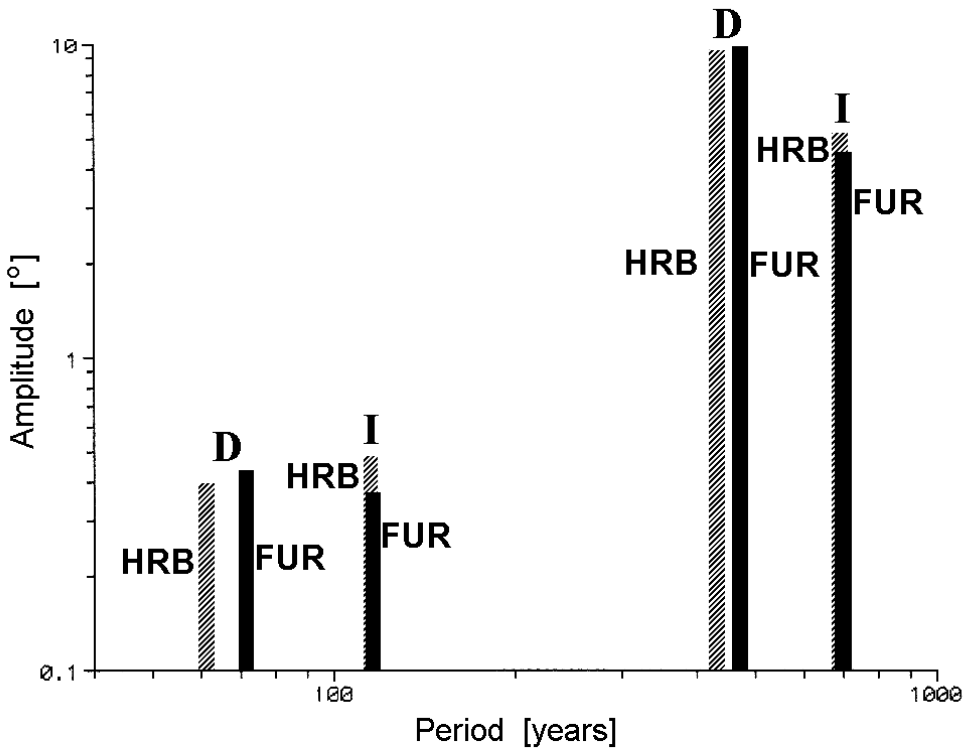

Fig. 5 The periods and amplitudes of the found variations.

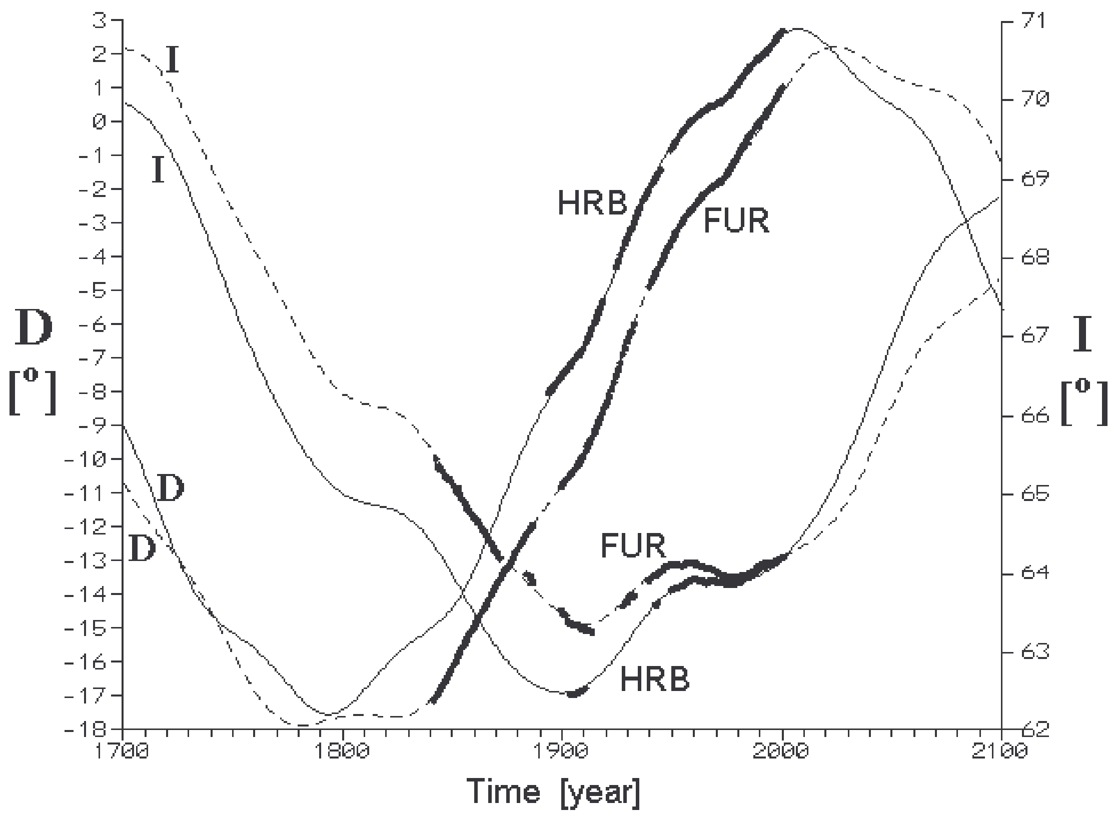

Fig. 6 Time series of declination and inclination at Hurbanovo and Fuerstenfeldbruck modelled on the basis of the found sinusoidal variations. Really observed parts of the curves are drawn as the thick parts of the curves.

Discussion

Fig. 6 shows declination and inclination for HRB and FUR modeled also beyond the time period with really carried out measurements (from 1700 to 2100). The model was made by superpositioning all the found sinusoidal variations. Fig. 7 shows these data drawn in the inclination vs declination form. According to the results the declination at HRB will increase until 2008.5 and will then decrease. For FUR such an extreme will occur in 2036.0. The westward drift calculated from these values is $0.25° . yr^{-1}$.

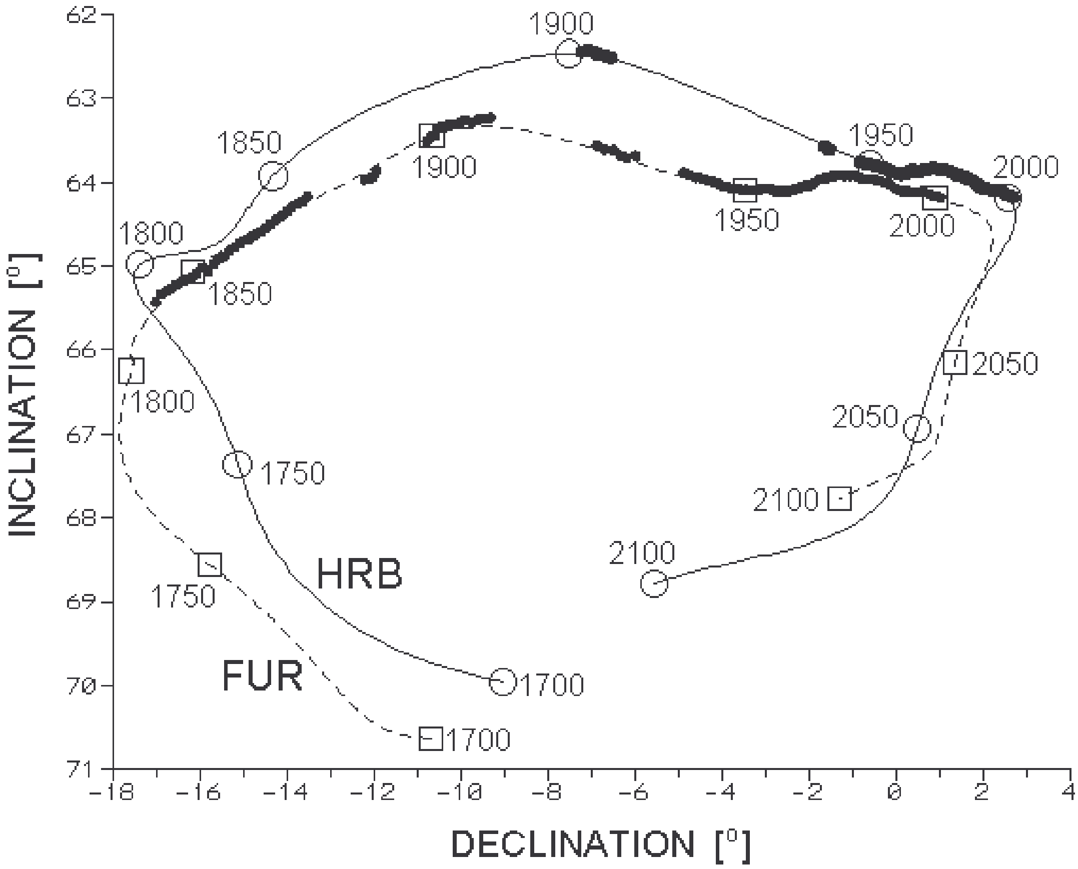

Fig. 7 Secular variations of declination and inclination at Hurbanovo and Fuerstenfeldbruck modeled on the basis of the found sinusoidal variations (Inclination vs Declination). Really observed parts of the curves are drawn as the thick parts of the curves.

The average westward drift calculated from all three local extremes, which are visible from the Figs. 6 and 7, is $0.5° . yr^{-1}$ ($0.93° . yr^{-1}$ for the 18th century from declination , $0.28° . yr^{-1}$ from inclination and $0.25° . yr^{-1}$ from the future maximum in declination).
Relatively realistic estimates of westward drift (comparing with [Merrill and McElhinny, 1983, Barraclough and Malin, 1999]) together with similar character of Figs. 1 and 7 in a certain extent confirm the proposed model.

Acknowledgements

The paper was prepared with the support of the Agency for Science VEGA grant No. 1118/2000. Geomagnetic data from the Fuerstenfeldbruck, Munich and Maisach Observatories are acknowledged.

References

Barraclough, D. R. and Malin, S. R. C. (1999), A fast-moving feature of westward drift, Annali di Geofisica, 42, 21-26.

Barta, Gy. (1954), On a 44 Years Period of the Secular Variation of the Geomagnetic Field. Geofizikai Közlemények, 3, 3-26.

Bucha, V. (1975), Geomagnetic Field and Its Contribution to Explaining of the Evolution of the Earth (in Czech), Academia, Prague.

Halley, E. (1692), An account of the cause of the change of the variation of the magnetic needle; with an hypothesis of the structure of the internal parts of the Earth, Philos. Trans. R. Soc. London, 17, 563-578.

Merrill, R. T. and McElhinny, M. W. (1983), The Earth's Magnetic Field / Its history, Origin and Planetary perspective, Academic Press, London.

Podsklan, J. (1977), Secular Variations of the Elements of the Geomagnetic Field at Hurbanovo, Contr. Geophys. Inst. Slov. Acad. Sci., 7, 65-70.

Soare, A., Cucu, G. and Mandea Alexandrescu, M. (1998), Historical geomagnetic measurements in Romania, 41 (4), 539-554.

Vestine, E. H. (1953), On variations of the geomagnetic field, fluid motions and the rate of the Earth's rotation. J. Geophys. Res., 58, 127-145.